Massimo Guiggiani

The Science of Vehicle Dynamics

Handling, Braking, and Ride of Road and Race Cars

Springer

The Science of Vehicle Dynamics

Massimo Guiggiani

The Science of Vehicle Dynamics

Handling, Braking, and Ride of Road and Race Cars

Springer

Massimo Guiggiani
Dip. di Ingegneria Civile e Industriale
Università di Pisa
Pisa, Italy

ISBN 978-94-017-8532-7 ISBN 978-94-017-8533-4 (eBook)
DOI 10.1007/978-94-017-8533-4
Springer Dordrecht Heidelberg New York London

Library of Congress Control Number: 2013958104

Printed on acid-free paper

Springer is part of Springer Science+Business Media (www.springer.com)

Preface

Vehicle dynamics should be a branch of Dynamics, but, in my opinion, too often it does not look like that. Dynamics is based on terse concepts and rigorous reasoning, whereas the typical approach to vehicle dynamics is much more intuitive. Qualitative reasoning and intuition are certainly very valuable, but they should be supported and confirmed by scientific and quantitative results.

I understand that vehicle dynamics is, perhaps, the most popular branch of Dynamics. Almost everybody has been involved in discussions about some aspects of the dynamical behavior of a vehicle (how to brake, how to negotiate a bend at high speed, which tires give best performance, etc.). At this level, we cannot expect a deep knowledge of the dynamical behavior of a vehicle.

But there are people who could greatly benefit from mastering vehicle dynamics. From having clear concepts in mind. From having a deep understanding of the main phenomena. This book is intended for those people who want to build their knowledge on sound explanations, who believe equations are the best way to formulate and, hopefully, solve problems. Of course along with physical reasoning and intuition.

I have been constantly alert not to give anything for granted. This attitude has led to criticize some classical concepts, such as self-aligning torque, roll axis, understeer gradient, handling diagram. I hope that even very experienced people will find the book interesting. At the same time, less experienced readers should find the matter explained in a way easy to absorb, yet profound. Quickly, I wish, they will feel not so less experienced any more.

Acknowledgments Over the last few years I have had interactions and discussions with several engineers from Ferrari Formula 1. The problems they constantly have to face have been among the motivations for writing this book. Moreover, their deep knowledge of vehicle dynamics has been a source of inspiration. I would like to express my gratitude to Maurizio Bocchi, Giacomo Tortora, Carlo Miano, Marco Fainello, Tito Amato (presently at Mercedes), and Gabriele Pieraccini (presently at Bosch).

I wish to thank Dallara Automobili and, in particular, Andrea Toso, Alessandro Moroni, and Luca Bergianti. They have helped me in many ways.

At the Università di Pisa there are an M.S. degree course in Vehicle Engineering (where I teach Vehicle Dynamics) and a Ph. D. program in Vehicle Engineering and Transportation Systems. This very lively environment has played a crucial role in the development of some of the most innovative topics in this book. In particular, I wish to acknowledge the contribution of my colleague Francesco Frendo, and of my former Ph. D. students Antonio Sponziello, Riccardo Bartolozzi, and Francesco Bucchi. Francesco Frendo and Riccardo Bartolozzi have also reviewed part of this book.

During the last six years I have been the Faculty Advisor of E-Team, the Formula Student team of the Università di Pisa. I thank all the team members. It has been a very interesting and rewarding experience, both professionally and personally.

Testing real vehicles is essential to understand vehicle dynamics. I wish to thank Danilo Tonani, director of FormulaGuidaSicura, for having given me the opportunity of becoming a safe driving instructor. Every year, he organizes an excellent safe driving course for the M.S. students in Vehicle Engineering of the Università di Pisa.

My collaborators and dear friends Alessio Artoni and Marco Gabiccini have carefully reviewed this book. I am most grateful to them for their valuable suggestions to correct and improve the text.

Pisa, Italy Massimo Guiggiani
October 2013

Contents

Chapter 1
Introduction

Vehicle dynamics is a fascinating subject, but it can also be very frustrating without the tools to truly understand it. We can try to rely on experience, but an objective knowledge needs a scientific approach. Something grounded on significant mathematical models, that is models complex enough to catch the essence of the phenomena under investigation, yet simple enough to be understood by a (well trained) human being. This is the essence of science, and vehicle dynamics is no exception.

But the really important point is in the mental attitude we should have in approaching a problem. We must be skeptical. We must be critical. We must be creative. Even if something is commonly accepted as obviously true, or if it looks very reasonable, it may be wrong, either totally or partially wrong. There might be room for some sort of improvement, for a fresh point of view, for something valuable.

Vehicle dynamics can be set as a truly scientific subject, it actually needs to be set as such to achieve a deep comprehension of what is going on when, e.g., a race car negotiates a bend.

When approached with open mind, several classical concepts of vehicle dynamics, like, e.g., the roll axis, the understeer gradient, even the wheelbase, turn out to be very weak concepts indeed. Concepts often misunderstood, and hence misused. Concepts that need to be revisited and redefined, and reformulated to achieve an objective knowledge of vehicle dynamics. Therefore, even experienced people will probably be surprised by how some topics are addressed and discussed here.

To formulate vehicle dynamics on sound concepts we must rely on clear definitions and model formulations, and then on a rigorous mathematical analysis. We must, indeed, "formulate" the problem at hand by means of mathematical formulæ [4]. There is no way out. Nothing is more practical than a good theory. However, although we will not refrain from using formulæ, at the same time we will keep the analysis as simple as possible, trying to explain what each formula tells us.

To help the reader, the Index of almost all mathematical symbols is provided at the end of this book. We believe an Index is more useful than a Glossary because it shows in which context each symbol is defined.

M. Guiggiani, *The Science of Vehicle Dynamics*, DOI 10.1007/978-94-017-8533-4_1,

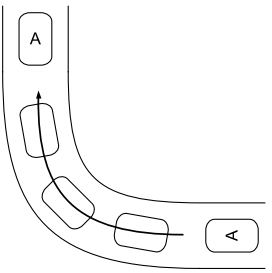

Fig. 1.1 Vehicle expected behavior when negotiating a curve

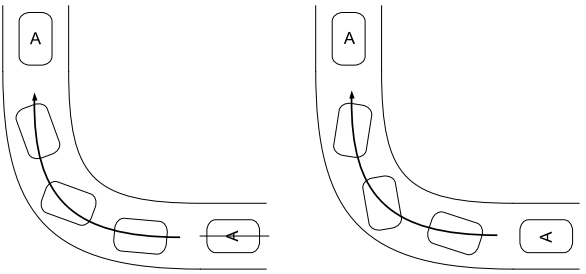

Fig. 1.2 Acceptable behaviors for a road vehicle

1.1 Vehicle Definition

Before embarking into the development of mathematical models, it is perhaps advisable to discuss a little what ultimately is (or should be) a *driveable road vehicle*. Since a road is essentially a long, fairly narrow strip, a vehicle must be an object with a clear *heading direction*.[1] For instance, a shopping kart is not a vehicle since it can go in any direction. Another common feature of road vehicles is that the driver is carried on board, thus undergoing the same dynamics (which, again, is not the case of a shopping kart).

Moreover, roads have curves. Therefore, a vehicle must have the capability to be driven in a fairly precise way. This basically amounts to controlling simultaneously the *yaw rate* and the magnitude and direction of the *vehicle speed*. To fulfill this task a car driver can act (at least) on the brake and accelerator pedals and on the steering wheel. And here it is where vehicle dynamics comes into play, since the outcome of the driver actions strongly depends on the vehicle dynamic features and state.

An example of proper turning of a road vehicle is something like in Fig. 1.1. Small deviations from this target behavior, like those shown in Fig. 1.2, may be tolerated. On the other hand, Fig. 1.3 shows two unacceptable ways to negotiate a bend.

[1] Usually, children show to have well understood this concept when they move by hand a small toy car.

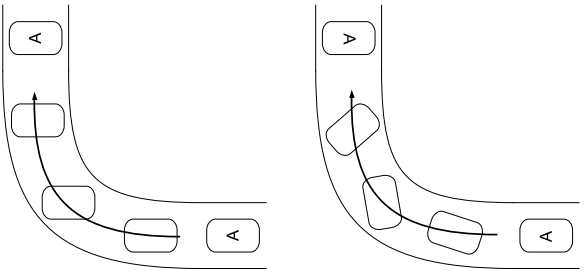

Fig. 1.3 Unacceptable behaviors for a road vehicle

All road vehicles have wheels, in almost all cases equipped with pneumatic tires. Indeed, also wheels have a clear heading direction. This is why the main way to steer a vehicle is by turning some (or all) of its wheels.[2]

To have good directional capability, the wheels in a vehicle are arranged such that their heading directions almost "agree", that is they do not conflict too much with each other. However, tires do work pretty well under small slip angles and, as will be shown, some amount of "disagreement" is not only tolerated, but may even be beneficial.

Wheel hubs are connected to the chassis (vehicle body) by means of suspensions. The number of possible different suspensions is virtually endless. However, suspension systems can be broadly classified into two main subgroups: dependent and independent. In a dependent suspension the two wheels of the same axle are rigidly connected together. In an independent suspension they are not, and each wheel is connected to the chassis by a linkage with "mainly" one degree of freedom. Indeed, the linkage has some compliance which, if properly tuned, can enhance the vehicle behavior.

1.2 Vehicle Basic Scheme

A mathematical model of a vehicle [5] should be *simple*, yet *significant* [1, 2]. Of course, there is not a unique solution. Perhaps, the main point is to state clearly the assumptions behind each simplification, thus making clear under which conditions the model can reliably predict the behavior of a real vehicle.

There are assumptions concerning the *operating conditions* and assumptions regarding the *physical model* of the vehicle.

Concerning the *operating conditions*, several options can be envisaged:

performance: the vehicle goes straight on a flat road, possibly braking or accelerating (nonconstant forward speed);
handling: the vehicle makes turns on a flat road, usually with an almost constant forward speed;
ride: the vehicle goes straight on a bumpy road, with constant forward speed.

[2] Broadly speaking, wheels location does not matter to the driver. But it matters to engineers.

Obviously, real conditions are a mixture of all of them.

A significant, yet simple, *physical model* of a car may have the following features:

(1) the vehicle body is a single rigid body;
(2) each wheel hub is connected to the vehicle body by a single degree-of-freedom linkage (independent suspension);
(3) the steering angle of each (front) wheel is mainly determined by the angular position δ_v of the steering wheel, as controlled by the driver;
(4) the mass of the wheels (unsprung mass) is very small if compared to the mass of the vehicle body (sprung mass);
(5) the wheels have pneumatic tires;
(6) there are springs and dampers (and, maybe, inerters) between the vehicle body and the suspensions, and, likely, between the two suspensions of the same axle (anti-roll bar). Front to rear interconnected suspensions are possible, but very unusual;
(7) there may be aerodynamic devices, like wings, that may significantly affect the downforce.

The first two assumptions ultimately disregard the elastic compliances of the chassis and of the suspension linkages, respectively, while the third assumption leaves room for vehicle models with compliant steering systems.

A vehicle basic scheme is shown in Fig. 1.4, which also serves the purpose of defining some fundamental geometrical parameters:

(1) the vehicle longitudinal axis x, and hence the vehicle heading direction $\mathbf{i}$;
(2) the height h from the road plane of the center of gravity G of the whole vehicle;
(3) the longitudinal distances a_1 and a_2 of G from the front and rear axles, respectively;
(4) the lateral position b of G from the axis;
(5) the wheelbase $l = a_1 + a_2$;
(6) the front and rear tracks t_1 and t_2;
(7) the geometry of the linkages of the front and rear suspensions;
(8) the position of the steering axis for each wheel.

All these distances are positive, except possibly b, which is usually very small and hence typically set equal to zero, like in Fig. 1.4.

It must be remarked that whenever during the vehicle motion there are suspension deflections, several of these geometrical parameters may undergo small changes. Therefore, it is common practice to take their reference value under the so called *static conditions*, which means with the vehicle moving straight on a flat road at constant speed, or, equivalently if there are no wings, when the vehicle is motionless on a horizontal plane.

Accordingly, the study of the performance and handling of vehicles is greatly simplified under the hypothesis of small suspension deflections, much like assuming

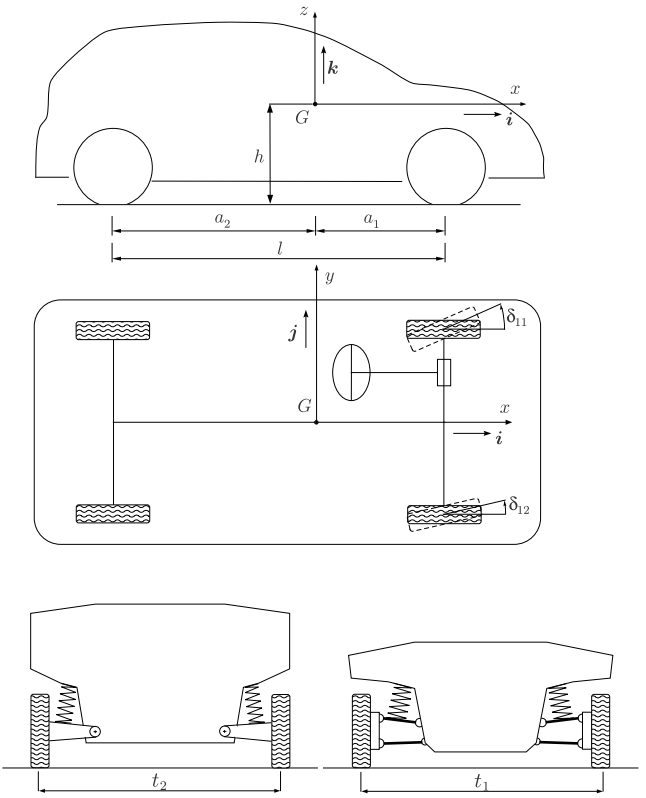

Fig. 1.4 Vehicle basic scheme

Fig. 1.5 Example of a double wishbone front suspension [6]

very stiff springs (which is often the case for race cars).[3] Yet, suspensions cannot be completely disregarded, at least not in vehicles with four or more wheels. This aspect will be thoroughly discussed.

The vehicle shown in Fig. 1.4 has a swing arm rear suspension and a double wishbone front suspension. Perhaps, about the worst and the best kind of independent suspensions [3]. They were selected to help explaining some concepts, and should not be considered as an example of a good vehicle design. An example of a double wishbone front suspension is shown in Fig. 1.5.

References

1. Arnold M, Burgermeister B, Führer C, Hippmann G, Rill G (2011) Numerical methods in vehicle system dynamics: state of the art and current developments. Veh Syst Dyn 49(7):1159–1207
2. Cao D, Song X, Ahmadian M (2011) Editors' perspectives: road vehicle suspension design, dynamics, and control. Veh Syst Dyn 49(1–2):3–28
3. Genta G, Morello L (2009) The automotive chassis. Springer, Berlin
4. Guiggiani M, Mori LF (2008) Suggestions on how not to mishandle mathematical formulæ. TUGboat 29:255–263
5. Heißing B, Ersoy M (eds) (2011) Chassis handbook. Springer, Wiesbaden
6. Longhurst C (2013). www.carbibles.com

[3] However, handling with roll will be covered in Chap. 9, although at the expense of quite a bit of additional work.

Chapter 2
Mechanics of the Wheel with Tire

All road vehicles have wheels and almost all of them have *wheels* with *pneumatic tires*. Wheels have been around for many centuries, but only with the invention, and enhancement, of the pneumatic tire it has been possible to conceive fast and comfortable road vehicles [3].

The main features of any tire are its *flexibility* and *low mass*, which allow for the contact with the road to be maintained even on uneven surfaces. Moreover, the rubber ensures *high grip*. These features arise from the highly composite structure of tires: a carcass of flexible, yet almost inextensible cords encased in a matrix of soft rubber, all inflated with air.[1] Provided the (flexible) tire is properly inflated, it can exchange along the bead relevant actions with the (rigid) rim. Traction, braking, steering and load support are the net result.

It should be appreciated that the effect of air pressure is to increase the structural stiffness of the tire, not to support directly the rim. How a tire carries a vertical load F_z if properly inflated is better explained in Fig. 2.1. In the lower part, the sidewalls bend and, thanks to the air pressure p_a, they apply more vertical forces F_a in the bead area than in the upper part. The overall effect on the rim is a vertical load F_z. The higher the air pressure p_a, the lower the sidewall bending.

The *contact patch*, or footprint, of the tire is the area of the tread in contact with the road. This is the area that transmits forces between the tire and the road via pressure and friction. To truly understand some of the peculiarities of tire mechanics it is necessary to get some insights on what happens in the contact patch.

Handling of road vehicles is strongly affected by the mechanical behavior of the wheels with tire, that is by the *relationship* between the *kinematics* of the rigid rim and the *force* exerted by the road. This chapter is indeed devoted to the analysis of experimental tests. The development of simple, yet significant, tire models is done in Chap. 10.

[1] Only in competitions it is worthwhile to employ special (and secret) gas mixtures instead of air. The use of nitrogen, as often recommended, is in fact completely equivalent to air, except for the cost.

M. Guiggiani, *The Science of Vehicle Dynamics*, DOI 10.1007/978-94-017-8533-4_2,

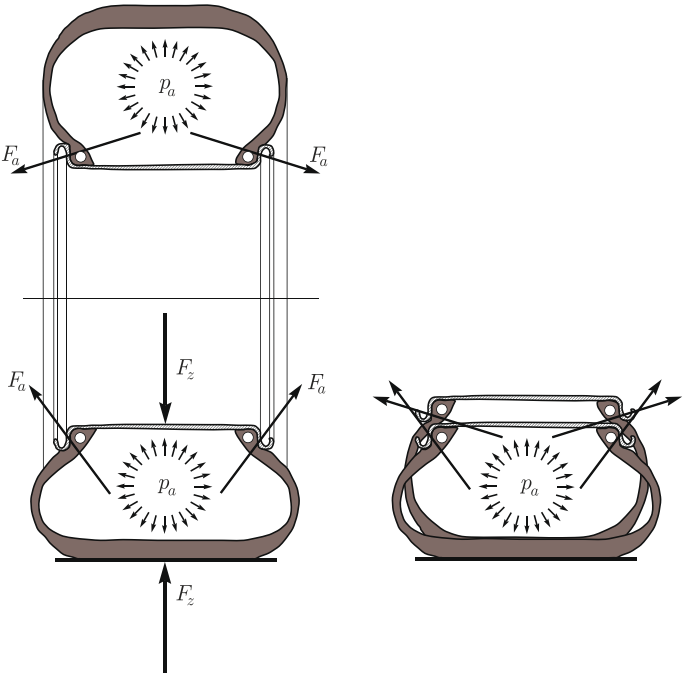

Fig. 2.1 How a tire carries a vertical load if properly inflated

2.1 The Tire as a Vehicle Component

A wheel with tire is barely a wheel, in the sense that it behaves quite differently from a rigid wheel.[2] This is a key point to really understand the mechanics of wheels with tires. For instance, a rigid wheel touches the (flat) road at one point C, whereas a tire has a fairly large contact patch. Pure rolling of a rigid wheel is a clear kinematic concept [12], but, without further discussion, it is not obvious whether an analogous concept is even meaningful for a tire. Therefore, we have to be careful in stating as clearly as possible the concepts needed to study the mechanics of wheels with tire.

Moreover, the analysis of tire mechanics will be developed with no direct reference to the dynamics of the vehicle. This may sound a bit odd, but it is not. The goal here is to describe the *relationship* between the *motion* and *position* of the rim and the *force* exchanged with the road through the contact patch:

$$\text{rim kinematics} \quad \Longleftrightarrow \quad \text{force and moment}$$

[2] A rigid wheel is essentially an axisymmetric convex rigid surface. The typical rigid wheel is a toroid.

Once this description has been obtained and understood, then it can be employed as one of the fundamental components in the development of suitable models for vehicle dynamics, but this is the subject of other chapters.

Three basic components play an active role in tire mechanics:

(1) the *rim*, which is assumed to be a rigid body;
(2) the flexible *carcass* of the inflated tire;
(3) the *contact patch* between the tire and the road.

2.2 Rim Position and Motion

For simplicity, the *road* is assumed to have a hard and *flat* surface, like a *geometric plane*. This is a good model for any road with high quality asphalt paving, since the texture of the road surface is not relevant for the definition of the rim kinematics (while it highly affects grip [8]).

The *rim* $\mathscr{R}$ is assumed to be a *rigid body*, and hence, in principle, it has six degrees of freedom. However, only two degrees of freedom (instead of six) are really relevant for the rim *position* because the road is *flat* and the wheel rim is *axisymmetrical*.

Let Q be a point on the rim axis y_c (Fig. 2.2). Typically, although not strictly necessary, a sort of midpoint is taken. The *position* of the rim with respect to the flat road depends only on the *height* h of Q and on the *camber angle* γ (i.e., the inclination) of the rim axis y_c. More precisely, h is the distance of Q from the road plane and γ is the angle between the rim axis and the road plane.

Now, we can address how to describe the rim velocity field.

The rim, being a rigid body, has a well defined angular velocity $\mathbf{\Omega}$. Therefore, the velocity of any point P of the (space moving with the) rim is given by the well known equation [7, p. 124]

$$\mathbf{V}_P = \mathbf{V}_Q + \mathbf{\Omega} \times QP \tag{2.1}$$

where $\mathbf{V}_Q$ is the velocity of Q and QP is the vector connecting Q to P. The three components of $\mathbf{V}_Q$ and the three components of $\mathbf{\Omega}$ are, e.g., the *six* parameters which completely determine the rim *velocity* field.

A moving reference system $\mathsf{S} = (x, y, z; O)$ is depicted in Fig. 2.2. It is defined in a fairly intuitive way. The y-axis is the intersection between a vertical plane containing the rim axis y_c and the road plane. The x-axis is given by the intersection of the road plane with a plane containing Q and normal to y_c. Axes x and y define the origin O as a point on the road. The z-axis is vertical, that is perpendicular to the road, with the positive direction upward.[3] The unit vectors marking the positive directions are $(\mathbf{i}, \mathbf{j}, \mathbf{k})$, as shown in Fig. 2.2.

[3] S is the system recommended by ISO (see, e.g., [14, Appendix 1]).

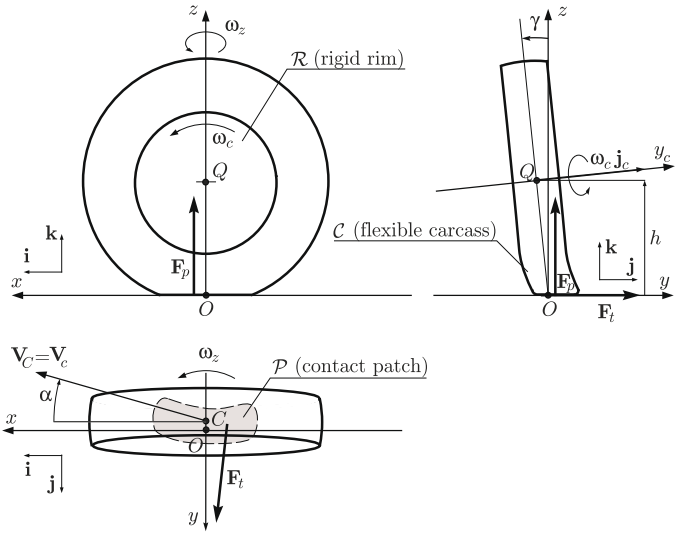

Fig. 2.2 Wheel with tire: nomenclature and reference system

An observation is in order here. The *directions* $(\mathbf{i}, \mathbf{j}, \mathbf{k})$ have a physical meaning, in the sense that they clearly mark some of the peculiar features of the rim with respect to the road. As a matter of fact, $\mathbf{k}$ is perpendicular to the road, $\mathbf{i}$ is perpendicular to both $\mathbf{k}$ and the rim axis $\mathbf{j}_c$, $\mathbf{j}$ follows accordingly. However, the *position* of the Cartesian axes (x, y, z) is arbitrary, since there is no physical reason to select a point as the origin O. This is an aspect whose implications are often underestimated.

The moving reference system $\mathsf{S} = (x, y, z; O)$ allows a more precise description of the rim kinematics. On the other hand, a reference system $\mathsf{S}_f = (x_f, y_f, z_f; O_f)$ fixed to the road is not very useful in this context.

Let $\mathbf{j}_c$ be the direction of the rim axis y_c

$$\mathbf{j}_c = \cos\gamma\,\mathbf{j} + \sin\gamma\,\mathbf{k} \tag{2.2}$$

where the *camber angle* γ of Fig. 2.2 is positive. The total *rim angular velocity* $\boldsymbol{\Omega}$ is

$$\begin{aligned}\boldsymbol{\Omega} &= \dot{\gamma}\mathbf{i} + \dot{\theta}\mathbf{j}_c + \dot{\zeta}\mathbf{k}\\ &= \dot{\gamma}\mathbf{i} + \omega_c\mathbf{j}_c + \omega_z\mathbf{k}\\ &= \dot{\gamma}\mathbf{i} + \omega_c\cos\gamma\,\mathbf{j} + (\omega_c\sin\gamma + \omega_z)\mathbf{k}\\ &= \Omega_x\mathbf{i} + \Omega_y\mathbf{j} + \Omega_z\mathbf{k}\end{aligned} \tag{2.3}$$

where $\dot{\gamma}$ is the time derivative of the camber angle, $\omega_c = \dot{\theta}$ is the angular velocity of the rim about its spindle axis, and $\omega_z = \dot{\zeta}$ is the yaw rate, that is the angular velocity of the reference system S.

It is worth noting that there are two distinct contributions to the *spin velocity* $\Omega_z \mathbf{k}$ of the rim, a camber contribution and a turn contribution[4]

$$\Omega_z = \omega_c \sin\gamma + \omega_z \tag{2.4}$$

Therefore, the same value of Ω_z can be the result of different operating conditions for the tire, depending on the amount of the camber angle γ and of the yaw rate ω_z.

By definition, the position vector OQ is (Fig. 2.2)

$$OQ = h(-\tan\gamma\,\mathbf{j} + \mathbf{k}) \tag{2.5}$$

This expression can be differentiated with respect to time to obtain

$$\begin{aligned}\mathbf{V}_Q - \mathbf{V}_O &= \dot{h}(-\tan\gamma\,\mathbf{j} + \mathbf{k}) + h\left(\omega_z \tan\gamma\,\mathbf{i} - \frac{\dot{\gamma}}{\cos^2\gamma}\mathbf{j}\right)\\ &= h\omega_z \tan\gamma\,\mathbf{i} - \left(\dot{h}\tan\gamma + h\frac{\dot{\gamma}}{\cos^2\gamma}\right)\mathbf{j} + \dot{h}\mathbf{k}\end{aligned} \tag{2.6}$$

since $\mathrm{d}\mathbf{j}/\mathrm{d}t = -\omega_z \mathbf{i}$. Even in steady-state conditions, that is $\dot{h} = \dot{\gamma} = 0$, we have $\mathbf{V}_Q = \mathbf{V}_O + h\omega_z \tan\gamma\,\mathbf{i}$ and hence the two velocities are not exactly the same, unless also $\gamma = 0$. The camber angle γ is usually very small in cars, but may be quite large in motorcycles.

The velocity of point O has, in general, longitudinal and lateral components

$$\mathbf{V}_o = \mathbf{V}_O = V_{o_x}\mathbf{i} + V_{o_y}\mathbf{j} \tag{2.7}$$

As already stated, the selection of point O is *arbitrary*, although quite reasonable. Therefore, the velocities V_{o_x} and V_{o_y} do not have much of physical meaning. A different choice for the point O would provide different values for the very same motion. However, a "wheel" is expected to have longitudinal velocities much higher than lateral ones, as will be discussed with reference to Fig. 10.23.

Summing up, the position of the rigid rim $\mathscr{R}$ with respect to the flat road is completely determined by the following six degrees of freedom:

$h(t)$ distance of point Q from the road;
$\gamma(t)$ camber angle;
$\theta(t)$ rotation of the rim about its axis y_c;
$x_f(t)$ first coordinate of point O w.r.t. S_f;
$y_f(t)$ second coordinate of point O w.r.t. S_f;
$\zeta(t)$ yaw angle of the rim.

However, owing to the circular shape of rim and the flatness of the road, the kinematics of the rigid rim $\mathscr{R}$ is also fully described by the following six functions of time:

[4] In the SAE terminology, it is $\omega_c \mathbf{j}_c$ that is called spin velocity [4, 11].

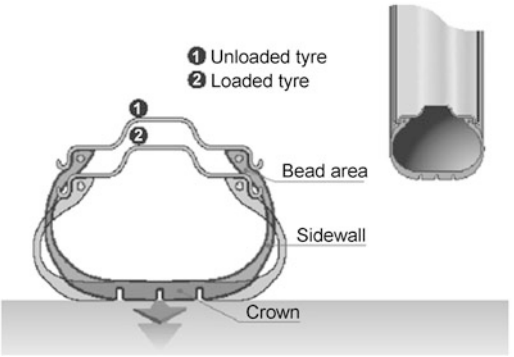

Fig. 2.3 Flexibility of the tire carcass [8]

Fig. 2.4 Structure of a radial tire [8]

$h(t)$ distance of point Q from the road;
$\gamma(t)$ camber angle;
$\omega_c(t)$ angular velocity of the rim about its axis y_c;
$V_{o_x}(t)$ longitudinal speed of O;
$V_{o_y}(t)$ lateral speed of O;
$\Omega_z(t)$ spin velocity of the rim.

The rim is in steady-state conditions if all these six quantities are constant in time. However, this is not sufficient for the wheel with tire to be in a stationary state. The flexible carcass and tire treads could still be under transient conditions.

2.3 Carcass Features

The tire carcass $\mathscr{C}$ is a highly composite and complex structure. Here we look at the tire as a vehicle component [13] and therefore it suffices to say that the inflated carcass, with its flexible sidewalls, is moderately compliant in all directions (Fig. 2.3). The external belt is also flexible, but quite inextensible (Fig. 2.4). For instance, its circumferential length is not very much affected by the vertical load

acting on the tire. The belt is covered with tread blocks whose elastic deformation and grip features highly affect the mechanical behavior of the wheel with tire [8–10].

Basically, the carcass can be seen as a nonlinear elastic structure with small hysteresis due to rate-dependent energy losses. It is assumed here that the carcass and the belt have negligible inertia, in the sense that the inertial effects are small in comparison with other causes of deformation. This is quite correct if the road is flat and the wheel motion is not "too fast".

2.4 Contact Patch

Tires are made from rubber, that is elastomeric materials to which they owe a large part of their grip capacity [17]. Grip implies contact between two surfaces: one is the tire surface and the other is the road surface.

The contact patch (or footprint) $\mathscr{P}$ is the region where the tire is in contact with the road surface. In Fig. 2.2 the contact patch is schematically shown as a single region. However, most tires have a tread pattern, with lugs and voids, and hence the contact patch is the union of many small regions (Fig. 2.5). It should be emphasized that the shape and size of the contact patch, and also its position with respect to the reference system, depend on the tire operating conditions.

Grip depends, among other things, on the *type* of road surface, its *roughness*, and whether it is *wet or not*. More precisely, grip comes basically from road roughness effects and molecular adhesion.

Road roughness effects, also known as indentation, require small bumps measuring a few microns to a few millimeters (Fig. 2.6), which dig into the surface of the rubber. On the other hand, *molecular adhesion* necessitates direct contact between the rubber and the road surface, i.e. the road must be dry.

Two main features of road surface geometry must be examined and assessed when considering tire grip, as shown in Fig. 2.6:

Macroroughness: this is the name given to the road surface texture when the distance between two consecutive rough spots is between 100 microns and 10 millimeters. This degree of roughness contributes to indentation, and to the drainage and storage of water. The load bearing surface, which depends on road macroroughness, must also be considered since it determines local pressures in the contact patch.

Microroughness: this is the name given to the road surface texture when the distance between two consecutive rough spots is between 1 and 100 microns. It is this degree of roughness which is mainly responsible for tire grip via the road roughness effects. Microroughness is related to the surface roughness of the aggregates and sands used in the composition of the road surface.

Fig. 2.5 Typical contact patch (if $\alpha = \gamma = 0$) with tread pattern

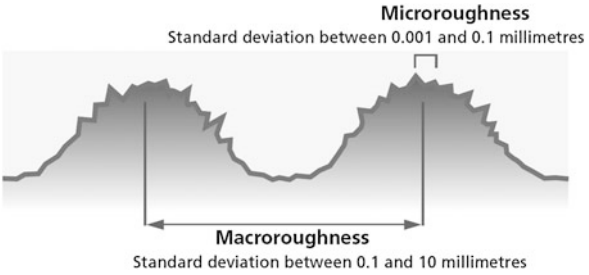

Fig. 2.6 Road roughness description [8]

2.5 Footprint Force

As well known (see, e.g., [18]), any set of forces or distributed load is statically equivalent to a force-couple system at a given (arbitrary) point O. Therefore, regardless of the degree of roughness of the road, the distributed normal and tangential loads in the footprint yield a resultant force $\mathbf{F}$ and a resultant couple vector $\mathbf{M}_O$

$$\begin{aligned} \mathbf{F} &= F_x\mathbf{i} + F_y\mathbf{j} + F_z\mathbf{k} \\ \mathbf{M}_O &= M_x\mathbf{i} + M_y\mathbf{j} + M_z\mathbf{k} \end{aligned} \tag{2.8}$$

The resultant couple $\mathbf{M}_O$ is simply the moment about the point O, but any other point could be selected. Therefore it has no particular physical meaning. However, if O is somewhere within the contact patch, the magnitude $|\mathbf{M}_O|$ is expected to be quite "small" for the wheel with tire to resemble a rigid wheel.

Traditionally, the components of $\mathbf{F}$ and $\mathbf{M}_O$ have the following names:

F_x longitudinal force;
F_y lateral force;
F_z vertical load or normal force;
M_x overturning moment;
M_y rolling resistance moment;
M_z self-aligning torque, called vertical moment here.

The names of the force components simply reaffirm their direction with respect to the chosen reference system S and hence with respect to the rim. On the other hand,

the names of the moment components, which would suggest a physical interpretation, are all quite questionable. Their values depend on the arbitrarily selected point O, and hence are arbitrary by definition.

For instance, let us discuss the name "self-aligning torque" of M_z, with reference to Fig. 2.2 and Eq. (2.10). The typical explanation for the name is that "M_z produces a restoring moment on the tire to realign the direction of travel with the direction of heading", which, more precisely, means that M_z and the slip angle α are both clockwise or both counterclockwise. But the sign and magnitude of M_z depend on the position of O, which could be anywhere! The selected origin O has nothing special, not at all. Therefore, the very same physical phenomenon, like in Fig. 2.2, may be described with O anywhere and hence by any value of M_z. The inescapable conclusion is that the name "self-aligning torque" is totally meaningless and even misleading.[5] For these reasons, here we prefer to call M_z the *vertical moment*. Similar considerations apply to M_x.

It is a classical result that any set of forces and couples in space, like $(\mathbf{F}, \mathbf{M}_O)$, is statically equivalent to a unique wrench [18]. However, in tire mechanics it is more convenient, although not mandatory, to represent the force-couple system $(\mathbf{F}, \mathbf{M}_O)$ by *two* properly located *perpendicular forces* (Fig. 2.2): a vertical force $\mathbf{F}_p = F_z\mathbf{k}$ having the line of action passing through the point with coordinates $(e_x, e_y, 0)$ such that

$$M_x = F_z e_y \quad \text{and} \quad M_y = -F_z e_x \tag{2.9}$$

and a tangential force $\mathbf{F}_t = F_x\mathbf{i} + F_y\mathbf{j}$ lying in the xy-plane and having the line of action with distance $|d_t|$ from O (properly located according to the sign of d_t)

$$M_z = \sqrt{F_x^2 + F_y^2}\, d_t = |\mathbf{F}_t| d_t \tag{2.10}$$

We remark that the two "displaced" forces $\mathbf{F}_p$ and $\mathbf{F}_t$ (Fig. 2.2) are completely equivalent to $\mathbf{F}$ and $\mathbf{M}_O$.

These forces are transferred to the rigid rim (apart for a small fraction due to the inertia and weight of the tire carcass and belt). Indeed, the equivalence of the distributed loads in the contact patch to concentrated forces and/or couples makes sense precisely because the rim is a rigid body.

For instance, the torque $\mathbf{T} = T\mathbf{j}_c$ that the distributed loads in the contact patch, and hence the force-couple system $(\mathbf{F}, \mathbf{M}_O)$, exert with respect to the wheel axis y_c is given by

$$\begin{aligned} \mathbf{T} = T\mathbf{j}_c &= \big((QO \times \mathbf{F} + \mathbf{M}_O) \cdot \mathbf{j}_c\big)\mathbf{j}_c \\ &= \left(-F_x \frac{h}{\cos\gamma} + M_y \cos\gamma + M_z \sin\gamma\right)\mathbf{j}_c \end{aligned} \tag{2.11}$$

[5] What is relevant in vehicle dynamics is the moment of $(\mathbf{F}, \mathbf{M}_O)$ with respect to the steering axis of the wheel. But this is another story.

where (2.2) and (2.5) were employed. This expression is particularly simple because the y_c-axis intersects the z-axis and is perpendicular to the x-axis (Fig. 2.2). If $\gamma = 0$, Eq. (2.11) becomes

$$T = -F_x h + M_y = -F_x h - F_z e_x \tag{2.12}$$

2.5.1 Perfectly Flat Road Surface

To perform some further mathematical investigations, it is necessary to discard completely the road roughness (Fig. 2.6) and to assume the road surface in the contact patch to be *perfectly flat*, exactly like a geometric plane (Fig. 2.2).[6] This is a fairly unrealistic assumption whose implications should not be underestimated.

Owing to the assumed flatness of the contact patch $\mathscr{P}$, we have that the *pressure* $p(x, y)\mathbf{k}$, by definition normal to the surface, is always vertical and hence forms a *parallel* distributed load. Moreover, the flatness of $\mathscr{P}$ implies that the *tangential stress* $\mathbf{t}(x, y) = t_x\mathbf{i} + t_y\mathbf{j}$ forms a *planar* distributed load. Parallel and planar distributed loads share the common feature that the resultant force and the resultant couple vector are perpendicular to each other, and therefore each force-couple system at O can be further reduced to a *single* resultant force applied along the *line of action* (in general not passing through O). A few formulae should clarify the matter.

The resultant force $\mathbf{F}_p$ and couple $\mathbf{M}_p^O$ of the distributed pressure $p(x, y)$ are given by

$$\begin{aligned} \mathbf{F}_p &= F_z\mathbf{k} = \mathbf{k}\iint_{\mathscr{P}} p(x, y)\mathrm{d}x\mathrm{d}y \\ \mathbf{M}_p^O &= M_x\mathbf{i} + M_y\mathbf{j} = \iint_{\mathscr{P}} (x\mathbf{i} + y\mathbf{j}) \times \mathbf{k}\, p(x, y)\mathrm{d}x\mathrm{d}y \end{aligned} \tag{2.13}$$

where

$$M_x = \iint_{\mathscr{P}} y p(x, y)\mathrm{d}x\mathrm{d}y = F_z e_y, \qquad M_y = -\iint_{\mathscr{P}} x p(x, y)\mathrm{d}x\mathrm{d}y = -F_z e_x \tag{2.14}$$

As expected, $\mathbf{F}_p$ and $\mathbf{M}_p^O$ are perpendicular. As shown in (2.14), the force-couple resultant $(\mathbf{F}_p, \mathbf{M}_p^O)$ can be reduced to a single force $\mathbf{F}_p$ having a vertical line of action passing through the point with coordinates $(e_x, e_y, 0)$, as shown in Fig. 2.2.

[6] More precisely, it is necessary to have a mathematical description of the shape of the road surface in the contact patch. The plane just happens to be the simplest.

The resultant tangential force $\mathbf{F}_t$ and couple $\mathbf{M}_t^O$ of the distributed tangential stress $\mathbf{t}(x, y) = t_x\mathbf{i} + t_y\mathbf{j}$ are given by

$$\begin{aligned}\mathbf{F}_t &= F_x\mathbf{i} + F_y\mathbf{j} = \iint_{\mathscr{P}} \big(t_x(x, y)\mathbf{i} + t_y(x, y)\mathbf{j}\big)\mathrm{d}x\mathrm{d}y \\ \mathbf{M}_t^O &= M_z\mathbf{k} = \iint_{\mathscr{P}} (x\mathbf{i} + y\mathbf{j}) \times (t_x\mathbf{i} + t_y\mathbf{j})\mathrm{d}x\mathrm{d}y \\ &= \mathbf{k}\iint_{\mathscr{P}} \big(xt_y(x, y) - yt_x(x, t)\big)\mathrm{d}x\mathrm{d}y = \mathbf{k}d_t\sqrt{F_x^2 + F_y^2}\end{aligned} \tag{2.15}$$

where

$$F_x = \iint_{\mathscr{P}} t_x(x, y)\mathrm{d}x\mathrm{d}y, \qquad F_y = \iint_{\mathscr{P}} t_y(x, y)\mathrm{d}x\mathrm{d}y \tag{2.16}$$

Also in this case $\mathbf{F}_t$ and $\mathbf{M}_t^O$ are perpendicular. As shown in (2.15), the force-couple resultant $(\mathbf{F}_t, \mathbf{M}_t^O)$ can be reduced to a tangential force $\mathbf{F}_t$, lying in the xy-plane and having a line of action with distance $|d_t|$ from O (properly located according to the sign of d_t), as shown in Fig. 2.2.

Obviously the more general (2.8) still holds

$$\begin{aligned}\mathbf{F} &= \mathbf{F}_p + \mathbf{F}_t \\ \mathbf{M}_O &= \mathbf{M}_p^O + \mathbf{M}_t^O\end{aligned} \tag{2.17}$$

2.6 Tire Global Mechanical Behavior

The analysis developed so far provides the tools for quite a precise description of the global mechanical behavior of a *real* wheel with tire interacting with a road. More precisely, as already stated at p. 8, we are interested in the *relationship* between the *motion* and *position* of the rim and the *force* exchanged with the road in the contact patch:

$$\text{rim kinematics} \quad \Longleftrightarrow \quad \text{force and moment}$$

We assume as given, and constant in time, both the wheel with tire (including its inflating pressure and temperature field) and the road type (including its roughness). Therefore we assume all grip features as given and constant in time.

2.6.1 Tire Transient Behavior

Knowing the mechanical behavior means knowing the relationships between the six kinematical parameters $(h, \gamma, \omega_c, V_{o_x}, V_{o_y}, \Omega_z)$ that fully characterize the position

and the motion of the rigid rim and the force-couple resultant $(\mathbf{F}, \mathbf{M}_O)$. We recall that the inertial effects of the carcass are assumed to be negligible.

Owing mostly to the flexibility of the tire structure, these relationships are of differential type, that is there exist *differential* equations

$$\begin{aligned} \mathbf{f}(\dot{\mathbf{F}}, \mathbf{F}, h, \gamma, \omega_c, V_{o_x}, V_{o_y}, \Omega_z) &= \mathbf{0} \\ \mathbf{g}(\dot{\mathbf{M}}_O, \mathbf{M}_O, h, \gamma, \omega_c, V_{o_x}, V_{o_y}, \Omega_z) &= \mathbf{0} \end{aligned} \tag{2.18}$$

In general, there might be the need of differential equations of higher order.

The identification of these differential equations by means solely of experimental tests is a formidable task. The point here is not to find them, but to appreciate that the transient behavior of a wheel with tire does indeed obey differential equations, maybe like in (2.18). Which also implies that initial conditions have to be included and the values of $(\mathbf{F}, \mathbf{M}_O)$ at time t depend on the time history.

Later on, suitable models will be developed that allow for a partial identification of (2.18) to be attempted.

2.6.2 Tire Steady-State Behavior

If all features are constant (or, at least, varying slowly) in time, the overall system is in steady-state conditions. Mathematically, it means that there exist, instead of (2.18), the following *algebraic* functions

$$\begin{aligned} \mathbf{F} &= \overline{\mathbf{F}}(h, \gamma, \omega_c, V_{o_x}, V_{o_y}, \Omega_z) \\ \mathbf{M}_O &= \overline{\mathbf{M}}_O(h, \gamma, \omega_c, V_{o_x}, V_{o_y}, \Omega_z) \end{aligned} \tag{2.19}$$

which relate the rim position and steady-state motion to the force and moment acting on the tire from the footprint. In other words, given the steady-state kinematics, we know the (constant in time) forces and couples (but not viceversa).

The algebraic functions in (2.19) are, by definition, the equilibrium states of the differential equations (2.18)

$$\begin{aligned} \mathbf{f}(\mathbf{0}, \overline{\mathbf{F}}, h, \gamma, \omega_c, V_{o_x}, V_{o_y}, \Omega_z) &= \mathbf{0} \\ \mathbf{g}(\mathbf{0}, \overline{\mathbf{M}}_O, h, \gamma, \omega_c, V_{o_x}, V_{o_y}, \Omega_z) &= \mathbf{0} \end{aligned} \tag{2.20}$$

Equations (2.19) can be split according to (2.17)

$$\begin{aligned} \mathbf{F}_p &= F_z\mathbf{k} = \overline{\mathbf{F}}_p(h, \gamma, \omega_c, V_{o_x}, V_{o_y}, \Omega_z) \\ \mathbf{F}_t &= F_x\mathbf{i} + F_y\mathbf{j} = \overline{\mathbf{F}}_t(h, \gamma, \omega_c, V_{o_x}, V_{o_y}, \Omega_z) \\ \mathbf{M}_p^O &= M_x\mathbf{i} + M_y\mathbf{j} = \overline{\mathbf{M}}_p^O(h, \gamma, \omega_c, V_{o_x}, V_{o_y}, \Omega_z) \\ \mathbf{M}_t^O &= M_z\mathbf{k} = \overline{\mathbf{M}}_t^O(h, \gamma, \omega_c, V_{o_x}, V_{o_y}, \Omega_z) \end{aligned} \tag{2.21}$$

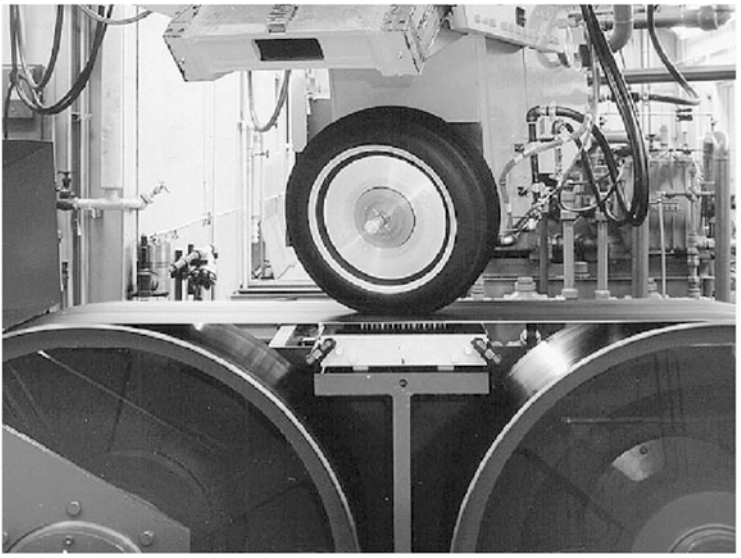

Fig. 2.7 Flat roadway testing machine (Calspan's Tire Research Facility)

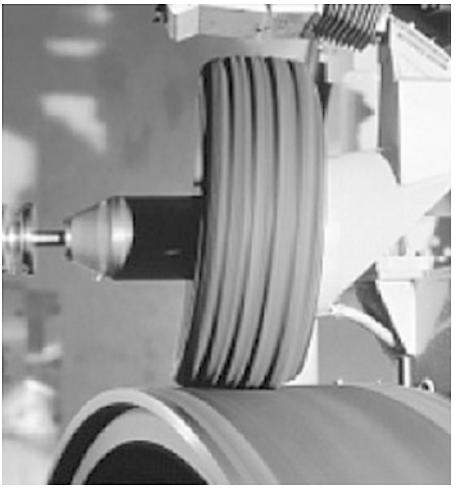

Fig. 2.8 Drum testing machine [8]

Typical *tire tests* (like in Figs. 2.7 and 2.8) aim at investigating some aspects of these functions. Actually, quite often the vertical load F_z takes the place of h as an independent variable, as discussed in Sect. 2.8. This is common practice, although it appears to be rather questionable in a neat approach to the analysis of tire mechanics. As already stated, a clearer picture arises if we follow the approach "impose the whole kinematics of the rim, measure all the forces in the contact patch" [14, p. 62].

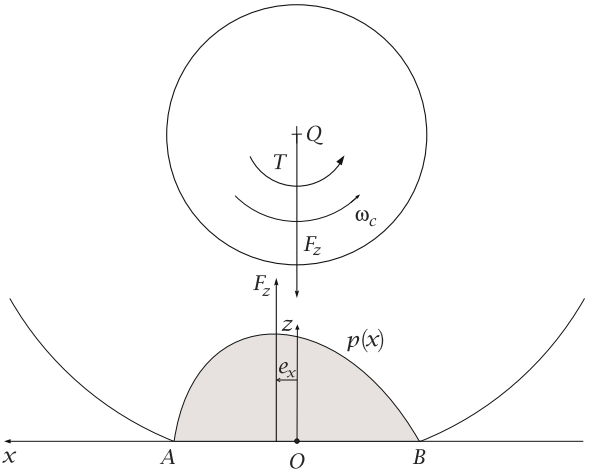

Fig. 2.9 Pure rolling: $F_x = 0$ and $T = F_z e_x$

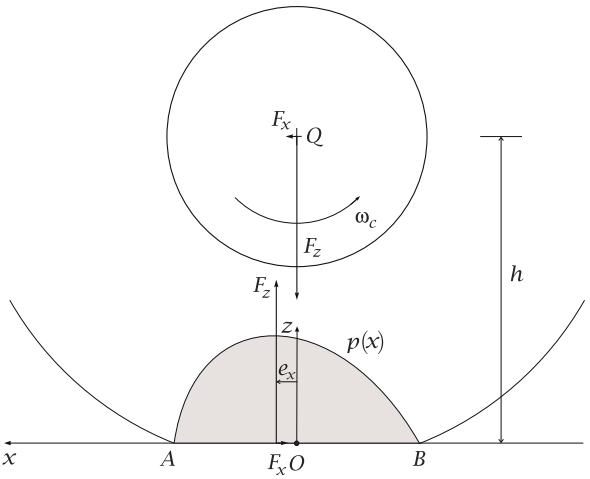

Fig. 2.10 Free rolling: $T = 0$ and $F_x h = F_z e_x$

2.6.3 Rolling Resistance

As shown schematically in Figs. 2.9 and 2.10, the rolling resistance arises because the normal pressure p in the leading half of the contact patch is higher than that in the trailing half. This is mainly caused by the hysteresis in the tire due to the deflection of the carcass while rolling. The vertical resultant $F_z\mathbf{k}$ of the pressure distribution is offset towards the front of the contact patch.

The main source of energy dissipation is therefore the visco-elasticity of the materials of which tires are made. Visco-elastic materials lose energy in the form of heat whenever they are deformed. Deformation-induced energy dissipation is the cause of about 90 % of rolling resistance [10, 19].

A number of tire operating conditions affect rolling resistance. The most important are load, inflation pressure and temperature. However, as speed increases, tire's internal temperature rises, offsetting some of the increased rolling resistance. Therefore, tire rolling resistance coefficients f are relatively constant on a relatively wide range of speeds. The values given by tire manufacturers are measured on test drums, usually at 80 km/h in accordance with ISO measurement standards.

2.6.4 Speed Independence (Almost)

Tire tests suggest that $\mathbf{F}_p$, $\mathbf{F}_t$, $\mathbf{M}_p^O$ and $\mathbf{M}_t^O$ are *almost speed independent*, if ω_c is not too high. Essentially, it means that (2.21) can be replaced by the following functions of only *five* variables:

$$\begin{aligned}
\mathbf{F}_p &= \widetilde{\mathbf{F}}_p\left(h, \gamma, \frac{V_{o_x}}{\omega_c}, \frac{V_{o_y}}{\omega_c}, \frac{\Omega_z}{\omega_c}\right) \\
\mathbf{F}_t &= \widetilde{\mathbf{F}}_t\left(h, \gamma, \frac{V_{o_x}}{\omega_c}, \frac{V_{o_y}}{\omega_c}, \frac{\Omega_z}{\omega_c}\right) \\
\mathbf{M}_p^O &= \widetilde{\mathbf{M}}_p^O\left(h, \gamma, \frac{V_{o_x}}{\omega_c}, \frac{V_{o_y}}{\omega_c}, \frac{\Omega_z}{\omega_c}\right) \\
\mathbf{M}_t^O &= \widetilde{\mathbf{M}}_t^O\left(h, \gamma, \frac{V_{o_x}}{\omega_c}, \frac{V_{o_y}}{\omega_c}, \frac{\Omega_z}{\omega_c}\right)
\end{aligned} \tag{2.22}$$

In other words, we assume that the steady-state forces and moments depend on the *geometrical* features of the rim motion (i.e., the trajectories), and not on how fast the motion develops in time. Therefore, we are discarding all inertial effects and any influence of speed on the phenomena related to grip. Of course, this may not be true at very high speeds, like in competitions.

2.6.5 Pure Rolling (not Free Rolling)

Pure rolling between two rigid surfaces that are touching at one point is a relevant topic, e.g., in robot manipulation. An in-depth discussion in the more general framework of contact kinematics can be found for instance in [12, p. 249].

Pure rolling in case of rigid bodies in *point contact* requires two kinematical conditions to be fulfilled: *no sliding* and *no mutual spin*. However, the two bodies may exchange tangential forces as far as the friction limit is not exceeded.

These concepts and results have, however, very little relevance, if any, for the (possible) definition of pure rolling of a wheel with tire. As a matter of fact, there are no rigid surfaces in contact and the footprint is certainly not a point (Fig. 2.5). Therefore, even if it is customary to speak of pure rolling of a wheel with tire, it

should be clear that it is a *totally different concept* than pure rolling between rigid bodies.

A reasonable definition of *pure rolling* for a wheel with tire, in steady-state conditions[7] and moving on a flat surface, is that the grip actions $\mathbf{t}$ have no global effect, that is

$$F_x = 0 \tag{2.23}$$

$$F_y = 0 \tag{2.24}$$

$$M_z = 0 \tag{2.25}$$

These equations do not imply that the local tangential stresses $\mathbf{t}$ in the contact patch are everywhere equal to zero, but only that their force-couple resultant is zero (cf. (2.15)). Therefore, the road applies to the wheel only a vertical force $\mathbf{F}_p = F_z\mathbf{k}$ and a horizontal moment $\mathbf{M}_p^O = M_x\mathbf{i} + M_y\mathbf{j}$.

The goal now is to find the kinematical conditions to be imposed to the rim to fulfill Eqs. (2.23)–(2.25). In general, the six parameters in Eq. (2.21) should be considered. However, it is more common to assume that *five* parameters suffice, like in (2.22) (as already discussed, it is less general, but simpler)

$$\widetilde{F}_x\left(h, \gamma, \frac{V_{ox}}{\omega_c}, \frac{V_{oy}}{\omega_c}, \frac{\Omega_z}{\omega_c}\right) = 0 \tag{2.26}$$

$$\widetilde{F}_y\left(h, \gamma, \frac{V_{ox}}{\omega_c}, \frac{V_{oy}}{\omega_c}, \frac{\Omega_z}{\omega_c}\right) = 0 \tag{2.27}$$

$$\widetilde{M}_z\left(h, \gamma, \frac{V_{ox}}{\omega_c}, \frac{V_{oy}}{\omega_c}, \frac{\Omega_z}{\omega_c}\right) = 0 \tag{2.28}$$

It is worth noting that *pure rolling* and *free rolling* are not the same concept [14, p. 65]. They provide different ways to balance the rolling resistance moment $M_y = -F_z e_x$. According to (2.12), we have pure rolling if $F_x = 0$ (Fig. 2.9), while free rolling means $T = 0$ (Fig. 2.10). However, the ratio $f = e_x/h$, called the *rolling resistance coefficient*, is typically less than 0.015 for car tires and hence there is not much quantitative difference between pure and free rolling.

2.6.5.1 Zero Longitudinal Force

First, let us consider Eq. (2.26) alone

$$\widetilde{F}_x\left(h, \gamma, \frac{V_{ox}}{\omega_c}, \frac{V_{oy}}{\omega_c}, \frac{\Omega_z}{\omega_c}\right) = 0 \tag{2.29}$$

[7] We have basically a steady-state behavior even if the operating conditions do not change "too fast".

which means that $F_x = 0$ if

$$\frac{V_{o_x}}{\omega_c} = f_x\left(h, \gamma, \frac{V_{o_y}}{\omega_c}, \frac{\Omega_z}{\omega_c}\right) \tag{2.30}$$

Under many circumstances there is experimental evidence that the relation above almost does not depend on V_{o_y} and can be recast in the following more explicit form[8]

$$\frac{V_{o_x}}{\omega_c} = r_r(h, \gamma) + \frac{\omega_z}{\omega_c} c_r(h, \gamma) \tag{2.31}$$

that is

$$V_{o_x} = \omega_c r_r(h, \gamma) + \omega_z c_r(h, \gamma) \tag{2.32}$$

This equation strongly suggests to take into account a *special point* C on the y-axis such that (Fig. 2.11 and also Fig. 2.2)

$$OC = c_r(h, \gamma)\mathbf{j} \tag{2.33}$$

where c_r is a (short) signed length. Point C would be the point of contact in case of a rigid wheel. Quite often point O and C have almost the same velocity, although their distance c_r may not be negligible (Fig. 2.11).

Equation (2.31) can be rearranged to get

$$\frac{V_{o_x} - \omega_z c_r(h, \gamma)}{\omega_c} = \frac{V_{c_x}}{\omega_c} = r_r(h, \gamma) \tag{2.34}$$

This is quite a remarkable result and clarifies the role of point C: the condition $F_x = 0$ requires $V_{c_x} = \omega_c r_r(h, \gamma)$, regardless of the value of ω_z (and also of V_{o_y}).

The function $r_r(h, \gamma)$ can be seen as a sort of longitudinal *pure rolling radius* [19, p. 18], although this name would be really meaningful only for a rigid wheel. Actually, rolling or sliding do not change the radius of a rigid wheel. As already stated, a wheel with tire has little to share with a rigid wheel.

The value of $r_r(h, \gamma)$ for given (h, γ) can be obtained by means of the usual indoor testing machines (Figs. 2.7 and 2.8) with $\omega_z = 0$. An additional, more difficult, test with $\omega_z \neq 0$ is required to obtain also $c_r(h, \gamma)$ and hence the position of C with respect to O. Car tires operate at low values of γ and hence have almost constant r_r.

In general, we can choose the origin O of the reference system to coincide with C when $\gamma = 0$. Therefore, only for large values of the camber angle, that is for motorcycle tires, the distance $|c_r|$ can reach a few centimeters (Fig. 2.11).

A rough estimate shows that the ratio $|\omega_z/\omega_c|$ is typically very small, ranging from zero (straight running) up to about 0.01. It follows that quite often $|(\omega_z/\omega_c)c_r|$

[8] However, in the brush model, and precisely at p. 294, the effect of the elastic compliance of the carcass on C is taken into account.

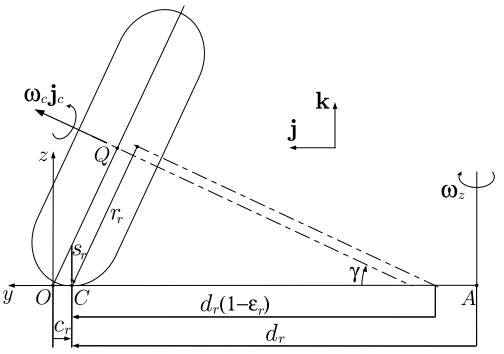

Fig. 2.11 Pure rolling of a cambered wheel

may be negligible and points O and C have almost the same velocity. However, particularly in competitions, it could be worthwhile to have a more detailed characterization of the behavior of the tire which takes into account even these minor aspects.

2.6.5.2 Zero Lateral Force

We can now discuss when the lateral force and the vertical moment are equal to zero.

According to (2.27), we have that $F_y = 0$ if

$$\widetilde{F}_y\left(h, \gamma, \frac{V_{ox}}{\omega_c}, \frac{V_{oy}}{\omega_c}, \frac{\Omega_z}{\omega_c}\right) = 0 \tag{2.35}$$

which means

$$\frac{V_{c_y}}{\omega_c} = f_y\left(h, \gamma, \frac{\Omega_z}{\omega_c}\right) \tag{2.36}$$

where, as suggested by the experimental tests, there is no dependence on the value of V_{c_x}. For convenience, the lateral velocity V_{c_y} of point C has been employed, instead of that of point O (Fig. 2.11). Nevertheless, it seems that (2.36) does not have a simple structure like (2.34).

2.6.5.3 Zero Vertical Moment

Like in (2.28), the vertical moment with respect to O is zero, that is $M_z = 0$ if

$$\widetilde{M}_z\left(h, \gamma, \frac{V_{ox}}{\omega_c}, \frac{V_{oy}}{\omega_c}, \frac{\Omega_z}{\omega_c}\right) = 0 \tag{2.37}$$

which provides

$$\frac{V_{c_y}}{\omega_c} = f_z\left(h, \gamma, \frac{\Omega_z}{\omega_c}\right) \tag{2.38}$$

where, like in (2.36), there is no dependence on the value of V_{c_x}. Also in this case, it is not possible to be more specific about the structure of this equation.

2.6.5.4 Zero Lateral Force and Vertical Moment

However, the fulfilment of *both* conditions (2.36) and (2.38) together, that is $F_y = 0$ and $M_z = 0$, yields these noteworthy results

$$V_{c_y} = \dot{\gamma} s_r(h, \gamma) \tag{2.39}$$

$$\Omega_z = \omega_c \sin\gamma \varepsilon_r(h, \gamma) \tag{2.40}$$

which have a simple structure. To have almost steady-state conditions, it has to be $|\dot{\gamma}| \ll \omega_c$, which is almost always the case. Indeed, in a wheel we do normally expect $|V_{c_x}| \gg |V_{c_y}|$ (Fig. 2.11).

The function $s_r(h, \gamma)$ is a sort of lateral pure rolling radius. It is significant in large motorcycle tires with toroidal shape (i.e., circular section with almost constant radius s_r).[9]

Sometimes $\varepsilon_r(h, \gamma)$ is called the *camber reduction factor* [14, p. 119], [15]. A car tire may have $0.4 < \varepsilon_r < 0.6$, while a motorcycle tire has ε_r almost equal to 0. The term $\sin\gamma$ in the r.h.s. of (2.40) simply states that the spin velocity Ω_z must be zero to have pure rolling with $\gamma = 0$.

Since $\Omega_z = \omega_z + \omega_c \sin\gamma$ (cf. (2.4)), Eq. (2.40) is equivalent to

$$\frac{\omega_z}{\omega_c} = -\sin\gamma\big(1 - \varepsilon_r(h, \gamma)\big) \tag{2.41}$$

Therefore, to have $F_y = 0$ and $M_z = 0$, a cambered wheel with tire must go round as shown in Fig. 2.12, with a suitable combination of ω_c and ω_z. Since no condition is set by (2.41) on the longitudinal velocity V_{c_x}, the radius of the circular path traced on the road by point C does not matter.

[9] In a toroidal *rigid* wheel with maximum radius r_0 and lateral radius s_r we would have $r_r = r_0 - s_r(1 - \cos\gamma)$, $c_r = -\tan\gamma s_r$ and $\varepsilon_r = 0$. It follows that $\dot{c}_r \neq -\dot{\gamma} s_r$.

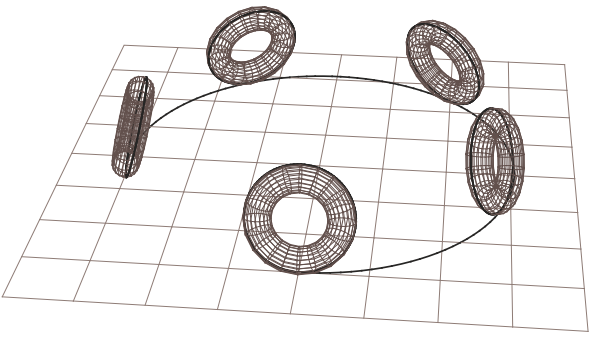

Fig. 2.12 Cambered toroidal wheel moving on a circular path (courtesy of M. Gabiccini)

2.7 Tire Slips

Summing up, we have obtained the following kinematic conditions for a wheel with tire to be in what we have defined *pure rolling* in (2.23)–(2.25):

$$
\begin{aligned}
F_x = 0 \quad &\Longleftrightarrow \quad \frac{V_{c_x}}{\omega_c} = r_r(h,\gamma) \\
\begin{cases} F_y = 0 \\ M_z = 0 \end{cases} \quad &\Longleftrightarrow \quad \begin{cases} \dfrac{V_{c_y}}{\omega_c} = \dfrac{\dot{\gamma}}{\omega_c} s_r(h,\gamma) \\ \dfrac{\Omega_z}{\omega_c} = \sin\gamma\, \varepsilon_r(h,\gamma) \end{cases}
\end{aligned}
\tag{2.42}
$$

with $OC = c_r(h,\gamma)\mathbf{j}$ (Fig. 2.11).

These equations provide a sort of *reference condition* for the behavior of a wheel with tire. Moreover, they are of key relevance for the subsequent definition of *tire slips*.

The fulfillment of only the first condition in (2.42) corresponds to longitudinal pure rolling.

It is worth recalling the main assumptions made (which are not always verified in real life):

- negligible inertial effects (five instead of six parameters);
- grip features unaffected by speed;
- point C not affected by ω_z;
- lateral velocity not affecting $F_x = 0$;
- longitudinal velocity not affecting $F_y = 0$ and $M_z = 0$.

2.7.1 Rolling Velocity

Point C and the first two equations in (2.42) provide the basis for the definition of the so-called *rolling velocity* $\mathbf{V}_r$ (Fig. 2.11)

$$\begin{aligned}\mathbf{V}_r &= \omega_c r_r(h,\gamma)\mathbf{i} + \dot{\gamma} s_r(h,\gamma)\mathbf{j} \\ &\approx \omega_c r_r \mathbf{i} = V_r \mathbf{i}\end{aligned} \tag{2.43}$$

Similarly, the third equation in (2.42) leads to the definition of the *rolling spin velocity* Ω_r

$$\Omega_r = \omega_c \sin\gamma\, \varepsilon_r(h,\gamma) \tag{2.44}$$

Therefore, for a wheel with tire to be in pure rolling it is necessary (according to (2.42)) that

$$\mathbf{V}_c = \mathbf{V}_r \quad \text{and} \quad \Omega_z = \Omega_r \tag{2.45}$$

To fulfill these conditions, in the case $\dot{\gamma} = 0$, we must move the wheel on a circular path centered at A (Figs. 2.12 and 2.11), with radius $AC = d_r(h,\gamma)\mathbf{j}$ such that

$$V_{c_x} = V_r = \omega_c r_r = -\omega_z d_r = \omega_c \sin\gamma\,(1-\varepsilon_r) d_r \tag{2.46}$$

which yields

$$d_r = \frac{r_r}{(1-\varepsilon_r)\sin\gamma} \tag{2.47}$$

Typically the rolling radius r_r is slightly bigger than the distance of point C from the rim axis (Fig. 2.11).

It is often stated that "a free-rolling tire with a camber angle would move on a circular path". This statement is clearly incorrect. It should be reformulated as "a tire with camber must be moved on a definite circular path to have pure/free rolling" (Fig. 2.12). We are not doing dynamics here, but only investigating the (almost) steady-state behavior of wheels with tire. Therefore, we can say nothing about what a wheel would do by itself.

2.7.2 Definition of Tire Slips

Let us consider a wheel with tire under real operating conditions, that is *not* necessarily in pure rolling. The velocity of point C (defined in (2.33)) is called the *speed of travel* $\mathbf{V}_c$ of the wheel (Fig. 2.11)

$$\mathbf{V}_c = V_{c_x}\mathbf{i} + V_{c_y}\mathbf{j} = (V_{o_x} - \omega_z c_r)\mathbf{i} + (V_{o_y} + \dot{c}_r)\mathbf{j} \tag{2.48}$$

The components of $\mathbf{V}_c$ also have specific names: V_{c_x} is the *forward velocity* and V_{c_y} is the *lateral velocity*.

To describe any steady-state conditions of a wheel with tire we need at least two parameters plus three kinematical quantities, as in (2.22). However, it is more informative to say how "distant" these three quantities are from pure rolling. It is therefore convenient to define the *slip velocity* $\mathbf{V}_s$ [16]

$$\mathbf{V}_s = \mathbf{V}_c - \mathbf{V}_r \tag{2.49}$$

as the difference between the speed of travel and the rolling velocity (2.43). Similarly, it is useful to define what can be called the *slip spin velocity* Ω_{s_z}

$$\begin{aligned} \Omega_{s_z} &= \Omega_z - \Omega_r \\ &= \Omega_z - \omega_c \sin\gamma\, \varepsilon_r(h,\gamma) \\ &= (\omega_z + \omega_c \sin\gamma) - \omega_c \sin\gamma\, \varepsilon_r \\ &= \omega_z + \omega_c \sin\gamma\,(1-\varepsilon_r) \end{aligned} \tag{2.50}$$

As already discussed, *the complete characterization of pure rolling conditions essentially means obtaining the following four functions* (Fig. 2.11)

$$c_r(h,\gamma), \qquad r_r(h,\gamma), \qquad s_r(h,\gamma), \qquad \varepsilon_r(h,\gamma) \tag{2.51}$$

Of them, the rolling radius r_r is the most important, followed by the camber reduction factor ε_r.

Once the pure rolling experimental investigation has been carried out, it is possible, and even advisable, to perform some simple changes of parameters based on (2.42), (2.49) and (2.50), which lead to the definition of the well known (wheel with) tire *slips* σ_x, σ_y and φ:

$$r_r(h,\gamma)\sigma_x = \frac{V_{c_x}}{\omega_c} - r_r(h,\gamma) = \frac{V_{s_x}}{\omega_c} \tag{2.52}$$

$$r_r(h,\gamma)\sigma_y = \frac{V_{c_y}}{\omega_c} - \frac{\dot\gamma}{\omega_c} s_r(h,\gamma) = \frac{V_{s_y}}{\omega_c} \tag{2.53}$$

$$r_r(h,\gamma)\varphi = -\left(\frac{\Omega_z}{\omega_c} - \sin\gamma\, \varepsilon_r(h,\gamma)\right) = \frac{\Omega_{s_z}}{\omega_c} \tag{2.54}$$

that is

$$\sigma_x = \frac{V_{c_x} - \omega_c r_r}{\omega_c r_r} = \frac{(V_{o_x} - \omega_z c_r(h,\gamma)) - \omega_c r_r(h,\gamma)}{\omega_c r_r(h,\gamma)} = \frac{V_{c_x}}{V_r} - 1 = \frac{V_{s_x}}{V_r} \tag{2.55}$$

$$\sigma_y = \frac{V_{c_y} - \dot\gamma s_r}{\omega_c r_r} = \frac{(V_{o_y} + \dot c_r(h,\gamma)) - \dot\gamma s_r(h,\gamma)}{\omega_c r_r(h,\gamma)} = -\frac{V_{c_x}\tan\alpha}{V_r} = \frac{V_{s_y}}{V_r} \tag{2.56}$$

$$\varphi = -\frac{\Omega_z - \omega_c \sin\gamma\, \varepsilon_r}{\omega_c r_r} = -\frac{\omega_z + \omega_c \sin\gamma(1-\varepsilon_r(h,\gamma))}{\omega_c r_r(h,\gamma)} = -\frac{\Omega_{s_z}}{V_r} \tag{2.57}$$

These quantities have the following names [14, 15]:

σ_x theoretical longitudinal slip ($\sigma_x > 0$ means breaking);
σ_y theoretical lateral slip;
φ spin slip.

The first two can be thought of as the components of the (*translational*) *theoretical slip* $\boldsymbol{\sigma}$

$$\boldsymbol{\sigma} = \sigma_x \mathbf{i} + \sigma_y \mathbf{j} = \frac{\mathbf{V}_c - \mathbf{V}_r}{V_r} = \frac{\mathbf{V}_s}{V_r} \tag{2.58}$$

while

$$\varphi = -\frac{\Omega_z - \Omega_r}{V_r} = -\frac{\Omega_{s_z}}{V_r} \tag{2.59}$$

The longitudinal and lateral slips are dimensionless, whereas the spin slip is not: $[\varphi] = \mathrm{m}^{-1}$.

Quite often tire tests are conducted with $\omega_z = 0$. In that case, the spin slip simply becomes

$$\varphi = -\frac{\sin\gamma\,(1 - \varepsilon_r(h, \gamma))}{r_r(h, \gamma)} \tag{2.60}$$

On the other hand, if there is only the yaw rate contribution (i.e., $\gamma = 0$) it is customary to speak of *turn slip* φ_t

$$\varphi_t = -\frac{\omega_z}{V_r} \tag{2.61}$$

Summing up, the *pure rolling* conditions (2.42) are therefore equivalent to

$$\begin{cases} \sigma_x = 0 \\ \sigma_y = 0 \\ \varphi = 0 \end{cases} \tag{2.62}$$

which look simpler, but are useless without the availability of r_r, c_r, s_r and ε_r in (2.51).

The theoretical slips could be defined with reference to point O instead of C (Fig. 2.11). In that case, according to (2.48), the correct definitions are

$$\sigma_x = \frac{(V_{o_x} - \omega_z c_r) - \omega_c r_r}{\omega_c r_r}, \qquad \sigma_y = \frac{(V_{o_y} + \dot{c}_r) - \dot{\gamma} s_r}{\omega_c r_r} \tag{2.63}$$

Although, as will be shown, the theoretical slip $\boldsymbol{\sigma}$ is a better way to describe the tire behavior, it is common practice to use the components of the *practical slip* $\boldsymbol{\kappa}$ instead

$$\kappa_x = \left(\frac{\omega_c r_r}{V_{c_x}}\right)\sigma_x = \frac{1}{1 + \sigma_x}\sigma_x = \frac{V_{c_x} - \omega_c r_r}{V_{c_x}} \tag{2.64}$$

$$\kappa_y = \left(\frac{\omega_c r_r}{V_{c_x}}\right)\sigma_y = \frac{1}{1 + \sigma_x}\sigma_y = -\tan\alpha \approx -\alpha \tag{2.65}$$

or, conversely

$$\sigma_x = \frac{1}{1-\kappa_x}\kappa_x = \kappa_x\left(1+\kappa_x+O\left(\kappa_x^2\right)\right) \tag{2.66}$$

$$\sigma_y = \frac{1}{1-\kappa_x}\kappa_y = \kappa_y\left(1+\kappa_x+O\left(\kappa_x^2\right)\right) \tag{2.67}$$

which also shows that practical and theoretical slips are almost equal only when the longitudinal slip is small.

The practical slip is only apparently simpler and its use should be discouraged. The *slip ratio* $\kappa = -\kappa_x$ is also often employed, along with the slip angle $\alpha \approx -\kappa_y$. The approximation is quite good because the slip angle normally does not exceed 15°, that is 0.26 rad.

As discussed in [11, p. 39] and also in [14, p. 597], a number of slip ratio definitions are used worldwide [1, 4–6, 19]. A check, particularly of the sign conventions, is therefore advisable. This can be easily done for some typical conditions like locked wheel ($\omega_c = 0$), or spinning wheel ($\omega_c = \infty$). For instance, with the definitions given here we have $\sigma_x = +\infty$, $\kappa_x = 1$ and $\kappa = -1$ for a traveling locked wheel.

It is worth remarking that *all these slip quantities are just a way to describe the motion of the rigid wheel rim, not of the tire*. Therefore they do not provide any direct information on the amount of sliding at any point of the contact patch. In this regard their names may be misleading. More precisely, *sliding* or *adhesion* is a *local* property of any point in the contact patch, whereas *slip* is a *global* property of the rim motion. They are completely different concepts.

2.7.3 Slip Angle

The *slip angle* α is defined as the angle between the rolling velocity $\mathbf{V}_r$ and the speed of travel $\mathbf{V}_c$. However, according to (2.48) and (2.43), when $\dot{\gamma} \approx 0$ it is almost equal to the angle between $\mathbf{i}$ and $\mathbf{V}_c$ (Fig. 2.2)[10]

$$\tan\alpha = -\frac{V_{c_y}}{V_{c_x}} \tag{2.68}$$

that is $V_{c_y} = -V_{c_x}\tan\alpha$. For convenience, α is *positive* when measured *clockwise*, that is when it is like in Fig. 2.2.[11]

Of course, a non-sliding rigid wheel has a slip angle constantly equal to zero. On the other hand, a tire may very well exhibit slip angles. However, as will be shown,

[10] Common definitions of the slip angle, like "α being the difference in wheel heading and direction" are not sufficiently precise.

[11] All other angles are positive angles if measured counterclockwise, as usually done in mathematical writing.

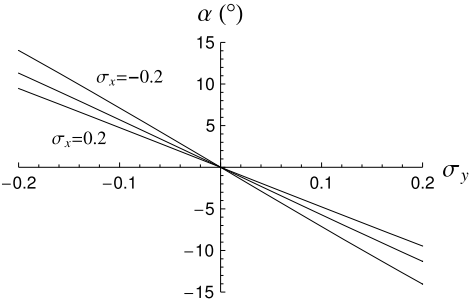

Fig. 2.13 Slip angle α as a function of σ_x and σ_y

a wheel with tire can exchange with the road very high longitudinal and lateral forces still with *small* slip angles (as shown in the important Fig. 10.23). This is one of the reasons that makes a wheel with tire behave quite close to a wheel, indeed.

More precisely, (2.68) can be rewritten as

$$\tan\alpha = -\frac{\sigma_y}{1+\sigma_x} = -\frac{\sigma_y}{\sigma_x}\left(\frac{\sigma}{\sigma+\sqrt{1+(\sigma_y/\sigma_x)^2}}\right) \tag{2.69}$$

which means that the slip angle is in the range $\pm 10 \circ$ if $\sigma < 0.2$, as shown in Fig. 2.13. This is why real tires are built in such a way to provide the best performances with values of σ below 0.2, as will also be discussed later on with reference to Fig. 10.23.

2.8 Grip Forces and Tire Slips

In (2.21) it was suggested that the steady-state global mechanical behavior of a wheel with tire could be described by means of forces and moments depending on (h, γ) to identify the rim position, and on other four kinematical parameters to determine the rim motion. We have shown that, by defining the *pure rolling* conditions and the *tire slips*, it is often possible to obtain a satisfactory description of the global mechanical behavior by means of only *three* kinematical parameters $(\sigma_x, \sigma_y, \varphi)$

$$\begin{aligned} F_x &= \widehat{F}_x(h, \gamma, \sigma_x, \sigma_y, \varphi) \\ F_y &= \widehat{F}_y(h, \gamma, \sigma_x, \sigma_y, \varphi) \\ M_z &= \widehat{M}_z(h, \gamma, \sigma_x, \sigma_y, \varphi) \end{aligned} \tag{2.70}$$

Instead of the vertical height h, it is customary to employ the vertical load F_z as an input variable. This can be safely done since

$$h = h(F_z, \gamma) \tag{2.71}$$

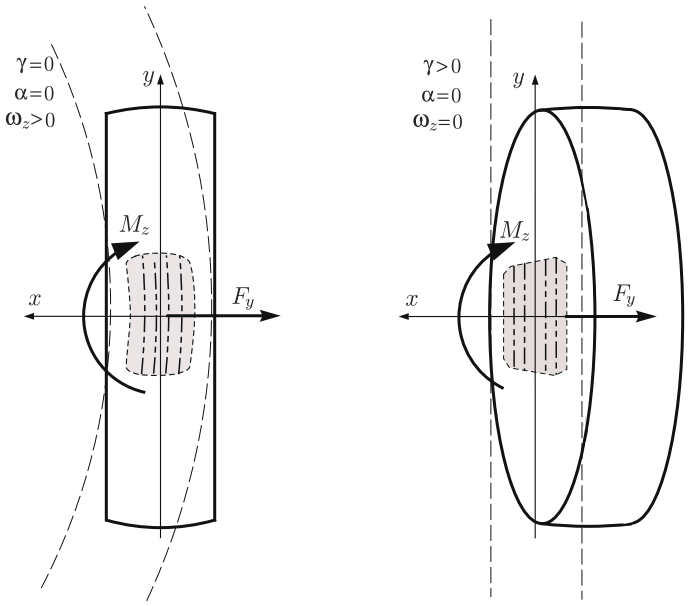

Fig. 2.14 Two different operating conditions, but with the same spin slip φ

with very little influence by the other parameters (cf. (2.21)). Therefore, the (almost) steady-state global mechanical behavior of a wheel with tire moving not too fast on a flat road is conveniently described by the following functions

$$\begin{aligned} F_x &= F_x(F_z, \gamma, \sigma_x, \sigma_y, \varphi) \\ F_y &= F_y(F_z, \gamma, \sigma_x, \sigma_y, \varphi) \\ M_z &= M_z(F_z, \gamma, \sigma_x, \sigma_y, \varphi) \end{aligned} \tag{2.72}$$

Similarly, (2.51) can be recast as

$$c_r = c_r(F_z, \gamma), \qquad r_r = r_r(F_z, \gamma), \qquad s_r = s_r(F_z, \gamma), \qquad \varepsilon_r = \varepsilon_r(F_z, \gamma) \tag{2.73}$$

It is often overlooked that F_x, F_y and M_z (Eqs. (2.70) and (2.72)) depend on *both* the camber angle γ and the spin slip φ. In other words, two operating conditions with the same φ, but obtained with different γ's, do not provide the same values of F_x, F_y and M_z, even if F_z, σ_x and σ_y are the same. For instance, the same value of φ can be obtained with no camber γ and positive yaw rate ω_z or with positive γ and no ω_z, as shown in Fig. 2.14. The two contact patches are certainly not equal to each other, and so the forces and moments. The same value of φ means that the rim has the same motion, but not the same position, if γ is different.

We remind that the moment M_z in (2.72) is with respect to a vertical axis passing through a point O chosen in quite an arbitrary way. Therefore, any attempt to attach a physical interpretation to M_z must take care of the position selected for O.

Unfortunately, it is common practice to employ the following functions, instead of (2.72)

$$\begin{aligned} F_x &= F_x^p(F_z, \gamma, \kappa_x, \alpha, \omega_z) \\ F_y &= F_y^p(F_z, \gamma, \kappa_x, \alpha, \omega_z) \\ M_z &= M_z^p(F_z, \gamma, \kappa_x, \alpha, \omega_z) \end{aligned} \tag{2.74}$$

They are, in principle, equivalent to (2.72). However, using the longitudinal practical slip κ_x, the slip angle α and the yaw rate ω_z provides a less systematic description of the tire mechanical behavior. It looks simpler, but ultimately it is not.

2.9 Tire Testing

Tire testing aims at the full identification of the three functions (2.72) or (2.74), that is of the *relationship* between the *motion* and *position* of the rim and the *force* and *moment* exchanged with the road in the contact patch

$$\text{rim kinematics} \quad \Longleftrightarrow \quad \text{force and moment}$$

Actually, this goal had already been stated in Sect. 2.1. The difference is that now we have defined the tire slips, that is a precise set of parameters to control the rim kinematics.

Indoor tire testing facilities (Figs. 2.7 and 2.8) usually have $\omega_z = 0$ in steady-state tests, and hence lack in generality by imposing a link between γ and φ (cf. (2.60)). However, in most practical applications in road vehicles we have $|\omega_z/\omega_c| < 0.01$ and ω_z can indeed be neglected.[12]

Owing to (2.42) and (2.62), it is meaningful to perform experimental tests for the so-called *pure slip conditions*. Basically it means setting $\gamma = \varphi = 0$ and either $\sigma_y = 0$ or $\sigma_x = 0$. In the first case we have pure longitudinal slip and hence only the longitudinal force $F_x = F_x(F_z, 0, \sigma_x, 0, 0)$, which is a very special case of (2.72). In the second case we have pure lateral slip, which allows for the experimental identification of the functions $F_y = F_y(F_z, 0, 0, \sigma_y, 0)$ and $M_z = M_z(F_z, 0, 0, \sigma_y, 0)$, which are also very special cases.

Unfortunately, the practical longitudinal slip κ_x and the slip angle α usually take the place of σ_x and σ_y, respectively [2].

[12] In a step steer the steering wheel of a car may reach $\omega_z = 20°/\text{s} = 0.35$ rad/s. At a forward speed of 20 m/s, the same wheels have about $\omega_c = 80$ rad/s. The contribution of ω_z to φ is therefore like a camber angle $\gamma \approx 0.5°$.

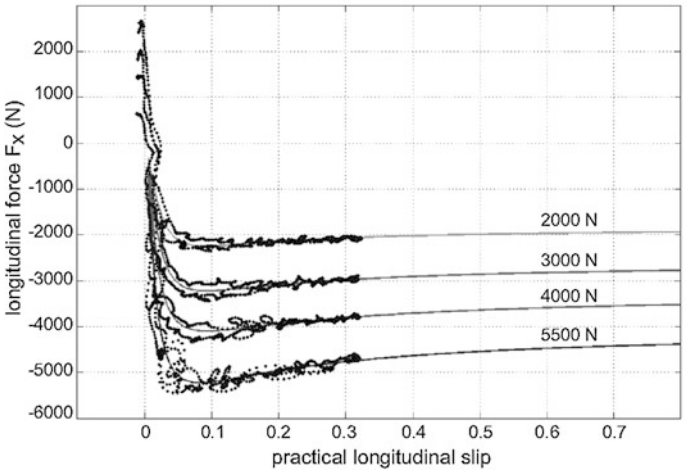

Fig. 2.15 Experimental results: longitudinal force F_x vs practical longitudinal slip κ_x for four values of the vertical load F_z

2.9.1 Pure Longitudinal Slip

Figure 2.15 shows the typical behavior of the longitudinal force F_x as a function of the practical longitudinal slip κ_x under pure braking conditions, for several values of the vertical load F_z. More precisely, it is the plot of $F_x^p(F_z, 0, \kappa_x, 0, 0)$. It is very important to note that:

- the maximum absolute value of F_x (i.e., the peak value $F_x^{\max}$) was obtained for $\kappa_x \approx 0.1$ (i.e., $\sigma_x = 0.11$);
- F_x grows *less than proportionally* with respect to the vertical load.

Both these aspects of tire behavior have great relevance in vehicle dynamics.

Also quite relevant are the values of the *longitudinal slip stiffness* C_{κ_x}, that is minus the slope of each curve at zero slip

$$C_{\kappa_x}(F_z) = -\left.\frac{\partial F_x^p}{\partial \kappa_x}\right|_{\kappa_x=0} \tag{2.75}$$

and the *global longitudinal friction coefficient* μ_p^x, that is the ratio between the peak value $F_x^{\max} = \max(|F_x^p|)$ and the corresponding vertical load

$$\mu_p^x(F_z) = \frac{F_x^{\max}}{F_z} \tag{2.76}$$

Typically, as shown in Fig. 2.16, it slightly decreases as the vertical load grows.

On the practical side, it is of some interest to observe that

- the experimental values are affected by significant errors;

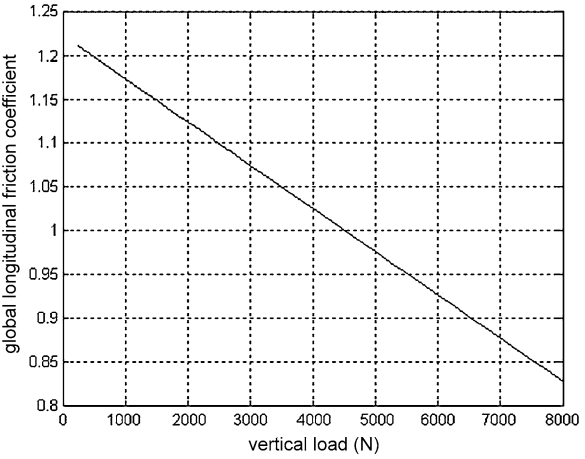

Fig. 2.16 Global longitudinal friction coefficient μ_p^x vs vertical load F_z

- the tests were carried out till $\kappa_x \approx 0.3$, to avoid wheel locking and excessive damage to the tire tread;
- the offset of F_x for $\kappa_x = 0$ is due to the rolling resistance: the wheel was (erroneously, but typically) under free rolling conditions, not pure rolling.

2.9.2 Pure Lateral Slip

Figure 2.17 shows the typical behavior of the lateral force F_y as a function of the slip angle α, for three values of F_z. More precisely, it is the plot of $F_y^p(F_z, 0, 0, \alpha, 0)$. It is very important to note that

- the maximum absolute value of F_y (i.e., the peak value $F_y^{\max}$) was obtained for $\alpha \approx \pm 8°$ (i.e., $\tan\alpha = -\sigma_y = \pm 0.14$);
- F_y grows *less than proportionally* with respect to the vertical load.

Also quite relevant are the values of the *lateral slip stiffness* C_α, also called *cornering stiffness*

$$C_\alpha(F_z) = \left.\frac{\partial F_y^p}{\partial \alpha}\right|_{\alpha=0} \tag{2.77}$$

that is the slope at the origin. As shown in Fig. 2.18, C_α grows less than proportionally with F_z, and actually it can even decrease at exceedingly high values of the vertical load.

Another important quantity is the *global lateral friction coefficient* μ_p^y, that is the ratio between the peak value $F_y^{\max} = \max(|F_y^p|)$ and the vertical load

$$\mu_p^y(F_z) = \frac{F_y^{\max}}{F_z} \tag{2.78}$$

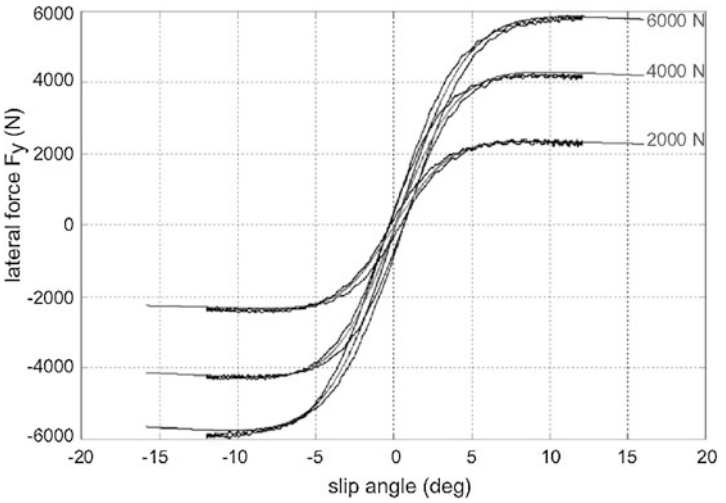

Fig. 2.17 Experimental results: lateral force F_y vs slip angle α for three values of the vertical load F_z

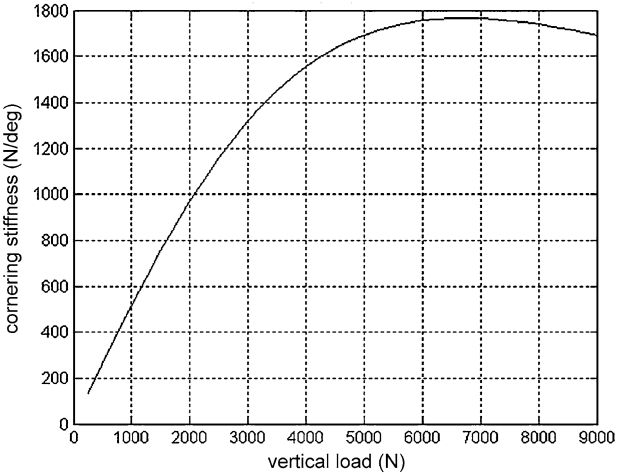

Fig. 2.18 Cornering stiffness C_α vs vertical load F_z

As shown in Fig. 2.19, it slightly decreases with F_z.

Comparing Figs. 2.16 and 2.19 we see that similar peak values for F_x and F_y are obtained for the same vertical load, that is $\mu_p^x \approx \mu_p^y$. Typically, μ_p^x is slightly greater than μ_p^y.

On the practical side it is to note that

- the experimental values are affected by small errors;
- the tests were carried out till $\alpha \approx 12°$, to avoid damaging the tire tread.

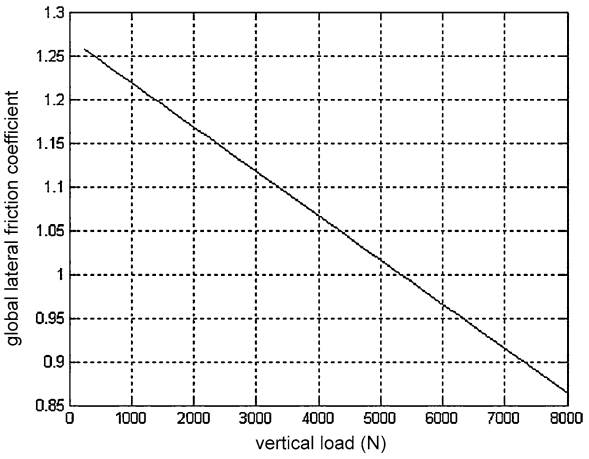

Fig. 2.19 Global lateral friction coefficient μ_p^y vs vertical load F_z

Figure 2.20 shows an example of the vertical moment M_z as a function of the slip angle α, for three values of F_z, that is the plot of $M_z^p(F_z, 0, 0, \alpha, 0)$. The tests are the same of Fig. 2.17 and similar observations apply.

The behavior of $M_z(\alpha)$ is obviously very much affected by the position of the z-axis, which should be always clearly stated. Therefore, it is hard to speak of "typical behavior" of M_z, unless there is general agreement on where to locate the origin O of the reference system. This aspect could be quite relevant in the comparison and interpretation of tests performed by different institutions, particularly for motorcycle tires at large camber angles.

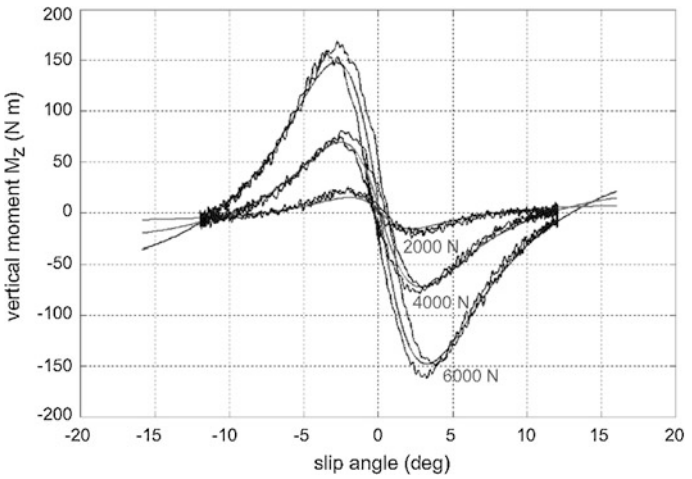

Fig. 2.20 Experimental results: vertical moment M_z vs slip angle α for three values of the vertical load F_z

2.10 Magic Formula

In vehicle dynamics it is useful to have mathematical functions that fit experimental tire response curves, like those in Figs. 2.15 and 2.17. Usually, these curves have similar shapes: they grow less than proportionally, reach a maximum and then tend to a horizontal asymptote. Among the very many functions that share all these features, there is one which is almost exclusively used in vehicle dynamics. It is called *Magic Formula* (MF).

Although, over the years, several versions of the Magic Formula have been developed, they are all based on the following function [14, 16]

$$y(x) = D \sin\{C \arctan[Bx - E(Bx - \arctan(Bx))]\} \tag{2.79}$$

where the four coefficients are usually referred to as

$$\begin{aligned} &B \quad \text{stiffness factor} \\ &C \quad \text{shape factor} \\ &D \quad \text{peak value} \\ &E \quad \text{curvature factor} \end{aligned} \tag{2.80}$$

Of course, y can be either F_x or F_y, with x being the corresponding practical or theoretical slip component.

The Magic Formula belongs to the so-called *empirical tire models*, in the sense that they mimic some experimental curves without any relation to the physical phenomena involved in tire mechanics.

Let $B > 0$. It is quite easy to show that

- $y(0) = 0$ and $y''(0) = 0$, since $y(x) = -y(-x)$ like any anti-symmetric function;
- the slope at the origin is given by $y'(0) = BCD$;
- the value of the horizontal asymptote is $y_a = \lim_{x \to +\infty} y(x) = D \sin(C\pi/2)$, if $E < 1$;
- the function is limited: $|y(x)| \leq D$;
- if $E < 1$ and $1 < C < 2$, then the function has a relative maximum $y_m = y(x_m) = D$, with

$$B(1 - E)x_m + E \arctan(Bx_m) = \tan(\pi/(2C)) \tag{2.81}$$

- $y'''(0) < 0$, if $-(1 + C^2/2) < E$.

Probably, the most relevant features of an experimental curve like in Fig. 2.17 are the peak value y_m with the corresponding abscissa x_m, the asymptotic value y_a and the slope at the origin $y'(0)$. Therefore, to determine the four coefficients a possible procedure is as follows. First set the peak value

$$D = y_m \tag{2.82}$$

then compute the shape factor C employing y_a[13]

$$C = 2 - \frac{2}{\pi} \arcsin\left(\frac{y_a}{D}\right) \tag{2.83}$$

obtain the stiffness factor B as

$$B = \frac{y'(0)}{CD} \tag{2.84}$$

and, finally, determine the curvature factor E from (2.81)

$$E = \frac{\tan(\pi/(2C)) - Bx_m}{\arctan(Bx_m) - Bx_m} \tag{2.85}$$

It is important that $y_a < y_m$. If they are equal (or almost equal), an unexpected plot may result. The Magic Formula usually does a good job at approximating experimental curves, although, with only four coefficients, the fitting may not be of uniform quality at all points. This aspect will be addressed in Figs. 10.16 and 10.17.

Quite often, some coefficients are made dependent on the vertical load F_z. According to Figs. 2.16 and 2.19, the global friction coefficient μ_p decreases almost linearly with F_z, and hence it is quite reasonable to assume

$$D = \mu_p F_z = (a_1 F_z + a_2) F_z \tag{2.86}$$

with $a_1 < 0$. To mimic the pattern shown in Fig. 2.18 for the slope at the origin $y'(0)$, the following formula has been suggested [16]

$$BCD = y'(0) = a_3 \sin\big(2 \arctan(F_z/a_4)\big) \tag{2.87}$$

Typical values may be $a_1 = -0.05\ \mathrm{kN}^{-1}$, $a_2 = 1$, $a_3 = 55$ kN/rad, $a_4 = 4$ kN.

An extensive description of the Magic Formula and all its subtleties can be found in [14].

2.11 Mechanics of Wheels with Tire

The most important aspects of tire behavior can be summarized in a few plots. They are not the whole story, and the interested reader will find in Chap. 10 many hints to better understand steady-state and also transient tire behavior. However, these plots are like a minimum common ground, i.e., something that any vehicle engineer should always have clear in mind.

Of course, they come from tire testing, either indoor or outdoor. Therefore, these plots are like the filtered (smoothed) version of the plots presented in Sect. 2.9. They were drawn employing the Magic Formula with the parameters reported below Eq. (2.87). The shape factor C was set equal to 1.65 for the plots of F_x, and equal to 1.3 for the plots of F_y.

[13] $\sin(C\pi/2) = \sin((2 - C)\pi/2)$, since $1 < C < 2$.

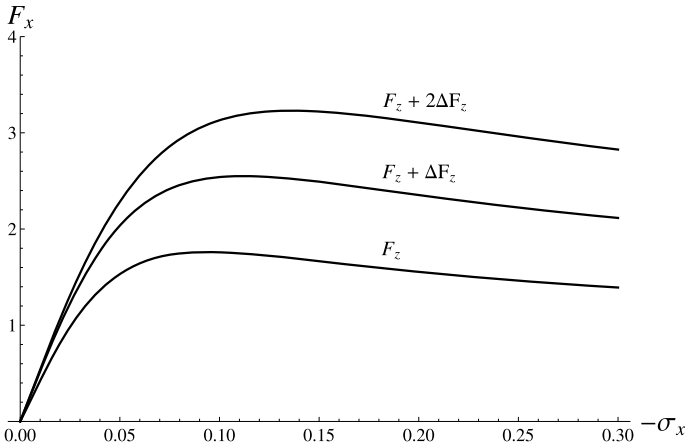

Fig. 2.21 Longitudinal force F_x due to pure longitudinal slip σ_x, for increasing vertical loads F_z. More precisely $F_x = F_x(F_z, 0, \sigma_x, 0, 0)$

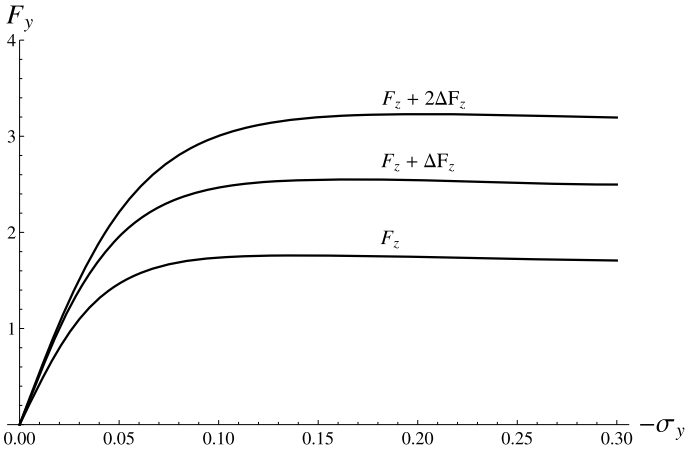

Fig. 2.22 Lateral force F_y due to pure lateral slip σ_y, for increasing vertical loads F_z. More precisely $F_y = F_y(F_z, 0, 0, \sigma_y, 0)$

Most tires under pure longitudinal slip behave like in Fig. 2.21. In particular, the effect of increasing the vertical load F_z is shown. As already mentioned at p. 34, the growth of F_x is less than proportional, particularly for low values of σ_x.

Similarly, most tires under pure lateral slip behave like in Fig. 2.22. In particular, the effect of increasing the vertical load F_z is shown. Again, as already mentioned at p. 35, the growth of F_y is less than proportional, particularly for low values of σ_y. It is precisely this nonlinearity that is, let us say, activated by anti-roll bars to modify the handling set-up of a car.

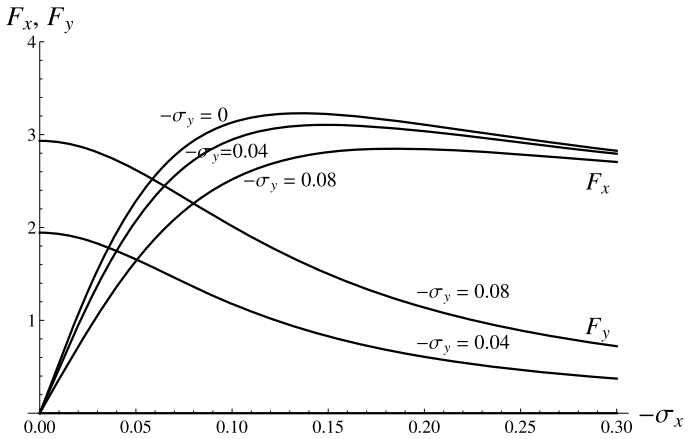

Fig. 2.23 Longitudinal force F_x and lateral force F_y due to combined longitudinal slip σ_x and lateral slip σ_y, for constant vertical load F_z. More precisely $F_y = F_y(F_z, 0, \sigma_x, \sigma_y, 0)$ and $F_y = F_y(F_z, 0, \sigma_x, \sigma_y, 0)$

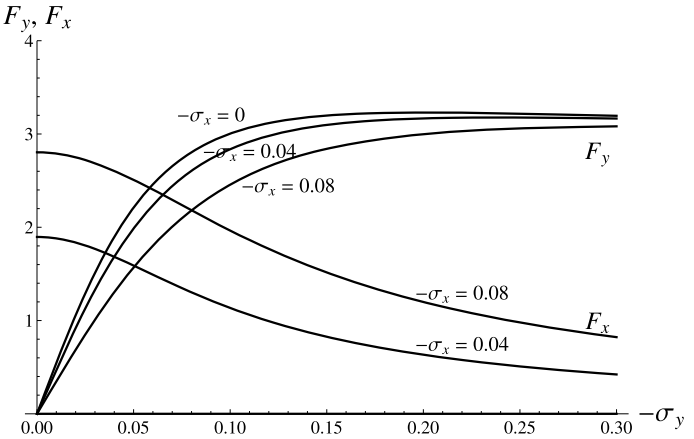

Fig. 2.24 Longitudinal force F_x and lateral force F_y due to combined longitudinal slip σ_x and lateral slip σ_y, for constant vertical load F_z. More precisely $F_y = F_y(F_z, 0, \sigma_x, \sigma_y, 0)$ and $F_y = F_y(F_z, 0, \sigma_x, \sigma_y, 0)$

The simultaneous application of σ_x and σ_y affects the grip forces F_x and F_y the way shown in Figs. 2.23 and 2.24. Basically, the total force $\mathbf{F}_t$, with components F_x and F_y, is directed like the slip vector $\boldsymbol{\sigma}$, with opposite sign, and has a magnitude almost dependent on $|\boldsymbol{\sigma}|$. These aspects will be thoroughly addressed in Chap. 10, were the tire brush model will be developed.

Also very relevant is the effect of the camber angle γ, alone or in combination with σ_y, on the lateral force F_y, as shown in Fig. 2.25 and, for better clarity, also in Fig. 2.26. We see that the camber effects are much stronger at low values of σ_y.

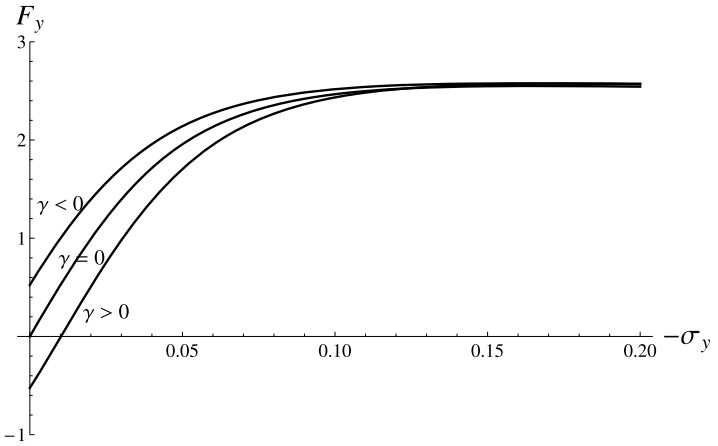

Fig. 2.25 Lateral force F_y due to lateral slip σ_y, for different values of the camber angle γ and constant vertical load F_z. More precisely $F_y = F_y(F_z, \gamma, 0, \sigma_y, 0)$

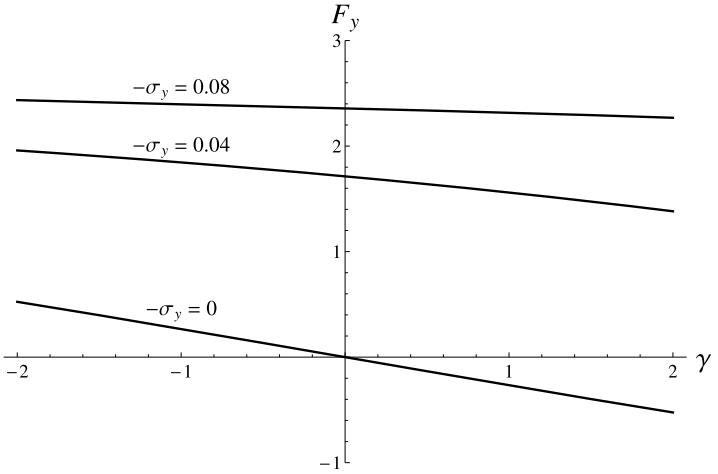

Fig. 2.26 Lateral force F_y due to camber angle γ, for different values of the lateral slip σ_y and constant vertical load F_z. More precisely $F_y = F_y(F_z, \gamma, 0, \sigma_y, 0)$

However, a right amount of camber can increase the maximum lateral force, thus improving the car handling performance.

Finally, the effect of the increasing the grip coefficient μ is investigated. We see in Figs. 2.27 and 2.28 that, as expected, we get higher maximum tangential forces. However, it should also be noted that changing the grip does not affect the slope of the curves near the origin.

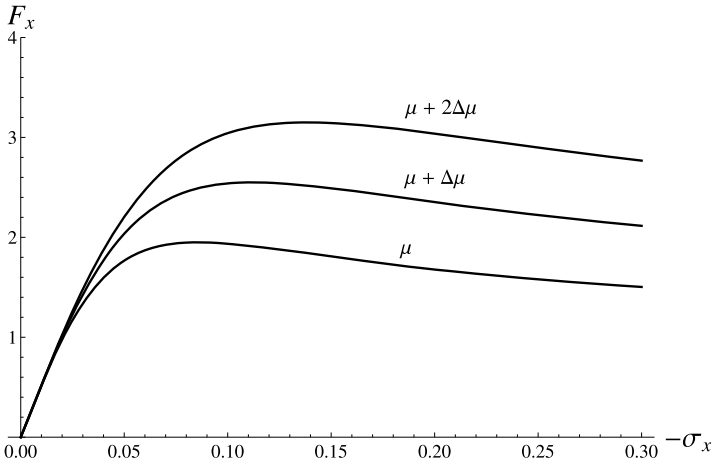

Fig. 2.27 Longitudinal force F_x due to pure longitudinal slip σ_x, for constant vertical load F_z and increasing grip

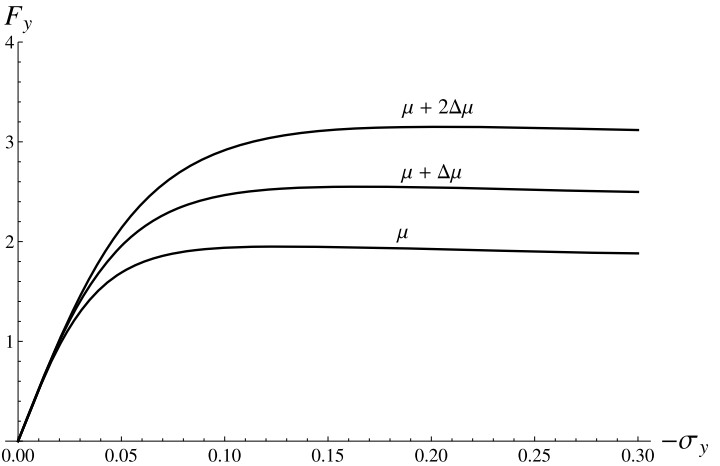

Fig. 2.28 Lateral force F_y due to pure lateral slip σ_y, for constant vertical load F_z and increasing grip

2.12 Summary

In this chapter we have first pursued the goal of clearly describing the relevant kinematics of a wheel with tire, mainly under steady-state conditions. This had led to the definitions of slips as a measure of the extent to which the wheel with tire departs from pure rolling conditions. The slip angle has been also defined and discussed. It has been shown that a wheel with tire resembles indeed a rigid wheel because slip angles are quite small. Tire experimental tests shows the relationships between the

kinematics and the forces/couples the tire exchanges with the road. The Magic Formula provides a convenient way to represent these functions. Finally, the mechanics of the wheel with tire has been summarized with the aid of a number of plots.

2.13 List of Some Relevant Concepts

p. 8 a wheel with tire is barely a wheel;
p. 11 there are two distinct contributions to the spin velocity of the rim;
p. 11 in a wheel, longitudinal velocities are expected to be much higher than lateral ones;
p. 15 the name "self-aligning torque" is meaningless and even misleading;
p. 21 rim kinematics depends on six variables, but often (not always) only five may be relevant for the tire;
p. 22 a reasonable definition of pure rolling for a wheel with tire is that the grip actions $\mathbf{t}$ have no global effect;
p. 20 pure rolling and free rolling are different concepts;
p. 27 tire slips measure the distance from pure rolling;
p. 30 tire slips do not provide any direct information on the amount of sliding at any point of the contact patch;
p. 32 tire forces and moments depend on both the camber angle γ and the spin slip φ.

References

1. Bastow D, Howard G, Whitehead JP (2004) Car suspension and handling, 4th edn. SAE International, Warrendale
2. Bergman W (1977) Critical review of the state-of-the-art in the tire and force measurements. SAE Preprint (770331)
3. Clark SK (ed) (2008) The pneumatic tire. NHTSA–DOT HS 810 561
4. Dixon JC (1991) Tyres, suspension and handling. Cambridge University Press, Cambridge
5. Font Mezquita J, Dols Ruiz JF (2006) La Dinámica del Automóvil. Editorial de la UPV, Valencia
6. Gillespie TD (1992) Fundamentals of vehicle dynamics. SAE International, Warrendale
7. Meirovitch L (1970) Methods of analytical dynamics. McGraw-Hill, New York
8. Michelin (2001) The tyre encyclopaedia. Part 1: grip. Société de Technologie Michelin, Clermont–Ferrand [CD-ROM]
9. Michelin (2002) The tyre encyclopaedia. Part 2: comfort. Société de Technologie Michelin, Clermont–Ferrand [CD-ROM]
10. Michelin (2003) The tyre encyclopaedia. Part 3: rolling resistance. Société de Technologie Michelin, Clermont–Ferrand [CD-ROM]
11. Milliken WF, Milliken DL (1995) Race car vehicle dynamics. SAE International, Warrendale
12. Murray RM, Li Z, Sastry SS (1994) A mathematical introduction to robot manipulation. CRC Press, Boca Raton
13. Pacejka HB (1996) The tyre as a vehicle component. In: 26th FISITA congress '96: engineering challenge human friendly vehicles, Prague, June 17–21, pp 1–19

14. Pacejka HB (2002) Tyre and vehicle dynamics. Butterworth–Heinemann, Oxford
15. Pacejka HB (2005) Slip: camber and turning. Veh Syst Dyn 43(Supplement):3–17
16. Pacejka HB, Sharp RS (1991) Shear force development by pneumatic tyres in steady state conditions: a review of modelling aspects. Veh Syst Dyn 20:121–176
17. Popov VL (2010) Contact mechanics and friction. Springer, Berlin
18. Pytel A, Kiusalaas J (1999) Engineering mechanics—statics. Brooks/Cole, Pacific Grove
19. Wong JY (2001) Theory of ground vehicles. Wiley, New York

Chapter 3
Vehicle Model for Handling and Performance

In Chap. 1 vehicle modeling has been approached in general terms. To get quantitative information there is the need to be more specific.

As already stated, in the study of handling and performance the road is assumed to be perfectly *flat* (no bumps) and with uniform features. Typically a good paved road, either dry or wet [1, 5].

The vehicle model fulfills all the assumptions listed at p. 4, with the addition of:

(1) negligible suspension deflections;
(2) negligible tire vertical deformations;
(3) small steering angles (otherwise, steering axes passing through the center of the corresponding wheel and perpendicular to the road);
(4) perfectly rigid steering system.

Mathematically these additional assumptions amount to having the vehicle always in its reference configuration, as shown in Fig. 1.4, with the exception of the steering angles δ_{ij} of each wheel (δ_{11} being front-left, δ_{12} front-right, etc.). More precisely, a_1, a_2, l, t_1, t_2 and h are all *constant* during the vehicle motion. This is fairly reasonable if the motion is not too harsh, that is if accelerations are not too big and do not change abruptly.

Typically, the steering axis (pivot line) is something like in Fig. 3.1, with a caster angle and a kingpin inclination angle. Therefore, there are a trail and a scrub radius. They are key quantities in the design of the steering system. However, their effects on the dynamics of the whole vehicle may be neglected in some cases, particularly with small steering angles and perfectly rigid steering systems (as assumed here).

The net effect of all these hypotheses is that the vehicle body has a *planar motion* parallel to the road. This is quite a remarkable fact since it greatly simplifies the analysis. Moreover, the wheel centers have a *fixed position* with respect to the vehicle body. This also helps a lot.

Notwithstanding its (apparent) simplicity, this vehicle model still shows a very rich and interesting dynamic behavior, and has proven to be a valuable tool to capture and understand many aspects of the dynamics of real vehicles. Of course, the

M. Guiggiani, *The Science of Vehicle Dynamics*, DOI 10.1007/978-94-017-8533-4_3,

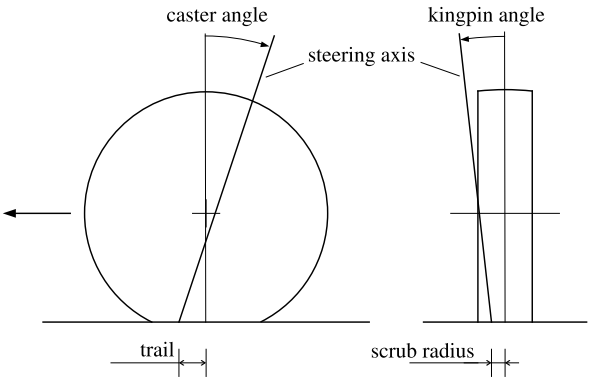

Fig. 3.1 Steering axis

underlying hypotheses impose some restrictions on its applicability, which a vehicle engineer should be well aware of.

3.1 Mathematical Framework

Basically, a vehicle model (like most physical models) is made of three separate sets of equations

- congruence (kinematic) equations;
- equilibrium equations;
- constitutive (tire) equations.

It may be convenient to consider first the whole vehicle and then the suspensions.

3.2 Vehicle Congruence (Kinematic) Equations

The analysis of the vehicle kinematics is based on Fig. 3.2.

It is good common practice to define the *body-fixed reference system* $\mathsf{S} = (x, y, z; G)$, with unit vectors $(\mathbf{i}, \mathbf{j}, \mathbf{k})$. It has origin in the center of mass G and axes fixed relative to the vehicle. The x-axis marks the forward direction, while the y-axis indicates the lateral direction. The z-axis is vertical, that is perpendicular to the road, with positive direction upward.

3.2.1 Velocities

The motion of the vehicle body may be completely described by its angular speed $\boldsymbol{\Omega}$ and by the velocity $\mathbf{V}_G$ of G, although any other point would do as well. Owing

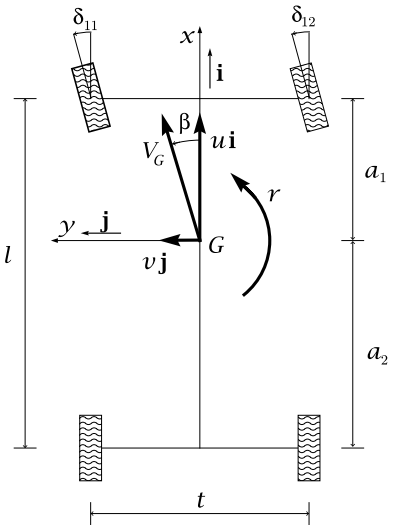

Fig. 3.2 Global kinematics of a vehicle in planar motion

to the assumed planarity of the vehicle motion, $\mathbf{V}_G$ is horizontal and $\boldsymbol{\Omega}$ is vertical. More precisely

$$\mathbf{V}_G = u\mathbf{i} + v\mathbf{j} \tag{3.1}$$

and

$$\boldsymbol{\Omega} = r\mathbf{k} \tag{3.2}$$

The component u is called vehicle *forward velocity*, while v is the *lateral velocity*. The quantity r is the vehicle *yaw rate*. Like in (2.1), the velocity of any point P of the vehicle body is given by the well known formula

$$\mathbf{V}_P = \mathbf{V}_G + \boldsymbol{\Omega} \times GP \tag{3.3}$$

Therefore, the kinematics of the vehicle body is completely described by, e.g., the three state variables $u(t)$, $v(t)$ and $r(t)$, as shown in Fig. 3.2.

Under normal operating conditions $u > 0$ and

$$u \gg |v| \quad \text{and} \quad u \gg |r|l \tag{3.4}$$

3.2.2 Yaw Angle and Trajectory

Let $\mathsf{S}_0 = (x_0, y_0, z_0; O_0)$ be a ground-fixed reference system, as shown in Fig. 3.3, with unit vectors $(\mathbf{i}_0, \mathbf{j}_0, \mathbf{k}_0)$. Therefore

$$\mathbf{i}_0 \cdot \mathbf{i} = \cos\psi \quad \text{and} \quad \mathbf{j}_0 \cdot \mathbf{i} = -\sin\psi \tag{3.5}$$

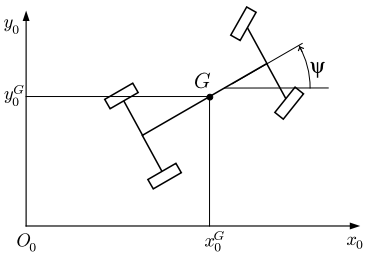

Fig. 3.3 Ground-fixed coordinate system and yaw angle ψ

where ψ is the vehicle *yaw angle*. Accordingly

$$\mathbf{V}_G = \dot{x}_0\mathbf{i}_0 + \dot{y}_0\mathbf{j}_0 = u\mathbf{i} + v\mathbf{j} \tag{3.6}$$

with

$$\begin{aligned} \dot{x}_0 &= u\cos\psi - v\sin\psi \\ \dot{y}_0 &= u\sin\psi + v\cos\psi \\ \dot{\psi} &= r \end{aligned} \tag{3.7}$$

The yaw angle ψ of the vehicle, at any time $t = \hat{t}$, is given by

$$\psi(\hat{t}) = \psi(0) + \int_0^{\hat{t}} r(t)\mathrm{d}t \tag{3.8}$$

Once the function of time $\psi(t)$ is known, the absolute position of G with respect to a frame fixed to the road is readily obtained by integrating the first two equations in (3.7)

$$\begin{aligned} x_0^G(\hat{t}) &= x_0^G(0) + \int_0^{\hat{t}} \dot{x}_0\mathrm{d}t = x_0^G(0) + \int_0^{\hat{t}} \big[u(t)\cos\psi(t) - v(t)\sin\psi(t)\big]\mathrm{d}t \\ y_0^G(\hat{t}) &= y_0^G(0) + \int_0^{\hat{t}} \dot{y}_0\mathrm{d}t = y_0^G(0) + \int_0^{\hat{t}} \big[u(t)\sin\psi(t) + v(t)\cos\psi(t)\big]\mathrm{d}t \end{aligned} \tag{3.9}$$

The two functions $x_0^G(t)$ and $y_0^G(t)$ are the parametric equations of the *trajectory* of G with respect to the fixed reference system S_0.

Equations (3.7) can be inverted to get

$$\begin{aligned} u(t) &= \cos\psi(t)\dot{x}_0(t) + \sin\psi(t)\dot{y}_0(t) \\ v(t) &= -\sin\psi(t)\dot{x}_0(t) + \cos\psi(t)\dot{y}_0(t) \\ r(t) &= \dot{\psi}(t) \end{aligned} \tag{3.10}$$

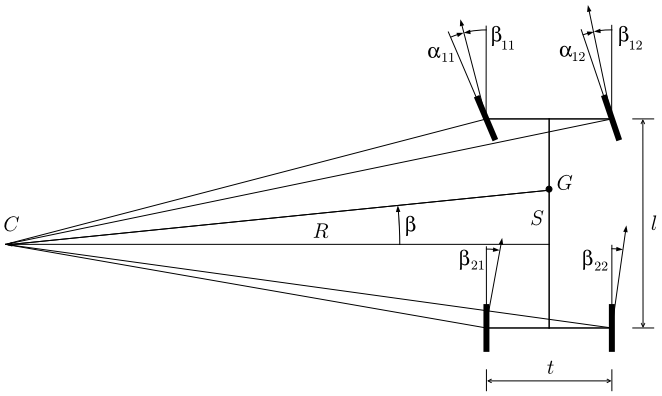

Fig. 3.4 Instantaneous velocity center C and definition of its coordinates S and R

These equations show that $u(t)$ and $v(t)$, despite being velocities, cannot be expressed as derivatives of other functions.[1] In other words, a formula like $v = \dot{y}$ is *totally meaningless*.

3.2.3 Velocity Center

As well known, if $r \neq 0$ any rigid body in planar motion has an *instantaneous center of zero velocity* C, that is a point such that $\mathbf{V}_C = \mathbf{0}$. With the aid of Fig. 3.4 it is easy to obtain the position of C of a vehicle in the body-fixed frame

$$GC = S\mathbf{i} + R\mathbf{j} \tag{3.11}$$

where

$$R = \frac{u}{r} \tag{3.12}$$

is the distance of C from the vehicle axis, and

$$S = -\frac{v}{r} \tag{3.13}$$

is the longitudinal position of C. Quite surprisingly, R is very popular, whereas S is hardly mentioned anywhere else.

The instantaneous center of zero velocity C, or *velocity center*, is often misunderstood. Indeed, it is correct to say that the velocity field of the rigid body is like a

[1] The reason is that $\mathrm{d}f = \cos\psi \mathrm{d}x_0 + \sin\psi \mathrm{d}y_0$ is not an exact differential since there does not exist a differentiable function $f(x_0, y_0, \psi)$.

pure rotation around C, that is

$$\mathbf{V}_P = r\mathbf{k} \times CP \tag{3.14}$$

but it is totally incorrect to think that the same property extends to the acceleration field. As a matter of fact, in general the acceleration $\mathbf{a}_C$ of point C is not zero. There is another point K, the *acceleration center* (described in Sect. 3.2.6) which has zero acceleration. Therefore, the velocity field is rotational around C, while the acceleration field is rotational around K. In other words, R is *not* a radius of curvature, unless $C = K$.

According to (3.35), the velocity center C has acceleration

$$\mathbf{a}_C = \left(a_x - r^2 S - \dot{r} R\right)\mathbf{i} + \left(a_y - r^2 R + \dot{r} S\right) = r(\dot{R}\mathbf{i} - \dot{S}\mathbf{j}) \tag{3.15}$$

3.2.4 Fundamental Ratios

Besides $R = u/r$ and $S = -v/r$, other ratios appear to be relevant in vehicle kinematics. They are

$$\beta = \frac{v}{u} = -\frac{S}{R} \tag{3.16}$$

and

$$\rho = \frac{r}{u} = \frac{1}{R} \tag{3.17}$$

The first is closely related to the *vehicle slip angle* $\hat{\beta}$

$$\hat{\beta} = \arctan(\beta) \tag{3.18}$$

that is the angle between $\mathbf{V}_G$ and $\mathbf{i}$.

Instead of ρ, it is usual to employ

$$l\rho = l\frac{r}{u} = \frac{l}{R} \tag{3.19}$$

This is the very classical *Ackermann angle*. However, in our opinion, ρ is more fundamental than l/R, as will be shown. For the moment it suffices to note that the wheelbase l is totally irrelevant for the description of the kinematics of the vehicle body. What matters are only u, v and r or their combinations (ratios). In this context, the wheelbase is quite an intruder. And by the way, what is the wheelbase in a three-axle vehicle?

3.2.5 Accelerations and Radii of Curvature

The angular acceleration is simply given by

$$\dot{\boldsymbol{\Omega}} = \dot{r}\mathbf{k} = \ddot{\psi}\mathbf{k} \tag{3.20}$$

A little more involved is the evaluation of the absolute acceleration $\mathbf{a}_G$ of G

$$\begin{aligned}\mathbf{a}_G = \frac{\mathrm{d}\mathbf{V}_G}{\mathrm{d}t} &= \dot{u}\mathbf{i} + ur\mathbf{j} + \dot{v}\mathbf{j} - vr\mathbf{i} \\ &= (\dot{u} - vr)\mathbf{i} + (\dot{v} + ur)\mathbf{j} \\ &= a_x\mathbf{i} + a_y\mathbf{j}\end{aligned} \tag{3.21}$$

where

$$\frac{\mathrm{d}\mathbf{i}}{\mathrm{d}t} = r\mathbf{j} \quad \text{and} \quad \frac{\mathrm{d}\mathbf{j}}{\mathrm{d}t} = -r\mathbf{i} \tag{3.22}$$

since the reference system S rotates with the vehicle body.

Equation (3.21) also defines the *longitudinal acceleration* a_x

$$\begin{aligned}a_x &= \dot{u} - vr \\ &= \dot{u} - u^2\beta\rho\end{aligned} \tag{3.23}$$

and the *lateral acceleration* a_y

$$\begin{aligned}a_y &= \dot{v} + ur \\ &= u\dot{\beta} + \dot{u}\beta + u^2\rho\end{aligned} \tag{3.24}$$

where longitudinal and lateral refer to the vehicle axis x, not to the trajectory. Again, a_x and a_y are not, in general, the second derivatives of some functions. In other words, a formula like $a_y = \ddot{y}$ is totally meaningless, and hence wrong.

Under *steady-state conditions* ($\dot{u} = \dot{v} = 0$), the lateral acceleration becomes

$$\tilde{a}_y = ur = u^2\rho = \frac{u^2}{R} \tag{3.25}$$

Whenever $\beta \neq 0$, the trajectory of G is not tangent to the vehicle axis x. The unit vector $\mathbf{t}$, directed like $\mathbf{V}_G$ (and hence tangent to the trajectory of G), is given by

$$\mathbf{t} = \frac{\mathbf{V}_G}{|\mathbf{V}_G|} = \cos\beta\mathbf{i} + \sin\beta\mathbf{j} \tag{3.26}$$

and the normal unit vector $\mathbf{n}$ by

$$\mathbf{n} = \mathbf{k} \times \mathbf{t} = -\sin\beta\mathbf{i} + \cos\beta\mathbf{j} \tag{3.27}$$

The acceleration $\mathbf{a}_G$ can be also expressed as

$$\mathbf{a}_G = a_t \mathbf{t} + a_n \mathbf{n} \tag{3.28}$$

with tangential component a_t (directed like $\mathbf{V}_G$)

$$a_t = \mathbf{a}_G \cdot \mathbf{t} = a_x \cos\beta + a_y \sin\beta = \frac{\dot{u}u + \dot{v}v}{\sqrt{u^2 + v^2}} \tag{3.29}$$

and centripetal component a_n (orthogonal to $\mathbf{V}_G$)

$$a_n = \mathbf{a}_G \cdot \mathbf{n} = -a_x \sin\beta + a_y \cos\beta = \frac{r(u^2 + v^2) + \dot{v}u - \dot{u}v}{\sqrt{u^2 + v^2}} \tag{3.30}$$

since $\sin\beta = v/V_G$ and $\cos\beta = u/V_G$, with $V_G = |\mathbf{V}_G| = u/\cos\beta$.

The *radius of curvature* R_G of the trajectory of G is readily obtained as

$$R_G = \frac{V_G^2}{a_n} = \frac{(u^2 + v^2)^{\frac{3}{2}}}{r(u^2 + v^2) + \dot{v}u - \dot{u}v} = \frac{V_G}{r + \frac{\dot{v}u - \dot{u}v}{V_G^2}} \tag{3.31}$$

It is worth remarking that the velocity center C is *not* the center of curvature of trajectories, unless $(\dot{v}u - v\dot{u}) = 0$.

Also useful is the curvature $\rho_G = 1/R_G$

$$\rho_G = \frac{r + \dot{\beta}}{u}\cos\beta = \frac{r}{\sqrt{u^2 + v^2}} + \frac{\dot{v}u - v\dot{u}}{(u^2 + v^2)^{\frac{3}{2}}} \tag{3.32}$$

Under normal operating conditions $|\beta| \ll 1$, i.e. $\beta \approx \hat{\beta}$, and hence

$$\rho_G \approx \frac{r + \dot{\beta}}{u} = \rho + \frac{\dot{\beta}}{u} \tag{3.33}$$

Quite a compact and interesting formula.

The acceleration of any point P of the vehicle body is given by the well known formula

$$\mathbf{a}_P = \mathbf{a}_G + \dot{\mathbf{\Omega}} \times GP + \mathbf{\Omega} \times (\mathbf{\Omega} \times GP) \tag{3.34}$$

which, in case of planar motion, simplifies into

$$\mathbf{a}_P = \mathbf{a}_G + \dot{r}\mathbf{k} \times GP - r^2 GP \tag{3.35}$$

3.2.6 Acceleration Center

The acceleration field of a rigid body in planar motion is like a pure rotation around the *acceleration center* K, that is a point which has $\mathbf{a}_K = \mathbf{0}$. According to (3.35),

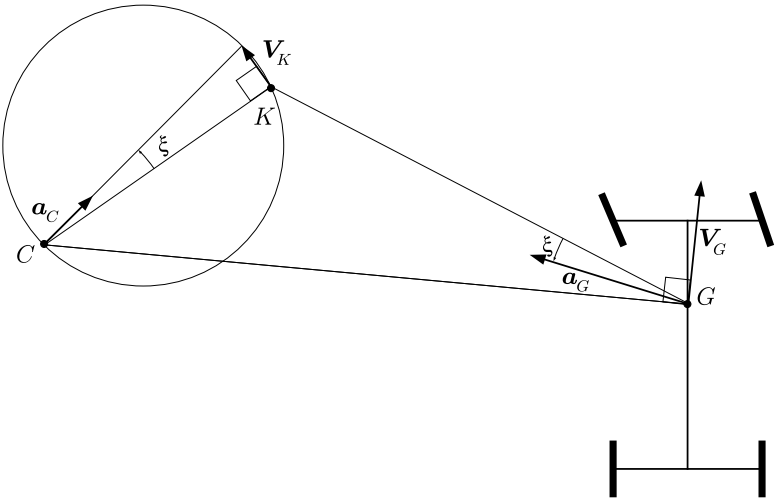

Fig. 3.5 Velocity center C, acceleration center K and inflection circle

the acceleration $\mathbf{a}_P$ of any point P must be given by

$$\mathbf{a}_P = \dot{r}\mathbf{k} \times KP - r^2 KP \tag{3.36}$$

Therefore, the angle ξ between $\mathbf{a}_P$ and PK is such that

$$\tan(\xi) = \frac{\dot{r}}{r^2} \tag{3.37}$$

By setting $P = G$ in (3.36), as shown in Fig. 3.5

$$\mathbf{a}_G = \dot{r}\mathbf{k} \times KG - r^2 KG \tag{3.38}$$

we obtain that

$$|KG| = \frac{a_G}{\sqrt{\dot{r}^2 + r^4}} \tag{3.39}$$

or, more precisely

$$GK = \frac{a_x r^2 - a_y \dot{r}}{r^4 + \dot{r}^2} + \frac{a_x \dot{r} + a_y r^2}{r^4 + \dot{r}^2} \tag{3.40}$$

The acceleration center lies necessarily on the *inflection circle*, which is the set of all points whose trajectories have an inflection point (Fig. 3.5). Actually, the velocity center C does not belong to the inflection circle, although it looks like. Point K spans the inflection circle depending on the value of the ratio $\dot{r}/r^2$, as shown in Fig. 3.5. This topic will be addressed in detail in Chap. 5, entirely devoted to the kinematics of cornering.

3.2.7 Tire Kinematics (Tire Slips)

So far only the kinematics of the vehicle body has been addressed. Roughly speaking, it is what that mostly matters to the driver. However, vehicle engineers are also interested in the kinematics of the wheels, since it strongly affects the forces exerted by the tires.

According to (3.3), the velocity of the center P_{11} of the left front wheel is given by

$$\mathbf{V}_{11} = \mathbf{V}_G + r\mathbf{k} \times GP_{11} = (u\mathbf{i} + v\mathbf{j}) + r\mathbf{k} \times \left(a_1\mathbf{i} + \frac{t_1}{2}\mathbf{j}\right) \tag{3.41}$$

Performing the same calculation for the centers of all wheels yields

$$\begin{aligned}
\mathbf{V}_{11} &= \left(u - \frac{rt_1}{2}\right)\mathbf{i} + (v + ra_1)\mathbf{j} \\
\mathbf{V}_{12} &= \left(u + \frac{rt_1}{2}\right)\mathbf{i} + (v + ra_1)\mathbf{j} \\
\mathbf{V}_{21} &= \left(u - \frac{rt_2}{2}\right)\mathbf{i} + (v - ra_2)\mathbf{j} \\
\mathbf{V}_{22} &= \left(u + \frac{rt_2}{2}\right)\mathbf{i} + (v - ra_2)\mathbf{j}
\end{aligned} \tag{3.42}$$

Therefore, the angles $\hat{\beta}_{ij}$ between the vehicle longitudinal axis $\mathbf{i}$ and $\mathbf{V}_{ij}$ can be obtained as (Fig. 3.4)

$$\begin{aligned}
\tan(\hat{\beta}_{11}) &= \frac{v + ra_1}{u - rt_1/2} = \beta_{11} = \tan(\delta_{11} - \alpha_{11}) \\
\tan(\hat{\beta}_{12}) &= \frac{v + ra_1}{u + rt_1/2} = \beta_{12} = \tan(\delta_{12} - \alpha_{12}) \\
\tan(\hat{\beta}_{21}) &= \frac{v - ra_2}{u - rt_2/2} = \beta_{21} = \tan(\delta_{21} - \alpha_{21}) \\
\tan(\hat{\beta}_{22}) &= \frac{v - ra_2}{u + rt_2/2} = \beta_{22} = \tan(\delta_{22} - \alpha_{22})
\end{aligned} \tag{3.43}$$

The tire slip angles α_{ij} of each wheel (positive if clockwise) are given by (Fig. 3.4)

$$\alpha_{ij} = \delta_{ij} - \hat{\beta}_{ij} \tag{3.44}$$

It is very important to realize that even small steering angles δ_{ij} may significantly affect α_{ij} and hence the tire friction forces.

As thoroughly discussed in Sect. 2.7.2, tire kinematics can, in most cases, be conveniently described by means of the translational slips σ_x and σ_y and the spin slip φ, defined in (2.55), (2.56) and (2.57), respectively.

According to (2.43), the rolling velocity of each wheel is equal to $\omega_{ij} r_i$, where ω_{ij} is the angular velocity of the rim and r_i is the rolling radius. The speed of travel $\mathbf{V}_{ij}$ of each wheel was obtained in (3.42). Considering also the steering angles δ_{ij}, we obtain for each tire

- longitudinal slips:

$$\begin{aligned}
\sigma_{x_{11}} &= \frac{[(u - rt_1/2)\cos(\delta_{11}) + (v + ra_1)\sin(\delta_{11})] - \omega_{11} r_1}{\omega_{11} r_1} \\
\sigma_{x_{12}} &= \frac{[(u + rt_1/2)\cos(\delta_{12}) + (v + ra_1)\sin(\delta_{12})] - \omega_{12} r_1}{\omega_{12} r_1} \\
\sigma_{x_{21}} &= \frac{[(u - rt_2/2)\cos(\delta_{21}) - (v - ra_2)\sin(\delta_{21})] - \omega_{21} r_2}{\omega_{21} r_2} \\
\sigma_{x_{22}} &= \frac{[(u + rt_2/2)\cos(\delta_{22}) - (v - ra_2)\sin(\delta_{22})] - \omega_{22} r_2}{\omega_{22} r_2}
\end{aligned} \tag{3.45}$$

- lateral slips:

$$\begin{aligned}
\sigma_{y_{11}} &= \frac{(v + ra_1)\cos(\delta_{11}) - (u - rt_1/2)\sin(\delta_{11})}{\omega_{11} r_1} \\
\sigma_{y_{12}} &= \frac{(v + ra_1)\cos(\delta_{12}) - (u + rt_1/2)\sin(\delta_{12})}{\omega_{12} r_1} \\
\sigma_{y_{21}} &= \frac{(v - ra_2)\cos(\delta_{21}) - (u - rt_2/2)\sin(\delta_{21})}{\omega_{21} r_2} \\
\sigma_{y_{22}} &= \frac{(v - ra_2)\cos(\delta_{22}) - (u - rt_2/2)\sin(\delta_{22})}{\omega_{22} r_2}
\end{aligned} \tag{3.46}$$

According to (2.57), the evaluation of the spin slips φ_{ij} requires also the knowledge of the camber angles γ_{ij}, of the wheel yaw rates $\dot{\zeta}_{ij} = r + \dot{\delta}_{ij}$ and of the camber reduction factors ε_i

$$\varphi_{ij} = -\frac{r + \dot{\delta}_{ij} + \omega_{ij} \sin\gamma_{ij} (1 - \varepsilon_i)}{\omega_{ij} r_i} \tag{3.47}$$

The sign conventions are like in Fig. 2.2. Therefore, under static conditions, the two wheels of the same axle have camber angles of opposite sign

$$\gamma_{i1}^0 = -\gamma_{i2}^0 \tag{3.48}$$

This is contrary to common practice, but more consistent and more convenient for a systematic treatment. The kinematic equations for camber variations due to roll motion will be discussed in Sect. 3.8.3.

Similarly, the kinematic equations for roll steer will be given in (3.123). Their presentation must be delayed till the suspension analysis has been completed.

Owing to (3.4), the expressions of the translational slips can be simplified under normal operating conditions and small steering angles

$$\begin{aligned}
\sigma_{x_{11}} &\simeq \frac{(u - rt_1/2) - \omega_{11} r_1}{\omega_{11} r_1}, & \sigma_{y_{11}} &\simeq \frac{(v + ra_1) - u\delta_{11}}{\omega_{11} r_1} \\
\sigma_{x_{12}} &\simeq \frac{(u + rt_1/2) - \omega_{12} r_1}{\omega_{12} r_1}, & \sigma_{y_{12}} &\simeq \frac{(v + ra_1) - u\delta_{12}}{\omega_{12} r_1} \\
\sigma_{x_{21}} &\simeq \frac{(u - rt_2/2) - \omega_{21} r_2}{\omega_{21} r_2}, & \sigma_{y_{21}} &\simeq \frac{(v - ra_2) - u\delta_{21}}{\omega_{21} r_2} \\
\sigma_{x_{22}} &\simeq \frac{(u + rt_2/2) - \omega_{22} r_2}{\omega_{22} r_2}, & \sigma_{y_{22}} &\simeq \frac{(v - ra_2) - u\delta_{22}}{\omega_{22} r_2}
\end{aligned} \tag{3.49}$$

3.3 Vehicle Constitutive (Tire) Equations

In any vehicle model we have to set up equations that relate the vehicle motion to the grip forces each tire exchanges with the road.

Two chapters are devoted to the analysis of the mechanical behavior of wheels with tires. The topic is quite complex. From that analysis, several tire models of increasing complexity can be formulated. However, in all of them the grip forces depend at least on the (theoretical) slips and the vertical loads acting on the tire. These two aspects cannot be omitted. Other effects, like the transient behavior can be included if necessary.

As discussed in Sect. 2.8, after having extensively tested a tire, the quantities listed in (2.73) should be available to the vehicle dynamicist to properly define the (steady-state) pure rolling conditions. Departing from pure rolling means having grip forces acting in the contact patch. Under steady-state conditions, it is often assumed that, for each wheel with tire, these grip forces and moments obey relations in the following form

$$\begin{aligned}
F_x &= F_x(F_z, \gamma, \sigma_x, \sigma_y, \varphi) \\
F_y &= F_y(F_z, \gamma, \sigma_x, \sigma_y, \varphi) \\
M_z &= M_z(F_z, \gamma, \sigma_x, \sigma_y, \varphi)
\end{aligned} \tag{3.50}$$

where γ is the camber angle, σ_x is the longitudinal theoretical slip, σ_y is the lateral theoretical slip and φ is the spin slip.

As shown in Sect. 3.5.3, and in particular in (3.58), the steering angles δ_{ij} have also to be taken into account to obtain the longitudinal and lateral forces with respect to the vehicle frame.

We recall that using the tire slips simplifies the analysis, but implicitly discards any possible influence of the forward speed on the tire behavior. In race cars, this influence may not be negligible.

3.4 Vehicle Equilibrium Equations

The classical dynamic equilibrium equations for a rigid body are [4]

$$\begin{aligned} m\mathbf{a}_G &= \mathbf{F} \\ \dot{\mathbf{K}}_G^r &= \mathbf{M}_G \end{aligned} \tag{3.51}$$

where m is the total mass of the vehicle and $\dot{\mathbf{K}}_G^r$ is the time rate of change of the angular momentum with respect to G.

The acceleration $\mathbf{a}_G$ of G has been obtained in (3.21)

$$\mathbf{a}_G = (\dot{u} - vr)\mathbf{i} + (\dot{v} + ur)\mathbf{j} = a_x\mathbf{i} + a_y\mathbf{j} \tag{3.21'}$$

The rate of change of the angular momentum $\dot{\mathbf{K}}_G^r$ can be conveniently expressed in terms of the inertia tensor in the body-fixed reference frame

$$\begin{aligned} \dot{\mathbf{K}}_G^r &= \left(-J_{zx}\dot{r} + J_{yz}r^2\right)\mathbf{i} + \left(-J_{zx}r^2 - J_{yz}\dot{r}\right)\mathbf{j} + J_z\dot{r}\mathbf{k} \\ &\approx -J_{zx}\left(\dot{r}\mathbf{i} + r^2\mathbf{j}\right) + J_z\dot{r}\mathbf{k} \end{aligned} \tag{3.52}$$

since $J_{yz} \approx 0$ and $|J_{zx}| \ll J_z$.

The total external force $\mathbf{F}$ and the total external couple $\mathbf{M}_G$ can be represented in terms of their components in the body-fixed reference system

$$\begin{aligned} \mathbf{F} &= X\mathbf{i} + Y\mathbf{j} + Z\mathbf{k} \\ \mathbf{M}_G &= L\mathbf{i} + M\mathbf{j} + N\mathbf{k} \end{aligned} \tag{3.53}$$

The components in (3.53) have the following standard names:

- X: longitudinal force;
- Y: lateral or side force;
- Z: vertical or normal force;
- L: rolling moment;
- M: pitching moment;
- N: yawing moment.

As already stated, the vehicle body has a planar motion. However, the forces acting on the vehicle do not form a planar system.

3.5 Forces Acting on the Vehicle

There are four different types of external forces acting on a road vehicle:

(1) weight (gravitational force);
(2) aerodynamic force;
(3) road-tire friction forces;
(4) road-tire vertical forces.

3.5.1 Weight

The *weight* $\mathbf{W}$ is simply given by

$$\mathbf{W} = -W\mathbf{k} = -mg\mathbf{k} \tag{3.54}$$

where g is the gravitational acceleration. As well known, the weight force is applied in G. Therefore, it does not contribute to $\mathbf{M}_G$.

3.5.2 Aerodynamic Force

The *aerodynamic force*

$$\mathbf{F}_a = -X_a\mathbf{i} + Y_a\mathbf{j} + Z_a\mathbf{k} \tag{3.55}$$

depends essentially on the vehicle shape and size, and on the relative speed $\mathbf{V}_a$ between the vehicle and the air. An in-depth discussion on vehicle aerodynamics is beyond the scope of the present work. Here it may suffice to state without proof that

$$X_a = \frac{1}{2}\rho_a V_a^2 C_x S_a, \qquad Y_a = \frac{1}{2}\rho_a V_a^2 C_y S_a, \qquad Z_a = \frac{1}{2}\rho_a V_a^2 C_z S_a \tag{3.56}$$

where ρ_a is the air density, $V_a = |\mathbf{V}_a|$, S_a is the area of the vehicle frontal projection (frontal area) and C_x, C_y, C_z are shape coefficients. Traditionally $C_x > 0$, which explains the minus sign in (3.55). If $\mathbf{V}_a$ is directed like the vehicle axis $\mathbf{i}$, that is $\mathbf{V}_a = -V_a\mathbf{i}$, the coefficient $C_y = 0$ and hence $Y_a = 0$.

In a modern car, the frontal area S_a is about 1.8 m^2 and the *drag coefficient* C_x ranges between 0.30 and 0.35. A Formula One car has a frontal area of about 1.3 m^2 and a drag coefficient which ranges between 0.7 and 1. It is quite usual to provide directly the product $S_a C_x$ as a more effective way to compare the aerodynamic efficiency of cars. For instance, a Formula One car has $S_a C_x$ of about 1.2 m^2, while a commercial one may have it below 0.6 m^2.

Formula 1 cars have C_z with very high *negative* values to achieve a very high aerodynamic downforce. Typically, $S_a C_z \simeq -5.2$ m^2.

In general, the aerodynamic force $\mathbf{F}_a$ in not applied at G (why should it be?) and therefore it contributes to $\mathbf{M}_G$ with an aerodynamic moment $\mathbf{M}_a = M_{a_x}\mathbf{i} + M_{a_y}\mathbf{j} + M_{a_z}\mathbf{k}$, the biggest component being M_{a_y} (pitch moment).

It is common practice to do like in Fig. 3.6, thus defining the front and rear aerodynamic vertical forces (positive upward) according to

$$\begin{aligned} Z_1^a &= \frac{1}{l}[Z_a a_2 - M_{a_y} + X_a h] = \frac{1}{2}\rho_a V_a^2 C_{z1} S_a \\ Z_2^a &= \frac{1}{l}[Z_a a_1 + M_{a_y} - X_a h] = \frac{1}{2}\rho_a V_a^2 C_{z2} S_a \end{aligned} \tag{3.57}$$

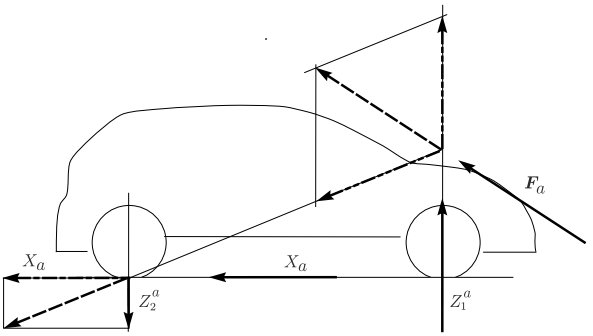

Fig. 3.6 Aerodynamic forces

where C_{z1} and C_{z2} have been introduced. In other words, in straight running, the aerodynamic force $\mathbf{F}_a$ is given as two vertical loads Z_1^a and Z_2^a acting directly on the front and rear tires, respectively, plus the aerodynamic drag X_a acting at road level.

3.5.3 Road-Tire Friction Forces

The *road-tire friction forces* $\mathbf{F}_{t_{ij}}$ are the resultant of the tangential stress in each footprint, as shown in (2.15). Typically, for each tire, the tangential force $\mathbf{F}_{t_{ij}}$ is split into a longitudinal component $F_{x_{ij}}$ and a lateral component $F_{y_{ij}}$, as shown in Fig. 3.7. It is very important to note that these two components refer to the wheel reference system shown in Fig. 2.2, not to the vehicle frame.

If δ_{ij} is the steering angle of a wheel, the components of the tangential force in the vehicle frame S are given by

$$\begin{aligned} \mathbf{F}_{t_{ij}} &= X_{ij}\mathbf{i} + Y_{ij}\mathbf{j} \\ \text{where } X_{ij} &= F_{x_{ij}}\cos(\delta_{ij}) - F_{y_{ij}}\sin(\delta_{ij}) \\ Y_{ij} &= F_{x_{ij}}\sin(\delta_{ij}) + F_{y_{ij}}\cos(\delta_{ij}) \end{aligned} \tag{3.58}$$

with obvious simplifications if δ_{ij} is very small.

To deal with shorter expressions, it is convenient to define

$$\begin{aligned} X_1 &= X_{11} + X_{12}, & X_2 &= X_{21} + X_{22} \\ Y_1 &= Y_{11} + Y_{12}, & Y_2 &= Y_{21} + Y_{22} \\ \Delta X_1 &= \frac{X_{12} - X_{11}}{2}, & \Delta X_2 &= \frac{X_{22} - X_{21}}{2} \\ \Delta Y_1 &= \frac{Y_{12} - Y_{11}}{2}, & \Delta Y_2 &= \frac{Y_{22} - Y_{21}}{2} \end{aligned} \tag{3.59}$$

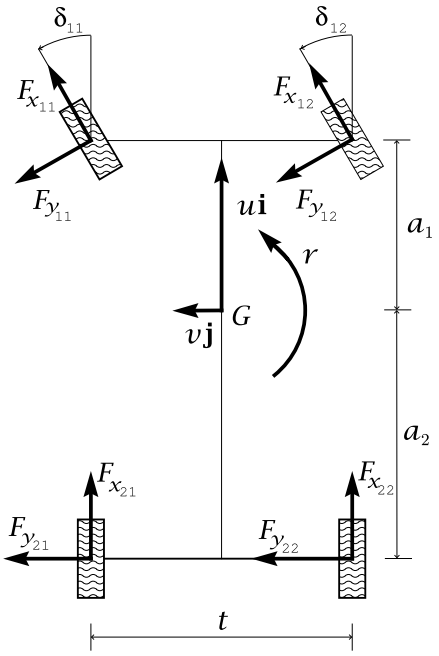

Fig. 3.7 Road-tire friction forces

Even for not so small steering angles, simpler expressions can be obtained by observing that small errors in the values of the steering angles δ_{ij} have marginal influence on the global equilibrium.[2] More precisely, in the equilibrium equations we can "force" the steering angles of the front wheels δ_{11} and δ_{12} both to be equal to $\delta_1 = (\delta_{11} + \delta_{12})/2$. Similarly, the rear wheels can be set to have the same (often zero) steering, that is $\delta_2 = (\delta_{21} + \delta_{22})/2$.

It should be clearly understood that often, in real vehicles, the two wheels of the same axle are intentionally slightly nonparallel. Assuming the two wheels to be parallel is harmless for the global equilibrium of the vehicle, whereas it would be quite influential on the tire behavior.

Strictly speaking, the tangential forces $F_{y_{ij}}$ are not applied at the center of the contact patch. In general, there are also vertical moments $M_{z_{ij}}$. However, these moments have negligible effects on the dynamics of the vehicle as a whole. Indeed, taking $M_{z_{ij}}$ into account would mean displacing by only a few centimeters the action lines of $\mathbf{F}_{t_{ij}}$.

On the other hand, vertical moments do affect quite a bit the steering system. In particular, they must be included in vehicle models with compliant steering system.

[2] But not on the tire slips.

3.5.4 Road-Tire Vertical Forces

The *road-tire vertical forces* $F_{z_{ij}}\mathbf{k}$ are the resultant of the normal pressure in each footprint, as in (2.13).

As discussed in Sect. 2.6.3, the displacement with respect to the center of the footprint of the line of action of the vertical forces is the main cause of rolling resistance. This phenomenon can be neglected when studying, e.g., extreme braking or handling, whereas it is of paramount importance for the estimation of fuel consumption or of power losses in general.

It is customary to add the vertical forces of the same axle

$$Z_1 = F_{z_{11}} + F_{z_{12}} \quad \text{and} \quad Z_2 = F_{z_{21}} + F_{z_{22}} \tag{3.60}$$

and to define the differences

$$\Delta Z_1 = \frac{F_{z_{12}} - F_{z_{11}}}{2} \quad \text{and} \quad \Delta Z_2 = \frac{F_{z_{22}} - F_{z_{21}}}{2} \tag{3.61}$$

usually called *lateral load transfers*.

Inverting these equations yields for the vertical load on each wheel

$$\begin{aligned} F_{z_{11}} &= \frac{Z_1}{2} - \Delta Z_1 = Z_{11}, & F_{z_{12}} &= \frac{Z_1}{2} + \Delta Z_1 = Z_{12} \\ F_{z_{21}} &= \frac{Z_2}{2} - \Delta Z_2 = Z_{21}, & F_{z_{22}} &= \frac{Z_2}{2} + \Delta Z_2 = Z_{22} \end{aligned} \tag{3.62}$$

3.6 Vehicle Equilibrium Equations (more Explicit Form)

The explicit expressions of all the force and moment components in (3.53) are obtained by collecting all the contributions of the external actions.

For a two-axle vehicle we obtain the forces

$$\begin{aligned} X &= X_1 + X_2 - X_a \\ Y &= Y_1 + Y_2 \\ Z &= Z_1 + Z_2 - (mg - Z_{a1} - Z_{a2}) \end{aligned}$$

and the moments (3.63)

$$\begin{aligned} L &= -\Delta Z_1 t_1 - \Delta Z_2 t_2 + (Y_1 + Y_2)h \\ M &= -Z_1 a_1 + Z_2 a_2 - (X_1 + X_2 - X_a)h - Z_{a1} a_1 + Z_{a2} a_2 \\ N &= Y_1 a_1 - Y_2 a_2 + \Delta X_1 t_1 + \Delta X_2 t_2 \end{aligned}$$

These expressions can be inserted into (3.63) and then into (3.51) to obtain the six *global equilibrium equations*.

Actually, it is more convenient to split them into the following two sets of equations. A first set of three equations, which deals explicitly with the vehicle motion

$$\begin{aligned} ma_x &= m(\dot{u} - vr) = X = X_1 + X_2 - X_a \\ ma_y &= m(\dot{v} + ur) = Y = Y_1 + Y_2 \\ J_z\dot{r} &= N = Y_1a_1 - Y_2a_2 + \Delta X_1t_1 + \Delta X_2t_2 \end{aligned} \tag{3.64}$$

and a second set that involves the constraint forces (vertical loads) to make the vehicle comply with the flatness of the road surface

$$\begin{aligned} 0 &= Z = Z_1 + Z_{a1} + Z_2 + Z_{a1} - mg \\ -J_{zx}\dot{r} &= L = (Y_1 + Y_2)h - \Delta Z_1t_1 - \Delta Z_2t_2 \\ -J_{zx}r^2 &= M = -(Z_1 + Z_{a1})a_1 + (Z_2 + Z_{a2})a_2 - (X_1 + X_2 - X_a)h \end{aligned} \tag{3.65}$$

Equations (3.64) and (3.65) are really important. If fully understood, they provide a lot of information on vehicle dynamics.

Combining (3.64) and (3.65), the second set can be recast in a form which better highlights the interplay between vertical loads and vehicle motion

$$\begin{aligned} Z_1 + Z_{a1} + Z_2 + Z_{a2} &= mg \\ \Delta Z_1t_1 + \Delta Z_2t_2 &= ma_yh + J_{zx}\dot{r} \\ (Z_1 + Z_{a1})a_1 - (Z_2 + Z_{a2})a_2 &= -ma_xh + J_{zx}r^2 \end{aligned} \tag{3.66}$$

where $J_{zx}\dot{r}$ and $J_{zx}r^2$ are usually negligible.

It is convenient to define

$$\begin{aligned} N_Y &= Y_1a_1 - Y_2a_2 \\ N_X &= \Delta X_1t_1 + \Delta X_2t_2 \end{aligned} \tag{3.67}$$

to highlight the different origin of the two contributions to the yawing moment

$$N = N_Y + N_X = J_z\dot{r} \tag{3.68}$$

N_Y is due to the lateral forces, while N_X comes from the difference between the longitudinal forces of the two wheels of the same axle.

From

$$\begin{aligned} Y &= Y_1 + Y_2 \\ N_Y &= Y_1a_1 - Y_2a_2 = J_z\dot{r} - N_X \end{aligned} \tag{3.69}$$

we obtain the lateral (grip) forces exerted by the road on each axle

$$Y_1 = \frac{Ya_2 + N_Y}{l} = \frac{Ya_2^b}{l} \quad \text{and} \quad Y_2 = \frac{Ya_1 - N_Y}{l} = \frac{Ya_1^b}{l} \tag{3.70}$$

where

$$a_1^b = a_1 - x_N \quad \text{and} \quad a_2^b = a_2 + x_N$$
$$\text{with } x_N = \frac{N_Y}{Y} \tag{3.71}$$

Therefore $a_1^b + a_2^b = a_1 + a_2 = l$.

An equivalent, more "dynamic", form of (3.70) is

$$Y_1 = \frac{ma_y a_2}{l} + \frac{N - N_X}{l} \quad \text{and} \quad Y_2 = \frac{ma_y a_1}{l} - \frac{N - N_X}{l} \tag{3.72}$$

where $N = J_z \dot{r}$.

Most classical vehicle dynamics assumes $N_Y = N$, that is $N_X = 0$; this is correct except when the vehicle:

- has a limited slip (or locked) differential;
- has ESP and it has been activated;
- is braking with locked wheels on a road with nonuniform grip coefficients.

3.7 Load Transfers

Load transfers ΔZ, ΔZ_1 and ΔZ_2 need additional discussion. Indeed, the vertical load acting on a tire does affect very much its behavior. Therefore, it is important to discuss the relationships between vehicle motion and vertical loads (3.62).

3.7.1 Longitudinal Load Transfer

From the first and last equations in (3.66) it is easy to obtain, for a two-axle vehicle, the vertical loads that the road applies on each axle

$$\begin{aligned} Z_1 &= Z_1^0 + \Delta Z - Z_1^a \\ Z_2 &= Z_2^0 - \Delta Z - Z_2^a \end{aligned} \tag{3.73}$$

where

$$\Delta Z = -\frac{ma_x h}{l} + \frac{J_{zx} r^2}{l} \simeq -\frac{ma_x h}{l} \tag{3.74}$$

is the *longitudinal load transfer* due to the longitudinal acceleration a_x, and

$$Z_1^0 = \frac{mga_2}{l}, \qquad Z_2^0 = \frac{mga_1}{l} \tag{3.75}$$

are the *static loads* on each axle. In a motionless vehicle the vertical loads have to balance only the vehicle weight.

During vehicle motion, the vertical loads change whenever there are accelerations. In case of substantial aerodynamic vertical loads, the vehicle speed also affects the vertical loads.

3.7.2 Lateral Load Transfers

Lateral load transfers ΔZ_1 and ΔZ_2 appear explicitly only in the second equation in (3.65), which may be recast as

$$\begin{aligned} \Delta Z_1 t_1 + \Delta Z_2 t_2 &= Yh + J_{zx}\dot{r} \\ &= ma_y h + J_{zx}\dot{r} \end{aligned} \tag{3.76}$$

where $a_y = \dot{v} + ur$ is the lateral acceleration. Of course, one equation is not enough to obtain ΔZ_1 and ΔZ_2. Even under *static conditions*, (3.76) yields, for a two-axle vehicle

$$\Delta Z_1^0 t_1 + \Delta Z_2^0 t_2 = 0 \tag{3.77}$$

which shows that the static lateral load transfers ΔZ_1^0 and ΔZ_2^0 may have in principle any value. However, with the aid of four scales, it is part of the set-up procedure to achieve $\Delta Z_1^0 = \Delta Z_2^0 = 0$.

Suspension geometry and compliances influence directly the ratio $\Delta Z_1/\Delta Z_2$. This is a fundamental aspect of vehicle dynamics.

3.7.3 Vertical Loads on Each Tire

The global amount of lateral load transfer is determined by (3.76), but how much of it goes to the front and how much to the rear cannot be found without looking at the suspensions and at the tires (unless the vehicle is a three-wheeler).

This is the motivation for the next Sect. 3.8, where some of the front and rear suspension features will be exploited.

Summing up, the vertical loads on each tire are

$$\begin{aligned} Z_{11} &= 0.5\left(Z_1^0 - Z_1^a + \Delta Z\right) - \Delta Z_1 \\ Z_{12} &= 0.5\left(Z_1^0 - Z_1^a + \Delta Z\right) + \Delta Z_1 \\ Z_{21} &= 0.5\left(Z_2^0 - Z_2^a - \Delta Z\right) - \Delta Z_2 \\ Z_{22} &= 0.5\left(Z_2^0 - Z_2^a - \Delta Z\right) + \Delta Z_2 \end{aligned} \tag{3.78}$$

or, more explicitly

$$
\begin{aligned}
Z_{11} &= \frac{1}{2}\left[\frac{mga_2}{l} - \frac{1}{2}\rho_a S_a C_{z1} u^2 - \frac{ma_x h - J_{zx} r^2}{l}\right] - \Delta Z_1 \\
Z_{12} &= \frac{1}{2}\left[\frac{mga_2}{l} - \frac{1}{2}\rho_a S_a C_{z1} u^2 - \frac{ma_x h - J_{zx} r^2}{l}\right] + \Delta Z_1 \\
Z_{21} &= \frac{1}{2}\left[\frac{mga_1}{l} - \frac{1}{2}\rho_a S_a C_{z2} u^2 + \frac{ma_x h - J_{zx} r^2}{l}\right] - \Delta Z_2 \\
Z_{22} &= \frac{1}{2}\left[\frac{mga_1}{l} - \frac{1}{2}\rho_a S_a C_{z2} u^2 + \frac{ma_x h - J_{zx} r^2}{l}\right] + \Delta Z_2
\end{aligned}
\tag{3.79}
$$

where ΔZ_i will be obtained after the suspension analysis (see Sect. 3.8.11).

3.8 Suspension First-Order Analysis

Consistently with the hypotheses listed at p. 47, the suspension mechanics will be analyzed assuming very small suspension deflections and tire deformations. This is what a first order analysis is all about. Of course, it is not the whole story, but it is a good starting point.[3]

More precisely, the following aspects will be addressed:

- suspension internal coordinates;
- suspension and tire stiffnesses;
- suspension internal equilibrium.

3.8.1 Suspension Reference Configuration

Figure 3.8 shows two possible suspensions in their reference configuration (vehicle going straight at constant speed). It also serves the purpose of defining some relevant quantities.

First of all, the reference configuration is supposed to be perfectly *symmetric*. More precisely, the left and right sides are exactly alike (including springs).

Points A_i mark the centers of the tire contact patches. Points B_i are the instantaneous centers of rotation of the wheel hub with respect to the vehicle body. Here, for simplicity, the suspension linkage is supposed to be *rigid* and *planar*. In a swing

[3] At first it may look paradoxical, but it is not. Actually it is common practice in engineering. Just take the most classical cantilever beam, of length l with a concentrated load F at its end. Strictly speaking, the bending moment at the fixed end is not exactly equal to Fl, since the beam deflection takes the force a little closer to the wall. But this effect is usually neglected.

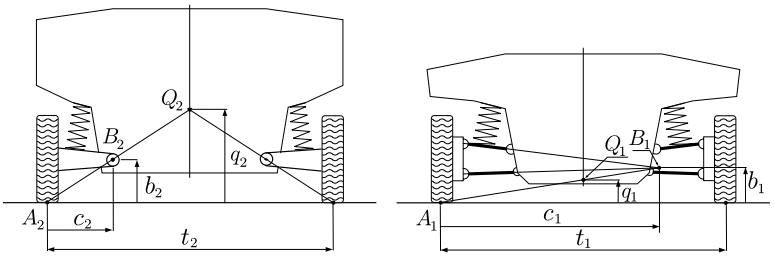

Fig. 3.8 Suspensions in their reference configuration: swing axle (*left*) and double wishbone suspension (*right*)

axle suspension, point B_2 is indeed the center of a joint, whereas in a double wishbone suspension (right) point B_1 has to be found by a well known method. In both cases, the distances c_i and b_i set the position of B_i with respect to A_i (Fig. 3.8). As usual, t_1 and t_2 are the front and rear track lengths.

Also shown in Fig. 3.8 are points Q_1 and Q_2. They are given by the intersection of the straight lines connecting A_i and B_i on both sides. Because of symmetry, they lay on the centerline at heights q_1 and q_2. Points Q_1 and Q_2 are the so-called *roll centers* and their role in vehicle dynamics will be addressed shortly.

3.8.2 Suspension Internal Coordinates

For each axle, *four* "internal" coordinates are necessary to monitor the suspension conditions with respect to a reference configuration. A possible selection of coordinates may be as follows (Fig. 3.9)

- body roll angle ϕ_i^s due to suspension deflections only;
- body vertical displacement z_i^s due to suspension deflections only (which results in track variation Δt_i);
- body roll angle ϕ_i^p due to tire deformations only;
- body vertical displacement z_i^p due to tire deformations only.

Figure 3.9 shows how each single coordinate changes the vehicle configuration for a swing axle suspension.[4] These four coordinates are, by definition, independent. It will depend on the vehicle dynamics whether they change or not. In other words, the kinematic schemes of Fig. 3.9 have nothing to do with real operating conditions. It is therefore legitimate, but not mandatory at all, to define, e.g., the roll ϕ_i^s of the vehicle body keeping the track t_i fixed and without any tire deformation, as in Fig. 3.9.

[4] A more precise definition of roll angle is given in Sect. 9.2.

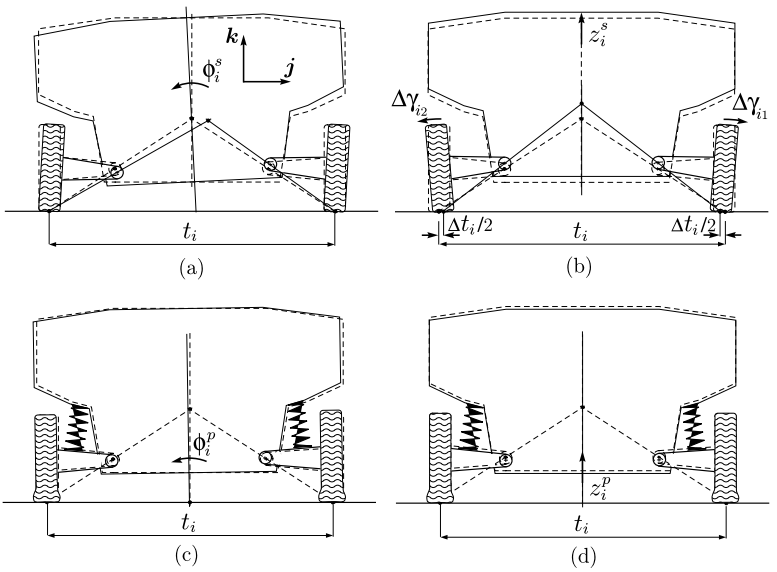

Fig. 3.9 Suggested selection of internal coordinates: (**a**) roll angle ϕ_i^s due to suspension deflections only, (**b**) track variation Δt_i, (**c**) roll angle ϕ_i^p due to tire deformations only, (**d**) vertical displacement z_i^p due to tire deformations only

The first order relationship between z_i^s and Δt_i is given by (Fig. 3.9)

$$z_i^s = -\frac{c_i}{2b_i}\Delta t_i = -\frac{t_i}{4q_i}\Delta t_i \tag{3.80}$$

which, because of *symmetry*, does not depend on ϕ_i^s and ϕ_i^p.

3.8.3 Camber Variation

Any other kinematic quantity is, by definition, a function of the selected set of coordinates $(\phi_i^s, \Delta t_i, \phi_i^p, z_i^p)$.

It is quite important to monitor the variation of the wheel *camber angle* γ_{ij} as a function of the selected coordinates $(\phi_i^s, \Delta t_i, \phi_i^p, z_i^p)$. In a first order analysis, the investigation is limited to the series expansion

$$\Delta\gamma_{ij} \approx \frac{\partial\gamma_{ij}}{\partial\phi_i^s}\phi_i^s + \frac{\partial\gamma_{ij}}{\partial\Delta t_i}\Delta t_i + \frac{\partial\gamma_{ij}}{\partial\phi_i^p}\phi_i^p + \frac{\partial\gamma_{ij}}{\partial z_i^p}z_i^p \tag{3.81}$$

where all derivatives are evaluated at the reference configuration. From Fig. 3.8 and also with the aid of Fig. 3.9, we obtain the following *general* results for *any*

symmetric planar suspension (cf. Fig. 9.5)

$$\begin{cases} \dfrac{\partial \gamma_{i1}}{\partial \phi_i^s} = \dfrac{\partial \gamma_{i2}}{\partial \phi_i^s} = -\dfrac{t_i/2 - c_i}{c_i} = -\dfrac{q_i - b_i}{b_i} \\ \dfrac{\partial \gamma_{i1}}{\partial \Delta t_i} = -\dfrac{\partial \gamma_{i2}}{\partial \Delta t_i} = \dfrac{1}{2b_i} \\ \dfrac{\partial \gamma_{i1}}{\partial \phi_i^p} = \dfrac{\partial \gamma_{i2}}{\partial \phi_i^p} = 1 \\ \dfrac{\partial \gamma_{ij}}{\partial z_i^p} = 0 \end{cases} \tag{3.82}$$

The sign convention for the camber variations $\Delta\gamma_{ij}$ is like in Fig. 2.2. Therefore, in Fig. 3.9(b) we have $\Delta\gamma_{i1} < 0$ and $\Delta\gamma_{i2} > 0$.

Equations (3.81) and (3.82) yield

$$\begin{aligned} \Delta\gamma_{i1} &\approx -\left(\frac{q_i - b_i}{b_i}\right)\phi_i^s + \phi_i^p + \frac{1}{2b_i}\Delta t_i \\ \Delta\gamma_{i2} &\approx -\left(\frac{q_i - b_i}{b_i}\right)\phi_i^s + \phi_i^p - \frac{1}{2b_i}\Delta t_i \end{aligned} \tag{3.83}$$

This is quite a remarkable formula. It is simple, yet profound. For instance, the two suspension schemes of Fig. 3.8, which look so different, do have indeed very different values of the first two partial derivatives in (3.82). On the other hand, it should not be forgotten that (3.81) is merely a kinematic relationship. There is no dynamics in it. Therefore, we must be careful not to attempt to extract from it information it cannot provide at all.

Another common mistake is to state, e.g., that a suspension scheme has a typical value of the partial derivative $\partial\gamma_{ij}/\partial\phi_i^s$, without specifying which are the other three internal coordinates. This is clearly meaningless. The value of the partial derivative is very much affected by which other coordinates are kept constant.

3.8.4 Vehicle Internal Coordinates

Three internal coordinates are necessary to monitor the *vehicle* condition with respect to a reference (often static) configuration. A suitable choice may be to take as coordinates the *vehicle body roll angle* ϕ and the front and rear vertical displacements z_1, z_2 of the vehicle centerline (Fig. 3.10). An alternative selection could be the roll angle ϕ and the track variations Δt_1 and Δt_2.

These three coordinates are, of course, independent. Whether they change or not will depend on the vehicle dynamics.

The total roll angle ϕ of the vehicle body is given by

$$\phi = \phi_1^s + \phi_1^p = \phi_2^s + \phi_2^p \tag{3.84}$$

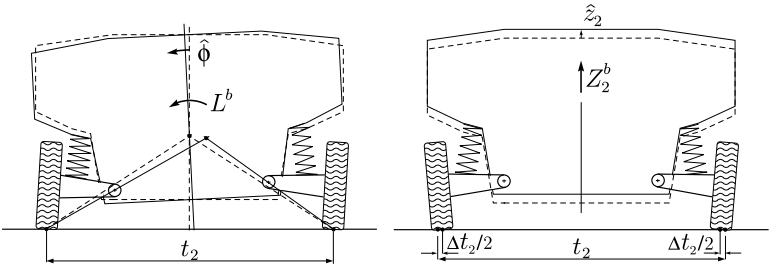

Fig. 3.10 Fictitious loads to obtain roll and vertical stiffnesses

that is, by the roll angle due to the suspension deflection plus the roll angle due to the tire deformation.

Similarly, the front and rear vertical displacements z_1, z_2 of the vehicle centerline are

$$z_1 = z_1^s + z_1^p \quad \text{and} \quad z_2 = z_2^s + z_2^p \tag{3.85}$$

where z_i^s are the vertical displacements of the vehicle centerline due to suspension deflections only and z_i^p are the vertical displacements due to the tire deformations only.

Equations (3.84) and (3.85) precisely relate the eight suspension internal coordinates to the three vehicle internal coordinates.

3.8.5 Roll and Vertical Stiffnesses

The goal of this section is to define the stiffness associated to each internal coordinate.

It is important to realize that the *symmetric* behavior of the two suspensions of the same axle plays a key role here. If, for some reason, the two suspensions were different, then we should also have to consider the cross-coupled stiffnesses.

3.8.5.1 Roll Stiffnesses

To this end, we assume to apply first a (small) pure rolling moment $L^b\mathbf{i}$ to the vehicle body.

As shown in Fig. 3.10, application of a (small) pure rolling moment $L^b\mathbf{i}$ to the vehicle body results in a (small) pure roll rotation $\hat{\phi}\mathbf{i}$ such that[5]

$$L^b = k_\phi \hat{\phi} = (k_{\phi_1} + k_{\phi_2})\hat{\phi} \tag{3.86}$$

[5]The symbol $\hat{\phi}$ (instead of just ϕ) is used to stress that this is not the roll angle under operating conditions.

where k_ϕ is, by definition, the *global roll stiffness* of the vehicle. Moreover, by measuring the corresponding load transfers

$$\Delta Z_1^L t_1 = k_{\phi_1}\hat{\phi} \quad \text{and} \quad \Delta Z_2^L t_2 = k_{\phi_2}\hat{\phi} \tag{3.87}$$

also the front and rear vehicle roll stiffnesses k_{ϕ_1} and k_{ϕ_2} can be obtained. The load transfers ΔZ_1^L and ΔZ_2^L depend on the combined deflections of suspensions and tires. Of course, $z_1 = z_2 = 0$, since they are not affected by L^b.[6]

For further developments, it is necessary to determine how much of $\hat{\phi}$ is due to the suspension springs and how much to the tire vertical deflections. More precisely, it is necessary to single out the *suspension* roll stiffnesses $k_{\phi_1}^s$ and $k_{\phi_2}^s$ from the *tire* roll stiffnesses $k_{\phi_1}^p$ and $k_{\phi_2}^p$.

Under a pure moment $L^b\mathbf{i}$, the tires and the suspensions of the same axle behave like springs in series. Therefore

$$k_{\phi_i} = \frac{k_{\phi_i}^s k_{\phi_i}^p}{k_{\phi_i}^s + k_{\phi_i}^p} \tag{3.88}$$

which means that, for each axle

$$\Delta Z_i^L t_i = k_{\phi_i}\hat{\phi} = k_{\phi_i}^s \hat{\phi}_i^s = k_{\phi_i}^p \hat{\phi}_i^p = L_i^b \quad \text{with } \hat{\phi} = \hat{\phi}_i^s + \hat{\phi}_i^p \tag{3.89}$$

where $\hat{\phi}_i^s$ and $\hat{\phi}_i^p$ are the roll angles due, respectively, to the suspension and tire deflections that the vehicle body undergoes under the action of a pure moment $L^b\mathbf{i}$. Of course, $L_1^b + L_2^b = L^b$.

If p_1 and p_2 are the vertical stiffnesses of a single front and rear tire, respectively (in a first-order analysis, a linear behavior can be safely assumed), the tire roll stiffnesses are given by

$$k_{\phi_i}^p = \frac{p_i t_i^2}{2} \tag{3.90}$$

which means that $L_i^b = \Delta Z_i^L t_i = k_{\phi_i}^p \hat{\phi}_i^p$. Once $k_{\phi_i}^p$ are known, the suspension roll stiffness $k_{\phi_i}^s$ for each axle can be obtained from (3.88).

3.8.5.2 Vertical Stiffnesses

Similarly, to obtain the vertical stiffnesses, small vertical loads Z_i^b are assumed to be applied over each axle.

[6] This is true only if the left and right suspensions have perfectly *symmetric* behavior. For instance, the so-called *contractive suspensions* do not behave the same way and, therefore, a pure rolling moment also yields some vertical displacement.

As shown in Fig. 3.10, application to the vehicle body centerline, exactly over the front axle, of an upward (small) vertical load $Z_1^b\mathbf{k}$ results only in a (small) vertical displacement $\hat{z}_1$ such that

$$Z_1^b = k_{z_1}\hat{z}_1 \tag{3.91}$$

which defines the *global front vertical stiffness* k_{z_1}. Doing the same on the rear axle provides

$$Z_2^b = k_{z_2}\hat{z}_2 \tag{3.92}$$

which defines the rear vertical stiffness k_{z_2}.

Again, to single out the suspension and tire contributions, first observe that the two tires of each axle have a vertical stiffness

$$k_{z_i}^p = 2p_i \tag{3.93}$$

Therefore, the corresponding suspension vertical stiffness $k_{z_i}^s$ can be obtained from

$$k_{z_i} = \frac{k_{z_i}^s k_{z_i}^p}{k_{z_i}^s + k_{z_i}^p} \tag{3.94}$$

which means that for each axle

$$k_{z_i}\hat{z}_i = k_{z_i}^s\hat{z}_i^s = k_{z_i}^p\hat{z}_i^p = Z_i^b \quad \text{with } \hat{z}_i = \hat{z}_i^s + \hat{z}_i^p \tag{3.95}$$

where $\hat{z}_i^s$ and $\hat{z}_i^p$ are the vertical displacements of the centerline due, respectively, to the suspension and tire deflections.

The four numbers $k_{\phi_1}^s$, $k_{z_1}^s$, $k_{\phi_2}^s$ and $k_{z_2}^s$ completely characterize the first-order *elastic* features of the front and rear *suspensions*. Similarly, the four numbers $k_{\phi_1}^p$, $k_{z_1}^p$, $k_{\phi_2}^p$ and $k_{z_2}^p$ completely characterize the first-order *elastic* features of the front and rear *tires*.

3.8.6 Suspension Internal Equilibrium

The forces exerted by the road on each tire are transferred to the vehicle body by the suspensions. It is important to find out how much of these loads goes *through the suspension linkages* and how much *through the springs and dampers*, thus requiring suspension deflections.

As already discussed in Sect. 3.5, each tire is subject to a force $X_{ij}\mathbf{i} + Y_{ij}\mathbf{j} + Z_{ij}\mathbf{k}$, which, for simplicity, is assumed to be applied at the center of the contact patch.

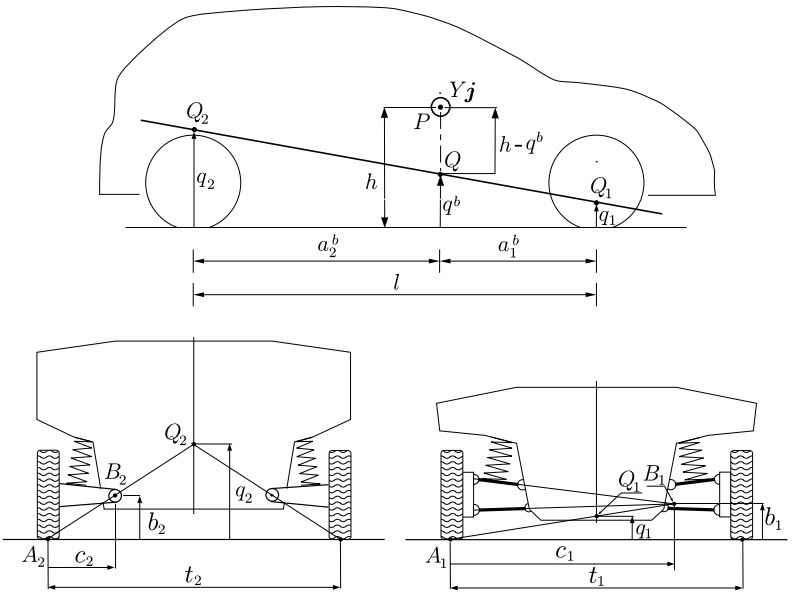

Fig. 3.11 No-roll centers and no-roll axis for a swing arm suspension (*left*) and a double wishbone suspension (*right*)

3.8.7 Effects of a Lateral Force

So far the suspension geometry has played no role (except in Sect. 3.8.3), at least not explicitly. This was done purposely to highlight which vehicle features are not directly related to the suspension kinematics.

The fundamental reason that makes the suspension geometry so relevant is that vehicle bodies are subject to *horizontal forces* (inertia and aerodynamic forces).

Starting from a reference configuration, and according to the equilibrium equation (3.64), let us apply to the vehicle body a *lateral force* $-Y\mathbf{j}$, with $Y = ma_y$. As shown in Fig. 3.11, be this force located at height h above the road and at distances a_1^b and a_2^b from the front and rear axles, respectively. As shown in (3.70), a_1^b and a_2^b differ from a_1 and a_2 whenever the yaw moment $N_Y \neq 0$.

Exactly like in (3.70), in a two-axle vehicle the lateral forces exerted by the road on each axle to balance Y are given by

$$Y_1 = \frac{Ya_2^b}{l} \quad \text{and} \quad Y_2 = \frac{Ya_1^b}{l} \tag{3.96}$$

It is very important to recall that these two forces can be obtained from the global equilibrium equations only. Therefore, they are not affected by the suspensions, by the type of tires, by the amount of grip, etc.

Moreover, like in (3.76),

$$\Delta Z_1 t_1 + \Delta Z_2 t_2 = Yh \tag{3.97}$$

This is all that can be achieved from global equilibrium.

Among the effects of $Y\mathbf{j}$ there is, in general, a (small) *roll angle* ϕ of the vehicle body. This angle ϕ is the sum of ϕ_i^s due to the suspension deformations and ϕ_i^p due to the tire deflections

$$\phi = \phi_1^s + \phi_1^p = \phi_2^s + \phi_2^p \tag{3.98}$$

From the definition of the tire roll stiffnesses (3.90), it immediately arises that

$$\Delta Z_1 t_1 = k_{\phi_1}^p \phi_1^p \quad \text{and} \quad \Delta Z_2 t_2 = k_{\phi_2}^p \phi_2^p \tag{3.99}$$

and hence, from (3.97)

$$Yh = k_{\phi_1}^p \phi_1^p + k_{\phi_2}^p \phi_2^p \tag{3.100}$$

However, to obtain ΔZ_1 and ΔZ_2, it is necessary to look at the suspension kinematics. More precisely, in a first-order analysis, it suffices to consider the roll centers and the roll axis, as discussed in the next section.

3.8.8 No-roll Centers and No-roll Axis

Let us start having a closer look at the suspension linkages. In case of purely transversal independent suspensions, like those shown, e.g., in Fig. 3.11, it is easy to obtain the instantaneous center of rotation B_i of each wheel hub with respect to the vehicle body. Another useful point is the center A_i of each contact patch.

The same procedure can be applied also to the MacPherson strut. The kinematic scheme is shown in Fig. 3.12, while a possible practical design is shown in Fig. 3.13. The MacPherson strut is the most widely used front suspension system, especially in cars of European origin. It is the only suspension to employ a slider, marked by number 2 in Fig. 3.12. Usually, the slider is the damper, which is then part of the suspension linkage. To obtain the instantaneous center of rotation B_i of each wheel hub with respect to the vehicle body it suffices to draw two lines, one along joints 3 and 4, and the other through joint 1 and perpendicular to the slider (not to the steering axis, which goes from joint 1 and 3, as also shown in Fig. 3.12).

In all suspension schemes, the intersection of lines connecting A_i and B_i on both side of the same axle provides, for each axle, the so-called *roll center* Q_i (Figs. 3.11 and 3.12). The signed distance of Q_i from the road is named q_i in Fig. 3.11. A roll center below the road level would have $q_i < 0$.

Therefore, a two-axle vehicle has two roll centers Q_1 and Q_2. The unique straight line connecting Q_1 and Q_2 is usually called the *roll axis* (Fig. 3.11).

Some comments are in order here:

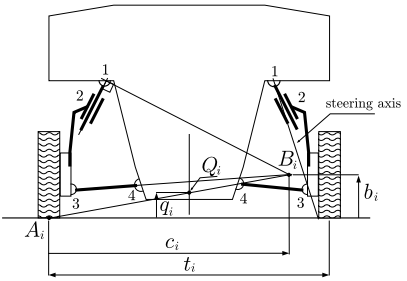

Fig. 3.12 No-roll center for a MacPherson strut

Fig. 3.13 Example of MacPherson strut [3]

- the procedure just described to obtain the roll centers Q_i is not ambiguous, provided the motion of the wheel hub with respect to the vehicle body is planar and has one degree of freedom;
- points A_i are well defined and are not affected by the tire vertical compliance;
- a three-axle vehicle has three points Q_i. Therefore, in general there is *not* a straight line connecting Q_1, Q_2 and Q_3. How to define, if possible, something like a roll axis for a three-axle vehicle will be addressed in Sect. 3.13.

But what is the motivation for having defined the roll centers, and afterwards the roll axis?

Figures 3.14 and 3.15 show how a lateral force Y_i, if applied at Q_i, is transferred to the ground *by the suspension linkage*, with no intervention of the springs. Therefore, a force applied at the roll center *does not produce any suspension roll*. This is the key feature of the roll centers Q_i, which should be better renamed *no-roll centers*.

The roll axis is useful because the two lateral forces Y_1 and Y_2 must be like in (3.96) for the global equilibrium to be fulfilled. A lateral force Y applied at any point of the line connecting Q_1 and Q_2 is indeed equivalent to a force Y_1 applied

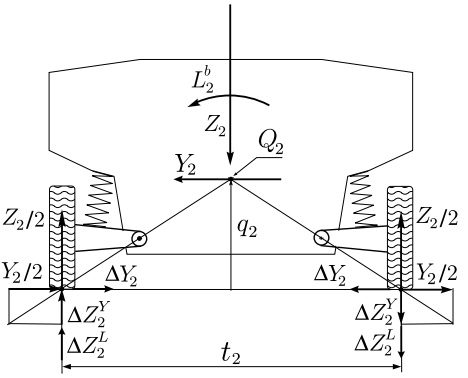

Fig. 3.14 Suspension internal force distribution

at Q_1 and a force Y_2 applied at Q_2 which obey (3.96). This is the motivation for defining the roll axis. Again, a better name would be *no-roll axis*.

Summing up, *application of a force to the vehicle body at any point of the roll axis does not produce suspension roll*. More precisely, a force (of any direction) applied to the vehicle body and whose line of action goes through the roll axis may affect the vehicle roll angle, but only because of tire deflections, with no contribution from the suspensions. In addition, there may be variations of z_1 and z_2.

3.8.9 Forces at the No-roll Centers

Let us go back to a purely lateral force $-Y\mathbf{j}$ applied at P (not necessarily the center of mass G), as shown in Fig. 3.11. Since the global equilibrium dictates in (3.96) the values of Y_1 and Y_2, we have to decompose the lateral force $-Y\mathbf{j}$ into a force $-Y_1\mathbf{j}$ applied at the front no-roll center Q_1 and a force $-Y_2\mathbf{j}$ applied at the other no-roll center Q_2, plus a suitable couple.

There is a simple two-step procedure to obtain this result. First, consider that $-Y\mathbf{j}$ at P is equivalent to the same force $-Y\mathbf{j}$ applied at point Q, on the no-roll axis

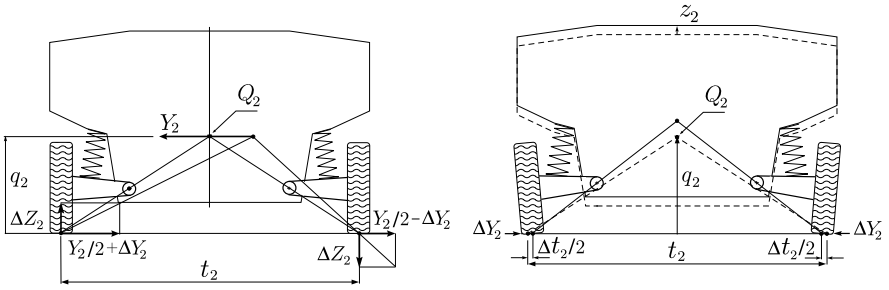

Fig. 3.15 Load transfer without suspension roll, but with vehicle raising

right below P, plus a pure (horizontal) roll moment

$$L^b\mathbf{i} = Y\big(h - q^b\big)\mathbf{i}, \quad \text{where } q^b = \frac{a_2^b q_1 + a_1^b q_2}{a_1^b + a_2^b} \tag{3.101}$$

Then, it is obvious that the force $-Y\mathbf{j}$ applied at Q is exactly equivalent to a force $-Y_1\mathbf{j}$ applied at the front no-roll center Q_1 and a force $-Y_2\mathbf{j}$ applied at the other no-roll center Q_2. Indeed

$$Yq^b = Y_1 q_1 + Y_2 q_2 \tag{3.102}$$

and $Y_1 a_1^b = Y_2 a_2^b$.

This way we have decomposed the lateral force into two forces at the two no-roll centers, each one of the magnitude imposed by the equilibrium equations, plus a horizontal moment. *It is important to note that it would be wrong to take the shortest distance from P to the roll axis to compute the moment. It is precisely the vertical distance $(h - q^b)$ that has to be taken as the force moment arm.*

Summing up, a lateral force $-Y\mathbf{j}$ at P is totally equivalent to a lateral force $-Y_1\mathbf{j}$ at Q_1 and another lateral force $-Y_2\mathbf{j}$ at Q_2, plus the horizontal moment $Y(h - q^b)\mathbf{i}$ (Fig. 3.11) applied to the vehicle body.

Figures 3.14 and 3.15 shows how each force Y_i at Q_i is transferred to the ground by the suspension linkage, *without producing any suspension roll*. This is the key feature of the roll center Q_i. Quite remarkably, this is true whichever the direction of the force there applied, and hence it is correct to speak of a (no-)roll center point (at first, Fig. 3.15 might suggest the idea of a roll center height q_i).

The moment $Y(h - q^b)$ is the sole responsible of *suspension roll*. More precisely

$$Y\big(h - q^b\big) = k_{\phi_1}^s \phi_1^s + k_{\phi_2}^s \phi_2^s = \Delta Z_1^L t_1 + \Delta Z_2^L t_2 \tag{3.103}$$

exactly like in (3.89).

The total lateral load transfer ΔZ_i on each axle is therefore given by

$$\Delta Z_i t_i = \big(\Delta Z_i^Y + \Delta Z_i^L\big) t_i = Y_i q_i + k_{\phi_i}^s \phi_i^s = k_{\phi_i}^p \phi_i^p \tag{3.104}$$

that is by the sum of the part due to the suspension linkage and the part due to the suspension springs (Eqs. (3.105) and (3.89)).

3.8.10 Suspension Jacking

However, no suspension roll does not mean no other effects at all. Indeed, there are always lateral load transfers (Fig. 3.15)

$$\Delta Z_i^Y t_i = Y_i q_i \tag{3.105}$$

and hence also some rolling of the vehicle body related to the tire vertical deflections.

Moreover, since the lateral forces exerted by the road on the left and right tires are not equal to each other (they will be equal to $Y_i/2 \pm \Delta Y_i$, where ΔY_i depends on the tire behavior), there is also a small *rising* z_i^s of the vehicle body (Fig. 3.15)

$$z_i^s = \Delta Y_i \frac{2b_i}{k_{z_i}^s c_i} = \Delta Y_i \frac{4q_i}{k_{z_i}^s t_i} \tag{3.106}$$

associated with a small *track variation* Δt_i

$$\Delta t_i = -\frac{2b_i}{c_i} z_i^s = -\frac{4q_i}{t_i} z_i^s = -\left(\frac{4q_i}{t_i}\right)^2 \frac{\Delta Y_i}{k_{z_i}^s} \tag{3.107}$$

and *suspension jacking*. The stiffness of the tires does not appear in (3.106) and (3.107).

3.8.11 Roll Angle and Lateral Load Transfers

All relevant equations for the first-order suspension analysis have been obtained. Solving them provides the relationship between Y and the total roll angle ϕ and, more importantly, the relationship between the front and rear load transfers ΔZ_1 and ΔZ_2.

The main equations are gathered here to have them available at a glance:

$$Y = Y_1 + Y_2 \tag{3.64′}$$

$$Yh = \Delta Z_1 t_1 + \Delta Z_2 t_2 \tag{3.76′}$$

$$Y_1 = \frac{Ya_2}{l} + \frac{N_Y}{l} = \frac{Ya_2^b}{l}, \qquad Y_2 = \frac{Ya_1}{l} - \frac{N_Y}{l} = \frac{Ya_1^b}{l} \tag{3.70′}$$

$$\phi = \phi_1^s + \phi_1^p, \qquad \phi = \phi_2^s + \phi_2^p \tag{3.98′}$$

$$\Delta Z_1 t_1 = k_{\phi_1}^p \phi_1^p, \qquad \Delta Z_2 t_2 = k_{\phi_2}^p \phi_2^p \tag{3.99′}$$

$$\Delta Z_1 t_1 = Y_1 q_1 + k_{\phi_1}^s \phi_1^s, \qquad \Delta Z_2 t_2 = Y_2 q_2 + k_{\phi_2}^s \phi_2^s \tag{3.104′}$$

$$q^b = \frac{a_2 q_1 + a_1 q_2}{l} + \frac{N_Y}{Y}\left(\frac{q_2 - q_1}{l}\right) = \frac{a_2^b q_1 + a_1^b q_2}{l} \simeq \frac{a_2 q_1 + a_1 q_2}{l} \tag{3.101′}$$

$$Y\left(h - q^b\right) = k_{\phi_1}^s \phi_1^s + k_{\phi_2}^s \phi_2^s \tag{3.103′}$$

$$Yh = k_{\phi_1}^p \phi_1^p + k_{\phi_2}^p \phi_2^p \tag{3.100′}$$

These equations are really of great relevance in vehicle dynamics.

The front and rear roll angles due to the suspension and tire deflections can be obtained solving the following system of equations

$$\begin{aligned} \phi &= \phi_1^s + \phi_1^p = \phi_2^s + \phi_2^p \\ Y\left(h - q^b\right) &= k_{\phi_1}^s \phi_1^s + k_{\phi_2}^s \phi_2^s \\ Y_1 q_1 + k_{\phi_1}^s \phi_1^s &= k_{\phi_1}^p \phi_1^p \\ Y_2 q_2 + k_{\phi_2}^s \phi_2^s &= k_{\phi_2}^p \phi_2^p \end{aligned} \tag{3.108}$$

The expressions are given here for the roll angles due to tire deflections

$$\begin{aligned} \phi_1^p &= \frac{1}{k_{\phi_1}^p} \frac{k_{\phi_1} k_{\phi_2}}{k_\phi} \left[\frac{Y(h - q^b)}{k_{\phi_2}} + \frac{Y_1 q_1}{k_{\phi_1}^s} + \frac{Y_1 q_1}{k_{\phi_2}^s} + \frac{Y_1 q_1 + Y_2 q_2}{k_{\phi_2}^p} \right] \\ \phi_2^p &= \frac{1}{k_{\phi_2}^p} \frac{k_{\phi_1} k_{\phi_2}}{k_\phi} \left[\frac{Y(h - q^b)}{k_{\phi_1}} + \frac{Y_2 q_2}{k_{\phi_1}^s} + \frac{Y_2 q_2}{k_{\phi_2}^s} + \frac{Y_1 q_1 + Y_2 q_2}{k_{\phi_1}^p} \right] \end{aligned} \tag{3.109}$$

and for the roll angles due to suspension (spring) deflections

$$\begin{aligned} \phi_1^s &= \frac{1}{k_{\phi_1}^s} \frac{k_{\phi_1} k_{\phi_2}}{k_\phi} \left[\frac{Y(h - q^b)}{k_{\phi_2}} + \frac{Y_1 q_1}{k_{\phi_1}^p} - \frac{Y_2 q_2}{k_{\phi_2}^p} \right] \\ \phi_2^s &= \frac{1}{k_{\phi_2}^s} \frac{k_{\phi_1} k_{\phi_2}}{k_\phi} \left[\frac{Y(h - q^b)}{k_{\phi_1}} + \frac{Y_2 q_2}{k_{\phi_1}^p} - \frac{Y_1 q_1}{k_{\phi_1}^p} \right] \end{aligned} \tag{3.110}$$

where

$$k_\phi = k_{\phi_1} + k_{\phi_2} = \frac{k_{\phi_1}^s k_{\phi_1}^p}{k_{\phi_1}^s + k_{\phi_1}^p} + \frac{k_{\phi_2}^s k_{\phi_2}^p}{k_{\phi_2}^s + k_{\phi_2}^p} \tag{3.111}$$

is the total roll stiffness, like in (3.86). Equations (3.109) and (3.110) show how the tire and suspension stiffnesses interact with each other and with the first-order suspension geometry (i.e., the no-roll axis position).

According to them, the total roll angle ϕ produced by a lateral force $Y\mathbf{j}$ applied at P (Fig. 3.11) is given by

$$k_\phi \phi = Y\left(h - q^b\right) + Y_1 q_1 \frac{k_{\phi_1}}{k_{\phi_1}^p} + Y_2 q_2 \frac{k_{\phi_2}}{k_{\phi_2}^p} \tag{3.112}$$

If q^b is almost constant (i.e., $q_1 \approx q_2$), then N_Y has little effect on the roll angle ϕ (see also (3.117)). However, N_Y affects quite strongly the lateral load transfers, because it redistributes the values of the lateral forces Y_1 and Y_2.

3.8.12 Explicit Expressions of Lateral Load Transfers

Lateral load transfers ΔZ_i are among the most influential quantities in vehicle dynamics. They can be obtained, e.g., combining (3.99) and (3.109)

$$\begin{aligned}
\Delta Z_1 t_1 &= \frac{k_{\phi_1} k_{\phi_2}}{k_\phi} \left[\frac{Y(h-q^b)}{k_{\phi_2}} + \frac{Y_1 q_1}{k^s_{\phi_1}} + \frac{Y_1 q_1}{k^s_{\phi_2}} + \frac{Y_1 q_1 + Y_2 q_2}{k^p_{\phi_2}} \right] \\
\Delta Z_2 t_2 &= \frac{k_{\phi_1} k_{\phi_2}}{k_\phi} \left[\frac{Y(h-q^b)}{k_{\phi_1}} + \frac{Y_2 q_2}{k^s_{\phi_1}} + \frac{Y_2 q_2}{k^s_{\phi_2}} + \frac{Y_1 q_1 + Y_2 q_2}{k^p_{\phi_1}} \right]
\end{aligned} \tag{3.113}$$

which can also be recast as

$$\begin{aligned}
\Delta Z_1 &= \frac{1}{t_1} \left[\frac{k_{\phi_1}}{k_\phi} Y\left(h-q^b\right) + Y_1 q_1 + \frac{k_{\phi_1} k_{\phi_2}}{k_\phi} \left(\frac{Y_2 q_2}{k^p_{\phi_2}} - \frac{Y_1 q_1}{k^p_{\phi_1}} \right) \right] \\
\Delta Z_2 &= \frac{1}{t_2} \left[\frac{k_{\phi_2}}{k_\phi} Y\left(h-q^b\right) + Y_2 q_2 + \frac{k_{\phi_1} k_{\phi_2}}{k_\phi} \left(\frac{Y_1 q_1}{k^p_{\phi_1}} - \frac{Y_2 q_2}{k^p_{\phi_2}} \right) \right]
\end{aligned} \tag{3.114}$$

It is worth noting that, in a first-order vehicle analysis, the lateral load transfers are linear functions of Y and N_Y, and hence of Y_1 and Y_2, that is

$$\begin{aligned}
\Delta Z_1 &= \xi_{11} Y_1 + \xi_{12} Y_2 \\
\Delta Z_2 &= \xi_{21} Y_1 + \xi_{22} Y_2
\end{aligned} \tag{3.115}$$

In these equations the interplay between stiffnesses and first-order suspension geometry is quite tricky. However, the simple Eq. (3.76) must always hold true.

Also interesting is to observe that, in a first-order analysis, the lateral load transfers ΔZ_i do not depend on the roll angle ϕ, although roll motion had to be taken into account to obtain ΔZ_i.

Since we are neglecting the inertial effects of roll motion, the lateral forces are simply given by

$$\begin{aligned}
Y &= m a_y = Y_1 + Y_2 \\
Y_1 &= \frac{m a_y a_2}{l} + \frac{J_z \dot{r} - (\Delta X_1 t_1 + \Delta X_2 t_2)}{l} = \frac{m a_y a_2}{l} + \frac{N_Y}{l} \\
Y_2 &= \frac{m a_y a_1}{l} - \frac{J_z \dot{r} - (\Delta X_1 t_1 + \Delta X_2 t_2)}{l} = \frac{m a_y a_1}{l} - \frac{N_Y}{l}
\end{aligned} \tag{3.116}$$

Therefore, ultimately, the lateral load transfers ΔZ_i are (linear) functions of the lateral acceleration a_y, and, just a little, of the angular acceleration $\dot{r}$. Moreover, in vehicle with limited slip differential or ESP, the contribution due to ΔX_i can be rather relevant.

3.8.13 Lateral Load Transfers with Rigid Tires

If the tire vertical deflections are neglected (i.e., $k_{\phi_i}^p \to \infty$ and $k_{\phi_i} \to k_{\phi_i}^s$), all expressions simplify considerably. For instance, Eq. (3.112) becomes

$$k_\phi \phi = Y\left(h - q^b\right) \tag{3.117}$$

This is a most classical result. Similarly, a much simpler expression is obtained for the lateral load transfers (3.104) or (3.113)

$$\Delta Z_i t_i = \frac{k_{\phi_i}}{k_\phi} Y\left(h - q^b\right) + Y_i q_i = k_{\phi_i} \phi + Y_i q_i \tag{3.118}$$

However, particularly in Formula cars, it may be not so safe to assume the tires to be perfectly rigid in the vertical direction (they are not at all!). Inclusion of tire compliance should be done according to (3.113), not by simply softening the suspension stiffness. Indeed, loosely speaking the tires counteract the rolling moment Yh, whereas the suspension springs have to deal with $Y(h - q^b)$. This point should not be underestimated.

3.9 Dependent Suspensions

In a dependent suspension the two wheels of the same axle are rigidly connected together. Nowadays very few cars are equipped with dependent suspensions. Nonetheless, it is still a type of suspension which is widely employed in commercial vehicles or the like, that is on vehicles that need to carry large loads compared to the vehicle weight.

Perhaps, the most classical lateral location linkage for dependent suspensions is the *Panhard rod* (also called Panhard bar or track bar), schematically shown in Fig. 3.16. A rendering of a complete dependent suspension with Panhard rod is shown in Fig. 3.17. The Panhard rod is a rigid bar running sideways in the same plane as the axle, connecting one end of the axle to the car body on the opposite side of the vehicle. The bar is attached at both ends with pivots that allow it to swivel upwards and downwards only, so that the axle can move in the vertical plane only. However, to effectively locate the axle longitudinally, it is usually used in conjunction with trailing arms. Obviously, the rigid axle has two degrees of freedom with respect to the vehicle body.

Most of the analysis developed for independent suspensions is applicable to dependent suspensions as well. For instance, the suspension internal coordinates listed at p. 69 are still meaningful (except track variation, which is obviously zero in the present case). Vertical stiffness and roll stiffness are also well defined. The only thing that needs to be addressed is the determination of the no-roll center Q_i.

Following the method explained in Sect. 3.8.8, we apply a lateral force Y_i, like in Fig. 3.18 (top). This force can be decomposed into a force H_i, which is counteracted by the Panhard rod, and a vertical force V_i, which must be counteracted

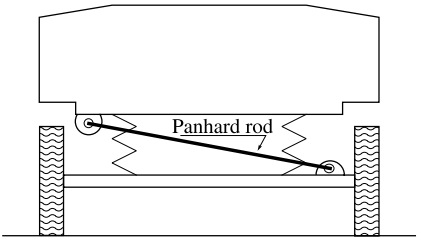

Fig. 3.16 Planar scheme of a dependent suspension with Panhard rod

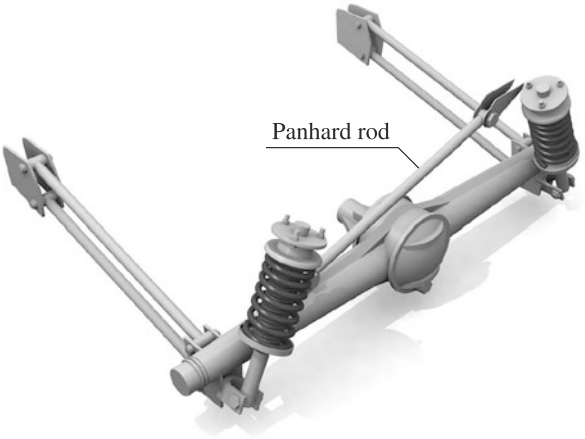

Fig. 3.17 Dependent suspension with Panhard rod [3]

by the springs, and whose line of action is located at a distance s_i from the vehicle centerline (Fig. 3.18 (bottom)). It is easy to obtain

$$\begin{aligned} H_i &= \frac{Y_i}{\cos \chi_i} \\ V_i &= Y_i \tan \chi_i \\ s_i &= \frac{h - q_i}{\tan \chi_i} \quad \text{and hence} \\ L_i^b &= V_i s_i = Y_i (h - q_i) \end{aligned} \tag{3.119}$$

where χ_i is the inclination of the Panhard rod. The lower χ_i, the better.

The moment $L_i^b = V_i s_i = Y_i (h - q_i)$ is the sole responsible of the vehicle body roll, as shown in Fig. 3.19 (top), and the force V_i is the only responsible for the body vertical displacement, as shown in Fig. 3.19 (bottom).

To have zero suspension roll we need zero moment, and this is possible if and only if $h = q_i$. Therefore, the *no-roll center* is point Q_i in Fig. 3.18.

In any case, we have a small body vertical displacement, either upward or downward, depending if we are turning left or right. The vertical displacement would be zero if and only if $\chi_i = 0$, which is clearly impossible in practice. Therefore,

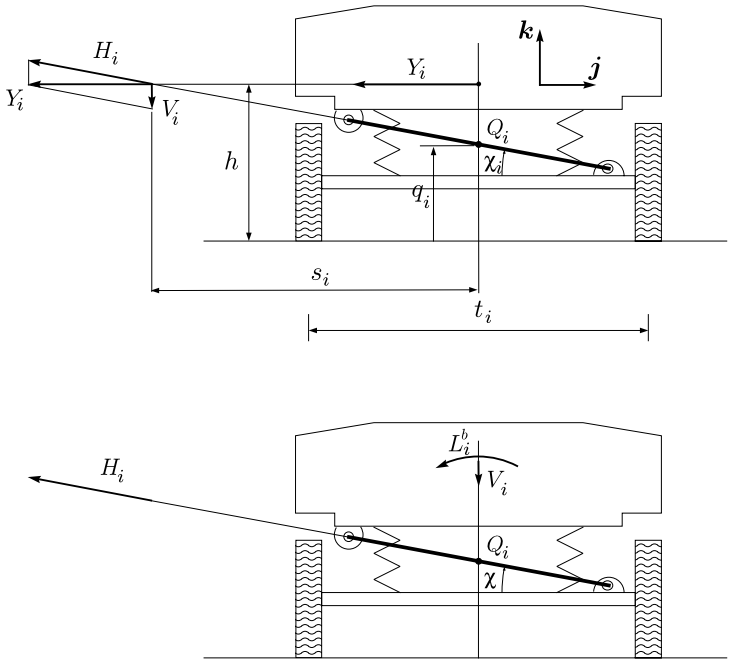

Fig. 3.18 Force distribution and no-roll center Q_i for a dependent suspension with Panhard rod

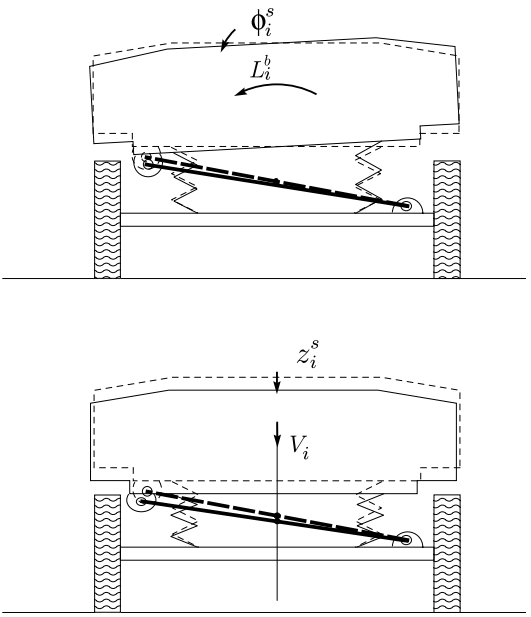

Fig. 3.19 Roll and vertical displacement of a dependent suspension with Panhard rod

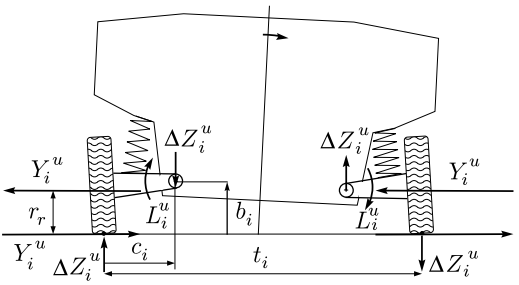

Fig. 3.20 Load distribution due to the inertia of the unsprung mass

the Panhard rod is a simple linkage, with the disadvantage of a certain degree of asymmetry.

Of course, dependent suspensions do not exhibit suspension jacking, nor camber variations.

3.10 Sprung and Unsprung Masses

In a vehicle like an automobile or a motorcycle, it is useful to distinguish between sprung mass and unsprung mass.

The sprung mass m_s is the portion of the vehicle's total mass that is supported *above* the suspension, thus including the body, frame, internal components, passengers and cargo. On the other hand, wheels, wheel bearings, brake rotors, calipers go into the unsprung mass m_u since they are not above the suspension. Of course, the total mass $m = m_s + m_u$.

The sprung mass is usually much bigger than the unsprung mass. Typically, $m_s/m_n = 5$–10. Therefore, it is often not a bad approximation to set $m \simeq m_s$, as it has been done in Sect. 3.8 to reduce the complexity of the model. However, a more accurate analysis is not much more difficult.

The load distribution due to the inertial effects of m_u is schematically shown in Fig. 3.20. Basically, a centrifugal force Y_i^u acts on each wheel. The equilibrium of the whole system and of each suspension requires

$$\begin{aligned} 2Y_i^u r_r &= \Delta Z_i^u t_i \\ Y_i^u r_r - \Delta Z_i^u c_i &= L_i^u \end{aligned} \tag{3.120}$$

which yield

$$Y_i^u r_r \left(1 - \frac{c_i}{t_i}\right) = L_i^u \tag{3.121}$$

The net effect is a small load transfer ΔZ_i^u and a very small suspension roll angle, particularly if $c_i \simeq t_i$ like in a double wishbone suspension, as shown in Fig. 3.8.

In practical terms, in (3.113) it suffices to set $Y = m_s a_y$, to modify Y_i accordingly, and to include an additional term $m_{u_i} a_y r_r$ for each axle, where m_{u_i} is the corresponding unsprung mass.

3.11 Vehicle Model for Handling and Performance

After quite a bit of work, we are now (almost) ready to set up our first-order vehicle model for handling and performance analyses. Essentially, setting up a model means collecting all relevant equations, their order being not important. Of course, a two-axle vehicle is considered.

3.11.1 Equilibrium Equations

We have three in-plane *equilibrium equations* (3.64)

$$\begin{aligned} ma_x &= m(\dot{u} - vr) = X = X_1 + X_2 - \frac{1}{2}\rho S C_x u^2 \\ ma_y &= m(\dot{v} + ur) = Y = Y_1 + Y_2 \\ J_z \dot{r} &= N = Y_1 a_1 - Y_2 a_2 + \Delta X_1 t_1 + \Delta X_2 t_2 \end{aligned} \tag{3.64′}$$

where the tangential (grip) forces are defined in (3.59) with respect to the vehicle frame (Fig. 3.7)

$$\begin{aligned} X_1 &= X_{11} + X_{12}, & X_2 &= X_{21} + X_{22} \\ Y_1 &= Y_{11} + Y_{12}, & Y_2 &= Y_{21} + Y_{22} \\ \Delta X_1 &= \frac{X_{12} - X_{11}}{2}, & \Delta X_2 &= \frac{X_{22} - X_{21}}{2} \\ \Delta Y_1 &= \frac{Y_{12} - Y_{11}}{2}, & \Delta Y_2 &= \frac{Y_{22} - Y_{21}}{2} \end{aligned} \tag{3.59′}$$

and in (3.58) to exploit the contribution of each single tire

$$\begin{aligned} \mathbf{F}_{t_{ij}} &= X_{ij}\mathbf{i} + Y_{ij}\mathbf{j} \\ \text{where} \quad X_{ij} &= F_{x_{ij}} \cos(\delta_{ij}) - F_{y_{ij}} \sin(\delta_{ij}) \\ Y_{ij} &= F_{x_{ij}} \sin(\delta_{ij}) + F_{y_{ij}} \cos(\delta_{ij}) \end{aligned} \tag{3.58′}$$

We also have other four out-of-plane equilibrium equations (3.79), which link the vertical loads acting on each tire to the vehicle motion

$$
\begin{aligned}
Z_{11} = F_{z_{11}} &= \frac{1}{2}\left[\frac{mga_2}{l} - \frac{1}{2}\rho_a S_a C_{z1} u^2 - \frac{ma_x h - J_{zx} r^2}{l}\right] - \Delta Z_1 \\
Z_{12} = F_{z_{12}} &= \frac{1}{2}\left[\frac{mga_2}{l} - \frac{1}{2}\rho_a S_a C_{z1} u^2 - \frac{ma_x h - J_{zx} r^2}{l}\right] + \Delta Z_1 \\
Z_{21} = F_{z_{21}} &= \frac{1}{2}\left[\frac{mga_1}{l} - \frac{1}{2}\rho_a S_a C_{z2} u^2 + \frac{ma_x h - J_{zx} r^2}{l}\right] - \Delta Z_2 \\
Z_{22} = F_{z_{22}} &= \frac{1}{2}\left[\frac{mga_1}{l} - \frac{1}{2}\rho_a S_a C_{z2} u^2 + \frac{ma_x h - J_{zx} r^2}{l}\right] + \Delta Z_2
\end{aligned}
\tag{3.79′}
$$

the lateral load transfers being as in (3.114)

$$
\begin{aligned}
\Delta Z_1 &= \frac{1}{t_1}\left[\frac{k_{\phi_1}}{k_\phi} Y\left(h - q^b\right) + Y_1 q_1 + \frac{k_{\phi_1} k_{\phi_2}}{k_\phi}\left(\frac{Y_2 q_2}{k^p_{\phi_2}} - \frac{Y_1 q_1}{k^p_{\phi_1}}\right)\right] \\
\Delta Z_2 &= \frac{1}{t_2}\left[\frac{k_{\phi_2}}{k_\phi} Y\left(h - q^b\right) + Y_2 q_2 + \frac{k_{\phi_1} k_{\phi_2}}{k_\phi}\left(\frac{Y_1 q_1}{k^p_{\phi_1}} - \frac{Y_2 q_2}{k^p_{\phi_2}}\right)\right]
\end{aligned}
\tag{3.114′}
$$

where

$$
q^b = \frac{a_2^b q_1 + a_1^b q_2}{a_1^b + a_2^b} \tag{3.101′}
$$

with a_1^b and a_2^b defined in (3.70). Of course, we also have the following inequalities

$$
\sqrt{X_i^2 + Y_i^2} \le \mu_p Z_i \quad \text{and} \quad Z_i \ge 0 \tag{3.122}
$$

Other six internal equilibrium equations involve the two roll angles due to the pneumatic tires

$$
\begin{aligned}
\phi_1^p &= \frac{1}{k^p_{\phi_1}} \frac{k_{\phi_1} k_{\phi_2}}{k_\phi}\left[\frac{Y(h - q^b)}{k_{\phi_2}} + \frac{Y_1 q_1}{k^s_{\phi_1}} + \frac{Y_1 q_1}{k^s_{\phi_2}} + \frac{Y_1 q_1 + Y_2 q_2}{k^p_{\phi_2}}\right] \\
\phi_2^p &= \frac{1}{k^p_{\phi_2}} \frac{k_{\phi_1} k_{\phi_2}}{k_\phi}\left[\frac{Y(h - q^b)}{k_{\phi_1}} + \frac{Y_2 q_2}{k^s_{\phi_1}} + \frac{Y_2 q_2}{k^s_{\phi_2}} + \frac{Y_1 q_1 + Y_2 q_2}{k^p_{\phi_1}}\right]
\end{aligned}
\tag{3.109′}
$$

the two roll angles due to the suspensions

$$\begin{aligned}\phi_1^s &= \frac{1}{k_{\phi_1}^s}\frac{k_{\phi_1}k_{\phi_2}}{k_\phi}\left[\frac{Y(h-q^b)}{k_{\phi_2}} + \frac{Y_1 q_1}{k_{\phi_1}^p} - \frac{Y_2 q_2}{k_{\phi_2}^p}\right] \\ \phi_2^s &= \frac{1}{k_{\phi_2}^s}\frac{k_{\phi_1}k_{\phi_2}}{k_\phi}\left[\frac{Y(h-q^b)}{k_{\phi_1}} + \frac{Y_2 q_2}{k_{\phi_1}^p} - \frac{Y_1 q_1}{k_{\phi_1}^p}\right]\end{aligned} \tag{3.110′}$$

and the two track variations

$$\Delta t_i = -\left(\frac{4q_i}{t_i}\right)^2 \frac{\Delta Y_i}{k_{z_i}^s} \tag{3.107′}$$

3.11.2 Constitutive (Tire) Equations

Each tire behaves according to its *constitutive equations* (2.72). Both the longitudinal force $F_{x_{ij}}$ and the lateral force $F_{y_{ij}}$ depend on the vertical load $F_{z_{ij}}$, the camber angle γ_{ij}, the translational slips $\sigma_{x_{ij}}$ and $\sigma_{y_{ij}}$, and the spin slip φ_{ij}

$$\begin{aligned}F_{x_{ij}} &= F_{x_{ij}}(F_{z_{ij}}, \gamma_{ij}, \sigma_{x_{ij}}, \sigma_{y_{ij}}, \varphi_{ij}) \\ F_{y_{ij}} &= F_{y_{ij}}(F_{z_{ij}}, \gamma_{ij}, \sigma_{x_{ij}}, \sigma_{y_{ij}}, \varphi_{ij})\end{aligned} \tag{2.72′}$$

3.11.3 Congruence (Kinematic) Equations

Congruence equations are, by definition, a link between kinematic quantities. In a vehicle they relate the vehicle motion to the tire kinematics (translational slips, spin slips, camber angles, steering angles).

The longitudinal and lateral slips were defined for a single wheel with tire in (2.55) and (2.56), respectively. For the four wheels of a vehicle they were given in (3.45) and (3.46):

- longitudinal slips:

$$\begin{aligned}\sigma_{x_{11}} &= \frac{[(u - rt_1/2)\cos(\delta_{11}) + (v + ra_1)\sin(\delta_{11})] - \omega_{11}r_1}{\omega_{11}r_1} \\ \sigma_{x_{12}} &= \frac{[(u + rt_1/2)\cos(\delta_{12}) + (v + ra_1)\sin(\delta_{12})] - \omega_{12}r_1}{\omega_{12}r_1} \\ \sigma_{x_{21}} &= \frac{[(u - rt_2/2)\cos(\delta_{21}) - (v - ra_2)\sin(\delta_{21})] - \omega_{21}r_2}{\omega_{21}r_2} \\ \sigma_{x_{22}} &= \frac{[(u + rt_2/2)\cos(\delta_{22}) - (v - ra_2)\sin(\delta_{22})] - \omega_{22}r_2}{\omega_{22}r_2}\end{aligned} \tag{3.45′}$$

- lateral slips:

$$\begin{aligned}
\sigma_{y_{11}} &= \frac{(v + ra_1)\cos(\delta_{11}) - (u - rt_1/2)\sin(\delta_{11})}{\omega_{11} r_1} \\
\sigma_{y_{12}} &= \frac{(v + ra_1)\cos(\delta_{12}) - (u + rt_1/2)\sin(\delta_{12})}{\omega_{12} r_1} \\
\sigma_{y_{21}} &= \frac{(v - ra_2)\cos(\delta_{21}) - (u - rt_2/2)\sin(\delta_{21})}{\omega_{21} r_2} \\
\sigma_{y_{22}} &= \frac{(v - ra_2)\cos(\delta_{22}) - (u - rt_2/2)\sin(\delta_{22})}{\omega_{22} r_2}
\end{aligned} \tag{3.46′}$$

According to (2.73), the rolling radii r_i should depend on the vertical load and the camber angle. However, in a car such dependence is so weak that they can be safely assumed as constant.

Suspension roll angles ϕ_i^s may affect the steering angles δ_{ij} of the wheels. It is the so-called *roll steer*. This feature is very important in vehicle handling and can be modelled by means of another set of kinematic equations

$$\begin{aligned}
\delta_{ij} &= \delta_{ij}\left(\delta_v, \phi_i^s\right) \\
&\simeq \delta_{ij}^0 + \delta_v \tau_{ij} + \Upsilon_{ij} \phi_i^s
\end{aligned} \tag{3.123}$$

where $\delta_{ij}^0 = \delta_{ij}(0, 0)$ is the toe-in (or toe-out) contribution, δ_v is the steering wheel rotation (as imposed by the driver) and τ_{ij} is the gear ratio of the whole steering system for each wheel. Most cars have $\tau_{2j} = 0$, that is no direct steering of the rear wheels. The roll steer contribution $\Upsilon_{ij}\phi_i^s$ can be given as linear functions of the suspension roll angles ϕ_i^s.

Ultimately, we have that

$$\begin{aligned}
\sigma_{x_{ij}} &= \sigma_{x_{ij}}\left(v, r, u, \delta_v, \phi_i^s, \omega_{ij}\right) \\
\sigma_{y_{ij}} &= \sigma_{y_{ij}}\left(v, r, u, \delta_v, \phi_i^s, \omega_{ij}\right)
\end{aligned} \tag{3.124}$$

The spin slip was defined for a single wheel with tire in (2.57). For the four wheels of a car they are

$$\varphi_{ij} = -\frac{r + \dot{\delta}_{ij} + \omega_{ij} \sin\gamma_{ij}(1 - \varepsilon_i)}{\omega_{ij} r_i} \tag{3.47′}$$

However, even in a Formula 1 car, the yaw rate r can be as high as 1 rad/s, that is 60°/s, while $\dot{\delta}_{ij}$ is about 4 times smaller. The bigger contribution comes from the last term, which ranges between 1 and 5 rad/s. Therefore,

$$\varphi_{ij} \simeq -\frac{\sin\gamma_{ij}(1 - \varepsilon_i)}{r_i} \tag{3.125}$$

which shows that, approximately, the spin slips affect the tire behavior like the camber angle. The camber reduction factor ε_i can be assumed as constant (cf. (2.73)).

Very important is the kinematic link between the suspension internal coordinates and the camber variations

$$\begin{aligned} \Delta\gamma_{i1} &\approx -\left(\frac{q_i - b_i}{b_i}\right)\phi_i^s + \phi_i^p + \frac{1}{2b_i}\Delta t_i \\ \Delta\gamma_{i2} &\approx -\left(\frac{q_i - b_i}{b_i}\right)\phi_i^s + \phi_i^p - \frac{1}{2b_i}\Delta t_i \end{aligned} \tag{3.83$'$}$$

Different suspensions with the same no-roll center behave differently.

3.11.4 Principles of Any Differential Mechanism

The non-driven wheels of a car can spin independently since there is no connection between them. But the driven wheels must be linked together so that a single engine and transmission can turn both wheels. The mechanism that links the two driven wheels of the same axle is called the *differential*. Basically, it is a device that splits the engine power two ways, allowing each output wheel to spin at a different speed [2]. But this is too loose an explanation. In this section the equations governing any differential are discussed in detail.

Regardless of the specific mechanical design, a differential is essentially a housing with two aligned shafts that must fulfill one very specific requirement: the two shafts must have opposite angular speeds with respect to the housing, as shown in Fig. 3.21, bottom.

Let ω_l, ω_h and ω_r be the absolute angular speeds of the left shaft, of the housing and of the right shaft, respectively (see Fig. 3.21 although the subscripts are different. Their meaning will be given shortly). Moreover, let M_l, M_h and M_r be the corresponding moments (torques) applied to them. All angular speeds are always positive, while the moments must be such that

$$M_l M_r \geq 0 \quad \text{and} \quad (M_l M_r) M_h \leq 0 \tag{3.126}$$

as will be shown in a while.

Every differential is governed by the following set of three equations:

$$\begin{aligned} &\frac{\omega_l - \omega_h}{\omega_r - \omega_h} = \frac{\hat{\omega}_l}{\hat{\omega}_r} = -1 \\ &M_h + M_l + M_r = 0 \\ &M_h\omega_h + M_l\omega_l + M_r\omega_r = W_d \end{aligned} \tag{3.127}$$

where $W_d > 0$ is the power lost *inside* the housing and

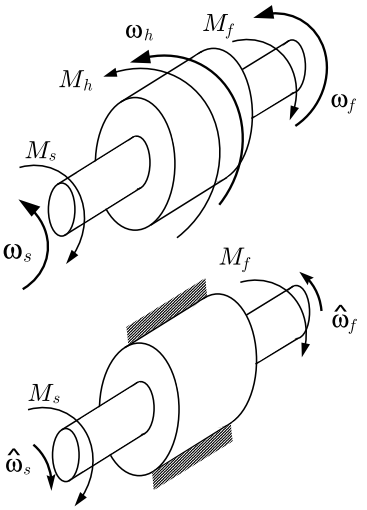

Fig. 3.21 Angular speeds and moments in any differential mechanism. *Top*: absolute speeds, *bottom*: relative speeds

$$\hat{\omega}_l = \omega_l - \omega_h \quad \text{and} \quad \hat{\omega}_r = \omega_r - \omega_h \tag{3.128}$$

are the *relative angular speeds* of the shafts with respect to the housing, usually very small. As already stated, under any working conditions we always have $\hat{\omega}_l = -\hat{\omega}_r$. The first equation in (3.127) is the Willis formula, the second equation is the torque balance and the third equation is the power balance.

The first equation can be better rewritten as

$$\omega_l + \omega_r = 2\omega_h \tag{3.129}$$

which shows a very important *kinematic* feature: if one wheel rotates *faster* than the housing, the other wheel must rotate *slower*. Let us call ω_f and ω_s these angular speeds, respectively, and M_f and M_s the corresponding torques (Fig. 3.21). Since the differential has two degrees of freedom, the Willis formula alone cannot say how big is the difference between the two rotation speeds ω_f and ω_s.

Combining the last two equations in (3.127), we get the internal power balance of the housing

$$\begin{aligned} M_l(\omega_l - \omega_h) + M_r(\omega_r - \omega_h) &= M_l\hat{\omega}_l + M_r\hat{\omega}_r \\ &= M_f(\omega_f - \omega_h) + M_s(\omega_s - \omega_h) = M_f\hat{\omega}_f + M_s\hat{\omega}_s \\ &= W_i - W_o = W_d \end{aligned} \tag{3.130}$$

where W_i is the input power and W_o is the output power, both assumed as positive. Obviously, by definition

$$(\hat{\omega}_f = \omega_f - \omega_h) > 0 \quad \text{and} \quad (\hat{\omega}_s = \omega_s - \omega_h) < 0 \tag{3.131}$$

with $\hat{\omega}_f = -\hat{\omega}_s$.

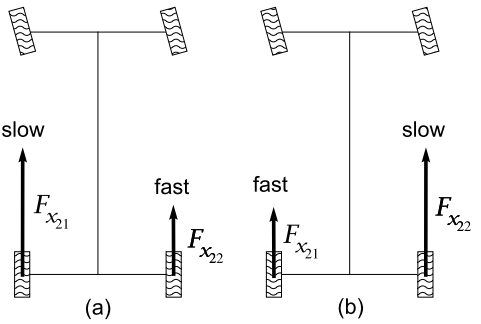

Fig. 3.22 Longitudinal forces during *power-on* in a vehicle equipped with a limited slip differential: (**a**) low lateral acceleration, (**b**) high lateral acceleration

The knowledge of the *internal efficiency* η_h of the housing is very helpful, since

$$\eta_h = \frac{W_o}{W_i} = \frac{W_i - W_d}{W_i} \leq 1 \tag{3.132}$$

Instead of η_h, it is common practice to use the Torque Bias Ratio (TBR) which is exactly equal to $1/\eta_h$

$$\text{TBR} = \frac{1}{\eta_h} \tag{3.133}$$

There are two possible working conditions:

(1) positive torque M_h from the engine (power-on), which means that both M_f and M_s are negative (for the differential, but positive for the wheels). Therefore, $-M_f\hat{\omega}_f = W_o$ and $M_s\hat{\omega}_s = W_i$ (Fig. 3.21);
(2) negative torque M_h from the engine (power-off), which means that both M_f and M_s are positive (for the differential, but negative for the wheel). Therefore, $-M_s\hat{\omega}_s = W_o$ and $M_f\hat{\omega}_f = W_i$.

Inserting these results in (3.132) we get

$$\begin{aligned} &\text{power-on} \quad \eta_h = \frac{-M_f\hat{\omega}_f}{M_s\hat{\omega}_s} = \frac{M_f}{M_s} \leq 1 \\ &\text{power-off} \quad \eta_h = \frac{-M_s\hat{\omega}_s}{M_f\hat{\omega}_f} = \frac{M_s}{M_f} \leq 1 \end{aligned} \tag{3.134}$$

As shown in Fig. 3.22, the outcome of a power-on condition strongly depends on the vertical loads acting on the two wheels. As a rule of thumb, *the slower wheel has always the higher torque*.[7] The power-off condition, instead, is more predictable, as shown in Fig. 3.23.

[7] Just consider that, since $\omega_h > \omega_s$, both M_s and $\hat{\omega}_s$ are negative and hence their product is positive, meaning input power for the differential mechanism inside the housing. Consistently, $M_f\hat{\omega}_f < 0$, which is an output power for the differential mechanism.

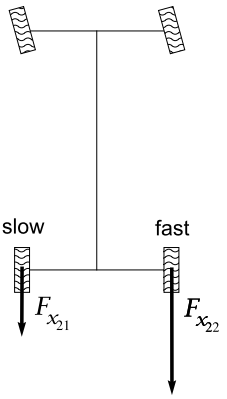

Fig. 3.23 Longitudinal forces during *power-off* (coasting mode) in a vehicle equipped with a limited slip differential (not locked)

For the purpose of practical implementation, it is useful to rewrite (3.134) in a more compact way. Let $\varsigma = \text{sign}(M_h)$; therefore $\varsigma = 1$ during power-on and $\varsigma = -1$ during power-off. We have that

$$M_f = \eta_h^{\varsigma} M_s \tag{3.135}$$

Moreover, let $\varphi = \text{sign}(\omega_r - \omega_l)$. We obtain

$$M_r = \left(\eta_h^{\varsigma}\right)^{\varphi} M_l \tag{3.136}$$

which covers all cases.

Most road cars are equipped with a so-called *open differential*, which has $\eta_h \simeq 1$ and hence $M_l = M_r$ under all working conditions.

On the other hand, off-road vehicles, race cars and other sports cars have a *limited slip differential* (also called self-locking). A low efficiency η_h (and hence a high TBR) can be achieved in several ways, but all rely on friction inside the housing. There are differentials with constant η_h (typically $\eta_h \simeq 1/4$), others which have some sort of clutches and have η_h sensitive to torque.

Many limited slip differentials which employ clutches behave like a *totally locked differential* whenever the difference $\Delta M = |M_l - M_r|$ is below a threshold value. In that case, there is no differential effect and both wheels rotate at the same angular speed $\omega_l = \omega_r = \omega_h$, the moments being any, provided they fulfill the equation $M_h + M_l + M_r = 0$. For instance, it is even possible to have the two longitudinal forces pointing in opposite directions, as shown in Fig. 3.24.

Summing up, the type of differential mechanism affects the handling behavior through the following equations:

open differential: $M_{i1} = M_{i2}$, and hence $\Delta X_i = 0$;

locked differential: $\omega_{i1} = \omega_{i2}$, and hence, in general, $\Delta X_i \neq 0$;

limited slip differential: $M_{i1} \neq M_{i2}$ and $\omega_{i1} \neq \omega_{i2}$ (more precisely, during power-on $|M_f| = \eta_h |M_s|$, with $\eta_h < 1$, that is the slower wheel receives by the engine the higher torque).

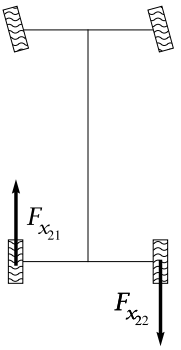

Fig. 3.24 Possible longitudinal forces in a vehicle equipped with a locked differential

3.12 The Structure of This Vehicle Model

The equations listed in the former section may look a bit complicated. It is important to observe that there are only three differential equations, namely the equilibrium equations. All other equations are algebraic. This means that, ultimately, the model is governed by three equations of motion, all first-order differential equations, in the unknown functions $u(t)$, $v(t)$ and $r(t)$.

However, it is advisable to extract simplified models tailored for specific vehicles and/or operating conditions. The goal is to obtain models simple enough for training human beings in learning and understanding vehicle dynamics. Of course, we will pay attention to state the additional assumptions needed for the simplified model to be meaningful.

A list of possible options can be:

(1) braking on a straight road with uniform grip;
(2) accelerating on a straight road with uniform grip;
(3) handling at constant and given speed u:

   (a) vehicle with open differential;
   (b) vehicle with locked differential;
   (c) vehicle with limited slip differential;
   (d) vehicle without wings (no downforce);
   (e) vehicle with wings.

In the next chapters, most of these options will be elaborated in detail. In addition, we will develop vehicle models for studying ride and road holding, and we will extend the handling model to take into account roll motion. A final chapter will address what happens in the contact patch between tire and road.

But there is one more topic to be discussed here.

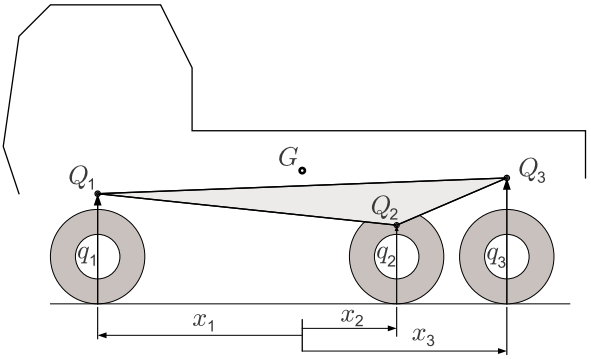

Fig. 3.25 Triangle of possible no-roll points ($x_2 < 0$ and $x_3 < 0$)

3.13 Three-Axle Vehicles

Most vehicles have two axles, but many have three (or more) [6, 7]. Just consider trucks. As we have already discussed, each axle has a no-roll center. So there are three no-roll centers, each at a differente height, in general (Fig. 3.25). But what about the no-roll axis? As a matter of fact, a straight line is defined by two points, not three!

It is quite amazing that such an (apparently) fundamental concept like the no-roll axis shows to be totally meaningless for an important class of vehicles. But what is even more surprising is that the vehicle dynamics community does not show any embarrassment for having grounded most of its theory on such a weak concept.

Having said that, let us address the problem with open mind. First of all, consider that the vehicle knows nothing about no-roll axis and the like. It behaves according to the fundamental laws of dynamics. And for sure, the vehicle body (assumed rigid) has an instantaneous screw axis, but it has nothing to do with the roll axis as commonly defined.

Actually, the really big difference between a vehicle with two and a vehicle with three (or more) axles is that with two axles we have in many respects a statically determinate (or isostatic) structure, whereas with three or more axles we have always to deal with a statically indeterminate (or hyperstatic) structure.

For instance, the *static* vertical loads in a two-axle vehicle can be obtained by the equilibrium equations only and are not affected by the suspension stiffnesses

$$Z_1^0 = \frac{mga_2}{l}, \qquad Z_2^0 = \frac{mga_1}{l} \tag{3.75'}$$

On the other hand, with three axles the static vertical loads cannot be obtained by the equilibrium equations only, that is without taking into account the suspension and tire vertical stiffnesses.

Let, $x_1 = a_1$, $x_2 = -a_2$ and x_3 be the longitudinal coordinate of each axle in the vehicle reference frame. The three static vertical loads on each axle must obey to the following equilibrium equations (in case of negligible aerodynamic loads)

$$\begin{aligned} 0 &= Z_1^0 + Z_2^0 + Z_3^0 - mg \\ 0 &= Z_1^0 x_1 + Z_2^0 x_2 + Z_3^0 x_3 \end{aligned} \tag{3.137}$$

We have two equations with three unknowns. Therefore, there are infinitely many solutions. For instance, we could set $X_3 = 0$ by raising the two wheels of the third axle, thus restoring the common two-axle architecture.

Exactly the same observation applies to the lateral forces Y_i: there are infinitely many possible combinations of lateral forces Y_1, Y_2 and Y_3 to balance Y.

Notwithstanding these difficulties, the analysis to *define* (and measure) the roll and vertical stiffnesses $k^s_{\phi_i}$, $k^p_{\phi_i}$, $k^s_{z_i}$, $k^p_{z_i}$ still applies entirely. We can then proceed to collect all relevant equations, like in Sect. 3.8.11.

$$Y = Y_1 + Y_2 + Y_3 \tag{3.138}$$

$$Yx_N = Y_1 x_1 + Y_2 x_2 + Y_3 x_3 \tag{3.139}$$

$$Yq^b = Y_1 q_1 + Y_2 q_2 + Y_3 q_3 \tag{3.140}$$

$$Yh = \Delta Z_1 t_1 + \Delta Z_2 t_2 + \Delta Z_3 t_3 \tag{3.141}$$

$$mg = Z_1 + Z_2 + Z_3 \tag{3.142}$$

$$Xh = -(Z_1 x_1 + Z_2 x_2 + Z_3 x_3) \tag{3.143}$$

$$\Delta Z_i t_i = k^p_{\phi_i} \phi^p_i \tag{3.144}$$

$$\Delta Z_i t_i = Y_i q_i + k^s_{\phi_i} \phi^s_i \tag{3.145}$$

$$Z_i^0 - Z_i = k^p_{z_i} z^p_i \tag{3.146}$$

$$Z_i^0 - Z_i = k^s_{z_i} z^s_i - \Delta Y_i \frac{4q_i}{t_i} \tag{3.147}$$

$$\phi = \phi^s_i + \phi^p_i \tag{3.148}$$

$$\frac{z_1 - z_3}{x_1 - x_3} = \frac{z_1 - z_2}{x_1 - x_2} \tag{3.149}$$

which imply

$$Yh = k^p_{\phi_1} \phi^p_1 + k^p_{\phi_2} \phi^p_2 + k^p_{\phi_3} \phi^p_3 \tag{3.150}$$

$$Y\left(h - q^b\right) = k^s_{\phi_1} \phi^s_1 + k^s_{\phi_2} \phi^s_2 + k^s_{\phi_3} \phi^s_3 \tag{3.151}$$

It is worth noting that the suspension jacking, as in (3.106), affects the vertical loads because the system is hyperstatic. Therefore it also interacts with lateral load transfers, with the lateral forces and, ultimately, with roll motion. In other words, in

a three-axle vehicle there is interaction between suspension jacking and roll angles. It was not so in a two-axle vehicle.

Moreover, under a given lateral force Y, the roll angles are also affected by the amount of grip of each axle, and vice versa.

But maybe the most interesting and, somehow, surprising result is that, as shown in Fig. 3.25, in a three-axle vehicle the no-roll axis must be replaced by a *triangle of possible no-roll points*. The three no-roll centers Q_i are the vertices of this triangle of possible no-roll points. The actual height q^b depends not only on the heights q_i of the no-roll centers, but also on the value of each lateral force Y_i.

This result generalizes the concept of no-roll axis and confirms that sentences like "The vehicle has two roll centers about which it rolls when cornering" are incorrect.

3.14 Summary

This is the main chapter of this book, the core of it. Therefore it covers a lot of topics.

At the beginning, the simplifying assumptions to formulate a simple, yet significant, vehicle model have been listed. Then the kinematics of the vehicle as a whole has been described in detail, followed by the kinematics of each wheel with tire. Formulation of the constitutive (tire) equations and of the global equilibrium equations has been the following step.

A lot of work has been devoted to load transfers, which has required an in-depth suspension analysis. This has led to the definition of suspension and vehicle internal coordinates, of no-roll centers and no-roll axis, for both independent and dependent suspensions. The case of three-axle vehicles has been also considered.

In the end, the vehicle model for handling and performance has been formulated in a synthetic, yet precise way. A general description of the mechanics of both open and limited-slip differential mechanisms has been included.

3.15 List of Some Relevant Concepts

p. 49 a vehicle can have a lateral velocity v, although it is normally much lower than the forward velocity u;
p. 50 the lateral and forward velocity cannot be expressed as derivatives of other functions;
p. 52 the velocity center C is not, in general, the center of curvature;
p. 69 for each axle, four internal coordinates are necessary to monitor the suspension conditions with respect to a reference configuration;
p. 78 application of a force to any point of the no-roll axis does not produce suspension roll;
p. 78 no suspension roll does not mean no other effects at all. There can be suspension jacking;

p. 95 in a three-axle vehicle, the no-roll axis must be replaced by a triangle of possible no-roll points;
p. 92 a fundamental parameter in a differential mechanism is its internal efficiency η_h.

References

1. Dixon JC (1991) Tyres, suspension and handling. Cambridge University Press, Cambridge
2. Genta G, Morello L (2009) The automotive chassis. Springer, Berlin
3. Longhurst C (2013) www.carbibles.com
4. Meirovitch L (1970) Methods of analytical dynamics. McGraw-Hill, New York
5. Milliken WF, Milliken DL (1995) Race car vehicle dynamics. SAE International, Warrendale
6. Williams DE (2011) On the equivalent wheelbase of a three-axle vehicle. Veh Syst Dyn 49(9):1521–1532
7. Williams DE (2012) Generalised multi-axle vehicle handling. Veh Syst Dyn 50(1):149–166

Chapter 4
Braking Performance

Driving a vehicle involves, among other things, braking [1]. Fortunately, most of the times, we brake very softly, far from the braking performance limit. Most drivers, perhaps, never need to experience the limit braking performance of their car in everyday traffic. However, engineers must know very well the mechanics of braking a vehicle, to allow it to stop as soon as possible in case of emergency. Actually, this problem has been somehow mitigated by the advent of ABS systems [2], which now equip every car. However, many race cars do not have ABS and hence brake design and balance is still a relevant topic in vehicle dynamics.

By *brake balance* or bias, we mean how much to brake the front wheels with respect to the rear wheels. The goal is to stop the vehicle as soon as possible, but avoiding wheel locking. Cars have only one pedal to brake all wheels and brake balance is left to the car. By the way, wheel locking should be avoided because, in order of importance:

(1) the steering/directional capability is totally impaired;
(2) the grip is lower;
(3) energy dissipation switches from the brakes to the contact patches and tires get damaged.

On the other hand, almost all motorcycles and bicycles have independent brake commands for the front wheel and for the rear wheel, thus leaving to the rider the duty of brake balance. Many bicyclists fear using the front brake because they believe it, in contrast to the rear brake, might cause the bicycle to overturn. Actually, overturning a bicycle with the front brake is much harder than it seems. Not using the front brake is a bad habit, since it drastically impairs the brake performance.

4.1 Pure Braking

As anticipated, we extract tailored models from the fairly general vehicle model developed in Chap. 3.

M. Guiggiani, *The Science of Vehicle Dynamics*, DOI 10.1007/978-94-017-8533-4_4,

When braking on a *flat*, *straight* road, with *uniform grip*, we know beforehand that

$$\begin{aligned} Y &= 0 \\ N &= 0 \\ \Delta X_i &= 0 \\ \Delta Z_i &= 0 \end{aligned} \tag{4.1}$$

that is, there are no lateral forces, no yaw moment and no lateral load transfers. Accordingly, the vehicle goes straight, with no lateral acceleration and yaw rate (and also no lateral velocity)

$$\begin{aligned} a_y &= 0 \\ \dot{r} &= 0 \\ v &= 0 \\ r &= 0 \end{aligned} \tag{4.2}$$

Other quantities are usually very small. In particular, if the wheels of the same axle have a bit of convergence (also called toe-in), that means that there are small steering angles and, accordingly, very small lateral slips. Similarly, if the wheels of the same axle have some camber, the tires are subject to a small spin slip:

$$\begin{aligned} \delta_{ij} &\simeq 0 \\ \sigma_{y_{ij}} &\simeq 0 \\ \varphi_{ij} &\simeq 0 \end{aligned} \tag{4.3}$$

At first, all these quantities can be set equal to zero.

4.2 Vehicle Model for Braking Performance

A simple, yet significant, model to study the limit braking performance of a road vehicle is shown in Fig. 4.1. We are dealing here with road vehicles, without significant aerodynamic downforces.

We suppose to brake on a flat and straight road, with uniform grip. Therefore, the vehicle goes straight. Moreover, we assume to apply a constant force to the brake pedal. Therefore, pitch oscillations are negligible.

Summing up, we can employ the two-dimensional model shown in Fig. 4.1. The vehicle is just a single rigid body with mass m, moving horizontally with forward speed u and forward acceleration $\dot{u} < 0$. Beside its own weight mg, it receives from the road two vertical forces Z_1 and Z_2, one per each axle, and two longitudinal (braking) forces X_1 and X_2, again one per each axle.

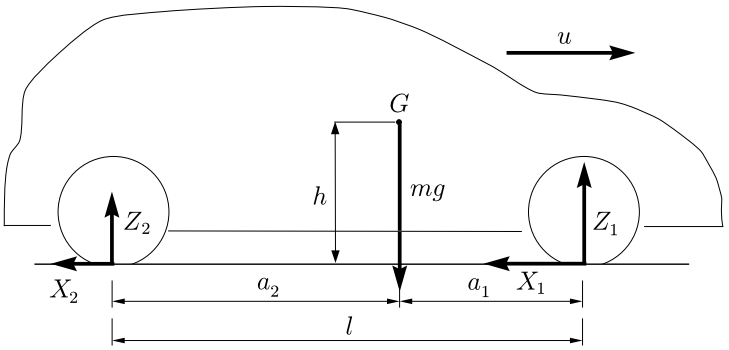

Fig. 4.1 Vehicle model for braking performance

In this chapter only we assume X_1 and X_2 to be positive if directed like in Fig. 4.1. It is more convenient to deal with positive quantities.

4.3 Equilibrium Equations

The three equilibrium equations are readily obtained from Fig. 4.1

$$\begin{aligned} m\dot{u} &= -(X_1 + X_2) \\ 0 &= Z_1 + Z_2 - mg \\ 0 &= (X_1 + X_2)h - Z_1 a_1 + Z_2 a_2 \end{aligned} \tag{4.4}$$

which must be supplemented by the following inequalities

$$|X_i| \le \mu_p^x Z_i \quad \text{and} \quad Z_i \ge 0 \tag{4.5}$$

where μ_p^x is the global longitudinal friction coefficient defined in (2.76). It is quite obvious that the braking forces cannot exceed the traction limit, nor the vertical forces be negative. For brevity, we will use the symbol μ for μ_p^x in this chapter.

The aerodynamic drag X_a has not been included because it is really small compared to the braking forces.

4.4 Longitudinal Load Transfer

When going at constant speed, that is with $\dot{u} = 0$, we have from (4.4) (or, directly, from (3.75)) that the static loads on each axle are

$$Z_1^0 = \frac{mga_2}{l}, \qquad Z_2^0 = \frac{mga_1}{l} \tag{4.6}$$

During braking with $\dot{u} < 0$, the two loads change, although their sum must be constantly equal to the vehicle weight mg. We have the so-called longitudinal load transfer ΔZ

$$Z_1 = Z_1^0 + \Delta Z \quad \text{and} \quad Z_2 = Z_2^0 - \Delta Z \tag{4.7}$$

where (cf. (3.74))

$$\Delta Z = -\frac{mh}{l}\dot{u} \tag{4.8}$$

with $\dot{u} < 0$. The front axle is subject to a higher load, while the rear axle to a lower load. It is worth noting that the load transfer does not depend on the type of suspensions.

We have *overturning* of the vehicle if $Z_2 = 0$, that is if

$$|\dot{u}| = a_1 g/h \tag{4.9}$$

This condition is never met in cars, whereas it may limit the brake performance in some motorcycles.

4.5 Maximum Deceleration

The best braking performance $|\dot{u}|_{\max}$ is obtained if both axles brake at their traction limit, that is if

$$X_1 = \mu Z_1 \quad \text{and} \quad X_2 = \mu Z_2 \tag{4.10}$$

From the equilibrium equations (4.4), it is straightforward to obtain the *limit deceleration*

$$|\dot{u}| = \mu g \tag{4.11}$$

Of course, the *maximum deceleration* is the minimum between (4.9) and (4.11)

$$|\dot{u}|_{\max} = \min(\mu g, a_1 g/h) \tag{4.12}$$

Cars have $\mu < a_1/h$, whereas in some motorcycles it can be the other way around. Here we are mainly dealing with cars, and therefore we have

$$|\dot{u}|_{\max} = \mu g \tag{4.13}$$

4.6 Brake Balance

When braking at the best braking performance, that is with $\dot{u} = -\mu g$, the longitudinal forces are

$$\begin{aligned} X_{1_P} &= \mu Z_{1_P} = \mu\left(Z_1^0 + \frac{mh}{l}\mu g\right) = \mu\frac{mg}{l}(a_2 + \mu h) \\ X_{2_P} &= \mu Z_{2_P} = \mu\left(Z_2^0 - \frac{mh}{l}\mu g\right) = \mu\frac{mg}{l}(a_1 - \mu h) \end{aligned} \tag{4.14}$$

The *brake balance* (or brake bias) β_P to have the *best braking performance* is promptly obtained as

$$\beta_P = \frac{X_{1_P}}{X_{2_P}} = \frac{Z_{1_P}}{Z_{2_P}} = \frac{a_2 + \mu h}{a_1 - \mu h} \tag{4.15}$$

Typical values in road cars are $\beta_P \simeq 2$ on dry asphalt ($\mu \simeq 0.8$) and $\beta_P \simeq 1.5$ on wet asphalt ($\mu \simeq 0.4$). More commonly the same concepts would be expressed as front/rear = 66/33 and front/rear = 60/40, respectively.

4.7 All Possible Braking Combinations

If the best braking performance is our ultimate goal, we should also look around to see what happens if we employ a brake balance not equal to β_P. All possible braking combinations can be visualized in a simple, yet very useful, figure.

First solve the equilibrium equations (4.4) with $X_1 = \mu Z_1$, thus getting

$$Z_1 = \frac{X_1}{\mu} = Z_1^0 + \frac{h}{l}(X_1 + X_2) \tag{4.16}$$

and hence

$$X_1 = \mu\left(\frac{Z_1^0 + \frac{h}{l}X_2}{1 - \mu\frac{h}{l}}\right) \tag{4.17}$$

This is the relationship between X_1 and X_2 to have limit (threshold) braking at the front wheels.

Similarly, solve the equilibrium equations (4.4) with $X_2 = \mu Z_2$, thus getting

$$X_2 = \mu\left(\frac{Z_2^0 - \frac{h}{l}X_1}{1 + \mu\frac{h}{l}}\right) \tag{4.18}$$

This is the relationship between X_1 and X_2 to have limit (threshold) braking at the rear wheels.

In the plane (X_2, X_1) we can now draw the two straight lines (4.17) and (4.18), as shown in Fig. 4.2. The region inside the two lines contains all possible (admissible) braking combinations. Trying to trespass the upper line means front wheels

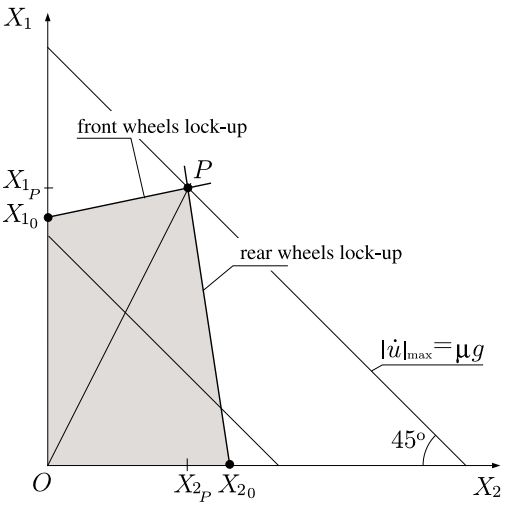

Fig. 4.2 Area of all admissible braking combinations

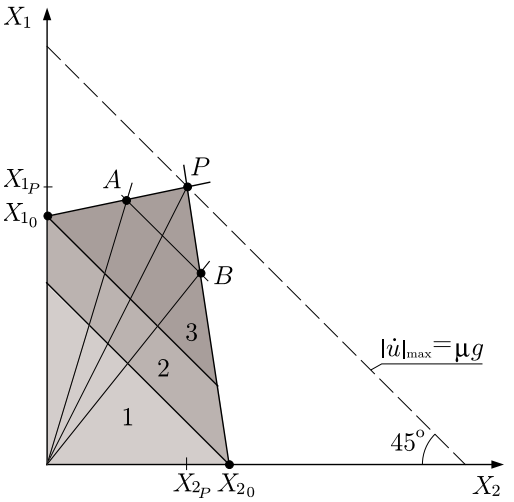

Fig. 4.3 Area of all admissible braking combinations with indication of some particular cases

lock-up. Trying to trespass the right line means rear wheels lock-up. Point P is the combination of braking forces X_{1_P} and X_{2_P} (best performance).

Points with the same level of deceleration all belong to straight lines with slope 45°, that is lines with constant $X_1 + X_2 = -m\dot{u}$. The maximum deceleration corresponds to the line passing through point P. Braking with balance β_P means moving along the line OP.

Some other relevant cases are shown in Fig. 4.3. Area 1 corresponds to low decelerations. So small that they can be obtained with any balance between front and rear braking forces (even only a rear braking force X_{2_0}). Area 2 needs necessarily some braking force at the front wheels, but even the front wheels alone, with a braking

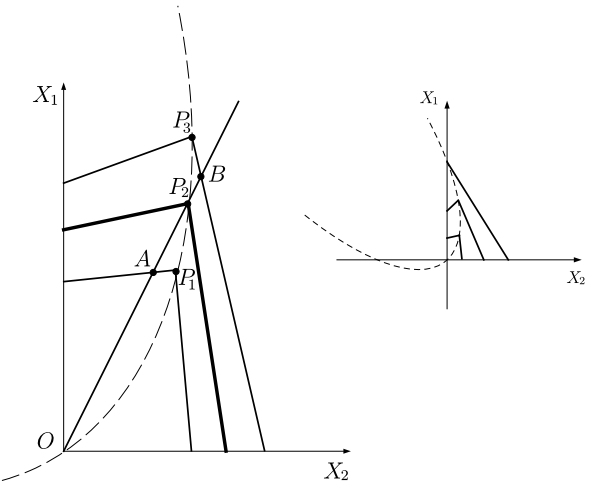

Fig. 4.4 Area of all admissible braking combinations for three different grip coefficients (*left*) and parabola of limit points (*right*)

force X_{1_0}, would do (front/rear = 100/0). Area 3, that is high decelerations, require intervention of both axles. The higher the deceleration, the narrower the range A–B.

To complete our discussion we have to address the effects of changing the grip coefficient μ and/or the position of G, that is a_1/a_2, and maybe h.

4.8 Changing the Grip

The formulation developed so far includes the grip coefficient as a parameter. Therefore, we have already obtained all formulas to deal with different values of μ. To understand what happens it is helpful to draw the admissible region for, say, three different values $\mu_1 < \mu_2 < \mu_3$ of the grip coefficient, as shown in Fig. 4.4.

Let us assume that our car has a brake balance that follows line OP_2, that is optimized for $\mu = \mu_2$. If the grip is lower there will be less load transfer ΔZ and a lower brake balance would be optimal. If we still follow line OP_2, we exit the admissible region at point A, that is for a deceleration lower than $\mu_1 g$ and with the front wheels at lock-up. It can be shown that the deceleration is equal to $\varepsilon_1 \mu_1 g$, with the *braking efficiency* $\varepsilon_1 < 1$ given by

$$\varepsilon_1 = \frac{a_2}{a_2 + h(\mu_2 - \mu_1)}, \quad \text{if } \mu_1 < \mu_2 \tag{4.19}$$

Efficiency lower than one is also obtained when the out-of-balance is due to a higher value of the grip coefficient. As shown in Fig. 4.4, we exit the admissible region at point B, which is not optimal. Rear wheels are about to lock up and the deceleration is equal to $\varepsilon_3 \mu_3 g$, with the braking efficiency $\varepsilon_3 < 1$ given by

$$\varepsilon_3 = \frac{a_1}{a_1 + h(\mu_3 - \mu_2)}, \quad \text{if } \mu_3 > \mu_2 \tag{4.20}$$

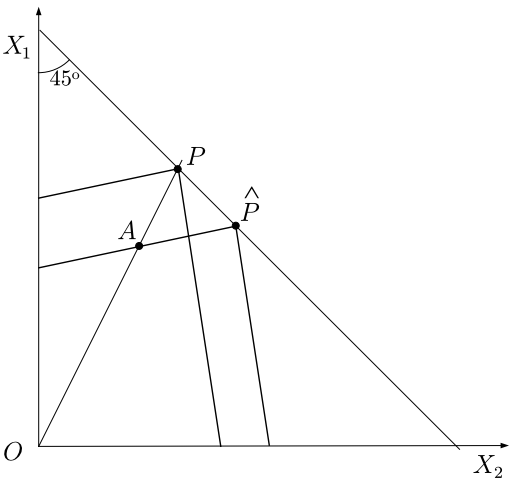

Fig. 4.5 Area of admissible braking combinations for two different weight distributions

Also shown in Fig. 4.4 is the parabola that collects all vertices P when varying the coefficient μ. Point P located on the X_1 axis means that maximum deceleration is limited by overturning.

4.9 Changing the Weight Distribution

The longitudinal position of G affects the static load distribution. Therefore, it affects the brake balance, but not the maximum deceleration μg. Accordingly, we get an admissible region like in Fig. 4.5, with a new vertex $\hat{P}$ still on the same line at 45°, and with sides parallel to those of the original region.

4.10 A Numerical Example

A numerical example may be useful to understand better the braking performance of a road car. We take a small car with the following features: mass $m = 1000$ kg, wheelbase $l = 2.4$ m, $a_1 = a_2 = l/2$, height of the center of mass $h = 0.5$ m.

Assuming a grip coefficient $\mu = 0.8$, the maximum deceleration is vehicle independent and it is equal to $|\dot{u}|_{\max} = \mu g = 7.84$ m/s^2, with $g = 9.81$ m/s^2.

According to (4.6), the static vertical loads for both axles are $Z_1^0 = Z_2^0 = 4900$ N. The load transfer at maximum deceleration is $\Delta Z = 1633$ N. Therefore, the vertical loads acting on each axle are $Z_{1_P} = 6533$ N and $Z_{2_P} = 3267$ N, which means a brake balance $\beta_P = 2$. This is the optimal value for that car if $\mu = 0.8$.

Should the grip coefficient drop to 0.4 because, e.g., of rain, we would end up with a braking efficiency $\varepsilon_1 = 0.86$. An increase of the grip coefficient up to 1.2 would still bring a reduced braking efficiency $\varepsilon_2 = 0.86$.

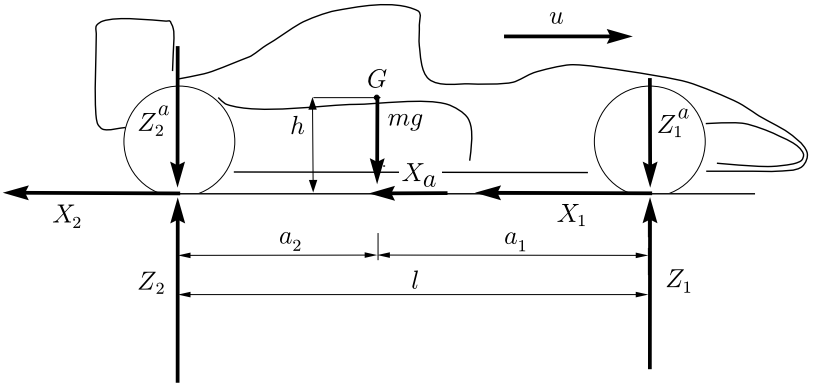

Fig. 4.6 Vehicle model for braking performance of a Formula car

4.11 Braking Performance of Formula Cars

Formula cars have aerodynamic wings that provide very high downforces at high speed, as briefly explained in Sect. 3.5.2. These loads affect braking pretty much. The first, obvious, effect is that the maximum longitudinal deceleration is speed dependent. In a Formula 1 car it can be up to $5g$ at 300 km/h, although the physical grip μ rarely exceeds 1.6. The second, perhaps less obvious, effect is that also the optimal brake balance is speed dependent.

4.11.1 Equilibrium Equations

The equilibrium equations (4.4) must be supplemented by the aerodynamic forces. According to Sect. 3.5.2 and as shown in Figs. 3.6 and 4.6, the aerodynamic loads are equivalent to three forces: a drag force X_a at road level and two vertical forces Z_1^a and Z_2^a acting directly on the front and rear axles, respectively. Therefore, the equilibrium equations become

$$\begin{aligned} m\dot{u} &= -(X_1 + X_2) - X_a \\ 0 &= Z_1 + Z_2 - mg - Z_1^a - Z_2^a \\ 0 &= (X_1 + X_2 + X_a)h - \left(Z_1 - Z_1^a\right)a_1 + \left(Z_2 - Z_1^a\right)a_2 \end{aligned} \tag{4.21}$$

Unlike in (3.64) and (3.65), here not only we assume X_1 and X_2 to be positive if directed like in Fig. 4.6, that is to be indeed braking forces, but also the aerodynamic vertical loads Z_1^a and Z_2^a are assumed to be positive if directed downward, again like in Fig. 4.6.

We recall that (cf. (3.56) and (3.57))

$$\begin{aligned} X_a &= \frac{1}{2}\rho_a C_x S_a u^2 = \xi u^2 \\ Z_1^a &= \frac{1}{2}\rho_a C_{z1} S_a u^2 = \zeta_1 u^2 \\ Z_2^a &= \frac{1}{2}\rho_a C_{z2} S_a u^2 = \zeta_2 u^2 \end{aligned} \tag{4.22}$$

where, as common practice among race engineers, $C_x > 0$ and $C_{zi} > 0$ (again, unlike in the other, more general, chapters).

For simplicity, although not strictly true, we assume all aerodynamic coefficients to be speed independent.

4.11.2 Longitudinal Load Transfer

The longitudinal load transfer ΔZ is not directly affected by the aerodynamic loads, in the sense that it is still given by

$$\Delta Z = -\frac{mh}{l}\dot{u} \tag{4.23}$$

with $\dot{u} < 0$, exactly like in (4.8). When braking, the front axle is subject to a higher load, while the rear axle to a lower load. It is a purely inertial effect.

The vertical loads on each axle are therefore given by the static loads, plus the aerodynamic (speed dependent) loads, plus or minus the load transfer

$$\begin{aligned} Z_1 &= \frac{mga_2}{l} + \zeta_1 u^2 + \Delta Z \\ Z_2 &= \frac{mga_1}{l} + \zeta_2 u^2 - \Delta Z \end{aligned} \tag{4.24}$$

4.11.3 Maximum Deceleration

The maximum deceleration is promptly obtained by assuming that both axles are at their limit braking conditions, that is $X_1 = \mu Z_1$ and $X_2 = \mu Z_2$

$$|\dot{u}|_{\max} = \mu\left(g + \frac{\zeta_1 + \zeta_2}{m}u^2\right) + \frac{\xi}{m}u^2 \tag{4.25}$$

This formula generalizes (4.13). Of course $|\dot{u}|_{\max}$ is very speed dependent.

4.11.4 Braking Balance

Having the right brake balance β_P is very important for lap performance:

$$\beta_P = \frac{(a_2 + h\mu)gm + u^2[(a_1 + a_2)\zeta_1 + h\xi + h(\zeta_1 + \zeta_2)\mu]}{(a_1 - h\mu)gm + u^2[(a_1 + a_2)\zeta_2 - h\xi - h(\zeta_1 + \zeta_2)\mu]} \tag{4.26}$$

which generalizes (4.15). As expected, now β_P is speed dependent, unless

$$(a_2 + h\mu) = (a_1 - h\mu) \tag{4.27}$$

and

$$\left[(a_1 + a_2)\zeta_1 + h\xi + h(\zeta_1 + \zeta_2)\mu\right] = \left[(a_1 + a_2)\zeta_2 - h\xi - h(\zeta_1 + \zeta_2)\mu\right] \tag{4.28}$$

which can be recast as

$$(a_1 + a_2 + 2h\mu)C_{z1} + 2h\mu C_x = (a_1 + a_2 - 2h\mu)C_{z2} \tag{4.29}$$

Although it is not possible (or not convenient) to fulfill these conditions, they can be taken as something to be considered during set-up.

4.11.5 Typical Formula 1 Braking Performance

A typical braking performance of a Formula 1 car is shown in Fig. 4.7. The deceleration grows suddenly up to about 38 m/s^2. Then, as the speed u decreases, also the aerodynamic load decreases, thus requiring the driver to gradually release the brake pedal. Meanwhile, the car is already negotiating the curve, as shown by the lateral acceleration and wheel steer angle. Also shown in Fig. 4.7 is the acceleration ($a_x > 0$) when the car exits the curve.

It is interesting to compare the total acceleration $\sqrt{a_x^2 + a_y^2}$ (lower line in Fig. 4.8) with the potential maximum acceleration (4.25) (upper line in Fig. 4.8). Whenever possible, the driver tries to stay as close as possible to the limit. This can be done in all curves that are grip limited. Of course, not in those curves that are speed limited.

4.12 Summary

The goal of this chapter has been to understand how to stop a vehicle as soon as possible, avoiding wheel locking. This result can be achieved only if the vehicle has the right brake balance. Unfortunately, brake balance is affected by the value of the grip and by the position of the center of mass. This topic has been addressed in detail, both analytically and graphically, through the region of all possible braking conditions. The peculiarity of the braking performance of a Formula car has been also discussed.

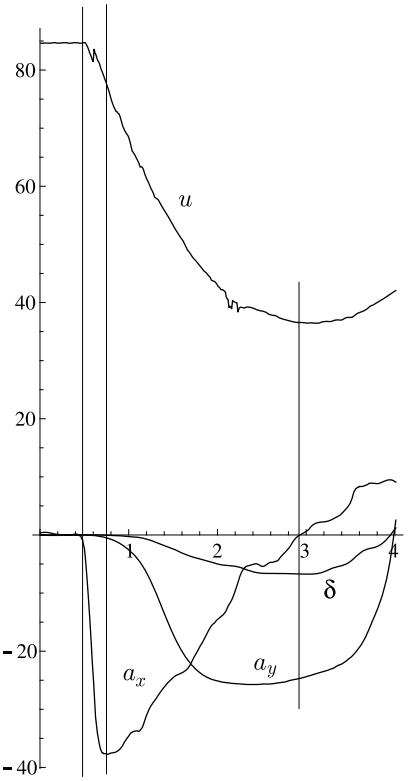

Fig. 4.7 Typical braking performance of a Formula 1 car

4.13 List of Some Relevant Concepts

p. 102 longitudinal load transfer do not depend on the type of suspensions;
p. 102 maximum deceleration is limited by either grip or overturning (supposing brakes are powerful enough);
p. 103 brake balance depends on grip and weight distribution;
p. 104 all possible braking combinations can be represented by a simple figure;

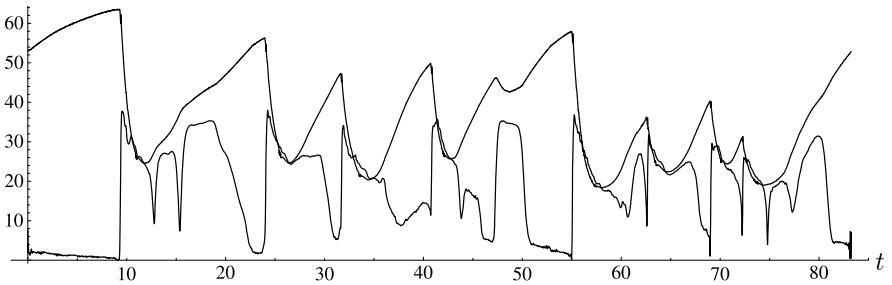

Fig. 4.8 Comparison between the total acceleration (*lower line*) and the potential maximum acceleration (*upper line*) of a Formula 1 car

p. 108 wings do not affect load transfer directly;
p. 109 brake balance is affected by wings.

References

1. Heißing B, Ersoy M (eds) (2011) Chassis handbook. Springer, Wiesbaden
2. Savaresi SM, Tanelli M (2010) Active braking control systems design for vehicles. Springer, London

Chapter 5
The Kinematics of Cornering

Cars have to negotiate corners. Everybody knows that. But not all cars do that the same way [4]. This is particularly evident in race cars, where the ability to negotiate a corner is a crucial aspect to minimize lap time.

In this chapter we will exploit the kinematics of a vehicle while taking a corner. At first sight, taking a corner looks quite a trivial task. But designing a vehicle that does it properly is one of the main challenges faced by a vehicle engineer [2]. Therefore, there is the need to investigate what really happens during the cornering process. It will be shown that some very significant kinematical quantities must follow precise patterns for the car to get around corner in a way that makes the driver happy. In some sense, the geometric features of the trajectory must adhere to some pretty neat criteria.

Before digging into the somehow mysterious kinematics of cornering, we will recall some kinematical concepts. Strangely enough, it appears that they have never been employed before in vehicle dynamics, although all of them date back to Euler or so.

5.1 Planar Kinematics of a Rigid Body

As discussed at the beginning of Chap. 3, in many cases a vehicle can be seen as a rigid body in planar motion. Basically, we need a flat road and small roll angles. The congruence (kinematic) equations for this case have been given in Sect 3.2. We will extensively use the symbols defined therein.

Here we recall some fundamental concepts of planar kinematics of a rigid body [1, 3, 5]. They will turn out to be very useful to understand how a car takes a corner.

5.1.1 Velocity Field and Velocity Center

In a rigid body, by definition, the distance between any two points is constant. Accordingly, taken two such points, say A and B, their velocities must have the same

M. Guiggiani, *The Science of Vehicle Dynamics*, DOI 10.1007/978-94-017-8533-4_5,

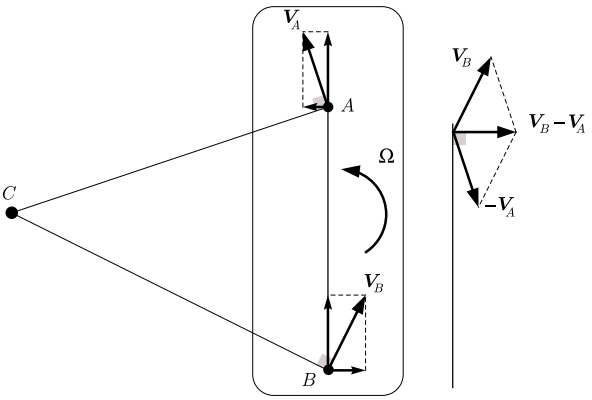

Fig. 5.1 Relationship between the velocities of two points of the same rigid body in planar motion

component along the direction AB, as shown in Fig. 5.1. More precisely, the two velocities are related by the following equation

$$\mathbf{V}_B = \mathbf{V}_A + \boldsymbol{\Omega} \times AB = \mathbf{V}_A + \mathbf{V}_{BA} \tag{5.1}$$

where $\boldsymbol{\Omega}$ is the angular speed. This is the fundamental equation of the kinematics of rigid bodies, planar or three-dimensional. It had been already given in (2.1) and (3.3).

It is worth noting that $\boldsymbol{\Omega}$ is the same for all points. It is a kinematic feature of the rigid body as a whole.

Another way to state the fundamental equation (5.1) is saying that the relative velocity $\mathbf{V}_{BA} = \mathbf{V}_B - \mathbf{V}_A$ is orthogonal to the segment AB and proportional to the length of AB, that is $|\mathbf{V}_{BA}| = |\boldsymbol{\Omega}||AB|$ (Fig. 5.1).

It can be shown [1, 3, 5] that in case of planar motion, that is $\boldsymbol{\Omega} = r\mathbf{k}$, and with $r \neq 0$, at any instant there is one point C of the (extended) rigid body that has zero velocity. Therefore, applying (5.1) to A and C, and then to B and C we have

$$\mathbf{V}_A = r\mathbf{k} \times CA \quad \text{and} \quad \mathbf{V}_B = r\mathbf{k} \times CB \tag{5.2}$$

as shown in Fig. 5.1.

Several different names are commonly in use to refer to point C:

- instantaneous center of velocity;
- velocity center;
- instantaneous center of zero velocity;
- instantaneous center of rotation.

As the body changes its position, the point of the rigid body with zero velocity changes as well. If we follow the positions of this sequence of points we obtain a curve σ_f in the fixed plane, called the *fixed centrode* or space centrode, and another curve σ_m on the moving plane, called the *moving centrode* or the body centrode. It can be shown that the moving centrode rolls without slipping on the fixed centrode, the point of rolling contact being C.

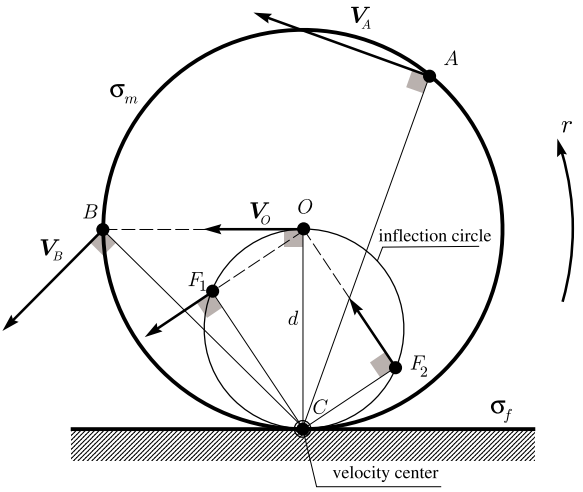

Fig. 5.2 Velocity field of a rigid wheel rolling on a flat road

A simple example should help clarify the matter. Just consider a rigid circle rolling without slipping on a straight line, as shown in Fig. 5.2. It is exactly like a rigid wheel rolling on a flat road. The two centrodes are the circle σ_m and the straight line σ_f. Point C as a point of the circle has zero velocity. However, the geometric point[1] $\hat{C}$ that at each instant coincides with C moves on the road with a speed

$$V_{\hat{C}} = rd \tag{5.3}$$

where d is the diameter of the inflection circle.

The velocity field is like a pure rotation around C (Fig. 5.1). But the acceleration field is not! In fact, the wheel is travelling on the road, not turning around C.

5.1.2 Acceleration Field, Inflection Circle and Acceleration Center

The counterpart of (5.1) for the accelerations of points of a rigid body is

$$\mathbf{a}_B = \mathbf{a}_A + \dot{\boldsymbol{\Omega}} \times AB + \boldsymbol{\Omega} \times (\boldsymbol{\Omega} \times AB) = \mathbf{a}_A + \mathbf{a}_{BA} \tag{5.4}$$

In case of planar motion it simplifies into (Fig. 5.3)

$$\mathbf{a}_B = \mathbf{a}_A + \dot{r}\mathbf{k} \times AB - r^2 AB \tag{5.5}$$

The relative acceleration $\mathbf{a}_{BA} = \mathbf{a}_B - \mathbf{a}_A$ between any two points is proportional to the length $|AB|$ and forms an angle ξ with the segment AB (Fig. 5.3)

$$\tan \xi = \frac{\dot{r}}{r^2} \tag{5.6}$$

[1] By geometric point we mean a point not belonging to the rigid body.

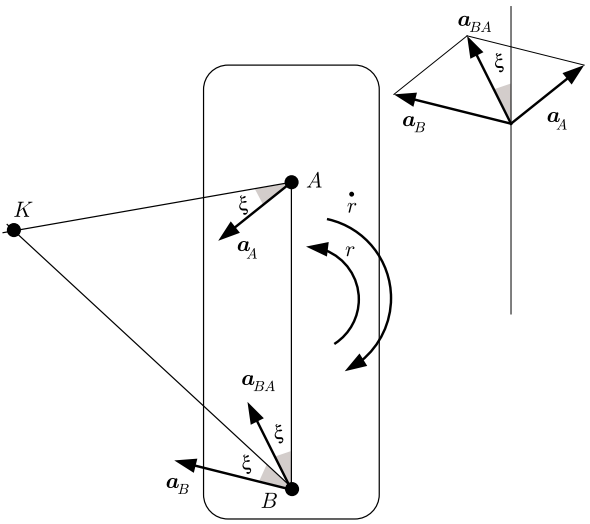

Fig. 5.3 Relationship between the acceleration of two points of the same rigid body in planar motion

It can be shown that in case of planar motion, that is $\boldsymbol{\Omega} = r\mathbf{k}$, and with $r \neq 0$, at any instant there is one point K of the (extended) rigid body that has zero acceleration. In general, $K \neq C$, unless the point C is truly a fixed point, like a fixed hinge. The absolute acceleration of any point A forms an angle ξ with the segment KA, as shown in Fig. 5.3.

Several different names are commonly in use to refer to point K:

- instantaneous center of acceleration;
- acceleration center;
- instantaneous center of zero acceleration.

The velocity and acceleration fields are superimposed in Fig. 5.4.

Let us consider again the rigid wheel rolling on a flat road. For the moment let us also assume that it rolls at constant speed. The center O of the wheel has zero acceleration, and hence it is the acceleration center K, as shown in Fig. 5.5. The acceleration field is centripetal towards $O = K$. It is worth noting that the acceleration of C is not zero

$$\mathbf{a}_C = \mathbf{n}r^2 d \tag{5.7}$$

Comparing Figs. 5.2 and 5.5, we see that there are points, like F_1 and F_2, whose velocity and acceleration have the same direction. They all belong to a circle, called the *inflection circle*. Even if we apply an angular acceleration $\dot{r}$, as in Fig. 5.6, the points on the inflection circle still have collinear velocity and acceleration. The points of the rigid body on the inflection circle, as the name implies, have a trajectory with an inflection point, that is a point with zero curvature.

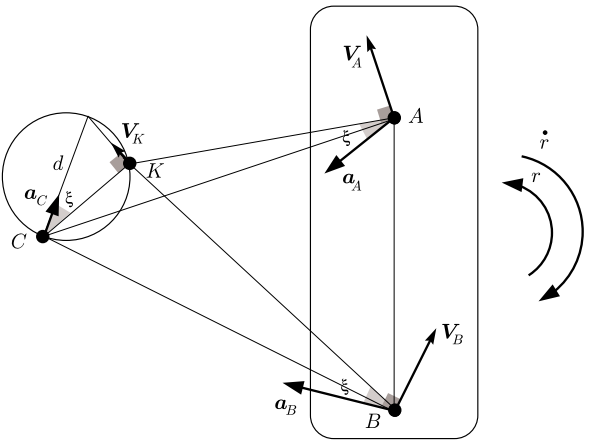

Fig. 5.4 Velocity center, acceleration center and inflection circle

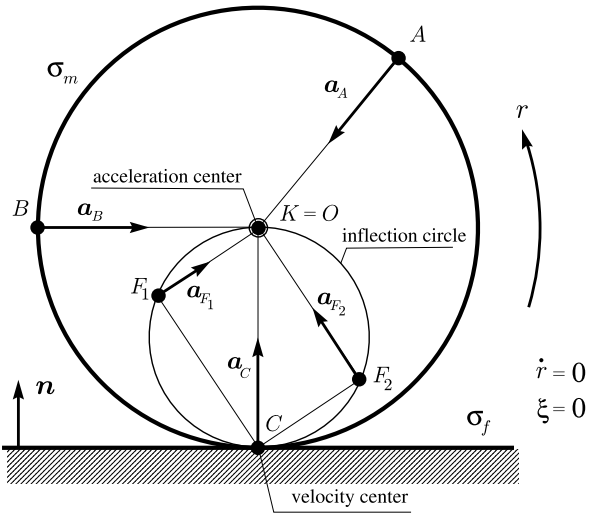

Fig. 5.5 Acceleration field of a rigid wheel rolling at *constant speed* on a flat road

Point C has a marvellous property: its acceleration is not affected by $\dot{r}$. In other words, Eq. (5.7) holds true even if $\dot{r} \neq 0$. Therefore, it is possible to obtain the diameter d of the inflection circle from the knowledge of $\mathbf{a}_C$ and $\dot{r}$.

The inflection circle turns out to be very useful to evaluate the *radius of curvature* of the trajectory of any point of the rigid body. The rule is very simple and it is exemplified in Fig. 5.7. Let us take point A. The center of curvature E_A of its trajectory must fulfill the following relationship

$$|AC|^2 = |AE_A||AF_A| \quad \text{or, more compactly} \quad a^2 = ef \tag{5.8}$$

where E_A and F_A are always on the same side with respect to A (this is why point A is always first in the three terms in (5.8)).

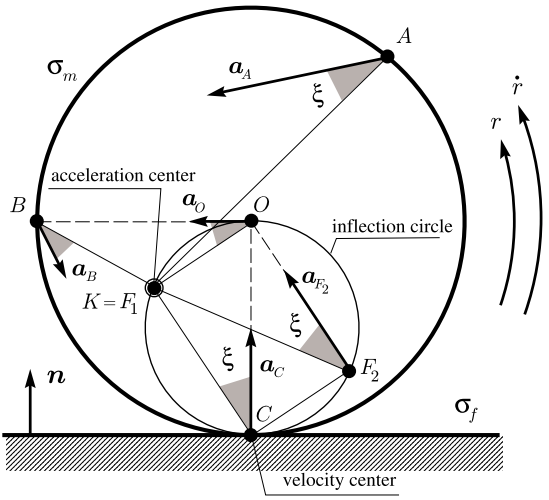

Fig. 5.6 Acceleration field of a rigid wheel rolling at *non-constant speed* on a flat road

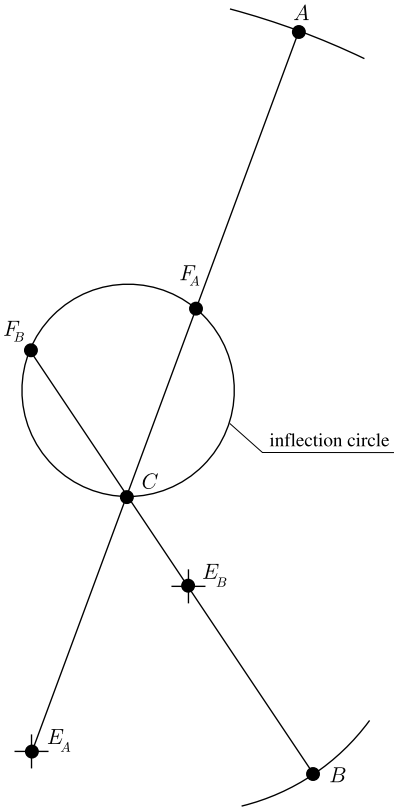

Fig. 5.7 How the inflection circle relates to the centers of curvature of the trajectories of the points of a rigid body

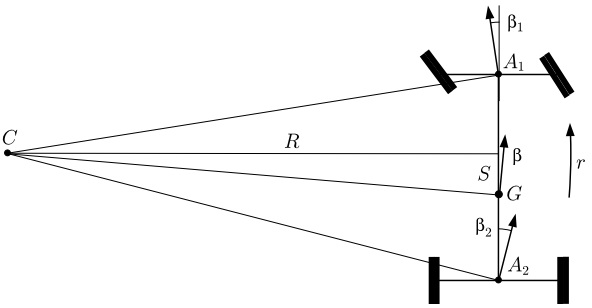

Fig. 5.8 Classical approach to the kinematics of a turning vehicle

Quite interestingly, we can obtain the following formula for the centripetal (normal) component of the acceleration of A

$$\mathbf{a}_A^n = \frac{V_A^2}{|AE_A|} = \frac{(ra)^2}{e} = r^2 f = r^2 |AF_A| \tag{5.9}$$

5.2 The Kinematics of a Turning Vehicle

Driving a vehicle to make a turn amounts, roughly speaking, at forcing it to follow a path with *variable radius of curvature*. The traditional approach looks only at the kinematics for a given instant of time, as shown in Fig. 5.8. This is a good starting point, but not the whole story. For instance, from Fig. 5.8 we cannot know the radius of curvature of the trajectory of G (which, of course, is not equal to CG, in general). But let us make the reasoning more precise.

A vehicle has infinitely many points and hence infinitely many trajectories. However, as a rigid body, these trajectories are not independent to each other. It suffices to look at the trajectory (path) of two points. It is perhaps advisable to select the midpoint A_1 of the front axle and the midpoint A_2 of the rear axle (Fig. 5.8). It is not mandatory at all, but maybe convenient.

Looking at the trajectories also implies monitoring the radii of curvature and how they relate to each other.

To monitor whether a vehicle is performing well, or not so well, we can consider also the fixed and moving centrodes, along with the inflection circle. Indeed, we should have clear in mind that the position of the velocity center C changes continuously in time, thus tracing the two centrodes. Therefore, the two centrodes "contain" all the geometric features of the kinematics of the turning vehicle.

5.2.1 Fixed and Moving Centrodes of a Turning Vehicle

The typical shape of the fixed and moving centrodes of a vehicle making a turn are shown in Figs. 5.9 and 5.10. We see that the moving centrode σ_m is pretty much

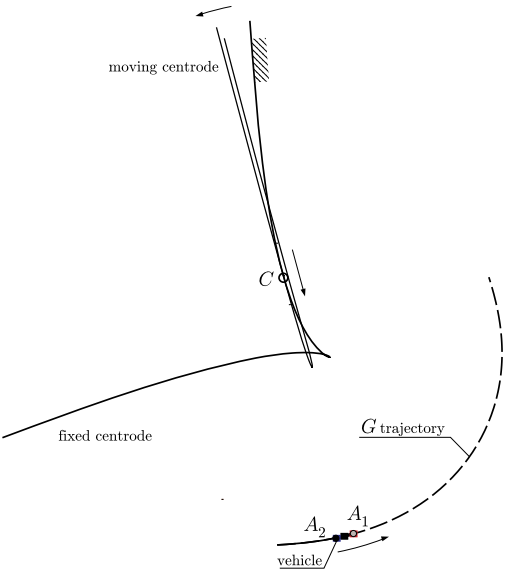

Fig. 5.9 Vehicle *entering a curve*: moving centrode rolling on the fixed centrode

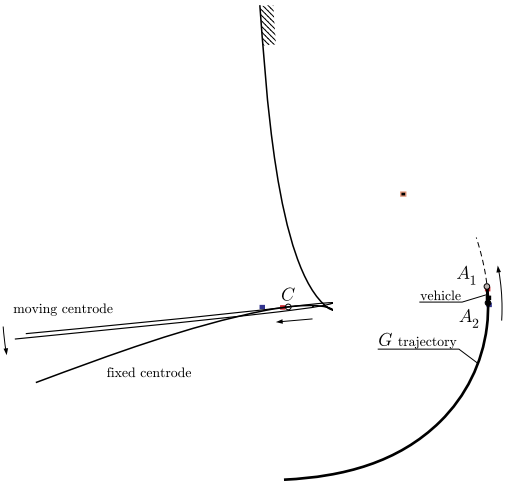

Fig. 5.10 Vehicle *exiting a curve*: moving centrode rolling on the fixed centrode

a straight line, while the fixed centrode σ_f is made of two distinct parts, as is the kinematics of turning: entering the curve and exiting the curve. The velocity center C is the point of rolling contact of the two centrodes.

By definition, the vehicle belongs precisely to the same rigid plane of the moving centrode. They move together.

Actually, the centrodes shown in Figs. 5.9 and 5.10 are typical of a vehicle making a curve the good way. The centrodes changes abruptly if the vehicle does not make the curve properly. This may happen, e.g., if the speed is too high. An example of "bad" centrodes, and hence of bad performance, is shown in Fig. 5.11. We

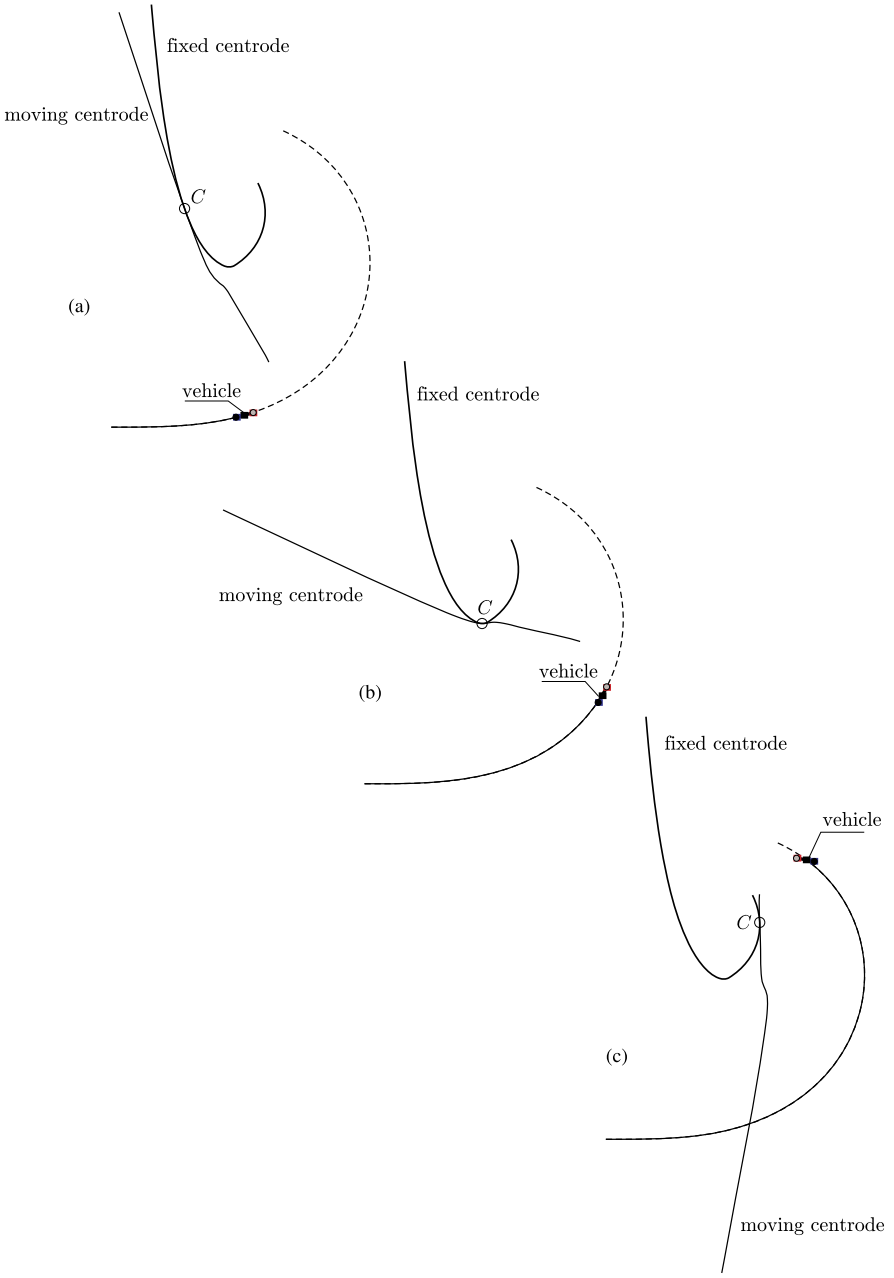

Fig. 5.11 Centrodes of a turning vehicle with handling misbehavior in the final part of the curve (the car goes into a spin)

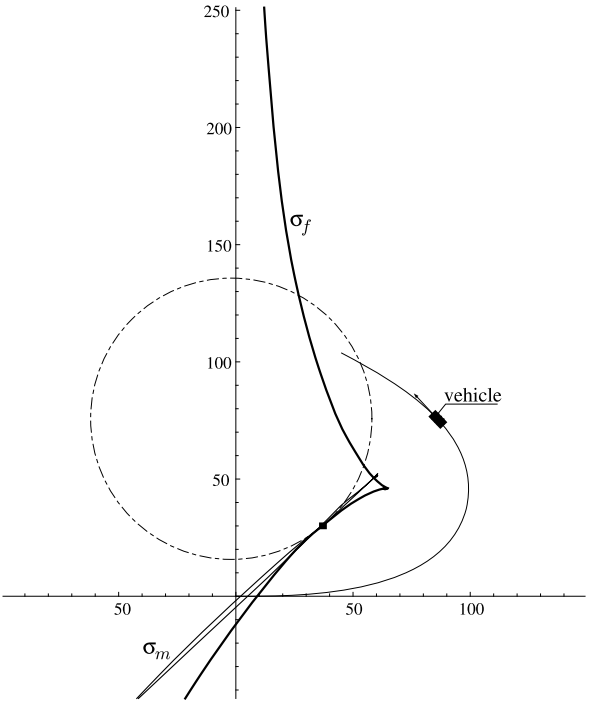

Fig. 5.12 Centrodes of a Formula car making Turn 5 of the Barcelona circuit (the inflection circle is also shown)

see that the centrodes for the exiting phase (Fig. 5.11(c)) are totally different with respect to Fig. 5.10. The vehicle goes into a spin.

Quite interestingly, as shown in Fig. 5.11(b), the two centrodes start having a bad shape although the vehicle still has an apparent good behavior. Therefore, the two centrodes could be used as a warning of handling misbehavior. They depart from the proper shape a little before the vehicle shows unwanted behavior.

To confirm that this is real stuff, we show in Fig. 5.12 the centrodes of a Formula car making Turn 5 of the Barcelona circuit. In this case everything was fine, as confirmed by the "good" shape of both centrodes. Also shown are the trajectory of G and the inflection circle.

But not all laps are the same. Figure 5.13 shows the centrodes for the same curve in a case in which the Formula car does not perform well.

The fixed centrodes for the two cases are compared in Fig. 5.14. The entering part is pretty much the same, whereas the central and the exiting parts are very different. It is worth noting that the trajectories of G are almost the same.

The moving centrodes are compared in Fig. 5.15. Again, they differ markedly in the exiting part.

By definition, the centrodes are generated by the successive positions of the velocity center C.

The moving centrode is given by the successive positions of C in the body-fixed reference system, that is with respect to the vehicle. As already obtained in (3.11),

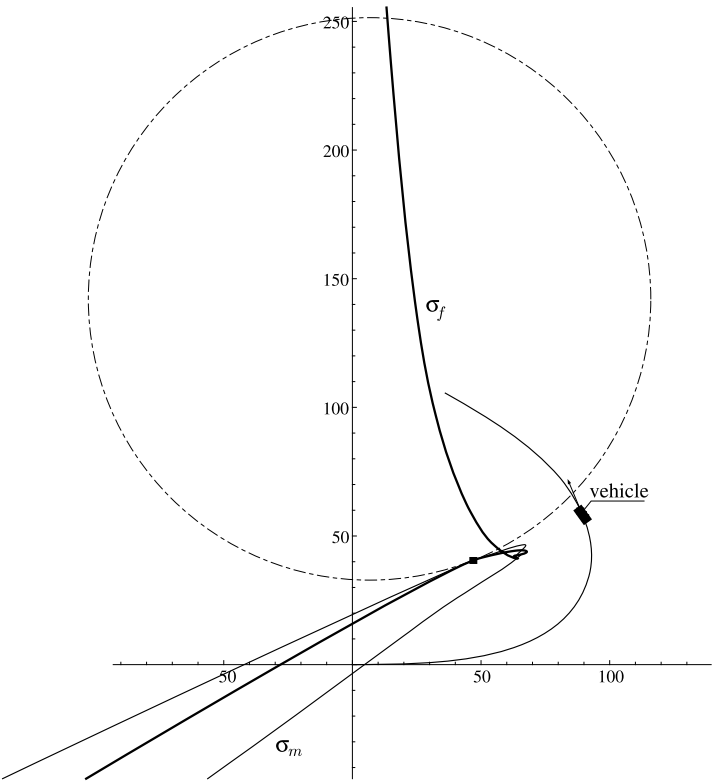

Fig. 5.13 Centrodes of a Formula car *badly* making Turn 5 of the Barcelona circuit (the inflection circle is also shown)

the position of C with respect to the vehicle is given by (Fig. 5.8)

$$GC = S\mathbf{i} + R\mathbf{j} = \mathbf{D} \tag{5.10}$$

where $S = -v/r$ and $R = u/r$. The coordinates (x_f, y_f) of the fixed centrode in the ground-fixed reference system can be obtained from the knowledge of the absolute coordinates of G, given in (3.9), and of the yaw angle (3.8)

$$\begin{aligned} x_f(t) &= x_0^G(t) + S(t)\cos\psi(t) - R(t)\sin\psi(t) \\ y_f(t) &= y_0^G(t) + S(t)\sin\psi(t) + R(t)\cos\psi(t) \end{aligned} \tag{5.11}$$

5.2.2 *Inflection Circle*

The inflection circle, that is all those points whose trajectory have an inflection point, can be easily obtained at any instant of time from the telemetry data. Here we list,

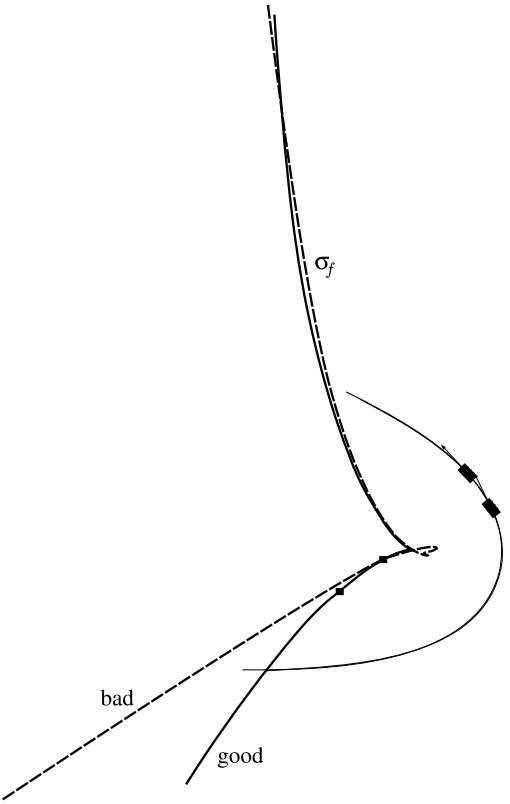

Fig. 5.14 Comparison of the fixed centrodes and of the trajectories of a Formula car making Turn 5 of the Barcelona circuit

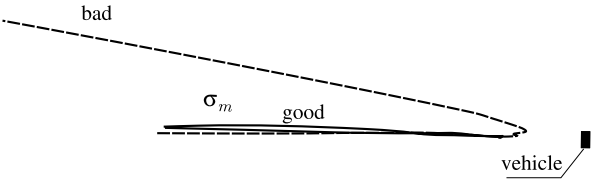

Fig. 5.15 Comparison of the moving centrodes of a Formula car making Turn 5 of the Barcelona circuit

with reference to Fig. 5.16, some relevant formulæ

$$d = \frac{1}{r^2}\sqrt{\left(\frac{\dot{v}r - v\dot{r}}{r}\right)^2 + \left(\frac{\dot{u}r - u\dot{r}}{r}\right)^2} = \sqrt{\frac{\dot{R}^2 + \dot{S}^2}{r^2}} \tag{5.12}$$

$$d\sin\chi = \left(\frac{\dot{v}r - v\dot{r}}{r}\right)\frac{1}{r^2} = -\frac{\dot{S}}{r} \tag{5.13}$$

$$d\cos\chi = \left(\frac{\dot{u}r - u\dot{r}}{r}\right)\frac{1}{r^2} = \frac{\dot{R}}{r} \tag{5.14}$$

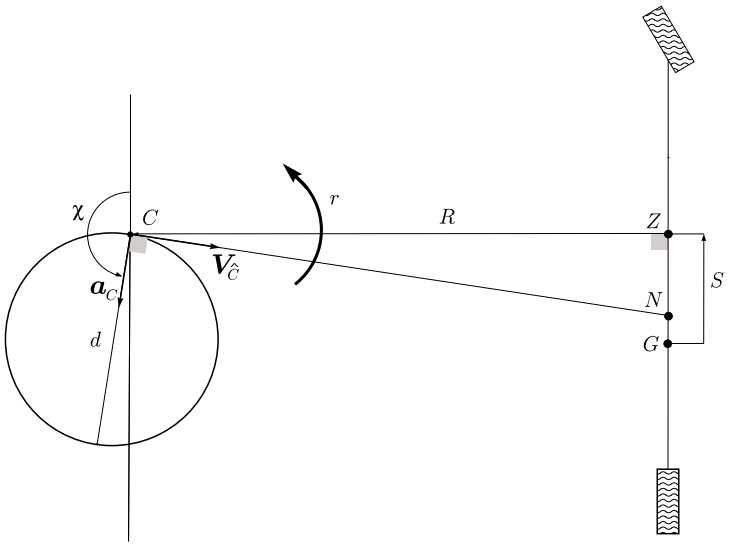

Fig. 5.16 Inflection circle and definition of some relevant quantities

$$\mathbf{d} = d\cos\chi\,\mathbf{i} + d\sin\chi\,\mathbf{j} = \frac{\dot{R}\mathbf{i} - \dot{S}\mathbf{j}}{r} \tag{5.15}$$

$$\mathbf{a}_C = r^2 d(\cos\chi\,\mathbf{i} + \sin\chi\,\mathbf{j}) = r^2\mathbf{d} = r(\dot{R}\mathbf{i} - \dot{S}\mathbf{j}) \tag{5.16}$$

$$\mathbf{V}_{\hat{C}} = rd(-\sin\chi\,\mathbf{i} + \cos\chi\,\mathbf{j}) = \dot{S}\mathbf{i} + \dot{R}\mathbf{j} \tag{5.17}$$

$$\dot{\mathbf{D}} = \dot{S}\mathbf{i} + \dot{R}\mathbf{j} - S\dot{\chi}\mathbf{j} + R\dot{\chi}\mathbf{i} = (\dot{S} + R\dot{\chi})\mathbf{i} + (\dot{R} - S\dot{\chi})\mathbf{j} \tag{5.18}$$

$$\dot{d} = \frac{1}{r^3 d}\left[r(\dot{R}\ddot{R} + \dot{S}\ddot{S}) - \dot{r}\left(\dot{R}^2 + \dot{S}^2\right)\right] \tag{5.19}$$

$$\frac{\mathrm{d}}{\mathrm{d}t}\left(\frac{\mathbf{D}}{d}\right) = \frac{\dot{\mathbf{D}}d - \mathbf{D}\dot{d}}{d^2} = \frac{1}{d^2}\left\{\left[(\dot{S} + R\dot{\chi})d - S\dot{d}\right]\mathbf{i} + \left[(\dot{R} - S\dot{\chi})d - R\dot{d}\right]\mathbf{j}\right\} \tag{5.20}$$

$$r(\mathbf{d}\cdot\mathbf{D}) = \dot{R}S - R\dot{S} \tag{5.21}$$

They cover many aspects, like:

- the diameter d of the inflection circle;
- its orientation χ with respect to the vehicle;
- the speed $\mathbf{V}_{\hat{C}}$ of the geometric point $\hat{C}$;
- the acceleration $\mathbf{a}_C$ of the velocity center C;
- the rate of change of d;
- the rate of change of $GC = \mathbf{D}$.

It is worth noting that almost all quantities depend on r, $\dot{R}$ and $\dot{S}$.

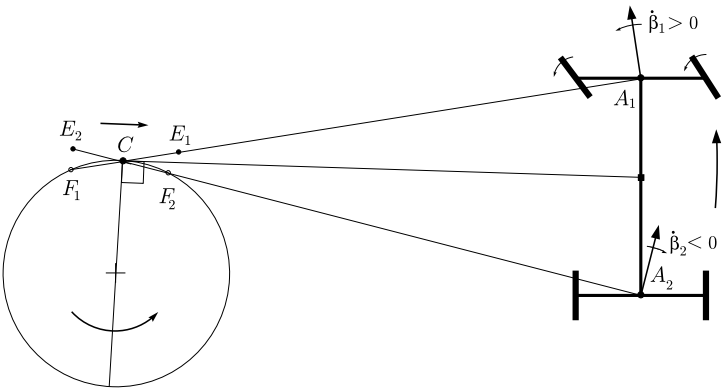

Fig. 5.17 Radii of curvature of a vehicle entering a turn properly

Along the axis of the vehicle there are, at any instant of time, some special points (Fig. 5.16). Point Z has zero slip angle, that is, $\beta_Z = 0$, or equivalently $\mathbf{V}_Z = u\mathbf{i}$. Point N has $\dot{\beta}_N = 0$.

5.2.3 Variable Curvatures

To truly understand the kinematics of a turning vehicle, we must also consider the curvature of the trajectories and how they change in time under the driver action on the steering wheel. In particular, we monitor the trajectories of the midpoints A_1 and A_2 of both axles, and their centers of curvature E_1 and E_2, respectively. There is a nice interplay between radii of curvature, the velocity center and the inflection circle.

The entering phase of making a turn is characterized by increasing steer angles and diminishing radii of curvature. Moreover, the velocity center C gets closer and closer to the vehicle. The corresponding kinematics is shown in Fig. 5.17. It is worth noting that, according to (5.8), the radius of curvature of point A_1 is equal to E_1A_1, and hence it is shorter than CA_1. On the contrary, the radius of curvature of point A_2 is equal to E_2A_2, which is longer than CA_2. This happens because the vehicle slip angle β_1 at point A_1 is increasing, while the vehicle slip angle β_2 at point A_2 is diminishing (in the sense that it gets bigger, but it is negative), as shown in Fig. 5.17.

The formulæ that substantiate this reasoning are as follows

$$\rho_G = \frac{r + \dot{\beta}}{u/\cos\beta} = \left[\frac{r}{u} + \frac{\dot{v}u - v\dot{u}}{u^3}\right]\cos\beta \tag{5.22}$$

$$\rho_1 = \frac{r + \dot{\beta}_1}{u/\cos\beta_1} = \left[\frac{r}{u} + \frac{(\dot{v} + a_1\dot{r})u - (v + a_1 r)\dot{u}}{u^3}\right]\cos\beta_1 \tag{5.23}$$

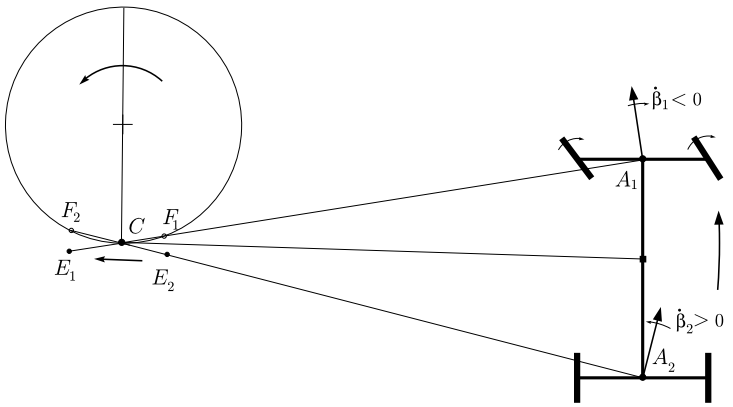

Fig. 5.18 Radii of curvature of a vehicle exiting a turn properly

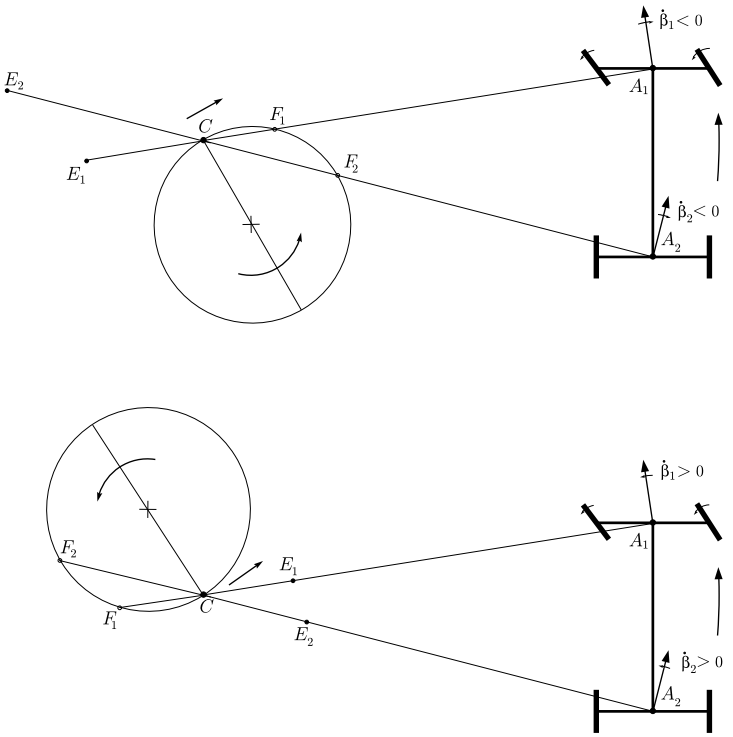

Fig. 5.19 Examples of undesirable kinematics in a turn

$$\rho_2 = \frac{r + \dot{\beta}_2}{u/\cos\beta_2} = \left[\frac{r}{u} + \frac{(\dot{v} - a_2\dot{r})u - (v - a_2 r)\dot{u}}{u^3}\right]\cos\beta_2 \tag{5.24}$$

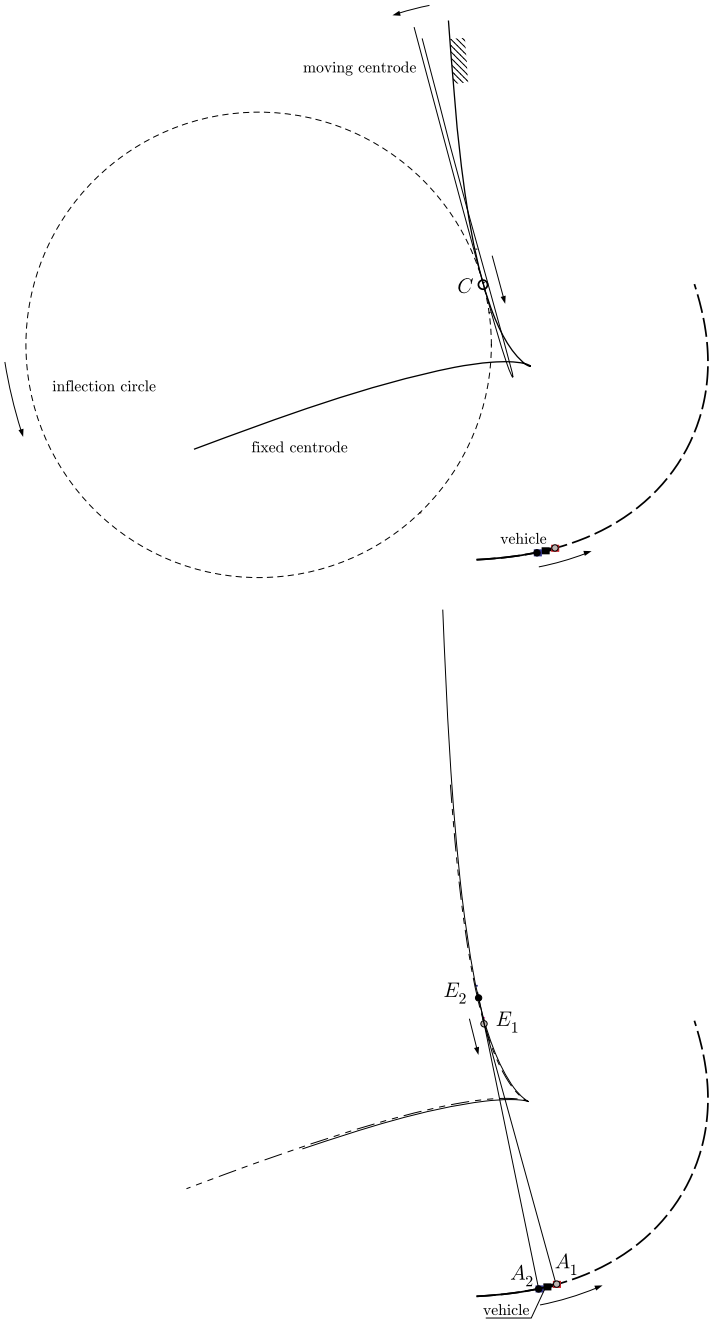

Fig. 5.20 Vehicle *entering* a curve: inflection circle (*top*) and centers of curvatures with the corresponding evolutes (*bottom*)

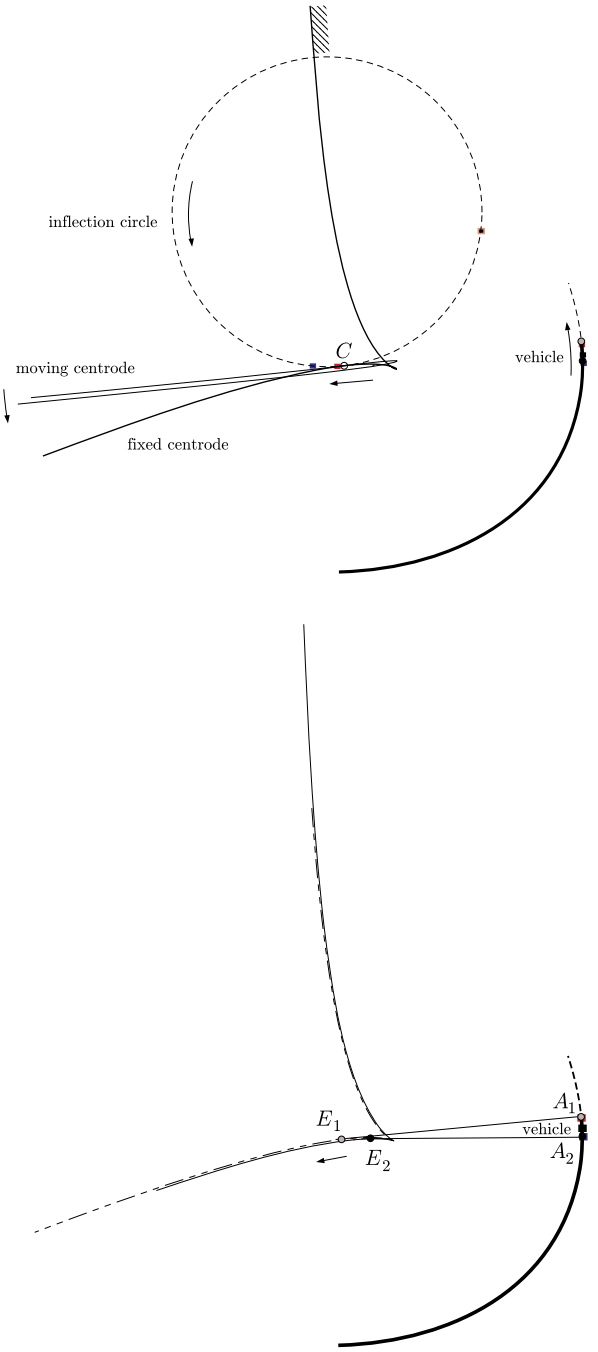

Fig. 5.21 Vehicle *exiting* a curve: inflection circle (*top*) and centers of curvatures with the corresponding evolutes (*bottom*)

$$\cos\beta = \frac{u}{\sqrt{u^2+v^2}} \tag{5.25}$$

$$\cos\beta_1 = \frac{u}{\sqrt{(v+a_1 r)^2+u^2}} \tag{5.26}$$

$$\cos\beta_2 = \frac{u}{\sqrt{(v-a_2 r)^2+u^2}} \tag{5.27}$$

$$\frac{\dot{\beta}_1}{u} \simeq \rho_1 - \frac{r}{u} \tag{5.28}$$

$$\frac{\dot{\beta}_2}{u} \simeq \rho_2 - \frac{r}{u} \tag{5.29}$$

where ρ_i are the curvatures, that is the inverse of the radii of curvature.

The kinematics of a vehicle exiting properly a turn is shown in Fig. 5.18. We see that many things go the other way around with respect to entering.

In both cases, the knowledge of the inflection circle immediately makes clear the relationship between the position of the velocity center C and the centers of curvature E_1 and E_2.

But things may go wrong. Bad kinematic behaviors are shown in Fig. 5.19. We see that the time derivatives of β_1 and β_2 are not as they should be. Indeed, point C is travelling also longitudinally. Again, the positions and orientations of the inflection circle immediately conveys the information about the unwanted kinematics.

But, let us go back to good turning. The *evolute* of a curve is the locus of all its centers of curvature. The evolutes of the trajectories of points A_1 and A_2, that is the midpoints of each axle, are shown in the lower part of Figs. 5.20 and 5.21. Also shown are the centers of curvature E_1 and E_2 at a given instant of time, along with the corresponding inflection circle (this one drawn in the upper part with the centrodes). We see that the two evolutes are almost coincident. The relative positions of E_1 and E_2 are consistent with Figs. 5.17 and 5.18.

References

1. Bottema O (1979) Theoretical kinematics. Dover, New York
2. Heißing B, Ersoy M (eds) (2011) Chassis handbook. Springer, Wiesbaden
3. Pytel A, Kiusalaas J (1999) Engineering mechanics—statics. Brooks/Cole, Pacific Grove
4. Rossa FD, Mastinu G, Piccardi C (2012) Bifurcation analysis of an automobile model negotiating a curve. Veh Syst Dyn 50(10):1539–1562
5. Waldron KJ, Kinzel GL (2004) Kinematics, dynamics and design of machinery. Wiley, New York

Chapter 6
Handling of Road Cars

Ordinary road cars are by far the most common type of motor vehicle. Almost all of them share the following features relevant to handling:

(1) four wheels (two axles);
(2) two-wheel drive;
(3) open differential;
(4) no wings (and hence, no significant aerodynamic downforces);
(5) no intervention by electronic active safety systems like ABS or ESP under ordinary operating conditions.

The handling analysis of this kind of vehicles is somehow the simplest that can be envisaged.[1] Moreover, it is typically assumed that the vehicle moves on a flat road at almost constant forward speed u, thus requiring small longitudinal forces by the tires.

The analysis developed here is based on the general vehicle model introduced in Chap. 3. Owing to the above listed features, it will be possible to study the handling of road cars by means of the celebrated *single track model*. However, all steps that lead to the single track model will be thoroughly discussed.

6.1 Open Differential

We start by investigating when, in the global equilibrium equations (3.64), the longitudinal forces do not contribute to the yaw moment N, that is

$$\Delta X_i = 0 \tag{6.1}$$

[1] Some sports cars and all race cars have a limited slip differential. Several race cars also have wings which provide fairly high aerodynamic downforces at high speed. The handling of these vehicles is somehow more involved than that of ordinary road cars and will be addressed in Chap. 7.

M. Guiggiani, *The Science of Vehicle Dynamics*, DOI 10.1007/978-94-017-8533-4_6,

The main requirement is that the vehicle be equipped with an *open differential*. Since there is almost no friction inside an open differential mechanism, we have $\eta_h \simeq 1$ in (3.132), and hence $M_l \simeq M_r$. In other words, the driving wheels receive the same torque by the engine.

Moreover, if the forward speed u is almost constant ($\dot{u} \simeq 0$) and the aerodynamic drag is not very high (like in ordinary cars, but not in a Formula 1 car, which, however, does not have an open differential),[2] the longitudinal forces are quite small. That means that also the *longitudinal slips are small and can be neglected*. Therefore,

$$\begin{aligned} F_{x_{ij}} &\simeq 0 \\ \sigma_{x_{ij}} &\simeq 0 \end{aligned} \tag{6.2}$$

which, according to (3.45), means that the rolling velocities ω_{ij} of each wheel are given by

$$\begin{aligned} \omega_{11} r_1 &= (u - rt_1/2)\cos(\delta_{11}) + (v + ra_1)\sin(\delta_{11}) \simeq u - rt_1/2 \\ \omega_{12} r_1 &= (u + rt_1/2)\cos(\delta_{12}) + (v + ra_1)\sin(\delta_{12}) \simeq u + rt_1/2 \\ \omega_{21} r_2 &= (u - rt_2/2)\cos(\delta_{21}) - (v - ra_2)\sin(\delta_{21}) \simeq u - rt_2/2 \\ \omega_{22} r_2 &= (u + rt_2/2)\cos(\delta_{22}) - (v - ra_2)\sin(\delta_{22}) \simeq u + rt_2/2 \end{aligned} \tag{6.3}$$

that is, all wheels are almost under longitudinal pure rolling conditions.

6.2 Fundamental Equations of Vehicle Handling

The vehicle has basically only lateral and yaw dynamics (often simply called lateral dynamics), described by the following differential equations (cf. (3.64))

$$\begin{aligned} ma_y &= Y = Y_1 + Y_2 \\ J_z \dot{r} &= N = Y_1 a_1 - Y_2 a_2 \end{aligned} \tag{6.4}$$

while

$$ma_x = mvr = X = X_1 + X_2 - \frac{1}{2}\rho S C_x u^2 \tag{6.5}$$

is now an algebraic equation, the unknown being $(X_1 + X_2)$.

[2] The left and right wheels of the same axle are normally equipped with the same kind of brake. Therefore, the braking torque is pretty much the same under ordinary operating conditions, and, again, (6.1) holds true. However, there are important exceptions. The left and right braking forces can be different if: (a) the grip is different and one wheel is locked; (b) the friction coefficients inside the two brakes is different (for instance, because of different temperatures, which is often the case in racing cars); (c) some electronic stability system, like ESP or ABS, has been activated.

With an open differential, it is easy to solve (6.4) with respect to the front and rear lateral forces

$$\begin{aligned} Y_1 &= \frac{ma_2}{l}a_y + \frac{J_z}{l}\dot{r} \simeq \frac{ma_2}{l}a_y \\ Y_2 &= \frac{ma_1}{l}a_y - \frac{J_z}{l}\dot{r} \simeq \frac{ma_1}{l}a_y \end{aligned} \tag{6.6}$$

where we took into account that $|J_z\dot{r}| \ll |ma_y a_i|$, since in a car $J_z < ma_1a_2$ and $|\dot{r}a_i| \ll |a_y|$. In a *two-axle* vehicle with *open differential* the lateral forces are *linear* functions of the lateral acceleration a_y. This is a very peculiar and important result, which greatly impacts on the whole vehicle model, as will be shown.

According to (3.114) and (3.115), the lateral load transfers are linear functions of Y_1 and Y_2. Employing (6.6) we obtain the following simplified equations for load transfers in vehicles with open differential

$$\begin{aligned} \Delta Z_1 &\simeq ma_y \frac{k_{\phi_1}k_{\phi_2}}{t_1 k_\phi}\left[\frac{h-q}{k_{\phi_2}} + \frac{a_2q_1}{lk^s_{\phi_1}} + \frac{a_2q_1}{lk^s_{\phi_2}} + \frac{a_2q_1 + a_1q_2}{lk^p_{\phi_2}}\right] = ma_y\eta_1 \\ \Delta Z_2 &\simeq ma_y \frac{k_{\phi_1}k_{\phi_2}}{t_2 k_\phi}\left[\frac{h-q}{k_{\phi_1}} + \frac{a_1q_2}{lk^s_{\phi_1}} + \frac{a_1q_2}{lk^s_{\phi_2}} + \frac{a_2q_1 + a_1q_2}{lk^p_{\phi_1}}\right] = ma_y\eta_2 \end{aligned} \tag{6.7}$$

The two constants η_1 and η_2 depend, in a peculiar way, on the roll stiffnesses, on the heights of the no-roll centers[3] and on the longitudinal position of the center of gravity.

Similarly, the suspension roll angles (3.110) can be set as functions of the lateral acceleration only[4]

$$\begin{aligned} \phi^s_1 &= ma_y \frac{1}{k^s_{\phi_1}}\frac{k_{\phi_1}k_{\phi_2}}{k_\phi}\left[\frac{h-q}{k_{\phi_2}} + \frac{a_2q_1}{lk^p_{\phi_1}} - \frac{a_1q_2}{lk^p_{\phi_2}}\right] = ma_y\rho^s_1 \\ \phi^s_2 &= ma_y \frac{1}{k^s_{\phi_2}}\frac{k_{\phi_1}k_{\phi_2}}{k_\phi}\left[\frac{h-q}{k_{\phi_1}} + \frac{a_1q_2}{lk^p_{\phi_1}} - \frac{a_2q_1}{lk^p_{\phi_1}}\right] = ma_y\rho^s_2 \end{aligned} \tag{6.8}$$

The same applies to tire roll angles ϕ^p_i

$$\begin{aligned} \phi^p_1 &= ma_y \frac{1}{k^p_{\phi_1}}\frac{k_{\phi_1}k_{\phi_2}}{k_\phi}\left[\frac{h-q}{k_{\phi_2}} + \frac{a_2q_1}{lk^s_{\phi_1}} + \frac{a_2q_1}{lk^s_{\phi_2}} + \frac{a_2q_1 + a_1q_2}{lk^p_{\phi_2}}\right] = ma_y\rho^p_1 \\ \phi^p_2 &= ma_y \frac{1}{k^p_{\phi_2}}\frac{k_{\phi_1}k_{\phi_2}}{k_\phi}\left[\frac{h-q}{k_{\phi_1}} + \frac{a_1q_2}{lk^s_{\phi_1}} + \frac{a_1q_2}{lk^s_{\phi_2}} + \frac{a_2q_1 + a_1q_2}{lk^p_{\phi_1}}\right] = ma_y\rho^p_2 \end{aligned} \tag{6.9}$$

If, for simplicity, the tires are supposed to be perfectly rigid, that is $k^p_{\phi_i} \to \infty$, we have $\rho^p_1 = \rho^p_2 = 0$, $\rho^s_1 = \rho^s_2 = (h-q)/k_\phi$ and the expressions of the lateral load

[3] We call no-roll center what is commonly called roll center. This aspect is discussed in Sect. 3.8.8.

[4] In this model the roll inertial effects are totally disregarded.

transfers become simpler

$$\begin{aligned}\Delta Z_1 &\simeq m a_y \frac{1}{t_1}\left[\frac{k_{\phi_1}(h-q)}{k_\phi}+\frac{a_2 q_1}{l}\right]=m a_y \eta_1\\ \Delta Z_2 &\simeq m a_y \frac{1}{t_2}\left[\frac{k_{\phi_2}(h-q)}{k_\phi}+\frac{a_1 q_2}{l}\right]=m a_y \eta_2\end{aligned} \tag{6.10}$$

as in (3.118).

The total vertical loads (3.79) on each tire can also be simplified by discarding the longitudinal load transfer. Moreover, cars with an open differential are not so sporty to have significant aerodynamic vertical loads. Therefore, combining (3.79) and (6.7), we get

$$\begin{aligned}Z_{11}=F_{z_{11}}&=\frac{mga_2}{2l}-m a_y \eta_1=\frac{Z_1^0}{2}-\Delta Z_1(a_y)\\ Z_{12}=F_{z_{12}}&=\frac{mga_2}{2l}+m a_y \eta_1=\frac{Z_1^0}{2}+\Delta Z_1(a_y)\\ Z_{21}=F_{z_{21}}&=\frac{mga_1}{2l}-m a_y \eta_2=\frac{Z_2^0}{2}-\Delta Z_2(a_y)\\ Z_{22}=F_{z_{22}}&=\frac{mga_1}{2l}+m a_y \eta_2=\frac{Z_2^0}{2}+\Delta Z_2(a_y)\end{aligned} \tag{6.11}$$

which shows that all vertical loads are (linear) function of the lateral acceleration.

According to (3.123) and taking into account (6.8), we get the following expression for the steering angles of the wheels

$$\begin{aligned}\delta_{ij}&=\delta_{ij}^0+\delta_v\tau_{ij}+\Upsilon_{ij}\phi_i^s(a_y)\\ &=\delta_{ij}^0+\delta_v\tau_{ij}+\Upsilon_{ij}\rho_i^s a_y\\ &=\delta_{ij}(\delta_v,a_y)\end{aligned} \tag{6.12}$$

which are functions of δ_v and, again, of the lateral acceleration a_y. More precisely, the term $\delta_v\tau_{ij}$ is the steer angle due to the steering wheel rotation δ_v, the term δ_{ij}^0 is the toe-in/out angle , and the term $\Upsilon_{ij}\phi_i^s(a_y)$ is the roll steer angle.

Under the assumed operating conditions (6.3), the tire lateral slips (3.49) become

$$\begin{aligned}\sigma_{y_{11}}&=\frac{(v+ra_1)-u\delta_{11}}{u-rt_1/2}\simeq\frac{v+ra_1}{u}-\delta_{11}\\ \sigma_{y_{12}}&=\frac{(v+ra_1)-u\delta_{12}}{u+rt_1/2}\simeq\frac{v+ra_1}{u}-\delta_{12}\end{aligned} \tag{6.13}$$

$$\sigma_{y_{21}} = \frac{(v - ra_2) - u\delta_{21}}{u - rt_2/2} \simeq \frac{v - ra_2}{u} - \delta_{21}$$
$$\sigma_{y_{22}} = \frac{(v - ra_2) - u\delta_{22}}{u + rt_2/2} \simeq \frac{v - ra_2}{u} - \delta_{22}$$

since $u \gg |rt_i/2|$ as discussed in (3.4). The lateral slips can be conveniently rewritten taking (6.12) into account

$$\begin{aligned}
\sigma_{y_{11}} &= \frac{v + ra_1}{u} - \delta_v \tau_{11} - \delta_{11}^0 - \Upsilon_{11}\rho_1^s a_y \\
\sigma_{y_{12}} &= \frac{v + ra_1}{u} - \delta_v \tau_{12} - \delta_{12}^0 - \Upsilon_{12}\rho_1^s a_y \\
\sigma_{y_{21}} &= \frac{v - ra_2}{u} - \delta_v \tau_{21} - \delta_{21}^0 - \Upsilon_{21}\rho_2^s a_y \\
\sigma_{y_{22}} &= \frac{v - ra_2}{u} - \delta_v \tau_{22} - \delta_{22}^0 - \Upsilon_{22}\rho_2^s a_y
\end{aligned} \tag{6.14}$$

or, more compactly[5]

$$\sigma_{y_{ij}} = \sigma_{y_{ij}}(v, r, u, \delta_v) = \sigma_{y_{ij}}(\beta, \rho, a_y, \delta_v) \tag{6.15}$$

Let, $\gamma_{i1}^0 = -\gamma_{i2}^0 = \gamma_i^0$ be the camber angles under static conditions, and let $\Delta\gamma_{i1} = \Delta\gamma_{i2} = \Delta\gamma_i$ be the camber variations. The camber angles of the two wheels of the same axle are thus given by

$$\gamma_{i1} = \gamma_i^0 + \Delta\gamma_i, \qquad \gamma_{i2} = -\gamma_i^0 + \Delta\gamma_i \tag{6.16}$$

where the camber variation $\Delta\gamma_i$, according to (3.83), (6.8) and (6.9), depends on the lateral acceleration a_y

$$\Delta\gamma_i \simeq m a_y \left[\left(\frac{q_i - b_i}{b_i} \right) \rho_i^s - \rho_i^p \right] = m a_y \chi_i \tag{6.17}$$

since the track variation term $\Delta t_i/(2b_i)$ is usually negligible.

The lateral forces exerted by the tires on the vehicle depend on many quantities, as shown in the second equation in (2.72). For sure, there is a strong dependence on the vertical loads Z_{ij} and on the lateral slips $\sigma_{y_{ij}}$, while, in this model, we can neglect the longitudinal slips $\sigma_{x_{ij}}$. The camber angles γ_{ij} need to be considered, since they are quite influential, even if small. According to (3.125), the spin slips φ_{ij} are directly related to γ_{ij}. Therefore, the simplified model for each lateral force is

$$F_{y_{ij}} = F_{y_{ij}}\left(Z_i^0/2 - \Delta Z_i(a_y), \gamma_i^0 + \Delta\gamma_i(a_y), \sigma_{y_{ij}}(v, r, u, \delta_v)\right) \cos\left(\delta_{ij}(\delta_v)\right) \tag{6.18}$$

[5] Here we are abusing the notation: different functions bear the same name. However, the meaning should be sufficiently clear and unambiguous.

The lateral force Y_i for each axle is obtained by adding the lateral forces of the left tire and of the right tire (cf. (3.58))

$$Y_i = F_{y_{i1}} \cos\big(\delta_{i1}(\delta_v)\big) + F_{y_{i2}} \cos\big(\delta_{i2}(\delta_v)\big) \tag{6.19}$$

or, more explicitly, taking also (6.15) into account

$$\begin{aligned} Y_1 &= F_{y_{11}}\big(Z_1^0/2 - \Delta Z_1(a_y), \gamma_1^0 + \Delta\gamma_1(a_y), \sigma_{y_{11}}(v, r, u, \delta_v)\big)\cos\big(\delta_{11}(\delta_v)\big) \\ &\quad + F_{y_{12}}\big(Z_1^0/2 + \Delta Z_1(a_y), -\gamma_1^0 + \Delta\gamma_1(a_y), \sigma_{y_{12}}(v, r, u, \delta_v)\big)\cos\big(\delta_{12}(\delta_v)\big) \\ &= Y_1(v, r, u, \delta_v) = Y_1(\beta, \rho, a_y, \delta_v) \\ Y_2 &= F_{y_{21}}\big(Z_2^0/2 - \Delta Z_2(a_y), \gamma_2^0 + \Delta\gamma_2(a_y), \sigma_{y_{21}}(v, r, u, \delta_v)\big)\cos\big(\delta_{21}(\delta_v)\big) \\ &\quad + F_{y_{22}}\big(Z_2^0/2 + \Delta Z_2(a_y), -\gamma_2^0 + \Delta\gamma_2(a_y), \sigma_{y_{22}}(v, r, u, \delta_v)\big)\cos\big(\delta_{22}(\delta_v)\big) \\ &= Y_2(v, r, u, \delta_v) = Y_2(\beta, \rho, a_y, \delta_v) \end{aligned} \tag{6.20}$$

The effects of a_y on the steering angles δ_{ij} can be neglected in the cosine terms because they are very small. On the other hand, these effects are very influential on the congruence equations (6.14).

It must be clearly understood that the functions in (6.20) are known functions.

6.3 Double Track Model

By double track model we mean actually a four-wheel dynamical model of the vehicle. The governing equations are promptly obtained. It suffices to insert (6.20) into (6.4)

$$\begin{aligned} m(\dot v + ur) &= Y_1(v, r, u, \delta_v) + Y_2(v, r, u, \delta_v) \\ J_z\dot r &= Y_1(v, r, u, \delta_v)a_1 - Y_2(v, r, u, \delta_v)a_2 \end{aligned} \tag{6.21}$$

The double track model is a dynamical system with two state variables (namely, but not necessarily, $v(t)$ and $r(t)$, as discussed in Sect. 6.5).

A general comment on this vehicle model is in order here: most quantities depend (linearly) on the lateral acceleration a_y. However, it must be remarked that this peculiarity needs an open differential, no aerodynamic forces, almost constant forward speed.

Unfortunately, the double track model is not as popular as the *single track model* (often and mistakenly also named "bicycle model"). The goal of the next sections is to present a comprehensive analysis of the single track model [1–4, 7, 8], thus showing also its limitations.

It is a useful model, particularly for educational purposes, but good vehicle engineers should be well aware of the steps taken to simplify the model, and hence realize that in some cases the single track model can be not only useless, but even misleading, depending on which aspects they are interested in.

In many courses on vehicle dynamics, unfortunately, the single track model is proposed without explaining in detail why, despite its awful appearance, it can provide useful insights into vehicle handling.

6.4 Single Track Model

To go from the double track to the single track model we need the following additional assumption: *the left and right gear ratio of the steering system are almost equal*, that is

$$(\tau_{11} = \tau_{12}) = \tau_1 \quad \text{and} \quad (\tau_{21} = \tau_{22}) = \tau_2 \tag{6.22}$$

which is consistent with small steering angles, that is $\cos(\delta_{ij}) \simeq 1$. This (not-so-true) hypothesis, if combined with (6.14), leads to

$$\begin{aligned}
\sigma_{y_{11}} &= \left(\frac{v + ra_1}{u} - \delta_v \tau_1\right) - \delta_{11}^0 - \Upsilon_{11}\rho_1^s a_y \\
\sigma_{y_{12}} &= \left(\frac{v + ra_1}{u} - \delta_v \tau_1\right) - \delta_{12}^0 - \Upsilon_{12}\rho_1^s a_y \\
\sigma_{y_{21}} &= \left(\frac{v - ra_2}{u} - \delta_v \tau_2\right) - \delta_{21}^0 - \Upsilon_{21}\rho_2^s a_y \\
\sigma_{y_{22}} &= \left(\frac{v - ra_2}{u} - \delta_v \tau_2\right) - \delta_{22}^0 - \Upsilon_{22}\rho_2^s a_y
\end{aligned} \tag{6.23}$$

Here, it is convenient to define (cf. (3.43)) what can be called the *apparent* slip angles α_1 and α_2 of the front and rear axle, respectively

$$\begin{aligned}
\alpha_1 &= \delta_v \tau_1 - \frac{v + ra_1}{u} = \alpha_1(v, r; u, \delta_v) \\
\alpha_2 &= \delta_v \tau_2 - \frac{v - ra_2}{u} = \alpha_2(v, r; u, \delta_v)
\end{aligned} \tag{6.24}$$

Combining (6.23) and (6.24), we obtain that both front lateral slips $\sigma_{y_{1i}}$ are *known* functions of only two variables, namely α_1 and a_y. Similarly, both rear lateral slips are *known* functions of α_2 and a_y

$$\begin{aligned}
\sigma_{y_{11}} &= -\alpha_1 - \delta_{11}^0 - \Upsilon_{11}\rho_1^s a_y = \sigma_{y_{11}}(\alpha_1, a_y) \\
\sigma_{y_{12}} &= -\alpha_1 - \delta_{12}^0 - \Upsilon_{12}\rho_1^s a_y = \sigma_{y_{12}}(\alpha_1, a_y) \\
\sigma_{y_{21}} &= -\alpha_2 - \delta_{21}^0 - \Upsilon_{21}\rho_2^s a_y = \sigma_{y_{21}}(\alpha_2, a_y) \\
\sigma_{y_{22}} &= -\alpha_2 - \delta_{22}^0 - \Upsilon_{22}\rho_2^s a_y = \sigma_{y_{22}}(\alpha_2, a_y)
\end{aligned} \tag{6.25}$$

This is the peculiar feature of the single track model (cf. (6.15)).

Indeed, owing to this result, the two constitutive equations (6.20) become

$$\begin{aligned} Y_1 &= F_{y_{11}}\big(F_{z_{11}}(a_y), \gamma_{11}(a_y), \sigma_{y_{11}}(\alpha_1, a_y)\big) + F_{y_{12}}\big(F_{z_{12}}(a_y), \gamma_{12}(a_y), \sigma_{y_{12}}(\alpha_1, a_y)\big) \\ &= F_{y_{11}}(\alpha_1, a_y) + F_{y_{12}}(\alpha_1, a_y) \\ &= F_{y_1}(\alpha_1, a_y) \\ Y_2 &= F_{y_{21}}\big(F_{z_{21}}(a_y), \gamma_{21}(a_y), \sigma_{y_{21}}(\alpha_2, a_y)\big) + F_{y_{22}}\big(F_{z_{22}}(a_y), \gamma_{22}(a_y), \sigma_{y_{22}}(\alpha_2, a_y)\big) \\ &= F_{y_{21}}(\alpha_2, a_y) + F_{y_{22}}(\alpha_2, a_y) \\ &= F_{y_2}(\alpha_2, a_y) \end{aligned} \tag{6.26}$$

As already obtained in (6.6), we have that the lateral forces are basically linear functions of a_y

$$Y_1 \simeq \frac{ma_2}{l} a_y \quad \text{and} \quad Y_2 \simeq \frac{ma_1}{l} a_y \tag{6.27}$$

Combining (6.26) and (6.27) we obtain

$$\frac{ma_2}{l} a_y = F_{y_1}(\alpha_1, a_y) \quad \text{and} \quad \frac{ma_1}{l} a_y = F_{y_2}(\alpha_2, a_y) \tag{6.28}$$

These equations can be solved with respect to the lateral acceleration

$$a_y = g_1(\alpha_1) \quad \text{and} \quad a_y = g_2(\alpha_2) \tag{6.29}$$

The final, crucial, step is to insert this result back into (6.27), thus obtaining the *axle characteristics*

$$\begin{aligned} Y_1 &= F_{y_1}\big(\alpha_1, g_1(\alpha_1)\big) = Y_1(\alpha_1) \\ Y_2 &= F_{y_2}\big(\alpha_2, g_2(\alpha_2)\big) = Y_2(\alpha_2) \end{aligned} \tag{6.30}$$

that is, two functions, one per each axle, that give the axle lateral force as a function of *only* the corresponding apparent slip angle (cf. (6.20)). In other words, each axle behaves pretty much as an equivalent single wheel with tire. The axle characteristics are so important that they need an in-depth discussion. This is done in Sect. 6.4.2.

6.4.1 Governing Equations of the Single Track Model

Summing up, the single track model is governed by the following set of six fairly simple equations:

- two equilibrium equations

$$\begin{aligned} m(\dot{v} + ur) &= Y = Y_1 + Y_2 = ma_y \\ J_z \dot{r} &= N = Y_1 a_1 - Y_2 a_2 \end{aligned} \tag{6.31}$$

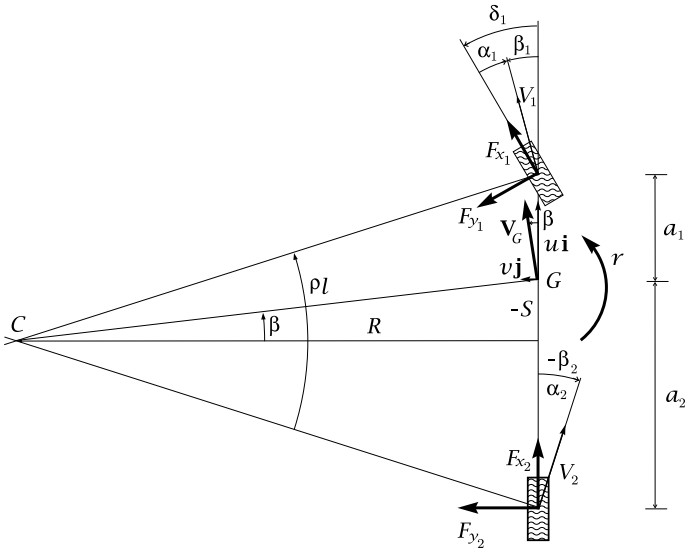

Fig. 6.1 Single track model

- two congruence equations

$$\begin{aligned} \alpha_1 &= \delta_v \tau_1 - \frac{v + r a_1}{u} \\ \alpha_2 &= \delta_v \tau_2 - \frac{v - r a_2}{u} \end{aligned} \tag{6.32}$$

- two constitutive equations (axle characteristics)

$$\begin{aligned} Y_1 &= Y_1(\alpha_1) \\ Y_2 &= Y_2(\alpha_2) \end{aligned} \tag{6.33}$$

A pictorial version of the single track model is shown in Fig. 6.1, where $\delta_1 = \delta_v \tau_1$ and $\delta_2 = \delta_v \tau_2$. Indeed, the equations governing such dynamical system are precisely (6.31), (6.32) and (6.33). Therefore, the system of Fig. 6.1 can be used as a shortcut to obtain the simplified equations of a vehicle. However, the vehicle model still has four wheels, lateral load transfers, camber and camber variations, roll steer. These aspects deserve further attention and will be addressed shortly.

The main feature of this model is that the two wheels of the same axle undergo the same *apparent* slip angle α_i, and hence can be replaced by a sort of equivalent wheel, like in Fig. 6.1. However, that does not imply that the real slip angles of the two wheels of the same axle are the same. Neither are the camber angles, the roll steer angles, the vertical loads. Therefore, the single track model is not really single track!

Among the governing equations, only the two equilibrium equations are differential equations, and both are first order. Therefore, the single track model is a dynamical system with two state variables (namely, but not necessarily, $v(t)$ and $r(t)$, as discussed in Sect. 6.5). The other four algebraic equations must be inserted into the equilibrium equations to ultimately obtain the two *dynamical equations* of the *single track model*

$$\begin{aligned} m(\dot{v} + ur) &= Y(v, r; u, \delta_v) \\ J_z \dot{r} &= N(v, r; u, \delta_v) \end{aligned} \tag{6.34}$$

or, more explicitly

$$\begin{aligned} \dot{v} &= \frac{1}{m}\left[Y_1\left(\delta_v \tau_1 - \frac{v + ra_1}{u}\right) + Y_2\left(\delta_v \tau_2 - \frac{v - ra_2}{u}\right)\right] - ur = f_v(v, r; u, \delta_v) \\ \dot{r} &= \frac{1}{J_z}\left[a_1 Y_1\left(\delta_v \tau_1 - \frac{v + ra_1}{u}\right) - a_2 Y_2\left(\delta_v \tau_2 - \frac{v - ra_2}{u}\right)\right] = f_r(v, r; u, \delta_v) \end{aligned} \tag{6.35}$$

To achieve this result and also to get some insights into the vehicle dynamic behavior, it is convenient to discuss how to obtain the axle characteristics and what is the net effect of the set-up parameters.

6.4.2 Axle Characteristics

By *axle characteristics* we mean two algebraic functions (one per each axle) of the form $Y_i = Y_i(\alpha_i)$, which provide the total lateral force as a function of the apparent slip angle only, with the effects, e.g., of the lateral load transfers already accounted for. They were obtained in (6.30) and (6.33), but the topic is so relevant to deserve an in-depth discussion.

According to (6.20), (6.25), (6.26) and (6.27), the general framework for a given vehicle is that

(1) there is a one-to-one correspondence between the lateral acceleration a_y and the following quantities:
   - lateral load transfers ΔZ_i, see (6.7);
   - camber angles γ_{ij}, see (6.16) and (6.17);
   - roll steer angles, see (6.12);

(2) both left and right tire lateral forces are known functions of the lateral acceleration a_y and of the *same apparent slip angle* α_i, see (6.26);
(3) each axle lateral force $F_{y_i}(\alpha_i, \tilde{a}_y)$ is the sum of the left and right tire lateral forces;

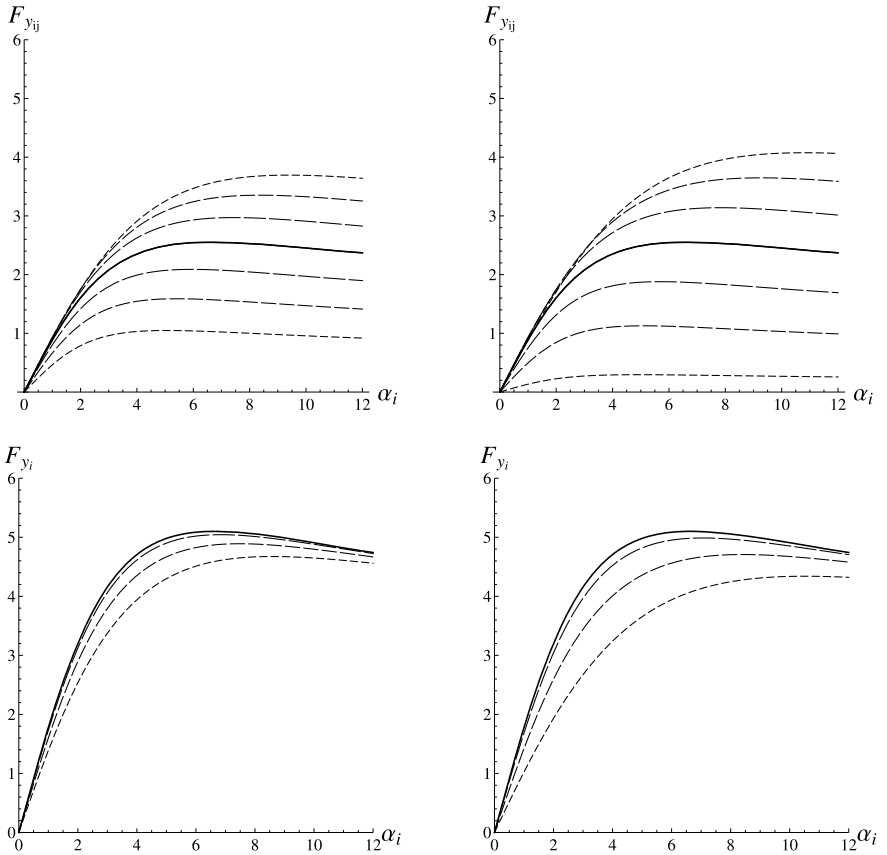

Fig. 6.2 Plots of $F_{y_{i1}}(\alpha_i, a_y)$ and $F_{y_{i2}}(\alpha_i, a_y)$ (*top*) and of their sum $F_{y_i}(\alpha_i, a_y)$ (*bottom*), for four values of $a_y \geq 0$ (*solid line*: $a_y = 0$) and two different set-ups: stiffer in the second case

(4) each axle lateral force Y_i is determined solely by the lateral acceleration a_y, see (6.27).

Therefore, for any given value of a_y, we can obtain the corresponding load transfers, camber angles and roll steer angles and, consequently, plot the lateral forces $F_{y_{i1}}(\alpha_i, a_y)$ and $F_{y_{i2}}(\alpha_i, a_y)$ of both wheels of the same axle, and also their sum $F_{y_i}(\alpha_i, a_y)$ (cf. (6.26)), all as functions of α_i *only*, that is using a_y as a parameter.

Two basic examples are shown in Fig. 6.2. They are basic in the sense that it is assumed that the parameter a_y affects the load transfer ΔZ_i only. More precisely, it is assumed that $\gamma_{ij} = \delta^0_{ij} = \Upsilon_{ij} = 0$.

In all plots in this section, the apparent slip angles are in degrees and forces are in kN. All curves with the same kind of dashing were obtained with the same lateral acceleration.

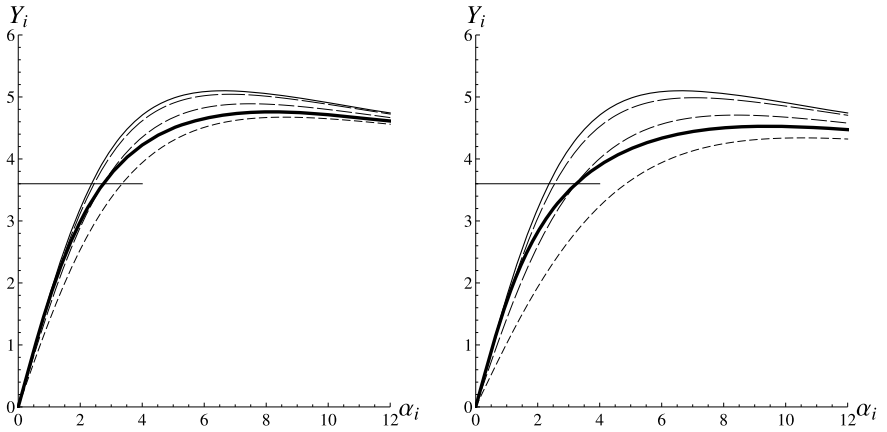

Fig. 6.3 Axle characteristics (*thick solid line*) for the two cases of Fig. 6.2

The two cases in Fig. 6.2 have different values of η_i, and hence different load transfers for the same lateral acceleration (higher load transfers in the second case, probably due to higher roll stiffness). A very relevant fact in vehicle dynamics, as stated in Sects. 2.9.2 and 2.11, is that the lateral force exerted by a single tire grows *less than proportionally* with respect to the vertical load. This is clearly shown in Fig. 6.2(top), and confirmed in Fig. 6.2(bottom) where the higher the lateral acceleration and hence the load transfer, the lower the resulting curve of $F_{y_i}(\alpha_i, a_y)$.

Once the functions F_{y_i} have been obtained as in Fig. 6.2(bottom), there is only one final step to obtain the axle characteristic. Indeed, only one point of each curve $F_{y_i}(\alpha_i, a_y)$ is actually a working point for the vehicle. The reason, as already discussed, is that there is a one-to-one correspondence between a_y and F_{y_i}. Mathematically, it amounts to solving Eq. (6.28), that is

$$F_{y_i}(\alpha_i, a_y) = \frac{m a_y (l - a_i)}{l} \tag{6.36}$$

as done in Fig. 6.3. The *axle characteristics* $Y_i(\alpha_i)$ (thick solid line) picks up just one point of each dashed curve. The higher η_i in (6.7) or (6.10), the lower the axle characteristic.

The effects of negative camber and of positive camber angles, i.e. $\gamma_{ij}^0 \neq 0$, are shown in Fig. 6.4, left and right, respectively. If the top of the wheel is farther out than the bottom (that is, away from the axle), it is called positive camber; if the bottom of the wheel is farther out than the top, it is called negative camber.

Similarly, the effects of toe-in and toe-out, i.e. $\delta_{ij}^0 \neq 0$, are shown in Fig. 6.5, left and right, respectively.

Also interesting is the case of roll steer, i.e. $\Upsilon_{ij} \neq 0$, shown in Fig. 6.6. While all other effects considered so far are symmetric with respect to the vehicle axis,

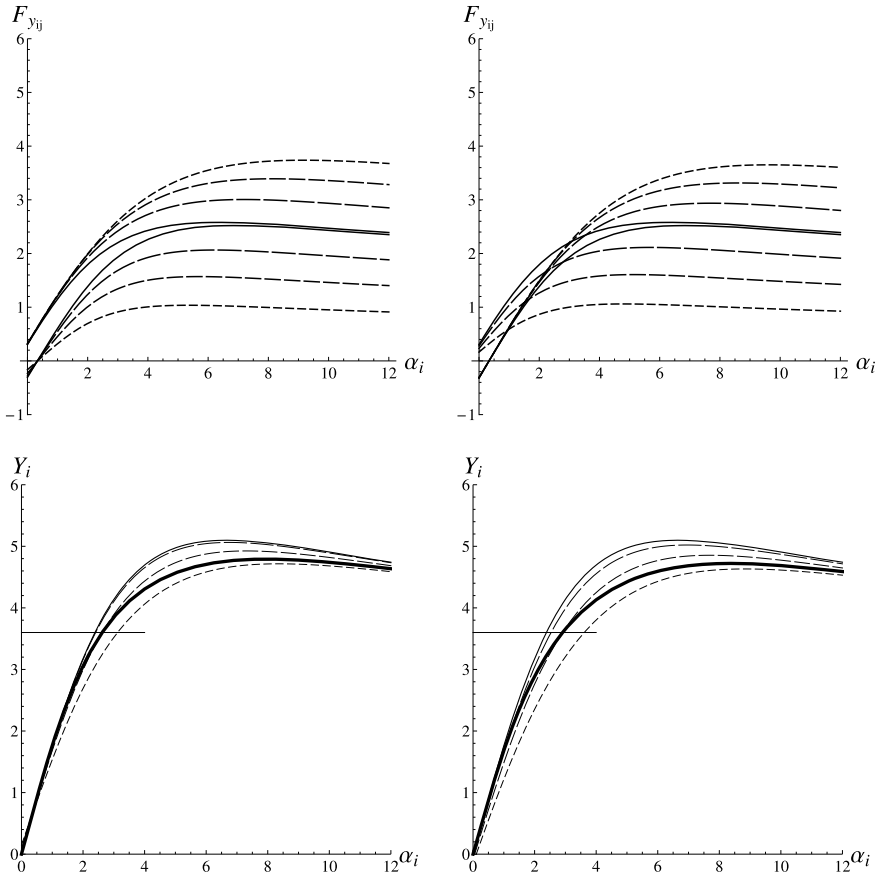

Fig. 6.4 As in Fig. 6.2(left), but with negative camber (*left*) or positive camber (*right*). Also shown the resulting axle characteristics, as in Fig. 6.3

and hence the contributions of the two wheels cancel each other at low lateral acceleration, the roll steer is anti-symmetric (usually $\Upsilon_{i1} = \Upsilon_{i2}$), and hence it affects the axle characteristic even at low lateral acceleration. The same applies to camber variations $\Delta\gamma_i$, as shown in Fig. 6.7.

Of course, all these effects may very well coexist in a real car. In Fig. 6.8, the curve in the middle is the axle characteristic of Fig. 6.3(left), the top curve was obtained including all parameters of the left-hand cases of Figs. 6.4–6.6, that is negative camber, toe-in and positive roll steer, whereas the lower curve was obtained including the parameters of all right-hand cases in the same figures (positive camber, toe-out, negative roll steer).

The curves differ in the initial slope (slip stiffness) and also in the maximum value. Both aspects have a big influence on vehicle handling. The axle characteris-

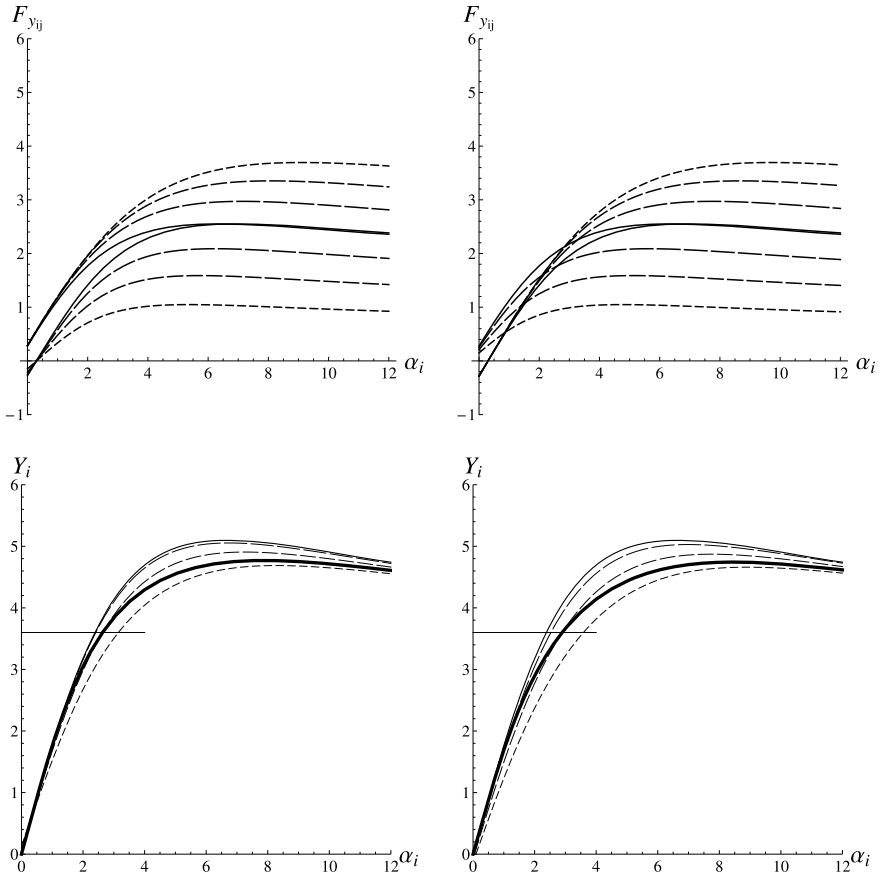

Fig. 6.5 As in Fig. 6.2(left), but with toe-in (*left*) or toe-out (*right*). Also shown the resulting axle characteristics, as in Fig. 6.3

tics are what characterize most vehicle dynamics, indeed. We remark that the axle characteristics, under an apparent simplicity, contain a lot of information about the vehicle features and set-up.

6.5 Alternative State Variables

The use of $v(t)$ and $r(t)$ as state variables is not mandatory, and other options can be envisaged. Here we suggest other possible couples of state variables, which may result in a more intuitive description of the vehicle motion. None of them is commonly employed, but nonetheless it is our opinion that they may provide some better insights into vehicle handling, if properly handled. It is worth remarking that these choices of state variables are by no means limited to the single track model.

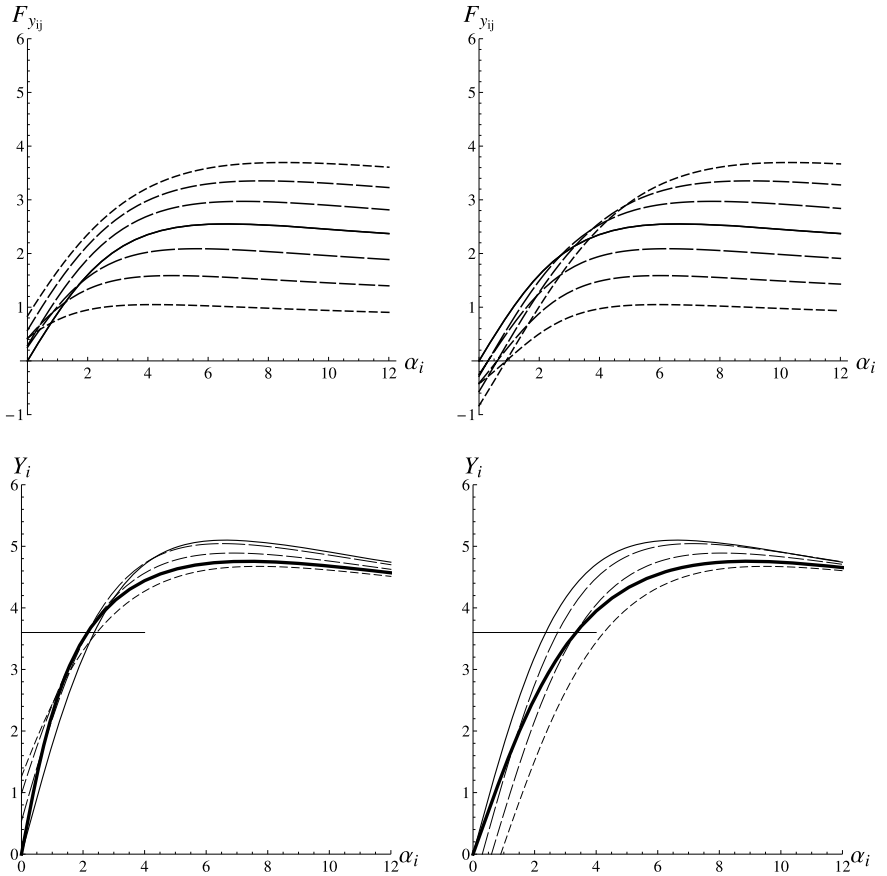

Fig. 6.6 As in Fig. 6.2(left), but with positive roll steer (*left*) or negative roll steer (*right*). Also shown the resulting axle characteristics, as in Fig. 6.3

6.5.1 β and ρ as State Variables

The first set, $\beta(t)$ and $\rho(t)$, has been already introduced in (3.16) and (3.17). They are repeated here for ease of reading (Fig. 6.1)

$$\beta = \frac{v}{u} = -\frac{S}{R} \tag{3.16'}$$

and

$$\rho = \frac{r}{u} = \frac{1}{R} \tag{3.17'}$$

The corresponding governing equations of the single track model becomes:

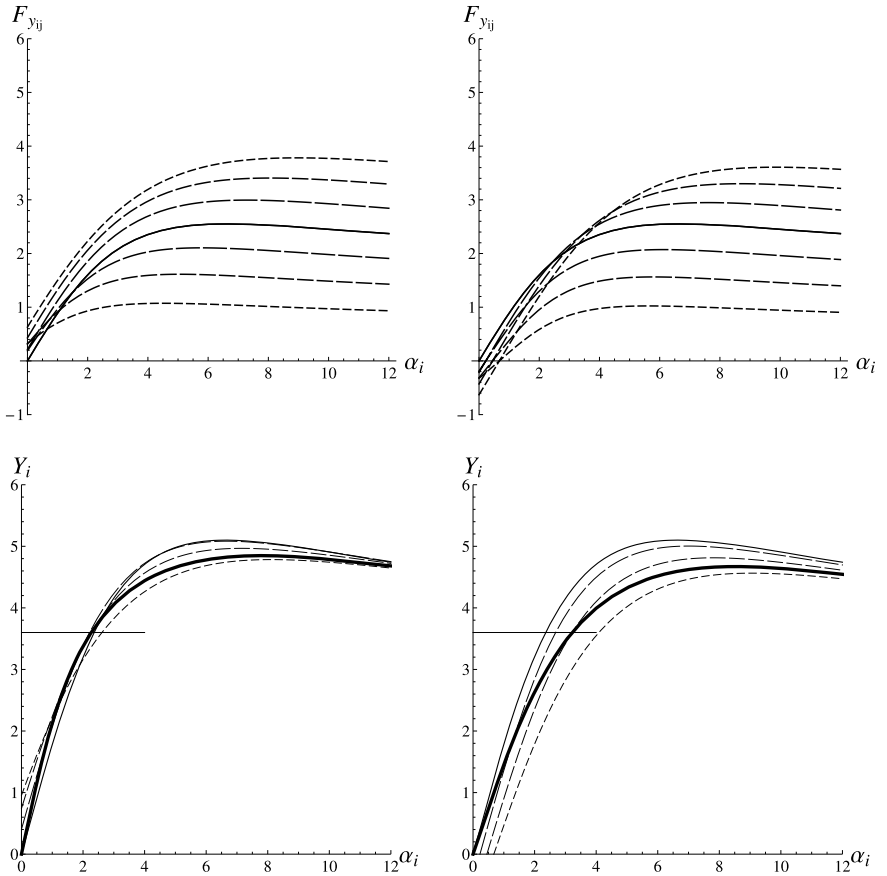

Fig. 6.7 As in Fig. 6.2(left), but with negative $\Delta\gamma_i$ (*left*) or positive $\Delta\gamma_i$ (*right*). Also shown the resulting axle characteristics, as in Fig. 6.3

- equilibrium equations

$$\begin{aligned} m\left(\dot{\beta}u + \beta\dot{u} + u^2\rho\right) &= Y \\ J_z(\dot{\rho}u + \rho\dot{u}) &= N \end{aligned} \tag{6.37}$$

- congruence equations

$$\begin{aligned} \alpha_1 &= \delta_v\tau_1 - \beta - \rho a_1 \\ \alpha_2 &= \delta_v\tau_2 - \beta + \rho a_2 \end{aligned} \tag{6.38}$$

- constitutive equations (from the axle characteristics)

$$\begin{aligned} Y &= Y(\alpha_1, \alpha_2) = Y_1(\alpha_1) + Y_2(\alpha_2) \\ N &= N(\alpha_1, \alpha_2) = Y_1(\alpha_1)a_1 - Y_2(\alpha_2)a_2 \end{aligned} \tag{6.39}$$

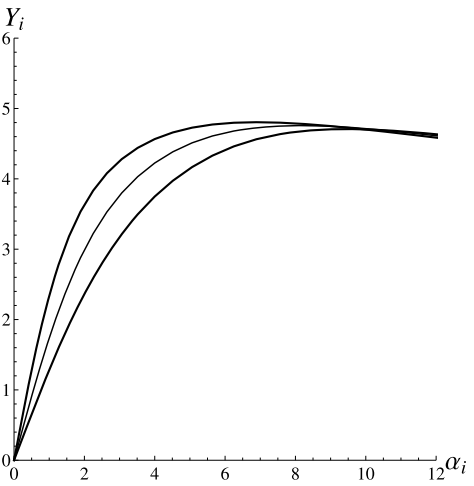

Fig. 6.8 Comparison of axle characteristics obtained with very different set-ups

The two first order differential equations (6.34), governing the single track model, become

$$\begin{aligned} m\left(\dot{\beta}u + \beta\dot{u} + u^2\rho\right) &= Y(\beta, \rho; \delta_v) \\ J_z(\dot{\rho}u + \rho\dot{u}) &= N(\beta, \rho; \delta_v) \end{aligned} \tag{6.40}$$

where the terms on the r.h.s. do not depend on u (vehicle without wings).

6.5.2 β_1 and β_2 as State Variables

Another useful set of state variables may be the vehicle slip angles at each axle midpoint (Fig. 6.1)

$$\begin{aligned} \beta_1 &= \beta + \rho a_1 \\ \beta_2 &= \beta - \rho a_2 \end{aligned} \tag{6.41}$$

The inverse equations are

$$\begin{aligned} \beta &= \frac{\beta_1 a_2 + \beta_2 a_1}{l} \\ \rho &= \frac{\beta_1 - \beta_2}{l} \end{aligned} \tag{6.42}$$

The corresponding governing equations of the single track model become:

- equilibrium equations

$$\begin{aligned}\dot{\beta}_1 u + \beta_1 \dot{u} + (\beta_1 - \beta_2)\frac{u^2}{l} &= \frac{Y}{m} + \frac{N}{J_z}a_1 \\ &= \frac{Y_1}{mJ_z}\left(J_z + ma_1^2\right) + \frac{Y_2}{mJ_z}(J_z - ma_1a_2) \\ \dot{\beta}_2 u + \beta_2 \dot{u} + (\beta_1 - \beta_2)\frac{u^2}{l} &= \frac{Y}{m} - \frac{N}{J_z}a_2 \\ &= \frac{Y_2}{mJ_z}\left(J_z + ma_2^2\right) + \frac{Y_1}{mJ_z}(J_z - ma_1a_2)\end{aligned} \tag{6.43}$$

- congruence equations

$$\begin{aligned}\alpha_1 &= \delta_v \tau_1 - \beta_1 \\ \alpha_2 &= \delta_v \tau_2 - \beta_2\end{aligned} \tag{6.44}$$

- constitutive equations (from the axle characteristics)

$$\begin{aligned}Y_1 &= Y_1(\alpha_1) \\ Y_2 &= Y_2(\alpha_2)\end{aligned} \tag{6.45}$$

The two first order differential equations (6.34) or (6.40), governing the dynamical system, become

$$\begin{aligned}&\dot{\beta}_1 u + \beta_1 \dot{u} + (\beta_1 - \beta_2)\frac{u^2}{l} \\ &\quad = \frac{Y_1(\delta_v \tau_1 - \beta_1)}{mJ_z}\left(J_z + ma_1^2\right) + \frac{Y_2(\delta_v \tau_2 - \beta_2)}{mJ_z}(J_z - ma_1a_2) \\ &\dot{\beta}_2 u + \beta_2 \dot{u} + (\beta_1 - \beta_2)\frac{u^2}{l} \\ &\quad = \frac{Y_2(\delta_v \tau_1 - \beta_2)}{mJ_z}\left(J_z + ma_2^2\right) + \frac{Y_1(\delta_v \tau_1 - \beta_1)}{mJ_z}(J_z - ma_1a_2)\end{aligned} \tag{6.46}$$

where, again, the terms on the r.h.s. do not depend on u.

These equations highlight an interesting feature. The last terms in both equations are often very small, and could even be purposely set equal to zero. Indeed, in road cars $J_z \simeq ma_1a_2$. Therefore, the coupling between the two equations is fairly weak.

6.5.3 S and R as State Variables

Another possible set of state variables may be (Fig. 6.1)

$$\begin{aligned} S &= -\frac{v}{r} = -\frac{\beta}{\rho} = -\frac{\beta_1 a_2 + \beta_2 a_1}{\beta_1 - \beta_2} \\ R &= \frac{u}{r} = \frac{1}{\rho} = \frac{l}{\beta_1 - \beta_2} \end{aligned} \tag{6.47}$$

already introduced in (3.12) and (3.13).

The corresponding governing equations of the single track model become:

- equilibrium equations

$$\begin{aligned} -\frac{u\dot{S}}{R} + \frac{u^2}{R} &= \frac{Y}{m} + \frac{N}{J_z} S \\ \frac{u\dot{R} - \dot{u}R}{R^2} &= -\frac{N}{J_z} \end{aligned} \tag{6.48}$$

- congruence equations

$$\begin{aligned} \alpha_1 &= \delta_v \tau_1 + \frac{S}{R} - \frac{a_1}{R} \\ \alpha_2 &= \delta_v \tau_2 + \frac{S}{R} + \frac{a_2}{R} \end{aligned} \tag{6.49}$$

- constitutive equations (from the axle characteristics)

$$\begin{aligned} Y_1 &= Y_1(\alpha_1) \\ Y_2 &= Y_2(\alpha_2) \end{aligned} \tag{6.50}$$

6.6 Inverse Congruence Equations

The state variables v and r appear in both congruence equations (6.32). However, it is possible to invert these equations to obtain two other equivalent equations, with r/u appearing only in the first equation and v/u only in the second equation

$$\begin{aligned} \frac{r}{u} &= \frac{\delta_1 - \delta_2}{l} - \frac{\alpha_1 - \alpha_2}{l} \\ \frac{v}{u} &= \frac{\delta_1 a_2 + \delta_2 a_1}{l} - \frac{\alpha_1 a_2 + \alpha_2 a_1}{l} \end{aligned} \tag{6.51}$$

where the more compact notation $\delta_1 = \delta_v \tau_1$ and $\delta_2 = \delta_v \tau_2$ has been introduced.

The same steps can be taken for (6.38) with respect to $\rho = r/u$ and $\beta = v/u$

$$\begin{aligned} \rho &= \frac{\delta_1 - \delta_2}{l} - \frac{\alpha_1 - \alpha_2}{l} \\ \beta &= \frac{\delta_1 a_2 + \delta_2 a_1}{l} - \frac{\alpha_1 a_2 + \alpha_2 a_1}{l} \end{aligned} \tag{6.52}$$

Equations (6.44) do not need any further manipulation, since they are already uncoupled. However, it is interesting to note that

$$\begin{aligned} \beta_d &= \beta_1 - \beta_2 = (\delta_1 - \delta_2) - (\alpha_1 - \alpha_2) = \rho(a_1 + a_2) \\ \beta_s &= \beta_1 + \beta_2 = (\delta_1 + \delta_2) - (\alpha_1 + \alpha_2) = 2\beta + \rho(a_1 - a_2) \end{aligned} \tag{6.53}$$

It is important to realize that all these inverse congruence equations are not limited to steady-state conditions, although they are mostly used for the evaluation of some steady-state features.

6.7 Vehicle in Steady-State Conditions

An essential step in understanding the behavior of a dynamical system, and therefore of a motor vehicle, is the determination of the steady-state (equilibrium) configurations (v_p, r_p). In physical terms, a vehicle is in steady-state conditions when, with fixed position δ_v of the steering wheel and at constant speed u, it goes round with perfectly circular trajectories of all of its points.

After having set $\dot{\delta}_v = 0$ and $\dot{u} = 0$, the mathematical conditions for the system being in steady state is to have $\dot{v} = 0$ and $\dot{r} = 0$ in (6.35). Accordingly, the *lateral acceleration* drops the $\dot{v}$ term and becomes

$$\tilde{a}_y = ur = \frac{u^2}{R} = u^2\rho \tag{6.54}$$

This equation was already introduced in (3.25), since it is not limited to the single track model.

Finding the equilibrium points (v_p, r_p) amounts to solving the system of two *algebraic* equations

$$\begin{aligned} 0 &= \frac{1}{m}\left[Y_1\left(\delta_v\tau_1 - \frac{v + ra_1}{u}\right) + Y_2\left(\delta_v\tau_2 - \frac{v - ra_2}{u}\right)\right] - ur = f_v(v, r; u, \delta_v) \\ 0 &= \frac{1}{J_z}\left[a_1 Y_1\left(\delta_v\tau_1 - \frac{v + ra_1}{u}\right) - a_2 Y_2\left(\delta_v\tau_2 - \frac{v - ra_2}{u}\right)\right] = f_r(v, r; u, \delta_v) \end{aligned} \tag{6.55}$$

to get (v_p, r_p) such that

$$f_v(v_p, r_p; u, \delta_v) = 0 \quad \text{and} \quad f_r(v_p, r_p; u, \delta_v) = 0 \tag{6.56}$$

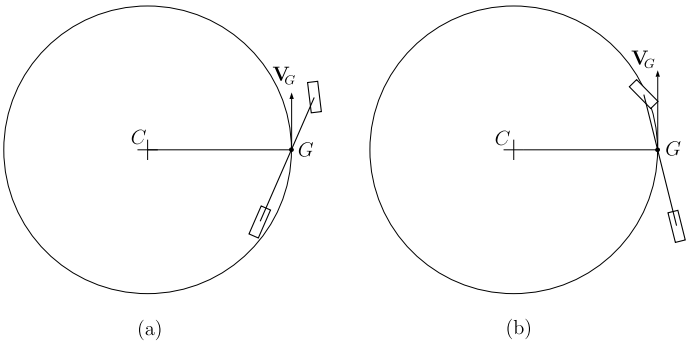

Fig. 6.9 Steady state behavior: (**a**) nose-out, (**b**) nose-in

Because of the nonlinearity of the axle characteristics, the number of possible solutions, for given (u, δ_v), is not known a priori.

Equations (6.56) define implicitly the two functions

$$v_p = v_p(u, \delta_v) \quad \text{and} \quad r_p = r_p(u, \delta_v) \tag{6.57}$$

that is, the totality of steady-state conditions as function of the forward speed u and of the steering wheel angle δ_v. This is quite obvious: given and kept constant the forward speed u and the steering wheel angle δ_v, after a while (a few seconds at most) the vehicle reaches the corresponding steady-state condition, characterized by a constant lateral speed v_p and a constant yaw rate r_p.

While the yaw rate r_p has necessarily the same sign as δ_v, the same does not apply to the lateral speed v_p. As shown in Fig. 6.9, in a left turn the vehicle slip angle $\beta_p = v_p/u$ can either be positive or negative. As a rule of thumb, at low forward speed the vehicle moves "nose-out", whereas at high speed the vehicle goes round "nose-in".

6.7.1 The Role of the Steady-State Lateral Acceleration

It is common practice to employ $(\tilde{a}_y, \delta_v)$, instead of (u, δ_v), as parameters to characterize a steady-state condition. This is possible because

$$\tilde{a}_y = u r_p(u, \delta_v) \quad \text{which can be solved to get } u = u(\tilde{a}_y, \delta_v) \tag{6.58}$$

At first it may look a bit odd to employ $(\tilde{a}_y, \delta_v)$ instead of (u, δ_v), but it is not, since it happens that some steady-state quantities are functions of $\tilde{a}_y$ only. This is quite a remarkable fact, but it should not be taken as a general rule.[6]

[6]For instance, vehicles equipped with locked differential and/or with relevant aerodynamic downforces always need (at least) two parameters.

The reason for such a fortunate coincidence in the case under examination is promptly explained. Just look at the equilibrium equations at steady state with the inclusion of the axle characteristics

$$\begin{aligned} m\tilde{a}_y &= Y_1(\alpha_1) + Y_2(\alpha_2) \\ 0 &= Y_1(\alpha_1)a_1 + Y_2(\alpha_2)a_2 \end{aligned} \tag{6.59}$$

They yield this noteworthy result

$$\frac{Y_1(\alpha_1)l}{ma_1} = \tilde{a}_y \quad \text{and} \quad \frac{Y_2(\alpha_2)l}{ma_2} = \tilde{a}_y \tag{6.60}$$

which can be more conveniently rewritten as

$$\frac{Y_1(\alpha_1)l}{mga_1} = \frac{Y_1(\alpha_1)}{Z_1^0} = \frac{\tilde{a}_y}{g} \quad \text{and} \quad \frac{Y_2(\alpha_2)l}{mga_2} = \frac{Y_2(\alpha_2)}{Z_2^0} = \frac{\tilde{a}_y}{g} \tag{6.61}$$

where Z_1^0 and Z_2^0 are the static vertical loads on each axle.

Therefore, if we take the monotone part of each axle characteristic, there is a one-to-one correspondence between $\tilde{a}_y$ and the apparent slip angles at steady state (Fig. 6.10)

$$\alpha_1 = \alpha_1(\tilde{a}_y) \quad \text{and} \quad \alpha_2 = \alpha_2(\tilde{a}_y) \tag{6.62}$$

This is the key fact for using $\tilde{a}_y$. Both slip angles only feel the lateral acceleration, no matter if the vehicle has small u and large δ_v or, vice versa, large u and small δ_v. In other words, the radius of the circular trajectory of the vehicle does not matter at all. Only $\tilde{a}_y$ matters to the lateral forces and hence to the apparent slip angles. Actually, this very same property has been already used to build the axles characteristics: Eq. (6.62) are just the inverse functions of (6.29). We remark that (6.62) must not be taken as a general rule, but rather as a fortunate coincidence (it applies only to vehicles with two axles, open differential, no wings and small steering angles).

Another very important result comes directly from (6.61)

$$\frac{Y_1(\alpha_1)}{Z_1^0} = \frac{Y_2(\alpha_2)}{Z_2^0} = \frac{\tilde{a}_y}{g} \tag{6.63}$$

that is, at steady state, the lateral forces are always proportional to the corresponding static vertical loads. Therefore, the *normalized axle characteristics*

$$\hat{Y}_1(\alpha_1) = \frac{Y_1(\alpha_1)}{Z_1^0} \quad \text{and} \quad \hat{Y}_2(\alpha_2) = \frac{Y_2(\alpha_2)}{Z_2^0} \tag{6.64}$$

are what really matters in vehicle dynamics. The normalized axle characteristics are non-dimensional. Their maximum value is equal to the grip available in the lateral direction and is, therefore, a very relevant piece of information.

6.7.2 Steady-State Analysis

We have already stated that the two functions (6.57) define all steady state conditions. However, the topic is so relevant to deserve additional attention and discussion.

From (6.62) and (6.52) we have, at *steady state*, the following functions

$$\begin{aligned}\rho = \rho_p(\tilde{a}_y, \delta_v) &= \frac{r_p}{u} = \frac{\tau_1 - \tau_2}{l}\delta_v - \frac{\alpha_1(\tilde{a}_y) - \alpha_2(\tilde{a}_y)}{l} \\ \beta = \beta_p(\tilde{a}_y, \delta_v) &= \frac{v_p}{u} = \frac{\tau_1 a_2 + \tau_2 a_1}{l}\delta_v - \frac{\alpha_1(\tilde{a}_y)a_2 + \alpha_2(\tilde{a}_y)a_1}{l}\end{aligned} \tag{6.65}$$

A vehicle has unique functions $\rho_p(\tilde{a}_y, \delta_v)$ and $\beta_p(\tilde{a}_y, \delta_v)$. As will be shown, they tell us a lot about the global vehicle steady-state behavior. In other words, these two maps fully characterize any steady-state conditions of the vehicle.

The two functions $\rho_p(\tilde{a}_y, \delta_v)$ and $\beta_p(\tilde{a}_y, \delta_v)$ can also be obtained experimentally, once a prototype vehicle is available, by performing some rather simple tests on a flat proving ground. With the vehicle driven at almost constant speed u and a slowly increasing steering wheel angle δ_v, it suffices to measure the following quantities: r_p, v_p, u, $\tilde{a}_y$ and δ_v. It is worth noting that none of these quantities does require to know whether the vehicle has two axles or more, or how long the wheelbase is. In other words, they are all well defined in any vehicle.

Of course, the r.h.s. part of (6.65) is strictly linked to the single track model, and it is useful to the vehicle engineer to understand how to modify the vehicle behavior.

A key feature, confirmed by tests on real road cars, is that the δ_v-dependence and the $\tilde{a}_y$-dependence are clearly separated.[7] Both maps in (6.65) are (in this model) *linear* with respect to the steering wheel angle δ_v, whereas they are certainly *strongly nonlinear* with respect to the steady-state lateral acceleration $\tilde{a}_y$. The linear parts are totally under control, in the sense that both of them are simple functions of the steer gear ratios and of a_1 and a_2. The nonlinear parts are more challenging, coming directly from the interplay of the axle characteristics.

6.7.2.1 Steady-State Gradients

It is informative, and hence quite useful, to define and compute/measure the *gradients* of the two functions in (6.65)

$$\begin{aligned}\operatorname{grad}\rho_p &= \left(\frac{\partial\rho_p}{\partial\tilde{a}_y}, \frac{\partial\rho_p}{\partial\delta_v}\right) = (\beta_y, \beta_\delta) = -(K_{\rho_y}, K_{\rho_\delta}) \\ \operatorname{grad}\beta_p &= \left(\frac{\partial\beta_p}{\partial\tilde{a}_y}, \frac{\partial\beta_p}{\partial\delta_v}\right) = (\rho_y, \rho_\delta) = -(K_{\beta_y}, K_{\beta_\delta})\end{aligned} \tag{6.66}$$

[7] We remark that this is no longer true in vehicles with locked differential and/or aerodynamic vertical loads.

As will be discussed shortly, only one out of four gradient components is usually employed in classical vehicle dynamics,[8] thus missing a lot of information. But this is not the only case in which classical vehicle dynamics turns out to be far from systematic and rigorous. This lack of generality of classical vehicle dynamics is the motivation for some of the next sections.

6.7.2.2 Understeer and Oversteer

For further developments, it is convenient to rewrite (6.65) in a more compact form

$$\begin{aligned} \rho &= \rho_p(\tilde{a}_y, \delta_v) = \frac{\tilde{a}_y}{u^2} = \left(\frac{\tau_1 - \tau_2}{l}\right)\delta_v - f_\rho(\tilde{a}_y) \\ \beta &= \beta_p(\tilde{a}_y, \delta_v) = \left(\frac{\tau_1 a_2 + \tau_2 a_1}{l}\right)\delta_v - f_\beta(\tilde{a}_y) \end{aligned} \tag{6.67}$$

where

$$\begin{aligned} f_\rho(\tilde{a}_y) &= \frac{\alpha_1(\tilde{a}_y) - \alpha_2(\tilde{a}_y)}{l} \\ f_\beta(\tilde{a}_y) &= \frac{\alpha_1(\tilde{a}_y)a_2 + \alpha_2(\tilde{a}_y)a_1}{l} \end{aligned} \tag{6.68}$$

are the nonlinear functions peculiar to each vehicle. They are called here *slip functions*. Let us discuss this topic by means of a few examples.

First, let us consider the normalized axle characteristics (multiplied by g) shown in Fig. 6.10(left). In this example, it has been assumed that both axles have the same lateral grip equal to 1. When inverted, they provide the apparent slip angles $\alpha_1(\tilde{a}_y)$ and $\alpha_2(\tilde{a}_y)$ shown in Fig. 6.10(right). We see that, in this case, $\alpha_1(\tilde{a}_y) > \alpha_2(\tilde{a}_y)$, which yields two slip functions f_ρ and f_β as in Fig. 6.11. A vehicle with a monotone increasing function $f_\rho(\tilde{a}_y)$ is said to be an *understeer* vehicle.

As a second example, let us consider the normalized axle characteristics (multiplied by g) shown in Fig. 6.12(left). They are like in Fig. 6.10, but interchanged. When inverted, they provide the two functions $\alpha_1(\tilde{a}_y)$ and $\alpha_2(\tilde{a}_y)$ shown in Fig. 6.12(right). In this case $\alpha_1(\tilde{a}_y) < \alpha_2(\tilde{a}_y)$, and hence the two slip functions f_ρ and f_β are as in Fig. 6.13. A vehicle with a monotone decreasing function $f_\rho(\tilde{a}_y)$ is said to be *oversteer*.

6.8 Handling Diagram—The Classical Approach

In classical vehicle dynamics only the function $f_\rho(\tilde{a}_y)$ is considered, while $f_\beta(\tilde{a}_y)$ is usually neglected. Moreover, it is customary to rewrite the first equation in (6.67)

[8] It is the well known understeer gradient K, defined in (6.71). Unfortunately, it is not a good parameter and should be replaced by the gradient components (6.66), as demonstrated in Sect. 6.15.1.

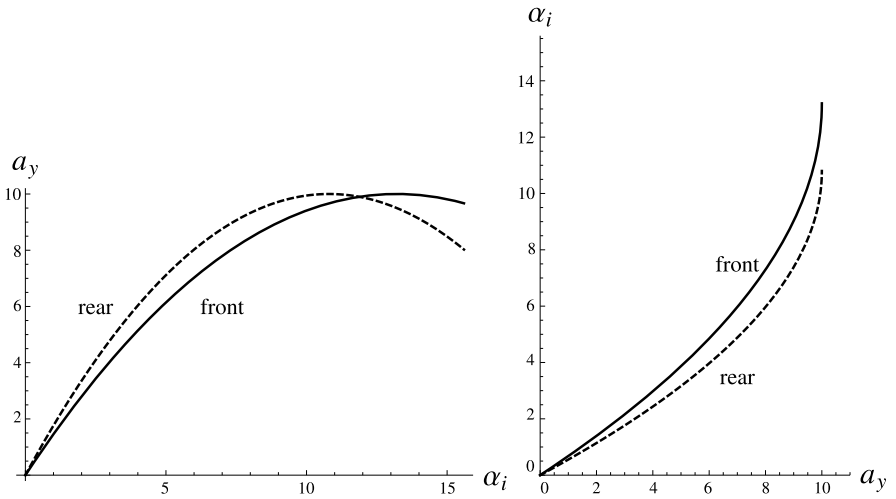

Fig. 6.10 Normalized axle characteristics of an understeer vehicle (*left*) and corresponding apparent slip angles (*right*)

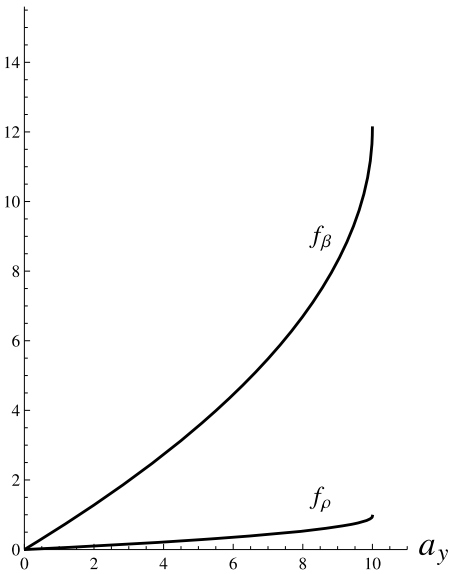

Fig. 6.11 Slip functions of an understeer vehicle

as a system of two equations

$$\begin{cases} y = \left(\dfrac{\tau_1 - \tau_2}{l}\right)\delta_v - \dfrac{\tilde{a}_y}{u^2} = \left(\dfrac{\tau_1 - \tau_2}{l}\right)\delta_v - \dfrac{1}{R} \\ y = f_\rho(\tilde{a}_y) = \dfrac{\alpha_1(\tilde{a}_y) - \alpha_2(\tilde{a}_y)}{l} \end{cases} \tag{6.69}$$

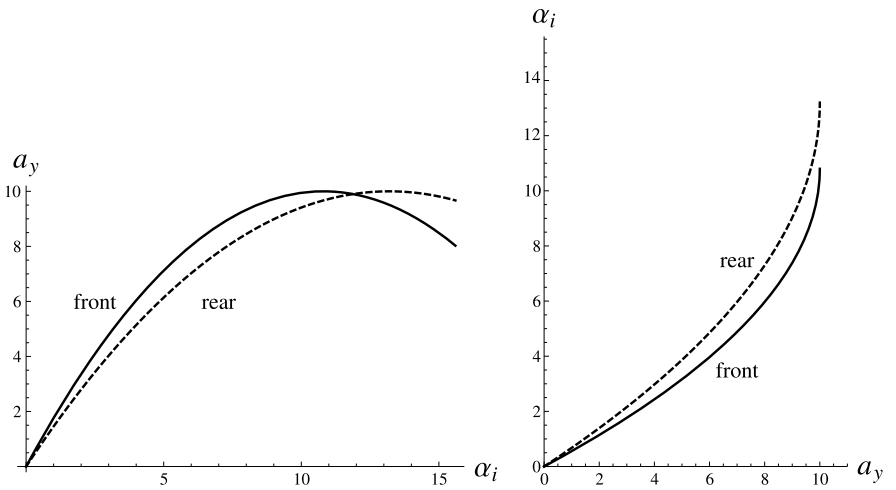

Fig. 6.12 Normalized axle characteristics of an oversteer vehicle (*left*) and corresponding apparent slip angles (*right*)

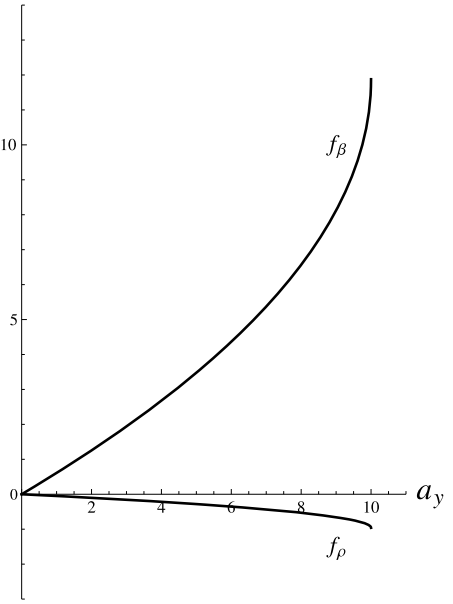

Fig. 6.13 Slip functions of an oversteer vehicle

since, at steady state, $\rho_p = \tilde{a}_y/u^2$. Solving this system amounts to obtaining the values of $(\tilde{a}_y, f_\rho)$ attained under the imposed operating conditions (u, δ_v). Geometrically, that can be seen as the intersection between a straight line and the so-called *handling curve* $y = f_\rho(\tilde{a}_y)$ [6–8], as shown in Fig. 6.14. Another way to recast the

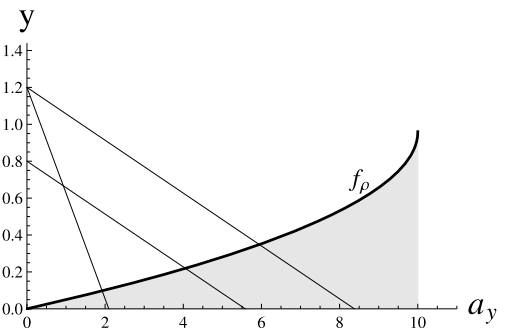

Fig. 6.14 Handling diagram of an understeer vehicle

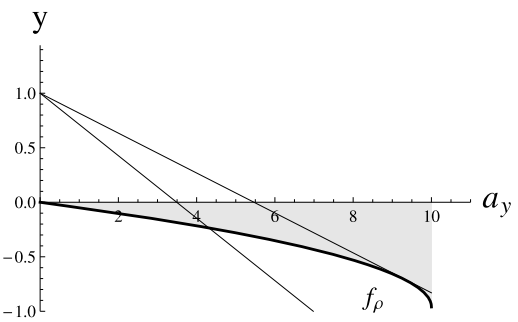

Fig. 6.15 Handling diagram of an oversteer vehicle

system (6.69) is

$$\delta - \frac{l}{R} = \alpha_1(\tilde{a}_y) - \alpha_2(\tilde{a}_y) \tag{6.70}$$

where $\delta = (\tau_1 - \tau_2)\delta_v$. This is by far the most classical way to write this equation.

Together, the handling curve and the straight lines, form the celebrated *handling diagram*.

The handling curve $y = f_\rho(\tilde{a}_y)$ is peculiar to each vehicle, since it depends on the normalized axle characteristics. The straight line depends on the selected operating conditions. In Fig. 6.14 two intersecting lines share the same value of δ_v, while the two parallel lines share the same value of u.

Perhaps, the best way to understand the handling diagram is by assuming that the steering wheel angle δ_v is kept constant, while the forward speed u is (slowly) increased. In Fig. 6.15, an increasing u results also in an increasing $\tilde{a}_y$. Therefore, from (6.70) with constant δ_v, the faster the vehicle, the larger the radius R. This is called *understeer behavior*. On the contrary, if the handling curve is, e.g., like in Fig. 6.15, the faster the vehicle with constant δ_v, the smaller the radius R. This is called *oversteer behavior*. Actually, when the straight line becomes tangent to the handling curve, as shown in Fig. 6.15, the vehicle becomes unstable. It means that the vehicle has reached the *critical speed* associated to that value of δ_v. The concept of critical speed will be discussed in another section in a more general framework.

Classical vehicle dynamics stops about here. In the next section a fresh, more comprehensive, global approach is developed. It brings new insights into the global

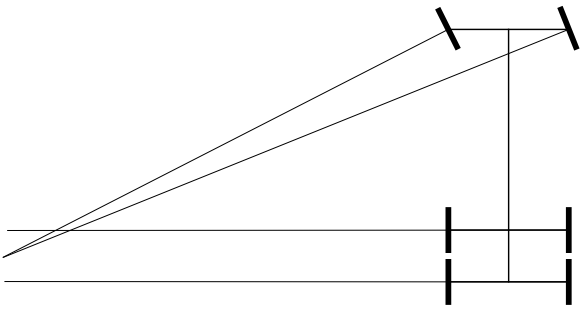

Fig. 6.16 Case not covered by the classical theory

steady-state behavior of vehicles, along with some new hints into the transient behavior.

6.9 Weak Concepts in Classical Vehicle Dynamics

Some "fundamental" concepts in vehicle dynamics are indeed very weak if addressed with open mind. They are either not well defined, particularly when we look at real vehicles, or they are commonly defined in an unsatisfactory way. This is a serious practical drawback that can lead to wrong results and conclusions.

According to SAE J266 Standard, *Steady-State Directional Control Test Procedures For Passenger Cars and Light Trucks*

> understeer/oversteer gradient K is defined as the difference between steer angle gradient and Ackermann steer angle gradient.

In formula, from (6.70)

$$K = \frac{\mathrm{d}}{\mathrm{d}\tilde{a}_y}\left(\delta - \frac{l}{R}\right) \tag{6.71}$$

Therefore, we need both the *steer angle* δ and the *Ackermann steer angle* l/R. Unfortunately, neither of them is clearly defined in a real vehicle. In fact, they are well defined only in the single track model, as it is done, e.g., in Fig. A1 in the SAE J266 Standard. In a real vehicle the two front wheels have typically different steer angles (Fig. 6.16). Therefore, the steer angle δ is not precisely defined. The Ackermann steer angle l/R also suffers whenever a vehicle has three or more axles, as the wheelbase l is no longer a clear concept (Fig. 6.16). Someone may object that almost all cars have two axles. But, nonetheless, we cannot ground a theory on such a weak concept.

The understeer gradient K has been an important performance metric in analyzing the handling behavior of vehicles. Unfortunately, it should not have been. It will be demonstrated here that it is not a good parameter to measure the handling behavior of a vehicle. Nor even of a single track model.

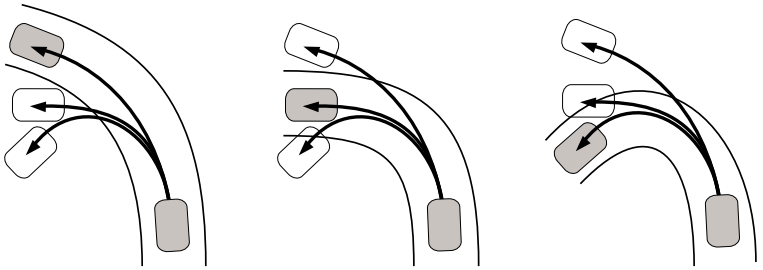

Fig. 6.17 What did the driver intend to do?

6.9.1 Popular Definitions of Understeer/Oversteer

Perhaps, the most astonishing case of the use of unclear concepts is the popular way to "define" understeer and oversteer:

> Oversteer is what occurs when a car steers by more than the amount commanded by the driver. Conversely, understeer is what occurs when a car steers less than the amount commanded by the driver.
> Understeer: a tendency of an automobile to turn less sharply than the driver intends (or would expect).
> The term understeer means that you have to give your car more steering input than the corner should require to get it to go around.

What is the "amount commanded by the driver"? What is the scientific, quantitative, meaning of what "the driver intends"? What does it mean "than the corner should require"?

Figure 6.17 exemplifies this paradoxical situation. Three different curves, three identical trajectories, only one is fine in each case. What about the understeer/oversteer behavior of the car? What did the driver intend?

6.10 Map of Achievable Performance (MAP)—A New Global Approach

The handling diagram, although noteworthy, does not provide a global picture of the handling behavior. Just consider that the use of $\tilde{a}_y$ as input variable, that is one variable instead of two, hides some features of the vehicle handling behavior.

Here we suggest a completely new approach, a global one. That is, an approach that unveils, at a glance, the overall steady-state features of the vehicle under investigation, thus making it easier to distinguish between a "good" vehicle and a "not-so-good" one.

As stated in Sect. 6.7, the steady-state handling behavior is completely described by the two functions (6.57)

$$v_p = v_p(u, \delta_v) \quad \text{and} \quad r_p = r_p(u, \delta_v) \tag{6.57'}$$

For further developments, it is convenient to solve the equation

$$\tilde{a}_y = u r_p(u, \delta_v) \tag{6.72}$$

with respect to $\tilde{a}_y$, thus getting the function $\tilde{a}_y(u, \delta_v)$, which can then be inserted back into (6.65) to obtain these new *handling maps*

$$\begin{aligned} \rho = \rho(u, \delta_v) &= \left(\frac{\tau_1 - \tau_2}{l}\right)\delta_v - \frac{\alpha_1(u, \delta_v) - \alpha_2(u, \delta_v)}{l} \\ \beta = \beta(u, \delta_v) &= \left(\frac{\tau_1 a_2 + \tau_2 a_1}{l}\right)\delta_v - \frac{\alpha_1(u, \delta_v)a_2 + \alpha_2(u, \delta_v)a_1}{l} \end{aligned} \tag{6.73}$$

These maps can be obtained experimentally or through simulations. Therefore, they are not limited to the single track model.

Actually, we can solve (6.72) also with respect to δ_v to obtain $\delta_v(\tilde{a}_y, u)$. Inserting this function into either (6.65) or (6.73), we get $\rho(\tilde{a}_y, u)$ and $\beta(\tilde{a}_y, u)$. This is a somehow unusual way to map the steady-state behavior, but which turns out to be quite useful.

To set the topic in an even more convenient framework, we define

$$\begin{aligned} (1 + \hat{\chi})\delta = \delta_1 &= \tau_1 \delta_v \\ \hat{\chi}\delta = \delta_2 &= \tau_2 \delta_v \end{aligned} \tag{6.74}$$

Usually, $\hat{\chi} = 0$ and hence δ is just the steering angle of the front wheels. However, $\hat{\chi} \neq 0$ leaves room for rear steering as well. In general,

$$\delta = \delta_1 - \delta_2 = (\tau_1 - \tau_2)\delta_v \tag{6.75}$$

and it is called *net steer angle* of the wheels. With this notation, the *handling maps* (6.73) become

$$\begin{aligned} \rho = \rho(u, \delta) &= \frac{\delta}{l} - \frac{\alpha_1(u, \delta) - \alpha_2(u, \delta)}{l} \\ \beta = \beta(u, \delta) &= \left(\frac{(1 + \hat{\chi})a_2 + \hat{\chi} a_1}{l}\right)\delta - \frac{\alpha_1(u, \delta)a_2 + \alpha_2(u, \delta)a_1}{l} \end{aligned} \tag{6.76}$$

Instead of doing as in (6.70), here we take a fresh approach and consider the handling maps of both ρ and β, and both as functions of two variables. This is a more general point of view that leads to a new global approach that we present here for the very first time and that we call *Map of Achievable Performance* (*MAP*).

Actually, under the acronym MAP we will present two types of possible handling maps, each one on the corresponding *achievable region*.

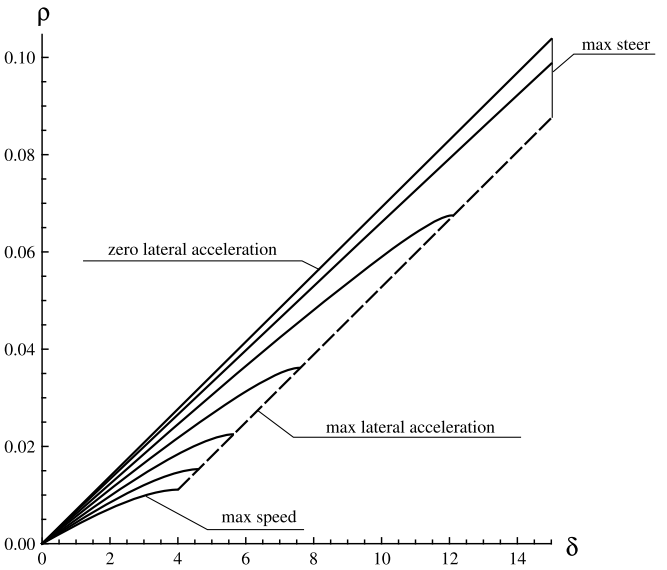

Fig. 6.18 Constant speed lines on the ρ–δ MAP for an understeer vehicle

6.10.1 MAP Curvature ρ vs Steer Angle δ

A central issue in vehicle dynamics is how a vehicle responds to the driver input commands (namely, the steering wheel angle δ_v and the forward speed u). Well, let us map it. The plane (δ, ρ) suits the purpose, as we are going to show here for the first time.

As a first example, let us consider a vehicle with the front and rear *normalized* axle characteristics (multiplied by g) shown in Fig. 6.10.[9] We recall that it is an understeer vehicle and that the corresponding slip functions and handling diagram are shown in Figs. 6.11 and 6.14, respectively.

If in the plane (δ, ρ) we draw the lines at constant speed u we get the plot shown in Fig. 6.18, if $\rho \geq 0$. In the same achievable region, we can draw the lines at constant lateral acceleration $\tilde{a}_y$, as shown in Fig. 6.19. According to (6.65), they are parallel straight lines. In Fig. 6.20 both lines at constant u and constant $\tilde{a}_y$ are drawn on the whole achievable region.

The *achievable region* is bounded by:

(1) maximum speed (dashed line in Fig. 6.19);
(2) maximum lateral acceleration (dashed line in Fig. 6.18);
(3) zero lateral acceleration;
(4) maximum steer angle.

[9]Moreover, to keep, for the moment, the analysis as simple as possible, we also assume that $\hat{Y}_1(x) = \hat{Y}_2(kx)$, with $k > 0$.

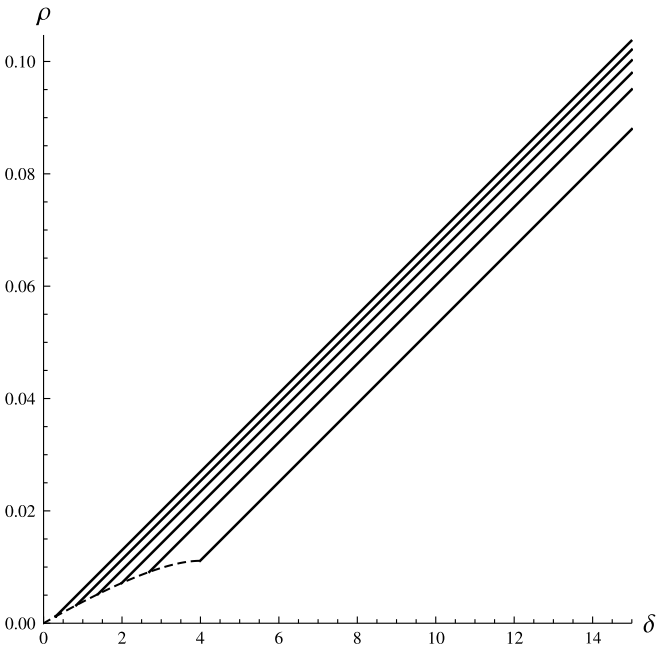

Fig. 6.19 Constant lateral acceleration lines on the ρ–δ MAP for an understeer vehicle

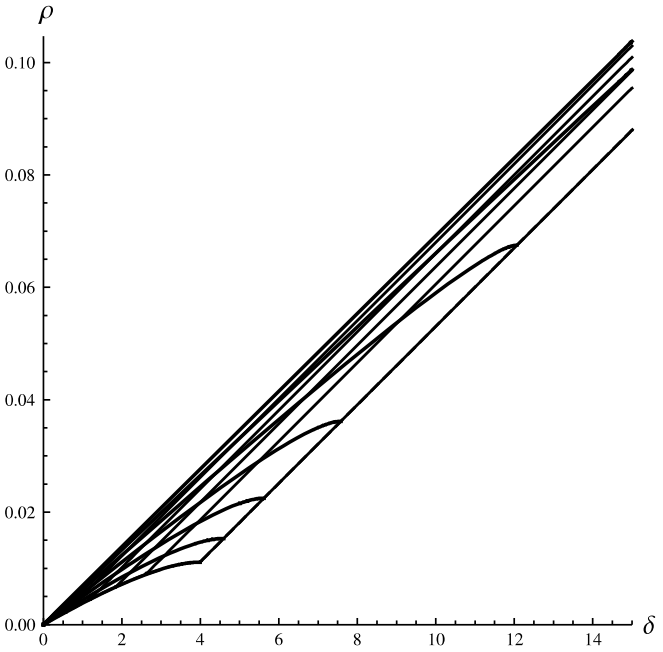

Fig. 6.20 ρ–δ MAP for an understeer vehicle

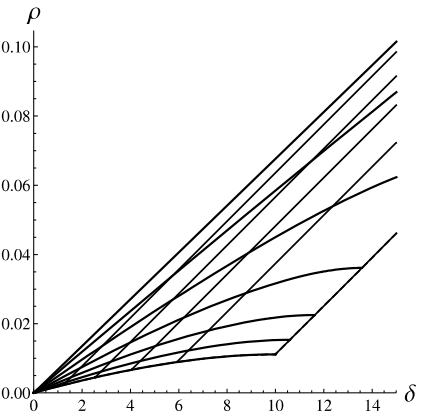

Fig. 6.21 ρ–δ MAP for a vehicle with too much understeer

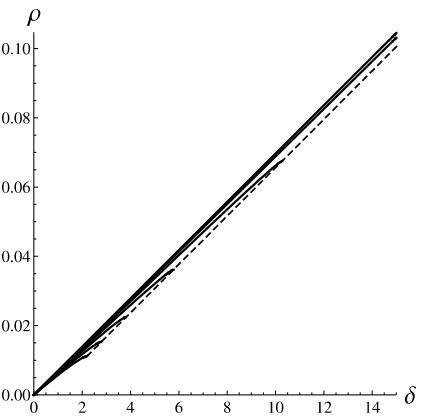

Fig. 6.22 Constant lateral acceleration lines on the ρ–δ MAP for a too little understeer vehicle

We see that the driver must act on both u and δ to control the vehicle, that is to drive it on a curve with curvature ρ and lateral acceleration $\tilde{a}_y$. But, the key feature is that it can be done fairly easily because the lines at constant speed are "well shaped", that is quite far apart from each other and neither too flat, nor too steep (Fig. 6.18).

In Fig. 6.20, all lines at constant speed intersect all lines at constant lateral acceleration. This is typical of all vehicle without significant aerodynamic vertical loads. This is another piece of information that is provided by this kind of maps on the achievable region.

An example of a not-so-nice achievable region is shown in Fig. 6.21. A vehicle with a map like in Fig. 6.21 shows too much understeer: the lines at high speed are too flat, showing that the driver can increase δ without getting a significant increase of ρ. Not a desirable behavior.

Another example of undesirable behavior, but for opposite reasons, is shown in Fig. 6.22. This is a vehicle with too little understeer. It has a very narrow achievable region, which means that the driver has a very heavy task in controlling the vehicle: the lines at zero and maximum lateral acceleration are very close together.

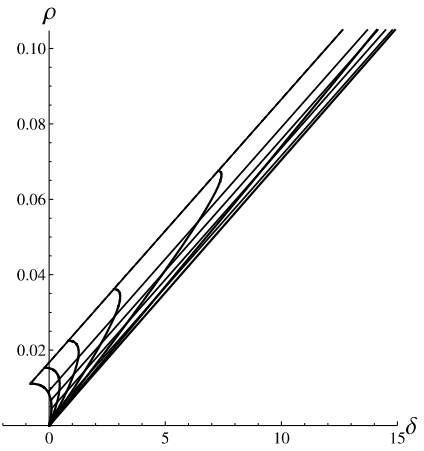

Fig. 6.23 Apparent achievable region on the ρ–δ MAP for an oversteer vehicle

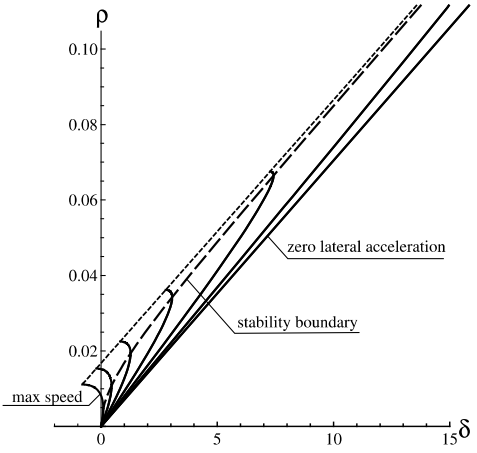

Fig. 6.24 Constant speed lines and truly achievable region on the ρ–δ MAP for an oversteer vehicle

An oversteer vehicle (whose corresponding slip functions and handling diagram are shown in Figs. 6.13 and 6.15, respectively) has an achievable region as in Fig. 6.23. The lines at constant $\tilde{a}_y$, shown in Fig. 6.24, are quite far apart like in Fig. 6.18, but the lines at constant speed u are very badly shaped. At high speed they are too steep, meaning that a small variation of δ drastically changes ρ and $\tilde{a}_y$.

Moreover, the vehicle becomes unstable when the u-lines have vertical slope. Accordingly, the truly achievable region becomes smaller, as shown in Fig. 6.24, where the truly achievable region is bounded by the stability boundary (long-dashed line).

All these examples show how the map *curvature* vs *steer angle* provides a very clear and global picture of the vehicle handling behavior. It makes clear why a well tuned vehicle must be moderately understeer. Too much or too little understeer are not desirable because the vehicle becomes much more difficult to be driven (for opposite reasons).

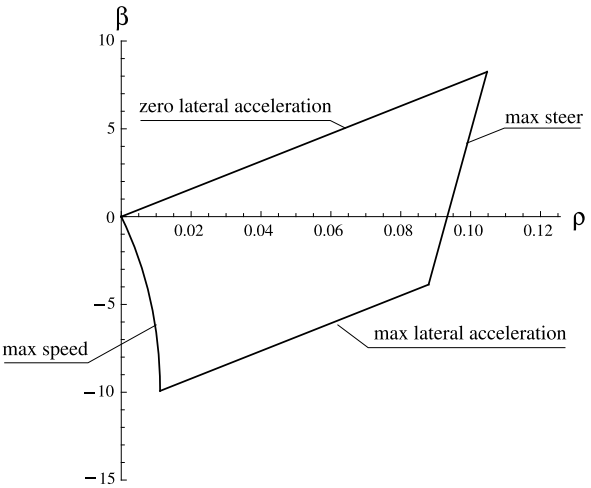

Fig. 6.25 Achievable region for an understeer vehicle in the plane (ρ, β)

The difference between understeer and oversteer is laid bare (Figs. 6.20 and 6.23). Both have far apart $\tilde{a}_y$-lines, but covering achievable regions on opposite sides. In fact, the u-lines are totally different.

The more one observes these handling maps on the corresponding achievable regions, the more the global handling behavior becomes clear.

6.10.2 MAP: Vehicle Slip Angle β vs Curvature ρ

Other very useful handling maps can be drawn in the plane (ρ, β), that is maps which show the relationship between the curvature ρ and the vehicle slip angle β. Again, it is possible at a glance to appreciate the difference between different vehicles.

The *achievable region* for an understeer vehicle is shown in Fig. 6.25. It is bounded by four lines, each with a precise physical meaning:

(1) upper line: zero lateral acceleration and forward speed;
(2) lower line: maximum lateral acceleration;
(3) left line: maximum forward speed;
(4) right line: maximum steer angle.

But more interesting are the MAPs (Map of Achievable Performance) that can be drawn inside the achievable region.

Curves at constant speed u and also lines at constant steer angle δ are shown in Fig. 6.26 for an understeer vehicle (the same of Fig. 6.20). As expected, moving top to bottom along the lines at constant steer angles, that is with increasing speed, brings smaller values of the curvature ρ. Also interesting is to observe that at low speed the slip angle β grows with δ, whereas at high speed it is the other way around. At intermediate speeds, β initially grows and then decreases.

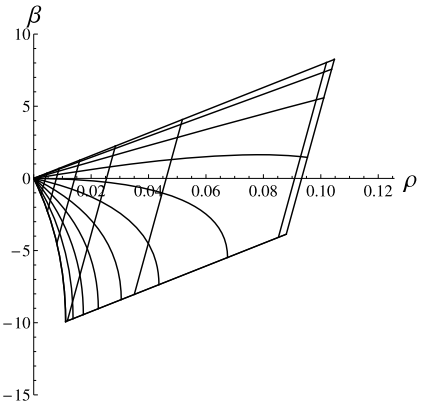

Fig. 6.26 Understeer vehicle: β–ρ MAP with curves at constant speed u and lines at constant steer angle δ

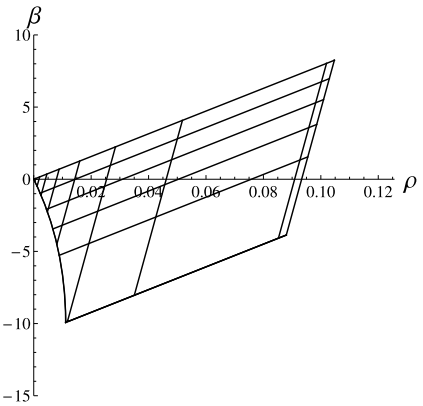

Fig. 6.27 Understeer vehicle: β–ρ MAP with curves at constant lateral acceleration $\tilde{a}_y$ and lines at constant steer angle δ

Lines at constant lateral acceleration $\tilde{a}_y$ along, again, with lines at constant δ, are shown in Fig. 6.27 for the same understeer vehicle. As expected, the vehicle slip angle β grows steadily if the steer angle δ is increased with constant lateral acceleration $\tilde{a}_y$.

Combining Figs. 6.26 and 6.27 we obtain Fig. 6.28: quite an informative picture to grasp the global vehicle behavior. We can appreciate the interplay between a lot of relevant handling quantities. Again, in Fig. 6.28, all lines at constant speed intersect all lines at constant lateral acceleration. This is typical of all vehicles without significant aerodynamic vertical loads.

The achievable region in the plane (ρ, β), that is the β–ρ MAP, for an oversteer vehicle (the same of Figs. 6.24 and 6.23) is shown in Fig. 6.29, along with curves at constant speed u and lines at constant steer angle δ. As expected, moving top to bottom along the lines at constant steer angles, that is with increasing speed, brings bigger values of the curvature ρ.

Very instructive is the comparison between Figs. 6.26 and 6.29, that is between an understeer and an oversteer vehicle. The two achievable regions have different

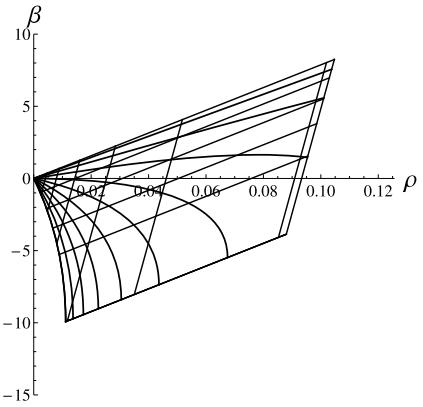

Fig. 6.28 Understeer vehicle: β–ρ MAP with lines at constant u, $\tilde{a}_y$ and δ

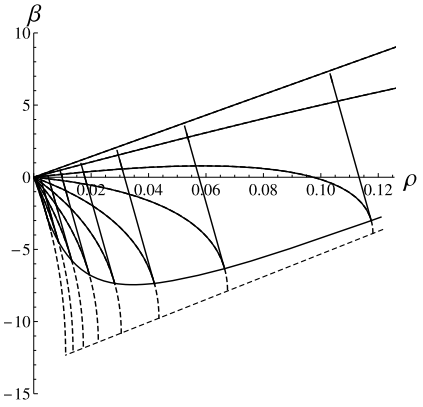

Fig. 6.29 Oversteer vehicle: β–ρ MAP with curves at constant speed u and lines at constant steer angle δ

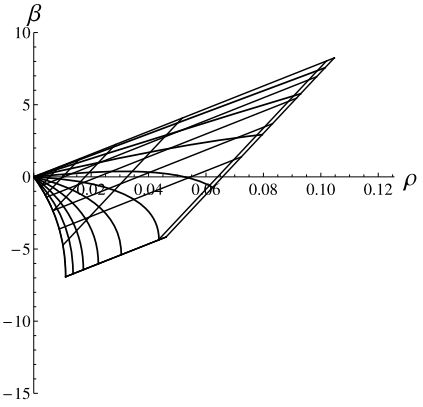

Fig. 6.30 Vehicle with too much understeer: β–ρ MAP with lines at constant u, $\tilde{a}_y$ and δ

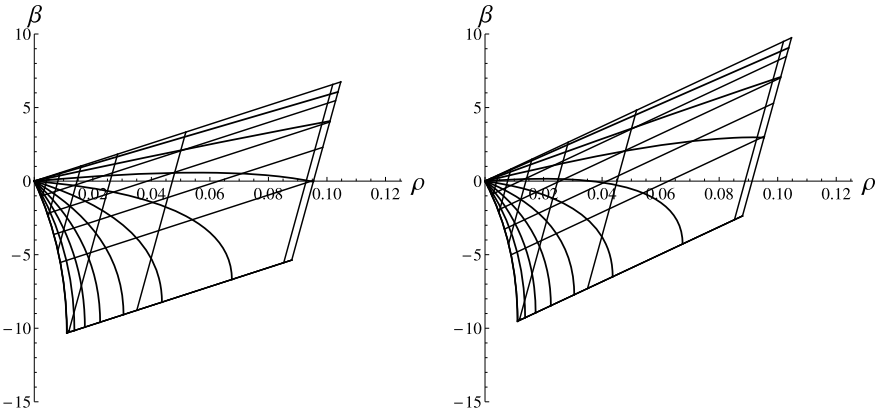

Fig. 6.31 Effects of rear steering on the achievable region: rear wheels turning opposite of the front wheels (*left*), rear wheels turning like the front wheels (*right*)

Fig. 6.32 Achievable region of a vehicle with rear wheels turning opposite of the front wheels at low speed and like the front wheels at high speed

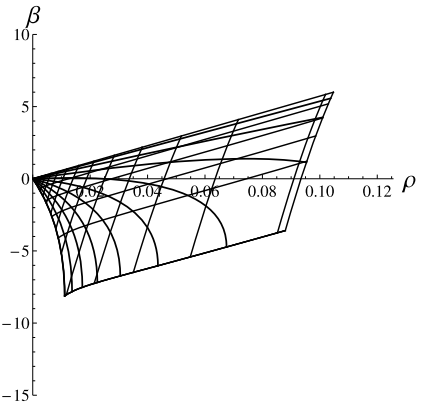

shapes also because an oversteer vehicle becomes *unstable* for certain combinations of speed and steer angle, as already pointed out when discussing Fig. 6.24. These critical combinations form a sort of stability boundary which collects all points where the u-curves and δ-lines are tangent to each other, as shown in both Figs. 6.24 and 6.29.

On the opposite side, a vehicle with too much understeer has an achievable region like in Fig. 6.30, which comes with Fig. 6.21.

The effects of rear steering (in addition to front steering, of course) are shown in Fig. 6.31. The picture on the left is for the case of rear wheels turning opposite of the front wheels, with $\hat{\chi} = -0.1$ in (6.74), whereas the picture on the right is for rear wheels turning like the front wheels, with $\hat{\chi} = 0.1$. The vehicle slip angle β is pretty much affected (cf. Fig. 6.28). Basically, a negative $\hat{\chi}$ moves the achievable region

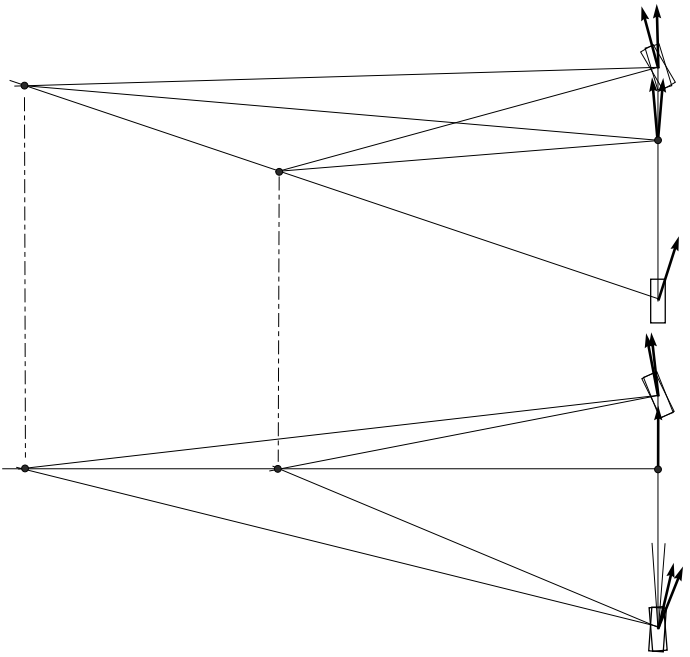

Fig. 6.33 Effect of steering on β: front steering only (*top*) and also rear steering (*bottom*). All cases have the same α_1 and α_2

upwards, and vice versa. On the other hand, $\hat{\chi}$ does not impinge on the available region in the plane (δ, ρ).

To have a narrower achievable region we have to move down the upper part and move up the lower part in the plane (ρ, β). This is indeed the effect of a steering system with rear wheels turning opposite of the front wheels at low speed, and turning like the front wheels at high speed. That is a steering system with, e.g., $\hat{\chi}(u) = -\hat{\chi}_0 \cos(\pi u/u_{\max})$. The net result can be appreciated by comparing Fig. 6.32 with Fig. 6.28. The vehicle behaves better if β spans a smaller range.

From all these figures, it is also clear for which combinations of δ and $\tilde{a}_y$ we have positive or negative β. The achievable region provides a much better insight into rear steering than by looking at, e.g., Fig. 6.33.

6.11 Vehicle in Transient Conditions (Stability and Control Derivatives)

Steady-state analysis cannot be the whole story. Indeed, a vehicle is quite often in transient conditions, that is with time varying quantities (forces, speeds, yaw rate, etc.). Addressing the transient behavior is, of course, more difficult than "simply" analyzing the steady state. More precisely, the steady-state conditions (also called

trim conditions) are just the equilibrium points from which a transient behavior can start.

The general way to study the transient behavior of any dynamical system is through in-time simulations. However, this approach has some drawbacks. Even after a large number of simulations it is quite hard to predict beforehand what the outcome of the next simulation will be.

One way to simplify the analysis of a non-linear dynamical system is to consider only small oscillations about steady-state (trim) conditions. This idea leads to the approach based on *stability derivatives* and *control derivatives* (as they are called in aerospace engineering).

The nonlinear equations of motion of the vehicle are (cf. (6.40))

$$\begin{aligned} m\left(u\dot{\beta} + \dot{u}\beta + u^2\rho\right) &= Y(\beta, \rho; u, \delta_v) \\ J_z(u\dot{\rho} + \dot{u}\rho) &= N(\beta, \rho; u, \delta_v) \end{aligned} \tag{6.77}$$

We prefer to use (β, ρ), instead of (v, r), as state variables because they provide a more "geometric" description of the vehicle motion. Since $\beta = v/u$ and $\rho = r/u$, it is pretty much like having normalized with respect to the forward speed u.

6.11.1 Steady-State Conditions (Equilibrium Points)

At steady-state we have, by definition, $\dot{v} = \dot{r} = 0$, that is $\dot{\beta} = \dot{\rho} = 0$. The driver has direct control on u and δ_v, which are kept constant and whose trim values are named u_a and δ_{va}. The equations of motion (6.77) become

$$\begin{aligned} mu_a^2\rho &= Y(\beta, \rho; u_a, \delta_{va}) \\ 0 &= N(\beta, \rho; u_a, \delta_{va}) \end{aligned} \tag{6.78}$$

which can be solved to get the steady-state maps

$$\begin{aligned} \beta_p &= \hat{\beta}_p(u_a, \delta_{va}) = \frac{v_p(u_a, \delta_{va})}{u_a} \\ \rho_p &= \hat{\rho}_p(u_a, \delta_{va}) = \frac{r_p(u_a, \delta_{va})}{u_a} \end{aligned} \tag{6.79}$$

It is customary, and perhaps more convenient, to use $\tilde{a}_y = u_a r_p(u_a, \delta_{va})$, which provides $u_a = u_a(\tilde{a}_y, \delta_{va})$ and hence

$$\begin{aligned} \beta_p &= \beta_p(\tilde{a}_y, \delta_{va}) = \hat{\beta}_p\left(u_a(\tilde{a}_y, \delta_{va}), \delta_{va}\right) \\ \rho_p &= \rho_p(\tilde{a}_y, \delta_{va}) = \hat{\rho}_p\left(u_a(\tilde{a}_y, \delta_{va}), \delta_{va}\right) \end{aligned} \tag{6.80}$$

These maps have been thoroughly discussed in Sect. 6.10, where the new concept of MAP (Map of Achievable Performance) has been also introduced. In a real vehicle,

these maps can also be obtained by means of classical steady-state tests. Therefore, they do not require departing from the traditional way of vehicle testing.

6.11.2 Linearization of the Equations of Motion

The basic idea is to linearize around an equilibrium point to get information about the dynamic behavior in its neighborhood. It is a standard approach for almost any kind of dynamical systems.

6.11.2.1 Free Oscillation (no Driver Action)

Assuming that the driver takes no action (i.e., both $u = u_a$ and $\delta_v = \delta_{va}$ are constant in time), the first order Taylor series expansion of the equations of motion (6.77) around the equilibrium point (β_p, ρ_p) are as follows

$$\begin{aligned} m\left(u_a\dot{\beta} + u_a^2\rho\right) &= Y_0 + Y_\beta(\beta - \beta_p) + Y_\rho(\rho - \rho_p) \\ J_z u_a \dot{\rho} &= N_0 + N_\beta(\beta - \beta_p) + N_\rho(\rho - \rho_p) \end{aligned} \tag{6.81}$$

where

$$Y_0 = Y(\beta_p, \rho_p; u_a, \delta_{va}) = m u_a^2 \rho_p, \qquad N_0 = N(\beta_p, \rho_p; u_a, \delta_{va}) = 0 \tag{6.82}$$

The *stability derivatives* Y_β, Y_ρ, N_β and N_ρ are simply the partial derivatives

$$Y_\beta = \frac{\partial Y}{\partial \beta}, \qquad Y_\rho = \frac{\partial Y}{\partial \rho}, \qquad N_\beta = \frac{\partial N}{\partial \beta}, \qquad N_\rho = \frac{\partial N}{\partial \rho} \tag{6.83}$$

all evaluated at $(\beta_p, \rho_p; u_a, \delta_{va})$. Obviously, each stability derivative depends on the whole set of chosen coordinates.

It is convenient to introduce the *shifted coordinates*

$$\beta_t = \beta - \beta_p \quad \text{and} \quad \rho_t = \rho - \rho_p \tag{6.84}$$

into the linearized system of Eq. (6.81), thus getting

$$\begin{aligned} m u_a \dot{\beta}_t &= Y_\beta \beta_t + \left(Y_\rho - m u_a^2\right)\rho_t \\ J_z u_a \dot{\rho}_t &= N_\beta \beta_t + N_\rho \rho_t \end{aligned} \tag{6.85}$$

where $\dot{\beta} = \dot{\beta}_t$ and $\dot{\rho} = \dot{\rho}_t$. The same system of equations can be rewritten as

$$\begin{bmatrix} \dot{\beta}_t \\ \dot{\rho}_t \end{bmatrix} = \begin{bmatrix} \dfrac{Y_\beta}{m u_a} & \dfrac{Y_\rho - m u_a^2}{m u_a} \\ \dfrac{N_\beta}{J_z u_a} & \dfrac{N_\rho}{J_z u_a} \end{bmatrix} \begin{bmatrix} \beta_t \\ \rho_t \end{bmatrix} = \mathbf{A} \begin{bmatrix} \beta_t \\ \rho_t \end{bmatrix} \tag{6.86}$$

As a further analytical step, we can reformulate the problem as two *identical* second order linear differential equations, one in $\rho_t(t)$ and the other in $\beta_t(t)$

$$\begin{aligned}
&\ddot{\rho}_t + \dot{\rho}_t\left(\frac{-mN_\rho - J_z Y_\beta}{J_z m u_a}\right) + \rho_t\left(\frac{Y_\beta N_\rho - (Y_\rho - mu_a^2)N_\beta}{J_z m u_a^2}\right) \\
&\quad = \ddot{\rho}_t - \mathrm{tr}(\mathbf{A})\dot{\rho}_t + \det(\mathbf{A})\rho_t \\
&\quad = \ddot{\rho}_t + 2\zeta\omega_n\dot{\rho}_t + \omega_n^2\rho_t = 0 \\
&\quad = \ddot{\beta}_t + 2\zeta\omega_n\dot{\beta}_t + \omega_n^2\beta_t = 0
\end{aligned} \tag{6.87}$$

The solutions of (6.86) depend on two initial conditions, i.e. $\beta_t(0)$ and $\rho_t(0)$. From the same system of equations we get $\dot{\beta}(0)$ and $\dot{\rho}(0)$, which are the two additional initial conditions needed in (6.87). Therefore, the two state variables have identical oscillatory behavior, but are not independent from each other.

The matrix $\mathbf{A}$ in (6.86) has eigenvalues

$$\lambda_j = -\zeta\omega_n \pm \omega_n\sqrt{\zeta^2 - 1}, \quad j = 1, 2 \tag{6.88}$$

with

$$\begin{aligned}
2\zeta\omega_n &= -\mathrm{tr}(\mathbf{A}) = -\frac{mN_\rho + J_z Y_\beta}{J_z m u_a} = -(\lambda_1 + \lambda_2) \\
\omega_n^2 &= \det(\mathbf{A}) = \frac{Y_\beta N_\rho - (Y_\rho - mu_a^2)N_\beta}{J_z m u_a^2} = \lambda_1\lambda_2
\end{aligned} \tag{6.89}$$

From (6.89) we can also obtain the damping coefficient

$$\zeta = -\frac{mN_\rho + J_z Y_\beta}{2\sqrt{J_z m}\sqrt{Y_\beta N_\rho - (Y_\rho - mu^2)N_\beta}} \tag{6.90}$$

and the natural angular frequency

$$\omega_s = \omega_n\sqrt{1 - \zeta^2} = \frac{mN_\rho + J_z Y_\beta}{2J_z m u} - \frac{\sqrt{Y_\beta N_\rho - (Y_\rho - mu^2)N_\beta}}{u\sqrt{J_z m}} \tag{6.91}$$

In ordinary road cars, ω_s is almost constant for moderate to high speeds.

All these equations show how the dynamical features of the dynamical system depend on *three stability derivatives* (6.83) (since $Y_\rho = N_\beta$), besides m, J_z and u_a. The characterization of the vehicle requires knowledge of these stability derivatives.

6.11.3 Stability

An equilibrium point can be either stable or unstable. A convenient way to assess whether there is stability or not is looking at the eigenvalues (6.88). As well known

$$\text{stability} \iff \text{Re}(\lambda_1) < 0 \quad \text{and} \quad \text{Re}(\lambda_2) < 0 \tag{6.92}$$

that is, both eigenvalues must have a negative real part. A convenient way to check this condition without computing the two eigenvalues is

$$\text{stability} \iff \big(\lambda_1 + \lambda_2 = \text{tr}(\mathbf{A})\big) < 0 \quad \text{and} \quad \big(\lambda_1\lambda_2 = \det(\mathbf{A})\big) > 0 \tag{6.93}$$

Typically, vehicles may become unstable because one of the two real eigenvalues becomes positive.

6.11.4 Forced Oscillations (Driver Action)

Linearized systems can also be used to study the effect of small driver actions on the forward speed and/or on the steering wheel angle to control the vehicle. More precisely, we have $u = u_a + u_t$ and $\delta_v = \delta_{va} + \delta_{vt}$.

The linearized inertial terms in (6.77) are

$$\begin{aligned} m\big(u\dot\beta + \dot u\beta + u^2\rho\big) &\simeq m\big(u_a\dot\beta + \dot u\beta_p + u_a^2\rho_p + u_a^2\rho_t + 2u_a u_t\rho_p\big) \\ J_z(u\dot\rho + \dot u\rho) &\simeq J_z(u_a\dot\rho + \dot u\rho_p) \end{aligned} \tag{6.94}$$

where $mu_a^2\rho_p = Y_0$, according to (6.78).

The linearized system becomes

$$\begin{aligned} m\big(u_a\dot\beta_t + \dot u\beta_p + u_a^2\rho_t + 2u_a\rho_p u_t\big) &= Y_\beta\beta_t + Y_\rho\rho_t + Y_u u_t + Y_\delta\delta_{vt} \\ J_z(u_a\dot\rho_t + \dot u\rho_p) &= N_\beta\beta_t + N_\rho\rho_t + N_u u_t + N_\delta\delta_{vt} \end{aligned} \tag{6.95}$$

where there are also four *control derivatives*

$$Y_\delta = \frac{\partial Y}{\partial\delta_v}, \qquad Y_u = \frac{\partial Y}{\partial u}, \qquad N_\delta = \frac{\partial N}{\partial\delta_v}, \qquad N_u = \frac{\partial N}{\partial u} \tag{6.96}$$

evaluated, like the others, at the equilibrium point $(\beta_p, \rho_p; u_a, \delta_{va})$. A better way to write (6.95) is

$$\begin{aligned} mu_a\dot\beta_t &= Y_\beta\beta_t + \big(Y_\rho - mu_a^2\big)\rho_t + (Y_u - 2mu_a\rho_p)u_t + Y_\delta\delta_{vt} - m\beta_p\dot u_t \\ J_z u_a\dot\rho_t &= N_\beta\beta_t + N_\rho\rho_t + N_u u_t + N_\delta\delta_{vt} - J_z\rho_p\dot u_t \end{aligned} \tag{6.97}$$

which generalizes (6.85). The most intuitive case is the driver acting only on the steering wheel, which is described by the simplified set of equations

$$\begin{aligned} mu_a\dot{\beta}_t &= Y_\beta\beta_t + \left(Y_\rho - mu_a^2\right)\rho_t + Y_\delta\delta_{vt} \\ J_z u_a\dot{\rho}_t &= N_\beta\beta_t + N_\rho\rho_t + N_\delta\delta_{vt} \end{aligned} \tag{6.98}$$

since $u_t = \dot{u} = 0$.

In matrix notation (6.97) become

$$\begin{bmatrix} \dot{\beta}_t \\ \dot{\rho}_t \end{bmatrix} = \mathbf{A}\begin{bmatrix} \beta_t \\ \rho_t \end{bmatrix} + \mathbf{B}\begin{bmatrix} u_t \\ \delta_{vt} \\ \dot{u} \end{bmatrix} = \mathbf{A}\begin{bmatrix} \beta_t \\ \rho_t \end{bmatrix} + \mathbf{b} \tag{6.99}$$

or, in an even more compact notation

$$\dot{\mathbf{w}} = \mathbf{A}\mathbf{w} + \mathbf{b} \tag{6.100}$$

Like in (6.87), we can recast the problem as two second order linear differential equations, only apparently independent from each other

$$\begin{aligned} \ddot{\rho}_t + 2\zeta\omega_n\dot{\rho}_t + \omega_n^2\rho_t &= -a_{22}b_1 + \dot{b}_1 + a_{12}b_2 = F_\beta \\ \ddot{\beta}_t + 2\zeta\omega_n\dot{\beta}_t + \omega_n^2\beta_t &= -a_{11}b_2 + \dot{b}_2 + a_{21}b_1 = F_\rho \end{aligned} \tag{6.101}$$

where

$$\begin{aligned} a_{11} &= Y_\beta/(mu_a), \qquad a_{12} = \left(Y_\rho - mu_a^2\right)/(mu_a) \\ a_{21} &= N_\beta/(J_z u_a), \qquad a_{22} = N_\rho/(J_z u_a) \end{aligned} \tag{6.102}$$

and

$$\begin{aligned} b_1 &= \frac{1}{mu_a}\left[(Y_u - 2mu_a\rho_p)u_t + Y_\delta\delta_{vt} - m\beta_p\dot{u}_t\right] \\ b_2 &= \frac{1}{J_z u_a}[N_u u_t + N_\delta\delta_{vt} - J_z\rho_p\dot{u}_t] \\ \dot{b}_1 &= \frac{1}{mu_a}\left[(Y_u - 2mu_a\rho_p)\dot{u}_t + Y_\delta\dot{\delta}_v - m\beta_p\ddot{u}_t\right] \\ \dot{b}_2 &= \frac{1}{J_z u_a}[N_u\dot{u}_t + N_\delta\dot{\delta}_v - J_z\rho_p\ddot{u}_t] \end{aligned} \tag{6.103}$$

Again, if the driver acts only on the steering wheel, like in (6.98), all these expressions become much simpler

$$b_1 = \frac{Y_\delta}{mu_a}\delta_{vt}, \qquad b_2 = \frac{N_\delta}{J_z u_a}\delta_{vt}, \qquad \dot{b}_1 = \frac{Y_\delta}{mu_a}\dot{\delta}_v, \qquad \dot{b}_2 = \frac{N_\delta}{J_z u_a}\dot{\delta}_v \tag{6.104}$$

The two equations (6.101) have identical values of ζ and ω_n, but different forcing terms.

The obvious conclusion of this analysis is that the dynamics of a vehicle in the neighborhood of an equilibrium point is fully characterized by a *finite number* of stability derivatives and control derivatives. The key point is how to measure (identify) all these stability and control derivatives. Their knowledge would be a very relevant practical information. The next section presents indeed a method to obtain these data from steady-state tests.

6.12 Relationship Between Steady State Data and Transient Behavior

Most classical vehicle dynamics deals with steady-state data. Understeer and oversteer are steady-state concepts. Or they are not? This is a crucial question. What does a professional driver mean when he/she complains about his car being understeer or oversteer? Does it have anything to do with the classical definition of understeer/oversteer as discussed in Sect. 6.7.2?

Two aspects should be carefully taken into account. While the concepts of velocity, acceleration, mass, stability etc. arise in any branch of mechanics, why do the concepts of understeer and oversteer only belong to vehicle dynamics? This is rather surprising. Why are vehicles so special dynamical systems that they need concepts conceived uniquely for them?

The other aspect is somehow more practical. Why should steady-state tests tell us anything about the transient behavior of a vehicle? In more technical terms, why should steady-state data be related to stability derivatives? Are they or not? If they are related, what is the relationship?

This section is devoted to the investigation of the link between the universe of steady-state data and the universe of dynamical, hence transient, behavior of a vehicle. It will be shown that a link does indeed exist, but it is not direct, not to mention obvious.

It is worth noting that this section is not strictly related to the single track model. The theory developed here is applicable to real road vehicles.

The starting point is a sort of mathematical trick. At steady state, the lateral force Y and the yawing moment N have very simple values, namely $Y_0 = m\tilde{a}_y$ and $N_0 = 0$. Nevertheless, they can be given, as functions, the following expressions

$$\begin{aligned} Y_0(\tilde{a}_y, \delta_{va}) &= Y\big(\beta_p(\tilde{a}_y, \delta_{va}), \rho_p(\tilde{a}_y, \delta_{va}); u_a(\tilde{a}_y, \delta_{va}), \delta_{va}\big) = m\tilde{a}_y \\ N_0(\tilde{a}_y, \delta_{va}) &= N\big(\beta_p(\tilde{a}_y, \delta_{va}), \rho_p(\tilde{a}_y, \delta_{va}); u_a(\tilde{a}_y, \delta_{va}), \delta_{va}\big) = 0 \end{aligned} \tag{6.105}$$

The key idea is taking the partial derivatives of the function $Y_0(\tilde{a}_y, \delta_{va})$, just defined in (6.105), thus getting

$$\begin{aligned} \frac{\partial Y_0}{\partial \tilde{a}_y} &= Y_\beta \frac{\partial \beta_p}{\partial \tilde{a}_y} + Y_\rho \frac{\partial \rho_p}{\partial \tilde{a}_y} + Y_u \frac{\partial u_a}{\partial \tilde{a}_y} = m\frac{\partial \tilde{a}_y}{\partial \tilde{a}_y} = m \\ \frac{\partial Y_0}{\partial \delta_{va}} &= Y_\beta \frac{\partial \beta_p}{\partial \delta_{va}} + Y_\rho \frac{\partial \rho_p}{\partial \delta_{va}} + Y_u \frac{\partial u_a}{\partial \delta_{va}} + Y_\delta = m\frac{\partial \tilde{a}_y}{\partial \delta_{va}} = 0 \end{aligned} \tag{6.106}$$

The same steps can be taken for the yawing moment $N_0(\tilde{a}_y, \delta_{va})$, getting

$$\begin{aligned} \frac{\partial N_0}{\partial \tilde{a}_y} &= N_\beta \frac{\partial \beta_p}{\partial \tilde{a}_y} + N_\rho \frac{\partial \rho_p}{\partial \tilde{a}_y} + N_u \frac{\partial u_a}{\partial \tilde{a}_y} = 0 \\ \frac{\partial N_0}{\partial \delta_{va}} &= N_\beta \frac{\partial \beta_p}{\partial \delta_{va}} + N_\rho \frac{\partial \rho_p}{\partial \delta_{va}} + N_u \frac{\partial u_a}{\partial \delta_{va}} + N_\delta = 0 \end{aligned} \tag{6.107}$$

In a road vehicle, that is without significant aerodynamic vertical loads, it is reasonable to assume $Y_u = N_u = 0$, if we take β and ρ as state variables to describe the vehicle motion. In other words, Y and N do not change if we modify only u, keeping constant β, ρ and δ_v (cf. (6.24)). It would not be so in Formula cars, that is in cars with aerodynamic wings.

The two equations in (6.106), with $Y_u = N_u = 0$, yield the system of linear equations

$$\begin{cases} Y_\beta \dfrac{\partial \beta_p}{\partial \tilde{a}_y} + Y_\rho \dfrac{\partial \rho_p}{\partial \tilde{a}_y} = m \\ Y_\beta \dfrac{\partial \beta_p}{\partial \delta_{va}} + Y_\rho \dfrac{\partial \rho_p}{\partial \delta_{va}} = -Y_\delta \end{cases} \tag{6.108}$$

and, similarly, from (6.107)

$$\begin{cases} N_\beta \dfrac{\partial \beta_p}{\partial \tilde{a}_y} + N_\rho \dfrac{\partial \rho_p}{\partial \tilde{a}_y} = 0 \\ N_\beta \dfrac{\partial \beta_p}{\partial \delta_{va}} + N_\rho \dfrac{\partial \rho_p}{\partial \delta_{va}} = -N_\delta \end{cases} \tag{6.109}$$

These two systems of equations have the same matrix

$$\begin{bmatrix} \beta_y & \rho_y \\ \beta_\delta & \rho_\delta \end{bmatrix} \begin{bmatrix} Y_\beta \\ Y_\rho \end{bmatrix} = \begin{bmatrix} m \\ -Y_\delta \end{bmatrix} \quad \text{and} \quad \begin{bmatrix} \beta_y & \rho_y \\ \beta_\delta & \rho_\delta \end{bmatrix} \begin{bmatrix} N_\beta \\ N_\rho \end{bmatrix} = \begin{bmatrix} 0 \\ -N_\delta \end{bmatrix} \tag{6.110}$$

whose coefficients are the four components of the *gradients* of the two steady-state *maps* (6.80)

$$\begin{aligned} \operatorname{grad} \rho_p &= \left(\frac{\partial \rho_p}{\partial \tilde{a}_y}, \frac{\partial \rho_p}{\partial \delta_v} \right) = (\beta_y, \beta_\delta) = -(K_{\rho_y}, K_{\rho_\delta}) \\ \operatorname{grad} \beta_p &= \left(\frac{\partial \beta_p}{\partial \tilde{a}_y}, \frac{\partial \beta_p}{\partial \delta_v} \right) = (\rho_y, \rho_\delta) = -(K_{\beta_y}, K_{\beta_\delta}) \end{aligned} \tag{6.66'}$$

After having performed the standard steady-state tests, all these gradient components (already introduced in Sect. 6.7.2.1) are known functions.

The four stability derivatives are the solution of the two systems of Eq. (6.110)

$$\begin{aligned} Y_\beta &= \frac{Y_\delta \rho_y + m\rho_\delta}{\beta_y \rho_\delta - \beta_\delta \rho_y}, \qquad & Y_\rho &= -\frac{Y_\delta \beta_y + m\beta_\delta}{\beta_y \rho_\delta - \beta_\delta \rho_y} \\ N_\beta &= \frac{N_\delta \rho_y}{\beta_y \rho_\delta - \beta_\delta \rho_y}, \qquad & N_\rho &= -\frac{N_\delta \beta_y}{\beta_y \rho_\delta - \beta_\delta \rho_y} \end{aligned} \tag{6.111}$$

Therefore, they are known functions of the gradient components and of the control derivatives Y_δ and N_δ. This is a relevant result, as it shows why steady-state data can indeed provide information about the transient behavior, although not in an obvious way.

Now, we can go back to the linearized equations of motion (6.98). The stability derivatives can be replaced by the expressions in (6.111), thus obtaining

$$\begin{aligned} m u_a \dot{\beta}_t &= \left(\frac{Y_\delta \rho_y + m\rho_\delta}{\beta_y \rho_\delta - \beta_\delta \rho_y} \right) \beta_t + \left(-\frac{Y_\delta \beta_y + m\beta_\delta}{\beta_y \rho_\delta - \beta_\delta \rho_y} - m u_a^2 \right) \rho_t + Y_\delta \delta_{vt} \\ J_z u_a \dot{\rho}_t &= \left(\frac{N_\delta \rho_y}{\beta_y \rho_\delta - \beta_\delta \rho_y} \right) \beta_t + \left(-\frac{N_\delta \beta_y}{\beta_y \rho_\delta - \beta_\delta \rho_y} \right) \rho_t + N_\delta \delta_{vt} \end{aligned} \tag{6.112}$$

where β_t and ρ_t are the shifted coordinates defined in (6.84). These equations can be rearranged to get

$$\begin{aligned} m u_a \dot{\beta}_t + m \left(u_a^2 \rho_t - \frac{\beta_t \rho_\delta - \rho_t \beta_\delta}{\beta_y \rho_\delta - \rho_y \beta_\delta} \right) &= Y_\delta \left(\frac{\beta_t \rho_y - \rho_t \beta_y}{\beta_y \rho_\delta - \rho_y \beta_\delta} \right) + Y_\delta \delta_{vt} \\ J_z u_a \dot{\rho}_t &= N_\delta \left(\frac{\beta_t \rho_y - \rho_t \beta_y}{\beta_y \rho_\delta - \rho_y \beta_\delta} \right) + N_\delta \delta_{vt} \end{aligned} \tag{6.113}$$

Quite a remarkable result. It shows how the data collected in steady-state tests are indeed informative about the dynamic (transient) behavior.

Moreover, it highlights the role of the control derivatives Y_δ and N_δ. For instance, let us consider a generalized *step steering input*, that is a sudden increase δ_{vt} of the steering wheel angle δ_v applied to a vehicle in a steady-state (equilibrium) configuration. We say "generalized" since it should and can be done from any steady-state configuration, not necessarily from a straight line trajectory. Since, by definition $\beta_t(0) = 0$ and $\rho_t(0) = 0$, from (6.112) we obtain

$$\frac{Y_\delta}{m} = \frac{u_a \dot{\beta}(0)}{\delta_{vt}} \quad \text{and} \quad \frac{N_\delta}{J_z} = \frac{u_a \dot{\rho}(0)}{\delta_{vt}} \tag{6.114}$$

The two coefficients $2\zeta\omega_n = -(\lambda_1 + \lambda_2)$ and $\omega_n^2 = \lambda_1\lambda_2$ defined in (6.89) now become

$$\begin{aligned} 2\zeta\omega_n &= \frac{1}{u_a(\beta_y\rho_\delta - \beta_\delta\rho_y)}\left[\left(\frac{N_\delta}{J_z}\beta_y - \frac{Y_\delta}{m}\rho_y\right) - \rho_\delta\right] = -\operatorname{tr}(\mathbf{A}) = n_1(\tilde{a}_y, \delta_{va}) \\ \omega_n^2 &= \frac{1}{(\beta_y\rho_\delta - \beta_\delta\rho_y)}\frac{N_\delta}{J_z}\left(\rho_y - \frac{1}{u_a^2}\right) = \det(\mathbf{A}) = n_2(\tilde{a}_y, \delta_{va}) \end{aligned} \tag{6.115}$$

Similarly, the two forcing terms F_β and F_ρ in (6.101) can be rewritten as

$$\begin{aligned} F_\beta &= -\frac{N_\delta}{J_z u_a^2}\left(\frac{\beta_\delta}{\beta_y\rho_\delta - \beta_\delta\rho_y} + u_a^2\right)\delta_{vt} + \frac{Y_\delta}{mu_a}\dot{\delta}_v \\ &= n_3(\tilde{a}_y, \delta_{va})\delta_{vt} + n_4(\tilde{a}_y, \delta_{va})\dot{\delta}_v \end{aligned} \tag{6.116}$$

and

$$\begin{aligned} F_\rho &= -\frac{N_\delta}{J_z u_a^2}\left(\frac{\rho_\delta}{\beta_y\rho_\delta - \beta_\delta\rho_y}\right)\delta_{vt} + \frac{N_\delta}{J_z u_a}\dot{\delta}_v \\ &= n_5(\tilde{a}_y, \delta_{va})\delta_{vt} + n_6(\tilde{a}_y, \delta_{va})\dot{\delta}_v \end{aligned} \tag{6.117}$$

Equations (6.115), (6.116) and (6.117) show that the dynamic behavior of a road vehicle in the neighborhood of an equilibrium point is fully described by six "magic functions" $n_i(\tilde{a}_y, \delta_{va})$. To help the reader, these six numbers are listed below:

$$\begin{aligned} n_1(\tilde{a}_y, \delta_{va}) &= \frac{1}{u_a(\beta_y\rho_\delta - \beta_\delta\rho_y)}\left[\left(\frac{N_\delta\beta_y}{J_z} - \frac{Y_\delta\rho_y}{m}\right) - \rho_\delta\right] = 2\zeta\omega_n \\ n_2(\tilde{a}_y, \delta_{va}) &= \frac{1}{(\beta_y\rho_\delta - \beta_\delta\rho_y)}\frac{N_\delta}{J_z}\left(\rho_y - \frac{1}{u_a^2}\right) = \omega_n^2 \\ n_3(\tilde{a}_y, \delta_{va}) &= -\frac{N_\delta}{J_z u_a^2}\left(\frac{\beta_\delta}{\beta_y\rho_\delta - \beta_\delta\rho_y} + u_a^2\right) \\ n_4(\tilde{a}_y, \delta_{va}) &= \frac{Y_\delta}{mu_a} \\ n_5(\tilde{a}_y, \delta_{va}) &= -\frac{N_\delta}{J_z u_a^2}\left(\frac{\rho_\delta}{\beta_y\rho_\delta - \beta_\delta\rho_y}\right) \\ n_6(\tilde{a}_y, \delta_{va}) &= \frac{N_\delta}{J_z u_a} \end{aligned} \tag{6.118}$$

We remark that all these quantities are, ultimately, combinations of the following six fundamental "bricks":

$$s_1 = \beta_y, \qquad s_2 = \rho_y, \qquad s_3 = \beta_\delta, \qquad s_4 = \rho_\delta, \qquad s_5 = \frac{N_\delta}{J_z}, \qquad s_6 = \frac{Y_\delta}{m} \tag{6.119}$$

all of them, in general, functions of two variables like, e.g., $\tilde{a}_y$ and δ_v. Two vehicles with the same s_i, and hence with the same n_i, have *identical handling behavior*, notwithstanding their size, weight, etc. In other words, they react in exactly the same way to given driver input.

On the practical side, we see that the components of the gradients (6.66) of the steady-state maps $\beta_p(\tilde{a}_y, \delta_v)$ and $\rho_p(\tilde{a}_y, \delta_v)$ provide four out of six "bricks", the other two being the control derivatives. Therefore, there is indeed a relationship between steady-state data and transient behavior of a vehicle. However, this relationship is far from obvious.

6.13 New Understeer Gradient

Let us discuss the new understeer gradient $\rho_y = -K_{\rho_y}$ in detail

$$\rho_y = \frac{\partial \rho_p}{\partial \tilde{a}_y} = \frac{\partial}{\partial \tilde{a}_y}\left(\frac{1}{R}\right) = -\frac{K}{l} = -K_{\rho_y} \tag{6.120}$$

This is similar to the definition of the classical understeer gradient K, but with a few fundamental differences. The definition of K_{ρ_y} does not involve any weak concept, like the wheelbase l or the Ackermann steer angle, as discussed in Sect. 6.9. Moreover, as will be shown in Sect. 6.15.1, it is the correct measure of understeer/oversteer, while K is not. This may look a bit surprising, but that is the way it is.

In general

$$K_{\rho_y} = K_{\rho_y}(\tilde{a}_y, \delta_{va}) \tag{6.121}$$

except in some noteworthy cases, like the single track model with open differential, where, according to (6.67), $K_{\rho_y} = K_{\rho_y}(\tilde{a}_y) = \mathrm{d}f_\rho/\mathrm{d}\tilde{a}_y$.

But there are other reasons that support K_{ρ_y} as a good handling parameter. Let us consider a *constant steering wheel test* and monitor the yaw rate $r_p = r_p(u_a; \delta_{va})$ as a function of the forward speed u_a, keeping constant the steering wheel angle δ_{va}. For brevity, let $r'_p = \mathrm{d}r_p/\mathrm{d}u_a$. Equation (6.120) can be rewritten as

$$\frac{\mathrm{d}\rho_p}{\mathrm{d}\tilde{a}_y} = \frac{\mathrm{d}(r_p/u_a)}{\mathrm{d}(r_p u_a)} = \frac{\mathrm{d}(r_p/u_a)}{\mathrm{d}u_a}\left(\frac{\mathrm{d}(r_p u_a)}{\mathrm{d}u_a}\right)^{-1} = \frac{1}{u_a^2}\left(\frac{r'_p u_a - r_p}{r'_p u_a + r_p}\right) = -K_{\rho_y} \tag{6.122}$$

This general equation provides a way to obtain the critical speed and the characteristic speed. The *characteristic speed* u_{char} is, by definition, the speed at which $r'_p = 0$. By letting $r'_p \to 0$ in (6.122), we obtain that the characteristic speed must satisfy the following equation

$$\frac{1}{u_a^2} = K_{\rho_y} \quad \text{that is } u_{\mathrm{char}} = \sqrt{\frac{1}{K_{\rho_y}}} \tag{6.123}$$

Similarly, the *critical speed* $u_{\rm cr}$ is, by definition, the speed at which $r'_p \to \infty$, which means

$$\frac{1}{u_a^2} = -K_{\rho_y} \quad \text{that is } u_{\rm cr} = \sqrt{-\frac{1}{K_{\rho_y}}} \tag{6.124}$$

Summing up:

- K_{ρ_y} has been defined without any recourse to weak concept, like a reference vehicle having Ackermann steer;
- K_{ρ_y} can be easily measured in constant steering wheel tests;
- the critical speed and the characteristic speed come out naturally as special cases.[10]

A similar treatment applies to the other gradient component $\beta_y = -K_{\beta_y}$. In this case $v_p = v_p(u_a; \delta_{va})$, thus getting

$$\beta_y = \frac{\mathrm{d}\beta_p}{\mathrm{d}\tilde{a}_y} = \frac{\mathrm{d}(v_p/u_a)}{\mathrm{d}(u_a r_p)} = \frac{1}{u_a^2}\left(\frac{v'_p u_a - v_p}{r'_p u_a + r_p}\right) = -K_{\beta_y} \tag{6.125}$$

In general

$$K_{\beta_y} = K_{\beta_y}(\tilde{a}_y, \delta_{va}) \tag{6.126}$$

except in cases like the single track model with open differential, where, according to (6.67), $K_{\beta_y} = K_{\beta_y}(\tilde{a}_y) = \mathrm{d}f_\beta/\mathrm{d}\tilde{a}_y$.

6.14 Stability (Again)

According to (6.93), an equilibrium point is stable if and only if $\mathrm{tr}(\mathbf{A}) < 0$ and $\det(\mathbf{A}) > 0$. These two conditions, after (6.115), can be expressed in terms of the six fundamental bricks (6.119) and the forward speed.

6.15 The Single Track Model Revisited

The suggested approach, which explains why steady-state data are also relevant for the transient behavior, is applied here to the single track model. The goal is to clarify the matter by an example.

[10] Actually, the real critical speed can be lower than the value predicted by (6.124), as shown in [5, pp. 216–219]. Basically, (6.124) may not predict the right value because in real vehicles we control the longitudinal force, not directly the forward speed. Therefore, a real vehicle is a system with three state variables, not just two. This additional degree-of-freedom does affect the critical speed, unless the vehicle is going straight.

For simplicity, we assume $u = u_a$ and $\dot{u} = 0$ and hence start with the linearized equations of motion (6.98). In the single track model (with open differential), the stability derivatives (6.83) can be given a more explicit form (cf. (6.59)) taking into account the axle characteristics

$$\begin{aligned} Y_\beta &= \frac{\partial Y_1}{\partial \alpha_1}\frac{\partial \alpha_1}{\partial \beta} + \frac{\partial Y_2}{\partial \alpha_2}\frac{\partial \alpha_2}{\partial \beta} = -\frac{\partial Y_1}{\partial \alpha_1} - \frac{\partial Y_2}{\partial \alpha_2} = -\Phi_1 - \Phi_2 \\ Y_\rho &= \frac{\partial Y_1}{\partial \alpha_1}\frac{\partial \alpha_1}{\partial \rho} + \frac{\partial Y_2}{\partial \alpha_2}\frac{\partial \alpha_2}{\partial \rho} = -a_1\frac{\partial Y_1}{\partial \alpha_1} + a_2\frac{\partial Y_2}{\partial \alpha_2} = -a_1\Phi_1 + a_2\Phi_2 \end{aligned} \tag{6.127}$$

and

$$\begin{aligned} N_\beta &= a_1\frac{\partial Y_1}{\partial \alpha_1}\frac{\partial \alpha_1}{\partial \beta} - a_2\frac{\partial Y_2}{\partial \alpha_2}\frac{\partial \alpha_2}{\partial \beta} = -a_1\frac{\partial Y_1}{\partial \alpha_1} + a_2\frac{\partial Y_2}{\partial \alpha_2} = -a_1\Phi_1 + a_2\Phi_2 \\ N_\rho &= a_1\frac{\partial Y_1}{\partial \alpha_1}\frac{\partial \alpha_1}{\partial \rho} - a_2\frac{\partial Y_2}{\partial \alpha_2}\frac{\partial \alpha_2}{\partial \rho} = -a_1^2\frac{\partial Y_1}{\partial \alpha_1} - a_2^2\frac{\partial Y_2}{\partial \alpha_2} = -a_1^2\Phi_1 - a_2^2\Phi_2 \end{aligned} \tag{6.128}$$

where

$$\Phi_1 = \frac{\partial Y_1}{\partial \alpha_1} \quad \text{and} \quad \Phi_2 = \frac{\partial Y_2}{\partial \alpha_2} \tag{6.129}$$

are the *slopes* of the axle characteristics at the equilibrium point. Obviously, $\Phi_i > 0$ in the monotone increasing part of the axle characteristics. These slopes are simple to be defined, but not so simple to be measured directly. It is also worth noting that

$$Y_\rho = N_\beta \tag{6.130}$$

To proceed further, let

$$\delta_1 = \tau_1\delta_v \quad \text{and} \quad \delta_2 = \tau_2\delta_v = \chi\tau_1\delta_v \tag{6.131}$$

thus linking the rear steering to the front steering. To have front steering only it suffices to set $\chi = 0$. We can now obtain also the more explicit expressions of the control derivatives

$$Y_\delta = (\Phi_1 + \chi\Phi_2)\tau_1, \qquad N_\delta = (\Phi_1 a_1 - \chi\Phi_2 a_2)\tau_1 \tag{6.132}$$

Therefore, the linearized equations of motions (6.98) are as follows, where Y and N do not depend on u

$$\begin{aligned} m\big(u_a\dot{\beta}_t + u_a^2\rho_t\big) &= -(\Phi_1 + \Phi_2)\beta_t - (\Phi_1 a_1 - \Phi_2 a_2)\rho_t + (\Phi_1 + \chi\Phi_2)\tau_1\delta_{vt} \\ J_z u_a\dot{\rho}_t &= -(\Phi_1 a_1 - \Phi_2 a_2)\beta_t - \big(\Phi_1 a_1^2 + \Phi_2 a_2^2\big)\rho_t + (\Phi_1 a_1 - \chi\Phi_2 a_2)\tau_1\delta_{vt} \end{aligned} \tag{6.133}$$

Formulæ (6.89) become, in this case

$$2\zeta\omega_n = -\operatorname{tr}(\mathbf{A}) = \frac{1}{u_a}\left(\frac{\Phi_1 + \Phi_2}{m} + \frac{\Phi_1 a_1^2 + \Phi_2 a_2^2}{J_z}\right) \tag{6.134}$$

and

$$\omega_n^2 = \det(\mathbf{A}) = \frac{1}{u_a^2 m J_z}\left[\Phi_1\Phi_2(a_1+a_2)^2 - m u_a^2(\Phi_1 a_1 - \Phi_2 a_2)\right] \tag{6.135}$$

and hence

$$\zeta = \frac{(\Phi_1+\Phi_2)J_z + (\Phi_1 a_1^2 + \Phi_2 a_2^2)m}{2\sqrt{J_z m}\sqrt{\Phi_1\Phi_2 l^2 - m u^2(\Phi_1 a_1 - \Phi_2 a_2)}} \tag{6.136}$$

These parameters characterize the handling behavior in the neighborhood of an equilibrium point. Actually, the fundamental "bricks" on which everything is built are the six design parameters

$$\frac{\Phi_1}{m}, \qquad \frac{\Phi_2}{m}, \qquad a_1, \qquad a_2, \qquad \frac{J_z}{m}, \qquad \chi \tag{6.137}$$

in addition to the control parameters u and $\delta_v(t)$, with constant u (τ_1 has no relevance).

At steady-state, the linearized equations of motion become a linear algebraic system of equations

$$\begin{aligned} m\tilde{a}_y = m u_a^2 \rho_p &= -(\Phi_1+\Phi_2)\beta_p - (\Phi_1 a_1 - \Phi_2 a_2)\rho_p + (\Phi_1 + \chi\Phi_2)\tau_1\delta_{va} \\ 0 &= -(\Phi_1 a_1 - \Phi_2 a_2)\beta_p - \left(\Phi_1 a_1^2 + \Phi_2 a_2^2\right)\rho_p + (\Phi_1 a_1 - \chi\Phi_2 a_2)\tau_1\delta_{va} \end{aligned} \tag{6.138}$$

which, when solved, provides the (linear approximation of the) *handling maps* in the neighborhood of the equilibrium point (cf. (6.80))

$$\begin{aligned} \beta_p = \beta_p(\tilde{a}_y, \delta_{va}) = \frac{v_p}{u_a} &= \left(\frac{a_2 + a_1\chi}{l}\right)\tau_1\delta_{va} - \frac{m}{l^2}\left(\frac{\Phi_1 a_1^2 + \Phi_2 a_2^2}{\Phi_1\Phi_2}\right)\tilde{a}_y \\ \rho_p = \rho_p(\tilde{a}_y, \delta_{va}) = \frac{r_p}{u_a} &= \left(\frac{1-\chi}{l}\right)\tau_1\delta_{va} - \frac{m}{l^2}\left(\frac{\Phi_2 a_2 - \Phi_1 a_1}{\Phi_1\Phi_2}\right)\tilde{a}_y \end{aligned} \tag{6.139}$$

We remark that this is a local linear approximation of the handling maps. In the suggested approach, these two maps fully describe the vehicle handling features at steady state.

The components of the gradients $\operatorname{grad}\beta_p$ and $\operatorname{grad}\rho_p$ (defined in (6.66)) are therefore given by

$$\begin{aligned} \beta_y &= -\frac{m}{l^2}\left(\frac{\Phi_1 a_1^2 + \Phi_2 a_2^2}{\Phi_1\Phi_2}\right) = -K_{\beta_y}, \qquad \beta_\delta = \tau_1\left(\frac{a_2 + \chi a_1}{l}\right) = -K_{\beta_\delta} \\ \rho_y &= -\frac{m}{l^2}\left(\frac{\Phi_2 a_2 - \Phi_1 a_1}{\Phi_1\Phi_2}\right) = -K_{\rho_y}, \qquad \rho_\delta = \tau_1\left(\frac{1-\chi}{l}\right) = -K_{\rho_\delta} \end{aligned} \tag{6.140}$$

As already stated, all these components can be obtained experimentally from standard steady-state tests, without having to bother about Ackermann steer angle and the like.

From the results displayed in the first column in (6.140) we get

$$\frac{\Phi_1}{m} = \frac{a_2}{l(K_{\beta_y} + a_1 K_{\rho_y})}, \qquad \frac{\Phi_2}{m} = \frac{a_1}{l(K_{\beta_y} - a_2 K_{\rho_y})} \tag{6.141}$$

which show that there may exist different vehicles with exactly the same values of $K_{\beta_y} = -\beta_y$ and $K_{\rho_y} = -\rho_y$. Therefore, more than two parameters are necessary.

Summing up, for the single track model, the six coefficients s_i in (6.119) are

$$\begin{aligned}
s_1 &= \beta_y = -\frac{m}{(a_1+a_2)^2}\left(\frac{\Phi_2 a_2^2 + \Phi_1 a_1^2}{\Phi_1 \Phi_2}\right) = -K_{\beta_y} \\
s_2 &= \rho_y = -\frac{m}{(a_1+a_2)^2}\left(\frac{\Phi_2 a_2 - \Phi_1 a_1}{\Phi_1 \Phi_2}\right) = -K_{\rho_y} \\
s_3 &= \beta_\delta = \tau_1 \frac{a_2 + \chi a_1}{a_1 + a_2} \\
s_4 &= \rho_\delta = \tau_1 \frac{1-\chi}{a_1 + a_2} \\
s_5 &= \frac{N_\delta}{J_z} = \tau_1 \frac{\Phi_1 a_1 - \chi \Phi_2 a_2}{J_z} \\
s_6 &= \frac{Y_\delta}{m} = \tau_1 \frac{C_1 + \chi \Phi_2}{m}
\end{aligned} \tag{6.142}$$

Of course, they depend on the six design parameters listed in (6.137): Φ_1/m, Φ_2/m, a_1, a_2, J_z/m, χ.

Assuming χ as given, we obtain from the first four equations in (6.142)

$$\begin{aligned}
\frac{\Phi_1}{m} &= \frac{\rho_\delta(\beta_\delta - \chi\tau_1)}{\tau_1(\chi-1)[\beta_y\rho_\delta - \rho_y(\beta_\delta - \tau_1)]} = \frac{s_4(s_3 - \chi\tau_1)}{\tau_1(\chi-1)[s_1 s_4 - s_2(s_3 - \tau_1)]} \\
\frac{\Phi_2}{m} &= \frac{\rho_\delta(\tau_1 - \beta_\delta)}{\tau_1(\chi-1)[\beta_y\rho_\delta - \rho_y(\beta_\delta - \chi\tau_1)]} = \frac{s_4(\tau_1 - s_3)}{\tau_1(\chi-1)[s_1 s_4 - s_2(s_3 - \chi\tau_1)]}
\end{aligned} \tag{6.143}$$

$$\begin{aligned}
a_1 &= \frac{\tau_1 - \beta_\delta}{\rho_\delta} = \frac{\tau_1 - s_3}{s_4} \\
a_2 &= \frac{\beta_\delta - \chi\tau_1}{\rho_\delta} = \frac{s_3 - \chi\tau_1}{s_4}
\end{aligned}$$

Then, also considering the fifth equation

$$\frac{J_z}{m} = \frac{1}{s_5}\frac{(\beta_y\rho_\delta - \rho_y\beta_\delta)(\beta_\delta - \chi\tau_1)(\beta_\delta - \tau_1)}{[\beta_y\rho_\delta - \rho_y(\beta_\delta - \tau_1)][\beta_y\rho_\delta - \rho_y(\beta_\delta - \chi\tau_1)]} \tag{6.144}$$

In the single track model there are not enough design parameters to fulfill all six equations. Therefore, the value of s_6 depends on the other five parameters s_i, $i = 1, \ldots, 5$.

Table 6.1 Features of vehicles with different amounts of rear steering χ, but with almost identical transient handling behavior. The old understeer gradient K conveys misleading information

χ	C_1 [N/rad]	C_2 [N/rad]	a_1 [m]	a_2 [m]	J_z [kg m^2]	m [kg]	K [deg/g]	K_{ρ_y} [deg/g]
−0.10	76 629	93 559	0.91	1.93	3 169	1 365	4.16	1.46
−0.05	74 900	91 452	0.91	1.80	2 759	1 365	3.97	1.46
0.00	73 000	90 000	0.91	1.67	2 400	1 365	3.78	1.46
+0.05	70 899	89 144	0.91	1.54	2 084	1 365	3.59	1.46
+0.10	68 565	88 851	0.91	1.41	1 803	1 365	3.40	1.46

6.15.1 Different Vehicles with Almost Identical Handling

It is kind of interesting to employ Eqs. (6.143) and (6.144) to obtain Φ_1/m, Φ_2/m, a_1, a_2 and J_z/m for given s_1–s_5, but different values of χ, that is with a different amount of rear steering. This way, it is possible to create vehicles that look very different, but which ultimately have almost exactly the same handling behavior. The little difference being due to the term s_6 that cannot be set to the same value for all vehicles, due to the lack of parameters in the single track model.

A vehicle with front steering only has $\chi = 0$, while, e.g., $\chi = -0.05$ means a rear steering angle $\delta_2 = -0.05\delta_1$, and so on.

But, let us do some numerical examples. Let us consider a vehicle with only front steering (i.e., $\chi = 0$), with the following features:

- $m = 1\,365$ kg;
- $J_z = 2\,400$ kg m^2;
- $a_1 = 0.912$ m;
- $a_2 = 1.668$ m;
- $\Phi_1 = C_1 = 73\,000$ N/rad;
- $\Phi_2 = C_2 = 90\,000$ N/rad.

From (6.142) we can compute all s_i for this vehicle.

Then we can set a non-zero value for χ and, employing the very same values of s_1, s_2, s_3, s_4 and s_5, compute the corresponding physical quantities C_1, C_2, a_1, a_2, J_z and m, according to (6.143) and (6.144). The results for some values of χ are shown in Table 6.1. The five vehicles there reported are strikingly different, yet they have (almost) the same handling behavior, and not limited to steady state. For the driver, they behave quite the same way even under transient conditions, like under a step steering input.

The amazing similarity of the handling dynamics between these five vehicles can be appreciated looking at Figs. 6.34, 6.35, 6.36 and 6.37, where the time-histories of some variables are shown and compared. All figures refer to a step steer $\delta_1 = 2.2°$, with $u = 30$ m/s, starting from a straight trajectory.

But perhaps the most astonishing result is that these vehicle, although with almost identical handling, do not have the same understeer gradient K. Just have a look at

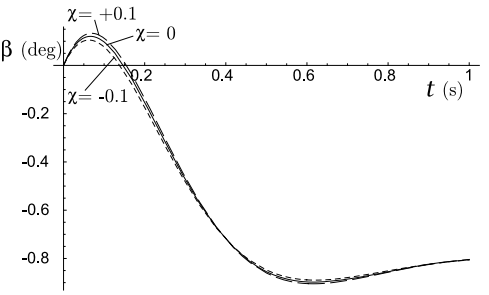

Fig. 6.34 Vehicle slip angle $\beta(t)$ after a step steering input

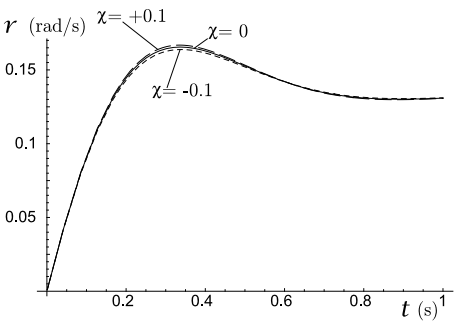

Fig. 6.35 Yaw rate $r(t)$ after a step steering input

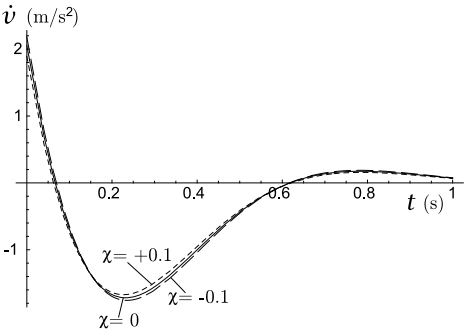

Fig. 6.36 Derivative $\dot{v}(t)$ of the lateral speed after a step steering input

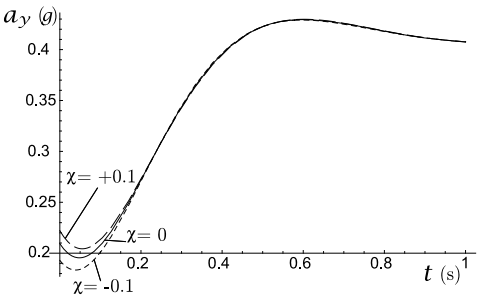

Fig. 6.37 Lateral acceleration $a_y(t) = \dot{v} + ur$ after a step steering input

the next to last column in Table 6.1. In other words, they would have been classified as very different if evaluated in terms of their understeer gradient K.

The conclusion is that the classical understeer gradient is *not* a good parameter and should be abandoned. It should be replaced by the gradient components proposed in (6.66) and discussed in Sect. 6.13, which have proven to really provide a measure of the dynamic features of a vehicle. In particular, the gradient component K_{ρ_y}, shown in the last column in Table 6.1, is the real measure of understeer/oversteer.

6.16 Road Vehicles with Locked or Limited Slip Differential

The handling of road cars equipped with either a locked or a limited slip differential is addressed in Sect. 7.5, that is in the chapter devoted to race car handling behavior. This has been done because the limited slip differential is a peculiarity of almost all race cars, whereas very few road cars have it.

6.17 Linear Single Track Model

The simplest dynamical systems are those governed by *linear* ordinary differential equations with *constant* coefficients. The single track model of Fig. 6.1 is governed by the *nonlinear* ordinary differential equations (6.111), unless the axle characteristics are replaced by linear functions

$$Y_1 = C_1\alpha_1 \quad \text{and} \quad Y_2 = C_2\alpha_2 \tag{6.145}$$

where

$$C_1 = \left.\frac{\mathrm{d}Y_1}{\mathrm{d}\alpha_1}\right|_{\alpha_1=0} \quad \text{and} \quad C_2 = \left.\frac{\mathrm{d}Y_2}{\mathrm{d}\alpha_2}\right|_{\alpha_2=0} \tag{6.146}$$

The *axle lateral slip stiffness* C_i is usually equal to twice the tire lateral slip stiffness, firstly introduced in (2.77). It is affected by the static vertical load (Fig. 2.18), but not by the load transfer, neither by the amount of grip. The influence of roll steer is quite peculiar (Fig. 6.6).

However, as shown in Fig. 6.38, this linear approximation is acceptable only if $|\alpha_i| < 2°$, that is for very low values of a_y.

The main advantage of the linear single track model is its simplicity, the main disadvantage is that it does not model the vehicle behavior at all, unless the lateral acceleration is really small (typically, $a_y < 0.2\ g$ on dry asphalt). In some sense, it is a "dangerous" model because you may be tempted to use it outside its range of validity.

Nevertheless, in some cases it is useful to have a model where everything can be obtained analytically.

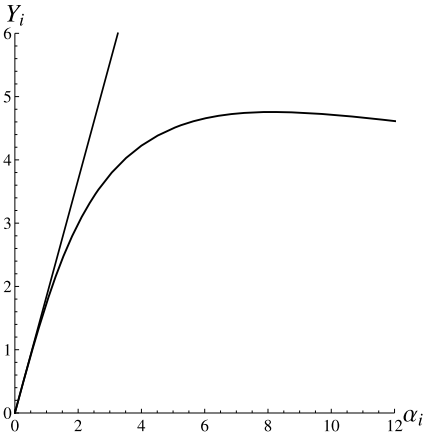

Fig. 6.38 Linear approximation of the axle characteristics

6.17.1 Governing Equations

The *linear* single track model differs from the more general nonlinear model only for the constitutive equations. However, we list here all relevant equations, that is equilibrium equations

$$\begin{aligned} m(\dot{v} + ur) &= Y = Y_1 + Y_2 \\ J_z\dot{r} &= N = Y_1 a_1 - Y_2 a_2 \end{aligned} \tag{6.147}$$

congruence equations (with $|\chi| \ll 1$, and often equal to zero)

$$\begin{aligned} \alpha_1 &= \tau_1 \delta_v - \frac{v + ra_1}{u} \\ \alpha_2 &= \chi\tau_1 \delta_v - \frac{v - ra_2}{u} \end{aligned} \tag{6.148}$$

and the *linear* constitutive equations

$$\begin{aligned} Y_1 &= C_1 \alpha_1 \\ Y_2 &= C_2 \alpha_2 \end{aligned} \tag{6.149}$$

Combining congruence and constitutive equations we get

$$\begin{aligned} Y_1 &= C_1\alpha_1 = C_1\left(\tau_1\delta_v - \frac{v + ra_1}{u}\right) \\ Y_2 &= C_2\alpha_2 = C_2\left(\tau_1\chi\,\delta_v - \frac{v - ra_2}{u}\right) \end{aligned} \tag{6.150}$$

which are linear in v and r, but not in u.

Inserting these equations into the equilibrium equations, we obtain the governing equations, that is two *linear* differential equations

$$\begin{aligned}\dot{v} &= -\left(\frac{C_1+C_2}{mu}\right)v - \left(\frac{C_1a_1-C_2a_2}{mu}+u\right)r + \frac{C_1+\chi C_2}{m}\tau_1\delta_v \\ \dot{r} &= -\left(\frac{C_1a_1-C_2a_2}{J_zu}\right)v - \left(\frac{C_1a_1^2+C_2a_2^2}{J_zu}\right)r + \frac{C_1a_1-\chi C_2a_2}{J_z}\tau_1\delta_v\end{aligned} \tag{6.151}$$

In matrix notation, (6.151) becomes

$$\dot{\mathbf{w}} = \mathbf{A}\mathbf{w} + \mathbf{b}\delta_v \tag{6.152}$$

where $\mathbf{w}(t) = (v(t), r(t))$ is the vector of state variables, the r.h.s. known vector is

$$\mathbf{b}(t) = \tau_1 \begin{bmatrix} \frac{C_1+\chi C_2}{m} \\ \frac{C_1a_1-\chi C_2a_2}{J_z} \end{bmatrix} \tag{6.153}$$

and

$$\mathbf{A} = \mathbf{A}\big(u(t)\big) = -\begin{bmatrix} \frac{C_1+C_2}{mu} & \frac{C_1a_1-C_2a_2}{mu}+u \\ \frac{C_1a_1-C_2a_2}{J_zu} & \frac{C_1a_1^2+C_2a_2^2}{J_zu} \end{bmatrix} \tag{6.154}$$

is the coefficient matrix. It is important to note that $\mathbf{A}$ depends on the forward speed u, but not on the steer angle δ_v, which multiplies the known vector $\mathbf{b}$.

6.17.2 Solution for Constant Forward Speed

As well known, the general solution $\mathbf{w}(t)$ of (6.152) is given by the solution $\mathbf{w}_o$ of the homogeneous equation plus a particular solution $\mathbf{w}_p$

$$\mathbf{w}(t) = \mathbf{w}_o(t) + \mathbf{w}_p(t) \tag{6.155}$$

Unfortunately, analytical solutions are not available if $u(t) \neq \text{const}$.

If u is *constant* ($\dot{u} = 0$), the system (6.152) has constant coefficients and the homogeneous solution must fulfill, with a constant matrix $\mathbf{A}$

$$\dot{\mathbf{w}}_o = \mathbf{A}\mathbf{w}_o \tag{6.156}$$

Assuming constant u is therefore a very relevant assumption. We look for a solution among the exponential functions

$$\mathbf{w}_o(t) = \big(v_o(t), r_o(t)\big) = \mathbf{x}e^{\lambda t} \tag{6.157}$$

which implies $\dot{\mathbf{w}}_o(t) = \lambda \mathbf{x} e^{\lambda t}$, and consequently yields an eigenvalue problem for the matrix $\mathbf{A}$

$$\mathbf{A}\mathbf{x} = \lambda \mathbf{x} \tag{6.158}$$

The eigenvalues are the solutions of the characteristic equation

$$\det(\mathbf{A} - \lambda \mathbf{I}) = 0 \tag{6.159}$$

that, for a (2×2) matrix, becomes

$$\lambda^2 - \operatorname{tr}(\mathbf{A})\lambda + \det(\mathbf{A}) = 0 \tag{6.160}$$

The two eigenvalues λ_1 and λ_2 are

$$\lambda_{1,2} = \frac{\operatorname{tr}(\mathbf{A}) \pm \sqrt{\operatorname{tr}(\mathbf{A})^2 - 4\det(\mathbf{A})}}{2} = -\zeta \omega_n \pm \omega_n \sqrt{\zeta^2 - 1} \tag{6.161}$$

If the discriminant is negative, that is if $\zeta < 1$, the dynamical system is underdamped and the eigenvalues are complex conjugates.

From (6.154) we get the trace

$$\operatorname{tr}(\mathbf{A}) = -\frac{1}{u}\left(\frac{C_1 + C_2}{m} + \frac{C_1 a_1^2 + C_2 a_2^2}{J_z}\right) < 0 \tag{6.162}$$

and the determinant

$$\det(\mathbf{A}) = \frac{1}{u^2 m J_z}\left[C_1 C_2 (a_1 + a_2)^2 - m u^2 (C_1 a_1 - C_2 a_2)\right] \tag{6.163}$$

These two quantities are very important because they provide handy information about the two eigenvalues λ_1 and λ_2 of $\mathbf{A}$, since

$$\operatorname{tr}(\mathbf{A}) = \lambda_1 + \lambda_2 \tag{6.164}$$

$$\det(\mathbf{A}) = \lambda_1 \lambda_2 \tag{6.165}$$

These two relationships can be obtained easily writing the characteristic equation as $(\lambda - \lambda_1)(\lambda - \lambda_2) = 0$.

Once the two eigenvalues have been obtained, we can compute the two eigenvectors $\mathbf{x}_1$ and $\mathbf{x}_2$.

Therefore, the solution of the homogeneous system is

$$\mathbf{w}_o(t) = \gamma_1 \mathbf{x}_1 e^{\lambda_1 t} + \gamma_2 \mathbf{x}_2 e^{\lambda_2 t} \tag{6.166}$$

where γ_1 and γ_2 are still to be determined constants. In components we have

$$\begin{aligned} v_o(t) &= \gamma_1 x_{11} e^{\lambda_1 t} + \gamma_2 x_{12} e^{\lambda_2 t} \\ r_o(t) &= \gamma_1 x_{21} e^{\lambda_1 t} + \gamma_2 x_{22} e^{\lambda_2 t} \end{aligned} \tag{6.167}$$

where $\mathbf{x}_1 = (x_{11}, x_{21})$ and $\mathbf{x}_2 = (x_{12}, x_{22})$.

The particular integral $\mathbf{w}_p(t) = (v_p(t), r_p(t))$ depends on the known vector $\mathbf{b}$ and on the steering wheel angle $\delta_v(t)$. The simplest case is for constant δ_v, but analytical solutions are available also when $\delta_v(t)$ is a polynomial or a trigonometric function.

Summing up, the general solution of the system (6.152) is

$$\mathbf{w}(t) = \mathbf{w}_o(t) + \mathbf{w}_p(t) = \gamma_1 \mathbf{x}_1 e^{\lambda_1 t} + \gamma_2 \mathbf{x}_2 e^{\lambda_2 t} + \mathbf{w}_p(t) \tag{6.168}$$

in which the two constants γ_1 and γ_2 appear to be determined from the initial conditions $\mathbf{w}(0) = (v(0), r(0))$, that is solving the system

$$\mathbf{S}\mathbf{y} = \mathbf{w}(0) - \mathbf{w}_p(0) \tag{6.169}$$

where $\mathbf{y} = (\gamma_1, \gamma_2)$ and $\mathbf{S}$ is the matrix whose columns are the two eigenvectors of $\mathbf{A}$.

6.17.3 Critical Speed

The two parts $\mathbf{w}_o$ and $\mathbf{w}_p$ of the general solution have distinct physical meanings. The particular integral is what the vehicle does asymptotically, that is basically at steady-state. The solution of the homogeneous system shows how the vehicle behaves before reaching the steady-state condition, if the vehicle is stable.

As already discussed in Sect. 6.11.3, the stability of the vehicle is completely determined by the two eigenvalues λ_1 and λ_2, or better, by the sign of their real parts $\mathrm{Re}(\lambda_1)$ and $\mathrm{Re}(\lambda_2)$. The rule is very simple: the system is asymptotically stable if and only if both eigenvalues have negative real parts

$$\text{stability} \iff \mathrm{Re}(\lambda_1) < 0 \quad \text{and} \quad \mathrm{Re}(\lambda_2) < 0 \tag{6.170}$$

If just one eigenvalue has a positive real part, the corresponding exponential solution grows without bound in time, and the system is unstable.

Fortunately, we can check the stability without computing the two eigenvalues explicitly, but simply looking at (6.164) and (6.165). To have an asymptotically stable vehicle it suffices to check that

$$\text{stability} \iff \mathrm{tr}(\mathbf{A}) < 0 \quad \text{and} \quad \det(\mathbf{A}) > 0 \tag{6.171}$$

From (6.162) we see immediately that $\mathrm{tr}(\mathbf{A}) < 0$ is always fulfilled. Stability is therefore completely due to the second condition in (6.171). Setting $\det(\mathbf{A}) = 0$ in (6.135) yields an equation in the unknown forward speed u, whose solution, if it exists, is the *critical speed* u_{cr}

$$u_{\mathrm{cr}} = \sqrt{\frac{C_1 C_2 l^2}{m(C_1 a_1 - C_2 a_2)}} \tag{6.172}$$

Beyond the critical speed the vehicle becomes unstable. It is worth noting that u_{cr} does not depend on J_z.

In the linear single track model, the critical speed exists if and only if

$$C_1 a_1 - C_2 a_2 > 0 \tag{6.173}$$

That is, if the vehicle is oversteer. In this vehicle model (which, we recall, has a very limited range of applicability), the critical speed is not affected by the steer angle.

6.17.4 Transient Vehicle Behavior

It may be of some interest to know how the eigenvalues evolve as the speed changes. To this end, it is useful to plot tr(**A**) vs det(**A**), which, according to (6.162) and (6.163), can be compactly expressed as[11]

$$\det(\mathbf{A}) = \frac{\alpha}{u^2} + \beta, \qquad \mathrm{tr}(\mathbf{A}) = -\frac{\gamma}{u} \tag{6.174}$$

where α and γ are always positive, while $\beta = (C_2 a_2 - C_1 a_1)/J_z$ can be either be positive or negative, depending on the vehicle being understeer or oversteer, respectively.

Both functions are monotone increasing in u (if $u > 0$). They can be combined to get

$$\det(\mathbf{A}) = \frac{\alpha}{\gamma^2}\,\mathrm{tr}(\mathbf{A})^2 + \beta \tag{6.175}$$

Moreover, it is easy to show that

$$\lim_{u \to +\infty} \mathrm{tr}(\mathbf{A}) = 0^-, \qquad \lim_{u \to +\infty} \det(\mathbf{A}) = \beta \tag{6.176}$$

Therefore, as u grows, we draw parabolas, as shown in Fig. 6.39, up to their vertex in $(0, \beta)$.

Also plotted in Fig. 6.39 is the parabola $\det = \mathrm{tr}^2/4$. According to (6.161), it corresponds to the points where $\lambda_1 = \lambda_2$. Below this parabola the two eigenvalues are real, whereas above it they are complex conjugates to each other.

It can be shown that

$$\left(\frac{\alpha}{\gamma^2} = \frac{C_1 C_2 k^2 l^2}{[k^2(C_1 + C_2) + C_1 a_1^2 + C_2 a_2^2]^2} \right) \leq \frac{1}{4} \tag{6.177}$$

where $J_z = mk^2$. Since it attains its maximum value $1/4$ when $C_1 a_1 = C_2 a_2$ (neutral vehicle) and $J_z = m a_1 a_2$, we see that all vehicles at sufficiently low speed have real negative eigenvalues.

As the speed increases, there can be the following possible evolutions. An oversteer vehicle (actually, an oversteer linear single track model) has always two real

[11] Here α, β and γ are just constants. They have no connection with slip and camber angles.

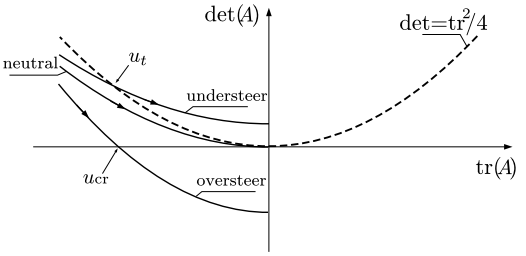

Fig. 6.39 Evolution of det(A) and tr(A) when u grows

eigenvalues. When the parabola in Fig. 6.39 crosses the horizontal axis (det = 0), one eigenvalue becomes positive and the vehicle becomes unstable. That happens for $u = u_{\rm cr}$.

An understeer vehicle has two negative real eigenvalues at low speed. For speeds higher than $u = u_t$ they become complex conjugate with negative real parts (Fig. 6.39): $\lambda_1 = -\zeta\omega_n + i\omega_n\sqrt{1-\zeta^2}$, $\lambda_2 = -\zeta\omega_n - i\omega_n\sqrt{1-\zeta^2}$. Therefore, at sufficiently high speed, the transient motion is a damped oscillation (very damped, indeed). The speed u_t is given by

$$u_t = \sqrt{\frac{\gamma^2 - 4\alpha}{4\beta}} = \sqrt{\frac{[J_z(C_1+C_2) + m(C_1a_1^2 + C_2a_2^2)]^2 - 4J_z m C_1 C_2 l^2}{4m^2 J_z(C_2a_2 - C_1a_1)}} \tag{6.178}$$

From Fig. 6.40, we see that the imaginary part of the eigenvalues, that is the angular frequency $\omega_s = \omega_n\sqrt{1-\zeta^2}$, is almost constant up to relatively high speeds. This is typical and makes the classical sine sweep test quite insensitive to the selected speed.

The general solution is given by (6.168). However, when the eigenvalues are complex conjugates, also the eigenvectors $\mathbf{x}_1$ and $\mathbf{x}_2$ and the constants γ_1 and γ_2 are complex conjugates. Having to deal with so many complex numbers to eventually get a real function $\mathbf{w}(t)$ is not very convenient. Fortunately, we can rearrange it in a way that it involves only real numbers. As well known, $\mathrm{e}^{(\zeta+i\omega)t} = \mathrm{e}^{\zeta t}[\cos(\omega t) + i\sin(\omega t)]$, and the general solution can be written as

$$\begin{aligned}
\mathbf{w}(t) &= \mathbf{w}_o(t) + \mathbf{w}_p(t) \\
&= \gamma_1\mathbf{x}_1\mathrm{e}^{\lambda_1 t} + \gamma_2\mathbf{x}_2\mathrm{e}^{\lambda_2 t} + \mathbf{w}_p(t) \\
&= \mathrm{e}^{-\zeta\omega_n t}\left[(\gamma_1\mathbf{x}_1 + \gamma_2\mathbf{x}_2)\cos(\omega_s t) + i(\gamma_1\mathbf{x}_1 - \gamma_2\mathbf{x}_2)\sin(\omega_s t)\right] + \mathbf{w}_p(t) \\
&= \mathrm{e}^{-\zeta\omega_n t}\left[\mathbf{z}_1\cos(\omega_s t) + \mathbf{z}_2\sin(\omega_s t)\right] + \mathbf{w}_p(t)
\end{aligned} \tag{6.179}$$

where $\omega_s = \omega_n\sqrt{1-\zeta^2}$.

To obtain $\mathbf{z}_1$ and $\mathbf{z}_2$ we can proceed as follows. Vector $\mathbf{z}_1$ is simply obtained setting $t = 0$ in the last expression in (6.179)

$$\mathbf{z}_1 = \mathbf{w}(0) - \mathbf{w}_p(0) \tag{6.180}$$

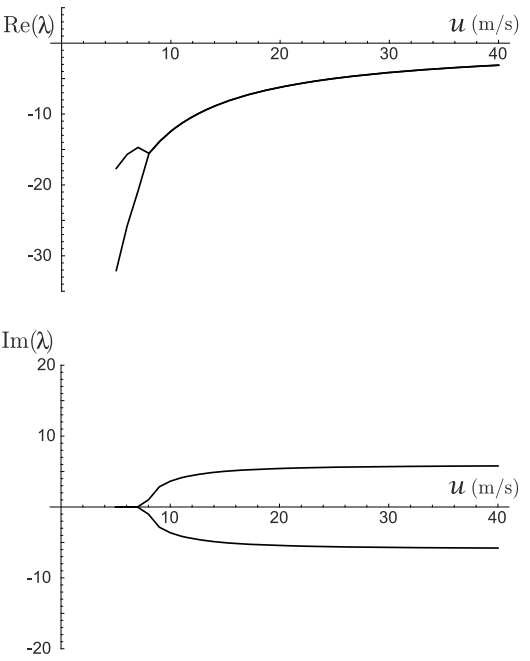

Fig. 6.40 Evolution of the real part and of the imaginary part of λ_1 and λ_2 as functions of the forward speed u, for an understeer vehicle

where $\mathbf{w}(0)$ is the vector of the initial conditions. To obtain the other vector, just consider that

$$\dot{\mathbf{w}}_o(0) = \mathbf{A}\mathbf{w}_o(0) = -\zeta\omega_n\mathbf{z}_1 + \omega_s\mathbf{z}_2 = \mathbf{z}_1 \tag{6.181}$$

and hence

$$\mathbf{z}_2 = \frac{1}{\omega_s}(\mathbf{A} + \zeta\omega_n\mathbf{I})\mathbf{z}_1 \tag{6.182}$$

6.17.5 Steady-State Behavior: Steering Pad

As already stated, the particular integral $\mathbf{w}_p(t) = (v_p(t), r_p(t))$ is determined, in this linear model, by the known vector $\mathbf{b}$, and hence by the function $\delta_v(t)$. The simplest case is when $\delta_v = \text{const}$.

Keeping the steering wheel in a fixed position and driving at constant speed makes the vehicle go round in a circle. This is called steering pad. To obtain the steady-state solution, we have to solve the system

$$-\mathbf{A}\mathbf{w}_p = \mathbf{b}\delta_v \tag{6.183}$$

thus getting

$$\begin{aligned} v_p &= \frac{[C_1C_2l(a_2+a_1\chi)-mu^2(C_1a_1-C_2a_2\chi)]u}{C_1C_2l^2-mu^2(C_1a_1-C_2a_2)}\tau_1\delta_v \\ r_p &= \frac{C_1C_2l(1-\chi)u}{mJu^2\det(\mathbf{A})}\tau_1\delta_v = \frac{C_1C_2l(1-\chi)u}{C_1C_2l^2-mu^2(C_1a_1-C_2a_2)}\tau_1\delta_v \end{aligned} \tag{6.184}$$

Once we have obtained v_p and r_p, we can easily compute all other relevant quantities, like the vehicle slip angle β_p and the Ackermann angle $\gamma_p = l/R_p$

$$\begin{aligned} \beta_p &= \frac{v_p}{u} = \frac{a_2+a_1\chi}{l}\tau_1\delta_v - \tilde{a}_y\frac{m}{l^2}\left(\frac{C_1a_1^2+C_2a_2^2}{C_1C_2}\right) = \frac{S_p}{R_p} \\ \gamma_p &= \frac{lr_p}{u} = (1-\chi)\tau_1\delta_v - \tilde{a}_y\frac{m}{l}\left(\frac{C_2a_2-C_1a_1}{C_1C_2}\right) = \frac{l}{R_p} \end{aligned} \tag{6.185}$$

According to (6.148), we can compute the steady-state front and rear slip angles

$$\begin{aligned} \alpha_{1p} &= \tau_1\delta_v - \frac{v_p+r_pa_1}{u} = \frac{ma_2}{lC_1}\tilde{a}_y \\ \alpha_{2p} &= \chi\tau_1\delta_v - \frac{v_p-r_pa_2}{u} = \frac{ma_1}{lC_2}\tilde{a}_y \end{aligned} \tag{6.186}$$

A non-zero lateral speed v_p at steady state may look a bit strange, at first sight. It simply means that the trajectory of G is not tangent to the vehicle longitudinal axis. As shown in Fig. 6.9(a), at low lateral acceleration we have very small slip angles α_{1p} and α_{2p} and, as a consequence, β_p has the same sign as δ_v. At high lateral acceleration, the large slip angles cause β_p to become of opposite sign with respect to δ_v, as shown in Fig. 6.9(b).

The speed u_β that makes $\beta_p = v_p = 0$ is given by (6.184) and is equal to (if $\chi = 0$)

$$u_\beta = \sqrt{\frac{C_2a_2l}{a_1m}} \tag{6.187}$$

It is called *tangent speed*.

6.17.6 Lateral Wind Gust

It is of some practical interest to study the behavior of a vehicle (albeit a very linear one) when suddenly subjected to a lateral force, like the force due to a lateral wind gust hitting the car when, e.g., exiting a tunnel. Actually, the same mathematical problem also covers the case of a car going straight along a banked road.

We have only to modify the equilibrium equations (6.147) by adding a lateral force $\mathbf{F}_l = -F_l\mathbf{j}$, applied at a distance x from G

$$\begin{aligned} m(\dot{v} + ur) &= F_{y_1} + F_{y_2} - F_l \\ J_z\dot{r} &= F_{y_1}a_1 - F_{y_2}a_2 - F_l x. \end{aligned} \tag{6.188}$$

where $x > 0$ if $\mathbf{F}_l$ is applied along a line closer to the front axle than G. The other equations are non affected directly by $\mathbf{F}_l$.

The equations of motion are like in (6.152), with the only difference that the term

$$\mathbf{b}_F = -\begin{bmatrix} 1/m \\ x/J \end{bmatrix} F_l \tag{6.189}$$

must be added to the known vector.

The steady-state conditions $\mathbf{w}_p$ are obtained, as usual, by solving the system of equations $-\mathbf{A}\mathbf{w}_p = \mathbf{b}_F$, with $\mathbf{A}$ as given in (6.154).

If we assume $\delta_v = 0$, we have the following quantities at steady-state

$$\begin{aligned} v_p &= \frac{[x(C_1a_1 - C_2a_2 + mu^2) - (C_1a_1^2 + C_2a_2^2)]u}{C_1C_2l^2 - mu^2(C_1a_1 - C_2a_2)} F_l \\ r_p &= \frac{[C_1a_1 - C_2a_2 - x(C_1 + C_2)]u}{C_1C_2l^2 - mu^2(C_1a_1 - C_2a_2)} F_l = \frac{-y(C_1 + C_2)u}{C_1C_2l^2 - mu^2(C_1a_1 - C_2a_2)} F_l \end{aligned} \tag{6.190}$$

where we set

$$x = e + y$$

with

$$e = \frac{C_1a_1 - C_2a_2}{C_1 + C_2} \tag{6.191}$$

Should the steer angle be non-zero, it suffices to superimpose the effects. This is legitimate because of the linearity of the equations.

This quantity e in (6.191) is often called *static margin*. The yaw rate is zero, that is $r_p = 0$, if and only if the lateral force is applied at a distance e from G. This is the distance that makes the vehicle translate diagonally under the action of a lateral force, as shown in Fig. 6.41. The point N_p on the axis of the vehicle at a distance e from G is called *neutral steer point*.

Obviously, the condition $r_p = 0$ with $\delta_v = 0$ is equivalent to $\alpha_{1p} = \alpha_{2p} = \alpha_p$. Inserting this condition into (6.188) we get

$$\begin{aligned} 0 &= (C_1 + C_2)\alpha_p - F_l \\ 0 &= (C_1a_1 - C_2a_2)\alpha_p - F_l e \end{aligned} \tag{6.192}$$

which provide another way to obtain e.

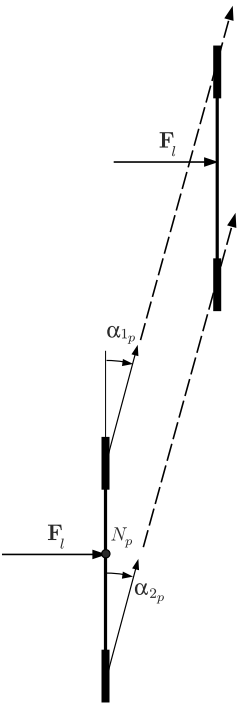

Fig. 6.41 Lateral force applied at the neutral point ($x = e$)

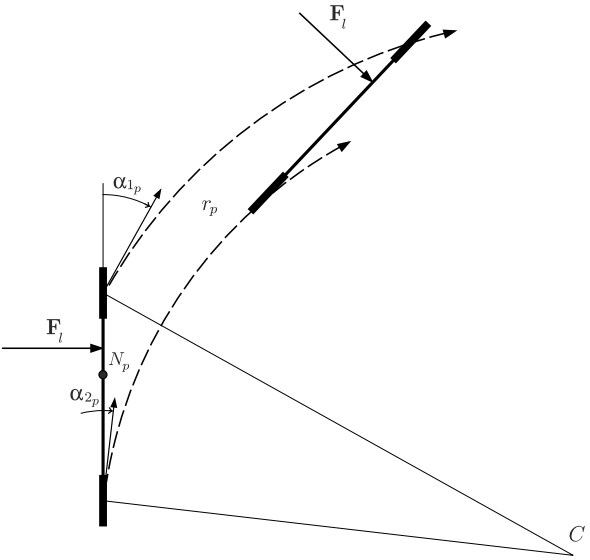

Fig. 6.42 Lateral force applied at a point ahead of the neutral point ($x > e$)

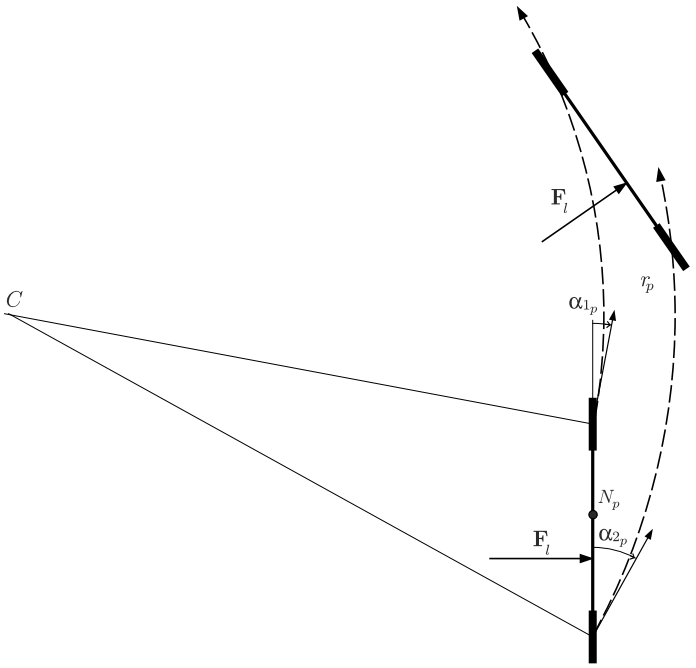

Fig. 6.43 Lateral force applied at a point behind the neutral point ($x < e$)

An oversteer vehicle has $e > 0$, whereas $e < 0$ in an understeer vehicle. In a medium size road car, we have $e/l \simeq -0.06$.

If $\delta_v = 0$, the steady-state distance R_p is

$$R_p = \frac{u}{r_p} = \frac{C_1 C_2 l^2 - mu^2(C_1 a_1 - C_2 a_2)}{-y(C_1 + C_2)F_l} \tag{6.193}$$

The numerator is always positive if $u < u_{\text{cr}}$. Therefore, $R_p > 0$ if $y < 0$ and vice versa.

If the point of application of the lateral force is located ahead of the neutral point, the vehicle behaves like in Fig. 6.42, turning in the same direction as the lateral force. This is commonly considered good behavior.

If the point of application of the lateral force is behind the neutral point, the vehicle behaves like in Fig. 6.43. This is commonly considered bad behavior.

Of course, since an oversteer vehicle has a neutral point ahead of G, the likelihood that a wind gust applies a force behind the neutral point is stronger, much stronger, than in an understeer vehicle.

To understand why the first case is considered good, while the second is considered bad, we have to look at the lateral forces that the tire have to exert. In the first case, the inertial effects counteract the wind gust, thus alleviating the tire job. In the second case, the inertial effects add to the lateral force, making the tire job harder.

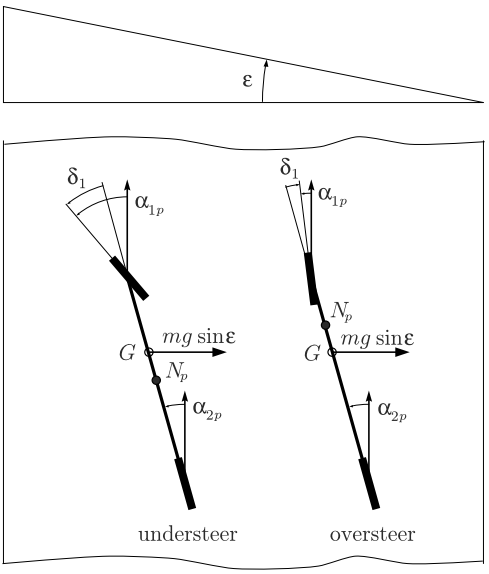

Fig. 6.44 Understeer ad oversteer vehicles going straight on a banked road

6.17.7 Banked Road

A car going straight on a banked road is subject to a lateral force due to its own weight. Therefore, it is a situation somehow similar to a lateral wind gust, but not equal. The main difference is that the lateral force is now applied at G.

Understeer and oversteer vehicles behave differently, as shown in Fig. 6.44. Both axles must exert lateral forces directed uphill to counteract the weight force $mg \sin \varepsilon$. Therefore, both must work with positive slip angles, like in Fig. 6.44. However, due to the different location of the neutral point N_p with respect to G, the two axles cannot have the same slip angle. To go straight, we must steer the front wheels uphill in an understeer vehicle and downhill in an oversteer vehicle, as in Fig. 6.44.

6.18 Compliant Steering System

Many modern cars use rack and pinion steering mechanisms. The steering wheel turns the pinion gear, which moves the rack, thus converting circular motion into linear motion. This motion applies steering torque to the front wheels via tie rods and a short lever arm called the steering arm.

So far we have assumed the steering system to be perfectly rigid, as stated at p. 47. More precisely, Eq. (3.123) have been used to relate the steer angles δ_{ij} of each wheel to the angle δ_v of the steering wheel.

In the single track model (Fig. 6.1) we have taken a further step, assuming that the left and right gear ratio of the steering system are almost equal, that is

$$(\tau_{11} = \tau_{12}) = \tau_1 \quad \text{and} \quad (\tau_{21} = \tau_{22}) = \tau_2 \tag{6.22'}$$

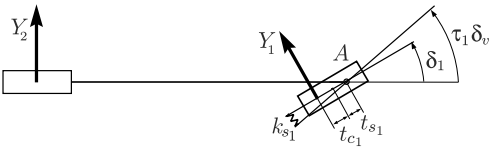

Fig. 6.45 Single track model with compliant steering system

thus getting (6.74)

$$\begin{aligned}(1+\hat{\chi})\delta &= \delta_1 = \tau_1\delta_v \\ \hat{\chi}\delta &= \delta_2 = \tau_2\delta_v\end{aligned} \tag{6.74′}$$

Now, in the framework of the *linear* single track model, we relax the assumption of rigid steering system. This means making a few changes in the congruence Eq. (6.148), since δ_1 and $\tau_1\delta_v$ are no longer equal to each other.

6.18.1 Governing Equations

As shown in Fig. 6.45, the steering system now has a finite angular stiffness k_{s_1} with respect to the axis about which the front wheel steers. In a turn, the lateral force Y_1 exerts a vertical moment with respect to the steering axis A because of the pneumatic trail t_{c_1} and also of the trail t_{s_1} due to the suspension layout (see Fig. 3.1). The effect of this vertical moment $Y_1(t_{c_1}+t_{s_1})$ on a compliant steering system is to make the front wheel to steer less than $\tau_1\delta_v$. More precisely, we have that (Fig. 6.45)

$$\delta_1 = \tau_1\delta_v - \frac{Y_1(t_{c_1}+t_{s_1})}{k_{s_1}} \tag{6.194}$$

The computation of the pneumatic trail t_{c_1} is discussed at p. 312.

Accordingly, the congruence equations (6.148) of the linear single track model become

$$\begin{aligned}\alpha_1 &= \delta_1 - \frac{v+ra_1}{u} \\ \alpha_2 &= \chi\tau_1\delta_v - \frac{v-ra_2}{u}\end{aligned} \tag{6.195}$$

with the additional equation (6.194).

On the other hand, the equilibrium equations

$$\begin{aligned}m(\dot{v}+ur) &= Y = Y_1+Y_2 \\ J_z\dot{r} &= N = Y_1a_1 - Y_2a_2\end{aligned} \tag{6.147′}$$

and the constitutive equations

$$\begin{aligned}Y_1 &= C_1\alpha_1 \\ Y_2 &= C_2\alpha_2\end{aligned} \tag{6.149′}$$

do not change at all.

6.18.2 Effects of Compliance

Equation (6.194) can be rewritten taking the first equation in (6.149) into account

$$\delta_1 = \tau_1 \delta_v - \frac{C_1(t_{c_1} + t_{s_1})}{k_{s_1}} \alpha_1 = \tau_1 \delta_v - \varepsilon \alpha_1 \tag{6.196}$$

where ε

$$\varepsilon = \frac{C_1(t_{c_1} + t_{s_1})}{k_{s_1}} \tag{6.197}$$

The first congruence equation becomes

$$(1 + \varepsilon)\alpha_1 = \tau_1 \delta_v - \frac{v + a_1 r}{u} \tag{6.198}$$

which leads naturally to define a fictitious slip angle

$$\tilde{\alpha}_1 = (1 + \varepsilon)\alpha_1 \tag{6.199}$$

and, consequently, a fictitious slip stiffness

$$\tilde{C}_1 = \frac{C_1}{1 + \varepsilon} \tag{6.200}$$

Summing up, the linear single track model with *compliant* steering system is governed by the set of equations

$$\begin{aligned} m(\dot{v} + ur) &= Y = Y_1 + Y_2 \\ J_z \dot{r} &= N = Y_1 a_1 - Y_2 a_2 \\ \tilde{\alpha}_1 &= \tau_1 \delta_v - \frac{v + r a_1}{u} \\ \alpha_2 &= \chi \tau_1 \delta_v - \frac{v - r a_2}{u} \\ Y_1 &= \tilde{C}_1 \tilde{\alpha}_1 \\ Y_2 &= C_2 \alpha_2 \end{aligned} \tag{6.201}$$

which is formally identical to the set governing the single track model with rigid steering system. Therefore, the analysis developed in Sect. 6.17 applies entirely, provided we take into account that $\tilde{C}_1 \to C_1$ and $\tilde{\alpha}_1 \to \alpha_1$.

Since $\tilde{C}_1 < C_1$, a compliant steering system makes the vehicle behavior more understeer.

6.19 Summary

Road cars are characterized by having an open differential and no significant aerodynamic downforces. These two aspects allow for some substantial simplifications of the vehicle model. With the additional assumption of equal gear ratios of the steering system for both front wheels, we have been able to formulate the single track model.

Quite contrary to common belief, we have shown that the axle characteristics can take into account many vehicle features, like toe in/out, roll steering, camber angles and camber angle variations.

The steady-state analysis has been carried out first using the classical handling diagram. Then, the new global approach MAP (Map of Achievable Performance), based on handling maps on achievable regions has been introduced and discussed in detail. This new approach shows the overall vehicle behavior at a glance.

Stability and control derivatives have been introduced to study the vehicle transient behavior. Moreover, the relationship between data collected in steady-state tests and the vehicle transient behavior has been thoroughly analyzed in a systematic framework. To prove the effectiveness of these results, a number of apparently different vehicles with almost the same handling characteristics has been generated.

6.20 List of Some Relevant Concepts

p. 131 road cars are normally equipped with an open differential;
p. 137 to go from the double track to the single track model we need the following additional assumption: the left and right gear ratio of the steering system are almost equal;
p. 139 the main feature of the single track model is that the two wheels of the same axle undergo the same apparent slip angle;
p. 151 some steady-state quantities are functions of the lateral acceleration only because of the open differential and no significant downforces;
p. 158 some "fundamental" concepts in vehicle dynamics are indeed very weak if addressed with open mind;
p. 179 the understeer gradient is not a good parameter and should be dismissed.

References

1. Bastow D, Howard G, Whitehead JP (2004) Car suspension and handling, 4th edn. SAE International, Warrendale
2. Dixon JC (1991) Tyres, suspension and handling. Cambridge University Press, Cambridge
3. Font Mezquita J, Dols Ruiz JF (2006) La Dinámica del Automóvil. Editorial de la UPV, Valencia
4. Gillespie TD (1992) Fundamentals of vehicle dynamics. SAE International, Warrendale
5. Guiggiani M (2007) Dinamica del Veicolo. CittaStudiEdizioni, Novara

6. Pacejka HB (1973) Simplified analysis of steady-state turning behaviour of motor vehicles, part 1: handling diagrams of simple systems. Veh Syst Dyn 2:161–172
7. Pacejka HB (1973) Simplified analysis of steady-state turning behaviour of motor vehicles, part 2: stability of the steady-state turn. Veh Syst Dyn 2:173–183
8. Pacejka HB (1973) Simplified analysis of steady-state turning behaviour of motor vehicles, part 3: more elaborate systems. Veh Syst Dyn 2:185–204
9. Popp K, Schiehlen W (2010) Ground vehicle dynamics. Springer, Berlin
10. Wong JY (2001) Theory of ground vehicles. Wiley, New York

Chapter 7
Handling of Race Cars

Race cars come in a number of shapes, sizes, engine power, type of wings, etc. However, most of them share the following features relevant to handling:

(1) four wheels (two axles);
(2) two-wheel drive;
(3) *limited slip or locked differential*;
(4) *wings* (and hence, significant aerodynamic downforces, along with significant aerodynamic drag);
(5) often no intervention by electronic active safety systems like ABS or ESP.

The handling analysis of this kind of vehicles is more involved than that of road cars. The non-open differential makes the vehicle behavior very sensitive also to the turning radius, while the aerodynamic effects make the vehicle handling behavior very sensitive to the forward speed.

The analysis developed here is based on the general vehicle model introduced in Chap. 3.

7.1 Locked and Limited Slip Differentials

The mechanics of any differential mechanism has been discussed in Sect. 3.11.4, where all relevant equations have been obtained. Here, we briefly summarized the topic.

A *locked differential* is actually not a differential. Indeed, a differential mechanism must convey power from a single shaft to two shafts while permitting different rotation speeds. A locked differential no longer has this degree of freedom and the *two wheels must rotate at the same angular speed*, regardless of the torques they receive. However, any locked differential can be unlocked, as its name implies.

Race cars are usually equipped with a *limited slip differential*. It is a differential with a torque bias, which can become totally locked in some cases. Actually, a better

M. Guiggiani, *The Science of Vehicle Dynamics*, DOI 10.1007/978-94-017-8533-4_7,

name would be just "differential", leaving the "open" attribute to those very special, albeit extremely common in road cars, differentials without significant internal friction.

Essentially, a differential must have the capability of splitting power according to the three fundamental laws (3.127). Let us consider a vehicle equipped with a *limited slip differential* at the driven axle, that is a differential whose internal efficiency $\eta_h \ll 1$, and hence with a TBR $\gg 1$. For definiteness, let us suppose to deal with a rear-wheel-drive vehicle.

As discussed in Sect. 3.11.4, a limited slip differential is built to have some sort of friction inside the housing, which makes the torques applied to the left and right shaft not equal to each other. It has been shown in (3.132) that during power on, it is always the slower wheel that receives the higher torque.

In a curve, counterintuitive as it may appear, the inside wheel has not necessarily an angular speed lower than the outside wheel. Just consider a race car accelerating while exiting a curve: since in most cases its inside wheel is barely touching the ground, its angular speed is certainly higher than that of the outer wheel (Fig. 3.22(b)). This phenomenon is one of the main reasons that renders a limited slip differential almost mandatory in a race car. Otherwise, that is with an open differential, the car would not accelerate much, as the maximum longitudinal force would be limited by the inner wheel (the one barely touching the ground).

On the other hand, if a vehicle is turning at low lateral acceleration the inside wheel will be turning slower than the outside wheel, and hence it will receive more torque (Fig. 3.22(a)).

In any case, as stated in (3.132), we have $\eta_h \ll 1$, and hence the two longitudinal forces $F_{x_{21}}$ and $F_{x_{22}}$ exerted by the rear tires on the vehicle are not equal to each other. Therefore we have a *yawing moment* coming from the longitudinal forces acting on the vehicle

$$\Delta X_2 t_2 \neq 0 \tag{7.1}$$

When compared with (6.1), that is with the case of open differential, it looks like a small difference, but it is not. The locked or limited slip differential does affect quite a bit the vehicle handling behavior, and, accordingly, the vehicle model becomes much more involved when compared with the model of a vehicle equipped with an open differential.

Another consequence is that we have significant longitudinal forces at the rear axles and, therefore, longitudinal slips, even when turning at constant forward speed

$$\begin{aligned} F_{x_{2j}} &\neq 0 \\ \sigma_{x_{2j}} &\neq 0 \end{aligned} \tag{7.2}$$

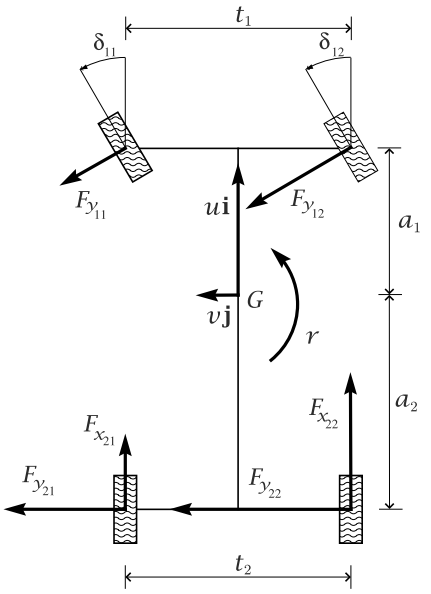

Fig. 7.1 Road-tire friction forces for a race car with limited slip differential

In other words, the longitudinal slips $\sigma_{x_{2j}}$ cannot be neglected, and, hence, the tire constitutive equations must include them for the two wheels of the driven axle.

7.2 Fundamental Equations of Race Car Handling

Owing to the presence of a limited slip differential ($\Delta X_2 \neq 0$) and of relevant aerodynamic loads (high downforce and hence high drag: $X_2 \neq 0$), the tires of the driven axle undergo significant longitudinal slips under almost all operating conditions. Therefore, it does not make much sense to restrict the analysis to steady state since the very beginning. However, to highlight the role of the limited slip differential, we do not consider the vehicle while braking, but only during power-on/power-off conditions. Therefore, we have at the front axle

$$F_{x_{11}} = F_{x_{12}} = 0 \tag{7.3}$$

and hence $\sigma_{x_{11}} = \sigma_{x_{12}} = 0$.

For a rear-wheel-drive race car, the equilibrium equations (3.64) become (Fig. 7.1)

$$\begin{aligned} ma_x &= m(\dot{u} - vr) = X = X_1 + X_2 - X_a \\ ma_y &= m(\dot{v} + ur) = Y = Y_1 + Y_2 \\ J_z\dot{r} &= N = Y_1 a_1 - Y_2 a_2 + \Delta X_1 t_1 + \Delta X_2 t_2 \end{aligned} \tag{7.4}$$

where, as discussed in Sect. 3.5.3,

$$\begin{aligned} X_1 &= -F_{y_{11}} \sin(\delta_{11}) - F_{y_{12}} \sin(\delta_{12}) \\ Y_1 &= F_{y_{11}} \cos(\delta_{11}) + F_{y_{12}} \cos(\delta_{12}) \\ \Delta X_1 &= \left[F_{y_{12}} \sin(\delta_{12}) - F_{y_{11}} \sin(\delta_{11})\right]/2 \simeq 0 \\ X_2 &= F_{x_{21}} + F_{x_{22}} \\ Y_2 &= F_{y_{21}} + F_{y_{22}} \\ \Delta X_2 &= (F_{x_{22}} - F_{x_{21}})/2 \end{aligned} \tag{7.5}$$

Depending on the type of differential mechanism, one of the following equations must supplement the equilibrium equations

$$\omega_{22} = \omega_{21} \qquad \text{(locked)} \tag{7.6}$$

$$F_{x_{22}} = \left(\left(\eta_h^{\varsigma}\right)^{\varphi}\right) F_{x_{21}} \qquad \text{(limited slip)} \tag{7.7}$$

$$F_{x_{22}} = F_{x_{21}} \qquad \text{(open)} \tag{7.8}$$

where, as already done in (3.136), $\varsigma = 1$ during power-on and $\varsigma = -1$ during power-off, and $\varphi = \text{sign}(\omega_{22} - \omega_{21})$.

The extra *yawing moment* $N_X = N_d$, due to the limited slip differential

$$N_d = \Delta X_2 t_2 \tag{7.9}$$

in the yaw equation, strongly affects the lateral forces, both quantitatively and qualitatively (cf. 6.6)

$$\begin{aligned} Y_1 &= \frac{1}{l}\left(ma_2 a_y + (J_z \dot{r} - N_d)\right) \simeq \frac{1}{l}(ma_2 a_y - N_d) \\ Y_2 &= \frac{1}{l}\left(ma_1 a_y - (J_z \dot{r} - N_d)\right) \simeq \frac{1}{l}(ma_1 a_y + N_d) \end{aligned} \tag{7.10}$$

A result already obtained in (3.72) and (3.116). The key point is that Y_1 and Y_2 are no longer functions of a_y only, as it was instead in (6.6). They also depend on the yawing moment N_d generated by the limited slip (or locked) differential.

The lateral load transfers ΔZ_i were obtained in (3.114) and (3.115) as linear functions of Y_1 and Y_2. Combining these equations with (7.10) we get

$$\begin{aligned} \Delta Z_1 &= ma_y \eta_1 + N_d \nu_1 \\ \Delta Z_2 &= ma_y \eta_2 + N_d \nu_2 \end{aligned} \tag{7.11}$$

The expressions (3.79) for the vertical loads on each tire must be taken in full, except for the $J_{zx} r^2$ term, which is almost certainly negligible. In compact form,

(3.79) can be recast as (cf. (6.11))

$$\begin{aligned}
Z_{11} &= \frac{m}{2l}(ga_2 - ha_x) + D_1u^2 - (ma_y\eta_1 + N_d\nu_1) = Z_{11}\big(a_x, u^2, a_y, N_d\big)\\
Z_{12} &= \frac{m}{2l}(ga_2 - ha_x) + D_1u^2 + (ma_y\eta_1 + N_d\nu_1) = Z_{12}\big(a_x, u^2, a_y, N_d\big)\\
Z_{21} &= \frac{m}{2l}(ga_1 + ha_x) + D_2u^2 - (ma_y\eta_2 + N_d\nu_2) = Z_{21}\big(a_x, u^2, a_y, N_d\big)\\
Z_{22} &= \frac{m}{2l}(ga_1 + ha_x) + D_2u^2 + (ma_y\eta_2 + N_d\nu_2) = Z_{22}\big(a_x, u^2, a_y, N_d\big)
\end{aligned} \tag{7.12}$$

where, according to (3.57)

$$D_1 = -\frac{1}{2}\rho_a S_a C_{z1} \quad \text{and} \quad D_2 = -\frac{1}{2}\rho_a S_a C_{z2} \tag{7.13}$$

A race car with wings has $C_{zi} < 0$, and hence $D_i > 0$. The comparison of (7.12) with (6.11) shows the effect of aerodynamic devices and of the limited slip differential.

Similarly, we have $\phi_i^s = \phi_i^s(a_y, N_d)$ and $\Delta\gamma_i = \Delta\gamma_i(a_y, N_d)$. They generalize (6.8) and (6.17).

Since, in general, the rear tires apply both longitudinal and lateral forces to the vehicle, the full form (3.124) of the tire slips must be taken

$$\begin{aligned}
\sigma_{x_{2j}} &= \sigma_{x_{2j}}\big(v, r, u, \delta_v, \phi_2^s(a_y, N_d), \omega_{2j}\big)\\
\sigma_{y_{2j}} &= \sigma_{y_{2j}}\big(v, r, u, \delta_v, \phi_2^s(a_y, N_d), \omega_{2j}\big)
\end{aligned} \tag{3.124′}$$

where ω_{21} and ω_{22} are the angular speed of the two rear wheels. They are not under longitudinal pure rolling condition.

At the front axle we have $\sigma_{x_{11}} = \sigma_{x_{12}} = 0$ (longitudinal pure rolling) and, accordingly, we can rely on the simplified expressions

$$\sigma_{y_{1j}} = \sigma_{y_{1j}}(v, r, u, \delta_v) = \sigma_{y_{1j}}(\beta, \rho, a_y, \delta_v) \tag{7.14}$$

as in (6.14).

Therefore, according to the constitutive equations (2.72), the load transfers (7.12) and the lateral slips (7.14), the front tire forces can be expressed as

$$\begin{aligned}
F_{x_{11}} &= 0\\
F_{y_{11}} &= F_{y_{11}}(Z_{11}, \gamma_{11}, \sigma_{y_{11}}) = F_{y_{11}}(v, r, u, \delta_v, N_d)\\
F_{x_{12}} &= 0\\
F_{y_{12}} &= F_{y_{12}}(Z_{12}, \gamma_{12}, \sigma_{y_{12}}) = F_{y_{12}}(v, r, u, \delta_v, N_d)
\end{aligned} \tag{7.15}$$

The rear tires are under combined slip conditions and, therefore, also the angular speed of rotation of each wheel has to be taken into account

$$\begin{aligned}
F_{x_{21}} &= F_{x_{21}}(Z_{21}, \gamma_{21}, \sigma_{x_{21}}, \sigma_{y_{21}}) = F_{x_{21}}(v, r, u, \delta_v, N_d, \omega_{21}) \\
F_{y_{21}} &= F_{y_{21}}(Z_{21}, \gamma_{21}, \sigma_{x_{21}}, \sigma_{y_{21}}) = F_{y_{21}}(v, r, u, \delta_v, N_d, \omega_{21}) \\
F_{x_{22}} &= F_{x_{22}}(Z_{22}, \gamma_{22}, \sigma_{x_{22}}, \sigma_{y_{22}}) = F_{x_{22}}(v, r, u, \delta_v, N_d, \omega_{22}) \\
F_{y_{22}} &= F_{y_{22}}(Z_{22}, \gamma_{22}, \sigma_{x_{22}}, \sigma_{y_{22}}) = F_{y_{22}}(v, r, u, \delta_v, N_d, \omega_{22})
\end{aligned} \tag{7.16}$$

All these tire forces have to be combined according to (7.5), because this is the way they are felt by the vehicle

$$\begin{aligned}
-F_{y_{11}} \sin(\delta_{11}) - F_{y_{12}} \sin(\delta_{12}) &= X_1(v, r, u, \delta_v, N_d) \\
F_{y_{11}} \cos(\delta_{11}) + F_{y_{12}} \cos(\delta_{12}) &= Y_1(v, r, u, \delta_v, N_d) \\
\left[F_{y_{12}} \sin(\delta_{12}) - F_{y_{11}} \sin(\delta_{11})\right]/2 &= \Delta X_1(v, r, u, \delta_v, N_d) t_1 \\
F_{x_{21}} + F_{x_{22}} &= X_2(v, r, u, \delta_v, N_d, \omega_{21}, \omega_{22}) \\
F_{y_{21}} + F_{y_{22}} &= Y_2(v, r, u, \delta_v, N_d, \omega_{21}, \omega_{22}) \\
(F_{x_{22}} - F_{x_{21}}) t_2/2 &= \Delta X_2(v, r, u, \delta_v, N_d, \omega_{21}, \omega_{22}) t_2
\end{aligned} \tag{7.17}$$

7.3 Double Track Race Car Model

After a bit of work, we are now ready to set up the fundamental governing equations for the handling of a car equipped with limited slip/locked differential and with aerodynamic wings. Just insert (7.17) into (7.4) and add one equation of (7.6), beside (3.129)

$$\begin{aligned}
m(\dot{u} - vr) &= X_1 + X_2 - X_a = X(v, r, u, \delta_v, N_d, \omega_{21}, \omega_{22}) \\
m(\dot{v} + ur) &= Y_1 + Y_2 = Y(v, r, u, \delta_v, N_d, \omega_{21}, \omega_{22}) \\
J_z \dot{r} &= Y_1 a_1 - Y_2 a_2 + N_d = N(v, r, u, \delta_v, N_d, \omega_{21}, \omega_{22}) \\
N_d &= (F_{x_{22}} - F_{x_{21}})/2 = \Delta X_2(v, r, u, \delta_v, N_d, \omega_{21}, \omega_{22}) \\
F_{x_{22}} &= \left(\left(\eta_h^{\varsigma}\right)^{\varphi}\right) F_{x_{21}} \quad \text{or} \\
\omega_{21} &= \omega_{22}, \qquad \omega_{21} + \omega_{22} = 2\omega_h
\end{aligned} \tag{7.18}$$

Perhaps, the most natural way to set up the problem is to assign the angular speed ω_h of the housing of the differential and the angular position δ_v of the steering wheel, and then solve a system of six differential-algebraic equations in the six unknown functions $(v, r, u, N_d, \omega_{21}, \omega_{22})$. This is more realistic than imposing directly the forward speed u.

The comparison of (7.18) with (6.21), that is with the governing equation for an ordinary road vehicle, clearly shows the increased complexity of the model. But this is no surprise: a race car exhibits indeed a much richer handling behavior. Fortunately, the *Map of Achievable Performance* (*MAP*), that is the new global approach first presented in Sect. 6.10, provides a useful tool for understanding the handling behavior of a race car. This aspect will be addressed shortly and thoroughly.

However, the question that naturally arises at this point is whether we can go "single track" or not, as has been done for road cars in Sect. 6.4. To answer this question we should recall that by single track [1–3, 7, 11] we meant a vehicle model having two axle characteristics (6.33), that is two constitutive equations, one per each axle, involving only a single kinematic variable each (namely, the axle apparent slip angle). This is no longer possible, nor even for the front axle, since there is a strong interaction between lateral and longitudinal tire forces. More precisely, the analysis developed in Sect. 6.7.1 about the role of lateral acceleration is no longer applicable.

Therefore, in this case we cannot end up with a single track model. However, we will find a way to achieve a fairly simple description of the vehicle handling behavior.

7.4 Tools for Handling Analysis

It is customary in vehicle dynamics to start with the steady-state analysis, that is with all time-derivatives in the governing equations (7.18) set equal to zero. That means having the vehicle go round along a circle of constant radius at constant forward speed. In practice, it is much more convenient to do a *slowly increasing steer* maneuver, also called *constant speed, variable steer* test. The vehicle is almost in steady-state conditions, but the test procedure is much faster.

Pretty much like in Sect. 6.7.2, everything is based on the steady-state maps

$$\rho = \rho(\tilde{a}_y, \delta_v) \quad \text{and} \quad \beta = \beta(\tilde{a}_y, \delta_v) \tag{7.19}$$

or, equivalently[1]

$$\rho = \rho(u, \delta_v) \quad \text{and} \quad \beta = \beta(u, \delta_v) \tag{7.20}$$

which, beside being important by themselves, make also possible to unambiguously define the gradients

$$\begin{aligned} \operatorname{grad} \rho_p &= \left(\frac{\partial \rho_p}{\partial \tilde{a}_y}, \frac{\partial \rho_p}{\partial \delta_v} \right) = (\beta_y, \beta_\delta) = -(K_{\rho_y}, K_{\rho_\delta}) \\ \operatorname{grad} \beta_p &= \left(\frac{\partial \beta_p}{\partial \tilde{a}_y}, \frac{\partial \beta_p}{\partial \delta_v} \right) = (\rho_y, \rho_\delta) = -(K_{\beta_y}, K_{\beta_\delta}) \end{aligned} \tag{6.66′}$$

[1] We apologize for abusing notation, but too many symbols would be confusing.

These quantities are well defined in any vehicle, including race cars.

The new global approach to handling called MAP, first developed in Sect. 6.10, turns out to be very informative for race cars as well, as will be shown shortly. The analysis will be particularly interesting when aerodynamics is taken into account.

In Eqs. (7.19) and (7.20) we have omitted, with respect to (6.65) and (6.73), the r.h.s. terms, that is those involving the apparent slip angles α_1 and α_2 (6.24) and the steering angles. This has been done for greater generality, because they are not well defined, unless we assume $\tau_{11} = \tau_{12}$,[2] as in (6.22). But the key point is that α_1 and α_2, even if well defined, no longer are functions of the lateral acceleration $\tilde{a}_y$ only. This aspect has a lot of important consequences. For instance, the classical handling diagram [8–10] does not exist any more. It has to be replaced by the *handling surface*, first introduced in [4–6], as will be shown in the next section.

7.5 The Handling Diagram Becomes the Handling Surface

Although, in our opinion, the handling surface has been superseded by the MAP approach, it still deserves to be explained.

The well known handling diagram is made up of the handling curve and a straight line. As already stated in Sect. 6.8, this is quite a fortunate coincidence. In general, the *handling curve* must be replaced by the *handling surface*. Indeed, any steady-state configuration depends on two parameters (as a minimum), like, e.g., the forward speed u and the steering angle δ_v. In vehicles with open differential and no wings, it happens that some quantities depend only on one parameter, namely the lateral acceleration $\tilde{a}_y$. More precisely, the handling surface becomes a cylinder, whose projection is the handling curve, as shown in [5]. But, let us elaborate this concept in detail.

7.5.1 Handling with Locked Differential (no Wings)

Before dealing with the handling of race cars with significant aerodynamic downforces, we address the effect of the locked differential alone, with respect to the open differential. To do this, we consider road cars, which have very little, if any, aerodynamic vertical forces (no wings and not too high speed).

7.5.1.1 Steady State

According to the classical theory, we perform a number of (almost) steady-state tests, like slowly increasing steer manoeuvres, first for a vehicle with open differential, and then for the same vehicle but with a locked differential.

[2] However, many race cars do have $\tau_{11} = \tau_{12}$, often called parallel steering.

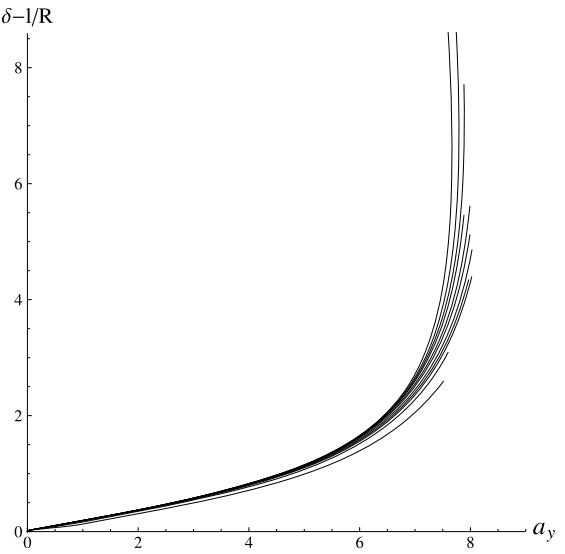

Fig. 7.2 Vehicle with *open* differential: handling curve(s) obtained in constant speed, variable steer tests

In all cases we monitor the forward speed u, the lateral speed v (or, equivalently, the vehicle slip angle $\beta = v/u$), the yaw rate r, the steering wheel angle δ_v. Although not strictly necessary, it is very convenient to monitor directly also the lateral acceleration $\tilde{a}_y = ur$. We also know the gear ratio τ_{ij} of the whole steering system for each wheel. Assuming, as in (6.22), $(\tau_{11} = \tau_{12}) = \tau_1$ for the front wheels, and $(\tau_{21} = \tau_{22}) = \tau_2$ for the rear wheels (although usually $\tau_2 = 0$), we can define the front steer angle $\delta_1 = \tau_1 \delta_v$ and the rear steer angle $\delta_2 = \tau_2 \delta_v$. The last useful piece of information is the wheelbase $l = a_1 + a_2$.[3]

The classical handling curve is the plot of $(\delta_1 - \delta_2) - l/R$ vs $\tilde{a}_y$, as discussed in Sect. 6.8. An understeer vehicle with open differential has a handling diagram like in Fig. 7.2. Basically, we get about the same curve regardless of the combination of forward speed and steer angle: only $\tilde{a}_y$ matters. On the other hand, performing constant speed, variable steer tests on the same vehicle, but with locked differential yields a different handling curve for each forward speed, as shown in Fig. 7.3.

The general framework to understand what is going on in all cases is the *handling surface*, that is the plot of

$$(\delta_1 - \delta_2) - \frac{l}{R} = \delta - \frac{l}{R} = f\left(\tilde{a}_y, \frac{l}{R}\right) \tag{7.21}$$

which is no longer a function of $\tilde{a}_y$ only, but needs another variable, like, e.g., l/R. Indeed, since there are two input quantities, like the forward speed and the steer angle, it is normal to have to deal with two variables at steady-state. The handling curves are just the *projections* of some *sections* of the handling surface onto the plane $(\tilde{a}_y, \delta - l/R)$. It happens that the handling surface is almost a cylinder for

[3] Actually, vehicle dynamics had better avoid using the wheelbase, as discussed in Sect. 6.9.

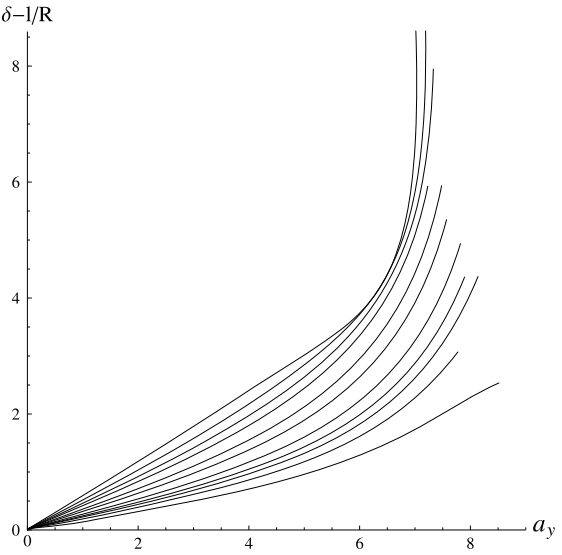

Fig. 7.3 Vehicle with *locked* differential: handling curves obtained in constant speed, variable steer tests

the open differential case, as shown in Fig. 7.4. Therefore, it always collapses into almost a single curve when projected. But more general vehicles (or better, less peculiar vehicles), that is all vehicles with at least one of the following features:

- locked differential;
- limited slip differential;
- aerodynamic wings;
- more than two axles;
- large steer angles;

they all exhibit a non-cylindrical handling surface, like the one shown in Fig. 7.5.

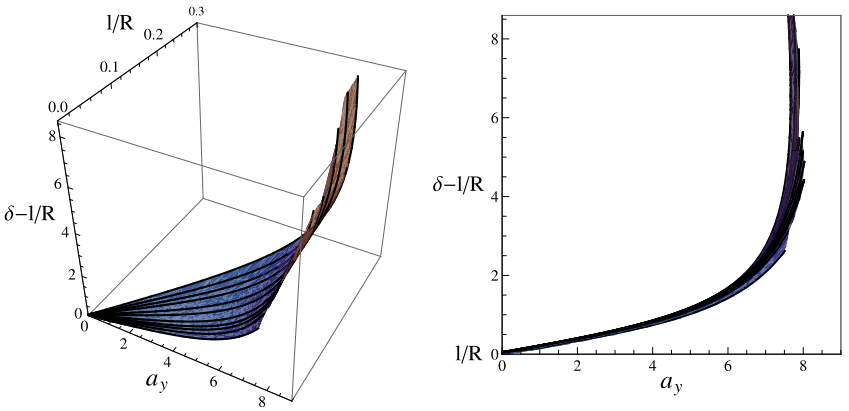

Fig. 7.4 Almost cylindrical handling surface for a vehicle with *open* differential

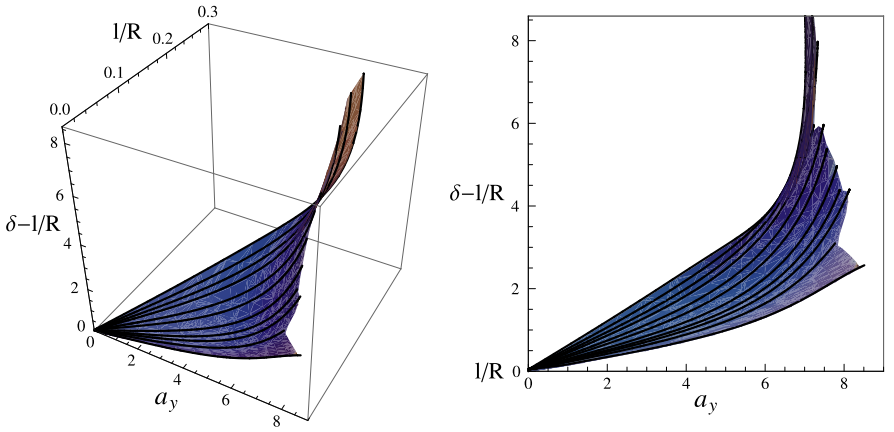

Fig. 7.5 Non-cylindrical handling surface for a vehicle with *locked* differential

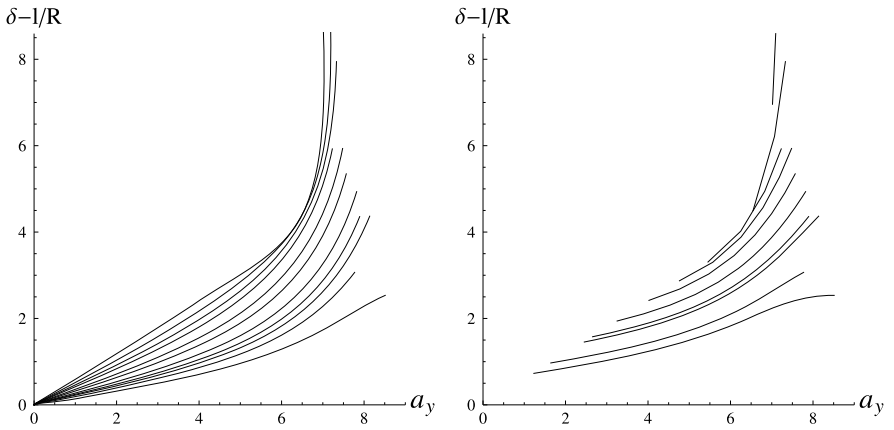

Fig. 7.6 Vehicle with *locked* differential: comparison between handling curves obtained in constant speed, variable steer tests (*left*) and constant steer, variable speed tests (*right*)

Therefore, drawing handling curves can be very confusing for a vehicle with locked differential, as the kind of test matters a lot. For instance, constant steer, variable speed tests yield curves that are totally different with respect to the constant speed, variable steer tests, as shown in Fig. 7.6. They are, however, just different sections of the very same handling surface. Again, if the differential is open, the handling surface is cylindrical, and all tests, that is all sections, project onto about the same curve, as shown in Fig. 7.7, regardless of the kind of maneuver.

To elaborate this idea further, we present Figs. 7.8 and 7.9 taken from [5]. The first figure shows sections of the handling surface for several values of the constant speed u. In the plane $(l/R, \tilde{a}_y) = (lr/u, ur)$, they appear as straight lines from the origin. The projections of each of these sections in the plane $(\tilde{a}_y, \delta - l/R)$ are

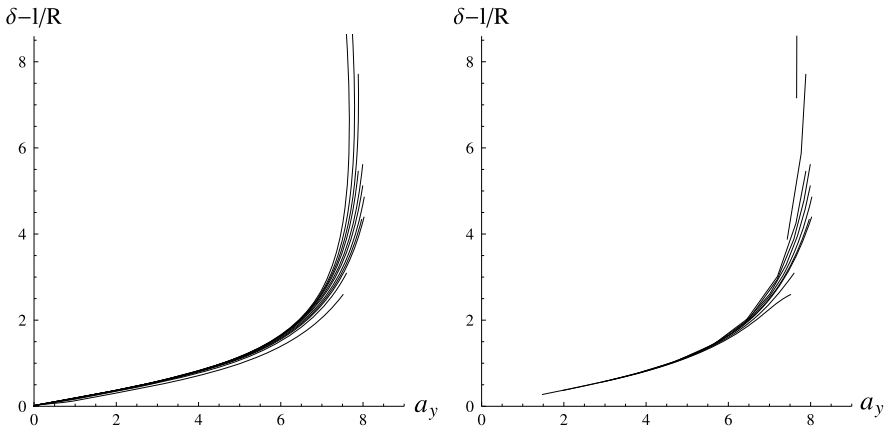

Fig. 7.7 Vehicle with *open* differential: comparison between handling curves obtained in constant speed, variable steer tests (*left*) and constant steer, variable speed tests (*right*)

shown in the left part. Similarly, the second figure shows sections of the handling surface for several values of the constant radius R. In the plane $(l/R, \tilde{a}_y)$, they appear as vertical straight lines. The projections of each of these sections in the plane $(\tilde{a}_y, \delta - l/R)$ are shown in the left part.

At low speed, like $u = 9$ m/s, and large steer angle $\delta_1 = 18°$, an ordinary road car receives from the road, more or less, the forces depicted in Fig. 7.10 when equipped with an open differential, and the forces shown in Fig. 7.11 when equipped with a locked differential. Also shown, in Fig. 7.12, is the case of a limited slip differential with internal efficiency $\eta_h = 0.33$. Similar figures can be found in Sect. 3.11.4. The three cases are deeply different. The yawing moment of the two longitudinal forces is obviously zero with open differential. With locked differential, at such low speed and high steer angle, the external wheel provides a braking force, which must be counteracted by the inner wheel: the yawing moment is so high to affect significantly both front and rear lateral forces. The limited slip case is something in between, with a small yawing moment coming from the longitudinal forces.

At much higher speed, say $u = 54$ m/s, and low steer angle, say $\delta_1 = 3°$, the moment due to the locked differential changes sign, as shown in Fig. 7.13. This is a typical and important phenomenon, due to the lateral load transfer. The inner wheel barely touches the ground and cannot provide much longitudinal force, thus limiting, with an open differential, the external force as well.

Superimposing the handling curves obtained in constant speed, variable steer tests for both open and locked differential, as shown in Fig. 7.14, we can appreciate the understeer effect at low lateral acceleration and the oversteer effect at high lateral acceleration. This is due to the yawing moment N_d, which has the typical behavior shown in Figs. 7.15 and 7.16 in case of locked differential. Of course, N_d is equal to zero when the differential is open.

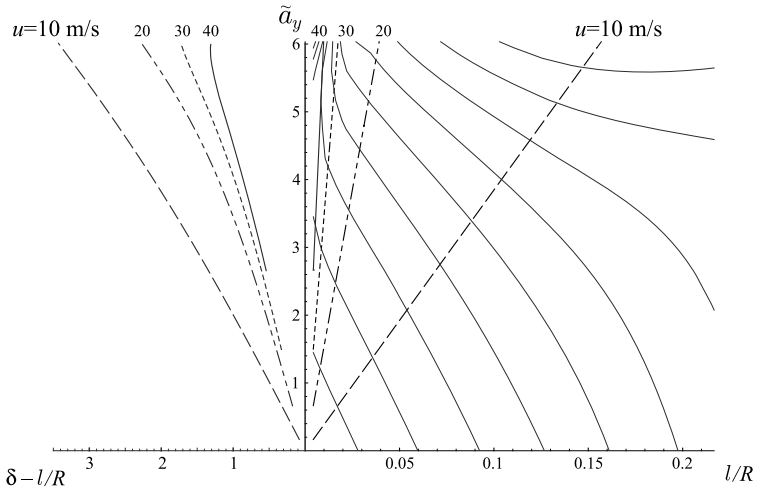

Fig. 7.8 Handling curves at constant speed (*left*) as sections of the handling surface (*right*) [5]

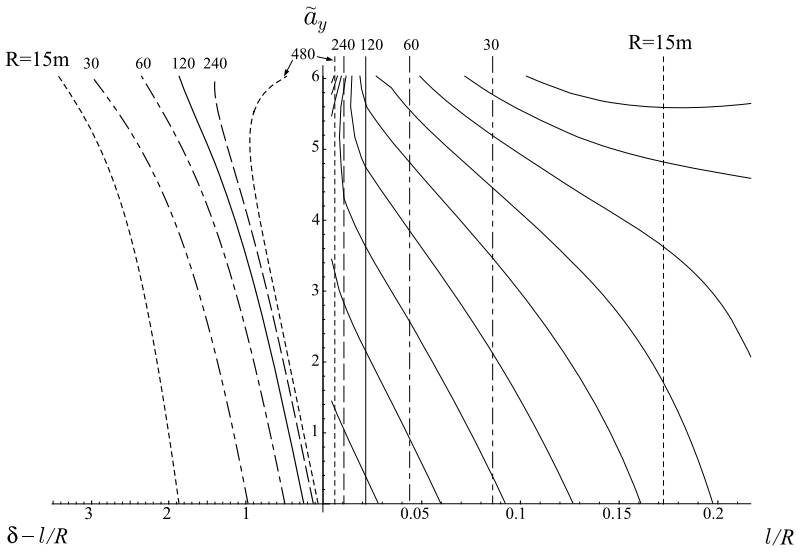

Fig. 7.9 Handling curves at constant turning radius (*left*) as sections of the handling surface (*right*) [5]

In case of limited slip differential with $\eta_h = 0.33$, the yawing moment N_d due to the longitudinal forces is something like in Figs. 7.17 and 7.18. It is worth noting the "knee" in some curves due to the internal wheel switching from slow wheel to fast wheel.

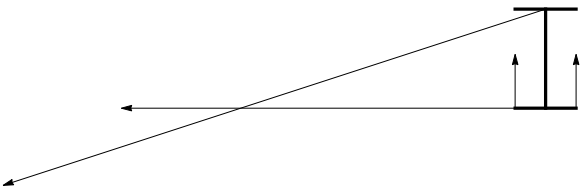

Fig. 7.10 Vehicle with open differential: forces received from the road at $u = 9$ m/s and $\delta_1 = 18°$

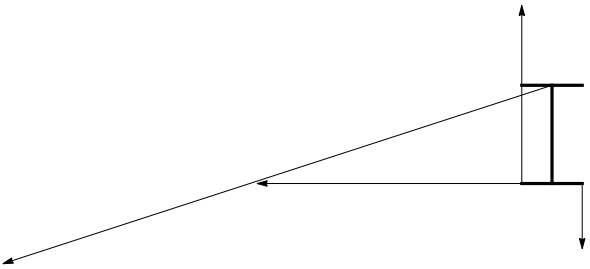

Fig. 7.11 Vehicle with locked differential: forces received from the road at $u = 9$ m/s and $\delta_1 = 18°$

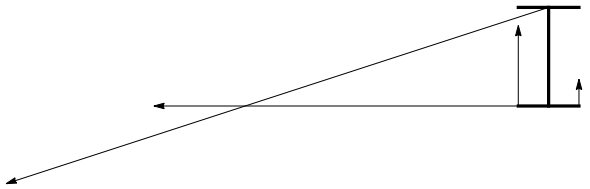

Fig. 7.12 Vehicle with limited slip differential ($\eta_h = 0.33$): forces received from the road at $u = 9$ m/s and $\delta_1 = 18°$

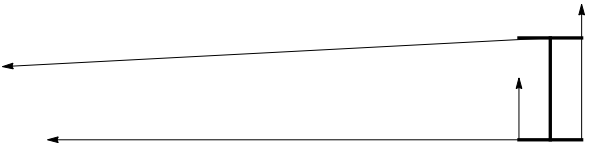

Fig. 7.13 Vehicle with locked differential: forces received from the road at $u = 54$ m/s and $\delta_1 = 3°$

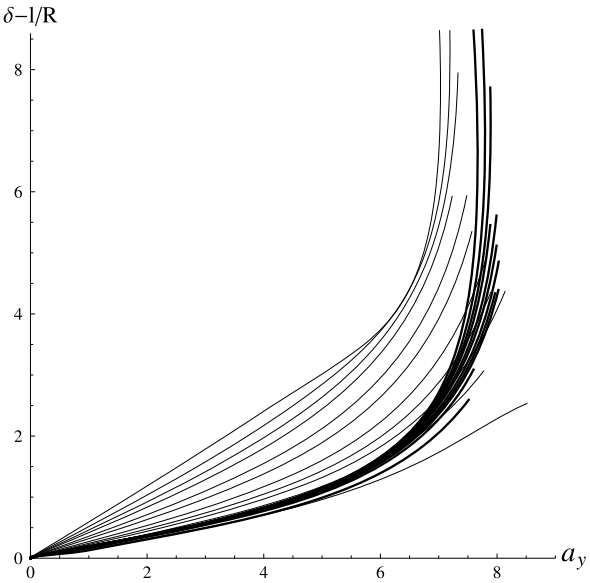

Fig. 7.14 Handling curves obtained in constant speed, variable steer tests: comparison between locked differential (*thin lines*) and open differential (*thick lines*)

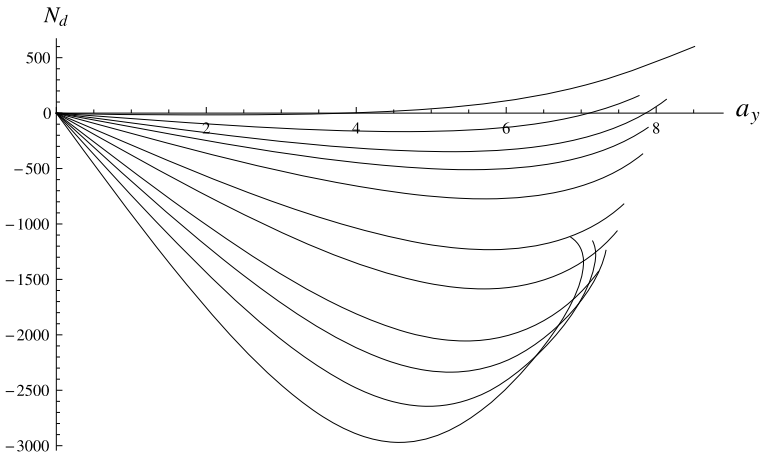

Fig. 7.15 Locked differential: yawing moment vs lateral acceleration for several speeds

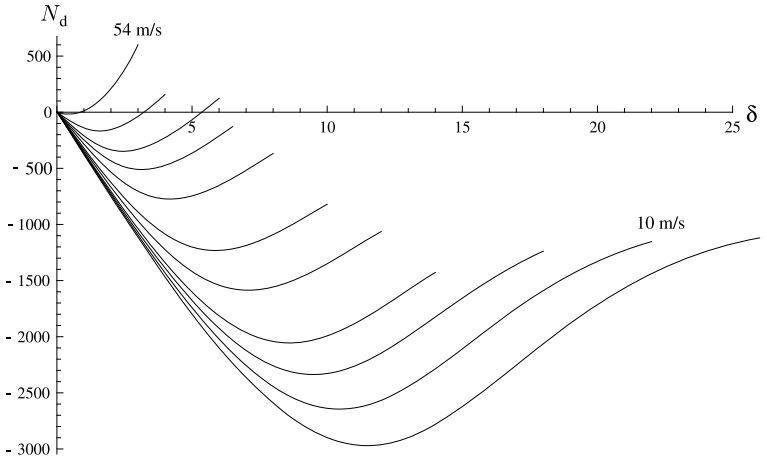

Fig. 7.16 Locked differential: yawing moment vs steer angle for several speeds

7.5.1.2 Power-off and Power-on

When braking using the engine, that is in *power-off* conditions, while negotiating a curve, the longitudinal forces are like in Fig. 7.19 in case of locked or limited slip differential. The corresponding yawing moments N_d are plotted in Figs. 7.20 and 7.21 vs the steer angle $\delta = \delta_1 - \delta_2$, for several values of the forward speed.

While during power-off it is always the external wheel that receives the highest (braking) longitudinal force, as shown in Fig. 7.19, under *power-on* conditions, while negotiating a curve with a vehicle with locked differential, there can be two possible cases, depending on the value of the lateral acceleration a_y (Fig. 7.22). This

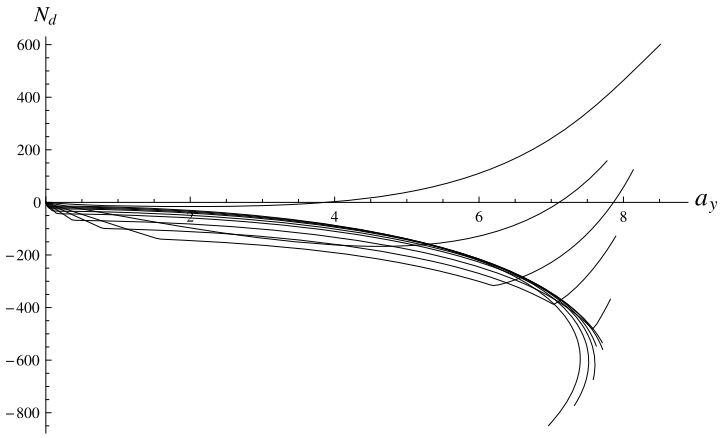

Fig. 7.17 Limited slip differential ($\eta_h = 0.33$): yawing moment vs lateral acceleration for several speeds

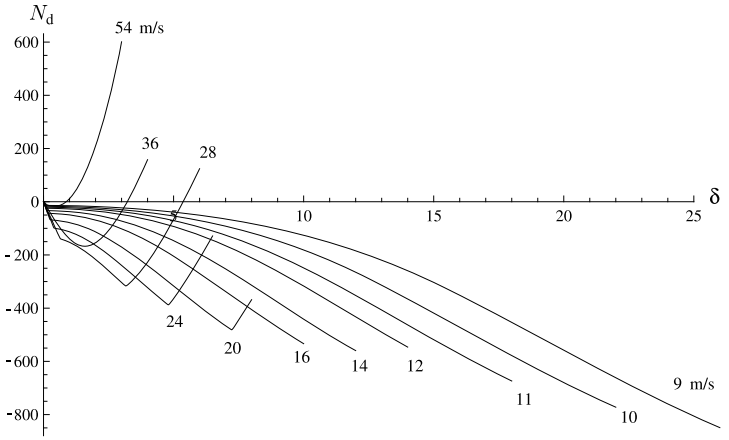

Fig. 7.18 Limited slip differential ($\eta_h = 0.33$): yawing moment vs steer angle for several speeds

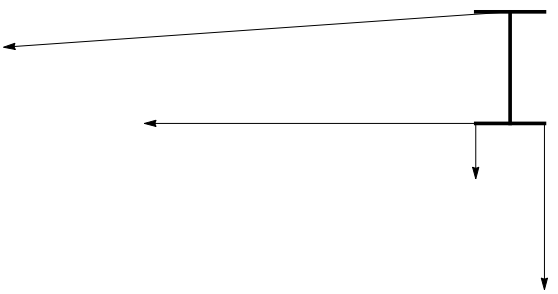

Fig. 7.19 Vehicle with locked or limited slip differential: forces received from the road during power-off

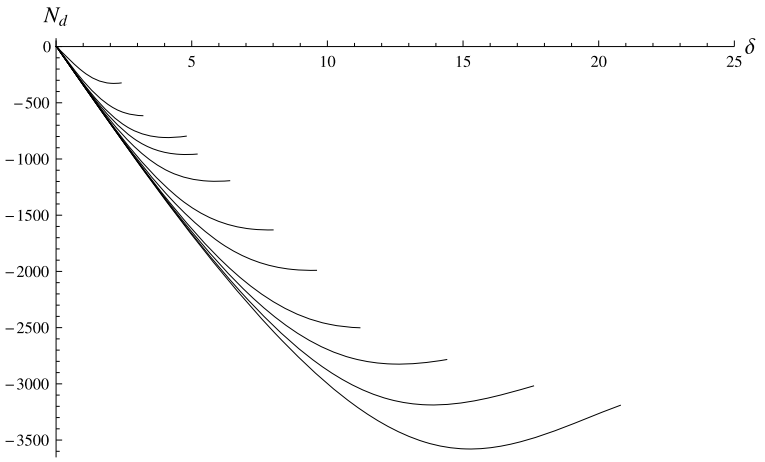

Fig. 7.20 Locked differential: yawing moment vs steer angle for several speeds during power-off

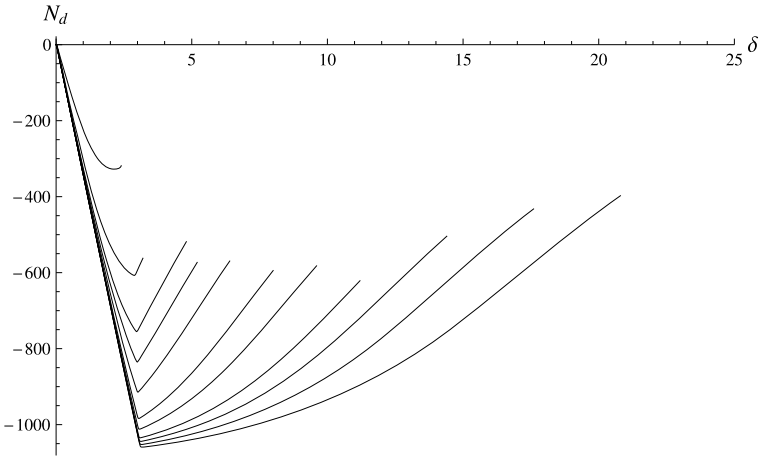

Fig. 7.21 Limited slip differential ($\eta_h = 0.33$): yawing moment vs steer angle for several speeds during power-off

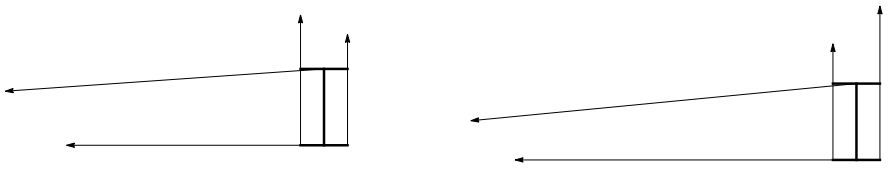

Fig. 7.22 Vehicle with locked or limited slip differential: forces received from the road during power-on

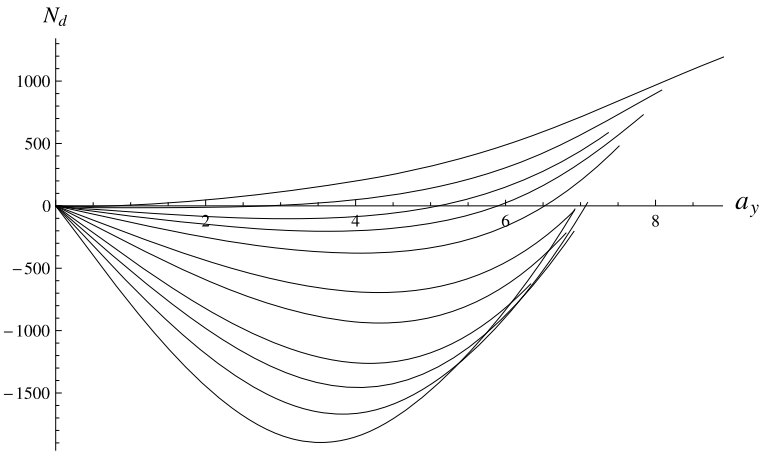

Fig. 7.23 Locked differential: yawing moment vs steer angle for several speeds during power-on

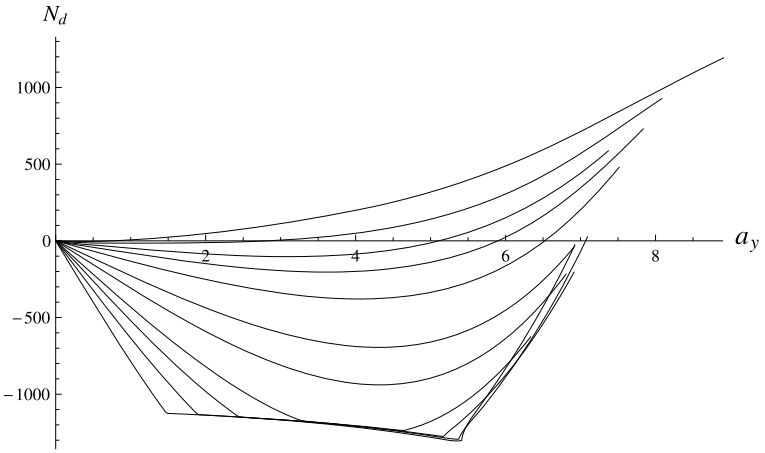

Fig. 7.24 Limited slip differential ($\eta_h = 0.33$): yawing moment vs lateral acceleration for several speeds during power-on

is better understood looking at the plot of N_d as a function of the lateral acceleration a_y, as shown in Fig. 7.23 for locked differential, and in Fig. 7.24 for limited slip differential, in both cases for several values of the forward speed u (ranging from 9 m/s up to 54 m/s): the moment can either be negative or positive, whereas in Figs. 7.20 and 7.21 it is always negative.

Although they are the main topic of the next section, we show the MAPs for the power-off and power-on cases of a road car. This new global approach has been already introduced and described in detail in Sect. 6.10 for steady-state handling analysis of road cars. The maps ρ–δ for locked differential are shown in Fig. 7.25, while the same maps for open differential are given in Fig. 7.26. The oversteer effect

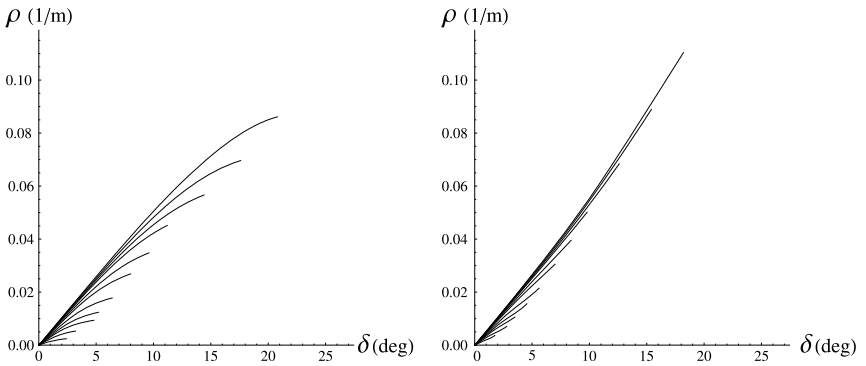

Fig. 7.25 Lines at constant speed u in the handling map ρ–δ during power-off (*left*) and power-on (*right*) for a road vehicle with *locked* differential

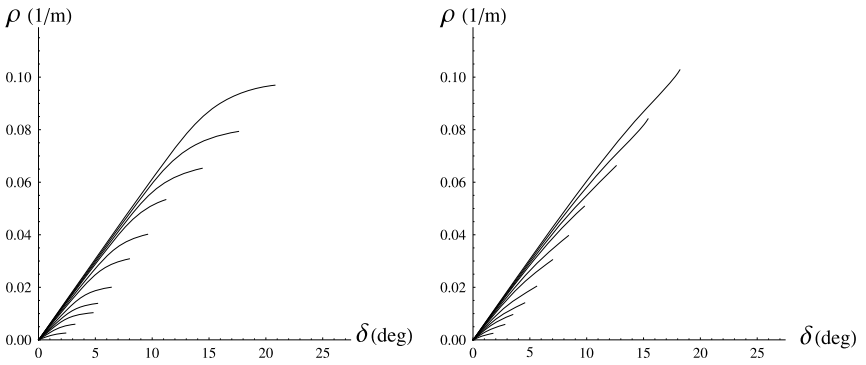

Fig. 7.26 Line at constant speed u in the handling map ρ–δ during power-off (*left*) and power-on (*right*) for a road vehicle with *open* differential

of power-on for a rear-wheel-drive car is evident in both cases. However, the locked differential makes this phenomenon stronger.

The maps β–ρ for power-off and power-on for a vehicle equipped with a locked differential are shown in Fig. 7.27. Again, the lines at constant steer angle clearly show, and do it in a quantitative way, the oversteer effect of power-on. For comparison, the same maps for a vehicle with open differential are given in Fig. 7.28.

7.6 Handling of Formula Cars

It is in the handling of Formula Cars that aerodynamics comes really into play (Fig. 7.29). Thanks to well designed wings, very high downforces are generated at high speeds, although at the price of high drag as well. A mathematical model that takes aerodynamics into account has been developed in Sect. 7.2. Here we discuss some of the main phenomena that make the handling of this kind of cars so

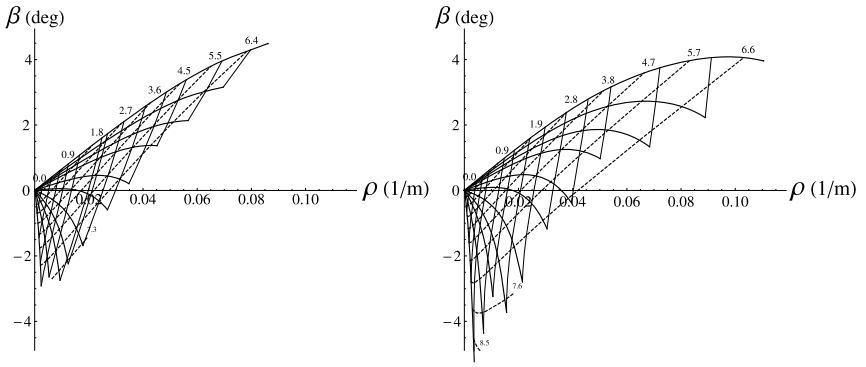

Fig. 7.27 Handling map β–ρ during power-off (*left*) and power-on (*right*) for a road vehicle with *locked* differential (constant u: *solid thick lines*, constant δ: *thin solid lines*, constant a_y: *dashed lines*)

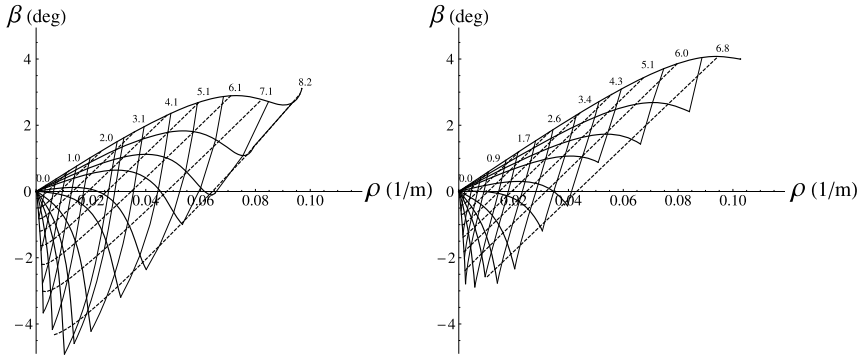

Fig. 7.28 Handling map β–ρ during power-off (*left*) and power-on (*right*) for a road vehicle with *open* differential (constant u: *solid thick lines*, constant δ: *thin solid lines*, constant a_y: *dashed lines*)

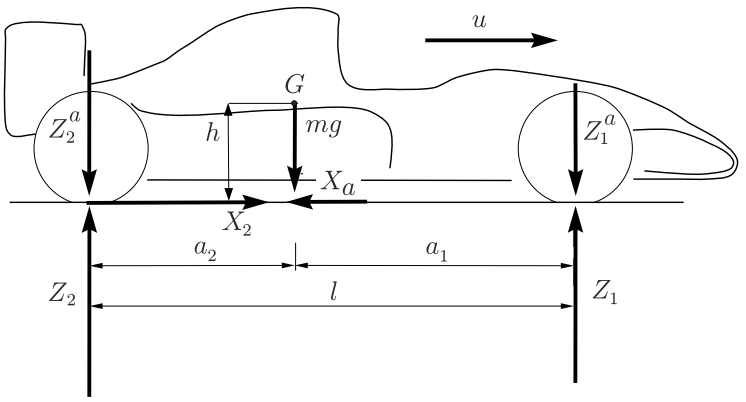

Fig. 7.29 Vehicle model for a Formula car

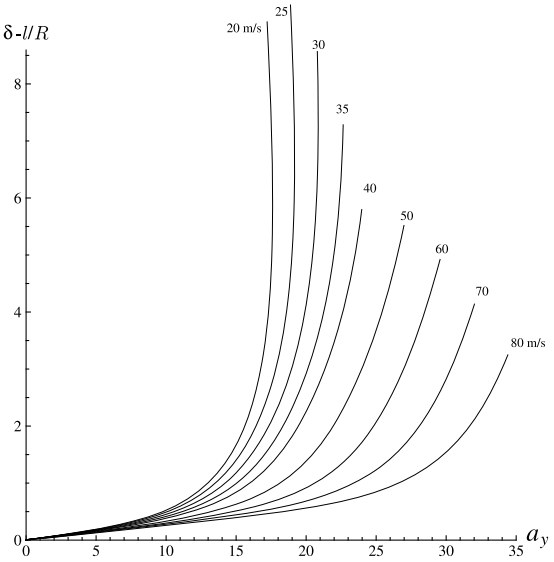

Fig. 7.30 Formula car with *open* differential: different handling curves obtained in constant speed, variable steer tests

peculiar. We start with the handling surface to move on to the maps of achievable performance (MAP's), first at steady state, and then during power-off and power-on.

Although these cars have a limited slip differential, at the center of a bend, that is when the vehicle is more or less close to steady state, the differential is basically open. Therefore, the steady-state analysis is more realistic if done with open differential, leaving the locked one for power-off and power-on. In all cases we consider speeds in the range 20–80 m/s.

7.6.1 Handling Surface

The handling surface has been introduced and discussed in Sect. 7.5. It is the plot of $\delta - l/r$ as a function of the lateral acceleration $\tilde{a}_y$ and the ratio $l/R = l\rho$. In case of significant aerodynamic effects, it is not cylindrical. This geometric feature is the counterpart of a very practical and obvious phenomenon: the speed matters a lot when a car is making a turn. The faster the car, the higher the lateral acceleration that can be achieved, assuming the same physical grip between the tires and the road. Therefore, once again, if we try to get the classical handling curve we will end up with a number of different handling curves, one for each testing condition. Tests at constant speed and variable steer will yield a different curve for each speed. Tests at constant steer and variable speed will produce a different set of curves, and so on.

These aspects are better understood looking at Fig. 7.30, which shows the handling curves for a Formula car with open differential as obtained in constant speed, slowly variable steer tests. It is evident that the higher the speed, the higher the lateral acceleration.

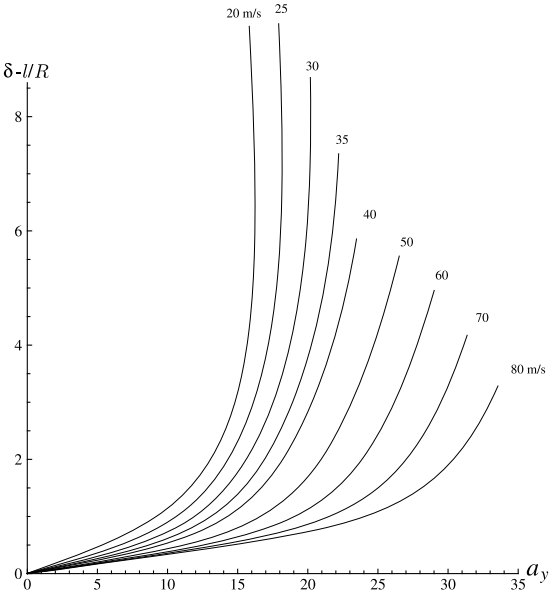

Fig. 7.31 Formula car with *locked* differential: different handling curves obtained in constant speed, variable steer tests

Locking completely the differential affects these handling curves, but not much, as shown in Fig. 7.31 (the aerodynamics is more influential). The main difference is, perhaps, that all curves in case of open differential share the same slope near the origin of the reference system, whereas in case of locked differential each one has a different slope, even when $\tilde{a}_y \simeq 0$.

As expected, performing constant steer, slowly variable speed tests yield different handling curves, as shown in Fig. 7.32. However, all these curves are just the projections of some sections of the *handling surface*, as shown in Fig. 7.33.

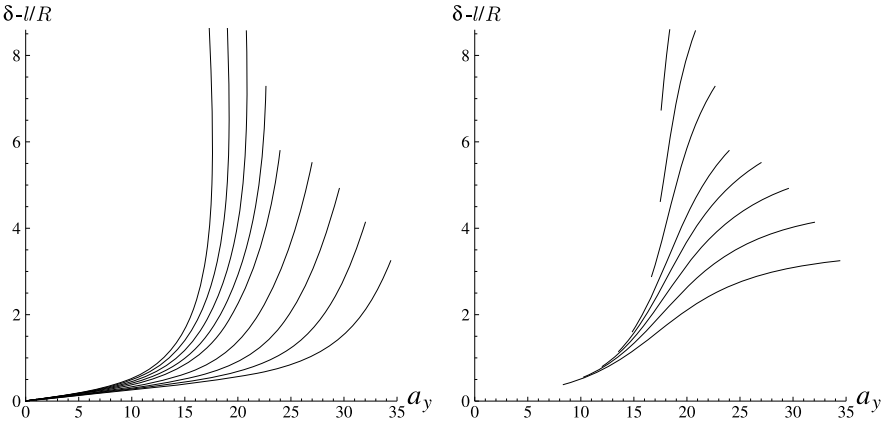

Fig. 7.32 Formula car with *open* differential: comparison between handling curves obtained in constant speed, variable steer tests (*left*) and constant steer, variable speed tests (*right*)

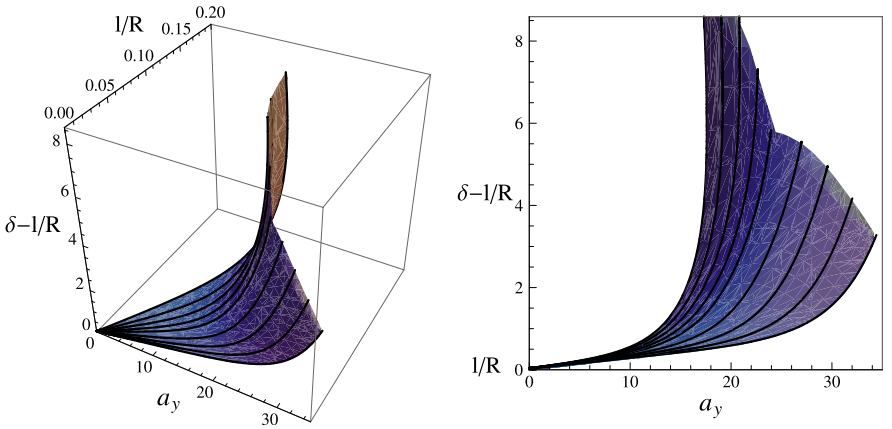

Fig. 7.33 Non-cylindrical handling surface for a Formula car with *open* differential

7.6.2 Map of Achievable Performance (MAP)

The global approach MAP has been introduced in Sect. 6.10. The emphasis there was on road cars, that is cars without any significant aerodynamic downforces and with open differential. However, this new approach is completely general, and its application to race cars is straightforward.

The basic idea, as discussed at p. 160, is to employ the maps

$$\begin{aligned} \rho &= \rho(u,\delta) = \frac{\delta}{l} - \frac{\alpha_1(u,\delta) - \alpha_2(u,\delta)}{l} \\ \beta &= \beta(u,\delta) = \left(\frac{(1+\hat{\chi})a_2 + \hat{\chi}a_1}{l}\right)\delta - \frac{\alpha_1(u,\delta)a_2 + \alpha_2(u,\delta)a_1}{l} \end{aligned} \tag{6.76′}$$

as functions of two variables to monitor the vehicle at steady state. This is a more general point of view than the handling surface (not to mention the handling diagram).

The maps in this section are typical for a Formula 1 car, year 2013. As usual, all quantities are in SI units, except angles that are in degrees.

7.6.2.1 ρ–δ MAP (Curvature-Steer Angle)

The first map to be considered is the curvature $\rho = r/u$ vs the wheel steer angle δ (although we could employ the steering wheel angle δ_v as well). In Fig. 7.34 we can see the lines at constant speed u, ranging from 20 to 80 m/s, and also the lines at constant lateral acceleration $\tilde{a}_y$, in case of open differential. In Fig. 7.35, we have the same picture, but for locked differential.

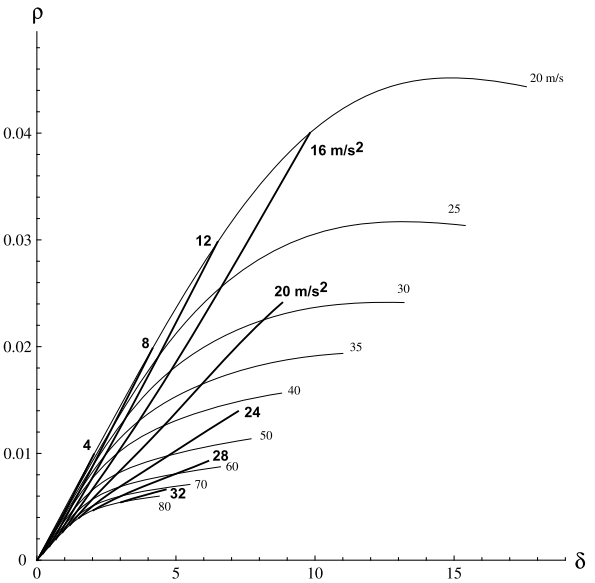

Fig. 7.34 ρ–δ MAP of a *Formula 1* car with *open* differential. Curves at constant speed u and curves at constant lateral acceleration $\tilde{a}_y$

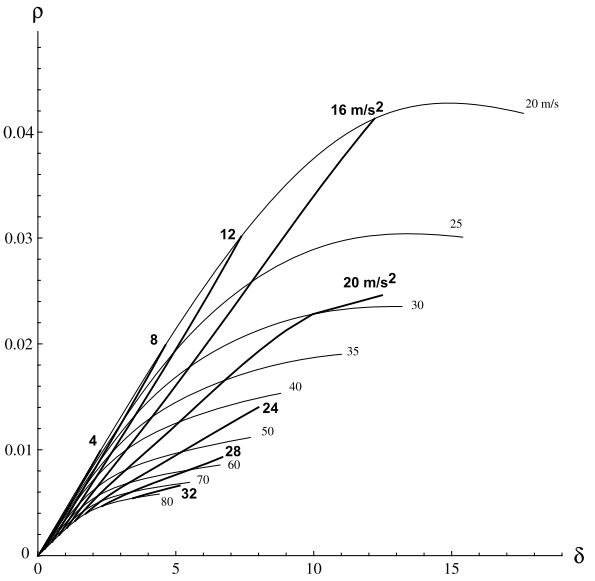

Fig. 7.35 ρ–δ MAP of a *Formula 1* car with *locked* differential. Curves at constant speed u and curves at constant lateral acceleration $\tilde{a}_y$

Lines at constant speed for open and locked differential are compared in Fig. 7.36. As expected, the locked differential makes the car turn on bigger radiuses (hence smaller values of ρ).

The strong influence of aerodynamics on the handling of the vehicle is highlighted by the pattern of the lines at constant lateral acceleration. Going back to Fig. 6.20, that is to the map for an ordinary road vehicle, we see that each line at

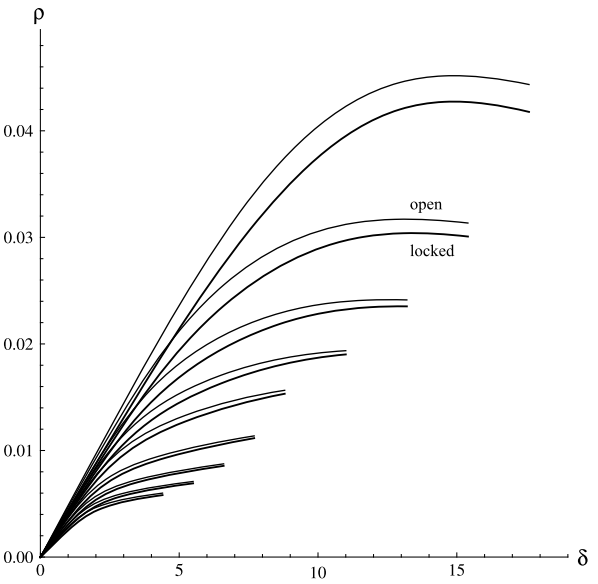

Fig. 7.36 Comparison between Figs. 7.34 and 7.35 for lines at constant speed

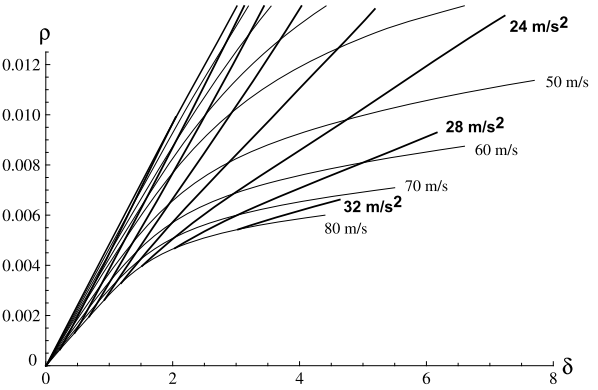

Fig. 7.37 Close-up of Fig. 7.34

constant $\tilde{a}_y$ intersects all lines at constant u. That means that the level of lateral acceleration that can be achieved is not affected by the forward speed (no wings). On the other hand, in Figs. 7.34 and 7.35, only lines up to about 16 m/s^2 intersect all constant speed lines. The lines for $\tilde{a}_y > 16$ m/s^2 only intersect lines for sufficiently high speed. Indeed, 1.6 is about the grip coefficient between the tire and the road, that is the "physical grip". The grip that does not need any aerodynamic contribution. Higher values of apparent grip do indeed need aerodynamic downforce and hence they can be achieved only for sufficiently high values of the forward speed u. The map shows this fact, and does so in a clear and global way. A close-up is shown in Fig. 7.37 for better clarity.

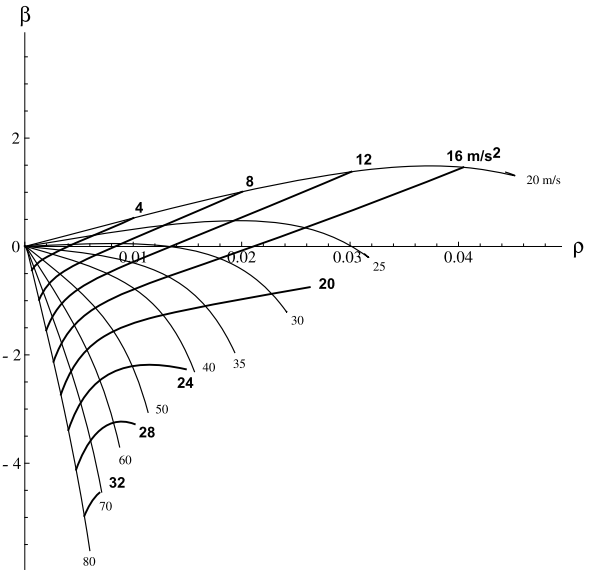

Fig. 7.38 β–ρ MAP for a Formula 1 car with open differential. Curves at constant speed u and curves at constant lateral acceleration $\tilde{a}_y$

7.6.2.2 β–ρ MAP (Vehicle Slip Angle-Curvature)

Also interesting is the handling β–ρ MAP, that is vehicle slip angle vs curvature. The lines at constant speed u and the lines at constant lateral acceleration $\tilde{a}_y$ are shown in Fig. 7.38. Again, only lines for $\tilde{a}_y < 16\ \mathrm{m/s^2}$ intersect all lines at constant speed, thus indicating that 1.6 is indeed the physical grip (of course we could be more precise by drawing more lines). Therefore, we have a tool to obtain a good approximation of the physical grip.

Also interesting is the overall picture, which shows how the control parameter u and δ are related to curvature and vehicle slip angle. For instance, if $u > 30\ \mathrm{m/s}$, we have basically $\beta \leq 0$ (in a left turn) at any speed.

Lines at constant steer angle are shown in Fig. 7.39. Looking at the slope of these curves, it immediately arises that the vehicle is more understeer at low speeds than at high speeds.

To help the reader catch other features in this map, all lines are shown in Fig. 7.40.

7.6.2.3 Set-up Identification

Another interesting application of the MAP's is to compare set-ups. This is done in Figs. 7.41 and 7.42 for two set-ups which have different aerodynamic balances. The second set-up (dashed lines) has higher aerodynamic load on the front axle and less aerodynamic load on the rear axle.

Very interesting is to observe that the lines at constant $\tilde{a}_y$ that are more affected are precisely those that need aerodynamic downforces to be achieved (Fig. 7.41).

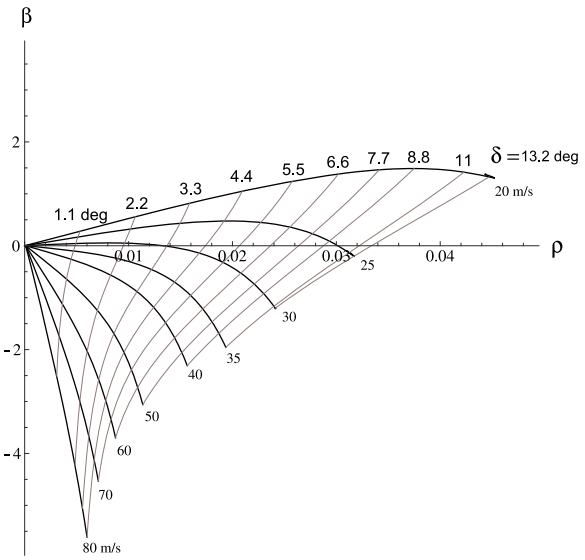

Fig. 7.39 β–ρ MAP or a Formula 1 car with open differential. Curves at constant speed u and curves at constant steer angle δ

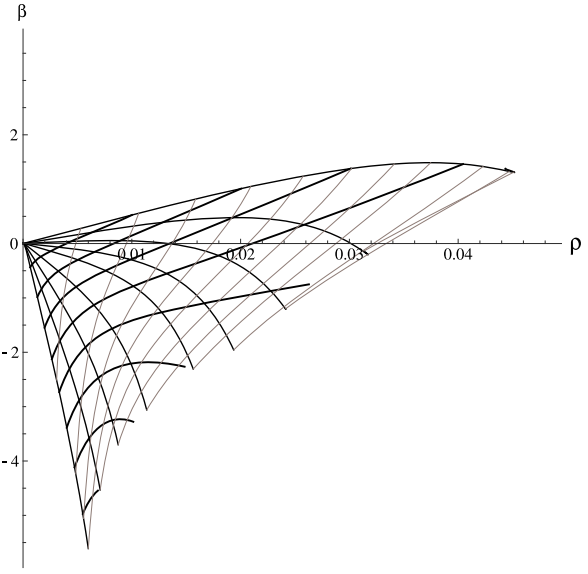

Fig. 7.40 β–ρ MAP for a Formula 1 car with open differential. Superimposition of Figs. 7.38 and 7.39

From Fig. 7.42 we see that the new aerodynamic balance does not affect the lines at constant δ in a uniform way. This may help understand which set-up is faster for a given circuit.

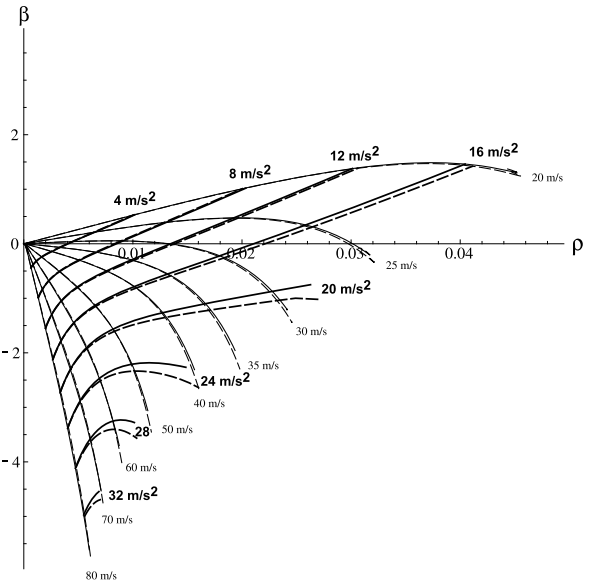

Fig. 7.41 Comparison of curve at constant lateral acceleration for two set-ups with different aerodynamic balance

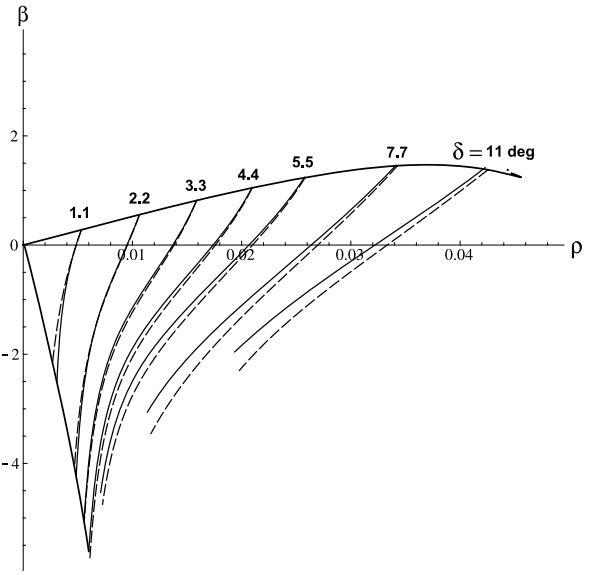

Fig. 7.42 Comparison of curve at constant steer angle for two set-ups with different aerodynamic balance

7.6.2.4 Power-off and Power-on

So far we have considered steady-state conditions. However, a Formula car is almost always under transient conditions, with the driver acting on the gas and/or brake pedals. The MAP's can be useful to monitor what is going on also during these more general working conditions. The trick is to do, e.g., constant speed, variable

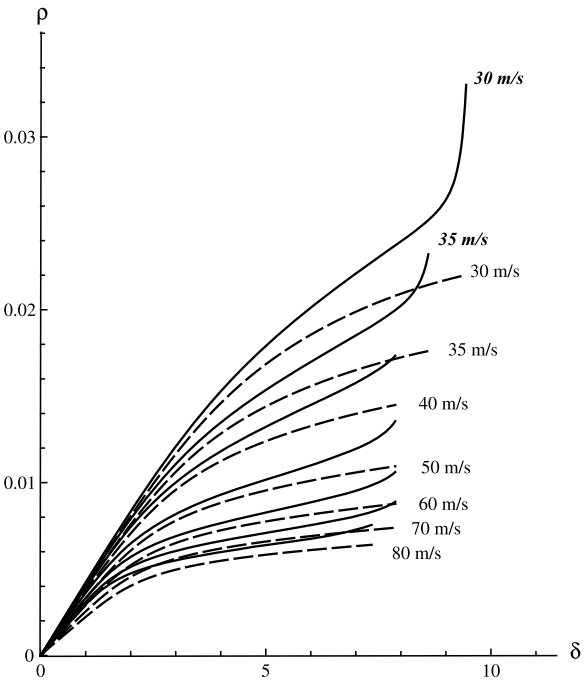

Fig. 7.43 Lines at constant speed in the ρ–δ MAP for a Formula 1 car during power-off (*dashed lines*) and power-on (*solid lines*)

steer simulations as if the car were constantly going uphill or downhill. This way, we have, strictly speaking, steady-state conditions, but the loads on the tires are pretty much like if the car were accelerating or slowing down with the engine (no braking), that is during power-on and power-off conditions.

During power-off and power-on, the differential of a Formula 1 car is locked. Therefore, all figures in this section are for locked differential.

A few figures are provided to show how the MAP's can be used to have a global view of the vehicle behavior even under pseudo-transient conditions. Figure 7.43 shows the ρ–δ map with lines at constant speed during power-off (dashed lines) and power-on (solid lines). Speeds below 30 m/s have been omitted. The two cases are for a longitudinal acceleration of ± 0.5 m/s^2. In Fig. 7.44 there is the comparison of power-off (dashed lines) and power-on (solid lines) in the plane β–ρ. At high steer angles and relatively low speeds there are, as expected, very big differences.

During power-on, the locked differential generates a yawing moment that can have either the same sign as the yaw rate (Fig. 7.45) or opposite sign (Fig. 7.46), depending on the operating conditions of the vehicle.

7.7 Summary

Limited slip differential and wings are typical of race cars. Both greatly impact on the vehicle handling (otherwise they would not be used). Therefore, the first part of

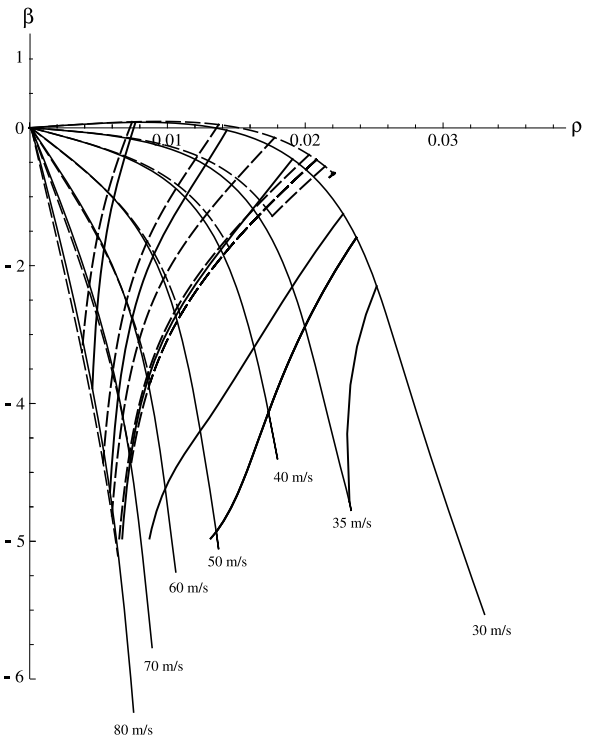

Fig. 7.44 Lines at constant u and constant δ in the $\beta-\rho$ MAP for a Formula 1 car during power-off (*dashed lines*) and power-on (*solid lines*)

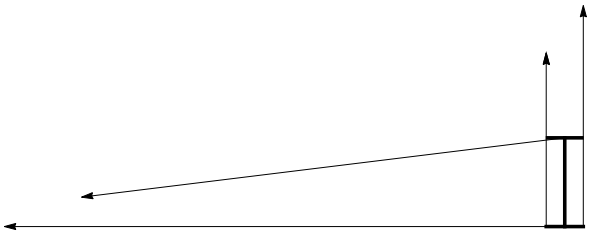

Fig. 7.45 Power-on with locked differential: forces received from the road at $u = 40$ m/s and $\delta = 7°$

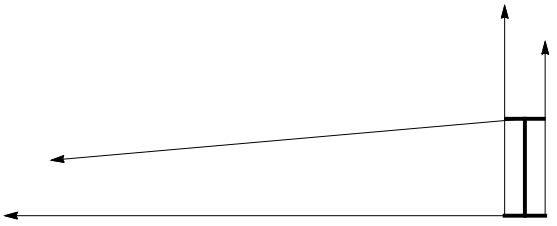

Fig. 7.46 Power-on with locked differential: forces received from the road at $u = 40$ m/s and $\delta = 5°$

this chapter has been devoted to the formulation of a suitable vehicle model, which, in this case, cannot be single track. As a matter of fact, there is a strong interaction between lateral and longitudinal forces.

The concept of handling diagram becomes inadequate and must be replaced by the handling surface. This fairly new tool has been introduced in the framework of handling of road cars with locked or limited slip differential.

The handling of Formula cars has been first addressed by means of the handling surface. However, a more powerful description has been provided by means of the *Maps of Achievable Performance—MAP*. With this new approach it is possible to better understand the effects of different vehicle set-ups at steady state and also in power-on/off conditions.

7.8 List of Some Relevant Concepts

p. 203 non-open differential makes vehicle behavior very sensitive also to the turning radius. Aerodynamic effects make the vehicle handling behavior very sensitive to the forward speed;
p. 210 the handling curve must be replaced by the handling surface;
p. 213 the curves on the handling diagram are the projections of sections of the handling surface;
p. 217 the yawing moment due to the limited slip differential can be either positive or negative;
p. 226 by means of the Map of Achievable Performance (MAP) it is possible to single out the physical grip.

References

1. Bastow D, Howard G, Whitehead JP (2004) Car suspension and handling, 4th edn. SAE International, Warrendale
2. Dixon JC (1991) Tyres, suspension and handling. Cambridge University Press, Cambridge
3. Font Mezquita J, Dols Ruiz JF (2006) La Dinámica del Automóvil. Editorial de la UPV, Valencia
4. Frendo F, Greco G, Guiggiani M (2006) Critical review of handling diagram and understeer gradient for vehicles with locked differential. Veh Syst Dyn 44:431–447
5. Frendo F, Greco G, Guiggiani M, Sponziello A (2007) The handling surface: a new perspective in vehicle dynamics. Veh Syst Dyn 45:1001–1016
6. Frendo F, Greco G, Guiggiani M, Sponziello A (2008) Evaluation of the vehicle handling performances by a new approach. Veh Syst Dyn 46:857–868
7. Gillespie TD (1992) Fundamentals of vehicle dynamics. SAE International, Warrendale
8. Pacejka HB (1973) Simplified analysis of steady-state turning behaviour of motor vehicles, part 1: handling diagrams of simple systems. Veh Syst Dyn 2:161–172
9. Pacejka HB (1973) Simplified analysis of steady-state turning behaviour of motor vehicles, part 2: stability of the steady-state turn. Veh Syst Dyn 2:173–183
10. Pacejka HB (1973) Simplified analysis of steady-state turning behaviour of motor vehicles, part 3: more elaborate systems. Veh Syst Dyn 2:185–204
11. Wong JY (2001) Theory of ground vehicles. Wiley, New York

Chapter 8
Ride Comfort and Road Holding

Real roads are far from flat. Even freshly paved highways have small imperfections that interact with the vehicle dynamics by exciting vehicle vertical vibrations.

The capability to smooth down road imperfections affects both the *comfort* and the *road holding* of the vehicle. Improving comfort means, basically, limiting the vertical acceleration fluctuations of the vehicle body and hence of passengers. Improving road holding means, among other things, limiting the fluctuations of the vertical force that each tire exchanges with the road.[1] The main parameters that affect both comfort and road holding are the suspension *stiffness* and *damping*.

The study of the vibrational behavior of a vehicle going straight at constant speed on a *bumpy road* is called *ride* [1–4, 7, 8]. More precisely, ride deals with frequencies in the range 0.25–25 Hz for road cars, a bit higher for race cars. Tires can, among other things, absorb small road irregularities at high frequency because of their vertical elasticity and low mass. However, for frequencies below 3 Hz the tires have little influence and can be considered as rigid. Therefore, the burden to absorb bigger bumps goes to the vehicle suspensions.

While when studying the handling of a vehicle we were also interested in the suspension geometry, we focus here on *springs* and *shock absorbers*. We look for criteria for selecting the right stiffness and the right amount of damping for each suspension.

Actually, this is only half the truth. Real suspensions have nonlinear springs and non linear shock absorbers, whose features cannot be reduced to a single number like in the linear case. However, suspensions with linear behavior are a good introduction to the study of ride and road holding.

Although standard suspension systems are based on two components—springs and shock absorbers (dampers)—there is a third component that can turn out to be useful in some cases. It is the so-called *inerter*. The inerter is a device that provides a force proportional to the relative *acceleration* between its attachment points, much

[1] Of course, we mean fluctuations due to road imperfections, not to load transfers.

M. Guiggiani, *The Science of Vehicle Dynamics*, DOI 10.1007/978-94-017-8533-4_8,

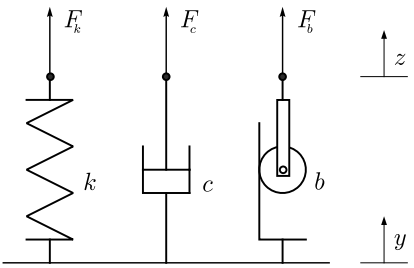

Fig. 8.1 Schematics for spring, shock absorber and inerter

like a shock absorber provides a force proportional to the relative velocity and a spring a force proportional to the relative displacement (Fig. 8.1)

$$\begin{aligned} F_k &= k(z-y) \\ F_c &= c(\dot{z}-\dot{y}) \\ F_b &= b(\ddot{z}-\ddot{y}) \end{aligned} \tag{8.1}$$

It was missing indeed, till quite recently [8]. A typical inerter incorporates a flywheel which rotates in proportion to the relative displacement between its two ends. So far, it has been employed in some Formula cars. We will show how it can improve, in some cases, the car road holding.

8.1 Vehicle Models for Ride and Road Holding

We are mostly interested in the vehicle vertical motion. To keep our ride analysis quite simple, we assume that the vehicle goes *straight* and at *constant speed*. Therefore, there are no handling and/or performance implications here. The ride analysis comes into play because of the *uneven road*. Actually, we ask for a very peculiar road, albeit uneven. It must have exactly the same profile for both wheels of the same axle, thus not inducing roll motion at all. That means that we can rely on a two-dimensional model.

The vehicle models set up for handling and performance are not suitable for ride. We need to develop a tailored model like, e.g., the four-degree-of-freedom model shown in Fig. 8.2. In this model there are three rigid bodies:

- the sprung mass m_s (with moment of inertia J_y w.r.t. its center of gravity G_s), which has vertical motion z_s and pitch motion θ;
- the front unsprung mass m_{n_1}, which has only vertical (hop) motion y_1;
- the rear unsprung mass m_{n_2}, which has only vertical (hop) motion y_2.

Also shown in Fig. 8.2 are the two suspension springs, with stiffnesses k_1 and k_2, and two shock absorbers, with damping coefficients c_1 and c_2, along with two springs p_1 and p_2 to model the tire vertical stiffnesses. Again, to keep the anal-

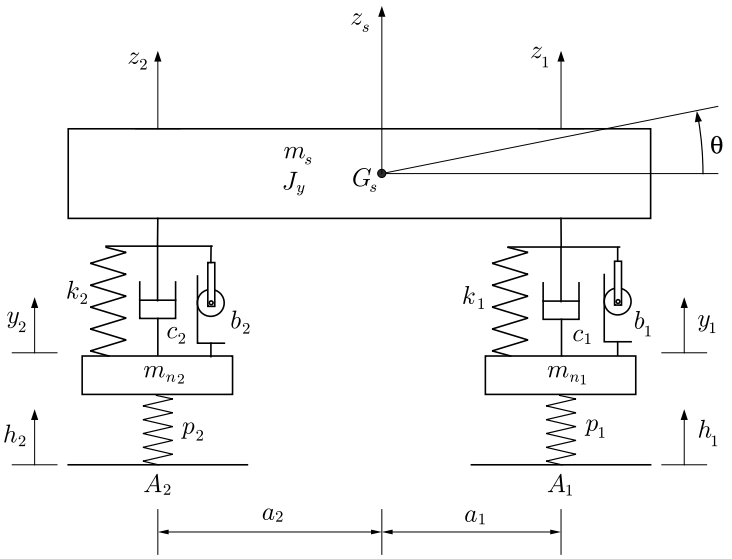

Fig. 8.2 Four-degree-of-freedom model to study ride and road holding

ysis simple, we assume that all these components have *linear* behavior. This is a very unrealistic hypothesis since real suspensions are designed to have hardening stiffness and are equipped with shock absorbers with more resistance during the extension cycle than the compression cycle.

Inerters, with inertances b_1 and b_2, are also shown in Fig. 8.2. They have been used sparingly and only in some race cars. They are included for greater generality.

The vehicle model shown in Fig. 8.2 has four degrees of freedom. Points A_1 and A_2 are the centers of the front axle contact patches and of the rear axle contact patches, respectively. The two functions $h_1(t)$ and $h_2(t)$ are the road profiles as "felt" by the car, that is through the tires.

The sprung mass has two degrees of freedom z_s and θ. Alternatively, we could use, e.g., the vertical displacements z_1 and z_2. All displacements and rotations are absolute and taken from the static equilibrium position of the vehicle. We are investigating the oscillations with respect to the equilibrium position, that is the configuration the vehicle would have on a perfectly flat road.

The vehicle model shown in Fig. 8.2 is governed by three sets of equations, as usual:

(1) congruence equations:

$$\begin{aligned} z_1 &= z_s + a_1\theta \\ z_2 &= z_s - a_2\theta \end{aligned} \tag{8.2}$$

that is a purely geometrical link between coordinates;

(2) equilibrium equations:

$$\begin{aligned} m_s\ddot{z}_s &= F_1 + F_2 \\ J_y\ddot{\theta} &= F_1 a_1 - F_2 a_2 \\ m_{n_1}\ddot{y}_1 &= N_1 - F_1 \\ m_{n_2}\ddot{y}_2 &= N_2 - F_2 \end{aligned} \tag{8.3}$$

that is a link between forces or couples and accelerations;

(3) constitutive equations:

$$\begin{aligned} F_1 &= -k_1(z_1 - y_1) - c_1(\dot{z}_1 - \dot{y}_1) - b_1(\ddot{z}_1 - \ddot{y}_1) = -(F_{k_1} + F_{c_1} + F_{b_1}) \\ F_2 &= -k_2(z_2 - y_2) - c_2(\dot{z}_2 - \dot{y}_2) - b_2(\ddot{z}_2 - \ddot{y}_2) = -(F_{k_2} + F_{c_2} + F_{b_2}) \\ N_1 &= -p_1(y_1 - h_1) \\ N_2 &= -p_2(y_2 - h_2) \end{aligned} \tag{8.4}$$

which model springs, shock absorbers and inerters.

By F_1 and F_2 we mean the vertical forces exchanged between the sprung mass and the two unsprung masses, respectively. By N_1 and N_2 we mean the forces exchanged by each axle with the road. All forces must be intended as perturbations with respect to the static equilibrium position. That is why the weight was not included in the equations.

Combining the above sets of equations, we end up with a system of four linear differential equations with constant coefficients. They are the governing equations of this vehicle model

$$\mathbf{M}\ddot{\mathbf{w}} + \mathbf{C}\dot{\mathbf{w}} + \mathbf{K}\mathbf{w} = \mathbf{h} \tag{8.5}$$

where $\mathbf{w} = \mathbf{w}(t) = (z_s(t), \theta(t), y_1(t), y_2(t))$ is the coordinate vector, and $\mathbf{h} = \mathbf{h}(t) = (0, 0, p_1 h_1(t), p_2 h_2(t))$ is the road excitation. We also have the mass matrix $\mathbf{M}$

$$\begin{aligned} \mathbf{M} &= \mathbf{M}_m + \mathbf{M}_b \\ &= \begin{bmatrix} m_s & 0 & 0 & 0 \\ 0 & J_y & 0 & 0 \\ 0 & 0 & m_{n_1} & 0 \\ 0 & 0 & 0 & m_{n_2} \end{bmatrix} + \begin{bmatrix} b_1 + b_2 & b_1 a_1 - b_2 a_2 & -b_1 & -b_2 \\ b_1 a_1 - b_2 a_2 & b_1 a_1^2 + b_2 a_2^2 & -b_1 a_1 & b_2 a_2 \\ -b_1 & -b_1 a_1 & b_1 & 0 \\ -b_2 & b_2 a_2 & 0 & b_2 \end{bmatrix} \end{aligned} \tag{8.6}$$

the damping matrix $\mathbf{C}$

$$\mathbf{C} = \begin{bmatrix} c_1 + c_2 & c_1 a_1 - c_2 a_2 & -c_1 & -c_2 \\ c_1 a_1 - c_2 a_2 & c_1 a_1^2 + c_2 a_2^2 & -c_1 a_1 & c_2 a_2 \\ -c_1 & -c_1 a_1 & c_1 & 0 \\ -c_2 & c_2 a_2 & 0 & c_2 \end{bmatrix} \tag{8.7}$$

and the stiffness matrix $\mathbf{K}$

$$\mathbf{K} = \mathbf{K}_k + \mathbf{K}_p$$
$$= \begin{bmatrix} k_1 + k_2 & k_1 a_1 - k_2 a_2 & -k_1 & -k_2 \\ k_1 a_1 - k_2 a_2 & k_1 a_1^2 + k_2 a_2^2 & -k_1 a_1 & k_2 a_2 \\ -k_1 & -k_1 a_1 & k_1 & 0 \\ -k_2 & k_2 a_2 & 0 & k_2 \end{bmatrix} + \begin{bmatrix} 0 & 0 & 0 & 0 \\ 0 & 0 & 0 & 0 \\ 0 & 0 & p_1 & 0 \\ 0 & 0 & 0 & p_2 \end{bmatrix} \tag{8.8}$$

A linear four-degree-of-freedom system is quite simple in principle, but also quite cumbersome to be dealt with analytically without the aid of a computer. Therefore, for educational purposes, it is useful to simplify this model further. The basic idea is to extract two models, both with two degrees of freedom. One model to study free vibrations and the other model to study forced vibrations. The two models are virtually obtained by cutting off the unnecessary parts (gray lines in Fig. 8.3) from the four-degree-of-freedom system.

The sprung mass m_s is always much higher than the total unsprung mass $m_n = m_{n_1} + m_{n_2}$. Typically we have $m_s \simeq 10 m_n$. Moreover, tire stiffness is, except in Formula cars, much higher than the suspension stiffness. Typically, $p_i = 6\text{–}12\ k_i$. Therefore, the tires have little influence on the free vibrations and can be considered as rigid, as done in Fig. 8.3(top). In Formula cars we have $p_i = 1\text{–}2\ k_i$.

On the other hand, the road disturbances involve also high frequencies, and tire stiffness has to be taken into account. For studying forced vibrations, the vehicle is then split into two half-car models, as in Fig. 8.3(bottom), where

$$m_{s_1} = m_s \frac{a_2}{l} \quad \text{and} \quad m_{s_2} = m_s \frac{a_1}{l} \tag{8.9}$$

Instead of the half-car model, it is customary to use the *quarter car model*, which is like the half-car model with all quantities divided by two.

Both models are rather crude approximations, but nevertheless they can provide very useful insights on how to choose the springs and shock absorbers (and, just in case, the inerters as well).

8.2 Quarter Car Model

The quarter car model is shown in Fig. 8.4. For simplicity we dropped the subscript in all quantities. The model consists of a sprung mass m_s connected via the primary suspension to the unsprung mass m_n of the axle. The suspension is supposed to have linear behavior with stiffness k and damping coefficient c. An inerter, with inertance b, is also included. The tire vertical elasticity is represented again by a linear spring p. The tire damping is so small that it can be neglected.

This model is mainly used to study the vibrational behavior of the vehicle when travelling on an uneven road. Therefore, the lowermost part of p receives from the road a sinusoidal displacement $h(t) = H \cos \Omega t$. Someone may object that real

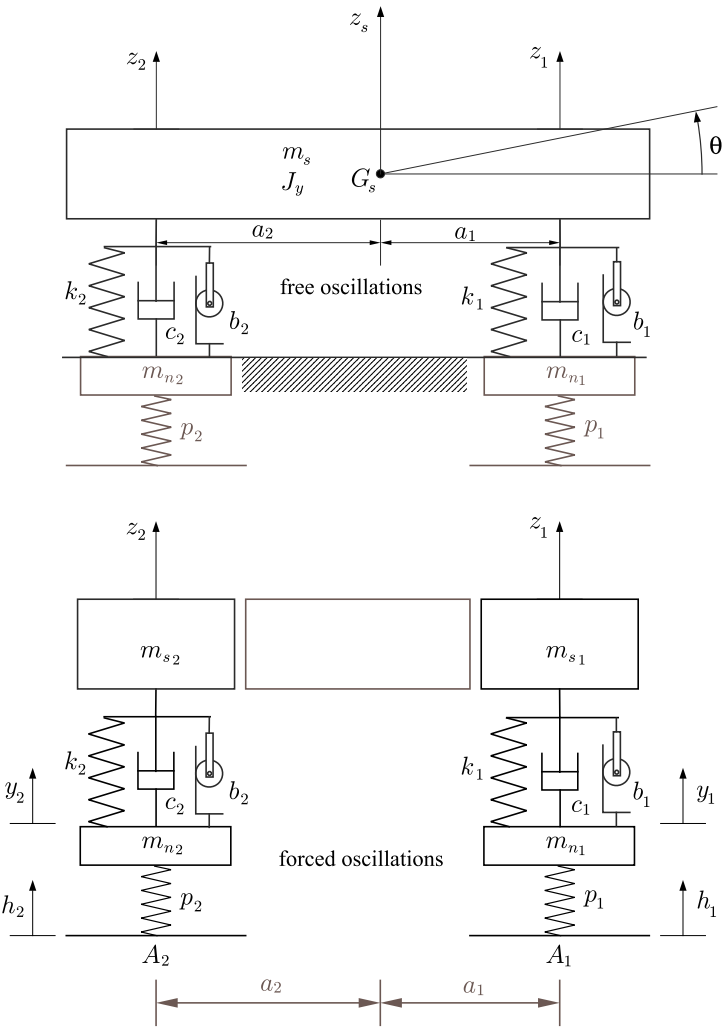

Fig. 8.3 "Extraction" of two-degree-of-freedom models to study free vibrations (*top*) and forced vibrations (*bottom*)

roads are not sinusoidal in shape. However, any road profile $g(x)$ of length L can be expressed by its Fourier series

$$g(x) = \sum_{n=0}^{\infty} \left[d_n \sin\left(\frac{2\pi n}{L} x\right) + e_n \cos\left(\frac{2\pi n}{L} x\right) \right] \tag{8.10}$$

that is as an infinite sum of trigonometric functions. Fortunately, it is possible to take only the first n terms without missing too much information. If the vehicle travels with speed u, the Fourier term with spatial period L/n acts as a forcing

Fig. 8.4 Quarter car model

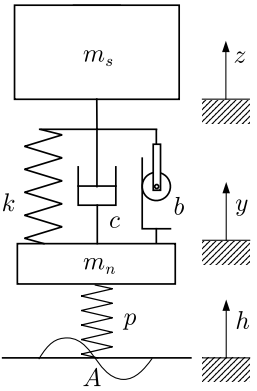

displacement of frequency $f_n = nu/L$. Therefore, the frequency of the excitation depends, obviously, on the speed of the vehicle.

Because of the assumed linearity of the quarter car model, we can take advantage of the superposition principle, and "feed" the system with one Fourier term at a time. Should the system be nonlinear, this trick would be meaningless and we could no longer apply a simple sinusoidal forcing function.

The quarter car model is a damped two-degree-of-freedom system. We employ as coordinates the vertical displacement z of the sprung mass and the vertical displacement y (hop) of the unsprung mass. The road surface vertical displacement $h(t)$ can be derived from the road surface profile and the car's speed. The equations of motion of the quarter car model are readily obtained from Fig. 8.4 (recommended), or as a special case of the equations given in Sect. 8.1

$$\begin{aligned} m_s\ddot{z} &= -b(\ddot{z} - \ddot{y}) - c(\dot{z} - \dot{y}) - k(z - y) \\ m_n\ddot{y} &= -b(\ddot{y} - \ddot{z}) - c(\dot{y} - \dot{z}) - k(y - z) - p(y - h) \end{aligned} \tag{8.11}$$

where, as already stated, $h(t) = H\cos\Omega t$ is the excitation due to the road asperities. The same equations in matrix notation become

$$\mathbf{M}\ddot{\mathbf{w}} + \mathbf{C}\dot{\mathbf{w}} + \mathbf{K}\mathbf{w} = \mathbf{h} \tag{8.12}$$

with mass matrix $\mathbf{M}$

$$\mathbf{M} = \mathbf{M}_m + \mathbf{M}_b = \begin{bmatrix} m_s & 0 \\ 0 & m_n \end{bmatrix} + \begin{bmatrix} b & -b \\ -b & b \end{bmatrix} = \begin{bmatrix} m_s + b & -b \\ -b & m_n + b \end{bmatrix} \tag{8.13}$$

damping matrix $\mathbf{C}$

$$\mathbf{C} = \begin{bmatrix} c & -c \\ -c & c \end{bmatrix} \tag{8.14}$$

and stiffness matrix $\mathbf{K}$

$$\mathbf{K} = \mathbf{K}_k + \mathbf{K}_p = \begin{bmatrix} k & -k \\ -k & k \end{bmatrix} + \begin{bmatrix} 0 & 0 \\ 0 & p \end{bmatrix} = \begin{bmatrix} k & -k \\ -k & k + p \end{bmatrix} \tag{8.15}$$

We are mainly interested in the steady-state response, that is in the particular integral of the system of differential equations (8.11). In a case like this, it can be expressed as

$$\begin{aligned} z(t) &= Z\cos(\Omega t+\varphi) \\ y(t) &= Y\cos(\Omega t+\psi) \end{aligned} \tag{8.16}$$

that is in oscillations with the same angular frequency Ω of the excitation, but also with nonzero phases φ and ψ.

The mathematical analysis is much simpler if complex numbers are employed. The forcing function is therefore given as

$$h(t) = H(\cos\Omega t + i\sin\Omega t) = H\mathrm{e}^{i\Omega t} \tag{8.17}$$

with $H\in\mathbb{R}$. The steady-state solution is

$$\begin{aligned} z(t) &= Z\big[\cos(\Omega t+\varphi)+i\sin(\Omega t+\varphi)\big] = Z\mathrm{e}^{i(\Omega t+\varphi)} = Z\mathrm{e}^{i\varphi}\mathrm{e}^{i\Omega t} = \mathsf{Z}\mathrm{e}^{i\Omega t} \\ y(t) &= Y\big[\cos(\Omega t+\psi)+i\sin(\Omega t+\psi)\big] = Y\mathrm{e}^{i(\Omega t+\psi)} = Y\mathrm{e}^{i\psi}\mathrm{e}^{i\Omega t} = \mathsf{Y}\mathrm{e}^{i\Omega t} \end{aligned} \tag{8.18}$$

where $\mathsf{Z}=Z\mathrm{e}^{i\varphi}$ and $\mathsf{Y}=Y\mathrm{e}^{i\psi}$ are complex numbers with modulus Z and Y, and phases φ and ψ.

Inserting these expressions into (8.11) and dropping $\mathrm{e}^{i\Omega t}$ provides the following algebraic system of equations in the complex unknowns Z and Y

$$\begin{cases} \big[\big(k-b\Omega^2\big)-m_s\Omega^2+ic\Omega\big]\mathsf{Z}-\big[\big(k-b\Omega^2\big)+ic\Omega\big]\mathsf{Y}=0 \\ -\big[\big(k-b\Omega^2\big)+ic\Omega\big]\mathsf{Z}+\big[p+\big(k-b\Omega^2\big)-m_n\Omega^2+ic\Omega\big]\mathsf{Y}=pH \end{cases} \tag{8.19}$$

whose solution is

$$\begin{aligned} \frac{\mathsf{Z}}{H} &= \frac{p[(k-b\Omega^2)+ic\Omega]}{[(k-b\Omega^2)-m_s\Omega^2+ic\Omega][p+(k-b\Omega^2)-m_n\Omega^2+ic\Omega]-[(k-b\Omega^2)+ic\Omega]^2} \\ &= p\frac{[(k-b\Omega^2)+ic\Omega]}{d(\Omega^2)+ic\Omega e(\Omega^2)} = \mathsf{G}_z(\Omega) \end{aligned} \tag{8.20}$$

and

$$\frac{\mathsf{Y}}{H} = p\frac{[(k-b\Omega^2)-m_s\Omega^2+ic\Omega]}{d(\Omega^2)+ic\Omega e(\Omega^2)} = \mathsf{G}_y(\Omega) \tag{8.21}$$

where, for compactness,

$$\begin{aligned} d\big(\Omega^2\big) &= m_sm_n\Omega^4-\big\{\big[p+\big(k-b\Omega^2\big)\big]m_s+\big(k-b\Omega^2\big)m_n\big\}\Omega^2+pk \\ e\big(\Omega^2\big) &= p-(m_s+m_n)\Omega^2 \end{aligned} \tag{8.22}$$

The non-dimensional complex functions $\mathsf{G}_z(\Omega)$ and $\mathsf{G}_y(\Omega)$, given in (8.20) and (8.21), can be directly employed to obtain the steady-state solution

$$\begin{aligned} z(t) &= H\mathsf{G}_z(\Omega)\mathrm{e}^{i\Omega t} \\ y(t) &= H\mathsf{G}_y(\Omega)\mathrm{e}^{i\Omega t} \end{aligned} \tag{8.23}$$

From a practical point of view, we are mostly interested in the *amplitude* of these oscillations as functions of Ω

$$\frac{Z}{H} = \frac{|\mathsf{Z}|}{H} = p\sqrt{\frac{(k-b\Omega^2)^2 + c^2\Omega^2}{d^2(\Omega^2) + c^2\Omega^2 e^2(\Omega^2)}} = \left|\mathsf{G}_z(\Omega)\right| \tag{8.24}$$

$$\frac{Y}{H} = \frac{|\mathsf{Y}|}{H} = p\sqrt{\frac{[(k-b\Omega^2) - m_s\Omega^2]^2 + c^2\Omega^2}{d^2(\Omega^2) + c^2\Omega^2 e^2(\Omega^2)}} = \left|\mathsf{G}_y(\Omega)\right| \tag{8.25}$$

However, the phases can be obtained as well

$$\tan\varphi = \frac{\mathrm{Im}(\mathsf{Z})}{\mathrm{Re}(\mathsf{Z})}, \qquad \tan\psi = \frac{\mathrm{Im}(\mathsf{Y})}{\mathrm{Re}(\mathsf{Y})} \tag{8.26}$$

The amplitude of the vertical accelerations of the sprung and unsprung masses are given by $\Omega^2 Z$ and $\Omega^2 Y$, respectively.

Due to the oscillations, there are fluctuations in the vertical force exchanged by the tires with the road. More precisely, we have a sinusoidal force $\mathsf{N}\mathrm{e}^{i\Omega t}$ superimposed on the constant force due to weight and, possibly, to aerodynamic downforces. From the quarter car model of Fig. 8.4 we get

$$\mathsf{N}\mathrm{e}^{i\Omega t} = p(h-y) = p(H-\mathsf{Y})\mathrm{e}^{i\Omega t} \tag{8.27}$$

From (8.21), we obtain the amplitude N as a function of the angular frequency Ω

$$\begin{aligned} \frac{N}{pH} = \frac{|\mathsf{N}|}{pH} &= \left|\frac{m_s m_n\Omega^4 - (m_s+m_n)\Omega^2[(k-b\Omega^2) + ic\Omega]}{d(\Omega^2) + ic\Omega e(\Omega^2)}\right| \\ &= \Omega^2\sqrt{\frac{[m_s m_n\Omega^2 - (k-b\Omega^2)(m_s+m_n)]^2 + c^2\Omega^2(m_s+m_n)^2}{d^2(\Omega^2) + c^2\Omega^2 e^2(\Omega^2)}} \end{aligned} \tag{8.28}$$

8.2.1 The Inerter as a Spring Softener

It is worth noting that all these expressions include the term $k - b\Omega^2$. This is the key to understand the *inerter* (also called J-Damper). It is pretty much like having a system whose suspension stiffness is sensitive to the frequency Ω of the excitation. At low frequencies $k - b\Omega^2 \simeq k$, but at high frequencies $k - b\Omega^2 \ll k$. The inertance b acts as a *spring softener*. This is a very interesting feature in Formula

cars, with high aerodynamic loads, because we can use very stiff springs, thus limiting the spring deflection due to variable aerodynamic downforces, but at the same time the car will be able to absorb the high frequency road asperities, as if it were equipped with not-so-stiff springs. We will elaborate this idea quantitatively and in more detail in Sect. 8.3.3.

8.2.2 *Quarter Car Natural Frequencies and Modes*

A linear two-degree-of-freedom vibrating system, damped or not, has two natural modes, each one associated with its natural frequency.

To obtain these two modes, we consider the homogeneous counterpart of the system of differential equations (8.12)

$$\mathbf{M}\ddot{\mathbf{w}}_o + \mathbf{C}\dot{\mathbf{w}}_o + \mathbf{K}\mathbf{w}_o = \mathbf{0} \tag{8.29}$$

We seek a solution like

$$\mathbf{w}_o = \mathbf{x}\mathrm{e}^{\mu t} \tag{8.30}$$

which, when inserted into (8.29), yields

$$\mathrm{e}^{\mu t}\left(\mu^2\mathbf{M} + \mu\mathbf{C} + \mathbf{K}\right)\mathbf{x} = \mathbf{0} \tag{8.31}$$

The four values of μ that make (8.30) truly a solution are the roots of the characteristic equation

$$\det\left(\mu^2\mathbf{M} + \mu\mathbf{C} + \mathbf{K}\right) = 0 \tag{8.32}$$

In an underdamped vibrating system, the four μ are complex numbers, complex conjugates in pairs

$$\begin{aligned} \mu_1 &= -\zeta_1\omega_1 + \mathrm{i}\omega_1\sqrt{1-\zeta_1^2}, \qquad & \mu_3 &= \bar{\mu}_1 = -\zeta_1\omega_1 - i\omega_1\sqrt{1-\zeta_1^2} \\ \mu_2 &= -\zeta_2\omega_2 + \mathrm{i}\omega_2\sqrt{1-\zeta_2^2}, \qquad & \mu_4 &= \bar{\mu}_2 = -\zeta_2\omega_2 - i\omega_2\sqrt{1-\zeta_2^2} \end{aligned} \tag{8.33}$$

where $0 \le \zeta_i < 1$ are the damping ratios (or damping factors), and ω_i are the natural angular frequencies of the undamped system. The two natural angular frequencies of the damped system (i.e., the quarter car model) are $\omega_{d_i} = \omega_i\sqrt{1-\zeta_i^2}$.

Once the four μ_i have been obtained, we can go back to (8.31) and obtain the corresponding generalized eigenvectors $\mathbf{x}_i \in \mathbb{C}^2$, again complex conjugates in pairs. The general solution of (8.29) is given as linear combination of complex exponential functions

$$\begin{aligned} \mathbf{w}_o(t) = {} & \gamma_1\mathbf{x}_1\mathrm{e}^{(-\zeta_1\omega_1 + i\omega_{d_1})t} + \bar{\gamma}_1\bar{\mathbf{x}}_1\mathrm{e}^{(-\zeta_1\omega_1 - i\omega_{d_1})t} \\ & + \gamma_2\mathbf{x}_2\mathrm{e}^{(-\zeta_2\omega_2 + i\omega_{d_2})t} + \bar{\gamma}_2\bar{\mathbf{x}}_2\mathrm{e}^{(-\zeta_2\omega_2 - i\omega_{d_2})t} \end{aligned} \tag{8.34}$$

As an introduction to the general case, it is useful to study first two very special cases, that is $c = 0$ and $c = \infty$.

8.2.2.1 Undamped Quarter Car Model

According to the expression of $d(\omega^2)$ in (8.22), the two natural angular frequencies ω_1 and ω_2 of the *undamped* system are the solutions of the equation

$$m_s m_n \omega^4 - \left\{\left[p + \left(k - b\omega^2\right)\right]m_s + \left(k - b\omega^2\right)m_n\right\}\omega^2 + pk = 0 \tag{8.35}$$

that is

$$\begin{aligned}\omega_{1,2}^2 = &\frac{k(m_n + m_s) + (b + m_s)p}{2m_n m_s + 2b(m_n + m_s)} \\ &\pm \frac{\sqrt{-4k[m_n m_s + b(m_n + m_s)]p + [k(m_n + m_s) + (b + m_s)p]^2}}{2m_n m_s + 2b(m_n + m_s)}\end{aligned} \tag{8.36}$$

which, if there is no inerter b, simplifies into

$$\begin{aligned}\omega_{1,2}^2 &= \frac{k(m_n + m_s) + m_s p \pm \sqrt{-4k(m_n m_s)p + [k(m_n + m_s) + m_s p]^2}}{2m_n m_s} \\ &= \frac{1}{2}\left[\frac{p + k}{m_n} + \frac{k}{m_s} \pm \sqrt{\left(\frac{p + k}{m_n} - \frac{k}{m_s}\right)^2 + \frac{4k^2}{m_n m_s}}\right]\end{aligned} \tag{8.37}$$

As already stated, in all road cars we have $m_s \gg m_n$ and $p \gg k$. Therefore, we can take the first-order Taylor expansion approximation of (8.37) for small values of m_n and k

$$\omega_1^2 \simeq \frac{kp}{(p + k)m_s} \quad \text{and} \quad \omega_2^2 \simeq \frac{p + k}{m_n} \tag{8.38}$$

In most cases, this very simple formulæ provide very accurate estimates of the natural frequencies of the undamped quarter car model. For instance, with the data reported in the caption of Fig. 8.6, we get the following values using first the exact formula and then the approximate one

$$\begin{aligned}f_1 &= \frac{\omega_1}{2\pi} = 1.254 \text{ Hz} \simeq 1.255 \text{ Hz} \\ f_2 &= \frac{\omega_2}{2\pi} = 12.64 \text{ Hz} \simeq 12.63 \text{ Hz}\end{aligned} \tag{8.39}$$

The results are almost identical. Typically, $f_2/f_1 \simeq 10$.

Of course there is a clear physical interpretation. The two approximate natural frequencies (8.38) would be the exact natural frequencies of the two one-degree-of-

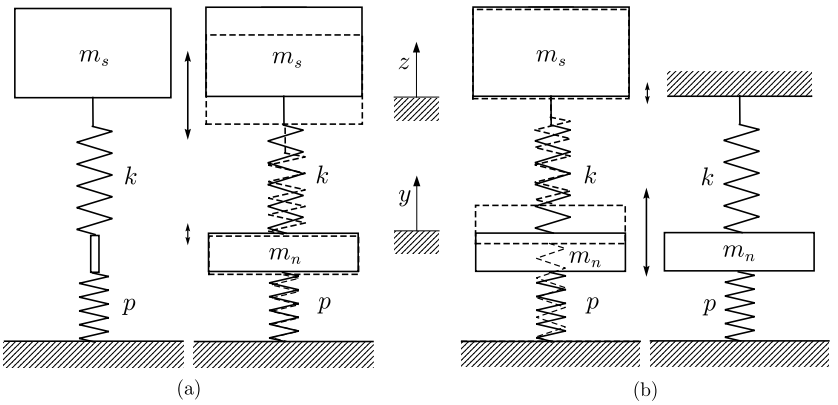

Fig. 8.5 One-degree-of-freedom systems for the approximate evaluation of the two natural frequencies of the quarter car model (road cars only)

freedom systems shown in Fig. 8.5. Indeed, as also shown in Fig. 8.5, the two natural modes of the undamped quarter car model are very peculiar. For instance, again with the same data, the first mode, the one with $f_1 = 1.2$ Hz, has $z(t) = 8.9y(t)$, whereas the second mode, with $f_2 = 12.6$ Hz, has $y(t) = -89.1z(t)$. That is, they look pretty much as if only one mass at the time were oscillating.

A Formula 1 car exhibits similar figures, although with some noteworthy differences. Typically, the undamped system has $f_1 \simeq 5$ Hz with $z(t) = 2.5y(t)$ and $f_2 \simeq 32$ Hz with $z(t) = -25y(t)$.

However, it is very important to know that while the first natural mode is quite insensitive to damping, the second natural mode is very damping dependent. For instance, in a road car having what will be called the *optimal damping* c_{opt}, the first mode has $f_1 = 1.21$ Hz, which is very close to $f_1 = 1.25$ Hz with no damping. Moreover, the amplitude of $z(t)$ is about 8.4 times the amplitude of $y(t)$, pretty much like in the undamped case. The second mode, on the other hand, has $f_2 = 11.1$ Hz instead of $f_2 = 12.6$ Hz with no damping. But the most striking difference is that the amplitude of $y(t)$ is only about 12 times the amplitude of $z(t)$, instead of about 90 times, as it was with no damping. This is to say that we should not extrapolate results obtained with no damping to the real case, when there is a lot of damping because of the shock absorbers.

8.2.2.2 Quarter Car with Stuck Shock Absorber

The other theoretical case is $c = \infty$, pretty much as travelling with a stuck shock absorber. The system behaves like a one-degree-of-freedom system with only one mass $m_s + m_n$ on top of a spring p. There is only one natural frequency $\omega_c = \sqrt{p/(m_s + m_n)}$, as shown in Fig. 8.6.

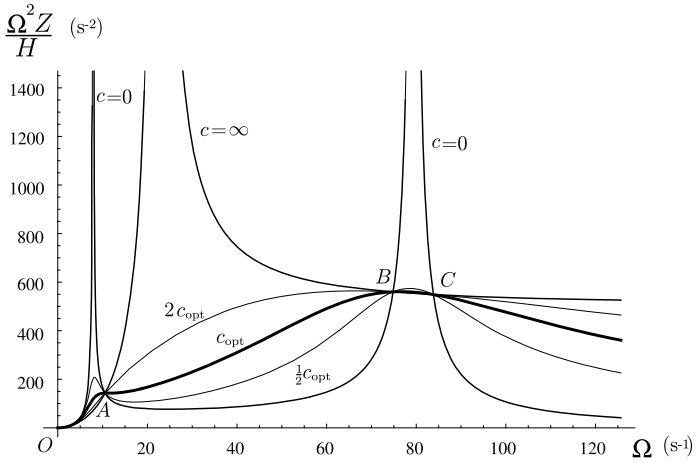

Fig. 8.6 Amplitude of the vertical acceleration of the sprung mass in a typical road car ($m_s = 1\,000$ kg, $m_n = 100$ kg, $k = 70$ kN/m and $p = 560$ kN/m)

8.3 Shock Absorber Tuning

The quarter car model can now be used as a tool for the selection of the damping coefficient c of the shock absorber. Of course, we have first to set up our goal. Typically, in road cars we are interested in minimizing the amplitude $\Omega^2 Z$ of the vertical acceleration $\ddot{z} = \Omega^2 \mathsf{Z} e^{i\Omega t}$ of the sprung mass, thus optimizing the passenger comfort. On the other hand, in race cars we are more interested in minimizing the amplitude N of the oscillating part of the vertical force $\mathsf{N} e^{i\Omega t}$, thus improving road holding.

8.3.1 Comfort Optimization

To select the right amount of damping to optimize passenger comfort, let us plot the normalized acceleration amplitude $\Omega^2 Z/H$ versus the angular frequency Ω of the road excitation. This is done in Fig. 8.6 for some values of c, including the two extreme cases $c = 0$ and $c = \infty$. The figure was obtained with $m_s = 1\,000$ kg, $m_n = 100$ kg, $k = 70$ kN/m and $p = 560$ kN/m, that is with $m_s = 10 m_n$ and $p = 8k$.

The plot for $c = 0$ and the plot for $c = \infty$ have four common points, marked by O, A, B and C in Fig. 8.6. Obviously, all other curves, for any value of c, must pass through the same points.

The best curve, and hence the best value of the damping coefficient c, is perhaps the one with *horizontal tangent at point A*. It is a good compromise, as suggested in 1950 by Bourcier de Carbon [2]. As also shown in Fig. 8.6, lower or higher values of c would yield less uniform plots.

To obtain this optimal value c_{opt}, we have to impose that the derivative at A be zero

$$\left.\frac{\partial(\Omega^2 Z(c,\Omega))}{\partial\Omega}\right|_{\Omega=\Omega_A} = 0 \tag{8.40}$$

where $Z = Z(c,\Omega)$ is given in (8.24). The result is the sought *optimal damping coefficient* c_{opt}

$$c_{\text{opt}} = \sqrt{\frac{m_s k}{2}}\sqrt{\frac{p+2k}{p}} \tag{8.41}$$

where the second square root is quite close to one. With the data used to draw Fig. 8.6 we get $c_{\text{opt}} = 5\,916.08 \times 1.118 = 6\,614.38$ Ns/m. With this value of the damping coefficient, we have that the two natural modes of the quarter car model have, respectively, $\zeta_1 = 0.34$ and $\omega_1\sqrt{1-\zeta_1^2} = 8.1$ rad/s for the first mode, and $\zeta_1 = 0.44$ and $\omega_1\sqrt{1-\zeta_1^2} = 77.0$ rad/s for the second mode. We see that both modes are underdamped ($\zeta_i < 1$), but with a far from negligible amount of damping. One observation is in order here. Although the two values of ζ_i are quite similar, the time-rate decaying of the two modes, which depend on $\zeta_i\omega_i$, are drastically different because the two ω_i are quite far apart. For instance, in one second the amplitude of the first mode drops from 1 to $\mathrm{e}^{-0.34\times 8.61} = 0.05$, while that of the second mode drops to $\mathrm{e}^{-0.44\times 85.7} = 10^{-17}$. Quite a big difference.

It is worth noting that c_{opt} does not depend on the unsprung mass m_n. Therefore, it is not necessary to change the shock absorbers when, for instance, mounting light alloy wheel rims. On the other hand, stiffer springs do require harder shock absorbers.

Saying that m_n does not affect c_{opt} does not imply that the unsprung mass has no influence at all. The comfort performances for three different values of the ratio m_n/m_s are shown in Fig. 8.7. The lower the unsprung mass, the better, because the resulting curve is more uniform.

The formula for the optimal value of the damping coefficient here obtained perhaps works to get a close to optimal damping coefficient for a Formula 1 car as well. Figure 8.8 is the counterpart of Fig. 8.6. We see that the two figures are quite different, but the c_{opt} curve is probably the best.

8.3.2 Road Holding Optimization

Needless to say that we need high vertical loads to have high friction forces. When the road is not flat, the vertical force fluctuations may impair road holding. Therefore, we are interested in how to determine the best shock absorber tuning to counteract these force fluctuations as much as possible. The quarter car model can be

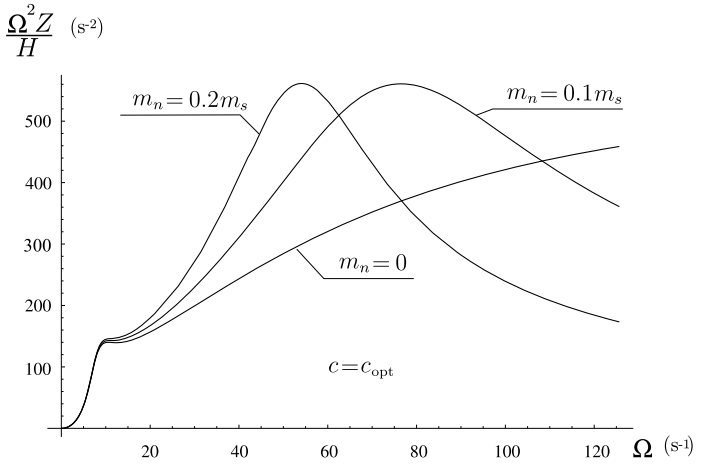

Fig. 8.7 Amplitude of the vertical acceleration of the sprung mass for three values of the unsprung mass (road car with $m_s = 1\,000$ kg, $c = c_{\text{opt}}$, $k = 70$ kN/m and $p = 560$ kN/m)

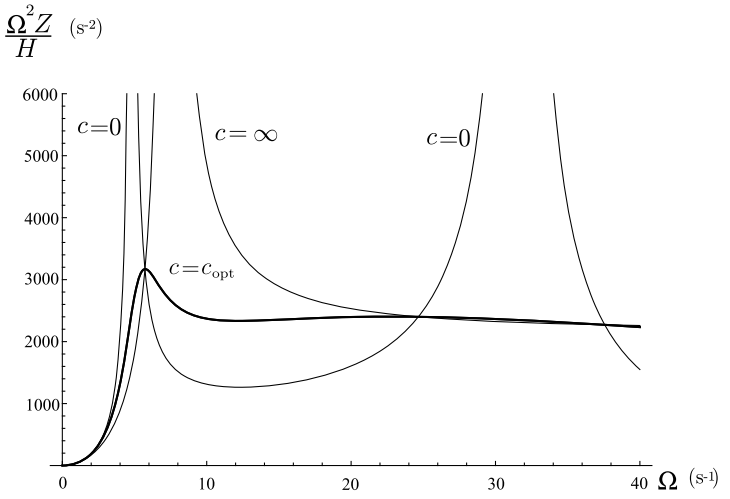

Fig. 8.8 Amplitude of the vertical acceleration of the sprung mass in a typical Formula 1 car

usefully employed to this end. We have already obtained in (8.28) the expression of the amplitude of the sinusoidal component of the vertical load. Of course, it is superimposed on the vertical load due to weight, load transfers and, possibly, aerodynamic downforces.

The plot of the normalized amplitude $N/(pH)$ versus Ω is shown in Fig. 8.9 for several values of the damping coefficient c. As before, there are the curves for the extreme cases $c = 0$ and $c = \infty$. In this case there are only three fixed points

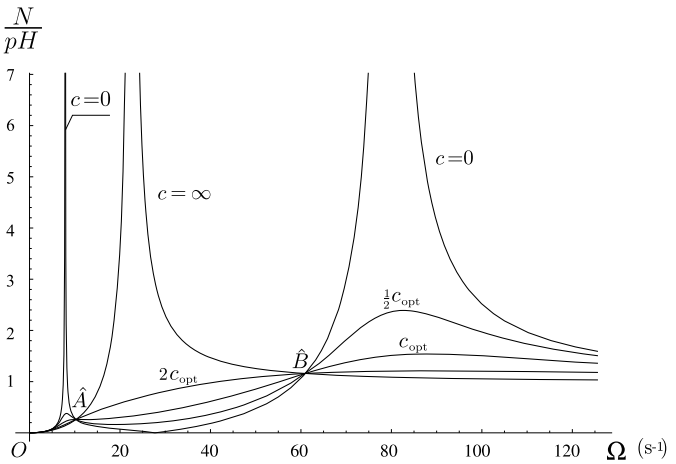

Fig. 8.9 Amplitude of the sinusoidal vertical load for a road car ($m_s = 1\,000$ kg, $m_n = 100$ kg, $k = 70$ kN/m and $p = 560$ kN/m)

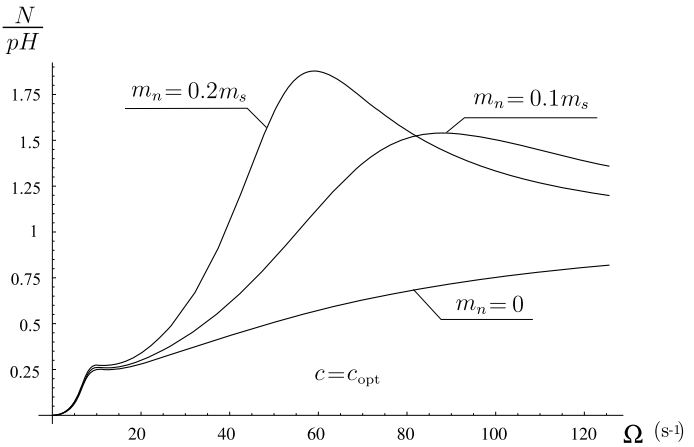

Fig. 8.10 Amplitude of the sinusoidal vertical load for a road car for three values of the unsprung mass and $c = c_{\text{opt}}$

O, $\hat{A}$ and $\hat{B}$. The curve corresponding to $c = \frac{1}{2}c_{\text{opt}}, c_{\text{opt}}, 2c_{\text{opt}}$ are also shown in Fig. 8.9. As before, we have assumed $m_s = 1\,000$ kg, $m_n = 100$ kg, $k = 70$ kN/m and $p = 560$ kN/m, that is $m_s = 10m_n$ and $p = 8k$.

The curve for $c = c_{\text{opt}}$ is not as good as it was with respect to comfort. For road holding optimization in road cars, it is better to use higher values of the damping coefficient c, that is $c > c_{\text{opt}}$.

Reducing the unsprung masses is very beneficial for road holding, as shown in Fig. 8.10. We see that the lower the unsprung mass, the lower the vertical force

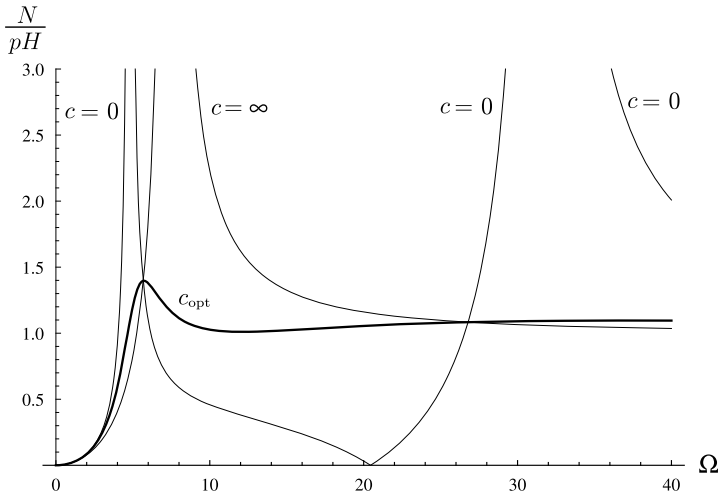

Fig. 8.11 Amplitude of the sinusoidal vertical load for a typical Formula 1 car

amplitude, and hence the better the road holding. Therefore, using light alloy wheels is certainly a way to improve road holding.

8.3.3 The Inerter as a Tool for Road Holding Tuning

Formula cars, and Formula 1 cars in particular, have wings that provide fairly high downforces at high speed. These devices are most efficient if kept at constant distance from the road surface. To reduce the spring deflections under variable aerodynamic loads, very stiff springs have to be used. However, stiff springs are not very good to absorb road irregularities. Here is where the *inerter* comes into play. It works as a sort of spring softener at high frequencies, while being almost irrelevant with respect to static or slowly varying loads.

Let us have a look at the counterpart of Fig. 8.9 for, e.g., a Formula 1 car. The plot of $N/(pH)$ versus Ω for a Formula 1 car is shown in Fig. 8.11. Interestingly enough, the value of c_{opt} is optimal indeed. Any other value would be worse.

But we are interested in increasing the spring stiffness k without impairing the suspension capability to filter down road irregularities. Unfortunately, simply stiffening the springs brings a worse plot of $N/(pH)$, as shown in Fig. 8.12 (dashed line). However, the inerter can help in balancing the stiffer spring, and, in fact we end up with a much better plot (thick solid line in Fig. 8.12). Typically, we can increase the stiffness by 10–20 %, with an inertance of 25–100 kg per wheel in a Formula Indy car.

It is worth noting that in ordinary road cars the inerter would not be beneficial. This is due to the totally different values of mass, stiffnesses, etc. Indeed, Figs. 8.9 and 8.11 are very different.

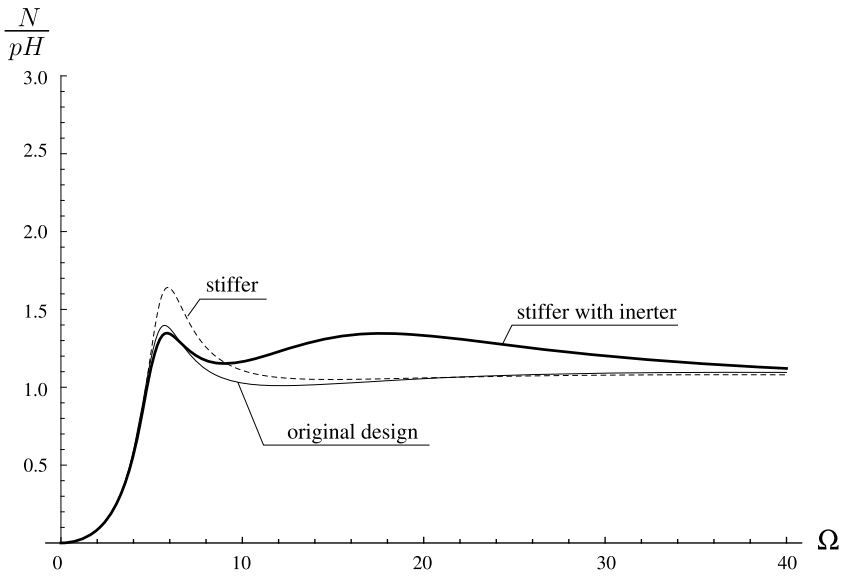

Fig. 8.12 Beneficial effect of the inerter in a Formula 1 car with stiffer springs

8.4 Road Profiles

In probability theory, stationary ergodic process is a random process which exhibits both stationarity and ergodicity. In essence this implies that the random process will not change its statistical properties with time and that its statistical properties (such as the theoretical mean and variance of the process) can be deduced from a single, sufficiently long sample of the process.

Road elevation profiles are stationary ergodic processes. This allows for fairly simple statistical treatment.

The Fourier transform $F(\omega)$ is a very powerful tool to obtain the frequency feature of a given function $f(x)$

$$F(\omega) = \int_{-\infty}^{+\infty} f(x)\mathrm{e}^{-i\omega x}\mathrm{d}x \tag{8.42}$$

The function $F(\omega) \in \mathbb{C}$ is precisely the frequency spectrum of $f(x)$.

We cannot apply directly the Fourier transform to a given road profile $g(x) \in \mathbb{R}$ because it does not tend to zero when $x \to \pm\infty$. However, we can introduce the spatial autocorrelation function $R_g(\tau)$ defined by

$$R_g(\tau) = \lim_{L\to\infty} \frac{1}{L} \int_{-L/2}^{+L/2} g(x)g(x+\tau)\mathrm{d}x \tag{8.43}$$

where L is the length of the road with profile $g(x)$, and then compute its *power spectral density* (PSD) as its Fourier transform

$$S_g(s) = \int_{-\infty}^{+\infty} R(\tau) \mathrm{e}^{-is\tau} \mathrm{d}\tau \tag{8.44}$$

The power spectral density is measured in m^2/(cycles/m), if g is in meters and s is in cycles/m. Therefore, s is the spatial frequency.

If the vehicle travels at constant speed u, we can switch from the profile $g(x)$ to the time history $h(t)$ by means of the simple formula $h(t) = g(ut)$. The PSD $S_h(f)$, measured in m/Hz, of $h(t)$ can be obtained from $S_g(s)$ using

$$S_h(f) = \frac{S_g(f/u)}{u} \tag{8.45}$$

In general, if we know the PSD $S_h(f)$ of the excitation $h(t)$ and the frequency gain $\mathsf{G}_z(\Omega)$ of the linear system at hand, we can easily obtain the PSD of the system response $z(t)$ as

$$S_z(f) = \left|\mathsf{G}_z(2\pi f)\right|^2 S_h(f) \tag{8.46}$$

where, as well known, $\Omega = 2\pi f$.

For instance, the PSD $S_a(f)$ of the vertical acceleration $\ddot{z}$ of the sprung mass of the quarter car model is

$$S_a(f) = \left|(2\pi f)^2 \mathsf{G}_z(2\pi f)\right|^2 S_h(f), \tag{8.47}$$

with $\mathsf{G}_z(\Omega) = \mathsf{G}_z(2\pi f)$ given in (8.20).

There is experimental evidence that the PSD of road profiles has a typical trend: the amplitude diminishes rapidly with the spatial frequency s. An often employed empirical formula for this behavior is

$$S_g(s) = Bs^{-k} \tag{8.48}$$

Unfortunately, there is not much agreement on the value of the exponent k. Typically it ranges between 2 and 4, including fractional values. The constant B characterizes the roughness of the road profile. The smoother the profile, the lower B. It is worth noting that the units to measure B are affected by the value of the exponent k.

According to (8.45), the counterpart of (8.48) in terms of time frequencies is

$$S_h(f) = Bu^{k-1} f^{-k} \tag{8.49}$$

which, obviously, shows that increasing the vehicle speed brings an increment in the PSD of the excitation.

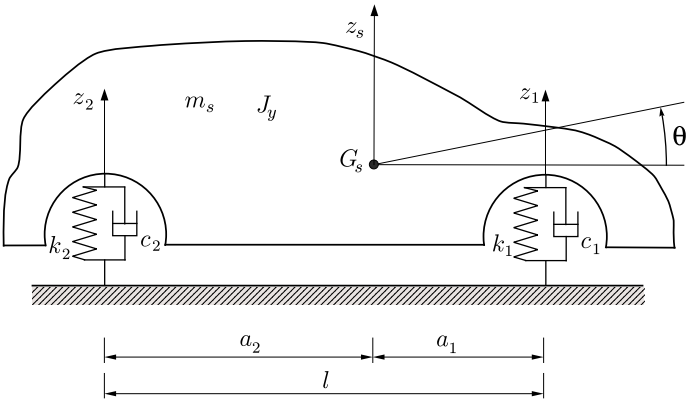

Fig. 8.13 Two-degree-of-freedom system for bounce and pitch analysis

8.5 Free Vibrations of Road Cars

The quarter car model looks at each axle as if it were alone. But it is not. Cars have two axles, and both take part in the vehicle body oscillations. Moreover, when we obtained the optimal value c_{opt} of the damping coefficient in (8.41) by means of the quarter car model, that was a function of the suspension stiffness k, beside the sprung mass m_s and the tire vertical stiffness p. But how was the stiffness k set? We do not have much freedom about m_s and p, and we may assume both of them as given for a certain kind of vehicle. But the stiffness k can be selected quite freely, for both front and rear axles.

Free oscillations are what happens right after the car has hit an isolated bump or hole. Since road cars usually do not employ the inerter, we use the even simpler two-degree-of-freedom model shown in Fig. 8.13, instead of the model of Fig. 8.3. As already discussed, we can safely consider the tires as rigid. The tires are indeed much stiffer than the springs, and at low frequencies (1–2 Hz) the unsprung masses oscillate very little. Moreover, the mode with higher natural frequency decays almost instantaneously, as already shown.

The analysis of the model of Fig. 8.13 will provide useful hints for the selection and tuning of the front and rear stiffnesses k_1 and k_2.

8.5.1 Governing Equations

To obtain all relevant equations for the two-degree-of-freedom vehicle model under investigation we follow the same path as in Sect. 8.1. We have (Fig. 8.13)

(1) congruence equations:

$$\begin{aligned} z_1 &= z_s + a_1\theta \\ z_2 &= z_s - a_2\theta \end{aligned} \tag{8.50}$$

that is a purely geometrical link between coordinates;
(2) equilibrium equations:

$$\begin{aligned} m_s\ddot{z}_s &= F_1 + F_2 \\ J_y\ddot{\theta} &= F_1 a_1 - F_2 a_2 \end{aligned} \tag{8.51}$$

that is a link between forces or couples and accelerations; and
(3) constitutive equations:

$$\begin{aligned} F_1 &= -k_1 z_1 - c_1 \dot{z}_1 \\ F_2 &= -k_2 z_2 - c_2 \dot{z}_2 \end{aligned} \tag{8.52}$$

When combined all together, they provide the governing equations

$$\begin{aligned} m_s\ddot{z}_s &= -k_1(z_s + a_1\theta) - c_1(\dot{z}_s + a_1\dot{\theta}) - k_2(z_s - a_2\theta) - c_2(\dot{z}_s - a_2\dot{\theta}) \\ J_y\ddot{\theta} &= \left[-k_1(z_s + a_1\theta) - c_1(\dot{z}_s + a_1\dot{\theta})\right]a_1 \\ &\quad - \left[-k_2(z_s - a_2\theta) - c_2(\dot{z}_s - a_2\dot{\theta})\right]a_2 \end{aligned} \tag{8.53}$$

that can also be written in matrix notation as

$$\mathbf{M}\ddot{\mathbf{w}}_o + \mathbf{C}\dot{\mathbf{w}}_o + \mathbf{K}\mathbf{w}_o = \mathbf{0} \tag{8.54}$$

where $\mathbf{w}_o = (z_s, \theta)$. Formally, they look like (8.5), except for being homogeneous now. The 2×2 matrices are

$$\mathbf{M} = \begin{bmatrix} m_s & 0 \\ 0 & J_y \end{bmatrix} \tag{8.55}$$

$$\mathbf{C} = \begin{bmatrix} c_1 + c_2 & c_1 a_1 - c_2 a_2 \\ c_1 a_1 - c_2 a_2 & c_1 a_1^2 + c_2 a_2^2 \end{bmatrix} \tag{8.56}$$

and

$$\mathbf{K} = \begin{bmatrix} k_1 + k_2 & k_1 a_1 - k_2 a_2 \\ k_1 a_1 - k_2 a_2 & k_1 a_1^2 + k_2 a_2^2 \end{bmatrix} \tag{8.57}$$

Quite surprisingly, it is common practice in the vehicle dynamic community to discard damping when studying free oscillations of a vehicle. Most books do that. But why?

Actually, vehicles have a lot of damping (in the quarter car model we obtained damping ratios ζ_i in the range 0.3–0.5). Perhaps they are the most damped system in mechanical engineering, and a good engineer cannot discard something which is not negligible at all. A rationale for neglecting damping should be provided, as a minimum. Unfortunately, in most cases there is just a sentence stating that damping will be neglected.

Free oscillations of undamped systems are much more predictable than those of a general damped system. Moreover, through modal analysis they can be treated as

a collection of single-degree-of-freedom oscillators. But, we insist, vehicles are not undamped. They are very damped systems.

Fortunately, there is a way to have a damped system behave pretty much like an undamped system: it must have *proportional viscous damping* (also called Rayleigh damping). Modes of proportionally damped systems preserve the simplicity of the real normal modes as in the undamped case.

8.5.2 Proportional Viscous Damping

The definition of proportional viscous damping is

$$\mathbf{C} = \alpha\mathbf{M} + \beta\mathbf{K} \tag{8.58}$$

that is the damping matrix must be a linear combination of the mass and stiffness matrices, for suitable constants α and β.

Systems with proportional viscous damping have exactly the same mode shapes as the corresponding undamped systems. This is the key property.

The proof is quite simple. Inserting (8.58) into (8.54) and assuming, as usual, $\mathbf{w}_o(t) = \mathbf{x}e^{\mu t}$, we get

$$\left(\mu^2 + \mu\alpha\right)\mathbf{M}\mathbf{x} + (\mu\beta + 1)\mathbf{K}\mathbf{x} = \mathbf{0} \tag{8.59}$$

that is

$$\left(\frac{\mu^2 + \mu\alpha}{\mu\beta + 1}\right)\mathbf{M}\mathbf{x} = -\mathbf{K}\mathbf{x} \tag{8.60}$$

With respect to the general case (8.31), we have only two matrices instead of three. And it makes quite a big difference.

Now, letting

$$\lambda = \frac{\mu^2 + \mu\alpha}{\mu\beta + 1} \quad \text{and} \quad \mathbf{A} = -\mathbf{M}^{-1}\mathbf{K} \tag{8.61}$$

we end up with exactly the same eigenvalue problem as the undamped system

$$\mathbf{A}\mathbf{x} = \lambda\mathbf{x} \tag{8.62}$$

which provides two real eigenvalues λ_1 and λ_2, and the corresponding *real* eigenvectors $\mathbf{x}_1$ and $\mathbf{x}_2$.

Solving the first equation in (8.61) with $\lambda = \lambda_1$, we obtain μ_1 and $\mu_3 = \bar{\mu}_1$. Similarly, solving with $\lambda = \lambda_2$ we obtain μ_2 and $\mu_4 = \bar{\mu}_2$. Therefore, we have apparently four μ_j and only two eigenvectors $\mathbf{x}_j$. The point is that the eigenvectors have real components, and hence coincide with their complex conjugates. Strictly speaking, we have two couples of identical eigenvectors.

The general solution, that is the free oscillations, for proportional damping (and hence also for no damping, which is just a special case of proportional damping) is[2]

$$\mathbf{w}_o(t) = \mathbf{x}_1\left(\gamma_1 \mathrm{e}^{\mu_1 t} + \gamma_3 \mathrm{e}^{\mu_3 t}\right) + \mathbf{x}_2\left(\gamma_2 \mathrm{e}^{\mu_2 t} + \gamma_4 \mathrm{e}^{\mu_4 t}\right) \tag{8.63}$$

Often, this equivalent expression is more convenient, which only involves real quantities (cf. (6.179))

$$\mathbf{w}_o(t) = \chi_1 \mathbf{x}_1 \mathrm{e}^{-\zeta_1 \omega_1 t} \sin(\omega_{d_1} t + \varphi_1) + \chi_2 \mathbf{x}_2 \mathrm{e}^{-\zeta_2 \omega_2 t} \sin(\omega_{d_2} t + \varphi_2) \tag{8.64}$$

where

$$\mu_1 = -\zeta_1 \omega_1 + \mathrm{i}\omega_{d_1} \quad \text{and} \quad \mu_2 = -\zeta_2 \omega_2 + \mathrm{i}\omega_{d_2} \tag{8.65}$$

As usual, ζ_j are the damping factors and ω_j are the angular frequencies of the corresponding undamped system, while $\omega_{dj} = \omega_j \sqrt{1 - \zeta_j^2}$ are the angular frequencies of the damped system. The undamped system has $\lambda = \mu^2$, and hence

$$\omega_j = \sqrt{-\lambda_j} \quad \text{and} \quad \zeta_j = 0 \tag{8.66}$$

The four unknown constants depend on the four initial conditions.

The undamped and proportionally damped system share almost everything, except the μ_j's. The really relevant aspect is that the eigenvectors $\mathbf{x}_j$ are exactly the same. This is the possible justification for "neglecting" the damping when studying the free oscillations of a vehicle. But the vehicle must be designed to have proportional viscous damping, indeed. And a good vehicle engineer should be well aware of this requirement.

8.5.3 Vehicle with Proportional Viscous Damping

Looking at the three matrices (8.55), (8.56) and (8.57) for the case at hand, we see that the matrix $\mathbf{C}$ and the matrix $\mathbf{K}$ share the very same structure. Therefore, the only way to have proportional damping in a vehicle (without inerter) is to set $\alpha = 0$ and select springs and shock absorbers such that

$$\beta = \frac{c_1}{k_1} = \frac{c_2}{k_2} \tag{8.67}$$

thus having $\mathbf{C} = \beta \mathbf{K}$. This can be done fairly easily.

[2] The quarter car model is a two-degree-of-freedom system whose damping is certainly not proportional. It is worth comparing (8.63) with the more general (8.34).

From (6.161) we obtain

$$\lambda_{1,2} = -\frac{1}{2J_y m_s}\Big[J_y(k_1+k_2) + m_s\big(k_1a_1^2 + k_2a_2^2\big) \mp \sqrt{\big[J_y(k_1+k_2) + m_s\big(k_1a_1^2 + k_2a_2^2\big)\big]^2 - 4J_y m_s(a_1+a_2)^2k_1k_2}\Big] \tag{8.68}$$

and the corresponding eigenvectors

$$\mathbf{x}_{1,2} = \left(\frac{1}{2(k_1a_1 - k_2a_2)m_s}\Big[J_y(k_1+k_2) - m_s\big(k_1a_1^2 + k_2a_2^2\big) \mp \sqrt{\big[J_y(k_1+k_2) + m_s\big(k_1a_1^2 + k_2a_2^2\big)\big]^2 - 4J_y m_s(a_1+a_2)^2k_1k_2}\Big], 1\right) \tag{8.69}$$

More compactly

$$\mathbf{x}_1 = \frac{Z_{s_1}}{1} = \frac{z_{s_1}(t)}{\theta_1(t)} \quad \text{and} \quad \mathbf{x}_2 = \frac{Z_{s_2}}{1} = \frac{z_{s_2}(t)}{\theta_2(t)} \tag{8.70}$$

which means that the free oscillations are the linear combination of the two natural modes

$$\begin{aligned} z_s(t) &= \chi_1 Z_{s_1} \mathrm{e}^{-\zeta_1\omega_1 t}\sin(\omega_{d_1}t + \varphi_1) + \chi_2 Z_{s_2}\mathrm{e}^{-\zeta_2\omega_2 t}\sin(\omega_{d_2}t + \varphi_2) \\ &= z_{s_1}(t) + z_{s_2}(t) \\ \theta(t) &= \chi_1 \mathrm{e}^{-\zeta_1\omega_1 t}\sin(\omega_{d_1}t + \varphi_1) + \chi_2\mathrm{e}^{-\zeta_2\omega_2 t}\sin(\omega_{d_2}t + \varphi_2) \\ &= \theta_1(t) + \theta_2(t) \end{aligned} \tag{8.71}$$

The time histories for each mode are shown in Fig. 8.14. The two coordinates move in a synchronous way.

Each natural mode is an oscillation around a point P_i which has constantly zero vertical velocity. These points P_1 and P_2 are called *nodes*[3] and are defined as those points at which no vertical motion occurs when the system oscillates according to only one mode. Their position can be immediately obtained from (8.70). Each node P_j is at a horizontal distance d_j from G_s equal to Z_{s_j}, taken in the positive direction if Z_{s_j} is negative, and vice versa. In some sense, in a vehicle the eigenvectors can be visualized with a yardstick. This is not magic, it suffices to solve the equation

$$0 = \dot{z}_{s_j}(t) + d_j\dot{\theta}_j(t) \quad \Longrightarrow \quad d_j = \frac{\dot{z}_{s_j}(t)}{\dot{\theta}_j(t)} = \frac{z_{s_j}(t)}{\theta_j(t)} = Z_{s_j} \tag{8.72}$$

taking (8.70) into account. The two natural modes and the corresponding nodes are shown in Fig. 8.15. Typically, the first mode, that is the one with lower natural frequency, has the node behind the rear axle. This mode is called *bounce*. The second mode has its node located ahead of G_s, near the front seat. This mode is called *pitch*.

[3] Other common names are motion centers or oscillation centers.

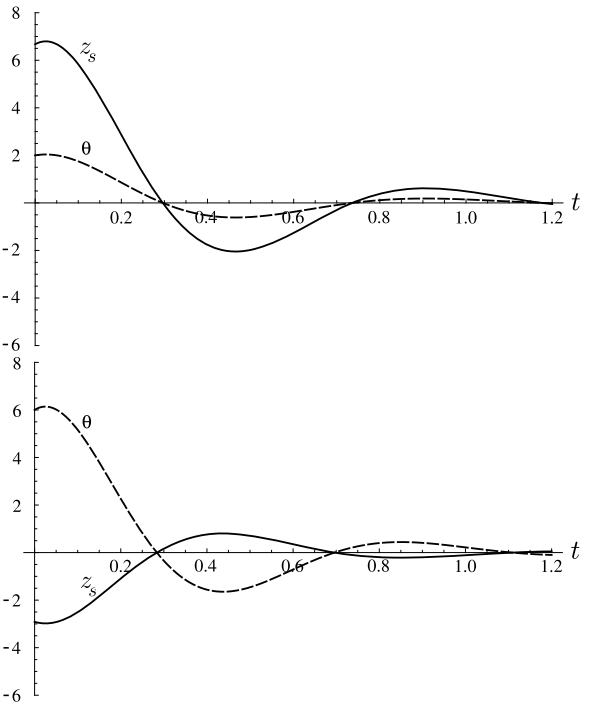

Fig. 8.14 Time histories for bounce (*top*) and pitch (*bottom*) in case of proportional damping (synchronous motion)

We remark that fixed nodes are a prerogative of proportionally damped systems. More general systems still have two natural modes, but in each mode the two coordinates $z_{s_j}(t)$ and $\theta_j(t)$ are no longer equal to zero simultaneously, i.e., the motion is not synchronous. Therefore, their ratio $d_j(t)$ is a function of time and ranges from $-\infty$ to $+\infty$. At each time instant there is a different fixed point. We will discuss further this topic in Sect. 8.7.

As already stated, the nodes also mark where the principal coordinates z_b and z_p are, as shown in Fig. 8.16. The system behaves precisely as if it were made up of two concentrated masses m_b and m_p, each one with its own spring k_b and k_p and shock absorber c_b and c_p, respectively.

All these quantities come from the diagonalization of the matrices. Let $\mathbf{S}$ be the matrix whose columns are the two eigenvectors (8.70), that is

$$\mathbf{S} = [\mathbf{x}_1 | \mathbf{x}_2] \tag{8.73}$$

We have that

$$\begin{bmatrix} m_b & 0 \\ 0 & m_p \end{bmatrix} = \mathbf{S}^T \mathbf{M} \mathbf{S}, \qquad \begin{bmatrix} c_b & 0 \\ 0 & c_p \end{bmatrix} = \mathbf{S}^T \mathbf{C} \mathbf{S}, \qquad \begin{bmatrix} k_b & 0 \\ 0 & k_p \end{bmatrix} = \mathbf{S}^T \mathbf{K} \mathbf{S} \tag{8.74}$$

In case of proportional damping, the shape of both modes (and hence the position of both nodes) depends on two nondimensional parameters. The first parameter is

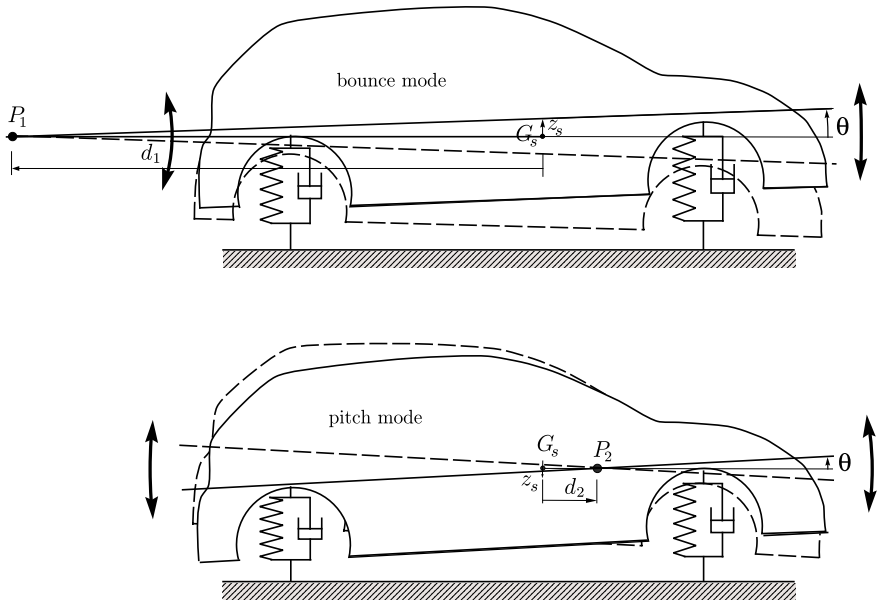

Fig. 8.15 Nodes of the two natural modes (proportional damping)

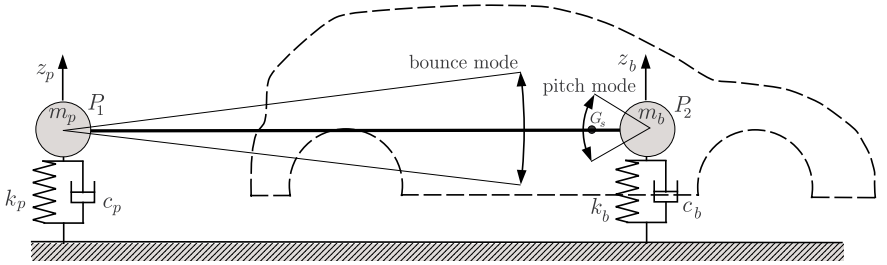

Fig. 8.16 Principal coordinates and equivalent system (proportional damping)

the *dynamic index*

$$\rho = \frac{J_y}{m_s a_1 a_2} \tag{8.75}$$

Usually, in ordinary road cars ρ ranges between 0.90 and 0.97. It is a measure of how far the vehicle mass is distributed from its center of mass. Of course, ρ depends on the whole vehicle architecture and it is very difficult to change it.

Another very useful parameter is the ratio η

$$\eta = \frac{k_1 a_1}{k_2 a_2} \tag{8.76}$$

which characterizes how the axle stiffnesses relate to each other.

For a deeper comprehension of the possible effects of these two parameters, we analyze the model of Fig. 8.13 in some special cases, before addressing how to tune the suspension stiffnesses in the general case.

For simplicity, we consider here the undamped system, whose governing equations are

$$\begin{aligned} m_s\ddot{z}_s + (k_1 + k_2)z_s + (k_1a_1 - k_2a_2)\theta = 0 \\ J_y\ddot{\theta} + (k_1a_1 - k_2a_2)z_s + \left(k_1a_1^2 + k_2a_2^2\right)\theta = 0 \end{aligned} \tag{8.77}$$

8.5.3.1 Case 1: $\eta = 1$

If the suspension stiffnesses are selected such that $\eta = 1$, that is

$$k_1a_1 = k_2a_2 \tag{8.78}$$

the two equations in (8.77) become uncoupled. Both matrices are diagonal, which means that z_s and θ are the principal coordinates. The two undamped natural angular frequencies are

$$\omega_1 = \sqrt{\frac{k_1 + k_2}{m_s}}, \qquad \omega_2 = \sqrt{\frac{k_1a_1^2 + k_2a_2^2}{J_y}} \tag{8.79}$$

Their ratio is equal, in this case, to the square root of the dynamic index

$$\left(\frac{\omega_1}{\omega_2}\right)^2 = \rho \tag{8.80}$$

The two eigenvalues are simply (cf. (8.69))

$$\mathbf{x}_1 = (1, 0) \quad \text{and} \quad \mathbf{x}_2 = (0, 1) \tag{8.81}$$

The bounce mode is a pure vertical translation and the pitch mode is a rotation around $G_s = P_2$.

8.5.3.2 Case 2: $\rho = 1$

Let us assume that a vehicle has $\rho = 1$, that is

$$J_y = ma_1a_2 \tag{8.82}$$

In this case the two principal coordinates are the vertical displacements z_1 and z_2 given in (8.2) and in Fig. 8.13, that is the displacements of the vehicle body at the two axles. After a little algebra, it is possible to rewrite the governing equations as

$$\begin{aligned} m_{s_1}\ddot{z}_1 + k_1z_1 = 0 \\ m_{s_2}\ddot{z}_2 + k_2z_2 = 0 \end{aligned} \tag{8.83}$$

where

$$m_{s_1} = m_s \frac{a_2}{a_1 + a_2}, \qquad m_{s_2} = m_s \frac{a_1}{a_1 + a_2} \tag{8.84}$$

The undamped natural frequencies are

$$\omega_1 = \sqrt{\frac{k_1}{m_{s_1}}}, \qquad \omega_2 = \sqrt{\frac{k_2}{m_{s_2}}} \tag{8.85}$$

Their ratio is, in this case, equal to the square root of η

$$\left(\frac{\omega_1}{\omega_2}\right)^2 = \frac{k_1 a_1}{k_2 a_2} = \eta \tag{8.86}$$

The two eigenvectors in the original coordinates z_s and θ are (cf. (8.69))

$$\mathbf{x}_1 = (a_2, 1) \quad \text{and} \quad \mathbf{x}_2 = (-a_1, 1) \tag{8.87}$$

The nodes are precisely over the front axle and the rear axle, as expected. Otherwise, z_1 and z_2 would not be the principal coordinates.

8.5.3.3 Case 3: $\eta = 1$ and $\rho = 1$

But what happens if we set both η and ρ equal to one? From (8.80) and (8.86) we obtain that

$$\left(\frac{\omega_1}{\omega_2}\right)^2 = 1 \tag{8.88}$$

that is the two undamped modes have exactly the same natural frequency.

The analysis of the shape of the two modes is more tricky. Apparently there is a paradox: the modes obtained for $\eta = 1$ are not consistent with those obtained for $\rho = 1$, and vice versa. Which prevails? There is only one way out. Any point can be a node, that is, any vector $\mathbf{x}$ is an eigenvector. This happens because the matrix $\mathbf{A} = -\mathbf{M}^{-1}\mathbf{K}$ is like the identity matrix $\mathbf{I}$, times a suitable constant.

A vehicle designed to have $\eta = \rho = 1$ would have a very unpredictable behavior. As a matter of fact, a real vehicle could fulfill this condition only approximately. Therefore, the two nodes would be quite randomly located. Certainly, not a desirable behavior.

8.6 Tuning of Suspension Stiffnesses

So far we have obtained the following results about the vehicle free oscillations:

(1) tires can be considered as rigid;

(2) damping should be proportional;
(3) the two natural frequencies of the undamped system are very close to the natural frequencies of the proportionally damped system;
(4) the shape of the modes of the undamped system are exactly equal to the shape of the modes of the proportionally damped system;
(5) $\eta = \rho = 1$ must be avoided.

Now we can proceed to discus how to choose k_1 and k_2. There are basically two requirements for road cars:

- both natural frequencies must fall in the range 1.0–1.5 Hz;
- the pitch mode should have its node located at about the front seat.

The first rule comes from the observation that oscillations at 1.0–1.5 Hz are quite comfortable for human beings. The second rule is an attempt to reduce the pitch motion of the driver. Pitch is typically more annoying than bounce.

As already stated, the value of ρ cannot be modified, unless the vehicle is completely redesigned. Modern road cars have $\rho \simeq 0.95$. To locate the pitch node on the front seat we can act on η, that is on the relative stiffnesses. Usually, a good value is $\eta \simeq 0.95$. With both η and ρ slightly lower than one, the car oscillations are like in Fig. 8.15.

8.6.1 Optimality of Proportional Damping

Summing up, for a good suspension design we have found that we should fulfill these requirements

- $c_j \simeq c_{\text{opt}}$;
- proportional viscous damping;
- $\eta \simeq 0.95$.

But do they conflict with each other or not? Let us develop this point.

Optimal damping requires (cf. (8.41))

$$c_1 \simeq \sqrt{\frac{m_{s_1} k_1}{2}} \quad \text{and} \quad c_2 \simeq \sqrt{\frac{m_{s_2} k_2}{2}} \tag{8.89}$$

where $m_{s_1} = m_s a_2/l$ and $m_{s_2} = m_s a_1/l$. At the same time, proportional damping requires $c_1/k_1 = c_2/k_2 = \beta$, which combined with the former expression means

$$\sqrt{\frac{m_{s_1} k_1}{2}} \frac{1}{k_1} \simeq \sqrt{\frac{m_{s_2} k_2}{2}} \frac{1}{k_2} \tag{8.90}$$

that is

$$\sqrt{\frac{m_s a_2}{k_1}} \simeq \sqrt{\frac{m_s a_1}{k_2}} \quad \Longrightarrow \quad k_1 a_1 \simeq k_2 a_2 \quad \Longrightarrow \quad \eta \simeq 1 \tag{8.91}$$

Therefore, we see that these three requirements do not conflict with each other.

8.6.2 A Numerical Example

Crunching numbers helps a lot to grasp what we are really doing.

Let a vehicle have these features:

- sprung mass $m_s = 1\,000$ kg and moment of inertia $J_y = 1\,620$ kg m^2;
- $a_1 = 1.2$ m and $a_2 = 1.5$ m;
- axle vertical stiffnesses $k_1 = 31\,500$ N/m and $k_2 = 28\,000$ N/m;
- proportional damping with $\beta = c_1/k_1 = c_2/k_2 = 0.0936$ s.

We obtain immediately the dynamic index

$$\rho = \frac{J_y}{m_s a_1 a_2} = \frac{1\,620}{1\,800} = 0.9 \tag{8.92}$$

and the ratio

$$\eta = \frac{k_1 a_1}{k_2 a_2} = \frac{31.5 \times 1.2}{28.0 \times 1.5} = 0.9 \tag{8.93}$$

Both ρ and η are lower than one, although $k_1 > k_2$.

The matrix A is

$$\mathbf{A} = -\begin{bmatrix} 59.5 & -4.2 \\ -2.592 & 66.89 \end{bmatrix} \tag{8.94}$$

with eigenvalues

$$\lambda_1 = -58.24 \text{ s}^{-2}, \qquad \lambda_2 = -68.15 \text{ s}^{-2} \tag{8.95}$$

and eigenvectors

$$\mathbf{x}_1 = (3.336, 1), \qquad \mathbf{x}_2 = (-0.486, 1) \tag{8.96}$$

The bounce mode has its node 3.336 m behind G_s, and hence $3.33 - 1.50 = 1.83$ m behind the rear axle (Fig. 8.15). The pitch mode has its node 0.486 m ahead of G_s.

Should the system be undamped, the natural frequencies would be

$$f_1 = \frac{\sqrt{-\lambda_1}}{2\pi} = 1.21 \text{ Hz}, \qquad f_2 = \frac{\sqrt{-\lambda_2}}{2\pi} = 1.31 \text{ Hz} \tag{8.97}$$

These frequencies could be estimated by means of the simple formulæ (8.79). The approximate values are $f_1 \simeq 1.23$ Hz and $f_2 \simeq 1.30$ Hz, quite close to the exact ones although $\eta \neq 1$.

With proportional damping, we have to solve (8.61)

$$\mu^2 - \beta\lambda_i \mu - \lambda_i = 0 \tag{8.98}$$

with $\beta = c_1/k_1 = c_2/k_2 = 0.0936$ s, thus getting

$$\mu_{1,3} = -2.73458 \pm \text{i}7.12481 \text{ s}^{-1}, \qquad \mu_{2,4} = -3.19975 \pm \text{i}7.60983 \text{ s}^{-1} \tag{8.99}$$

From the imaginary part we obtain the natural frequencies of the damped system

$$f_{s1} = \frac{\mathrm{Im}(\mu_1)}{2\pi} = 1.13 \text{ Hz}, \qquad f_{s2} = \frac{\mathrm{Im}(\mu_3)}{2\pi} = 1.21 \text{ Hz} \tag{8.100}$$

They are about 10 % lower than those of the undamped system. Both fall within the acceptable range. The bounce and pitch modes have $\zeta_1 = 0.36$ and $\zeta_2 = 0.39$, respectively. There is quite a lot of damping indeed.

If, just to see what happens, we set $J_y = 1980\,\mathrm{kg\,m^2}$, thus having $\rho = 1.1$, we get that the bounce mode has $f_1 = 1.24$ Hz and its node located 2.93 m ahead of G_s, while the pitch mode has $f_2 = 1.16$ Hz and its node located at 0.67 m behind G_s. As expected, many things have been inverted, like the node positions and the frequency order.

8.7 Non-proportional Damping

We have insisted many times about having a vehicle with springs and shock absorbers tuned to have proportional damping. As shown in Fig. 8.15, fixed nodes are a prerogative of proportionally damped systems. This is the outcome of having synchronous motion of both degrees of freedom in each natural mode, as shown in Fig. 8.14.

On the contrary, a vehicle with non-proportional damping has non-synchronous motion, as shown in Fig. 8.17, where the front damping coefficient has been reduced by 10 %, while the rear damping coefficient has been increased by 10 %. Also shown in Fig. 8.17 are the plots of $d_1(t)$ and $d_2(t)$, that is the time-varying positions of the nodes w.r.t. G_s

$$0 = \dot{z}_{s_j}(t) + d_j(t)\dot{\theta}_j(t) \quad \Longrightarrow \quad d_j(t) = \frac{\dot{z}_{s_j}(t)}{\dot{\theta}_j(t)} \tag{8.101}$$

These positions are functions of time and cycle from zero (when $\dot{z}_s = 0$) to $\pm\infty$ (when $\dot{\theta} = 0$). Therefore, the vehicle still has two modes, but their shapes are somehow mixed up. They are not so neatly different as they are with proportional damping.

Actually, in some sense, both modes share some fundamental features. In both modes there are time instants in which $\dot{z}_s = 0$ and hence the vehicle body is rotating around G_s, and other time instants in which $\dot{\theta} = 0$ and hence the vehicle body is having a pure vertical translation.

8.8 Interconnected Suspensions

So far we have employed the model of Fig. 8.13. Implicitly, we have considered it to be quite a general model for studying the ride of a two-axle vehicle. But it is not. Let us address the problem from a fresh point of view.

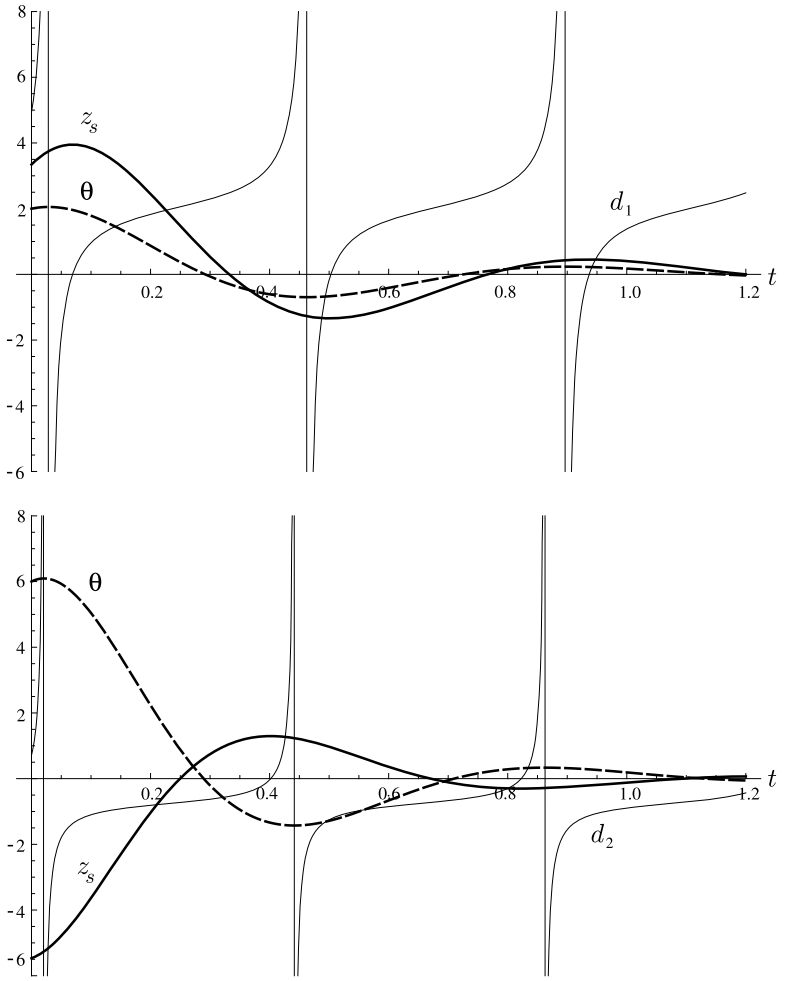

Fig. 8.17 Time histories for bounce (*top*) and pitch (*bottom*) in case of non-proportional damping (non-synchronous motion)

Still using z_s and θ as coordinates, a more general form of the equations of motion (8.77) for a linear two-degree-of-freedom undamped system are

$$\begin{aligned} m_s\ddot{z}_s + k_{zz}z_s + k_{z\theta}\theta = 0 \\ J_y\ddot{\theta} + k_{\theta z}z_s + k_{\theta\theta}\theta = 0 \end{aligned} \tag{8.102}$$

where $k_{z\theta} = k_{\theta z}$.

Each stiffness has a clear physical meaning. Let us impose a pure translation z_s to the system, that is with $\theta = 0$. The system reacts with a force $-k_{zz}z_s$ and a couple

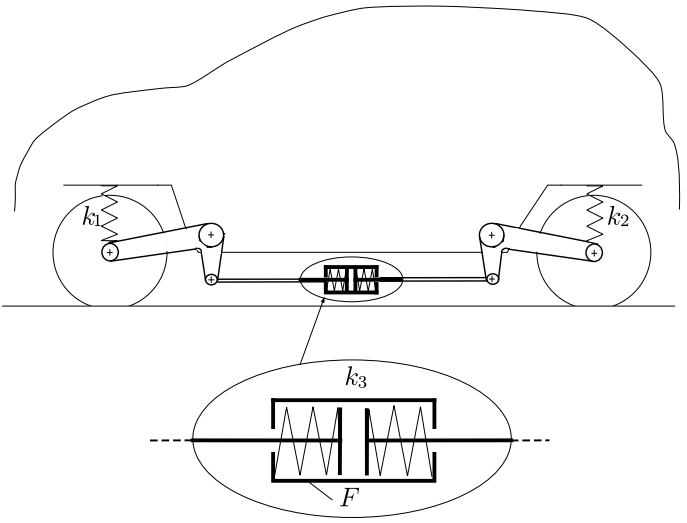

Fig. 8.18 Schematic for interconnected suspensions

$-k_{\theta z} z_s$. Similarly, imposing a pure rotation around G_s, the system reacts with a force $-k_{z\theta}\theta$ and a couple $-k_{\theta\theta}\theta$.

In general, any 2×2 stiffness matrix is characterized by three coefficients. But in the system of Fig. 8.13 we have only two parameters, namely k_1 and k_2. Therefore the following equations

$$\begin{aligned} k_1 + k_2 &= k_{zz} \\ k_1 a_1 - k_2 a_2 &= k_{z\theta} \\ k_1 a_1^2 + k_2 a_2^2 &= k_{\theta\theta} \end{aligned} \tag{8.103}$$

may not all be fulfilled. As anticipated, the scheme of Fig. 8.13 is not as general as it may seem at first. We need a suspension layout with three springs, although we still have only two axles.

Interconnected suspensions are the solution to this apparent paradox. A very basic scheme of interconnected suspensions is shown in Fig. 8.18. Its goal is to explain the concept, not to be a solution to be adopted in real cars (although, it was actually employed many years ago).

To understand how it works, first suppose the car bounces, as in Fig. 8.19. The springs contained in the floating device F get compressed, thus stiffening both axles. On the other hand, if the car pitches, as in Fig. 8.20, the floating device F just translates longitudinally, without affecting the suspension stiffnesses. This way we have introduced the third independent spring k_3 in our vehicle.

Obviously, hydraulic interconnections are much more effective, but the principle is the same. We have an additional parameter to tune the vehicle oscillatory behavior.

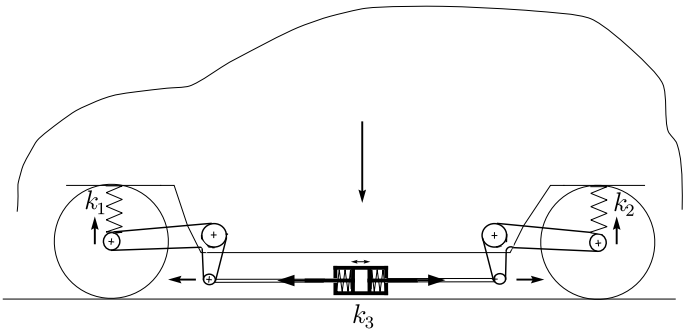

Fig. 8.19 Interconnected suspensions activated when bouncing

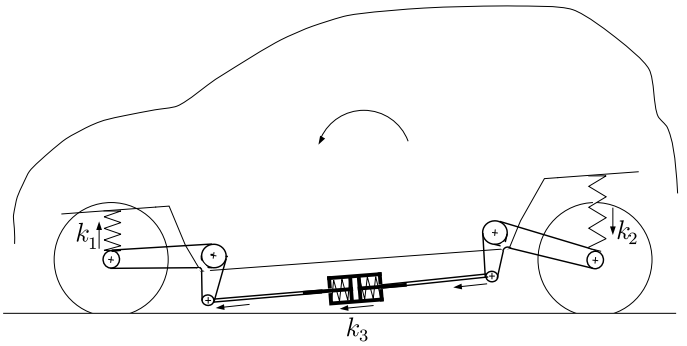

Fig. 8.20 Interconnected suspensions not activated when pitching

Although only a few cars have longitudinal interconnection, almost all cars are equipped with torsion (anti-roll) bars, and hence they have transversal interconnection. An example is shown in Fig. 8.21.

Using interconnected suspensions may lead to non-proportional damping, if proper counteractions are not taken, that is if the floating device F adds a stiffness k_3 without also adding a damping coefficient c_3.

8.9 Summary

In this chapter, the ride behavior of vehicles has been investigated. To keep the analysis very simple, two two-degree-of-freedom models have been formulated. The first, called quarter car model, has been used for determining the right amount of damping to have good comfort and/or road holding when the vehicle travels on a bumpy road (forced oscillations). In this framework, the inerter has been also introduced and discussed.

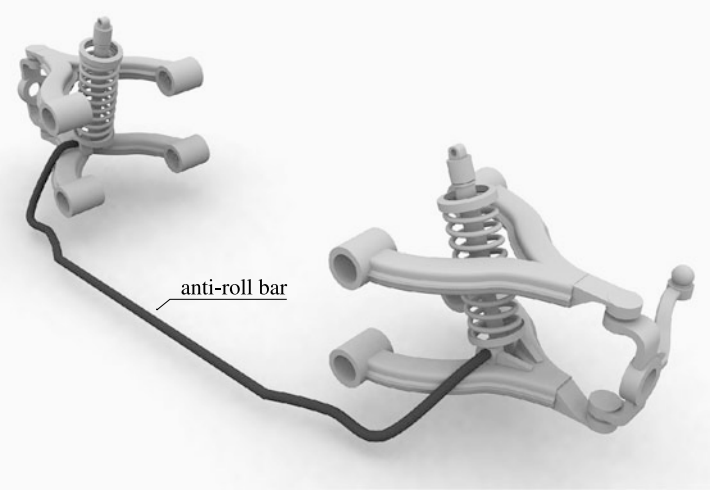

Fig. 8.21 Transversal interconnection by means of the anti-roll bar [6]

Free oscillations have been studied assuming the tires are perfectly rigid. The importance of proportional damping has been highlighted. This analysis has given indications on how to select spring stiffnesses.

Interconnected suspensions have been mentioned to show how to have a very general stiffness matrix.

8.10 List of Some Relevant Concepts

p. 236 the inerter is a device that provides a force proportional to the relative acceleration between its attachment points;
p. 241 the quarter car model is mainly used to study the vibrational behavior of a vehicle travelling on an uneven road;
p. 243 the inertance acts as a spring softener at high frequencies;
p. 247 the quarter car model is a tool for the selection of the damping coefficient of the shock absorbers;
p. 256 systems with proportional viscous damping have exactly the same mode shapes as the corresponding undamped systems;
p. 258 only vehicles with proportional viscous damping have simple bounce and pitch modes.

References

1. Bastow D, Howard G, Whitehead JP (2004) Car suspension and handling, 4th edn. SAE International, Warrendale

2. Bourcier de Carbon C (1950) Theorie mathématique et réalisation pratique de la suspension amortie des véhicules terrestres. In: 3rd Congres Technique de l'Automobile, Paris
3. Dixon JC (1991) Tyres, suspension and handling. Cambridge University Press, Cambridge
4. Font Mezquita J, Dols Ruiz JF (2006) La Dinámica del Automóvil. Editorial de la UPV, Valencia
5. Gillespie TD (1992) Fundamentals of vehicle dynamics. SAE International, Warrendale
6. Longhurst C (2013) www.carbibles.com
7. Popp K, Schiehlen W (2010) Ground vehicle dynamics. Springer, Berlin
8. Smith MC (2002) Synthesis of mechanical networks: the inerter. IEEE Trans Autom Control 47:1648–1662
9. Wong JY (2001) Theory of ground vehicles. Wiley, New York

Chapter 9
Handling with Roll Motion

So far we have investigated the handling behavior of a vehicle under the assumption of negligible roll. Actually, we have not completely discarded roll angles, as they are absolutely necessary for evaluating, e.g., lateral load transfers. But we have not considered, for instance, the inertial effects of roll motion.

In this chapter, the roll motion is taken into account (Fig. 9.1). It is hard work, as the analysis becomes more involved [7]. However, it also sheds light onto one of the most controversial concepts in vehicle dynamics: the roll axis [1–4, 8], in this book renamed no-roll axis. This concept has been already discussed in Sect. 3.8.8, but it will be considered again here.

We state from the very beginning what the outcome of our analysis will be: the roll axis, as that axis about which the vehicle rolls, does not exist. Or, in other words, the concept of an axis about which the vehicle rolls is meaningless. We understand it sounds harsh, but that is the way it is. There is no such thing as an axis about which the vehicle rolls, albeit the vehicle rolls indeed. A similar conclusion was also obtained in [5]. The no-roll axis, as defined in Sect. 3.8.8, maintains its validity.

9.1 Vehicle Position and Orientation

Defining the position and orientation of a vehicle when roll is assumed to be zero is a simple matter. As shown in Fig. 3.3, the motion is two-dimensional and hence it suffices to know, with respect to a ground-fixed reference system, the two coordinates of the center of mass G and the yaw angle ψ.

Including roll (and, perhaps, also pitch) means having to deal with a full three-dimensional problem. Therefore, we must employ more sophisticated tools. Quite paradoxically, it turns out that it is easier to define unambiguously the *orientation* of the vehicle body, rather than the *position* of the vehicle. The reason is that the concept of "position of the vehicle" is not so clear anymore. As a matter of fact, roll causes point G to move sideways with respect to the wheels, but this movement does not change the "position of the vehicle" directly. In other words, we pretend

M. Guiggiani, *The Science of Vehicle Dynamics*, DOI 10.1007/978-94-017-8533-4_9,

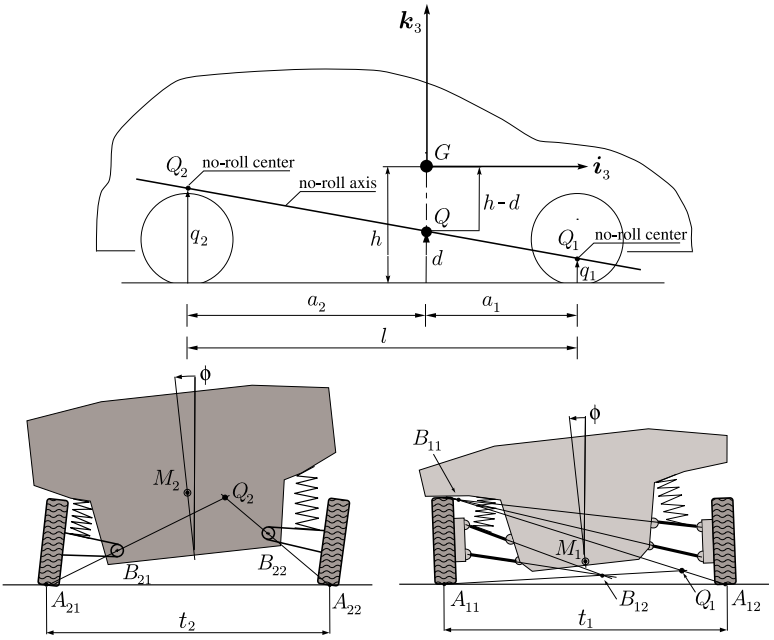

Fig. 9.1 Vehicle basic scheme including roll motion ϕ

that the lateral velocity v of the vehicle does not contain any roll contribution. We will address this important aspect shortly. First, some other concepts need to be introduced.

9.2 Yaw, Pitch and Roll

Although everybody has an intuitive notion of roll, pitch and yaw of a vehicle, we need a more precise definition at this stage. The goal is to know the *orientation* of the vehicle body (assumed to be a rigid body) with respect to a ground-fixed reference system S_0. A typical approach is to give a *sequence* of three *elemental* rotations, that is rotations about the axes of a chain of coordinate systems.

The three elemental rotations must follow a definite order. In other words, the same rotations in a different order provide a different orientation. This aspect can be appreciated by a simple example. In Fig. 9.2(a), a parallelepiped is rotated by 90 degrees about the axis **i** and then by -90 degree about the axis **j**. In Fig. 9.2(b), the same parallelepiped is subject to the same two rotations, but in reverse order. The final orientation is totally different, thus confirming that finite rotations are not commutative.[1]

[1] Rotation matrices are a tool to represent finite rotation. As well known, the product of matrices is not commutative, in general.

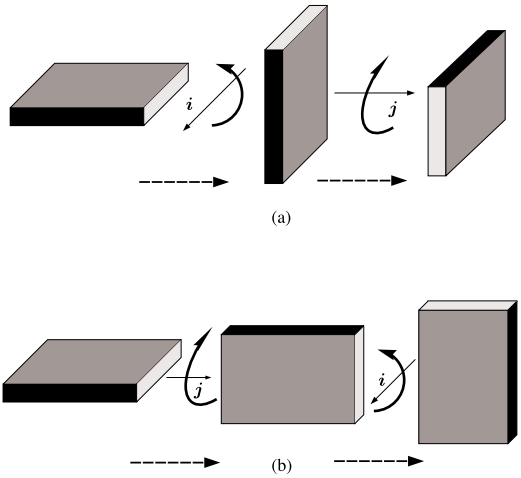

Fig. 9.2 Rotations are not commutative (i.e., their order is important)

Human beings are comfortable with two-dimensional rotations, and Euler was, perhaps, no exception when he invented the technique of three *elemental* rotations, often referred to as Euler angles. The basic idea is to generate a sequence of four Cartesian reference systems S_i, each one sharing one axis with the preceding system and another axis with the next one. Therefore, we can go from one system to the next by means of a two-dimensional rotation about their common axis.[2]

In vehicle dynamics it is convenient to use the following sequence of reference systems (Fig. 9.3)

$$(\mathbf{i}_0, \mathbf{j}_0, \mathbf{k}_0) \xrightarrow[\mathbf{k}_0=\mathbf{k}_1]{\psi} (\mathbf{i}_1, \mathbf{j}_1, \mathbf{k}_1) \xrightarrow[\mathbf{j}_1=\mathbf{j}_2]{\theta} (\mathbf{i}_2, \mathbf{j}_2, \mathbf{k}_2) \xrightarrow[\mathbf{i}_2=\mathbf{i}_3]{\phi} (\mathbf{i}_3, \mathbf{j}_3, \mathbf{k}_3) \tag{9.1}$$

to go from the ground-fixed reference system S_0, with directions $(\mathbf{i}_0, \mathbf{j}_0, \mathbf{k}_0)$, to the vehicle-fixed reference system S_3, with directions $(\mathbf{i}_3, \mathbf{j}_3, \mathbf{k}_3)$. This vehicle-fixed reference system has been already introduced in Fig. 1.4, although with a slightly different notation (no subscripts). When the vehicle is at rest, direction $\mathbf{k}_3 = \mathbf{k}$ is orthogonal to the road (hence directed like $\mathbf{k}_0$) and direction $\mathbf{i}_3 = \mathbf{i}$ is parallel to the road and pointing forward (hence like $\mathbf{i}_1$, Fig. 9.1).

During the vehicle motion, S_3 moves accordingly. At any instant of time, the key step is the definition of the auxiliary direction $\mathbf{j}_1 = \mathbf{j}_2$

$$\mathbf{j}_1 = \mathbf{j}_2 = \frac{\mathbf{k}_0 \times \mathbf{i}_3}{|\mathbf{k}_0 \times \mathbf{i}_3|} = \frac{\mathbf{k}_1 \times \mathbf{i}_2}{|\mathbf{k}_1 \times \mathbf{i}_2|} \tag{9.2}$$

often called the *line of nodes*, which is *orthogonal* to both $\mathbf{k}_0 = \mathbf{k}_1$ and $\mathbf{i}_2 = \mathbf{i}_3$. This direction $\mathbf{j}_1 = \mathbf{j}_2$ is the link between the ground-fixed and the vehicle-fixed reference systems. This way, we have that we can go from S_0 to S_1 with an elemental rotation

[2] More precisely, the axis must share the same direction. The origin can be different.

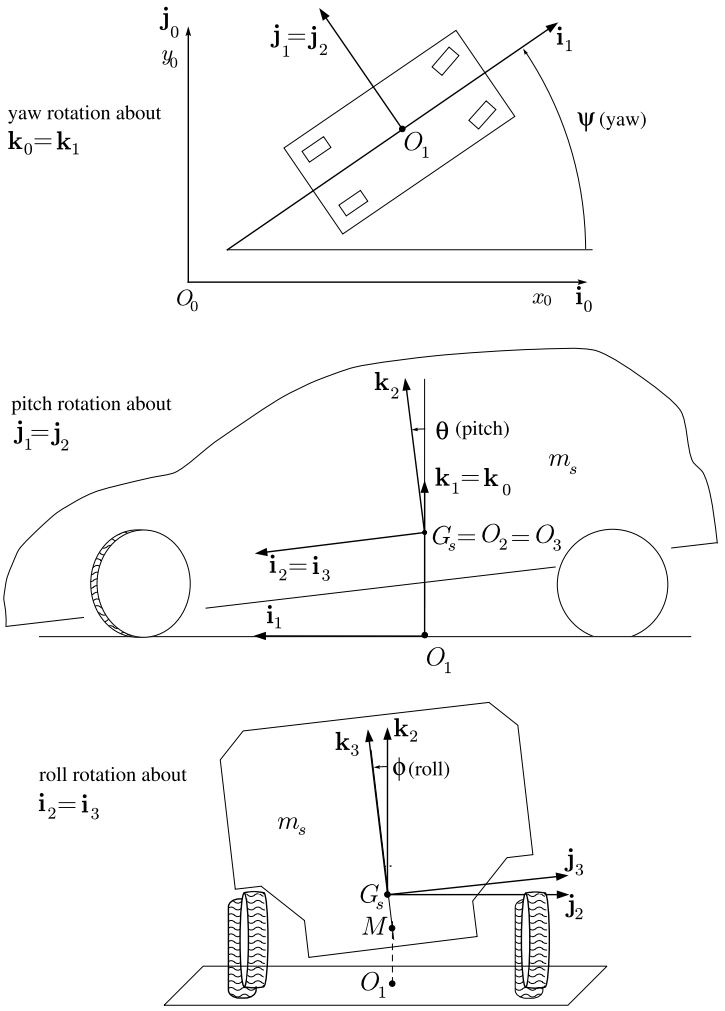

Fig. 9.3 Definition of yaw, pitch and roll

ψ about $\mathbf{k}_0 = \mathbf{k}_1$, and so on. Any two consecutive reference systems differ by a two-dimensional rotation, as shown in (9.1).

More precisely, as shown in Fig. 9.3, the first rotation ψ (yaw) is about the third axis $\mathbf{k}_0 = \mathbf{k}_1$, which S_0 and S_1 have in common, the second rotation θ (pitch) is about the second axis $\mathbf{j}_1 = \mathbf{j}_2$, shared by S_1 and S_2, and the third rotation ϕ (roll) is about the first common axis $\mathbf{i}_2 = \mathbf{i}_3$ of S_2 and S_3. This is why this sequence of elemental rotations is marked (3, 2, 1), or yaw, pitch and roll.[3] In vehicle dynamics, the pitch and roll angles are very small.

[3] Classical Euler angles use the sequence (3, 1, 3).

9.3 Angular Velocity

With this sequence of reference systems, the angular velocity of the vehicle body $\boldsymbol{\Omega}$ is given by

$$\boldsymbol{\Omega} = \dot{\phi}\mathbf{i}_2(\psi,\theta) + \dot{\theta}\mathbf{j}_1(\psi) + \dot{\psi}\mathbf{k}_0 \tag{9.3}$$

This is a simple and intuitive equation, but it has the drawback that the three unit vectors are not mutually orthogonal (Fig. 9.3). Therefore, our goal is to obtain the following equation[4]

$$\boldsymbol{\Omega} = p\mathbf{i}_3 + q\mathbf{j}_3 + r\mathbf{k}_3 \tag{9.4}$$

where the vector $\boldsymbol{\Omega}$ is expressed in terms of its components in the vehicle-fixed reference system S_3.[5]

The expressions of p, q and r can be easily obtained by means of the rotation matrices

$$\begin{aligned}\begin{bmatrix} p \\ q \\ r \end{bmatrix} &= \mathbf{R}_1(\phi)\begin{bmatrix} \dot{\phi} \\ 0 \\ 0 \end{bmatrix} + \mathbf{R}_1(\phi)\mathbf{R}_2(\theta)\begin{bmatrix} 0 \\ \dot{\theta} \\ 0 \end{bmatrix} + \mathbf{R}_1(\phi)\mathbf{R}_2(\theta)\mathbf{R}_3(\psi)\begin{bmatrix} 0 \\ 0 \\ \dot{\psi} \end{bmatrix} \\ &= \begin{bmatrix} \dot{\phi} \\ 0 \\ 0 \end{bmatrix} + \mathbf{R}_1(\phi)\begin{bmatrix} 0 \\ \dot{\theta} \\ 0 \end{bmatrix} + \mathbf{R}_1(\phi)\mathbf{R}_2(\theta)\begin{bmatrix} 0 \\ 0 \\ \dot{\psi} \end{bmatrix}\end{aligned} \tag{9.5}$$

where, as well known, the rotation matrices for elemental rotations are as follows, for a generic angle α

– rotation around the first axis

$$\mathbf{R}_1(\alpha) = \begin{bmatrix} 1 & 0 & 0 \\ 0 & \cos\alpha & \sin\alpha \\ 0 & -\sin\alpha & \cos\alpha \end{bmatrix} \tag{9.6}$$

– rotation around the second axis

$$\mathbf{R}_2(\alpha) = \begin{bmatrix} \cos\alpha & 0 & -\sin\alpha \\ 0 & 1 & 0 \\ \sin\alpha & 0 & \cos\alpha \end{bmatrix} \tag{9.7}$$

– rotation around the third axis

$$\mathbf{R}_3(\alpha) = \begin{bmatrix} \cos\alpha & \sin\alpha & 0 \\ -\sin\alpha & \cos\alpha & 0 \\ 0 & 0 & 1 \end{bmatrix} \tag{9.8}$$

[4] In this chapter the symbol q is a component of $\boldsymbol{\Omega}$. Therefore, we use the symbol d for the height of the no-roll center Q (Fig. 9.1).

[5] The components p, q and r of $\boldsymbol{\Omega}$ cannot be given, in general, as time derivatives of an angle.

The final result is

$$\begin{aligned} p &= \dot{\phi} - \dot{\psi}\sin\theta \\ q &= \dot{\theta}\cos\phi + \dot{\psi}\sin\phi\cos\theta \\ r &= \dot{\psi}\cos\phi\cos\theta - \dot{\theta}\sin\phi \end{aligned} \tag{9.9}$$

which can be simplified in

$$\begin{aligned} p &\simeq \dot{\phi} - \dot{\psi}\theta \\ q &\simeq \dot{\theta} + \dot{\psi}\phi \\ r &\simeq \dot{\psi} \end{aligned} \tag{9.10}$$

because of the small values of pitch and roll. Therefore, the angular velocity of the vehicle body can be expressed as

$$\boldsymbol{\Omega} \simeq (\dot{\phi} - \dot{\psi}\theta)\mathbf{i}_3 + (\dot{\theta} + \dot{\psi}\phi)\mathbf{j}_3 + \dot{\psi}\mathbf{k}_3 \tag{9.11}$$

in the vehicle-fixed reference system.

Moreover, if there is no pitch, that is $\theta = \dot{\theta} = 0$, we have a further simplification

$$\begin{aligned} p &\simeq \dot{\phi} \\ q &\simeq \dot{\psi}\phi \\ r &\simeq \dot{\psi} \end{aligned} \tag{9.12}$$

A lot of work for getting such a simple result.

This definition of roll, pitch and yaw is quite general. It only needs the reasonable assumption that the vehicle body be considered as perfectly rigid. It is worth remarking that what matters in the definition of roll, pitch and yaw are only the *directions* of the axes of the four reference systems S_i. Their positions, that is the positions of their origins O_i, have no relevance at all.

It is useful to obtain the expressions of the unit vectors $(\mathbf{i}_3, \mathbf{j}_3, \mathbf{k}_3)$ in terms of $(\mathbf{i}_1, \mathbf{j}_1, \mathbf{k}_1)$

$$\begin{aligned} \mathbf{i}_3 &= \cos(\theta)\mathbf{i}_1 - \sin(\theta)\mathbf{k}_1 \\ \mathbf{j}_3 &= \sin(\theta)\sin(\phi)\mathbf{i}_1 + \cos(\phi)\mathbf{j}_1 + \cos(\theta)\sin(\phi)\mathbf{k}_1 \\ \mathbf{k}_3 &= \sin(\theta)\cos(\phi)\mathbf{i}_1 - \sin(\phi)\mathbf{j}_1 + \cos(\theta)\cos(\phi)\mathbf{k}_1 \end{aligned} \tag{9.13}$$

which can be simplified into

$$\begin{aligned} \mathbf{i}_3 &\simeq \mathbf{i}_1 - \theta\mathbf{k}_1 \\ \mathbf{j}_3 &\simeq \mathbf{j}_1 + \phi\mathbf{k}_1 \\ \mathbf{k}_3 &\simeq \theta\mathbf{i}_1 - \phi\mathbf{j}_1 + \mathbf{k}_1 \end{aligned} \tag{9.14}$$

9.4 Angular Acceleration

The angular acceleration $\dot{\boldsymbol{\Omega}}$ is promptly obtained by differentiating (9.4) with respect to time

$$\begin{aligned}\dot{\boldsymbol{\Omega}} &= \dot{p}\mathbf{i}_3 + \dot{q}\mathbf{j}_3 + \dot{r}\mathbf{k}_3 + \boldsymbol{\Omega} \times \boldsymbol{\Omega} \\ &= \dot{p}\mathbf{i}_3 + \dot{q}\mathbf{j}_3 + \dot{r}\mathbf{k}_3\end{aligned} \tag{9.15}$$

where, according to (9.10)

$$\begin{aligned}\dot{p} &\simeq \ddot{\phi} - \ddot{\psi}\theta - \dot{\psi}\dot{\theta} \\ \dot{q} &\simeq \ddot{\theta} + \ddot{\psi}\phi + \dot{\psi}\dot{\phi} \\ \dot{r} &\simeq \ddot{\psi}\end{aligned} \tag{9.16}$$

9.5 Vehicle Lateral Velocity

The vehicle lateral velocity v was introduced in (3.1) in the case of negligible roll motion. Now we need to extend that definition when the roll motion is taken into account. This task is not as simple as it may seem. Intuitively, we would like to obtain an expression of v independent of ϕ. Therefore, we are looking for a point which, broadly speaking, follows the vehicle motion, without being subject to roll. A point that is like G, except that it does not roll. More precisely, we are looking for the origin O_1 of the reference system S_1 in Fig. 9.3, that is a reference system which yaws, but does not pitch and roll.

For simplicity, we assume the tires are perfectly rigid in this chapter.

9.5.1 Track Invariant Points

Roll motion is part of vehicle dynamics. However, it is useful to start with a purely kinematic analysis to get an idea of the several effects of roll motion. This kinematic analysis should be seen as a primer for better investigating roll dynamics.

Figure 3.11 shows how to determine the no-roll centers Q_i for a swing arm suspension and a double wishbone suspension. The same method is applied in Fig. 3.12 to a MacPherson strut. In all these cases, the vehicle is in its reference configuration (no roll). When the vehicle rolls, the no-roll centers Q_i migrate with respect to the vehicle body. They can be obtained, as shown in Fig. 9.1, using the same procedure of Fig. 3.11, i.e., as the intersection of the two lines passing through points A_{ij} and B_{ij}.

However, determining the current position of Q_i has little relevance in this context. Much more important are the following definitions.

We define point M_1 as the point *of the vehicle body* that coincides with Q_1 in the vehicle reference configuration (Fig. 9.1). The same idea, applied to the rear axle,

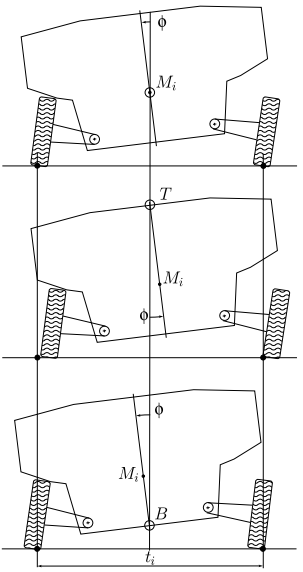

Fig. 9.4 Roll rotations about different points and comparison of the relative contact patch positions

leads to the definition of M_2. These points are called here *track invariant points*. Let us investigate their properties.

In Fig. 9.4, the vehicle body is rotated, in turn, by the same roll angle ϕ about three different points, namely M_i, T, and B. We see that in all cases the track length t_i is almost constant. However, in general, the two contact patches move sideways with respect to the point. The only exception is with point M_i, which remains midway between the two contact patches. This is the reason why it has been called track invariant point.

The property that a roll rotation about the track invariant point M_i does not affect the positions of the tire contact patches with respect to M_i itself holds true for any suspension type, as shown in Fig. 9.5.[6]

However, the vehicle does not care much about which point we applied the roll rotation. This is demonstrated in Fig. 9.6, where we superimposed the three vehicle rotations shown in Fig. 9.4. They are almost indistinguishable, suggesting that the notion of a roll axis about which the vehicle rolls is meaningless. For the vehicle, all points between, say, T and B are pretty much equivalent.

In general, in addition to roll, there may be some suspension jacking, which results in a vehicle vertical displacement z_i, as discussed in Sect. 3.8.10. Figure 9.7 shows the same axle with and without suspension jacking. The roll angle is the same. It is evident, particularly when comparing the two cases, as it is done in Fig. 9.7 (bottom), that the combination of roll and suspension jacking is like a rotation about a point Q_z.

[6] In Fig. 9.5 it is also quite interesting to note the camber variations due to pure roll in each type of suspension. This topic has been addressed in Sect. 3.8.3.

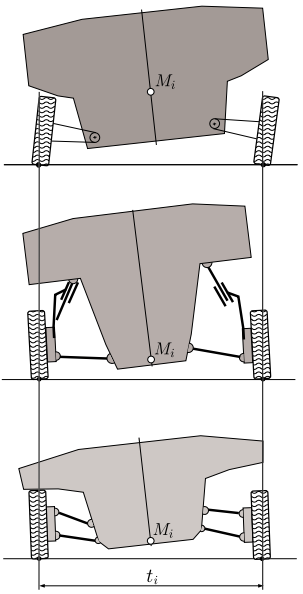

Fig. 9.5 Roll rotations about the track invariant point M_i for three different suspension layouts (*top* to *bottom*): swing arm, MacPherson strut, double wishbone

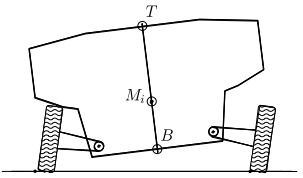

Fig. 9.6 Comparison of roll rotations about different points: they have almost the same effect on the vehicle

We recall that suspension jacking occurs whenever the lateral forces exerted by the two tires of the same axle are not equal, which is always the case, indeed. However, it is a small effect that can be safely neglected, particularly in more sophisticated suspensions, like the double wishbone or the MacPherson strut.

9.5.2 Vehicle Invariant Point (VIP)

Now let us look at both axles together, that is at the vehicle as a whole, as done in Fig. 9.8. For simplicity, let us assume the front and rear tracks to be equal to each other, that is $t_1 = t_2$, and that they are not affected by roll (no suspension jacking).

Points M_1 and M_2 have, in general, different heights. Therefore, roll motion makes the front and rear tracks "slide" a little bit with respect to each other (Fig. 9.8). We remark that we know the *direction* $\mathbf{i}_3$ about which the vehicle (by definition) rolls, but we cannot say anything about an elusive *axis* about which the vehicle rolls.

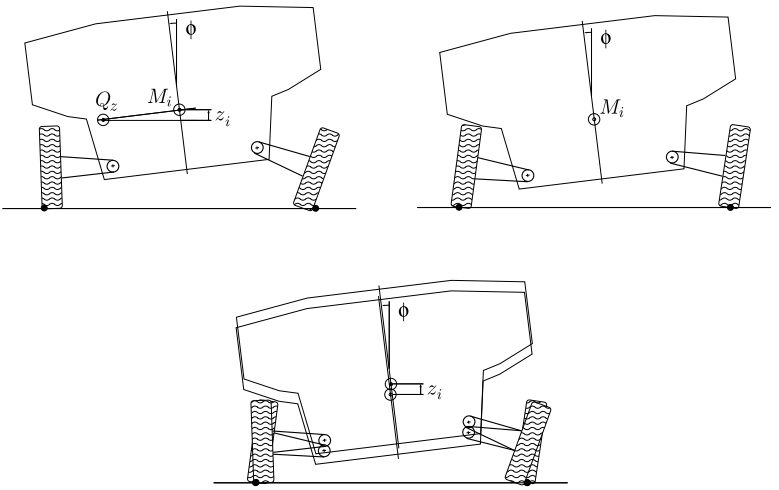

Fig. 9.7 Roll rotations with and without suspension jacking

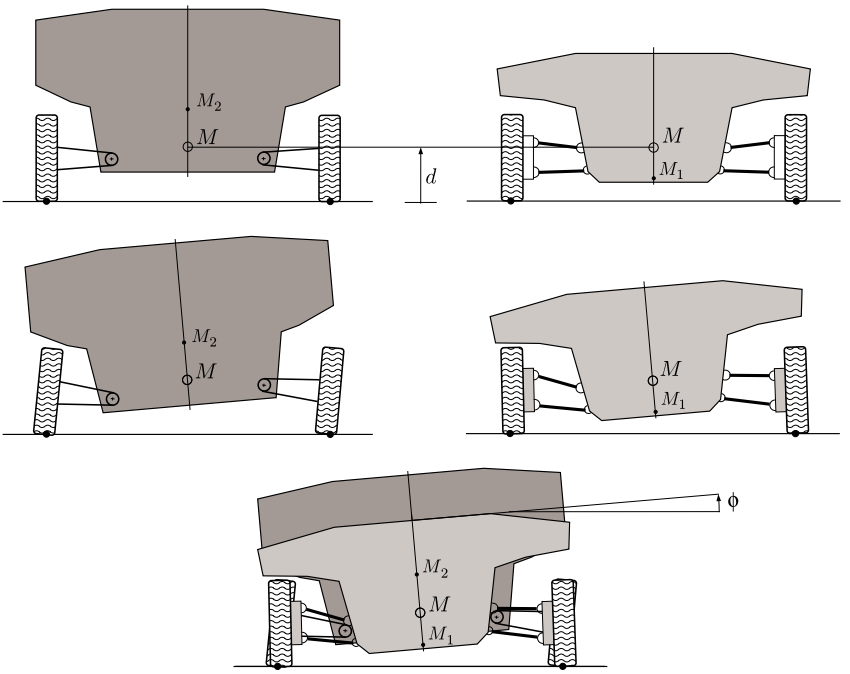

Fig. 9.8 Roll motion explained without the recourse to any roll axis

We are looking for a point of the vehicle body that, regardless of the roll angle ϕ, remains most centered with respect to the four contact patches. Figure 9.8 suggests that the point that is most insensitive to roll is indeed a point M between M_1 and M_2.

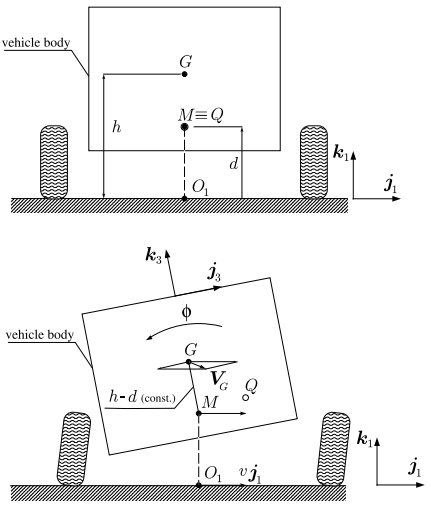

Fig. 9.9 Schematic for the definition of points M and O_1, and hence for the definition of the lateral velocity v of the vehicle

Therefore, we define point M as the point *of the vehicle body* that, in the reference configuration, coincides with the no-roll center Q. We call M *vehicle invariant point* (VIP). Point O_1 is the point on the ground always below M, as shown in Fig. 9.9.

The selection of point M as the best suited to represent the vehicle position purged by the roll motion, is reasonable (we believe), but nonetheless arbitrary.[7] However, this is what is commonly done in vehicle dynamics, although often without providing an explicit explanation. We repeat that point M, and hence also O_1, are basically in the middle of the vehicle, even when it rolls. This is the reason that makes them the best option to monitor the vehicle position.

9.5.3 Lateral Velocity and Acceleration

The vehicle velocity is, by definition, that of the *vehicle invariant point* M. Therefore, pretty much like in (3.1)

$$\mathbf{V}_M = u\mathbf{i}_1 + v\mathbf{j}_1 \tag{9.17}$$

where u is the forward velocity and v is the lateral velocity. We recall that we have assumed the tires to be rigid, and hence there is no roll motion due to tire deformation.

The vehicle acceleration is given by a formula identical to (3.21)

$$\begin{aligned}\mathbf{a}_M &= (\dot{u} - v\dot{\psi})\mathbf{i}_1 + (\dot{v} + u\dot{\psi})\mathbf{j}_1 \\ &\simeq (\dot{u} - vr)\mathbf{i}_1 + (\dot{v} + ur)\mathbf{j}_1\end{aligned} \tag{9.18}$$

[7] The use of the center of mass G to represent the vehicle position in Chaps. 3–7 was arbitrary as well.

Actually, point M may also have a vertical velocity, due to uneven road or suspension jacking. Here we assume the road to be perfectly flat and suspension jacking to be negligible.

Point M inherits almost everything that was obtained for G in Chaps. 3–7, in the sense that now we have to use M (or O_1) to define the vehicle slip angle β, trajectory, etc.

9.6 Three-Dimensional Vehicle Dynamics

We have assumed the vehicle sprung mass m_s to be a rigid body. If roll motion is taken into account, it has a three-dimensional dynamics. For simplicity, at least at the beginning, it is useful to suppose the unsprung mass m_n to be negligible (i.e., $m = m_s$).

Like in (3.51), the classical force and torque equations for the dynamics of a single rigid body are [6]

$$\begin{aligned} m\mathbf{a}_G &= \mathbf{F} \\ \dot{\mathbf{K}}_G^r &= \mathbf{M}_G \end{aligned} \tag{9.19}$$

where $m = m_s$ is the total mass of the vehicle, $\mathbf{a}_G$ is the acceleration of its center of mass, $\mathbf{F}$ is the resultant of all forces applied to the vehicle body, $\dot{\mathbf{K}}_G^r$ is the rate of change of the angular momentum of the vehicle body with respect to $G = G_s$, and $\mathbf{M}_G$ is the global moment (torque) of all forces, again with respect to G.

If the second equation is written with respect to the freshly defined vehicle invariant point M, it generalizes into

$$\dot{\mathbf{K}}_G^r + MG \times m\mathbf{a}_G = \dot{\mathbf{K}}_M^r + MG \times m\mathbf{a}_M = \mathbf{M}_M \tag{9.20}$$

9.6.1 Velocity and Acceleration of G

Dynamics cannot get rid of G. We have to compute its velocity and acceleration.

Both points M and G belong to the same rigid body. Therefore, we can use again the fundamental formula (5.1) to relate the velocity of G to the velocity of M, plus the roll contribution

$$\mathbf{V}_G = \mathbf{V}_M + \boldsymbol{\Omega} \times MG \tag{9.21}$$

where, by definition

$$\begin{aligned} MG &= (h-d)\mathbf{k}_3 \\ &\simeq (h-d)(\theta\mathbf{i}_1 - \phi\mathbf{j}_1 + \mathbf{k}_1) \end{aligned} \tag{9.22}$$

Therefore

$$\begin{aligned}\mathbf{V}_G &= u\mathbf{i}_1 + v\mathbf{j}_1 - p(h-d)\mathbf{j}_3 + q(h-d)\mathbf{i}_3 \\ &= u\mathbf{i}_1 + v\mathbf{j}_1 - (\dot{\phi} - \dot{\psi}\theta)(h-d)\mathbf{j}_3 + (\dot{\theta} + \dot{\psi}\phi)(h-d)\mathbf{i}_3\end{aligned} \tag{9.23}$$

where in the last equation we employed the approximate expression (9.11).

We can proceed in a similar way for accelerations, that is using the fundamental formula (5.4)

$$\mathbf{a}_G = \mathbf{a}_M + \dot{\boldsymbol{\Omega}} \times MG + \boldsymbol{\Omega} \times (\boldsymbol{\Omega} \times MG) \tag{9.24}$$

that is

$$\begin{aligned}\mathbf{a}_G = {} & (\dot{u} - v\dot{\psi})\mathbf{i}_1 + (\dot{v} + u\dot{\psi})\mathbf{j}_1 \\ & - \dot{p}(h-d)\mathbf{j}_3 + \dot{q}(h-d)\mathbf{i}_3 \\ & + (h-d)\big[-p(p\mathbf{k}_3 - r\mathbf{i}_3) + q(r\mathbf{j}_3 - q\mathbf{k}_3)\big]\end{aligned} \tag{9.25}$$

which can be rewritten as

$$\begin{aligned}\mathbf{a}_G = {} & (\dot{u} - v\dot{\psi})\mathbf{i}_1 + (\dot{v} + u\dot{\psi})\mathbf{j}_1 \\ & + (h-d)[-\dot{p}\mathbf{j}_3 + \dot{q}\mathbf{i}_3] \\ & + (h-d)\big[r(p\mathbf{i}_3 + q\mathbf{j}_3) - \big(p^2 + q^2\big)\mathbf{k}_3\big]\end{aligned} \tag{9.26}$$

Each term has a clear physical meaning. The acceleration $\mathbf{a}_G$ is one of the fundamental bricks in the force equation in (9.19).

The acceleration $\mathbf{a}_G$ can be expressed in S_1

$$\begin{aligned}\mathbf{a}_G = {} & (\dot{u} - v\dot{\psi})\mathbf{i}_1 + (\dot{v} + u\dot{\psi})\mathbf{j}_1 \\ & + (h-d)\big[-\dot{p}(\mathbf{j}_1 + \phi\mathbf{k}_1) + \dot{q}(\mathbf{i}_1 - \theta\mathbf{k}_1)\big] \\ & + (h-d)\big\{r\big[p(\mathbf{i}_1 - \theta\mathbf{k}_1) + q(\mathbf{j}_1 + \phi\mathbf{k}_1)\big] - \big(p^2 + q^2\big)(\theta\mathbf{i}_1 - \phi\mathbf{j}_1 + \mathbf{k}_1)\big\}\end{aligned} \tag{9.27}$$

which can be rearranged as

$$\begin{aligned}\mathbf{a}_G = {} & (\dot{u} - v\dot{\psi})\mathbf{i}_1 + (\dot{v} + u\dot{\psi})\mathbf{j}_1 \\ & + (h-d)\big[\dot{q} + rp - \big(p^2 + q^2\big)\theta\big]\mathbf{i}_1 \\ & + (h-d)\big[-\dot{p} + rq + \big(p^2 + q^2\big)\phi\big]\mathbf{j}_1 \\ & + (h-d)\big[-\dot{p}\phi - \dot{q}\theta - rp\theta + rq\phi - \big(p^2 + q^2\big)\big]\mathbf{k}_1\end{aligned} \tag{9.28}$$

Taking (9.16) into account, and discarding the small terms, we get

$$\begin{aligned}\mathbf{a}_G \simeq\ & (\dot{u} - v\dot{\psi})\mathbf{i}_1 + (\dot{v} + u\dot{\psi})\mathbf{j}_1 \\ & + (h-d)\big[(\ddot{\theta} + \ddot{\psi}\phi + \dot{\psi}\dot{\phi}) + \dot{\psi}(\dot{\phi} - \dot{\psi}\theta)\big]\mathbf{i}_1 \\ & + (h-d)\big[-(\ddot{\phi} - \ddot{\psi}\theta - \dot{\psi}\dot{\theta}) + \dot{\psi}(\dot{\theta} + \dot{\psi}\phi)\big]\mathbf{j}_1 \end{aligned} \tag{9.29}$$

If also $\dot{\psi}$ and $\ddot{\psi}$ are small

$$\mathbf{a}_G \simeq (\dot{u} - v\dot{\psi})\mathbf{i}_1 + (\dot{v} + u\dot{\psi})\mathbf{j}_1 + (h-d)[\ddot{\theta}\mathbf{i}_1 - \ddot{\phi}\mathbf{j}_1] \tag{9.30}$$

9.6.2 Rate of Change of the Angular Momentum

It is very convenient to use, as already done in Sect. 9.2, a reference system S_3 attached to the vehicle body and with its origin in the center of gravity of the sprung mass G_s.

As already stated, when the vehicle is at rest, direction $\mathbf{k}_3$ of S_3 is orthogonal to the road and direction $\mathbf{i}_3$ is parallel to the road pointing forward (like in Fig. 1.4, where the body-fixed axes do not have the subscript 3, or in Fig. 9.1). Therefore, in general, S_3 is not directed as the principal axes of inertia. Consequently, the expression of $\dot{\mathbf{K}}^r_G$ is a little involved

$$\begin{aligned}\dot{\mathbf{K}}^r_G =\ & \big[J_x\dot{p} - (J_y - J_z)qr - J_{xy}(\dot{q} - rp) - J_{yz}\big(q^2 - r^2\big) - J_{zx}(\dot{r} - pq)\big]\mathbf{i}_3 \\ & + \big[J_y\dot{q} - (J_z - J_x)rp - J_{yz}(\dot{r} - pq) - J_{zx}\big(r^2 - p^2\big) - J_{xy}(\dot{p} - qr)\big]\mathbf{j}_3 \\ & + \big[J_z\dot{r} - (J_x - J_y)pq - J_{zx}(\dot{p} - qr) - J_{xy}\big(p^2 - q^2\big) - J_{yz}(\dot{q} - rp)\big]\mathbf{k}_3 \end{aligned} \tag{9.31}$$

Actually, most vehicles have $(J_{xy} = J_{yz}) \simeq 0$, and hence we can use the simplified expression

$$\begin{aligned}\dot{\mathbf{K}}^r_G =\ & \big[J_x\dot{p} - (J_y - J_z)qr - J_{zx}(\dot{r} - pq)\big]\mathbf{i}_3 \\ & + \big[J_y\dot{q} - (J_z - J_x)rp - J_{zx}\big(r^2 - p^2\big)\big]\mathbf{j}_3 \\ & + \big[J_z\dot{r} - (J_x - J_y)pq - J_{zx}(\dot{p} - qr)\big]\mathbf{k}_3 \end{aligned} \tag{9.32}$$

This very same quantity can be expressed in S_1, if (9.14) is taken into account

$$\begin{aligned}\dot{\mathbf{K}}^r_G =\ & \big[J_x\dot{p} - (J_y - J_z)qr - J_{zx}(\dot{r} - pq)\big](\mathbf{i}_1 - \theta\mathbf{k}_1) \\ & + \big[J_y\dot{q} - (J_z - J_x)rp - J_{zx}\big(r^2 - p^2\big)\big](\mathbf{j}_1 + \phi\mathbf{k}_1) \\ & + \big[J_z\dot{r} - (J_x - J_y)pq - J_{zx}(\dot{p} - qr)\big](\theta\mathbf{i}_1 - \phi\mathbf{j}_1 + \mathbf{k}_1) \end{aligned} \tag{9.33}$$

That is, with some further simplifications because θ, ϕ, p and q are small

$$\begin{aligned}\dot{\mathbf{K}}_G^r = &\left[J_x\dot{p} - (J_y - J_z)qr - J_{zx}\dot{r} + J_z\dot{r}\theta\right]\mathbf{i}_1\\ &+\left[J_y\dot{q} - (J_z - J_x)rp - J_{zx}r^2 - J_z\dot{r}\phi\right]\mathbf{j}_1\\ &+\left[J_z\dot{r} + J_{zx}\left(\dot{r}\theta - r^2\phi - \dot{p} + qr\right)\right]\mathbf{k}_1\end{aligned} \tag{9.34}$$

And finally, taking (9.16) into account (cf. (3.52))

$$\begin{aligned}\dot{\mathbf{K}}_G^r = &\left[J_x(\ddot{\phi} - \ddot{\psi}\theta - \dot{\psi}\dot{\theta}) - (J_y - J_z)(\dot{\theta} + \dot{\psi}\phi)\dot{\psi} - J_{zx}\ddot{\psi} + J_z\ddot{\psi}\theta\right]\mathbf{i}_1\\ &+\left[J_y(\ddot{\theta} + \ddot{\psi}\phi + \dot{\psi}\dot{\phi}) - (J_z - J_x)\dot{\psi}(\dot{\phi} - \dot{\psi}\theta) - J_{zx}\dot{\psi}^2 - J_z\ddot{\psi}\phi\right]\mathbf{j}_1\\ &+\left[J_z\ddot{\psi} + J_{zx}(2\ddot{\psi}\theta - \ddot{\phi} + 2\dot{\psi}\dot{\theta})\right]\mathbf{k}_1\end{aligned} \tag{9.35}$$

If also $\dot{\psi}$ and $\ddot{\psi}$ are small (obviously, ψ is not small)

$$\dot{\mathbf{K}}_G^r = (J_x\ddot{\phi} - J_{zx}\ddot{\psi})\mathbf{i}_1 + J_y\ddot{\theta}\mathbf{j}_1 + (J_z\ddot{\psi} - J_{zx}\ddot{\phi})\mathbf{k}_1 \tag{9.36}$$

Of course, all inertia terms J_x, J_{xz}, etc. are constant because the reference system S_3 is fixed to the vehicle body. We see that the definition of roll, pitch and yaw is crucial in these equations.

9.6.3 Completing the Torque Equation

Once that $\mathbf{a}_G$ has been obtained, we can also compute the term $MG \times m\mathbf{a}_G$ in the torque equation (9.20). To keep the analysis fairly simple, we employ the simplified expressions (9.22) and (9.30)

$$\begin{aligned}MG \times m\mathbf{a}_G \simeq &\left\{\left[(h-d)(\theta\mathbf{i}_1 - \phi\mathbf{j}_1 + \mathbf{k}_1)\right]\right.\\ &\left.\times\left[(\dot{u} - v\dot{\psi})\mathbf{i}_1 + (\dot{v} + u\dot{\psi})\mathbf{j}_1 + (h-d)(\ddot{\theta}\mathbf{i}_1 - \ddot{\phi}\mathbf{j}_1)\right]\right\}\end{aligned} \tag{9.37}$$

which provides

$$\begin{aligned}MG \times m\mathbf{a}_G \simeq m\big\{&\left[(h-d)^2\ddot{\phi} - (h-d)(\dot{v} + u\dot{\psi})\right]\mathbf{i}_1\\ &+\left[(h-d)^2\ddot{\theta} + (h-d)(\dot{u} - v\dot{\psi})\right]\mathbf{j}_1\\ &+(h-d)\dot{u}\phi\mathbf{k}_1\big\}\end{aligned} \tag{9.38}$$

9.6.4 Equilibrium Equations

We have obtained all inertia terms of the force and torque equations (left hand side terms). Considering (9.30), (9.36), and (9.38), we get the following explicit (linearized) form of the equilibrium equations (9.19) and (9.20) for a vehicle that can

roll and pitch

$$\begin{aligned}
&m\left[(\dot{u}-vr)+(h-d)\ddot{\theta}\right]=ma_x=X\\
&m\left[(\dot{v}+ur)-(h-d)\ddot{\phi}\right]=ma_y=Y\\
&0=Z\\
&\left[J_x+m(h-d)^2\right]\ddot{\phi}-J_{zx}\dot{r}-m(h-d)(\dot{v}+ur)=L_M\\
&\left[J_y+m(h-d)^2\right]\ddot{\theta}+m(h-d)(\dot{u}-vr)=M_M\\
&J_z\dot{r}-J_{zx}\ddot{\phi}+m(h-d)\dot{u}\phi=N_M=N
\end{aligned}\tag{9.39}$$

where, according to (9.10), we set $r=\dot{\psi}$. It is useful to compare these equations with (3.64) and (3.65), that is with the equilibrium equations obtained when the inertial effects of pitch and roll are neglected.

Interestingly enough, the last three equations in (9.39) can be rewritten as

$$\begin{aligned}
&J_x\ddot{\phi}-J_{zx}\dot{r}-ma_y(h-d)=L_M\\
&J_y\ddot{\theta}+ma_x(h-d)=M_M\\
&J_z\dot{r}-J_{zx}\ddot{\phi}+ma_x(h-d)\phi=N_M=N
\end{aligned}\tag{9.40}$$

Of course, everything looks like the car rolls about point M, but it is not so. Actually, the car rolls about the point M as it does with respect to *any other of its points* (Fig. 9.6). It is just the fundamental law (9.21) of the kinematics of rigid bodies. Therefore, we should avoid sentences like "the car rolls about the roll axis", simply because they have no physical meaning at all.

9.6.5 Including the Unsprung Mass

If the unsprung mass m_n cannot be neglected, Eq. (9.39) become

$$\begin{aligned}
&m(\dot{u}-vr)+m_s(h-d)\ddot{\theta}=X\\
&m(\dot{v}+ur)-m_s(h-d)\ddot{\phi}=Y\\
&0=Z\\
&\left[J_x+m_s(h-d)^2\right]\ddot{\phi}-\tilde{J}_{zx}\dot{r}-m_s(h-d)(\dot{v}+ur)=L_M\\
&\left[J_y+m_s(h-d)^2\right]\ddot{\theta}+m_s(h-d)(\dot{u}-v\dot{\psi})=M_M\\
&\tilde{J}_z\dot{r}-J_{zx}\ddot{\phi}+m_s(h-d)\dot{u}\phi=N
\end{aligned}\tag{9.41}$$

where $\tilde{J}_z$ and $\tilde{J}_{zx}$ take into account both m_s and m_n.

9.7 Handling with Roll Motion

The analysis carried out in Chap. 3 can now be extended taking roll and pitch into account. However, as already stated, we assume here that the tires are rigid, as in Sect. 3.8.13. Otherwise, the theory would become too involved, and some physical aspects would not be clear enough.

9.7.1 Equilibrium Equations

The inertia terms of the equilibrium equations have been already obtained in (9.39), and rewritten in an alternative form in (9.40). Therefore, we have to complete the equilibrium equations by including the resultant $\mathbf{F}$ and the moment $\mathbf{M}_M$ (right-hand side terms). Of course, now we have to include the effects of the shock absorbers, which are sensitive to the roll time rate $\dot{\phi}$.

We call c_ϕ the global damping coefficients with respect to roll, much like k_ϕ is the global stiffness with respect to roll. More precisely, as in (3.86), we have

$$k_\phi = k_{\phi_1} + k_{\phi_2} \quad \text{and} \quad c_\phi = c_{\phi_1} + c_{\phi_2} \tag{9.42}$$

Similarly, according to (8.53), we have the following global stiffness and global damping coefficient with respect to pitch

$$k_\theta = k_1 a_1^2 + k_2 a_2^2 \quad \text{and} \quad c_\theta = c_1 a_1^2 + c_2 a_2^2 \tag{9.43}$$

Therefore, the right-hand side terms to be inserted into the equilibrium equations (9.39) are as follows (cf. (3.64) and (3.65))

$$\begin{aligned} X &= X_1 + X_2 - \frac{1}{2}\rho S C_x u^2 \\ Y &= Y_1 + Y_2 \\ Z &= Z_1 + Z_{a1} + Z_2 + Z_{a1} - mg \\ L_M &= -k_\phi \phi - c_\phi \dot{\phi} + mg(h-d)\phi \\ M_M &= -k_\theta \theta - c_\theta \dot{\theta} \\ N_M &= N = N_Y + N_X = (Y_1 a_1 - Y_2 a_2) + (\Delta X_1 t_1 + \Delta X_2 t_2) \end{aligned} \tag{9.44}$$

9.7.2 Load Transfers

Having roll $\phi(t)$ and $\theta(t)$ as functions of time requires some other equations of the vehicle model developed in Chap. 3 to be updated. More precisely, we have to take shock absorbers and inertia terms into account.

The lateral load transfers (3.104) now become

$$\begin{aligned} \Delta Z_1 t_1 &= Y_1 q_1 + k_{\phi_1}\phi + c_{\phi_1}\dot{\phi} \\ \Delta Z_2 t_2 &= Y_2 q_2 + k_{\phi_2}\phi + c_{\phi_2}\dot{\phi} \end{aligned} \tag{9.45}$$

which, if added, provide

$$\begin{aligned} \Delta Z_1 t_1 + \Delta Z_2 t_2 &= (k_{\phi_1} + k_{\phi_2})\phi + (c_{\phi_1} + c_{\phi_2})\dot{\phi} + Y_1 q_1 + Y_2 q_2 \\ &= k_\phi \phi + c_\phi \dot{\phi} + Yd = k_\phi \phi + c_\phi \dot{\phi} + m a_y d \end{aligned} \tag{9.46}$$

since, as in (3.102), $Yd = Y_1 q_1 + Y_2 q_2$.

Combining (9.40), (9.44) and (9.46), we obtain

$$Y(h-d) + mg(h-d)\phi = k_\phi \phi + c_\phi \dot{\phi} + J_x \ddot{\phi} - J_{zx}\dot{r} \tag{9.47}$$

which generalizes (3.117). With a little algebra, we can obtain also

$$\Delta Z_1 t_1 + \Delta Z_2 t_2 = m a_y h + mg(h-d)\phi - (J_x \ddot{\phi} - J_{zx}\dot{r}) \tag{9.48}$$

which generalizes (3.76).

For the longitudinal load transfer ΔZ we can follow a similar line of reasoning, thus obtaining

$$\Delta Z = -\frac{Xh + J_y \ddot{\theta}}{l} = -\frac{m a_x h + J_y \ddot{\theta}}{l} \tag{9.49}$$

which generalizes (3.74).

The main difference with respect to the model developed in Chap. 3, and summarized at p. 86, is that load transfers now depend explicitly on the angular accelerations of the vehicle body.

9.7.3 Constitutive (Tire) Equations

Taking explicitly into account the roll and pitch motions does not affect directly the tire equations. Therefore, the analysis developed in Chap. 3 applies entirely.

9.7.4 Congruence (Kinematic) Equations

The congruence equations listed in Sect. 3.11.3 can be employed even when the vehicle model has the roll and pitch degrees of freedom. Actually, according to Fig. 9.8, the lateral velocities of the front and rear axles should be, respectively

$$v_1 = v + r a_1 + (d - q_1)\dot{\phi} \quad \text{and} \quad v_2 = v - r a_2 + (d - q_2)\dot{\phi} \tag{9.50}$$

that is they include small contributions due to the different heights of the vehicle invariant point M and the two track invariant points M_1 and M_2. However, the additional terms are really very small, and hence can be neglected.

9.8 Steady-State and Transient Analysis

Obviously, including the roll and pitch motions into the vehicle model has very little, if any, influence on the vehicle steady-state behavior. We should not forget that the steady-state roll angle was part of the analyses carried out in Chaps. 3–7. On the other hand, the transient behavior, in particular when entering or exiting a curve, can be rather different.

9.9 Summary

The vehicle orientation has been defined by means of the yaw-pitch-roll elemental rotations. Then, to define the vehicle position, a careful analysis of what happens when the vehicle rolls has been performed. The key result is the definition of the Vehicle Invariant Point (VIP) as the best option for monitoring the vehicle position, and also for defining the lateral velocity and acceleration.

VIP allows for a simple and systematic analysis of the vehicle three-dimensional dynamics. Among other things, it has been shown that the well known roll-axis, as the axis about which the vehicle rolls, is nonsense.

9.10 List of Some Relevant Concepts

p. 273 finite rotations are not commutative;
p. 273 yaw, pitch, and roll are the three elemental rotations commonly and conveniently employed in vehicles;
p. 277 track invariant points belong to the vehicle body;
p. 280 vehicle invariant point (VIP) belongs to the vehicle body and it is the point best suited to represent the vehicle position, lateral velocity, and lateral acceleration;
p. 280 roll motion is better explained without recourse to the roll axis;
p. 288 load transfers depend also on angular accelerations.

References

1. Bastow D, Howard G, Whitehead JP (2004) Car suspension and handling, 4th edn. SAE International, Warrendale

2. Dixon JC (1991) Tyres, suspension and handling. Cambridge University Press, Cambridge
3. Font Mezquita J, Dols Ruiz JF (2006) La Dinámica del Automóvil. Editorial de la UPV, Valencia
4. Gillespie TD (1992) Fundamentals of vehicle dynamics. SAE International, Warrendale
5. Innocenti C (2007) Questioning the notions of roll center and roll axis for car suspensions. In: Deuxieme Congres International Conception et Modelisation des Systemes Mecaniques, Monastir
6. Meirovitch L (1970) Methods of analytical dynamics. McGraw-Hill, New York
7. Shim T, Velusamy PC (2011) Improvement of vehicle roll stability by varying suspension properties. Veh Syst Dyn 49(1–2):129–152
8. Wong JY (2001) Theory of ground vehicles. Wiley, New York

Chapter 10
Tire Models

The global mechanical behavior of the wheel with tire has been addressed in Chap. 2. Basically, we have first found a way to describe the kinematics of a wheel with tire. This effort has led to the definition of the tire slips, as quantities that measure how far a tire is from pure rolling conditions. Then, the forces and couples that a tire receives from the road have been defined. The final step has been to investigate experimentally the link between these kinematic parameters and forces/couples. That was about enough for the chapters dealing with the dynamical behavior of the whole vehicle.

In Chap. 2 no attempt was made to analyze what happens in the contact patch. That is, how the forces and couples are built by the elementary actions that arise at each point of the contact patch. This kind of analysis, however, is quite relevant for a real comprehension of the subtleties of vehicle set-up.

In this chapter, what happens in the contact patch will be investigated by means of the so-called *brush model*. Great care will be devoted to clearly stating the assumptions on which this model is based. Moreover, the investigation will also cover the transient tire behavior. The final results are really interesting and enlightening.

10.1 Brush Model Definition

The *brush model* is perhaps the simplest *physical* tire model, yet it is quite significant and interesting. It is a tool to analyze qualitatively what goes on in the contact patch and to understand why the global mechanical behavior of a wheel with tire is, indeed, like in Figs. 2.15–2.28. Due to its simplicity, the brush model is not always able to provide quantitative results. However, it is of great help in grasping some of the fundamental aspects of tire mechanics.

The Magic Formula provides curves that fit fairly well the experimental results, while the brush model attempts to describe the complex interaction between the tire and the road and how forces are generated. They are complementary approaches.

Basically, in the brush model, a belt equipped with infinitely many flexible bristles (the thread) is wrapped around a cylindrical rigid body (the rim), which moves

M. Guiggiani, *The Science of Vehicle Dynamics*, DOI 10.1007/978-94-017-8533-4_10,

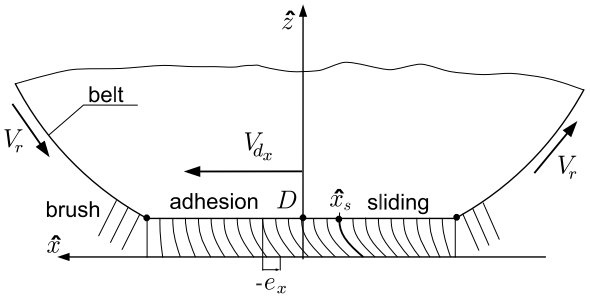

Fig. 10.1 Schematic of the brush model

on a flat surface (the roadway). In a well defined area (the contact patch), the tips of the bristles touch the ground, thus exchanging with the road normal pressures p and tangential stresses $\mathbf{t}$, provided the bristles also have a horizontal deflection $\mathbf{e}$. Each bristle is undistorted ($\mathbf{e} = \mathbf{0}$) when it enters the contact patch. A schematic of the brush model is shown in Fig. 10.1.

The brush model, as any mathematical model, relies on very many assumptions, more or less realistic. An attempt is made to clearly establish all of them, so that the impact of possible improvements can be better appreciated.

For generality, the model is formulated for transient conditions.

10.1.1 Roadway and Rim

The brush model, like the tire, is something that connects the rim to the road. The roadway is assumed to be perfectly *flat*, like a geometric plane. The rim is modeled like a non-rolling cylindrical rigid body moving on the road, carrying on its outer surface a belt to simulate the rolling of the wheel. The belt slides on the rigid body (to simulate rolling) and is equipped with infinitely many flexible bristles (like a brush) which touch the road in the contact patch.

10.1.2 Shape of the Contact Patch

As shown in Fig. 10.2, the contact patch $\mathscr{P}$ is assumed to be a convex, simply connected region. Therefore, it is quite different from a real contact patch, like the one in Fig. 2.5 at p. 14, which usually has lugs and voids.

It is useful to define a reference system $\hat{\mathsf{S}} = (\hat{x}, \hat{y}, \hat{z}; D)$, with directions $(\mathbf{i}, \mathbf{j}, \mathbf{k})$ and origin at point D. Usually D is the center of the contact patch, as in Fig. 10.2. Directions $(\mathbf{i}, \mathbf{j}, \mathbf{k})$ resemble those of Fig. 2.2, in the sense that $\mathbf{k}$ is perpendicular to the road and $\mathbf{i}$ is the direction of the wheel pure rolling.

More precisely, the contact patch is defined as the region between the *leading edge* $\hat{x} = \hat{x}_0(\hat{y})$ and the *trailing edge* $\hat{x} = -\hat{x}_0(\hat{y})$, that is

$$\mathscr{P} = \left\{(\hat{x}, \hat{y}) : \hat{x} \in \left[-\hat{x}_0(\hat{y}), \hat{x}_0(\hat{y})\right], \hat{y} \in [-b, b]\right\} \tag{10.1}$$

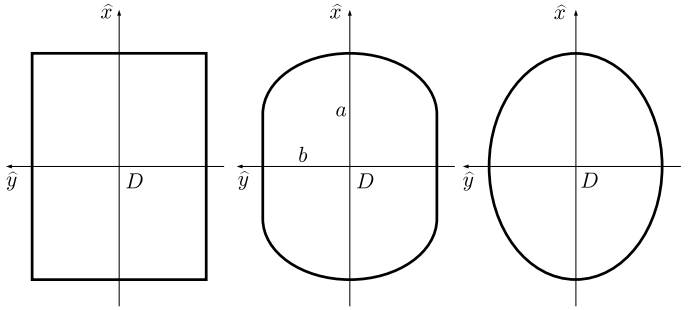

Fig. 10.2 Possible shapes of the contact patch

It is assumed for simplicity that the *shape* and *size* of the contact patch are not affected by the operating conditions, including the camber angle γ. Of course, this is not true in real tires.

For mathematical convenience, the contact patch is assumed here to be either a *rectangle*, centered at D, of length $2a$ and width $2b$ (Fig. 10.2(left)), or an *ellipse*, again with axes of length $2a$ and $2b$ (Fig. 10.2(right)). In the first case we have $\hat{x}_0 = a$, whereas in the second case

$$\hat{x}_0(\hat{y}) = \sqrt{a^2\left(1 - \frac{\hat{y}^2}{b^2}\right)} \tag{10.2}$$

Typical values for a and b are in the range 0.04–0.08 m. The rectangular shape is not a bad approximation of the contact patch of car tires (Fig. 2.5), while the elliptical one is better for motorcycle tires (Fig. 10.5).

10.1.3 Force-Couple Resultant

Exactly like in (2.15), the tangential stresses $\mathbf{t}(\hat{x}, \hat{y}, t)$ exerted by the road on the tire at each point of the contact patch yield a tangential force $\mathbf{F}_t$

$$\mathbf{F}_t(t) = F_x\mathbf{i} + F_y\mathbf{j} = \int_{-b}^{b} \mathrm{d}\hat{y} \int_{-\hat{x}_0(\hat{y})}^{\hat{x}_0(\hat{y})} \mathbf{t}(\hat{x}, \hat{y}, t)\mathrm{d}\hat{x} \tag{10.3}$$

and a vertical moment M_z^D with respect to point D

$$M_z^D(t)\mathbf{k} = \int_{-b}^{b} \mathrm{d}\hat{y} \int_{-\hat{x}_0(\hat{y})}^{\hat{x}_0(\hat{y})} (\hat{x}\mathbf{i} + \hat{y}\mathbf{j}) \times \mathbf{t}(\hat{x}, \hat{y}, t)\mathrm{d}\hat{x} \tag{10.4}$$

All inertial effects, of any nature, are neglected.

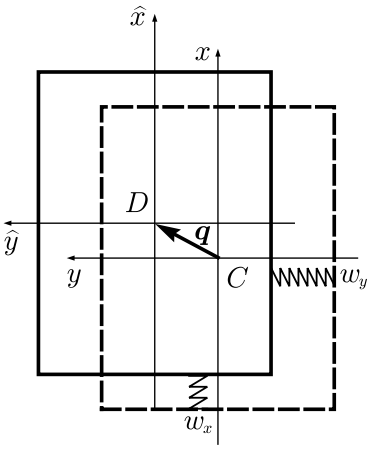

Fig. 10.3 Model for the carcass compliance

10.1.4 Position of the Contact Patch

Let C be the position of D under pure rolling steady-state conditions, that is $F_x = F_y = M_z = 0$. Owing to the geometrical effect of camber, point C may not coincide with O, as shown in Eq. (2.33) and in Fig. 2.11.

Under general operating conditions, points D and C may have different positions on the road, mainly due to the *elastic compliance* of the carcass. Therefore, as also shown in Fig. 10.3

$$CD = \mathbf{q}(t) = q_x(t)\mathbf{i} + q_y(t)\mathbf{j} \tag{10.5}$$

and, for any other point P in the contact patch

$$CP = CD + DP = CD + \hat{x}\mathbf{i} + \hat{y}\mathbf{j} = (\hat{x} + q_x)\mathbf{i} + (\hat{y} + q_y)\mathbf{j} \tag{10.6}$$

Differentiating (10.5) provides the velocity $\mathbf{V}_d$ of point D

$$\mathbf{V}_d - \mathbf{V}_c = \dot{\mathbf{q}} = \dot{q}_x\mathbf{i} + \dot{q}_y\mathbf{j} + \omega_z\mathbf{k} \times \mathbf{q} \tag{10.7}$$

However, as discussed at p. 33, in most cases ω_z is very small and hence

$$\dot{\mathbf{q}} \approx \dot{q}_x\mathbf{i} + \dot{q}_y\mathbf{j} \tag{10.8}$$

To approximately model the lateral and longitudinal compliance of the carcass, it has been assumed that the contact patch (with its reference system $\hat{\mathrm{S}}$) can have small rigid displacements q_x and q_y, without changing its orientation. A linear relationship between $\mathbf{F}_t$ and $\mathbf{q}$ is the simplest option

$$\mathbf{F}_t = \mathbf{W}\mathbf{q} \tag{10.9}$$

that is

$$F_x = w_x q_x(t) \quad \text{and} \quad F_y = w_y q_y(t) \tag{10.10}$$

if

$$\mathbf{W} = \begin{bmatrix} w_x & 0 \\ 0 & w_y \end{bmatrix} \tag{10.11}$$

with constant *stiffnesses* w_x and w_y. More general symmetric matrices are possible.

The displacements q_x and q_y are usually quite small (i.e., $|q_x|, |q_y| \ll a$) and hence they can be neglected with respect to some phenomena, as will be discussed.

More advanced tire models may also include small rigid rotations of the contact patch [9], or employ the stretched string approach to model the carcass flexibility [1, 6, 8].

10.1.5 Pressure Distribution

Figures 10.4 and 10.5 show a typical pressure distribution as measured in a real motionless tire. The average ground pressure in the tire contact patch, considered as a single region, is not much higher than the tire inflation pressure. Of course there are high peaks near the tread edges.

A very simple pressure distribution $p(\hat{x}, \hat{y})$ on the contact patch $\mathscr{P}$, which roughly mimics the experimental results, may be parabolic along $\hat{x}$

$$p = p(\hat{x}, \hat{y}) = p_0(\hat{y}) \frac{(\hat{x}_0(\hat{y}) - \hat{x})(\hat{x}_0(\hat{y}) + \hat{x})}{\hat{x}_0(\hat{y})^2} \tag{10.12}$$

where $p_0(\hat{y}) = p(0, \hat{y})$ is the pressure peak value. The corresponding vertical load is given by

$$F_z = \int_{-b}^{b} \mathrm{d}\hat{y} \int_{-\hat{x}_0(\hat{y})}^{\hat{x}_0(\hat{y})} p(\hat{x}, \hat{y}) \mathrm{d}\hat{x} \tag{10.13}$$

Other pressure distributions may be used as well in the brush model, including non-symmetric ones like in Fig. 2.10 to include the rolling resistance.

On a rectangular contact patch $\hat{x}_0(\hat{y}) = a$. Equation (10.12), with uniform p_0, becomes simply

$$p = p(\hat{x}, \hat{y}) = p_0 \left[1 - \left(\frac{\hat{x}}{a} \right)^2 \right] \tag{10.14}$$

and hence

$$F_z = \int_{-b}^{b} \mathrm{d}\hat{y} \int_{-a}^{a} p(\hat{x}, \hat{y}) \mathrm{d}\hat{x} = \frac{2}{3} p_0 2a 2b \tag{10.15}$$

which yields

$$p_0 = \frac{3}{2} \frac{F_z}{(2a)(2b)} \tag{10.16}$$

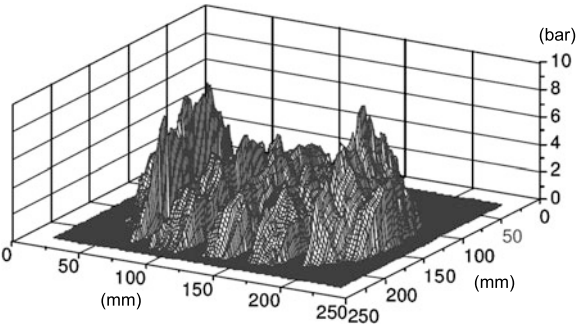

Fig. 10.4 Experimental results: pressure distribution for a motionless motorcycle tire [4]

On an elliptical contact patch (10.12) and (10.2) provide

$$p = p(\hat{x}, \hat{y}) = p_0 \left[1 - \frac{\hat{x}^2}{a^2(1 - \frac{y^2}{b^2})} \right] \tag{10.17}$$

again with the same peak value p_0 for any y.

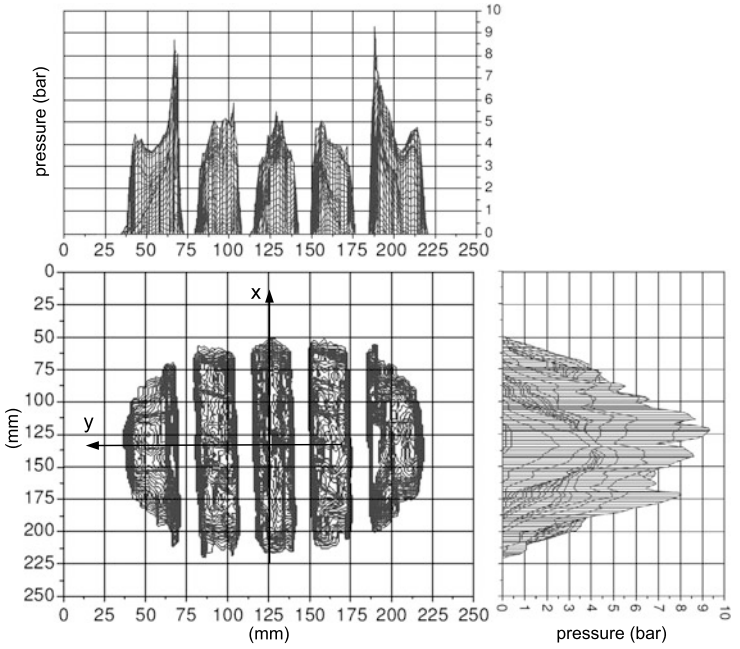

Fig. 10.5 Experimental results: contact patch and envelope of pressure distribution for a motionless motorcycle tire [4]

10.1.6 Friction

Let $V_\mu = |\mathbf{V}_\mu|$ be the magnitude of the *sliding velocity* $\mathbf{V}_\mu$, that is the velocity of the bristle tip with respect to the road, and μ the *local friction coefficient*.[1] Fairly general rules for *adhesion* and *sliding* between the bristle tip and the road are as follows

$$|\mathbf{t}| < \mu p \quad \Longleftrightarrow \quad V_\mu = 0 \quad \text{(adhesion)} \tag{10.18}$$

$$\mathbf{t} = -\mu p \frac{\mathbf{V}_\mu}{V_\mu} \quad \Longleftrightarrow \quad V_\mu \neq 0 \quad \text{(sliding)} \tag{10.19}$$

Equation (10.19) simply states that, at sliding, $\mathbf{t}$ and $\mathbf{V}_\mu$ have opposite direction and $|\mathbf{t}| = \mu p$.

If thermal effects are neglected, μ may reasonably depend on the local value of the pressure p and of V_μ

$$\mu = \mu(p, V_\mu) \tag{10.20}$$

It is common practice to call $\mu_0 = \mu(p, 0)$ the *coefficient of static friction* and $\mu_1 = \mu(p, V_\mu \neq 0)$ the *coefficient of kinetic friction*. In the present analysis, to keep it simple, we assume μ_0 and μ_1 to be *constant* all over the contact patch

$$\mu_0 = (1 + \chi)\mu_1, \quad \text{with } \chi > 0 \tag{10.21}$$

thus discarding all dependencies on p and V_μ, except the switch from μ_0 to μ_1. Typically, $\mu_0 \approx 1.2\mu_1$, that is $\chi \approx 0.2$. More advanced models can be found, e.g., in [2, 3, 9].

10.1.7 Constitutive Relationship

The brush model owes its name to this section. It is indeed the constitutive relation that makes it possible to think of this model as having a moving belt equipped with infinitely many *independent* flexible bristles (Fig. 10.1).

Each massless bristle, while traveling in the contact patch, may have a horizontal deflection $\mathbf{e}(\hat{x}, \hat{y}, t) = e_x\mathbf{i} + e_y\mathbf{j}$. The key point is to assume that this deflection $\mathbf{e}(\hat{x}, \hat{y})$ does depend solely on the tangential stress $\mathbf{t}(\hat{x}, \hat{y}, t) = t_x\mathbf{i} + t_y\mathbf{j}$ at the very same point in the contact patch. In other words, each bristle behaves independently of the others: the constitutive relation is purely *local*. It is quite a strong assumption. Not very realistic, but terribly useful to get a simple model.

Actually, a truly simple model requires three further assumptions. The constitutive relation need to be *linear*, *isotropic* and *homogeneous*, that is simply

$$\mathbf{t}(\hat{x}, \hat{y}, t) = k\mathbf{e}(\hat{x}, \hat{y}, t) \tag{10.22}$$

[1] Not to be confused with the global friction coefficients (2.76) and (2.78).

where k is the *bristle stiffness*. Usually, k ranges between 30 and 60 MN/m^3.

A linear but anisotropic and non homogeneous constitutive relation would be like

$$\mathbf{t}(\hat{x}, \hat{y}, t) = \begin{bmatrix} k_{xx}(\hat{x}, \hat{y}) & k_{xy}(\hat{x}, \hat{y}) \\ k_{yx}(\hat{x}, \hat{y}) & k_{yy}(\hat{x}, \hat{y}) \end{bmatrix} \mathbf{e}(\hat{x}, \hat{y}, t) \tag{10.23}$$

with $k_{xy} = k_{yx}$ and often equal to zero.

It is worth noting that in (10.22) (and also in (10.23)) all quantities, including $\mathbf{t}$ and $\mathbf{e}$, are associated with the coordinates of the root, not of the tip of the bristle. Much like in the classical theory of linear elasticity, we are assuming that the problem can be safely formulated with reference to the undeformed state. This is reasonable provided the deflections $\mathbf{e}$ are small, that is $|\mathbf{e}| \ll a$. In other words, the root and the tip of each bristle are almost coincident.

10.1.8 Kinematics

There are two fundamental global motions in the kinematics of a real wheel with tire:

(1) the continuous flow of undeformed rubber tread in the contact patch;
(2) the motion of the contact patch with respect to the road.

For an in-depth discussion of these topics, along with the definition of the translational slip $\boldsymbol{\sigma}$ and of the spin slip φ, we refer to Sect. 2.7.

The first motion is modeled by assuming that the belt (i.e., the root of each bristle) moves with respect to the rim, and hence to the contact patch, with a velocity equal to minus the rolling velocity $-\mathbf{V}_r = -V_r\mathbf{i}$ (defined in (2.43)). This flow is always along parallel lines directed like $-\mathbf{i}$. In the brush model the rolling velocity may change in time ($V_r = V_r(t)$), but it must be the same at all points of the contact patch (it is a *global* parameter). This property makes it possible to define a sort of global *rolling distance* $s(t)$

$$s(t) = \int_0^t V_r(t)\mathrm{d}t \quad \text{that is} \quad \frac{\mathrm{d}s}{\mathrm{d}t} = V_r(t) \tag{10.24}$$

If $V_r > 0$, the function $s(t)$ is one-to-one. It will be shown that, in some cases, the use of s as the independent variable is more convenient than the use of t.

As already stated, the forefront border of the contact patch is called the leading edge. It is very important to realize that it is through the leading edge that *undeformed* rubber tread enters the contact patch.

The second motion is modeled by considering the contact patch $\mathscr{P}$ as a rigid region that moves with respect to the road with angular velocity equal to the slip spin velocity $\Omega_{s_z}\mathbf{k}$ (defined in (2.50)) and whose center D has velocity $\mathbf{V}_d$ given by (cf. (10.7) and (10.8))

$$\mathbf{V}_d = \mathbf{V}_c + \dot{\mathbf{q}} = \mathbf{V}_c + \dot{q}_x\mathbf{i} + \dot{q}_y\mathbf{j} + \omega_z\mathbf{k} \times \mathbf{q} \tag{10.25}$$

where $\mathbf{V}_c$, that is the velocity of point C, is set equal to the *speed of travel*, defined in (2.48) for a real wheel. From (2.49) and (2.58) it follows that $\mathbf{V}_c = \mathbf{V}_r + \mathbf{V}_s = \mathbf{V}_r + V_r\boldsymbol{\sigma}$, and hence

$$\mathbf{V}_d = \mathbf{V}_c + \dot{\mathbf{q}} = \mathbf{V}_r + V_r\boldsymbol{\sigma} + \dot{\mathbf{q}} \tag{10.26}$$

The generic point $P = (\hat{x}, \hat{y})$ of $\mathscr{P}$ has therefore a velocity equal to[2]

$$\mathbf{V}_P = \mathbf{V}_d + \Omega_{s_z}\mathbf{k} \times CP = \mathbf{V}_c + \dot{\mathbf{q}} + \Omega_{s_z}\mathbf{k} \times (\hat{x}\mathbf{i} + \hat{y}\mathbf{j}) \tag{10.27}$$

The two global motions affect the *local kinematics*, that is the motion of each *single bristle*. The *root* of the bristle (momentarily) at point $(\hat{x}, \hat{y}) = (\hat{x}_b(t), \hat{y})$ of the contact patch has a velocity $\mathbf{V}_t$ with respect to the ground given by the superimposition of the two global motions

$$\begin{aligned}\mathbf{V}_t(\hat{x}, \hat{y}, t) &= \mathbf{V}_P(\hat{x}, \hat{y}, t) - \mathbf{V}_r(t)\\ &= (\mathbf{V}_c - \mathbf{V}_r) + \Omega_{s_z}\mathbf{k} \times (\hat{x}\mathbf{i} + \hat{y}\mathbf{j}) + \dot{\mathbf{q}}\\ &= \mathbf{V}_s + \Omega_{s_z}(\hat{x}\mathbf{j} - \hat{y}\mathbf{i}) + \dot{\mathbf{q}}\\ &= V_r\big[\boldsymbol{\sigma} - \varphi(\hat{x}\mathbf{j} - \hat{y}\mathbf{i})\big] + \dot{\mathbf{q}}\end{aligned} \tag{10.28}$$

The local velocity $\mathbf{V}_t$ of each bristle root may be called the *skating velocity*.[3] It is usually quite small, and everywhere zero in pure rolling conditions.

Equation (10.28) suggests to define the *skating slip* $\boldsymbol{\varepsilon}$

$$\begin{aligned}\boldsymbol{\varepsilon} = \frac{\mathbf{V}_t}{V_r} &= \boldsymbol{\sigma} - \varphi(\hat{x}\mathbf{j} - \hat{y}\mathbf{i}) + \frac{\dot{\mathbf{q}}}{V_r}\\ &= \boldsymbol{\rho} - \varphi(\hat{x}\mathbf{j} - \hat{y}\mathbf{i}) = \boldsymbol{\varepsilon}(\hat{x}, \hat{y}, t)\end{aligned} \tag{10.29}$$

and also the *transient translational slip*

$$\boldsymbol{\rho}(t) = \boldsymbol{\sigma}(t) + \frac{\dot{\mathbf{q}}(t)}{V_r(t)} \tag{10.30}$$

The translational slip $\boldsymbol{\sigma}$ and the spin slip φ were defined also for real wheels with tires, whereas the local skating slip $\boldsymbol{\varepsilon}$ and the global transient translational slip $\boldsymbol{\rho}$ are meaningful in the brush model only, as they involve $\dot{\mathbf{q}}$.

To study the possible *sliding* of each bristle *tip* on the ground, let us consider the bristle root (momentarily) with coordinates $(\hat{x}, \hat{y}) = (\hat{x}_b(t), \hat{y})$. According to (10.28), its root moves with respect to the road with a skating velocity $\mathbf{V}_t(\hat{x}, \hat{y}, t)$. At the same time, its tip has, by definition, a velocity $\dot{\mathbf{e}} = \mathrm{d}\mathbf{e}/\mathrm{d}t$ with respect to

[2] In the brush model there is slip spin velocity Ω_{s_z} only within the contact patch, as if it were entirely due to the camber angle.

[3] The use of the practical slip $\boldsymbol{\kappa}$ would not have provided an equally neat formula.

the root.[4] However, exactly like in fluid dynamics, it is more convenient to take a so-called Eulerian approach,[5] which provides

$$\dot{\mathbf{e}} = \frac{\mathrm{d}\mathbf{e}(\hat{x}_b(t), \hat{y}, t)}{\mathrm{d}t} = \frac{\partial \mathbf{e}}{\partial \hat{x}} \frac{\mathrm{d}\hat{x}_b}{\mathrm{d}t} + \frac{\partial \mathbf{e}}{\partial t} = -\mathbf{e}_{,\hat{x}} V_r + \mathbf{e}_{,t} \tag{10.31}$$

since $\mathrm{d}\hat{y}/\mathrm{d}t = 0$ and where, for brevity, $\mathbf{e}_{,\hat{x}} = \partial \mathbf{e}/\partial \hat{x}$ and $\mathbf{e}_{,t} = \partial \mathbf{e}/\partial t$. Therefore, the possible *sliding velocity* $\mathbf{V}_\mu$ of a bristle tip with respect to the road is given by

$$\begin{aligned} \mathbf{V}_\mu(\hat{x}, \hat{y}, t) &= \mathbf{V}_t + \dot{\mathbf{e}} \\ &= V_r \boldsymbol{\varepsilon} - V_r \mathbf{e}_{,\hat{x}} + \mathbf{e}_{,t} \\ &= V_r \big[\boldsymbol{\sigma} - \varphi(\hat{x}\mathbf{j} - \hat{y}\mathbf{i})\big] + \dot{\mathbf{q}} - V_r \mathbf{e}_{,\hat{x}} + \mathbf{e}_{,t} \\ &= V_r \big[\boldsymbol{\rho} - \varphi(\hat{x}\mathbf{j} - \hat{y}\mathbf{i})\big] - V_r \mathbf{e}_{,\hat{x}} + \mathbf{e}_{,t} \end{aligned} \tag{10.32}$$

Of course, there is *adhesion* between the tip and the road if $V_\mu = 0$, like in (10.18).

10.2 General Governing Equations of the Brush Model

The brush model has been completely defined in the previous section. A schematic was shown in Fig. 10.1. Its distinguishing feature is that each bristle behaves independently of the others.

The fundamental governing equations for the *transient* behavior are to be obtained by combining all the relationships given in the brush model definition.

Whenever there is *adhesion*, as defined in (10.18), between the tip and the road, the deflection $\mathbf{e}$ grows with the following time rate, according to (10.32) with $\mathbf{V}_\mu = \mathbf{0}$

$$\dot{\mathbf{e}} = -\mathbf{V}_t \quad \Longleftrightarrow \quad |\mathbf{t} = k\mathbf{e}| < \mu_0 p \quad \text{(adhesion)} \tag{10.33}$$

As soon as the friction limit is reached ($|\mathbf{t}| = \mu_0 p$), the bristle tip starts *sliding* with velocity $\mathbf{V}_\mu \neq \mathbf{0}$ and the governing equation changes abruptly into (10.19), which, owing to (10.32) and (10.22), is equivalent to

$$k\mathbf{e} = -\mu_1 p \frac{\mathbf{V}_t + \dot{\mathbf{e}}}{|\mathbf{V}_t + \dot{\mathbf{e}}|} \quad \Longleftrightarrow \quad |\mathbf{V}_t + \dot{\mathbf{e}}| \neq 0 \quad \text{(sliding)} \tag{10.34}$$

This vectorial differential equation states that, whenever there is sliding, we have $k|\mathbf{e}| = \mu_1 p$ and the vectors $\mathbf{t} = k\mathbf{e}$ and $\mathbf{V}_\mu$ have the same, unknown, direction.

[4] The total time derivative is evaluated within $\hat{\mathsf{S}}$, that is as if $\mathbf{i}$ and $\mathbf{j}$ were fixed.

[5] As reported in [11, p. 4], this approach is actually due to d'Alembert.

According to (10.31) and (10.32), Eqs. (10.33) and (10.34) can be recast as follows, where $\boldsymbol{\varepsilon} = \boldsymbol{\rho} - \varphi(\hat{x}\mathbf{j} - \hat{y}\mathbf{i})$

$$\mathbf{e}_{,\hat{x}} - \frac{\mathbf{e}_{,t}}{V_r} = \boldsymbol{\varepsilon} = \boldsymbol{\sigma}(t) + \frac{\dot{\mathbf{q}}}{V_r} - \varphi(t)(\hat{x}\mathbf{j} - \hat{y}\mathbf{i}) \quad \Longleftrightarrow \quad k|\mathbf{e}| < \mu_0 p \quad \text{(adhesion)} \tag{10.35}$$

$$k\mathbf{e} = -\mu_1 p \frac{\boldsymbol{\varepsilon} - \mathbf{e}_{,\hat{x}} + \mathbf{e}_{,t}/V_r}{|\boldsymbol{\varepsilon} - \mathbf{e}_{,\hat{x}} + \mathbf{e}_{,t}/V_r|} \quad \Longleftrightarrow \quad |\boldsymbol{\varepsilon} - \mathbf{e}_{,\hat{x}} + \mathbf{e}_{,t}/V_r| \neq 0 \quad \text{(sliding)} \tag{10.36}$$

with given boundary conditions (like $\mathbf{e}(\hat{x}_0(\hat{y}), \hat{y}, t) = 0$ at the leading edge) and initial conditions (like $\mathbf{e}(\hat{x}, \hat{y}, 0) = \mathbf{e}_0(\hat{x}, \hat{y})$). This is a two-state system, in the sense that only one partial differential equation applies at each point of the contact patch: we can either have adhesion or sliding, but not both (or none). By definition, adhesion means $|\mathbf{V}_\mu| = 0$ and the differential equation (10.36) of sliding is indeed meaningless.

A closer look shows that we have a different two-state system for any value of $\hat{y}$. Indeed, the spatial derivatives in (10.35) and (10.36) are only with respect to $\hat{x}$, that is in the direction $\mathbf{i}$ of the rolling velocity $V_r\mathbf{i}$. The rubber flows along parallel lines that do not interact (in this model!).

However, the problem needs an additional vectorial equation since $\dot{\mathbf{q}}$ is unknown, and so is $\boldsymbol{\rho}(t)$. Differentiating (10.9) with respect to time and taking (10.30) into account provides

$$\dot{\mathbf{F}}_t = \mathbf{W}\dot{\mathbf{q}} = \mathbf{W}(\boldsymbol{\rho} - \boldsymbol{\sigma})V_r \tag{10.37}$$

Also useful is to insert the constitutive relationship (10.22) into (10.3) and then differentiate with respect to time

$$\dot{\mathbf{F}}_t = k \int_{-b}^{b} \mathrm{d}\hat{y} \int_{-\hat{x}_0(\hat{y})}^{\hat{x}_0(\hat{y})} \mathbf{e}_{,t}\mathrm{d}\hat{x} \tag{10.38}$$

Combining (10.37) and (10.38) yields the missing governing equation

$$k \int_{-b}^{b} \mathrm{d}\hat{y} \int_{-\hat{x}_0(\hat{y})}^{\hat{x}_0(\hat{y})} \mathbf{e}_{,t}\mathrm{d}\hat{x} = \mathbf{W}\dot{\mathbf{q}} = \mathbf{W}(\boldsymbol{\rho} - \boldsymbol{\sigma})V_r \tag{10.39}$$

Summing up, the behavior of the *transient* brush model, that is the functions $\mathbf{e}(\hat{x}, \hat{y}, t)$ and $\boldsymbol{\rho}(t)$, for given boundary conditions $\mathbf{e}(\hat{x}_0(\hat{y}), \hat{y}, t) = \mathbf{0}$ at the leading edge and initial conditions $\mathbf{e}(\hat{x}, \hat{y}, 0) = \mathbf{e}_0(\hat{x}, \hat{y})$ and $\boldsymbol{\rho}(0) = \boldsymbol{\rho}_0$, is completely defined by the *governing equations* (10.35) or (10.36), and (10.39).

Actually, a somehow more compact formulation of the very same problem can be obtained employing, instead of time t, the rolling distance s, defined in (10.24). Since there is a one-to-one correspondence between t and s, that is $t = t(s)$, and all time derivatives in the brush model are divided by $V_r(t) = \mathrm{d}s/\mathrm{d}t$, the general

governing equations can be reformulated in terms of $\mathbf{e}(\hat{x}, \hat{y}, s)$ in the following way

$$\mathbf{e}_{,\hat{x}} - \mathbf{e}_{,s} = \boldsymbol{\varepsilon} \qquad \Longleftrightarrow \qquad k|\mathbf{e}| < \mu_0 p \qquad \text{(adhesion)} \qquad (10.40)$$

$$k\mathbf{e} = -\mu_1 p \frac{\boldsymbol{\varepsilon} - \mathbf{e}_{,\hat{x}} + \mathbf{e}_{,s}}{|\boldsymbol{\varepsilon} - \mathbf{e}_{,\hat{x}} + \mathbf{e}_{,s}|} \qquad \Longleftrightarrow \qquad |\boldsymbol{\varepsilon} - \mathbf{e}_{,\hat{x}} + \mathbf{e}_{,s}| \neq 0 \qquad \text{(sliding)} \qquad (10.41)$$

along with

$$k \int_{-b}^{b} \mathrm{d}\hat{y} \int_{-\hat{x}_0(\hat{y})}^{\hat{x}_0(\hat{y})} \mathbf{e}_{,s} \mathrm{d}\hat{x} = \mathbf{W}\mathbf{q}' = \mathbf{W}(\boldsymbol{\rho} - \boldsymbol{\sigma}) \qquad (10.42)$$

where $\mathbf{e}_{,s} = \partial \mathbf{e}/\partial s$ and $\mathbf{q}' = \mathrm{d}\mathbf{q}/\mathrm{d}s$. This formulation shows that the rolling velocity $V_r(t)$ does not have any influence on the behavior of the brush model with respect to the rolling distance s. The main reason is that all inertial effects have been neglected, as in (2.22).

Either in terms of t or s, this is quite a difficult mathematical problem if tackled in its full generality. Fortunately, under suitable simplifying assumptions it becomes much simpler. However, it should be appreciated that the transient behavior of a real wheel with tire (cf. (2.18)) is a rather difficult matter.

10.2.1 Data for Numerical Examples

Almost all figures from here onwards in this chapter are obtained with the following numerical values:

$$\begin{array}{lll} a = 7.5 \text{ cm}, & b = 5.6 \text{ cm}, & r_r = 25 \text{ cm} \\ \mu_0 = 1, & \chi = 0.2, & p_0 = 0.3 \text{ MPa} \\ k = 30 \text{ MN/m}^3, & w_x = 500 \text{ kN/m}, & w_y = 125 \text{ kN/m} \end{array} \qquad (10.43)$$

10.3 Brush Model Steady-State Behavior

The main, and most common, simplification is assuming the model to be in steady-state conditions, that is that

- $\mathbf{e}_{,t} = \mathbf{0}$, and hence $\mathbf{e} = \mathbf{e}(\hat{x}, \hat{y})$;
- $\dot{\mathbf{q}} = \mathbf{0}$, which means that $\boldsymbol{\rho} = \boldsymbol{\sigma}$ is known.

The problem is substantially simpler, since there are only *ordinary* differential equations, and the only unknown function is $\mathbf{e}(\hat{x}, \hat{y})$.

More in detail, the skating slip (10.29) becomes

$$\boldsymbol{\varepsilon}(\hat{x}, \hat{y}) = \frac{\mathbf{V}_t(\hat{x}, \hat{y}, t)}{V_r(t)} = \boldsymbol{\sigma} - \varphi(\hat{x}\mathbf{j} - \hat{y}\mathbf{i}) \qquad (10.44)$$

with *constant* σ and φ. Therefore, the skating slip $\boldsymbol{\varepsilon}$ is a given quantity, a known input to the model. It is worth noting that some quantities may be time dependent, like $\mathbf{V}_t$ and V_r.

According to (10.31), the total time derivative of the bristle tip is given by

$$\frac{\dot{\mathbf{e}}}{V_r(t)} = -\mathbf{e}'(\hat{x}, \hat{y}) \tag{10.45}$$

where $\mathbf{e}' = \mathbf{e}_{,\hat{x}}$ to stress that it is a total derivative here.

10.3.1 Governing Equations

According to (10.44) and (10.45), in the steady-state case the governing equations (10.35) and (10.36) of the brush model become (cf. [1, p. 761] and [8, p. 83])

$$\mathbf{e}' = \boldsymbol{\varepsilon} \quad \Longleftrightarrow \quad k|\mathbf{e}| < \mu_0 p \quad \text{(adhesion)} \tag{10.46}$$

$$k\mathbf{e} = -\mu_1 p \frac{\boldsymbol{\varepsilon} - \mathbf{e}'}{|\boldsymbol{\varepsilon} - \mathbf{e}'|} \quad \Longleftrightarrow \quad \left|\boldsymbol{\varepsilon} - \mathbf{e}'\right| \neq 0 \quad \text{(sliding)} \tag{10.47}$$

These first-order differential equations in the unknown function $\mathbf{e}(\hat{x}, \hat{y})$, along with the boundary conditions at the leading edge, completely describe the behavior of the brush model.[6] Indeed, in this case the other equation (10.39) simply states $\boldsymbol{\rho} - \boldsymbol{\sigma} = \mathbf{0}$.

As already remarked, this is a two-state system, since at each point there is, obviously, either adhesion or sliding. To distinguish between the solutions in the *adhesion* and in the *sliding* regions, we will use the symbols $\mathbf{e}_a$ and $\mathbf{e}_s$, respectively.

10.3.2 Adhesion and Sliding Zones

Each bristle, which behaves independently of the others, is undeformed when it enters the contact patch through the leading edge $\hat{x}_0(\hat{y})$. Its tip sticks to the ground and, due to the skating velocity $\mathbf{V}_t$ between the bristle root and the road, a deflection $\mathbf{e}$ immediately starts to build up, along with a tangential stress $\mathbf{t} = k\mathbf{e}$.

To better understand the roles played by adhesion and sliding, we refer to Fig. 10.6, where a fairly unusual pressure pattern has been depicted.

[6] More convenient governing equations for the sliding state are given in (10.52) and (10.53).

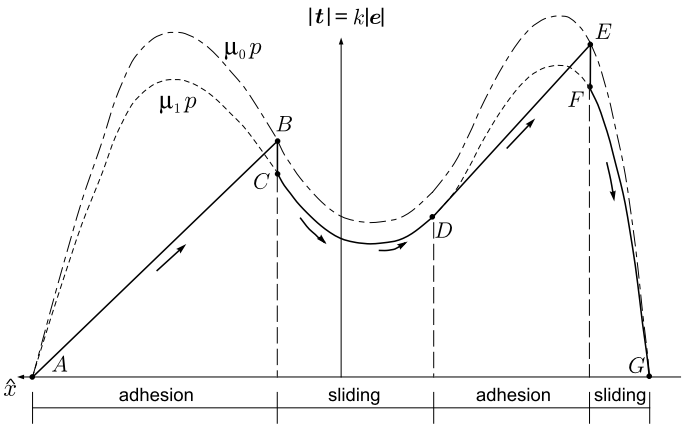

Fig. 10.6 Adhesion and sliding zones in the case $\boldsymbol{\varepsilon} = \boldsymbol{\sigma} = \text{const}$

10.3.2.1 Adhesion

At first there is adhesion, and Eq. (10.46) applies with initial condition $\mathbf{e}_a = \mathbf{0}$ at $\hat{x}_0$ (point A in Fig. 10.6). A simple integration provides the behavior of the bristle deflection $\mathbf{e}_a$ in the adhesion zone

$$\begin{aligned}\mathbf{e}_a(\hat{x}, \hat{y}) &= \int_{\hat{x}_0}^{\hat{x}} \mathbf{e}' \mathrm{d}\hat{x} = \int_{\hat{x}_0}^{\hat{x}} \boldsymbol{\varepsilon} \mathrm{d}\hat{x} = \int_{\hat{x}_0}^{\hat{x}} \left[\boldsymbol{\sigma} - \varphi(\hat{x}\mathbf{j} - \hat{y}\mathbf{i})\right] \mathrm{d}\hat{x} \\ &= -\boldsymbol{\sigma}(\hat{x}_0 - \hat{x}) + \varphi\left[\frac{(\hat{x}_0 - \hat{x})(\hat{x}_0 + \hat{x})}{2}\mathbf{j} - \hat{y}(\hat{x}_0 - \hat{x})\mathbf{i}\right] \end{aligned} \tag{10.48}$$

It is worth noting that this expression is linear with respect to $\boldsymbol{\sigma}$ and φ. Moreover, it is not affected by the pressure distribution.

The magnitude of $\mathbf{e}_a$ is given by

$$|\mathbf{e}_a| = \sqrt{\mathbf{e}_a \cdot \mathbf{e}_a} = (\hat{x}_0 - \hat{x}) \sqrt{(\sigma_x + \varphi\hat{y})^2 + \left(\sigma_y - \varphi\frac{\hat{x}_0 + \hat{x}}{2}\right)^2} \tag{10.49}$$

Expressions (10.48) and (10.49) simplify considerably if $\varphi = 0$, that is $\boldsymbol{\varepsilon} = \boldsymbol{\sigma} = \text{const}$.

Line A–B in Fig. 10.6 shows an example of linear growth ($\boldsymbol{\varepsilon} = \boldsymbol{\sigma}$). According to (10.46), the adhesion state is maintained as far as $k|\mathbf{e}_a| < \mu_0 p$, that is up to $\hat{x}_s = \hat{x}_s(\boldsymbol{\sigma}, \varphi, \hat{y})$ (point B in Fig. 10.6) where

$$|\mathbf{t}| = k\left|\mathbf{e}_a(\hat{x}_s, \hat{y})\right| = \mu_0 p(\hat{x}_s, \hat{y}) \tag{10.50}$$

In the proposed model, as soon as the static friction limit is reached at point $\hat{x} = \hat{x}_s$, the following sudden change in the deflection (massless bristle) occurs

$$\mathbf{e}_s(\hat{x}_s, \hat{y}) = \frac{\mu_1}{\mu_0}\mathbf{e}_a(\hat{x}_s, \hat{y}) \tag{10.51}$$

Therefore, at the transition from adhesion to sliding the deflection preserves its direction, but with a sudden reduction in magnitude (line B–C in Fig. 10.6).

10.3.2.2 Sliding

The sliding state starts with $\mathbf{e}_s(\hat{x}_s, \hat{y})$ as initial condition and evolves according to (10.47). Apparently, (10.47) is a system of two nonlinear first-order ordinary differential equations. However, it can be recast in a simpler, more convenient form

$$\begin{aligned} \mathbf{e}_s \cdot \mathbf{e}_s &= \left(\frac{\mu_1 p}{k}\right)^2 \\ \left(\mathbf{e}_s \times \left(\boldsymbol{\varepsilon} - \mathbf{e}_s'\right)\right) \cdot \mathbf{k} &= 0 \end{aligned} \tag{10.52}$$

that is, using components

$$\begin{aligned} e_x^2 + e_y^2 &= \left(\frac{\mu_1 p}{k}\right)^2 \\ e_x\left(\varepsilon_y - e_y'\right) &= e_y\left(\varepsilon_x - e_x'\right) \end{aligned} \tag{10.53}$$

which is a differential-algebraic system. Indeed, the sliding state requires

- the magnitude of the tangential stress $\mathbf{t}$ to be equal to the kinetic coefficient of friction times the pressure (curved line C–D in Fig. 10.6);
- the direction of $\mathbf{t}$ (and hence of $\mathbf{e}$) to be the same as that of the sliding velocity $\mathbf{V}_\mu = V_r(\boldsymbol{\varepsilon} - \mathbf{e}_s')$.

These are precisely the two conditions stated by (10.52) or (10.53).

Although, in general, the exact solution cannot be obtained by analytical methods, some features of the solution are readily available.

Let $\mathbf{s}$ be a unit vector directed like the sliding velocity $\mathbf{V}_\mu$, that is such that

$$\mathbf{V}_\mu = |\mathbf{V}_\mu|\mathbf{s} \tag{10.54}$$

or, equivalently, $\mathbf{t} = -|\mathbf{t}|\mathbf{s}$ and $\mathbf{e} = -|\mathbf{e}|\mathbf{s}$.

As well known, for any unit vector we have $\mathbf{s} \cdot \mathbf{s}' = 0$, where $\mathbf{s}' = \partial\mathbf{s}/\partial\hat{x}$. Therefore, $\mathbf{m} = \mathbf{s}'/|\mathbf{s}'|$ is a unit vector orthogonal to $\mathbf{s}$ (and hence to $\mathbf{V}_\mu$), and the skating slip $\boldsymbol{\varepsilon}$ can be expressed as

$$\boldsymbol{\varepsilon} = (\boldsymbol{\varepsilon} \cdot \mathbf{s})\mathbf{s} + (\boldsymbol{\varepsilon} \cdot \mathbf{m})\mathbf{m} \tag{10.55}$$

Moreover, according to (10.47)

$$\mathbf{e}_s = -\frac{\mu_1 p}{k}\mathbf{s} \quad \Longrightarrow \quad \mathbf{e}_s' = -\frac{\mu_1 p'}{k}\mathbf{s} - \frac{\mu_1 p}{k}\mathbf{s}' \tag{10.56}$$

Combining (10.54), (10.55) and (10.56) we get

$$\begin{aligned}\frac{\mathbf{V}_\mu}{V_r} &= \frac{|\mathbf{V}_\mu|\mathbf{s}}{V_r} = \boldsymbol{\varepsilon} - \mathbf{e}_s' \\ &= (\boldsymbol{\varepsilon}\cdot\mathbf{s})\mathbf{s} + (\boldsymbol{\varepsilon}\cdot\mathbf{m})\mathbf{m} + \frac{\mu_1 p'}{k}\mathbf{s} + \frac{\mu_1 p}{k}|\mathbf{s}'|\mathbf{m} \\ &= \left(\boldsymbol{\varepsilon}\cdot\mathbf{s} + \frac{\mu_1 p'}{k}\right)\mathbf{s}\end{aligned} \tag{10.57}$$

which shows which terms actually contribute to the sliding velocity.

In most cases, the sliding regime is preserved up to the trailing edge, that is till the end of the contact patch. However, it is interesting to find the conditions that can lead the bristle to switch back to adhesion (point D in Fig. 10.6). From (10.57) it immediately arises that

$$|\mathbf{V}_\mu| = 0 \quad \Longleftrightarrow \quad \boldsymbol{\varepsilon}\cdot\mathbf{s} + \frac{\mu_1 p'}{k} = 0 \tag{10.58}$$

Since $\mathbf{s}$ depends on the solution $\mathbf{e}_s$ of the algebraic-differential system of equations (10.53), this condition has to be checked at each numerical integration step.

The governing equation (10.47) of the sliding state deserves some further discussion. The "annoying" term $(\boldsymbol{\varepsilon} - \mathbf{e}_s')/|\boldsymbol{\varepsilon} - \mathbf{e}_s'|$ is simply equal to $\boldsymbol{\varepsilon}/|\boldsymbol{\varepsilon}|$ if $\mathbf{e}_s$ and $\boldsymbol{\varepsilon}$ are parallel vectors. This observation may suggest the following approximate approach to (10.47)

$$\begin{aligned} k\mathbf{e}_f &= -\mu_1 p\frac{\boldsymbol{\varepsilon} - \mathbf{e}_f'}{|\boldsymbol{\varepsilon}|} \\ k\tilde{\mathbf{e}}_s &= -\mu_1 p\frac{\mathbf{e}_f}{|\mathbf{e}_f|}\end{aligned} \tag{10.59}$$

First we solve two *separate linear* differential equations (not a system) for the two components of the "fictitious" deflection $\mathbf{e}_f$. Then, we obtain the *approximate* deflection $\tilde{\mathbf{e}}_s$ in the sliding region as a vector with magnitude $\mu_1 p/k$ and directed like $\mathbf{e}_f$. We remind that linear first-order differential equations can always be solved by integration (see, e.g., [12, p. 410]).[7] In many cases $\tilde{\mathbf{e}}_s$ is a very good approximation of $\mathbf{e}_s$.

[7] The solution of $y' + f(x)y = g(x)$ is

$$y(x) = \exp\left(-\int^x f(t)\mathrm{d}t\right)\left[\int^x \exp\left(\int^z f(t)\mathrm{d}t\right)g(z)\mathrm{d}z + C\right].$$

An even simpler, less accurate, but often employed idea is to assume that the governing equation in the sliding state is just an algebraic equation

$$k\hat{\mathbf{e}}_s = -\mu_1 p \frac{\boldsymbol{\varepsilon}}{|\boldsymbol{\varepsilon}|} \tag{10.60}$$

Therefore, we allow a sudden discontinuity in the direction of the deflection at the transition from adhesion to sliding. This is not correct, but very appealing because of its simplicity. Of course, as already mentioned, (10.60) is exact if $\mathbf{e}_s$ and $\boldsymbol{\varepsilon}$ happen to be parallel throughout the whole sliding region, that is if $\varphi = 0$ and hence $\boldsymbol{\varepsilon} = \boldsymbol{\sigma}$.

10.3.3 Force-Couple Resultant

The solution of the steady-state brush model shows whether there is adhesion or sliding at each point of the contact patch $\mathscr{P}$ and provides the corresponding bristle deflection $\mathbf{e}_a(\hat{x}, \hat{y})$ or $\mathbf{e}_s(\hat{x}, \hat{y})$. Therefore, the tangential stress $\mathbf{t}$ at each point of $\mathscr{P}$ is

$$\mathbf{t}(\hat{x}, \hat{y}) = \begin{cases} \mathbf{t}_a = k\mathbf{e}_a(\hat{x}, \hat{y}) & \text{(adhesion)} \\ \mathbf{t}_s = k\mathbf{e}_s(\hat{x}, \hat{y}) & \text{(sliding)} \end{cases} \tag{10.61}$$

Like in (2.15) and (10.3), the tangential force $\mathbf{F}_t = F_x\mathbf{i} + F_y\mathbf{j}$ that the road applies on the tire model is given by the integral of $\mathbf{t}$ over the contact patch

$$\mathbf{F}_t(\boldsymbol{\sigma}, \varphi) = \int_{-b}^{b} \mathrm{d}\hat{y} \int_{-\hat{x}_0(\hat{y})}^{\hat{x}_0(\hat{y})} \mathbf{t}(\hat{x}, \hat{y})\mathrm{d}\hat{x} \tag{10.62}$$

which is a function, among other things, of the global slips $\boldsymbol{\sigma}$ and φ.[8]

It may be convenient to use the nondimensional or *normalized* tangential force $\mathbf{F}_t^n$ and its components [7]

$$\mathbf{F}_t^n = F_x^n\mathbf{i} + F_y^n\mathbf{j} = \frac{\mathbf{F}_t}{F_z} = \frac{F_x\mathbf{i} + F_y\mathbf{j}}{F_z} \tag{10.63}$$

Of course, under whichever operating condition of the brush model, we always have $|\mathbf{F}_t^n| < \mu_0$. It is quite interesting to find the combination of σ_x, σ_y and φ which provides the highest possible value. Equations (2.76) and (2.78) address a similar issue in an experimental context.

The overall moment of the tangential stresses with respect to point D is given by

$$M_z^D(\boldsymbol{\sigma}, \varphi)\mathbf{k} = \int_{-b}^{b} \mathrm{d}\hat{y} \int_{-\hat{x}_0(\hat{y})}^{\hat{x}_0(\hat{y})} (\hat{x}\mathbf{i} + \hat{y}\mathbf{j}) \times \mathbf{t}(\hat{x}, \hat{y})\mathrm{d}\hat{x} \tag{10.64}$$

[8] Since the tangential force is constant in time, it is possible to exploit its dependence on the given slips.

However, in general, we are more interested in the vertical moment (usually called self-aligning torque) M_z, that is the moment with respect to the origin O of S. According to (10.5) and (10.10), we have to take into account the effects of the carcass compliance and of camber (Fig. 2.11) to locate D with respect to O

$$\begin{aligned} M_z(\gamma, \boldsymbol{\sigma}, \varphi) &= M_z^D - F_x\big(c_r(\gamma) + q_y\big) + F_y q_x \\ &= M_z^D - F_x\left(c_r(\gamma) + \frac{F_y}{w_y}\right) + F_y\frac{F_x}{w_x} \\ &= M_z^D - F_x c_r(\gamma) + F_x F_y \frac{w_y - w_x}{w_x w_y} \end{aligned} \tag{10.65}$$

To gain insights into the steady-state brush model behavior, we will address some particular cases. Some of them can be solved analytically, while others require a numerical approach.

The shape of the contact patch is taken to be rectangular or elliptical, although it would not be much more difficult to deal with more realistic shapes, like the one in the center of Fig. 10.2.

Figure 10.7, obtained with the data listed in (10.43), shows the tangential stress pattern in rectangular contact patches, along with the adhesion and sliding regions, for four combinations of $(\sigma_x, \sigma_y, \varphi)$. The corresponding values of the normalized longitudinal and lateral forces are also reported. As typical in car tires, the value of φ is small.

Similarly, in Fig. 10.8, four cases for elliptical contact patches are shown. The spin slip is quite high, as typical in motorcycle tires.

10.4 Adhesion Everywhere (Linear Behavior)

If the magnitude of the skating slip $\boldsymbol{\varepsilon}$ is everywhere very small, then there is adhesion almost everywhere on the contact patch. More precisely, small skating slips means

$$|\boldsymbol{\varepsilon}| \ll \frac{\mu_0 p_0}{2ak} \tag{10.66}$$

that is $|\boldsymbol{\varepsilon}| < 0.03$ on a dry paved road.

According to (10.48) and (10.62), the tangential force is

$$\begin{aligned} \mathbf{F}_t(\boldsymbol{\sigma}, \varphi) &= F_x\mathbf{i} + F_y\mathbf{j} \\ &= \int_{-b}^{b} \mathrm{d}\hat{y} \int_{-\hat{x}_0(\hat{y})}^{\hat{x}_0(\hat{y})} k\mathbf{e}_a(\hat{x}, \hat{y})\mathrm{d}\hat{x} \end{aligned}$$

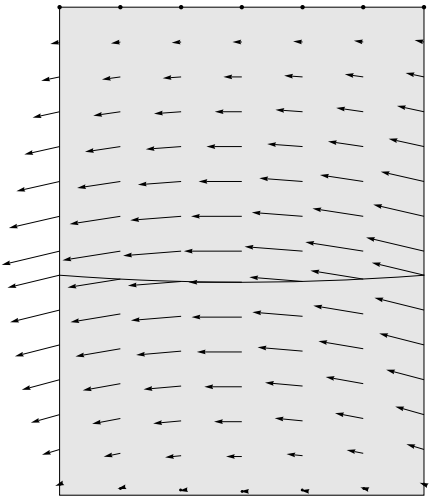

(a) $(\sigma_x, \sigma_y, \varphi) = (0, -0.1, 0.5)$, $(F_x^n, F_y^n) = (0, 0.77)$

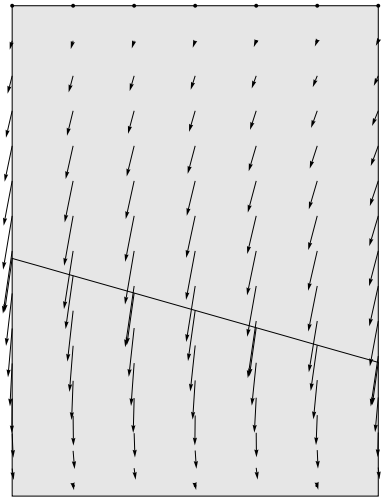

(b) $(\sigma_x, \sigma_y, \varphi) = (0.1, 0, 0.5)$, $(F_x^n, F_y^n) = (-0.69, 0.11)$

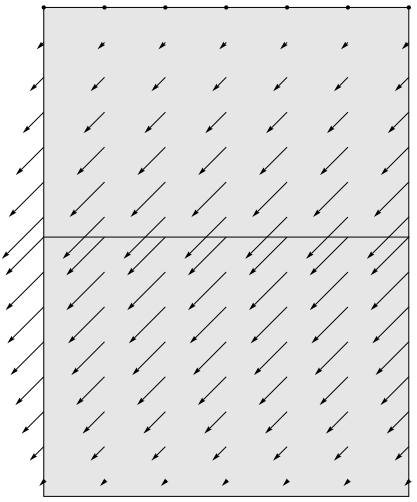

(c) $(\sigma_x, \sigma_y, \varphi) = (0.1, -0.1, 0)$, $(F_x^n, F_y^n) = (-0.57, 0.57)$

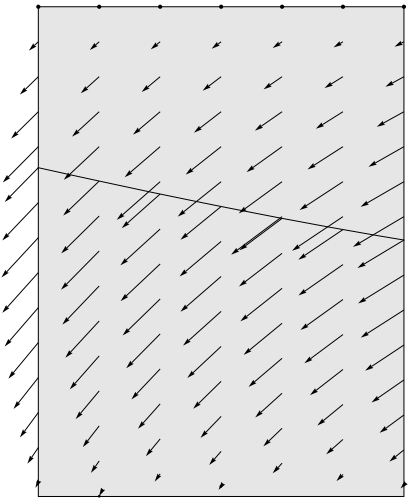

(d) $(\sigma_x, \sigma_y, \varphi) = (0.1, -0.1, 0.5)$, $(F_x^n, F_y^n) = (-0.54, 0.63)$

Fig. 10.7 Examples of tangential stress distributions in rectangular contact patches. Also shown the *line* separating the adhesion region (*top*) and the sliding region (*bottom*). Values of φ are in m^{-1}

$$
\begin{aligned}
&= \int_{-b}^{b} \mathrm{d}\hat{y} \int_{-\hat{x}_0}^{\hat{x}_0} k\left(-\boldsymbol{\sigma}(\hat{x}_0 - \hat{x}) + \varphi\left[\frac{(\hat{x}_0 - \hat{x})(\hat{x}_0 + \hat{x})}{2}\mathbf{j} - \hat{y}(\hat{x}_0 - \hat{x})\mathbf{i}\right]\right)\mathrm{d}\hat{x} \\
&= -C_\sigma \boldsymbol{\sigma} + C_\varphi \varphi \mathbf{j} \\
&= -C_\sigma \sigma_x \mathbf{i} - (C_\sigma \sigma_y - C_\varphi \varphi)\mathbf{j}
\end{aligned} \tag{10.67}
$$

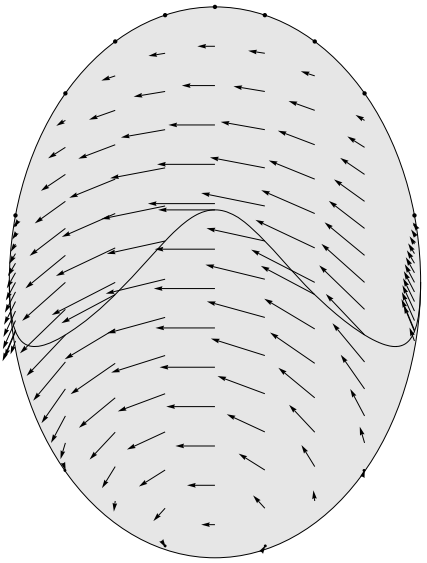

(a) $(\sigma_x, \sigma_y, \varphi) = (0, -0.05, 2.5)$,
$(F_x^n, F_y^n) = (0, 0.70)$

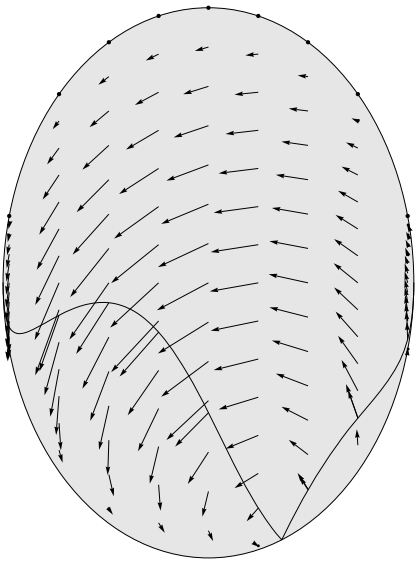

(b) $(\sigma_x, \sigma_y, \varphi) = (0.05, 0, 2.5)$,
$(F_x^n, F_y^n) = (-0.29, 0.47)$

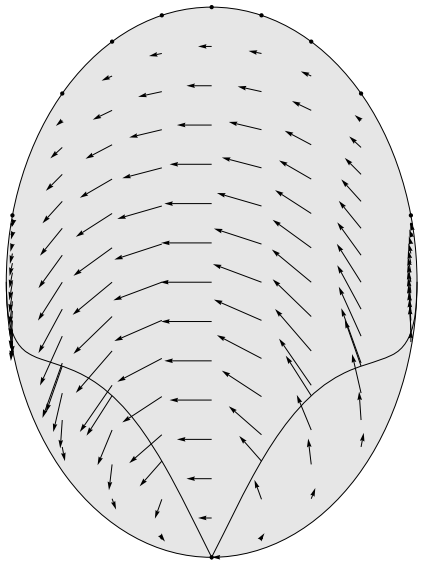

(c) $(\sigma_x, \sigma_y, \varphi) = (0, 0, 2.5)$,
$(F_x^n, F_y^n) = (0, 0.50)$

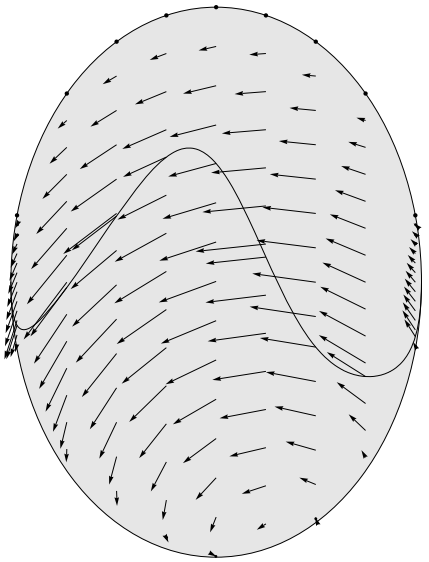

(d) $(\sigma_x, \sigma_y, \varphi) = (0.05, -0.05, 2.5)$,
$(F_x^n, F_y^n) = (-0.25, 0.66)$

Fig. 10.8 Examples of tangential stress distributions in elliptical contact patches. Also shown the *line* separating the adhesion region (*top*) and the sliding region(s) (*bottom*). Values of φ are in m^{-1}

which, as expected, is linear in both $\boldsymbol{\sigma}$ and φ. The longitudinal force F_x is a function of σ_x only, whereas the lateral force F_y depends on both σ_y and φ.

The coefficient C_σ may be called *slip stiffness*. In the brush model, C_σ is the same for any direction of the tangential force, that is for any combination of σ_x and σ_y. Moreover, in the brush model

$$C_\sigma = C_\alpha = C_{\kappa_x} \tag{10.68}$$

where C_α and C_{κ_x} were defined in (2.77) and (2.75).

The coefficient C_φ is the *spin stiffness* for the lateral force. Owing to the symmetric shape of the contact patch, the spin slip does not contribute to the longitudinal force.

It is possible to insert (2.66) and (2.67), that is the practical slip components, into (10.67), but the resulting function is no longer linear

$$\mathbf{F}_t(\boldsymbol{\kappa}, \varphi) = F_x\mathbf{i} + F_y\mathbf{j} = -C_\sigma \frac{\kappa_x\mathbf{i} + \kappa_y\mathbf{j}}{1 - \kappa_x} + C_\varphi\varphi\mathbf{j} \tag{10.69}$$

Once again, the practical slip does not do a good job.

As shown in (2.60), if the yaw rate ω_z is zero or at least negligible (as discussed at p. 33), the spin slip φ becomes a function of γ only (besides F_z). In this case, we can define the *camber stiffness* C_γ

$$C_\gamma = -\frac{C_\varphi}{r_r}(1 - \varepsilon_r) < 0 \tag{10.70}$$

and obtain ($\sin\gamma \approx \gamma$)

$$\mathbf{F}_t(\boldsymbol{\sigma}, \gamma) = F_x\mathbf{i} + F_y\mathbf{j} = -C_\sigma(\sigma_x\mathbf{i} + \sigma_y\mathbf{j}) + C_\gamma\gamma\mathbf{j} \tag{10.71}$$

Typically, $F_z/C_\gamma \approx 1$ for a motorcycle tire. Quite often, $-C_\sigma\sigma_y\mathbf{j}$ is called *cornering force* and $C_\gamma\gamma\mathbf{j}$ is called *camber force* (or camber thrust). Obviously, only under the very strong assumption of adhesion all over the contact patch, that is for very small values of the skating slip $\boldsymbol{\varepsilon}$, we have two separate and independent contributions to the lateral force.

Under the same conditions and according to (10.65) we can compute the vertical moment with respect to the center D of the contact patch

$$\begin{aligned} M_z^D(\sigma_y, \varphi)\mathbf{k} &= \int_{-b}^{b} \mathrm{d}\hat{y} \int_{-\hat{x}_0(\hat{y})}^{\hat{x}_0(\hat{y})} (\hat{x}\mathbf{i} + \hat{y}\mathbf{j}) \times k\mathbf{e}_a(\hat{x}, \hat{y})\mathrm{d}\hat{x} \\ &= (C_{M_\sigma}\sigma_y + C_{M_\varphi}\varphi)\mathbf{k} = -F_y t_c\mathbf{k} \end{aligned} \tag{10.72}$$

where t_c is the *pneumatic trail* with respect to the contact center D. The last expression states quite a remarkable fact: that $F_y = 0$ means $M_z^D = 0$ as well. The minus sign makes $t_c > 0$ under standard operating conditions.

Combining (10.65), (10.67) and (10.72) we obtain the vertical moment with respect to point O

$$M_z(\gamma, \boldsymbol{\sigma}, \varphi) = C_{M_\sigma}\sigma_y + C_{M_\varphi}\varphi + C_\sigma \sigma_x \left[c_r(\gamma) + \frac{w_x - w_y}{w_x w_y}(-C_\sigma \sigma_y + C_\varphi \varphi) \right] \tag{10.73}$$

For a *rectangular* contact patch (i.e., $x_0(\hat{y}) = a$) we have

$$C_\sigma = 4ka^2 b \tag{10.74}$$

and

$$C_\varphi = C_{M_\sigma} = \frac{a}{3} C_\sigma, \qquad C_{M_\varphi} = \frac{b^2}{3} C_\sigma, \qquad C_\gamma = -\frac{a(1-\varepsilon_r)}{3r_r} C_\sigma \tag{10.75}$$

Typically, $C_\gamma \ll |C_\sigma|$. From (10.67), (10.72) and (10.75) we can obtain the pneumatic trail t_c for a rectangular contact patch

$$t_c = \frac{\sigma_y a + \varphi b^2}{3(\sigma_y - \varphi a)} \tag{10.76}$$

Special, but quite important cases are $\varphi = 0$, which yields

$$t_c = \frac{a}{3} \tag{10.77}$$

and $\sigma_y = 0$

$$t_c = -\frac{b^2}{3a} \tag{10.78}$$

For an *elliptical* contact patch the algebra is a bit more involved. The final expression of the tangential force $\mathbf{F}_t$ is exactly like in (10.67), but with the following stiffnesses

$$C_\sigma = \frac{8}{3} ka^2 b \quad \text{and} \quad C_\varphi = C_{M_\sigma} = \frac{3\pi a}{32} C_\sigma \tag{10.79}$$

10.5 Wheel with Pure Translational Slip ($\sigma \neq 0$, $\varphi = 0$)

The investigation of the steady-state behavior of the brush model is quite a simple matter if there is no spin slip φ.

According to (10.44), if $\varphi = 0$ all points in the contact patch $\mathscr{P}$ have the same skating slip $\boldsymbol{\varepsilon}$, which is simply equal to $\boldsymbol{\sigma}$

$$\boldsymbol{\varepsilon} = \boldsymbol{\sigma} \tag{10.80}$$

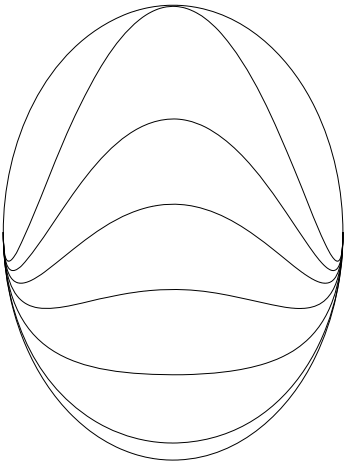

Fig. 10.9 *Lines* separating the adhesion region (*top*) and the sliding region (*bottom*) for $\sigma = (0.01, 0.05, 0.10, 0.15, 0.20, 0.266)$ and $\varphi = 0$. Pressure distribution as in (10.17)

Therefore, the governing equation (10.46) in the *adhesion* region becomes

$$\mathbf{e}_a' = \boldsymbol{\sigma} = \text{const} \tag{10.81}$$

whose solution, which is a linear function of $\hat{x}$, is readily obtained as a special case of (10.48)

$$\mathbf{e}_a(\hat{x}, \hat{y}) = -\boldsymbol{\sigma}\big(\hat{x}_0(\hat{y}) - \hat{x}\big) = -\sigma\mathbf{s}\big(\hat{x}_0(\hat{y}) - \hat{x}\big) \tag{10.82}$$

All vectors $\mathbf{e}_a$ have the same constant direction $\mathbf{s} = \boldsymbol{\sigma}/\sigma$, with $\sigma = |\boldsymbol{\sigma}|$.

Like in (10.50), the adhesion state is maintained up to $\hat{x}_s = \hat{x}_s(\sigma, \hat{y})$, which marks the point where the friction limit is reached

$$k\big|\mathbf{e}_a(\hat{x}_s, \hat{y})\big| = \kappa\sigma\big(\hat{x}_0(\hat{y}) - \hat{x}_s\big) = \mu_0 p(\hat{x}_s, \hat{y}) \tag{10.83}$$

For the parabolic pressure distribution (10.12) we obtain

$$\hat{x}_s(\sigma, \hat{y}) = \hat{x}_0(\hat{y})\left[\frac{\kappa\hat{x}_0(\hat{y})}{\mu_0 p_0(\hat{y})}\sigma - 1\right] \tag{10.84}$$

It is worth noting that, if $\varphi = 0$, the line separating the adhesion and the sliding regions depends solely on the magnitude σ of the slip. It is not affected by the direction $\mathbf{s}$ of $\boldsymbol{\sigma}$. Figure 10.9 shows, for an elliptical contact patch, the lines between adhesion and sliding for a sequence of growing values of σ.

At $\hat{x}_s$ the friction coefficient switches to its kinetic value μ_1 and the sliding state starts according to (10.51), that is with

$$k\mathbf{e}_s(\hat{x}_s, \hat{y}) = -\mu_1 p(\hat{x}_s, \hat{y})\mathbf{s} \tag{10.85}$$

The really important aspect is that sliding begins with the bristle deflection $\mathbf{e}_a$ that has already the *same constant direction* $\mathbf{s}$ as $\boldsymbol{\varepsilon} = \boldsymbol{\sigma}$. Therefore, also $\mathbf{e}_s'$ is directed

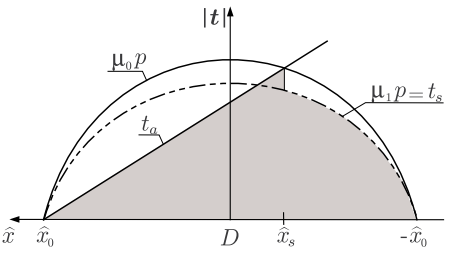

Fig. 10.10 Typical pattern of the tangential stress in the adhesion region (*left*) and in the sliding region (*right*)

like $\mathbf{s}$, and the governing equation (10.47) (or (10.52)) for the *sliding* region becomes simply

$$k\mathbf{e}_s(\hat{x},\hat{y}) = -\mu_1 p(\hat{x},\hat{y})\mathbf{s} \tag{10.86}$$

which is no longer a differential equation. Actually this is already the definition of $\mathbf{e}_s$ in the sliding region.

Equations (10.82) and (10.86) provide the complete solution for this case. Therefore, the tangential stress $\mathbf{t}$ at each point of the contact patch $\mathscr{P}$ is given by

$$\mathbf{t}(\hat{x},\hat{y}) = \begin{cases} \mathbf{t}_a = -t_a\mathbf{s} = -\sigma k(\hat{x}_0(\hat{y}) - \hat{x})\mathbf{s}, & \text{(adhesion)} \\ \mathbf{t}_s = -t_s\mathbf{s} = -\mu_1 p(\hat{x},\hat{y})\mathbf{s}, & \text{(sliding)} \end{cases} \tag{10.87}$$

where $\mathbf{s} = \boldsymbol{\sigma}/\sigma$, $t_a = |\mathbf{t}_a|$ and $t_s = |\mathbf{t}_s|$. Actually, as in Fig. 10.10, we have assumed that, for any $\mathbf{y}$, a single adhesion region ($\hat{x}_s(\sigma,\hat{y}) \le \hat{x} \le \hat{x}_0(\hat{y})$) is followed by a single sliding region ($-\hat{x}_0(\hat{y}) \le \hat{x} < \hat{x}_s(\sigma,\hat{y})$), as it is normally the case. However, as shown in Fig. 10.6 for a fairly unrealistic pressure distribution, it is possible, at least in principle, to have multiple regions.

Summing up, we have the following features (Fig. 10.10):

- the tangential stress $\mathbf{t}$ is directed like $\boldsymbol{\sigma}$, with opposite sign;
- t_a grows linearly in the adhesion region;
- t_s follows the $\mu_1 p$ pattern in the sliding region;
- both t_a and t_s are not affected by the direction of $\boldsymbol{\sigma}$;
- the higher σ, the steeper the growth of t_a and hence the closer the transition point $\hat{x}_s$ to the leading edge $\hat{x}_0$.

All these features can be appreciated in Figs. 10.11 and 10.12, which show the tangential stress pattern, as predicted by the brush model, in rectangular and elliptical contact patches under pure translational slip $\boldsymbol{\sigma}$.

The global tangential force $\mathbf{F}_t = F_x\mathbf{i} + F_y\mathbf{j}$ that the road applies to the tire model is given by the integral of $\mathbf{t}$ on the contact patch, like in (10.62). Of course, here the analysis will provide $\mathbf{F}_t(\boldsymbol{\sigma}, 0)$. Since all tangential stresses $\mathbf{t}$ have the same direction $-\mathbf{s}$, the computation simply amounts to integrating $|\mathbf{t}|$ (shaded area in Fig. 10.10)

$$\mathbf{F}_t = -\mathbf{s}F_t(\sigma) = -\mathbf{s}\left[\int_{-b}^{b} \mathrm{d}\hat{y} \int_{\hat{x}_s(\sigma,\hat{y})}^{\hat{x}_0(\hat{y})} t_a(\sigma,\hat{x},\hat{y})\mathrm{d}\hat{x} + \int_{-b}^{b} \mathrm{d}\hat{y} \int_{-\hat{x}_0(\hat{y})}^{\hat{x}_s(\sigma,\hat{y})} t_s(\hat{x},\hat{y})\mathrm{d}\hat{x}\right] \tag{10.88}$$

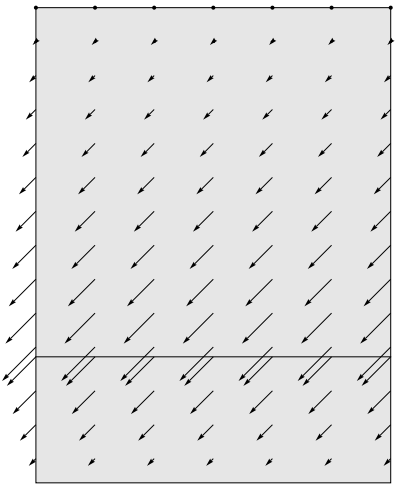

(a) $(\sigma_x, \sigma_y, \varphi) = (0.05, -0.05, 0)$,
$(F_x^n, F_y^n) = (-0.41, 0.41)$

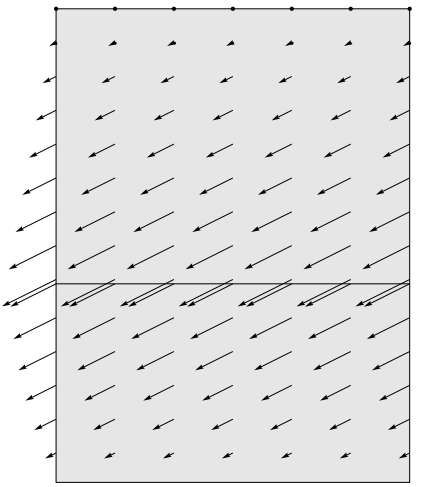

(b) $(\sigma_x, \sigma_y, \varphi) = (0.05, -0.10, 0)$,
$(F_x^n, F_y^n) = (-0.33, 0.66)$

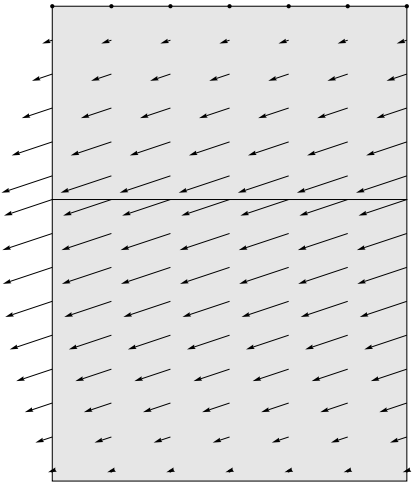

(c) $(\sigma_x, \sigma_y, \varphi) = (0.05, -0.15, 0)$,
$(F_x^n, F_y^n) = (-0.26, 0.78)$

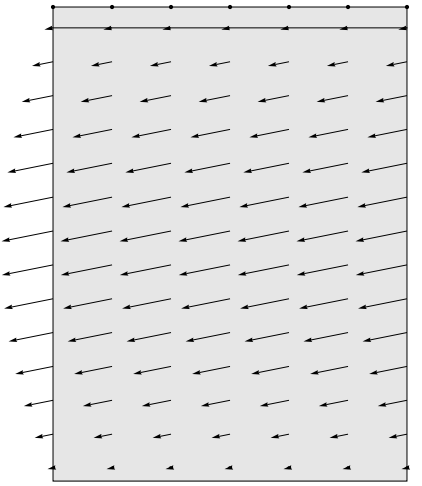

(d) $(\sigma_x, \sigma_y, \varphi) = (0.05, -0.25, 0)$,
$(F_x^n, F_y^n) = (-0.16, 0.82)$

Fig. 10.11 Examples of tangential stress distributions in rectangular contact patches under *pure translational slip* $\boldsymbol{\sigma}$. Also shown is the *line* separating the adhesion region (*top*) and the sliding region (*bottom*)

where $F_t = |\mathbf{F}_t|$. The two components, that is the longitudinal force F_x and the lateral force F_y, are given by

$$F_x = F_x(\sigma_x, \sigma_y) = -\frac{\sigma_x}{\sigma} F_t(\sigma), \qquad F_y = F_y(\sigma_x, \sigma_y) = -\frac{\sigma_y}{\sigma} F_t(\sigma) \tag{10.89}$$

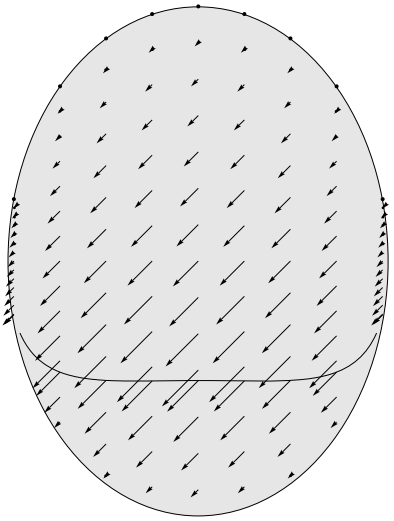

(a) $(\sigma_x, \sigma_y, \varphi) = (0.05, -0.05, 0)$,
$(F_x^n, F_y^n) = (-0.36, 0.36)$

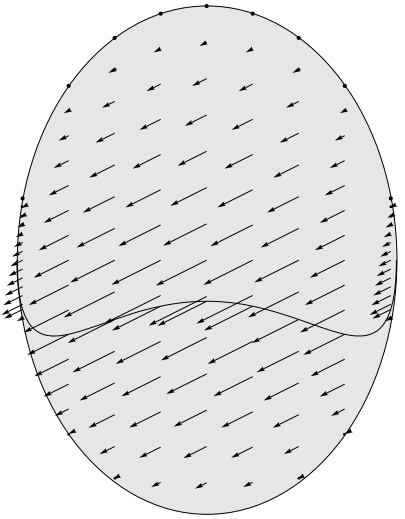

(b) $(\sigma_x, \sigma_y, \varphi) = (0.05, -0.10, 0)$,
$(F_x^n, F_y^n) = (-0.30, 0.60)$

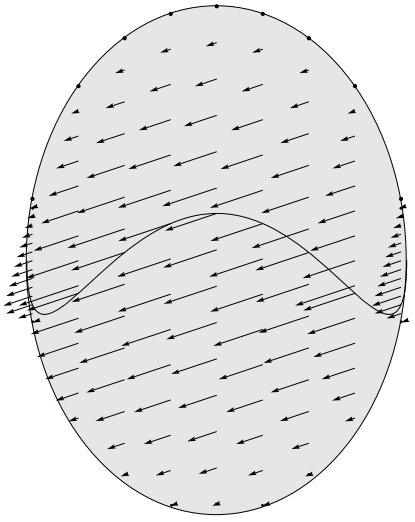

(c) $(\sigma_x, \sigma_y, \varphi) = (0.05, -0.15, 0)$,
$(F_x^n, F_y^n) = (-0.25, 0.76)$

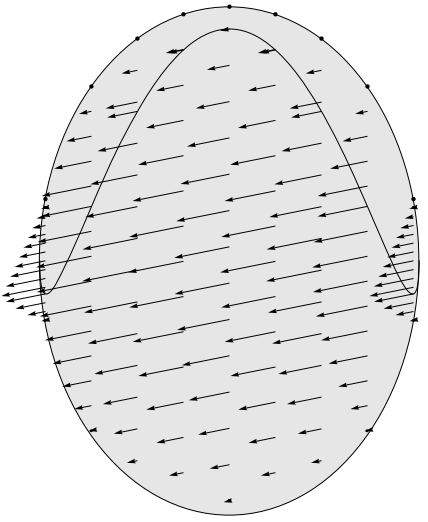

(d) $(\sigma_x, \sigma_y, \varphi) = (0.05, -0.25, 0)$,
$(F_x^n, F_y^n) = (-0.16, 0.81)$

Fig. 10.12 Examples of tangential stress distributions in elliptical contact patches under *pure translational slip* $\boldsymbol{\sigma}$. Also shown is the *line* separating the adhesion region (*top*) and the sliding region (*bottom*)

which imply $\sigma_x / F_x = \sigma_y / F_y$.

Summing up, in the brush model with $\varphi = 0$, the magnitude $F_t(\sigma)$ of the tangential force $\mathbf{F}_t$ depends on the magnitude $\sigma = \sqrt{\sigma_x^2 + \sigma_y^2}$ of the translational slip. The vectors $\mathbf{F}_t$ and $\boldsymbol{\sigma}$ have the same direction, but opposite signs.

Partial derivatives can be readily obtained from (10.89)

$$\begin{aligned} -\frac{\partial F_x}{\partial \sigma_x} &= \frac{\partial}{\partial \sigma_x}\left(\frac{\sigma_x}{\sigma} F_t(\sigma)\right) = \left(\frac{\sigma_x}{\sigma}\right)^2 \left(F_t' - \frac{F_t}{\sigma}\right) + \frac{F_t}{\sigma}, \\ -\frac{\partial F_x}{\partial \sigma_y} &= \frac{\partial}{\partial \sigma_y}\left(\frac{\sigma_x}{\sigma} F_t(\sigma)\right) = \left(\frac{\sigma_x \sigma_y}{\sigma^2}\right)\left(F_t' - \frac{F_t}{\sigma}\right) \end{aligned} \tag{10.90}$$

Those of F_y simply need interchanging x and y.

Equation (10.64) provides the vertical moment M_z^D with respect to point D. However, it can be considerably simplified in the case of $\varphi = 0$. As a matter of fact, we see from (10.87) that $\mathbf{t}(\hat{x}, \hat{y}) = \mathbf{t}(\hat{x}, -\hat{y})$[9] and hence

$$M_z^D(\sigma_x, \sigma_y) = -\frac{\sigma_y}{\sigma}\left[\int_{-b}^{b} \mathrm{d}\hat{y} \int_{\hat{x}_s(\sigma,\hat{y})}^{\hat{x}_0(\hat{y})} \hat{x} t_a(\sigma, \hat{x}, \hat{y}) \mathrm{d}\hat{x} + \int_{-b}^{b} \mathrm{d}\hat{y} \int_{-\hat{x}_0(\hat{y})}^{\hat{x}_s(\sigma,\hat{y})} \hat{x} t_s(\hat{x}, \hat{y}) \mathrm{d}\hat{x}\right] \tag{10.91}$$

It may be convenient to recast this equation in the following form

$$M_z^D(\sigma_x, \sigma_y) = \frac{\sigma_y}{\sigma} F_t(\sigma) t_c(\sigma) = -F_y(\sigma_x, \sigma_y) t_c(\sigma) \tag{10.92}$$

which is, indeed, the definition of the *pneumatic trail* t_c, that is the (signed) distance from the contact center D of the line of action of the lateral force $F_y \mathbf{j}$. A positive t_c stands for a lateral force behind D, which is the standard case.

10.5.1 Rectangular Contact Patch

Assuming a rectangular shape (Fig. 10.2) essentially means setting $\hat{x}_0(\hat{y}) = a$ as the equation of the leading edge. Therefore, any dependence on $\hat{y}$ disappears and the problem becomes one-dimensional, that is $\mathbf{e}_a = \mathbf{e}_a(\hat{x})$ and $\mathbf{e}_s = \mathbf{e}_s(\hat{x})$.

As shown in Fig. 10.11, in this case the line between the adhesion and the sliding regions is simply a straight line directed like $\mathbf{j}$

$$\hat{x}_s(\sigma) = a\left(\frac{\kappa a}{\mu_0 p_0}\sigma - 1\right) = a\left(2\frac{\sigma}{\sigma_s} - 1\right) \tag{10.93}$$

where

$$\sigma_s = \frac{2\mu_0 p_0}{ka} = \frac{3\mu_0 F_z}{C_\sigma} = \frac{\mu_0}{k}\left|p'(a)\right| \tag{10.94}$$

[9] If, as usual, also $\hat{x}_0(\hat{x}, \hat{y}) = \hat{x}_0(\hat{x}, -\hat{y})$ and $p(\hat{x}, \hat{y}) = p(\hat{x}, -\hat{y})$.

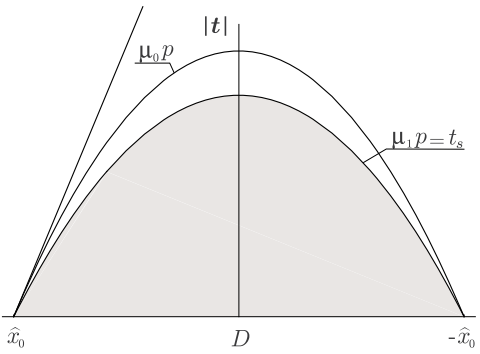

Fig. 10.13 Tangential stress if $\sigma = \sigma_s$ (total sliding)

If $\sigma \geq \sigma_s$, regardless of the direction of $\boldsymbol{\sigma}$, there is sliding on the whole rectangular contact patch, that is $\hat{x}_s = a$. For instance, with the numerical values of (10.43) at p. 302, we have $\sigma_s = 0.27$, that is a fairly low value. At first, it may be surprising to have full sliding without wheel locking (i.e., $\sigma = \infty$). The phenomenon is explained in Fig. 10.13: to have total sliding it suffices that the straight line to be tangent to the upper parabola at the leading edge. The value (10.94) of σ_s predicted by the brush model is therefore quite "weak", in the sense that it is very much affected by the assumed pressure distribution. However, the existence of full sliding without (necessarily) wheel locking is an important result.

Application of (10.88) with $\hat{x}_0 = a$ and $\hat{x}_s(\sigma)$ as in (10.93) (and hence $0 \leq \sigma \leq \sigma_s$), provides the expression of the magnitude F_t of the tangential force

$$F_t = F_t(\sigma) = C_\sigma \sigma \left[1 - \frac{\sigma}{\sigma_s} \left(\frac{1+2\chi}{1+\chi} \right) + \left(\frac{\sigma}{\sigma_s} \right)^2 \left(\frac{1+3\chi}{3(1+\chi)} \right) \right] \tag{10.95}$$

where $\mu_0 = (1+\chi)\mu_1$ as in (10.21). In this model and under these specific operating conditions, $F_t(\sigma)$ is a polynomial function of σ, whose typical behavior is shown in Fig. 10.14, along with its linear approximation ("good" only up to $\sigma \approx 0.03$). From Fig. 10.15 we can also appreciate how the adhesion and sliding regions contribute separately to build up the total tangential force.

The derivative of $F_t(\sigma)$ is

$$F_t'(\sigma) = \frac{\mathrm{d}F_t}{\mathrm{d}\sigma} = C_\sigma \left[1 - 2\frac{\sigma}{\sigma_s} \left(\frac{1+2\chi}{1+\chi} \right) + \left(\frac{\sigma}{\sigma_s} \right)^2 \left(\frac{1+3\chi}{1+\chi} \right) \right] \tag{10.96}$$

which, among other things, clearly provides the important result

$$\left. \frac{\mathrm{d}F_t}{\mathrm{d}\sigma} \right|_{\sigma=0} = C_\sigma \tag{10.97}$$

As expected, the force with total sliding is

$$F_t(\sigma_s) = \mu_1 F_z \tag{10.98}$$

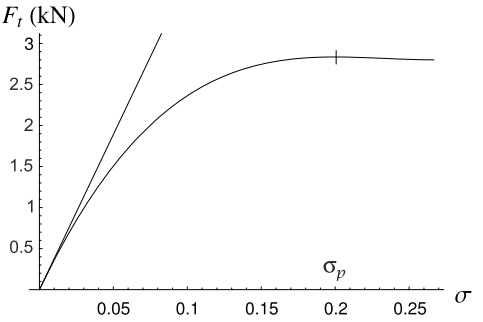

Fig. 10.14 Magnitude F_t of the tangential force as a function of σ, and corresponding linear approximation

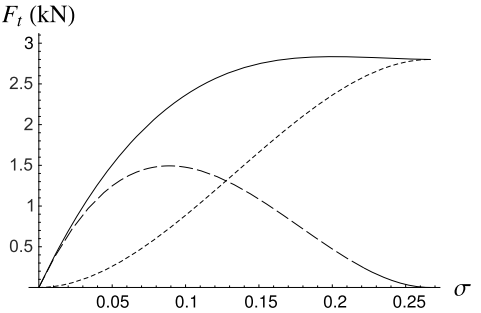

Fig. 10.15 Contributions to F_t (*solid line*) of the adhesion region (*long-dashed line*) and of the sliding region (*short-dashed line*)

since all tangential stresses $\mathbf{t}$ have the same direction.

The peak value of F_t is

$$F_t^{\max} = F_t(\sigma_p) = \mu_0 \left[\frac{4 - 3(\mu_1/\mu_0)}{[3 - 2(\mu_1/\mu_0)]^2} \right] F_z = \mu_1 \left[1 + \frac{4\chi^3}{(3\chi + 1)^2} \right] F_z = \mu_p F_z \tag{10.99}$$

and it is achieved at $\sigma = \sigma_p$ (Fig. 10.14)

$$\sigma_p = \frac{1 + \chi}{1 + 3\chi} \sigma_s \tag{10.100}$$

Typically, as in Fig. 10.14, good tires have low values of σ_p. In this model, the global friction coefficient μ_p is given by (cf. (2.76) and (2.78))

$$\mu_p = \frac{F_t^{\max}}{F_z} = \mu_1 \left[1 + \frac{4\chi^3}{(3\chi + 1)^2} \right] \tag{10.101}$$

which means that, as expected

$$\mu_1 < \mu_p \ll \mu_0 \tag{10.102}$$

For instance, if $\mu_0 = 1.2\mu_1$, we have $F_t^{\max} = 0.84\mu_0 F_z = 1.013\mu_1 F_z$, that is a value only marginally higher than $F_t(\sigma_s)$. Indeed, as shown in Fig. 10.16, the mechanics of the tire makes it very difficult to have tangential stresses close to $\mu_0 p$. In practical terms, attempts at increasing μ_1 are more worthwhile than those at increasing μ_0.

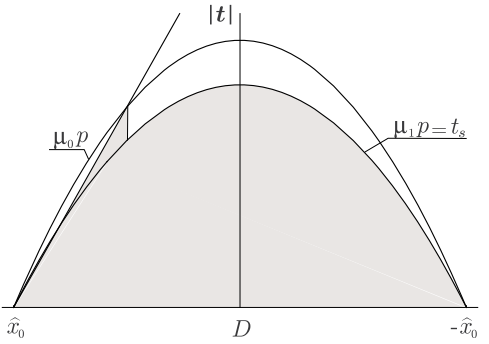

Fig. 10.16 Tangential stress if $\sigma = \sigma_p$ (maximum tangential force)

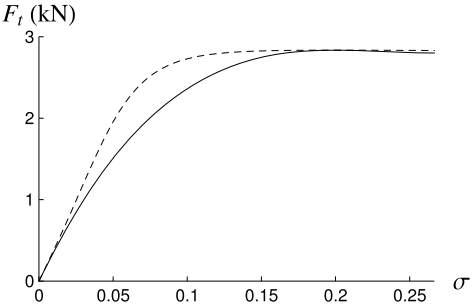

Fig. 10.17 Brush model curve (*solid line*) and the corresponding classical fitting by the Magic Formula (*dashed line*)

It may be interesting to fit the curve of $F_t(\sigma)$ shown in Fig. 10.14 by means of the Magic Formula $y(x)$ given in (2.79). According to Sect. 2.10, the four unknown coefficients can be obtained by matching the peak value $y_m = F_t(\sigma_p) = 2.84$ kN, the asymptotic value $y_a = F_t(\sigma_s) = 2.80$ kN, the slope at the origin $y'(0) = C_\sigma = 37.8$ kN/rad and the abscissa of the peak value $x_m = \sigma_p = 0.2$. The resulting coefficients are $B = 12.1$, $C = 1.10$, $D = 2.835$ kN and $E = -3.63$. The comparison is shown in Fig. 10.17. The agreement between the two curves is quite poor. Particularly unacceptable is the initial increase of the slope, which is never found in experimental curves (cf. Figs. 2.15 and 2.17). Indeed, $E < -(1 + C^2/2)$ and hence $y'''(0) > 0$.

A better agreement is shown in Fig. 10.18, where the asymptotic value was arbitrarily lowered to $y_a = 0.7 F_t(\sigma_s)$, thus obtaining $B = 8.81$, $C = 1.51$, $D = 2.84$ kN and $E = 0.1$. The lesson to be learnt is, perhaps, that the Magic Formula may occasionally provide unexpected results and, therefore, should be used with care.

Going back to the brush model, the explicit expressions of $F_x(\sigma_x, \sigma_y)$ and $F_y(\sigma_x, \sigma_y)$, that is of the longitudinal and lateral components, can be obtained by inserting (10.95) into (10.89). Figure 10.19 illustrates the combined effect of σ_x and σ_y. Quite remarkable is the effect on the slope at the origin, that is on the generalized slip stiffness $\widetilde{C}_\sigma$. From (10.90) and (10.95) it follows that

$$\widetilde{C}_\sigma(\sigma_y) = -\left.\frac{\partial F_x}{\partial \sigma_x}\right|_{\sigma_x=0} = C_\sigma \left[1 - \frac{|\sigma_y|}{\sigma_s}\frac{1+2\chi}{1+\chi} + \left(\frac{\sigma_y}{\sigma_s}\right)^2 \frac{1+3\chi}{3(1+\chi)}\right] \tag{10.103}$$

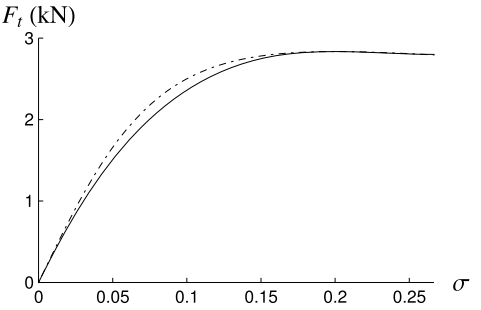

Fig. 10.18 Brush model curve (*solid line*) and another possible fitting by the Magic Formula (*dot-dashed line*)

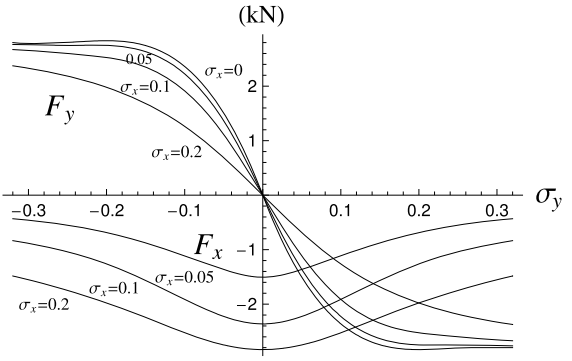

Fig. 10.19 F_y and F_x as functions of σ_y, for $\sigma_x = (0, 0.05, 0.1, 0.2)$

and, interchanging x and y

$$\widetilde{C}_\sigma(\sigma_x) = -\left.\frac{\partial F_y}{\partial \sigma_y}\right|_{\sigma_y=0} = C_\sigma\left[1 - \frac{|\sigma_x|}{\sigma_s}\frac{1+2\chi}{1+\chi} + \left(\frac{\sigma_x}{\sigma_s}\right)^2 \frac{1+3\chi}{3(1+\chi)}\right] \tag{10.104}$$

Of course $\widetilde{C}_\sigma(0) = C_\sigma$. This stiffness reduction has strong practical implications on the handling behavior of vehicles.

It should be observed that the generalized cornering stiffness $\widetilde{C}_\alpha(\sigma_x)$ is no longer equal to $\widetilde{C}_\sigma(\sigma_x)$ (cf. (10.68))

$$\widetilde{C}_\alpha(\sigma_x) = (1+\sigma_x)\widetilde{C}_\sigma(\sigma_x) \tag{10.105}$$

whereas $\widetilde{C}_{\kappa_x}(\sigma_y) = \widetilde{C}_\sigma(\sigma_y)$.

Another useful plot is the one shown in Fig. 10.20. For any combination of (σ_x, σ_y), a point in the plane (F_x, F_y) is obtained such that $\sigma_x/\sigma_y = F_x/F_y$. All these points fall within a circle of radius $F_t^{\max}$, usually called the *friction circle*. Lines with constant σ_y are also drawn in Fig. 10.20. Because of the symmetry of this tire model, lines with constant σ_x are identical, but rotated of 90 degrees around the origin.

More often, the plot employed is the one in Fig. 10.21, where lines with constant slip angle α are drawn. Since α is a function of σ_x and σ_y (Eq. (2.69)), the two plots contain exactly the same information. While the lines in Fig. 10.20 are symmetric

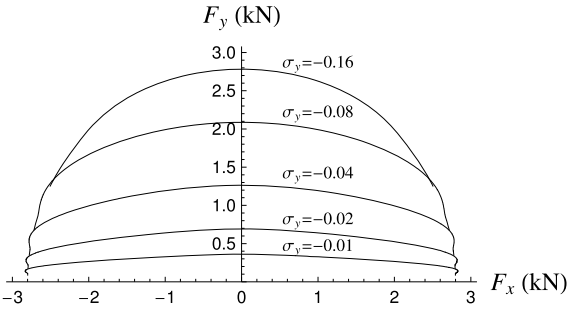

Fig. 10.20 Friction circle with lines at constant σ_y

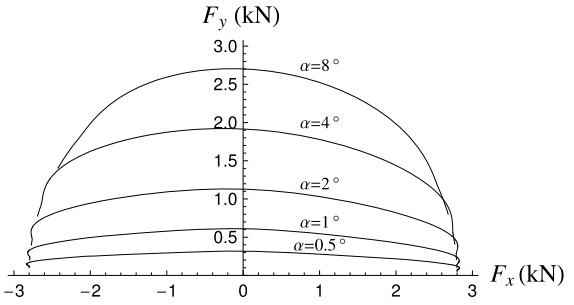

Fig. 10.21 Friction circle of Fig. 10.20, but with lines at constant α

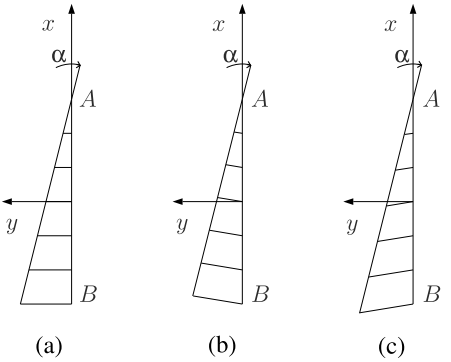

Fig. 10.22 Same slip angle α with (**a**) $\sigma_x = 0$, (**b**) $\sigma_x < 0$ (driving), (**c**) $\sigma_x > 0$ (braking)

with respect to the vertical axis, lines in Fig. 10.21 are not. The asymmetry arises simply because the slip angle is not the parameter to be used for a neat description of the tire mechanics. Indeed, as schematically shown in Fig. 10.22, the bristles may have different lateral deformations under the same slip angle.

As already mentioned at p. 31, tires have to be built in such a way to provide the maximum tangential force $\mathbf{F}_t$ *in any direction* with small slip angles α, as shown in Fig. 10.23. This is a fundamental requirement for a wheel with tire to behave almost like a wheel, that is to have a *directional capability*. In other words, while $\mathbf{F}_t$ can have any direction, the speed of travel $\mathbf{V}_c$ must undergo just small deviations α. According to (2.69), this condition will be fulfilled if and only if the tire exhibits the peak value of $\mathbf{F}_t$ for small values of the theoretical slip σ_p, typically below 0.2. On

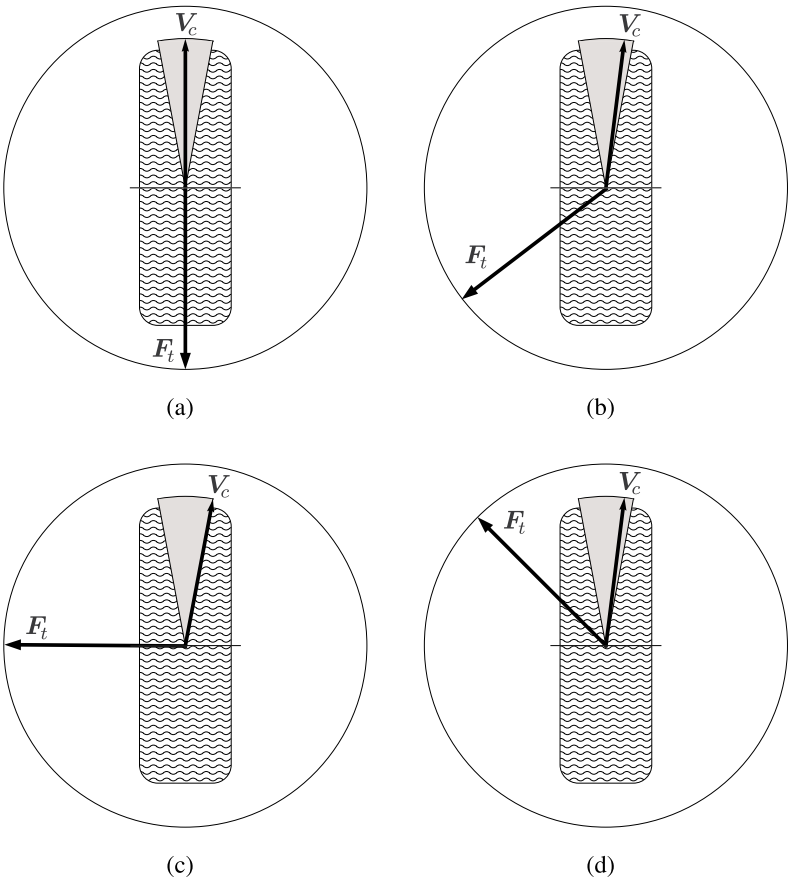

Fig. 10.23 Typical relationships between the tangential force $\mathbf{F}_t$ and the speed of travel $\mathbf{V}_c$ for a tire rolling with theoretical slip $0 < \sigma < \sigma_p$

the contrary, in a locked wheel the two vectors $\mathbf{F}_t$ and $\mathbf{V}_c$ always point in opposite directions.

Equation (10.91), with $\hat{x}_0 = a$ and $\hat{x}_s$ as in (10.93), provides the vertical moment M_z^D with respect to the center D of the rectangular contact patch

$$M_z^D(\sigma_x, \sigma_y) = \sigma_y C_\sigma \frac{a}{3}\left[1 - 3\frac{\sigma}{\sigma_s}\frac{1+2\chi}{1+\chi} + 3\left(\frac{\sigma}{\sigma_s}\right)^2 \frac{1+3\chi}{1+\chi} - \left(\frac{\sigma}{\sigma_s}\right)^3 \frac{1+4\chi}{1+\chi}\right]$$
$$= \frac{\sigma_y}{\sigma} F_t(\sigma) t_c(\sigma) = -F_y(\sigma_x, \sigma_y) t_c(\sigma) \tag{10.106}$$

where t_c is the pneumatic trail. The typical behavior of M_z^D is shown in Fig. 10.24.

However, under combined slip conditions, to obtain M_z with respect to point O it is necessary to take into account the *carcass compliance*, according to (10.65).

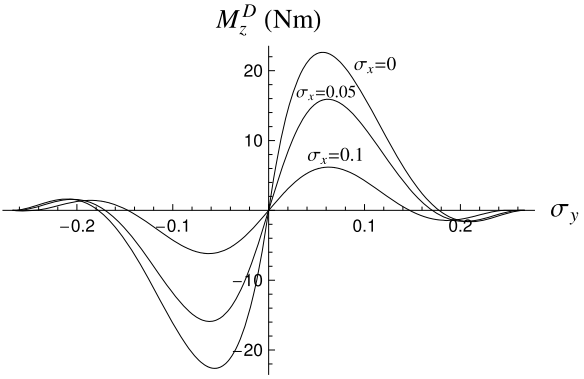

Fig. 10.24 Vertical moment M_z^D versus σ_y, at constant σ_x

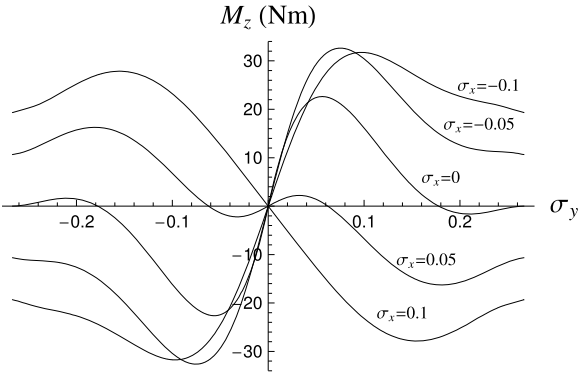

Fig. 10.25 Vertical moment M_z versus σ_y, at constant σ_x and $\gamma = 0$

The typical behavior of $M_z(\sigma_x, \sigma_y)$ is shown in Fig. 10.25. The difference with Fig. 10.24 is quite relevant.

Also of practical interest may be the plots of M_z vs F_x (Fig. 10.26) and of F_y vs $-M_z$ (Fig. 10.27), this one being often called *Gough plot* if $\sigma_x = 0$.

The three functions $F_x(\sigma_x, \sigma_y)$, $F_y(\sigma_x, \sigma_y)$ and $M_z(\sigma_x, \sigma_y)$ can be seen as the parametric equations of a three-dimensional surface that fully describes, at constant vertical load F_z, the tire mechanical behavior. Such surface is shown in Fig. 10.28(a), along with its three projections, which are precisely like Figs. 10.19, 10.26 and 10.27, respectively. The surface in Fig. 10.28(a) is called here the *tire action surface*.

As already mentioned, a wheel with tire can be called a wheel because:

(1) the tire action surface is regular, in the sense that it does not fold onto itself, for a limited set of values (σ_x, σ_y). It has therefore a limited contour and, hence, the slip angle α is always quite low, according to (2.69). The goal of ABS [10] is to avoid wheel locking and also to keep $|\alpha|$ very low, thus maintaining the *directional capability* of the wheels;
(2) the vertical moment M_z is always moderate. A wheel must provide forces applied not far from the center of the contact patch.

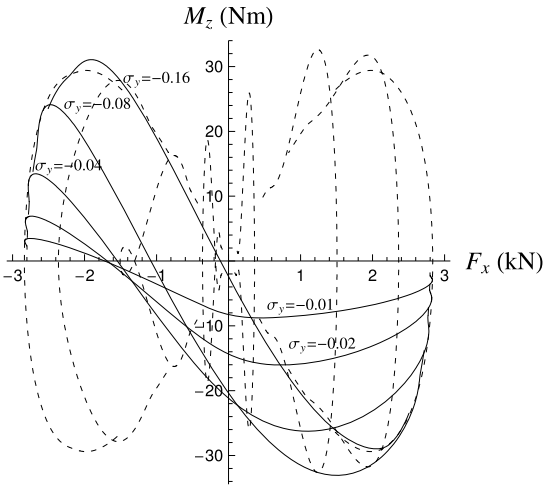

Fig. 10.26 Vertical moment M_z versus longitudinal force F_x, with lines at constant σ_y (*solid*) and constant σ_x (*dashed*: ± 0.01, ± 0.05, ± 0.1, ± 0.2)

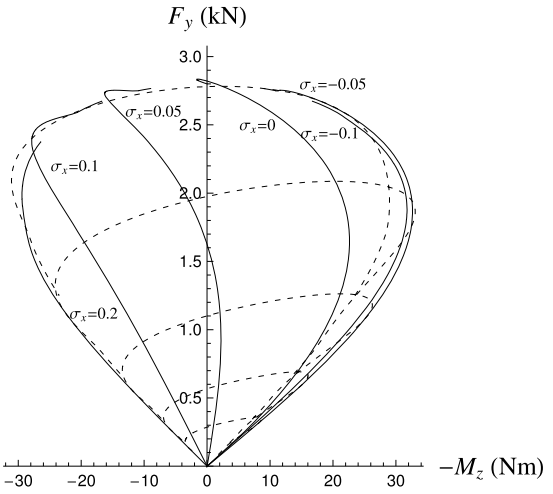

Fig. 10.27 Lateral force F_y versus vertical moment M_z, with lines at constant σ_x (*solid*) and constant σ_y (*dashed*: -0.01, -0.02, -0.04, -0.08, -0.16)

10.5.2 Elliptical Contact Patch

Assuming an elliptical shape (Fig. 10.2) essentially means setting $\hat{x}_0(\hat{y})$ according to (10.2). As shown in Figs. 10.9 and 10.12, in this case the line between the adhesion and the sliding regions is *curved*. Its explicit equation is obtained inserting (10.2) into (10.84). To have sliding on the whole elliptical contact patch, a very high value of σ is necessary (Fig. 10.9).

Application of (10.88) with suitable $\hat{x}_0(\hat{y})$ and $\hat{x}_s(\sigma, \hat{y})$ provides the expression of the magnitude F_t of the tangential force

$$F_t = F_t(\sigma) = C_\sigma \sigma \left[1 - \frac{18\pi}{64} \frac{\sigma}{\sigma_s} \left(\frac{1+2\chi}{1+\chi} \right) + \frac{12}{45} \left(\frac{\sigma}{\sigma_s} \right)^2 \left(\frac{1+3\chi}{1+\chi} \right) \right] \quad (10.107)$$

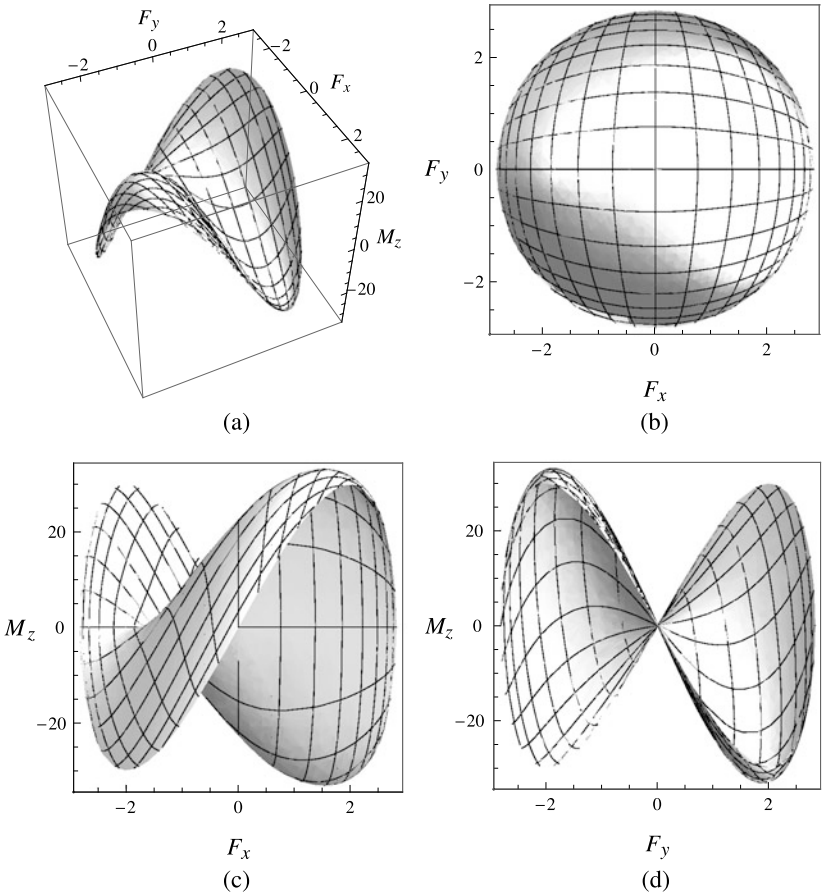

Fig. 10.28 Tire action surface for $\sigma < \sigma_p$, and its three projections (forces in kN and moments in Nm)

where C_σ was obtained in (10.79) and σ_s is as in (10.94), although it has no special meaning in this case. Again, $F_t(\sigma)$ is a polynomial function of σ, whose typical behavior is much like in Fig. 10.14, but with a less evident peak.

10.6 Wheel with Pure Spin Slip ($\sigma = 0$, $\varphi \neq 0$)

The investigation of the behavior of the brush model becomes much more involved if there is *spin slip* φ. Even if $\boldsymbol{\sigma} = \mathbf{0}$, the problem in the sliding region has to be solved in full generality according to the governing equations (10.53). Therefore, numerical solutions have to be sought.

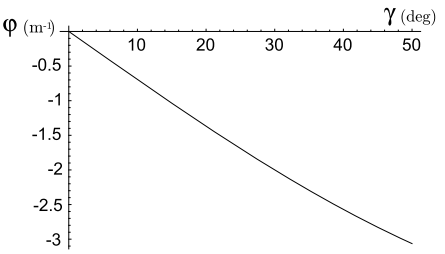

Fig. 10.29 Relationship between the camber angle γ and the spin slip φ, if $\omega_z = 0$, $\varepsilon_r = 0$ and $r_r = 0.25$ m

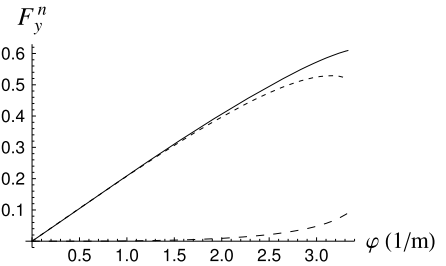

Fig. 10.30 Normalized lateral force versus spin slip (*solid line*). Also shown is the contribution of the adhesion zone (*short-dashed line*) and of the sliding zone (*long-dashed line*)

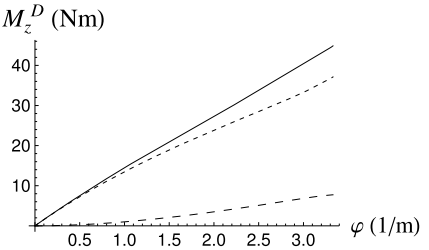

Fig. 10.31 Vertical moment versus spin slip (*solid line*). Also shown is the contribution of the adhesion zone (*short-dashed line*) and of the sliding zone (*long-dashed line*)

The definition of φ was given in (2.57) and is repeated here

$$\varphi = -\frac{\omega_z + \omega_c \sin\gamma\,(1 - \varepsilon_r)}{\omega_c r_r} \tag{2.57'}$$

It involves ω_z, $\sin\gamma$, ε_r, ω_c and r_r. However, in most applications spin slip means camber angle γ, since $\omega_z/\omega_c \approx 0$. Figure 10.29 reports an example of the relationship between γ and φ, if $\varepsilon_r = 0$ (motorcycle tire), $r_r = 0.25$ m and $\omega_z = 0$.

Large values of φ are attained only in motorcycles.[10] Therefore, in this section the analysis is restricted to *elliptical* contact patches. Figure 10.30 shows the almost linear growth of the (normalized) lateral force $F_y^n(\mathbf{0}, \varphi) = F_y^n(\varphi) = F_y/F_z$, even for very large values of the spin slip. A similar pattern can be observed in Fig. 10.31 for the vertical moment $M_z^D = M_z$. In both cases, the main contribution comes from the adhesion regions.

[10]More generally, in tilting vehicles, which may have three wheels, like *MP3* by *Piaggio*, or even four.

The lateral force plotted in Fig. 10.30 is precisely what is usually called the *camber force*, that is the force exerted by the road on a tire under pure spin slip.

Some examples of tangential stress distributions are shown in Fig. 10.32. They are quite informative. There is adhesion along the entire central line, and the stress has a parabolic pattern. The value of φ does not affect the direction of the arrows in the adhesion region, but only their magnitude. Even at $\varphi = 3.33\ \mathrm{m}^{-1}$, i.e. a very high value, the two symmetric sliding regions have spread only on less than half the contact patch.

Another important observation is that there are longitudinal components of the tangential stress, although the longitudinal force $F_x = 0$. In some sense, these components are wasted, and keeping them as low as possible is a goal in the design of real tires.

The comparison of Figs. 10.32(d) and 10.33 gives an idea of the effect of the shape of the contact patch. In the second case the lengths of the axes have been inverted, while all other parameters are unchanged. Nevertheless, the normalized lateral force is much lower (0.36 vs 0.61).

In the brush model developed here, the lateral force and the vertical moment depend on φ, but not directly on γ. Therefore, there is no distinction between operating conditions with the same spin slip φ, but different camber angle γ as in Fig. 2.14. This is a limitation of the model with respect to what stated at p. 32.

It should be appreciated that a cambered wheel under pure spin slip cannot be in free rolling conditions. According to (2.11), there must be a torque $\mathbf{T} = M_z \sin\gamma\,\mathbf{j}_c = T\mathbf{j}_c$ with respect to the wheel axis. Conversely, $T = 0$ requires a longitudinal force F_x and hence a longitudinal slip σ_x.

10.7 Wheel with Both Translational and Spin Slips

From the tire point of view, there are fundamentally two kinds of vehicles: cars, trucks and the like, whose tires may operate at relatively large values of translational slip and small values of spin slip, and motorcycles, bicycles and other tilting vehicles, whose tires typically operate with high camber angles and small translational slips. In both cases, the interaction between $\boldsymbol{\sigma}$ and φ in the mechanics of force generation is of great practical relevance. The tuning of a vehicle often relies on the right balance between these kinematical quantities.

10.7.1 Rectangular Contact Patch

Rectangular contact patches mimic those of car tires. Therefore, we will address the effect of just a bit of spin slip on the lateral force of a wheel mainly subjected to lateral slips. The goal is to achieve the highest possible value of F_y^n. Unfortunately, it is not possible to obtain analytical results and a numerical approach has to be pursued.

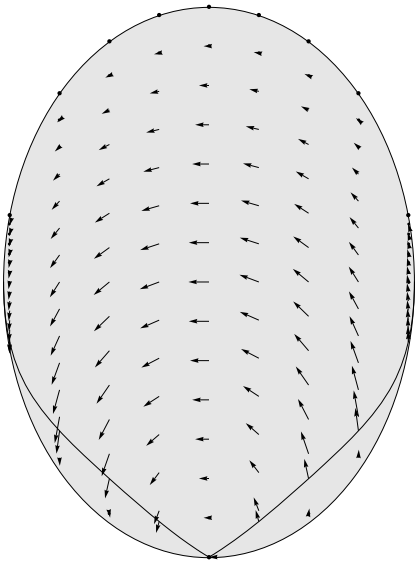

(a) $(\sigma_x, \sigma_y, \varphi) = (0, 0, 1.0)$,
$(F_x^n, F_y^n) = (0, 0.21)$

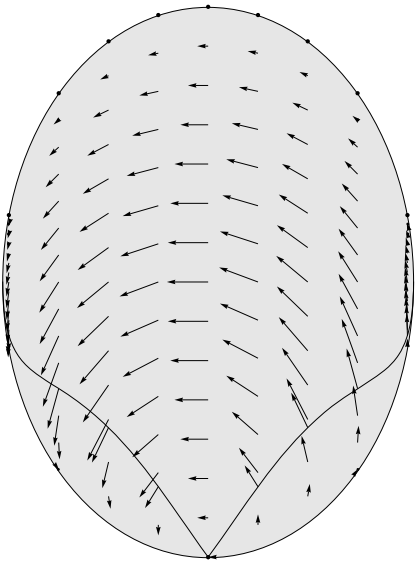

(b) $(\sigma_x, \sigma_y, \varphi) = (0, 0, 2.0)$,
$(F_x^n, F_y^n) = (0, 0.41)$

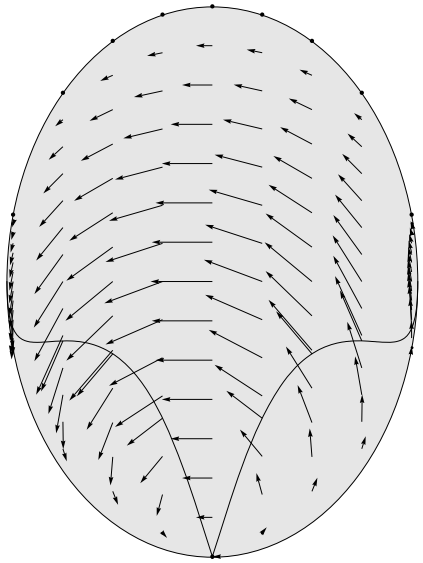

(c) $(\sigma_x, \sigma_y, \varphi) = (0, 0, 3.0)$,
$(F_x^n, F_y^n) = (0, 0.57)$

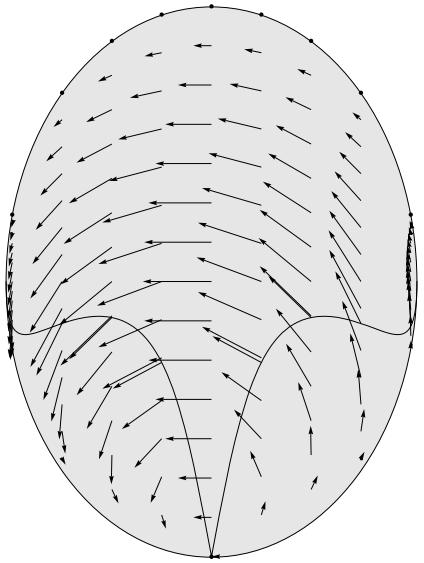

(d) $(\sigma_x, \sigma_y, \varphi) = (0, 0, 3.33)$,
$(F_x^n, F_y^n) = (0, 0.61)$

Fig. 10.32 Examples of tangential stress distributions in elliptical contact patches under *pure spin slip* φ. Also shown is the *line* separating the adhesion region (*top*) and the two sliding regions (*bottom*). Values of φ are in m^{-1}

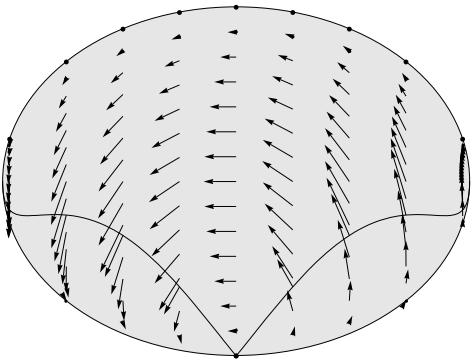

Fig. 10.33 Elliptical contact patch with inverted proportions. $(\sigma_x, \sigma_y, \varphi) = (0, 0, 3.33)$, $(F_x^n, F_y^n) = (0, 0.36)$

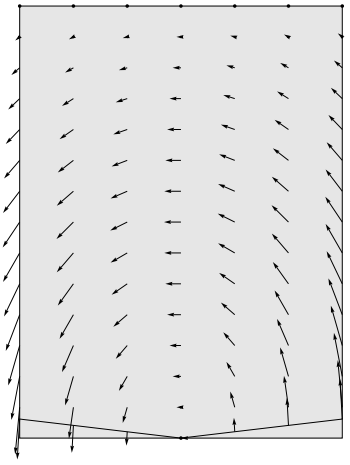

Fig. 10.34 Rectangular contact patch under pure spin slip (*arrows* magnified by a factor 5 with respect to the other figures). $(\sigma_x, \sigma_y, \varphi) = (0, 0, 0.21)$, $(F_x^n, F_y^n) = (0, 0.06)$

A rectangular contact patch under pure spin slip (arrows magnified by a factor 5) is shown in Fig. 10.34. The global effect is a small lateral force, usually called camber force.

Indeed, as shown in Fig. 10.35, the effect of a small amount of spin slip φ is, basically, to translate *horizontally* the curve of the lateral force versus σ_y.[11] However, the peak value is also affected, as more clearly shown in Fig. 10.36. By means of a trial-and-error procedure it has been found, in the case at hand, that $\varphi = 0.21\ \mathrm{m}^{-1}$ does indeed provide the highest positive value of F_y^n. In general, car tires need just a few degrees of camber to provide the highest lateral force as a function of the lateral slip σ_y (Fig. 10.37).

Such small values of spin slip have very little influence on longitudinal force generation.

[11] Of course, the effect cannot be to "add" the camber force, that is to translate the curve vertically.

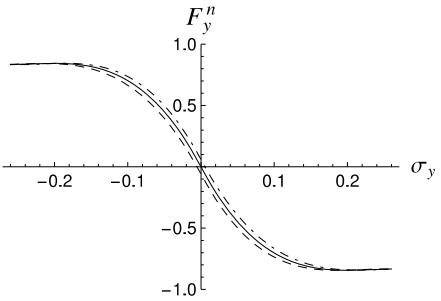

Fig. 10.35 Normalized lateral force F_y^n versus σ_y, for $\varphi = 0$ (*solid line*), $\varphi = -0.21\ \mathrm{m}^{-1}$ (*dashed line*), $\varphi = 0.21\ \mathrm{m}^{-1}$ (*dot-dashed line*). $\sigma_x = 0$ in all cases

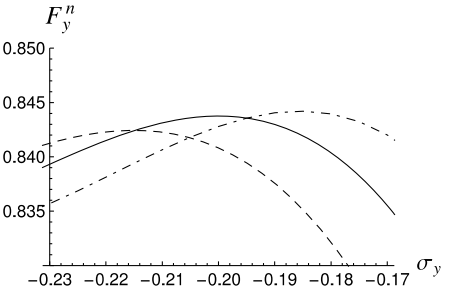

Fig. 10.36 Detail of Fig. 10.35 showing different peak values

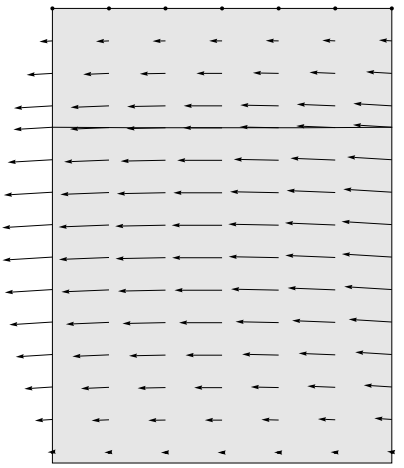

Fig. 10.37 Rectangular contact patch under lateral and spin slips. $(\sigma_x, \sigma_y, \varphi) = (0, -0.185, 0.21)$, $(F_x^n, F_y^n) = (0, 0.84)$

10.7.2 Elliptical Contact Patch

Elliptical contact patches mimic those of motorcycle tires. Therefore, in this case we will study the effect of just a bit of lateral slip σ_y on the lateral force of a cambered wheel. Again, the goal is to achieve the highest possible value of F_y^n.

The large effect of even a small amount of σ_y on the normalized lateral force F_y^n as a function of φ is shown in Fig. 10.38. However, this is quite an expected result

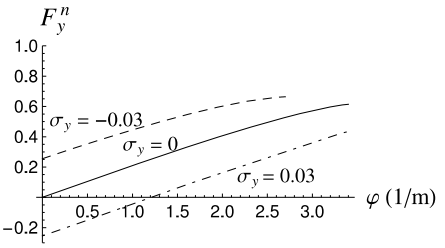

Fig. 10.38 Normalized lateral force vs spin slip, at different values of lateral slip

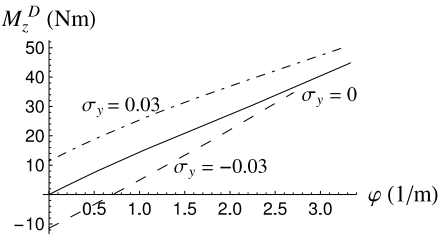

Fig. 10.39 Vertical moment vs spin slip, at different values of lateral slip

after (10.79). Consistently, also the vertical moment M_z^D changes a lot under the influence of small variations of σ_y (Fig. 10.39).

Figure 10.40 provides a pictorial representation of the tangential stress in two relevant cases, that is those that yield the highest lateral force. Quite remarkably, a 10 % higher value of F_y^n is achieved in case (b) with respect to case (a). In general, a little σ_y has a great influence on the stress distribution in the contact patch. Conversely, the same lateral force can be obtained by infinitely many combinations (σ_y, φ). This is something most riders know intuitively. Obviously, $F_x = 0$ in all cases of Fig. 10.40.

Under these operating conditions, according to (2.69), the slip angle α never exceeds two degrees. Therefore, the wheel has excellent directional capability.

It should be observed that the larger value of F_y^n of case (b) in Fig. 10.40 is associated with a smaller value of M_z^D. Basically, it means that the tangential stress distribution in the contact patch is *better organized* to yield the lateral force, without wasting much in the vertical moment (mainly due to useless longitudinal stress components). The comparison shown in Fig. 10.40(c) confirms this conclusion.

A lateral slip in the "wrong" direction, like in Fig. 10.40(d), yields a reduction of the lateral force and an increase of the vertical moment.

As reported in Figs. 10.38 and 10.39, there are particular combinations of (σ_y, φ) which provide either $F_y^n = 0$ or $M_z^D = 0$. The stress distributions in such two cases are shown in Fig. 10.41.

The interaction of longitudinal slip σ_x and spin slip φ yields the effects reported in Fig. 10.42 on the longitudinal and lateral forces. A fairly high value $\sigma_x = -0.15$ has been employed. Examples of stress distributions are given in Fig. 10.43.

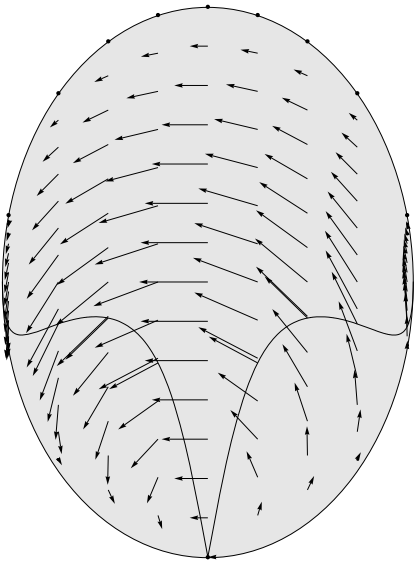

(a) $(\sigma_x, \sigma_y, \varphi) = (0, 0, 3.33)$,
$F_y^n = 0.61$, $M_z^D = 44.9$ Nm

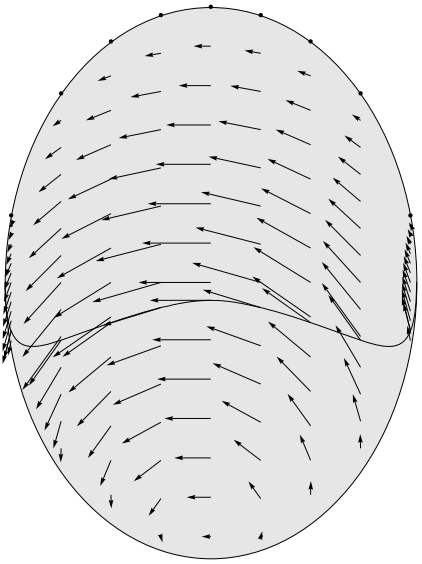

(b) $(\sigma_x, \sigma_y, \varphi) = (0, -0.03, 2.7)$,
$F_y^n = 0.66$, $M_z^D = 34.7$ Nm

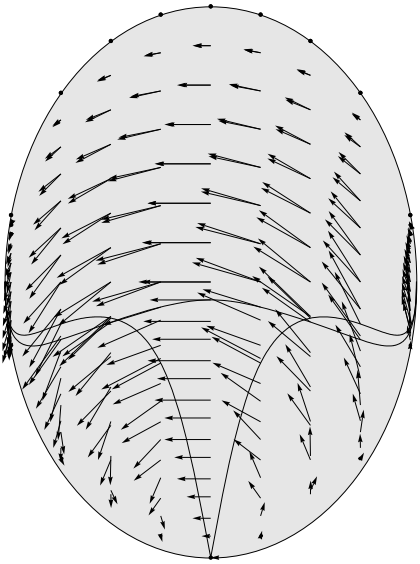

(c) Comparison of (a) and (b)

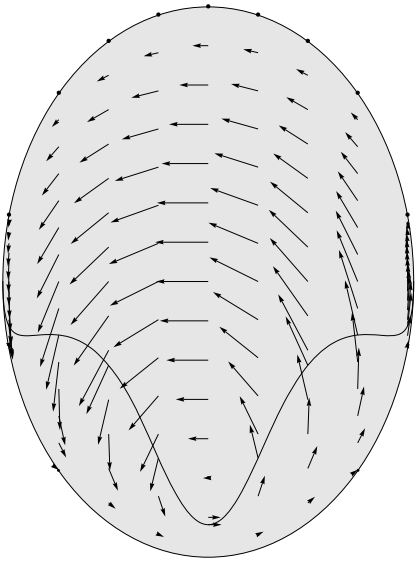

(d) $(\sigma_x, \sigma_y, \varphi) = (0, 0.03, 3.33)$,
$F_y^n = 0.42$, $M_z^D = 50.4$ Nm

Fig. 10.40 Comparison between contact patches under (**a**) large spin slip only and (**b**) still quite large spin slip with the addition of a little of lateral slip. Case (**d**) shown for completeness. Values of φ are in m^{-1}

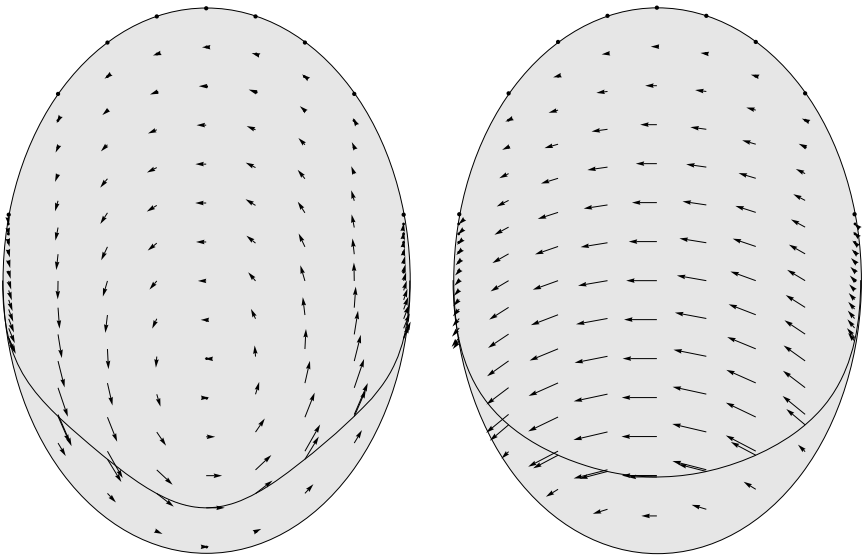

(a) $(\sigma_x, \sigma_y, \varphi) = (0, 0.03, 1.21)$, $F_y^n = 0$, $M_z^D = 28.0\,\text{Nm}$

(b) $(\sigma_x, \sigma_y, \varphi) = (0, -0.03, 0.70)$, $F_y^n = 0.39$, $M_z^D = 0$

Fig. 10.41 Special cases: (**a**) zero lateral force and (**b**) zero vertical moment

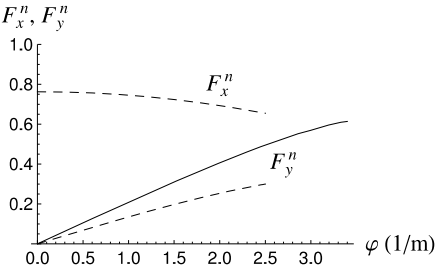

Fig. 10.42 Normalized longitudinal and lateral forces vs spin slip, at $\sigma_x = 0$ (*solid line*) and $\sigma_x = -0.15$ (*dashed lines*)

10.8 Brush Model Transient Behavior

Understanding and describing the transient behavior of wheels with tires has become increasingly important with the advent of electronic systems like ABS [10] or traction control, which may impose very rapidly varying slip conditions (up to tens of cycles per second).

Addressing the problem in its full generality like in Sect. 10.2, even in the simple brush model, looks prohibitive. However, with the aid of some additional simplifying assumptions, some interesting results can be achieved which, at least, give some hints on what is going on when a tire is under transient operating conditions.

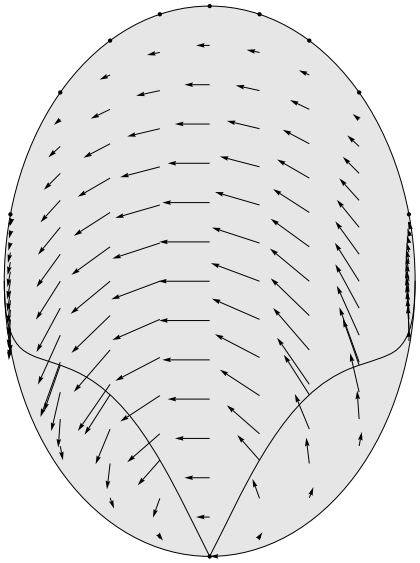

(a) $(\sigma_x, \sigma_y, \varphi) = (0, 0, 2.5)$,
$(F_x^n, F_y^n) = (0, 0.50)$

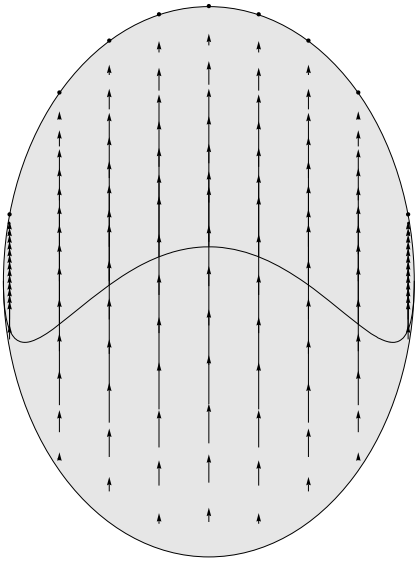

(b) $(\sigma_x, \sigma_y, \varphi) = (-0.15, 0, 0)$,
$(F_x^n, F_y^n) = (0.76, 0)$

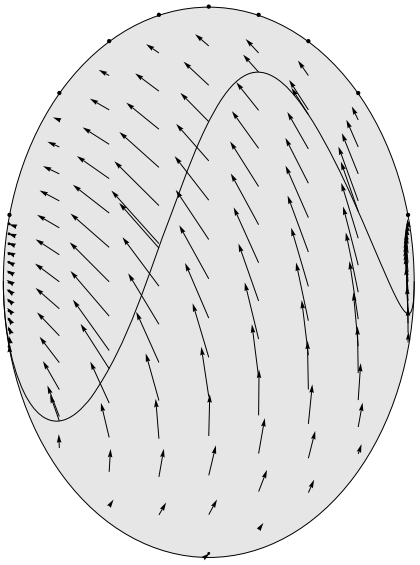

(c) $(\sigma_x, \sigma_y, \varphi) = (-0.15, 0, 2.5)$,
$(F_x^n, F_y^n) = (0.65, 0.30)$

Fig. 10.43 Examples of tangential stress distributions: (**a**) pure spin slip φ, (**b**) pure longitudinal slip σ_x and (**c**) both φ and σ_x. Values of φ are in m^{-1}

In the next sections two possible simplified approaches will be developed. They lead to complementary transient models. In both cases, inertia effects are totally neglected.

10.8.1 Transient Model with Carcass Compliance only

A possible way to partly generalize the steady-state brush model discussed in Sect. 10.3 is to relax only the second condition of p. 302, while still retaining the first one, that is:

- $\mathbf{e}_{,t} = \mathbf{0}$;
- $\dot{\mathbf{q}} \neq \mathbf{0}$.

This approach, which leads to quite a simple and very popular transient tire model, discards the transition in the bristle deflection pattern and takes care only of the transient deformation of the carcass.[12] Therefore, although rarely stated explicitly, it can be safely employed whenever the carcass stiffnesses w_x and/or w_y are much lower than the tread stiffness $K_t = 4abk$

$$w_i \ll 4abk, \quad i = x, y \tag{10.108}$$

Indeed, this condition makes $\dot{\mathbf{F}}_t \neq \mathbf{0}$ in (10.38) although $\mathbf{e}_{,t} \approx \mathbf{0}$.

The general governing equations (10.35) and (10.36), with the assumption $\mathbf{e}_{,t} = \mathbf{0}$, become

$$\mathbf{e}' = \boldsymbol{\rho} - \varphi(\hat{x}\mathbf{j} - \hat{y}\mathbf{i}) = \boldsymbol{\varepsilon} \quad \Longleftrightarrow \quad k|\mathbf{e}| < \mu_0 p \quad \text{(adhesion)} \tag{10.109}$$

$$k\mathbf{e} = -\mu_1 p \frac{\boldsymbol{\varepsilon} - \mathbf{e}'}{|\boldsymbol{\varepsilon} - \mathbf{e}'|} \quad \Longleftrightarrow \quad \left|\boldsymbol{\varepsilon} - \mathbf{e}'\right| \neq 0 \quad \text{(sliding)} \tag{10.110}$$

formally *identical* to the governing equations (10.46) and (10.47) of the steady-state case, but with $\boldsymbol{\rho} = \boldsymbol{\sigma} + \mathbf{q}'$ in place of $\boldsymbol{\sigma}$. Therefore, the whole analysis developed in Sect. 10.3 holds true in this case as well, with the only difference that $\boldsymbol{\rho}$ replaces any occurrence of $\boldsymbol{\sigma}$. Of particular importance is to understand that the global tangential force $\mathbf{F}_t = \mathbf{F}_t(\boldsymbol{\rho}, \varphi)$ is exactly the *same function* of (10.62). For instance, in a rectangular contact patch with $\varphi = 0$ the magnitude of $\mathbf{F}_t$ is given by a formula like in (10.95)

$$F_t = F_t\big(\rho(t)\big) = C_\sigma \rho \left[1 - \frac{\rho}{\sigma_s}\left(\frac{1+2\chi}{1+\chi}\right) + \left(\frac{\rho}{\sigma_s}\right)^2 \left(\frac{1+3\chi}{3(1+\chi)}\right)\right] \tag{10.111}$$

with $\rho = |\boldsymbol{\rho}|$, while the components $F_x(\rho_x, \rho_y)$ and $F_y(\rho_x, \rho_y)$ and their partial derivatives are given by (10.89) and (10.90), respectively. Of course, $\boldsymbol{\rho} = \rho_x \mathbf{i} + \rho_y \mathbf{j}$.

[12] This kind of models are often referred to as single contact point transient tire models [8].

However, since $\boldsymbol{\rho}(t) = \boldsymbol{\sigma}(t) + \dot{\mathbf{q}}(t)/V_r(t)$, the transient slip $\boldsymbol{\rho}(t)$ is an unknown function and an additional vectorial equation is necessary (it was not so in the steady-state case, which had $\dot{\mathbf{q}} = \mathbf{0}$). The key step is obtaining $\dot{\mathbf{F}}_t$ and inserting it into (10.37), as already done in Sect. 10.2. The simplification with respect to the transient general case is that here $\mathbf{F}_t(\boldsymbol{\rho}, \varphi)$ is a known function and hence

$$\begin{cases} \dot{F}_x = \dfrac{\partial F_x}{\partial \rho_x}\dot{\rho}_x + \dfrac{\partial F_x}{\partial \rho_y}\dot{\rho}_y + \dfrac{\partial F_x}{\partial \varphi}\dot{\varphi} = w_x V_r(\rho_x - \sigma_x) \\ \dot{F}_y = \dfrac{\partial F_y}{\partial \rho_x}\dot{\rho}_x + \dfrac{\partial F_y}{\partial \rho_y}\dot{\rho}_y + \dfrac{\partial F_y}{\partial \varphi}\dot{\varphi} = w_y V_r(\rho_y - \sigma_y) \end{cases} \tag{10.112}$$

where, as shown in (10.90), the partial derivatives are known functions. This is a system of linear differential equations with nonconstant coefficients in the unknown functions $\rho_x(t)$ and $\rho_y(t)$. In general, it requires a numerical solution. *Generalized relaxation lengths* can be defined in (10.112)

$$\begin{aligned} s_{xx} &= -\frac{\partial F_x}{\partial \rho_x}\frac{1}{w_x}, \qquad & s_{xy} &= -\frac{\partial F_x}{\partial \rho_y}\frac{1}{w_x} \\ s_{yx} &= -\frac{\partial F_y}{\partial \rho_x}\frac{1}{w_y}, \qquad & s_{xy} &= -\frac{\partial F_y}{\partial \rho_y}\frac{1}{w_y} \end{aligned} \tag{10.113}$$

Of course, they are functions of ρ_x and ρ_y. In [8, p. 346] this kind of model is called fully nonlinear.

The most popular version of (10.112) assumes, more or less explicitly, a linear function $\mathbf{F}_t(\boldsymbol{\rho}, \varphi) = -C_\sigma(\rho_x \mathbf{i} + \rho_y \mathbf{j}) + C_\varphi \varphi \mathbf{j}$, exactly like in (10.67). Accordingly, Eqs. (10.112) become

$$\begin{aligned} -C_\sigma \dot{\rho}_x &= w_x V_r(\rho_x - \sigma_x) \\ -C_\sigma \dot{\rho}_y &= w_y V_r(\rho_y - \sigma_y) - C_\varphi \dot{\varphi} \end{aligned} \tag{10.114}$$

often conveniently rewritten as

$$\begin{aligned} s_x \dot{\rho}_x + V_r \rho_x &= V_r \sigma_x \\ s_y \dot{\rho}_y + V_r \rho_y &= V_r \sigma_y + s_\varphi \dot{\varphi} \end{aligned} \tag{10.115}$$

where the constants

$$s_x = \frac{C_\sigma}{w_x} \quad \text{and} \quad s_y = \frac{C_\sigma}{w_y} \tag{10.116}$$

are called, respectively, longitudinal and lateral *relaxation lengths*. Obviously, $s_x \le s_{xx}$ and $s_y \le s_{yy}$. The term $s_\varphi \dot{\varphi}$, with $s_\varphi = C_\varphi / w_y$, is usually discarded because it is really very small. The two equations in (10.115) are no longer a system of equations, which simplifies further the model. With the data listed in (10.43), we have $s_x = a$ and $s_y = 4a$.

Consistently with the assumption of linear tire behavior, inserting $\mathbf{F}_t = -C_\sigma \boldsymbol{\rho}$ into (10.115) leads to the most classical *transient linear tire model* ($i = x, y$)

$$s_i \dot{F}_i + V_r(t) F_i = -V_r(t) C_\sigma \sigma_i(t) \tag{10.117}$$

that is, to nonhomogeneous linear first-order differential equations [5]. The simplest case is with constant V_r, which makes the equations with constant coefficients. The homogeneous counterpart of (10.117) has solution

$$F_i^O(t) = \mathscr{A} \mathrm{e}^{-\frac{V_r}{s_i} t} \tag{10.118}$$

If also σ_i is constant, a particular solution is simply $F_i^p = -C_\sigma \sigma_i$. Therefore, in this case the general solution of (10.117) with initial condition $F_i(0) = 0$ is

$$F_i(t) = -C_\sigma \sigma_i \left(1 - \mathrm{e}^{-\frac{V_r}{s_i} t}\right) \tag{10.119}$$

Under these very peculiar operating conditions, $F_i(s_i / V_r) = -0.63 C_\sigma \sigma_i$, which is often employed as a way to measure experimentally the relaxation length s_i. Also interesting is the particular solution if $\sigma_i(t) = \sigma_0 \sin(\omega t)$ (the homogeneous solution decays very rapidly)

$$F_i^p(t) = -\frac{C_\sigma \sigma_0}{\sqrt{1 + (\omega s_i / V_r)^2}} \sin\left(\omega t - \arctan(\omega s_i / V_r)\right) \tag{10.120}$$

It is worth noting how the term $\omega s_i / V_r$ affects both the amplitude (reducing it) and the phase shift. The tire force is delayed with respect to the input.

Finally, it should be remarked that it is very common in the vehicle dynamics community to employ (10.115), instead of (10.112), with a nonlinear function for the tangential force, like, e.g., $\mathbf{F}_t = -(\boldsymbol{\rho}/\rho) F_t(\rho)$ as in (10.89). Things are a bit mixed up, but the allure of simplicity is quite powerful. Indeed, the differential equations in (10.112) are much more involved than those in (10.115), while employing a nonlinear function for $\mathbf{F}_t$ is fairly straightforward. In [8, p. 345] this kind of model is called semi-nonlinear.

10.8.2 Transient Model with Carcass and Tread Compliance

If the carcass and tread stiffnesses are comparable, that is if (10.108) does not hold, the effects of $\mathbf{e}_{,t}$ should also be taken into account, particularly under severe transient conditions. Therefore, both conditions listed at p. 302 are relaxed, that is:

- $\mathbf{e}_{,t} \neq \mathbf{0}$;
- $\dot{\mathbf{q}} \neq \mathbf{0}$.

To keep the formulation rather simple, while still grasping the main phenomena, it is useful to work under the following simplifying assumptions:

- rectangular shape of the contact patch, which means $x_0(\hat{y}) = a$;
- no spin slip φ;
- either pure longitudinal slip σ_x or pure lateral slip σ_y, but not both;
- $\mu_0 = \mu_1$, that is both equal to μ.

It is worth noting that complete adhesion in the contact patch is *not* assumed (cf. [8, p. 220]). Like in Sect. 10.2, boundary conditions at the leading edge and initial conditions on the whole contact patch need to be supplied, that is

$$\mathbf{e}(a, \hat{y}, t) = 0, \quad \text{and} \quad \mathbf{e}(\hat{x}, \hat{y}, 0) = \mathbf{0} \tag{10.121}$$

Nonzero initial conditions are possible, but may lead to more involved formulations.

Like in Sect. 10.5.1, the first two simplifying assumptions, along with zero initial conditions, make $\mathbf{e}$, and actually the whole formulation, not dependent on $\hat{y}$. The additional effect of the third assumption is to have $\mathbf{e}(\hat{x}, t)$ and $\boldsymbol{\rho}(t)$ with only one nonzero component (directed like either $\mathbf{i}$ or $\mathbf{j}$).

With $\varphi = 0$, the first general governing equation (10.35) (adhesion region) becomes

$$V_r \mathbf{e}_{,\hat{x}} - \mathbf{e}_{,t} = V_r \boldsymbol{\rho} \tag{10.122}$$

which is a nonhomogeneous transport equation in the unknown function $\mathbf{e}(\hat{x}, t) = \mathbf{e}_a(\hat{x}, t)$. The tangential stress in the adhesion region is given by $\mathbf{t}_a(\hat{x}, t) = k\mathbf{e}_a$.

The adhesion state starts at the leading edge $\hat{x} = a$ and is maintained up to $\hat{x} = \hat{x}_s(t)$, which marks, at time t, the moving point where the friction limit is reached

$$k\left|\mathbf{e}_a\big(\hat{x}_s(t), t\big)\right| = \mu p\big(\hat{x}_s(t)\big) \tag{10.123}$$

and hence where the sliding region begins.

Exactly like in (10.86), the onset of sliding is with the bristle deflection that has the *same direction* as $\mathbf{e}_a(\hat{x}_s(t), t)$. Therefore, the governing equation (10.36) for the *sliding* region becomes simply

$$\mathbf{t}_s(\hat{x}) = k\mathbf{e}_s(\hat{x}) = \mu p(\hat{x}) \frac{\mathbf{e}_a(\hat{x}_s(t), t)}{|\mathbf{e}_a(\hat{x}_s(t), t)|}, \quad \text{with } -a \le \hat{x} < \hat{x}_s(t) \tag{10.124}$$

which is already the definition of $\mathbf{e}_s$ and hence of $\mathbf{t}_s$. It is important to note that in the sliding region the bristle deflections $\mathbf{e}_s$ do not depend on time and, therefore, are known. It is the moving transition point $\hat{x}_s(t)$ that has to be found as a function of time.

The global tangential force $\mathbf{F}_t(t) = F_x\mathbf{i} + F_y\mathbf{j}$ that the road applies to the tire model is given by the integral of $\mathbf{t} = k\mathbf{e}$ on the contact patch, like in (10.62), with all tangential stresses $\mathbf{t}$ having the same direction

$$\mathbf{F}_t(t) = -\mathbf{s}F_t(t) = k\left[2b\int_{\hat{x}_s(t)}^{a} \mathbf{e}_a(\hat{x}, t)\mathrm{d}\hat{x} + 2b\int_{-a}^{\hat{x}_s(t)} \mathbf{e}_s(\hat{x})\mathrm{d}\hat{x}\right] \tag{10.125}$$

Since also $\boldsymbol{\rho}(t) = \boldsymbol{\sigma}(t) + \dot{\mathbf{q}}(t)/V_r(t)$ is unknown, an additional equation is necessary. Exactly like in (10.38), it is obtained by differentiating $\mathbf{F}_t(t)$. But here, owing to the simplifying assumptions, some further steps can be carried out,[13] thus getting

$$\begin{aligned}\dot{\mathbf{F}}_t &= 2bk \int_{\hat{x}_s(t)}^{a} \mathbf{e}_{,t} \mathrm{d}\hat{x} = 2bkV_r \int_{\hat{x}_s(t)}^{a} (\mathbf{e}_{,\hat{x}} - \boldsymbol{\rho}) \mathrm{d}\hat{x} \\ &= 2bkV_r \big[-\mathbf{e}\big(\hat{x}_s(t), t\big) - \big(a - \hat{x}_s(t)\big)\boldsymbol{\rho}(t) \big] \end{aligned} \tag{10.126}$$

since $\mathbf{e}(a, t) = 0$. This result can be inserted into (10.39) to get the sought equation

$$-2bk \big[\mathbf{e}\big(\hat{x}_s(t), t\big) + \big(a - \hat{x}_s(t)\big)\boldsymbol{\rho}(t) \big] = \mathbf{W}\big[\boldsymbol{\rho}(t) - \boldsymbol{\sigma}(t)\big] \tag{10.127}$$

where $\mathbf{W}$ is a diagonal matrix, as in (10.11).

Summing up, the problem is therefore governed by either of the two following (formally identical) systems of differential-algebraic equations, with suitable boundary and initial conditions

$$\begin{cases} V_r e_{x,\hat{x}} - e_{x,t} = V_r \rho_x \\ k \big| e_x\big(\hat{x}_s(t), t\big) \big| = \mu p\big(\hat{x}_s(t)\big) \\ \rho_x(t) = \dfrac{w_x \sigma_x(t) - 2bk e_x(\hat{x}_s(t), t)}{w_x + 2bk(a - \hat{x}_s(t))} \\ e_x(a, t) = 0 \\ e_x(\hat{x}, 0) = 0 \end{cases} \qquad \begin{cases} V_r e_{y,\hat{x}} - e_{y,t} = V_r \rho_y \\ k \big| e_x\big(\hat{x}_s(t), t\big) \big| = \mu p\big(\hat{x}_s(t)\big) \\ \rho_y(t) = \dfrac{w_y \sigma_y(t) - 2bk e_y(\hat{x}_s(t), t)}{w_y + 2bk(a - \hat{x}_s(t))} \\ e_y(a, t) = 0 \\ e_y(\hat{x}, 0) = 0 \end{cases} \tag{10.128}$$

where, possibly, $V_r = V_r(t)$. Zero initial conditions imply that $\rho_i(0) = w_i \sigma_i(0)/(w_i + 4abk)$.

It should be remarked that, unlike the commonly used approaches described in the previous section, the proposed model accounts not only for the transient deformation of the carcass (i.e., $\dot{\mathbf{q}} \neq \mathbf{0}$), but also for the transient behavior of the bristle deflection pattern (i.e., $\mathbf{e}_{,t} \neq \mathbf{0}$). It will be shown that this last effect may be far from negligible in some important cases, particularly in braking/driving wheels. More

[13] The main points are: $\mathbf{e}_s$ not depending on time, $\mathbf{e}_a(\hat{x}_s, t) = \mathbf{e}_s(\hat{x}_s)$.

precisely, the larger any of the ratios

$$\theta_x = \frac{w_x}{K_t}, \qquad \theta_y = \frac{w_y}{K_t} \tag{10.129}$$

where $K_t = 4abk$ is the tread stiffness, the more relevant the effect of the bristle deflection in that direction. Since $w_x \gg w_y$, the transient behavior in the bristle deflection pattern has more influence when the wheel is subject to time-varying longitudinal slip. For instance, with the data reported at p. 302, we have $\theta_x = 1$ and $\theta_y = 0.25$.

10.8.3 Numerical Examples

The proposed models for the transient behavior of tires are compared on a few numerical tests. The goal is to show the range of applicability and to warn about employing a model without really understanding its capabilities.

In particular, three models of increasing complexity are compared. All tests are performed with the data listed in (10.43), except for $\chi = 0$, and under either pure longitudinal slip or pure lateral slip. Moreover, a brush model with rectangular contact patch and parabolic pressure distribution is assumed.

The *first model* (semi-nonlinear single contact point) takes into account only the carcass compliance and employs a constant relaxation length s_i, with $i = x, y$. According to (10.115), the model is defined by

$$\begin{cases} s_i \dot{\rho}_i + V_r \rho_i = V_r \sigma_i \\ \rho_i(0) = 0 \end{cases} \tag{10.130}$$

where $s_i = C_\sigma / w_i$, with $C_\sigma = 4ka^2b$ as in (10.74). Once the function $\rho_i(t)$ has been obtained, the global tangential force is given by the nonlinear function

$$F_i(\rho_i) = -C_\sigma \rho_i \left[1 - \frac{|\rho_i|}{\sigma_s} + \frac{1}{3} \left(\frac{\rho_i}{\sigma_s} \right)^2 \right] \tag{10.131}$$

much like in (10.89) with (10.95).

The *second model* (nonlinear single contact point) is similar, but employs a non-constant relaxation length, as in (10.112)

$$\begin{cases} -\dfrac{F_i'(\rho_i)}{w_i} \dot{\rho}_i + V_r \rho_i = V_r \sigma_i \\ \rho_i(0) = 0 \end{cases} \tag{10.132}$$

where (cf. (10.96) with $\chi = 0$)

$$F_i'(\rho_i) = -C_\sigma \left[1 - 2\frac{|\rho_i|}{\sigma_s} + \left(\frac{\rho_i}{\sigma_s} \right)^2 \right] \tag{10.133}$$

A numerical solution is usually required. Again, the function $\rho_i(t)$ is then inserted into (10.131).

The *third model* (nonlinear full contact patch) takes into account both the carcass and tread compliances, as in (10.128)

$$\begin{cases} V_r e_{i,\hat{x}} - e_{i,t} = V_r \rho_i \\ k\left|e_i\left(\hat{x}_s(t), t\right)\right| = \mu p\left(\hat{x}_s(t)\right) \\ \rho_i(t) = \dfrac{w_i \sigma_i(t) - 2bk e_i(\hat{x}_s(t), t)}{w_i + 2bk(a - \hat{x}_s(t))} \\ e_i(a, t) = 0 \\ e_i(\hat{x}, 0) = 0 \end{cases} \tag{10.134}$$

To obtain a numerical solution, an iterative method can be employed. First make an initial guess for $\rho_i^{(0)}(t)$ (for instance $\rho_i^{(0)}(t) = (\sigma_i(t) + \rho_i^s(t))/2$, where $\rho_i^s(t)$ is the solution of (10.130)). By means of the first equation, numerically obtain $e_x^{(0)}(\hat{x}, t)$, and then, using the second equation, evaluate the function $\hat{x}_s^{(0)}$. At this stage, the first iteration can be completed by computing $\rho_i^{(1)}(t)$ by means of the third equation. The whole procedure has to be repeated (usually 5 to 15 times) until convergence is attained.

Once a good approximation of $e_i(\hat{x}, t)$ and $\hat{x}_s(t)$ (and also of $\rho_i(t)$) has been computed, the tangential force can be obtained from the following integral over the contact patch

$$F_i(t) = 2bk\left[\int_{\hat{x}_s(t)}^{a} e_i(\hat{x}, t)\mathrm{d}\hat{x} + \mu\,\mathrm{sign}\left(e_i\left(\hat{x}_s(t), t\right)\right)\int_{-a}^{\hat{x}_s(t)} p(\hat{x})\mathrm{d}\hat{x}\right] \tag{10.135}$$

A *step change* in the input (forcing) function $\sigma_i(t)$ works well to highlight the differences between the three models. With the data of (10.43), except $\chi = 0$, the static tangential force (10.131) has maximum magnitude for $\sigma = 0.266$. To test the models in both the (almost) linear and nonlinear ranges, a small ($\sigma_i = -0.07$) and a large ($\sigma_i = -0.21$) step have been selected. Since $w_x = 4w_y$, both longitudinal and lateral numerical tests are performed.

In all cases, results are plotted versus the rolling distance s, instead of time, thus making $V_r(t)$ irrelevant.

10.8.3.1 Longitudinal Step Input

The longitudinal force $F_x(s)$, as obtained from the three tire models with step inputs $\sigma_x = -0.07$ and $\sigma_x = -0.21$, is shown in Fig. 10.44. Because of the high value of the longitudinal carcass stiffness w_x (equal to the tread stiffness K_t), the transient phenomenon is quite fast. Indeed, in the first model (*dashed line*) the relaxation length $s_x = 7.5$ cm.

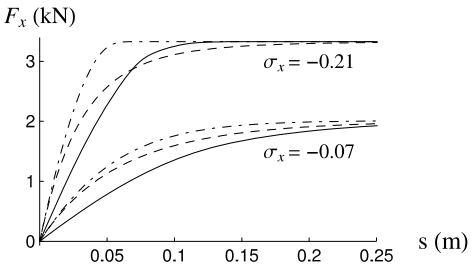

Fig. 10.44 Longitudinal force response to small and large step changes in σ_x. Comparison of three tire models: semi-nonlinear single contact point (*dashed line*), nonlinear single contact point (*dot-dashed line*), nonlinear full contact patch (*solid line*)

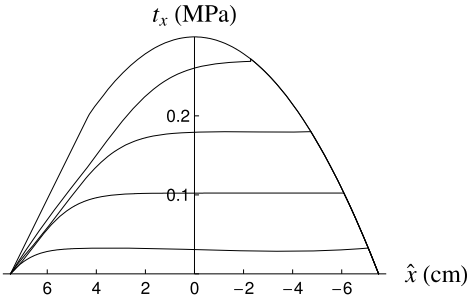

Fig. 10.45 Transient patterns of the tangential stress t_x in the contact patch (third model)

Quite remarkably, the three models provide very different results, thus showing that the selection of the transient tire model may be a crucial aspect in vehicle dynamics, particularly when considering vehicles equipped with ABS.

The behavior of the first model (*dashed lines*) is the same in both cases, except for a vertical scaling. This is not the case for the second model (*dot-dashed lines*) because of the nonconstant generalized relaxation length. The more detailed third model (*solid lines*) behaves in quite a peculiar way, thus confirming that the contribution of the transient tread deflection is far from negligible.

Figure 10.45 shows the transient pattern of the tangential longitudinal stress t_x in the contact patch as provided by the third model with $\sigma_x = -0.21$. It is worth noting how greatly, in the adhesion region, the pattern departs from the linear behavior of the static case (Fig. 10.10).

10.8.3.2 Lateral Step Input

The lateral force $F_y(s)$, as obtained from the three tire models with step inputs $\sigma_y = -0.07$ and $\sigma_y = -0.21$, is shown in Fig. 10.46. Because of the low value of the lateral carcass stiffness w_y (equal to one fourth of the tread stiffness K_t), the transient phenomenon is not as fast as in the longitudinal case. Indeed, in the first model the relaxation length $s_y = 30$ cm.

In this case, the three models provide not very different results in the linear range, while they depart significantly in the nonlinear range, that is with $\sigma_y = -0.21$. Therefore, the selection of the transient tire model may be crucial in lateral dynamics as well.

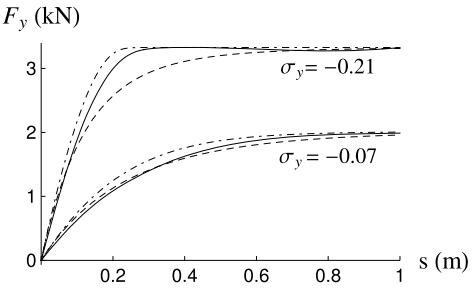

Fig. 10.46 Lateral force response to small and large step changes in σ_y. Comparison of three tire models: semi-nonlinear single contact point (*dashed line*), nonlinear single contact point (*dot-dashed line*), nonlinear full contact patch (*solid line*)

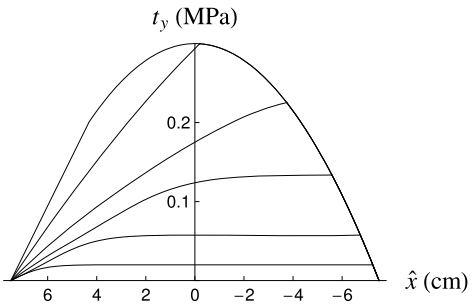

Fig. 10.47 Transient patterns of the tangential stress t_y in the contact patch (third model)

It should be observed from Figs. 10.44 and 10.46 that the first and second models have the same "formal" behavior. Therefore, changing the carcass stiffness results only in a horizontal scaling. This is not true for the third model.

Figure 10.47 shows the transient pattern of the tangential lateral stress in the contact patch as provided by the third model with $\sigma_y = -0.21$. There are still differences with respect to the static case, although not as much as in Fig. 10.45.

10.9 Summary

In this chapter a relatively simple, yet significant, tire model has been developed. It is basically a brush model, but with some noteworthy additions with respect to more common formulations. For instance, the model takes care of the transient phenomena that occur in the contact patch. A number of figures show the pattern of the local actions within the contact patch (rectangular and elliptical).

10.10 List of Some Relevant Concepts

p. 299 the skating slip takes into account both transient translational slip and spin slip;
p. 304 each bristle is undeformed when it enters the contact patch;

p. 312 the analysis of the steady-state behavior of the brush model is quite simple if there is no spin slip;
p. 318 full sliding does not imply wheel locking;
p. 322 the slip angle α is not a good parameter for a neat description of tire mechanics;
p. 323 tires have to be built in such a way to provide the maximum tangential force in any direction with small slip angles. This is a fundamental requirement for a wheel with tire to have a directional capability;
p. 324 the tire action surface summarizes the tire characteristics under a constant vertical load;
p. 326 the tire action surface summarizes the steady-state behavior of a tire;
p. 332 good wheel directional capability means small slip angles.

References

1. Clark SK (ed) (1971) Mechanics of pneumatic tires. National Bureau of Standards, Washington
2. Deur J, Asgari J, Hrovat D (2004) A 3D brush-type dynamic tire friction model. Veh Syst Dyn 42:133–173
3. Deur J, Ivanovic V, Troulis M, Miano C, Hrovat D, Asgari J (2005) Extension of the LuGre tyre friction model related to variable slip speed along the contact patch length. Veh Syst Dyn 43(Supplement):508–524
4. Hüsemann T (2007) Tire technology: simulation and testing. Tech rep, Institut für Kraftfahrwesen, Aachen. http://www.ika.rwth-aachen.de/lehre/kfz-labor/2_tires_en.pdf
5. Kreyszig E (1999) Advanced engineering mathematics, 8th edn. Wiley, New York
6. Lugner P, Pacejka H, Plöchl M (2005) Recent advances in tyre models and testing procedures. Veh Syst Dyn 43:413–436
7. Milliken WF, Milliken DL (1995) Race car vehicle dynamics. SAE International, Warrendale
8. Pacejka HB (2002) Tyre and vehicle dynamics. Butterworth–Heinemann, Oxford
9. Pacejka HB, Sharp RS (1991) Shear force development by pneumatic tyres in steady state conditions: a review of modelling aspects. Veh Syst Dyn 20:121–176
10. Savaresi SM, Tanelli M (2010) Active braking control systems design for vehicles. Springer, London
11. Truesdell C, Rajagopal KR (2000) An introduction to the mechanics of fluids. Birkhäuser, Boston
12. Zwillinger D (ed) (1996) CRC standard mathematical tables and formulae, 30th edn. CRC Press, Boca Raton

Index

M. Guiggiani, *The Science of Vehicle Dynamics*, DOI 10.1007/978-94-017-8533-4,